2020

Chirality-Assisted Synthesis of Single-Handed Freeform Helical Ladder Polymers

Kyle Everett Murphy
University of Vermont

CHIRALITY-ASSISTED SYNTHESIS OF SINGLE-HANDED FREEFORM HELICAL LADDER POLYMERS

A Dissertation Presented

by

Kyle Everett Murphy

to

The Faculty of the Graduate College

of

The University of Vermont

In Partial Fulfillment of the Requirements
for the Degree of Doctor of Philosophy
Specializing in Chemistry

May, 2020

Defense Date: December 10, 2019
Dissertation Examination Committee:

Severin T. Schneebeli, Ph.D., Advisor
Scott W. Morrical, Ph.D., Chairperson
Matthias Brewer, Ph.D.
Rory Waterman, Ph.D.
Cynthia J. Forehand, Ph.D., Dean of the Graduate College

ABSTRACT

In nature, shape defines function, and as such scientists have long since attempted to mimic nature in a pursuit to reach a similar level of fidelity. Complex macromolecular structures and shapes have been developed with interesting and unique functionalities—such as the design and synthesis of molecular machines. However, macromolecular structures such as these are difficult to synthesize. My work in the Schneebeli group builds upon this challenge, where I have developed a strategy to precisely control the shape of macromolecules to generate well-defined structures. This was accomplished with stereoisomerically pure triptycene-like derivatives as the building block pieces which have an inherent three-dimensional scaffold. With my own developed methodology by which they can be exactly functionalized, these building blocks can then couple together in a unique fashion not unlike Lego pieces. This synthetic technology leads to controlled growth of a molecular structure with precisely predictable shapes. In particular, my work involves the generation of short molecular strips, both linear and with a helical bend, as well as ladder polymer molecular helices of different pitches, which were probed for their spring-like motions. The development of these three-dimensional building blocks, their affinity for coupling in a controllable fashion, and their ability to be functionalized with through-space directed aromatic nitration methodology, laid the foundation for much of the research in the Schneebeli group related to chirality-assisted synthesis (CAS).

CITATION

Material from this dissertation has been published in the following form:

Murphy, K. E.; Bocanegra, J. L.; Liu, X.; Chau, H. Y. K.; Lee, P. C.; Li, J.; Schneebeli, S. T.. **2017**. Precise through-space control of an abiotic electrophilic aromatic substitution reaction. *Nature Communications*, *8*, 14840.

DEDICATION

I dedicate this work to my parents, for trusting me enough to let me pursue my passions.

ACKNOWLEDGMENTS

It would be difficult to imagine my graduate school career without many of the people I've come to know here. First, I have to give my greatest appreciations to my advisor Severin Schneebeli. Without Severin's constant advice, enthusiasm, and his own passion for science, I don't think I'd be half the chemist I am today. I can say for sure I certainly picked up his enthusiasm for learning, and determination to struggle through any challenging hurdle in my way.

I've been very fortunate to spend my time with a lot of like-minded individuals, next to none, they were like family. All of who I treasure their friendship and all of the time we spent together, dearly. Whether we were idly chatting in the hallway, lab, or off in the organic office, it was an incredible time. Playing DnD in particular helped bolster my creativity in ways I couldn't imagine. And, so often we would make each other laugh, mouth filled with drink or food downtown after a week of work. It was always an absolute pleasure to be able to be around everyone. After a tough time at school, it was a relief to be able to think about something else for a while, or simply to vent about the issues I had been having. I'll always remember those times together.

In no particular order, I'd like to give shout outs to: Brandon Ackley, Adam Dyer, Ramya Srinivasan, Dillon McCarthy, Kyle McKay, Jonathan Hollin, Nick Dodge, Magenta Hensinger, Joseph Campbell, Mona Sharafi, Teruki Watanabe, Evan Howard, Mark Mancini, Rebecca Bogart, Jordan Tocher, Ariel Schuelke-Sanchez, and Eleanor Fortner-Buczala. Without you all and your support and friendship, I'm not sure I would be the person I am today. I hope we'll able to see each other again and stay in touch.

TABLE OF CONTENTS

LIST OF FIGURES

Figure **Page**

LIST OF SCHEMES

Scheme **Page**

LIST OF ABBREVIATIONS

^{13}C NMR ..... Carbon nuclear magnetic resonance

^{1}H NMR ..... Proton nuclear magnetic resonance

B_2pin_2 ..... Bis(pinacolato)diboron

CAS ..... Chirality-assisted synthesis

CD ..... Circular Dichroism

COSY ..... Correlated Spectroscopy

DCC ..... Dynamic covalent chemistry

DCM ..... Dichloromethane

DFT ..... Density functional theory

DMATS ..... Dimethylallyl tryptophan synthase

DMF ..... Dimethylformamide

DMSO ..... Dimethylsulfoxide

DOSY ..... Diffusion Ordered Spectroscopy

EAS ..... Electrophilic aromatic substitution

EDG ..... Electron-donating group

EtOAC ..... Ethyl acetate

EWG ..... Electron-withdrawing group

HOAc ..... Acetic acid

HOMO ..... Highest occupied molecular orbital

HRMS ..... High-resolution mass spectrometry

LAH ..... Lithium aluminum hydride

LRMS ..... Low-resolution mass spectrometry

LUMO ..... Lowest unoccupied molecular orbital

M_n ..... Number average molar mass

m/z ..... Mass-to-charge ratio

NMR ..... Nuclear magnetic resonance

NOE ..... Nuclear Overhauser effect

PAH ..... Polycyclic aromatic hydrocarbon

PDI ..... Polydispersity Index

ROESY ..... Rotating-frame Overhauser effect correlation Spectroscopy

S_EAr ..... Aromatic electrophilic substitution

TFA ..... Trifluoroacetic acid

TFAA ..... Trifluoroacetic anhydride

TLC ..... Thin-layer chromatography

TMS ..... Tetramethylsilane

CHAPTER 1: INTRODUCTION

1.1 Chirality-Assisted Synthesis

Nature is able to control the sequences and shapes of large macromolecules precisely in 3D. In many instances, this exquisite level of natural shape-control is made possible by the chiral building blocks (e.g. amino acids or glycosides) employed as the monomers. The well-defined shapes adopted by most biological macromolecules are vital to enabling highly selective recognition, complex self-assembly, and efficient catalysis that are crucial for life. As postulated in Anfinsen's dogma,[1] the structure of a protein is determined only by its amino acid sequence—or more simply, sequence defines structure. Nevertheless, most biological macromolecules only adopt well-defined shapes under specific conditions (e.g. in a certain solvent, at a certain pH, at a certain temperature, at a certain ionic strength, etc.). For this reason, learning how to generalize macromolecular shape control so that it becomes more predictable and less dependent on the environmental conditions has been a long sought after endeavor of biomimetic and supramolecular chemistry.[2, 3] One of the ultimate goals of this biomimetic research certainly is to create synthetic, sequence-defined polymers, which consistently fold into programmable three-dimensional shapes, regardless of the solvent, the temperature, the pH, and the ionic strength employed. Such a universal synthetic shape control system will likely outperform the natural way of controlling macromolecular shape in terms of predictability and programmability.

CAS was recently reported by the Schneebeli group as a universal method to precisely control the shapes of large molecular strips.[4] The method makes use of selective

double-amination reactions to couple chiral building blocks in a specific, programmable manner. Moreover, my own reaction methodology, as in addition to its ramifications for reaction design, has allowed for findings of precise, through-space directed S_EAr reactivity (**Chapter 2**) which also has practical implications for CAS. Thanks to biomimetic selective aromatic nitrations, designing stereomerically pure and thus well-defined molecular building blocks became possible. CAS employs chiral building blocks to assemble 3D molecular strips with predictable geometries. In general, a CAS monomer is defined as a shape-defined chiral building block, which forms at least two new bonds with another monomer in a regio- and stereospecific fashion with well-defined linkage geometry, much like a ladder polymer. As **Figure 1.1** illustrates, if we couple a mixture of achiral building blocks, a mixture of *syn*- and *anti*-products results. However, CAS with chiral building blocks leads to only a single product, which is *syn* in the example shown.

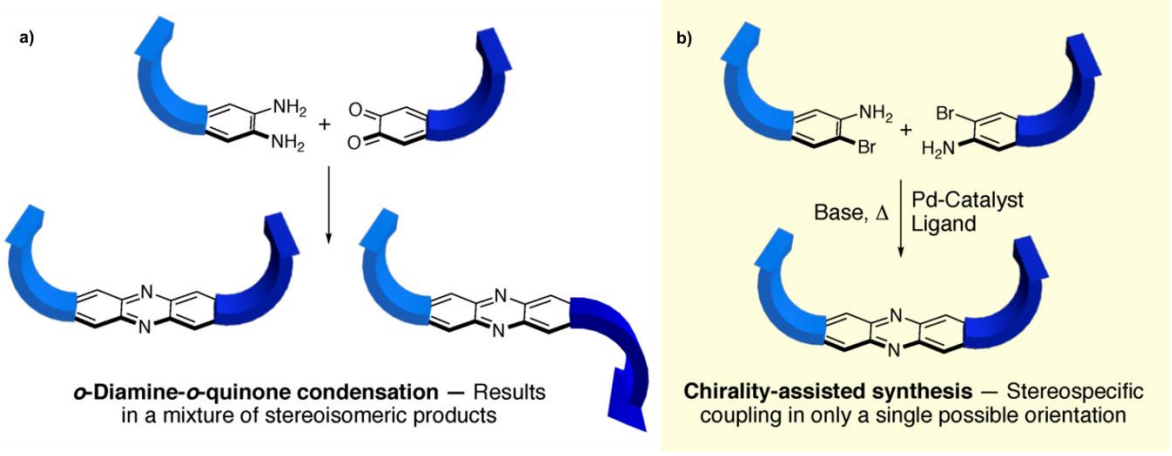

Figure 1.1. Illustrating the enhanced shape-control abilities CAS offers for polyaromatic phenazine strips. (**a**) With achiral building blocks, a mixture of *syn*- and *anti*-products

results. (**b**) CAS with chiral building blocks leads to only a single *syn* product—the selectivity can be switched to *anti* by changing the chirality of one of the monomers. (Reproduced with permission[5]).

CAS-based coupling of two identical strips (**Figure 1.1b**) leads solely to the *syn*-isomer, in a fully stereospecific and thus predictable manner. The most powerful aspect of the CAS concept is that the *syn*-stereospecificity can, in principle, be readily converted to anti, by simply changing the chirality of one of the coupling partners. CAS therefore encompasses an intrinsic ability to program (**Figure 1.2**) a wide-variety of molecular shapes in a deterministic fashion by simply adjusting the sequence and chirality of the building blocks. This unique programmability aspect is what sets CAS apart from complementary methods (e.g. alternating *exo*/*endo* selective Diels–Alder reactions[6]) that can be used to control the shapes of molecular strips.

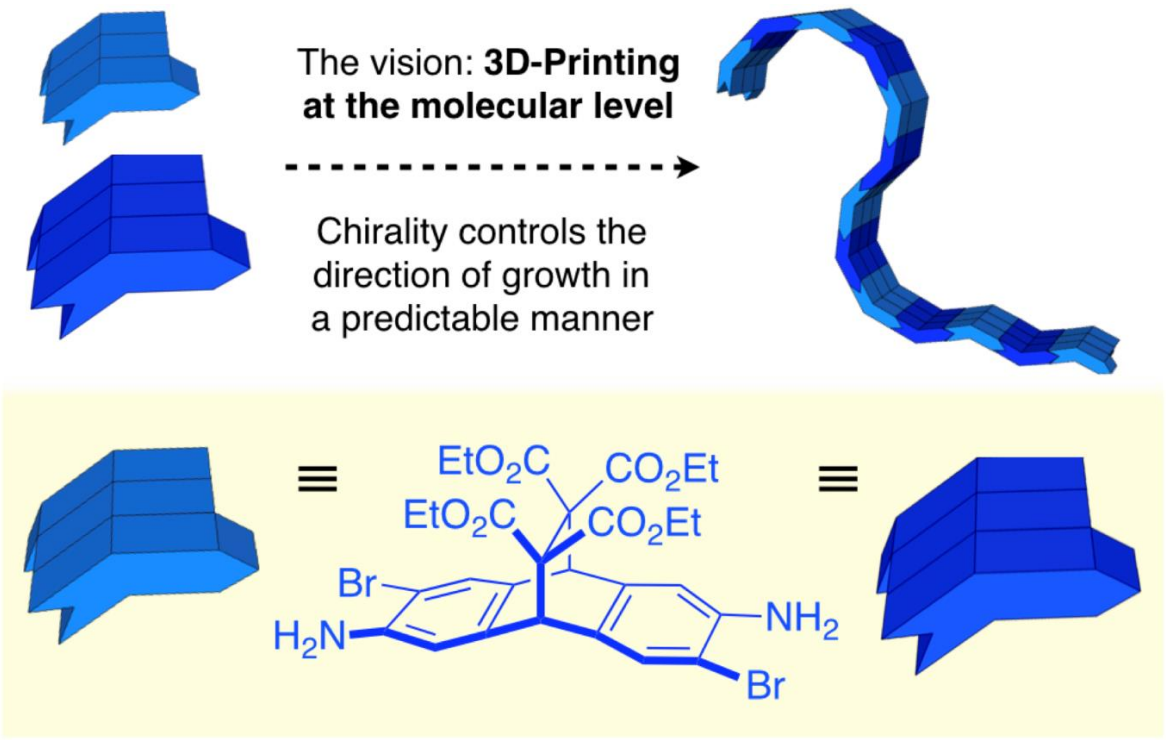

Figure 1.2. A perspective of how chirality-assisted synthesis will allow for programmable molecular shape control in the future. (Reproduced with permission[5]).

1.1.1. Previous Work in the Schneebeli Group on Chirality-Assisted Synthesis

Creating C-shaped molecular strips with large internal cavities efficiently has proven challenging, since mixtures of *syn*- and *anti*-stereoisomers are obtained (**Figure 1.1a**) with traditional coupling methods like *o*-dianiline/*o*-quinone condensations.[7] As previously described, CAS now overcomes this fundamental synthetic challenge, which allowed previous group member Dr. Xiaoxi Liu to synthesize (**Scheme 1.1**) some of the largest C-shaped molecular strips created to date with the help of CAS.[4] This early CAS work showed that if concave, enantiopure, monomeric, building blocks can be formed,

then the desired curvature and chirality of the overall C-shaped strip is fully defined by the chirality of the monomers. For the CAS growth, *o*-bromoaniline containing monomers were synthesized, the enantiomers were resolved with a unique diastereoselective gelation methodology (**Figure 1.4**), and the monomers were coupled (**Scheme 1.1**) with double Buchwald–Hartwig aminations. Owing to their well-defined shapes, structures created with CAS often exhibit unique properties, such as the C-shaped strips' ability to encapsulate pillar[5]arene macrocycles[4] (found by Dr. Xiaoxi Liu) and stacks of perylenediimide dyes (found by Dr. Mona Sharafi).[8]

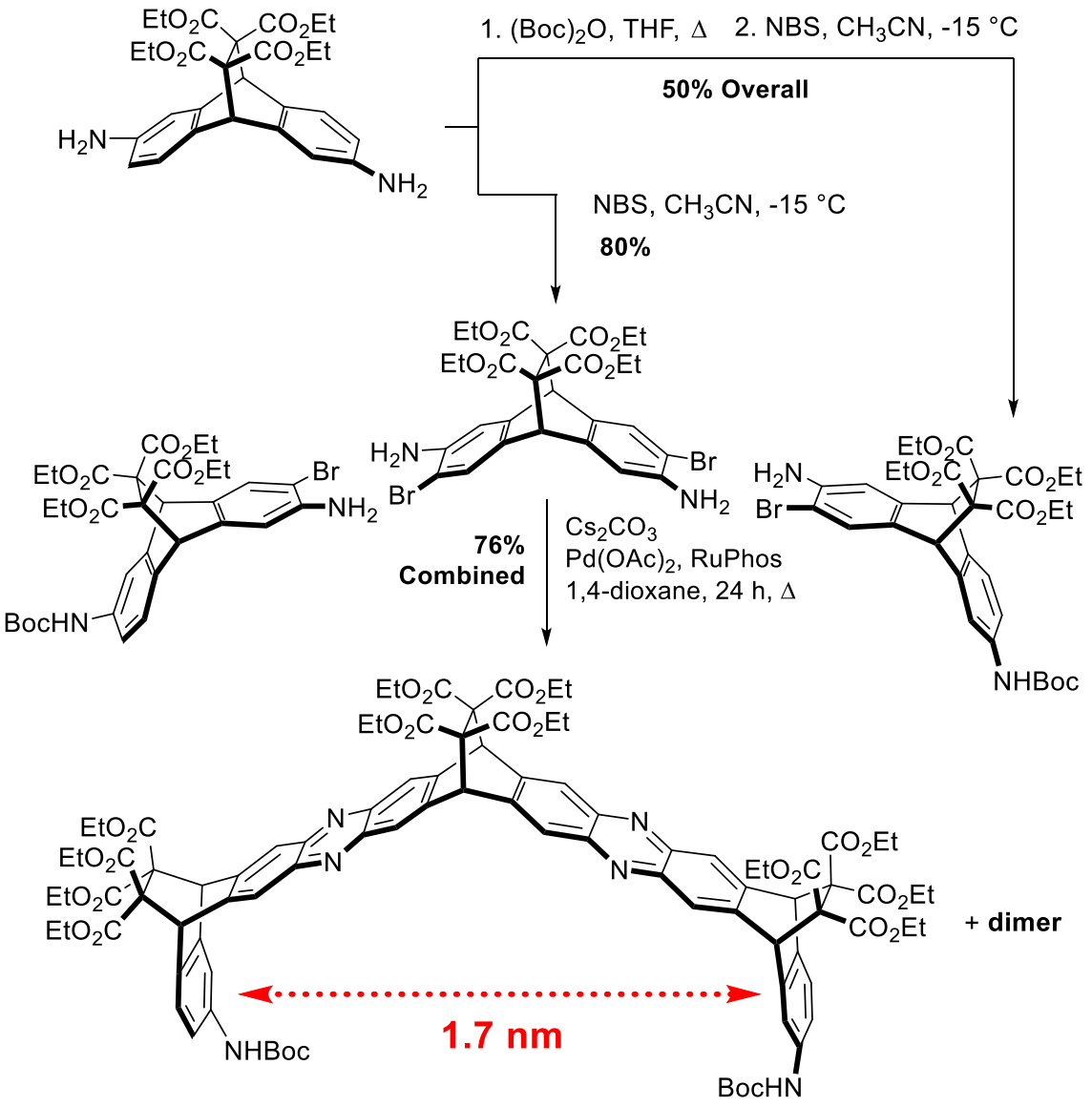

Scheme 1.1. Chirality-assisted couplings of *o*-bromoanilines leading to C-shaped molecular strips with large internal cavities.

Each of the C-shaped strips formed in this manner with CAS contains a prominent chiral cavity (**Scheme 1.1**), which is also able to achieve supramolecular shape recognition. For example—based on NMR evidence and all-atom molecular dynamics (MD) simulations—the CAS-based strips were found to encircle (**Figure 1.3**)

pillar[5]arene macrocycles. Up to the tetrameric strip, the association constants for the **pillar[5]arene@C-shaped-strip** complexes were measured to increase consistently with increasing lengths of the molecular strips. This finding is likely rooted in stronger π-π stacking interactions being present between the hosts and the guest for longer strips. Furthermore, the affinity of a third guest (e.g. viologen) for the central cavity of the pillar[5]arene ring increases, when a C-shaped strip is bound to the perimeter of the pillar[5]arene. This observed cooperative binding interaction between the C-shaped strips, the pillararene, and the viologen is likely caused by the C-shaped strip surrounding the pillar[5]arene—not unlike a molecular wrench.

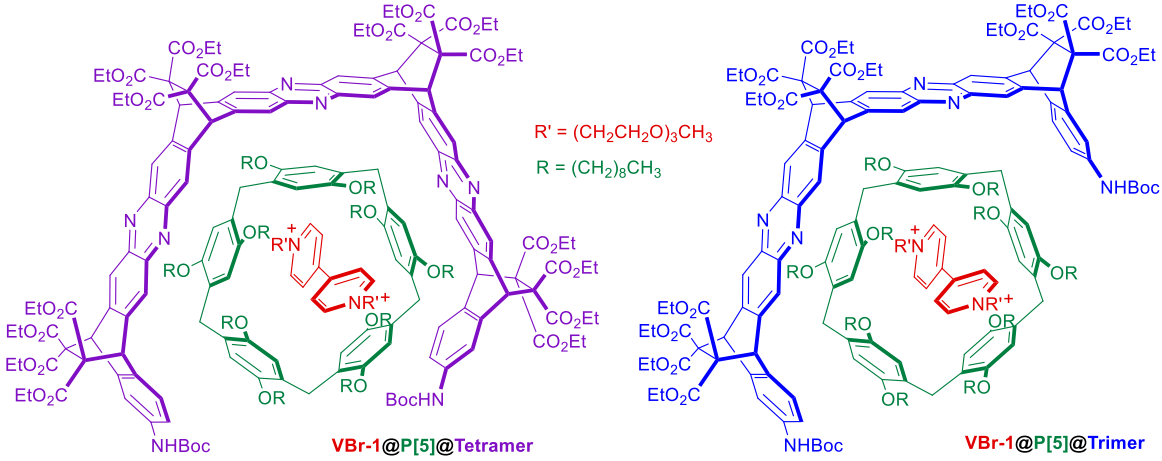

Figure 1.3. CAS-created molecular strips recognize pillar[5]arene macrocycles, and furthermore the generated complexes increase affinity to viologen.

Moreover, Dr. Xiaoxi Liu discovered that diastereoselective gelation, brought about by simply mixing a racemic acetonitrile solution of the diamine with dibenzoyl-*D*-tartaric acid, represents an effective means to isolate (**Figure 1.4**) the chiral (*S*,*S*)-diamine

in 98% *ee* on a multi-gram scale. While this chiral resolution-based approach is scalable, 50% of the material (the undesired enantiomer) is generally wasted during the resolution. The only exceptions are dynamic kinetic resolutions;[9] however such processes require stereoisomers to be in equilibrium with each other, which is not the case for the S_EAr nitration methodology currently used to access CAS monomers. Therefore, it is generally preferable to pursue stereoselective syntheses of the monomers required for CAS instead, as higher yields of the desired enantiomers are obtainable with regio- and stereoselective synthetic methodology.

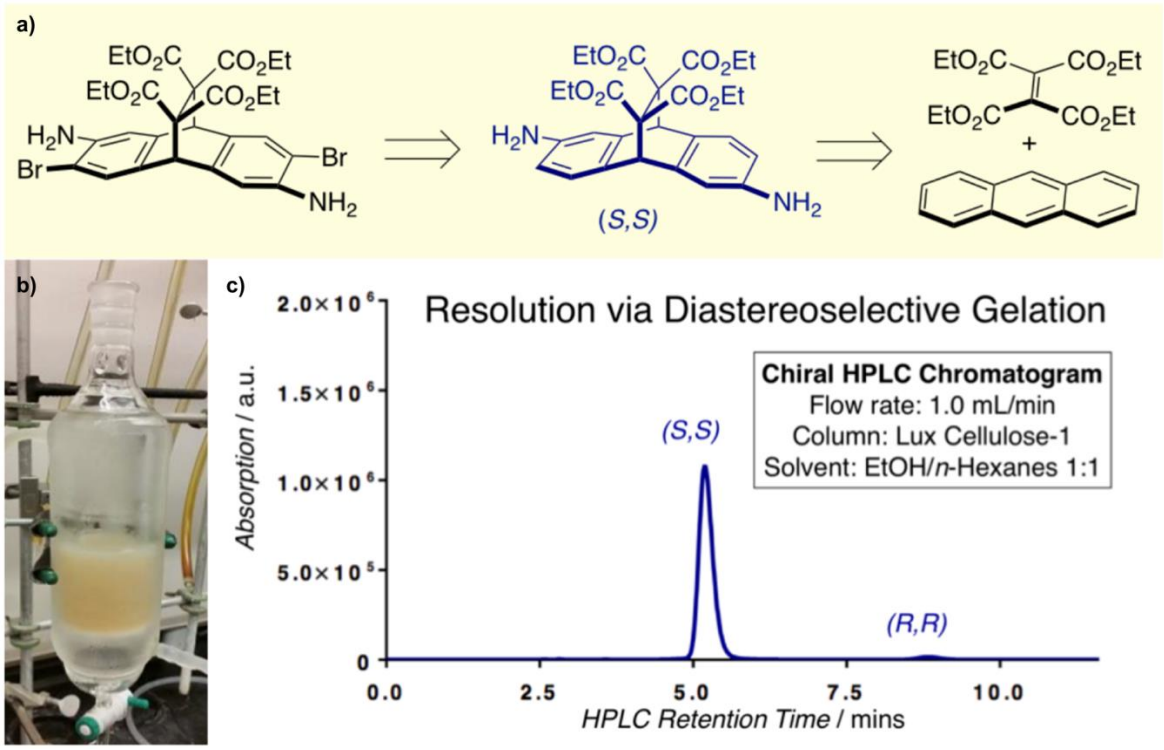

Figure 1.4. Resolution of chiral monomers for CAS by diastereoselective gelation. (**a**) Retrosynthesis of the chiral CAS building block, with gelation-based resolution occurring at the diamine stage. (**b**) Custom glassware (an ice-water cooled chromatography column) used for the gelation-based, chiral resolution process. (**c**) Chiral HPLC trace of the (*S*,*S*)-diamine, which was subjected twice to the gelation-based resolution process. (Reproduced with permission[5]).

Thus, CAS can be utilized in constructing large molecular architectures so long as the molecular building blocks are (i) stereomerically pure, (ii) have the functionality to generate ladder-type linkages upon coupling, and (iii) possess a stiff core to promote some rigidity throughout the final molecular scaffold. To again pull from Anfinsen's dogma, which certainly rings true of non-biological systems as well, sequence defines

structure. In any case, these combined qualities are utilized in my own 3D building blocks in generating molecular shapes with CAS to form an exact sequence with a precisely-known shape as well be discussed over the next following chapters.

1.2 Ladder Polymers

Polymers are long connective chains comprised of many smaller repeat units, monomers, which make up their backbone and are typically connected to another monomer by only a singular bond.[10] While linear polymers are the most simplistic form in terms of structure, more architecturally complex polymers, and polymerization techniques, need to be investigated, since polymers branching, size, connectivity to monomer units, folding, and other architectural features affect many of its physical properties.[11]

Ladder polymers then, are a unique type of polymer where rather than only two connective sites on each "end" of a monomer, several connective sites exists—therein a ladder polymer is a double-stranded polymer with four interconnected bonds.[12] The links connecting the strands of ladder polymers look very similar to the rungs of a ladder, giving the uninterrupted sequence of repeat units a wholly unique structural motif. They exhibit unique physical properties due to their connectivity, such as great thermal stability and (not unrelated) shape-persistency due to the constrained subunits which comprise the backbone of organic ladder polymers (**Figure 1.5**).[13, 14] While constraints of the backbone can lead to interesting physical properties, issues with ladder polymers can also arise for the same reasons, particularly with more conjugated systems, including (i)

solubility, (ii) structural defects in the polymerization process, and (iii) difficulties related to structural elucidation.[15]

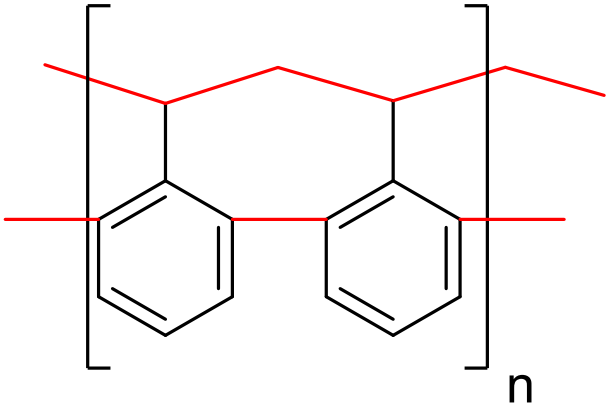

Ladder Polymer

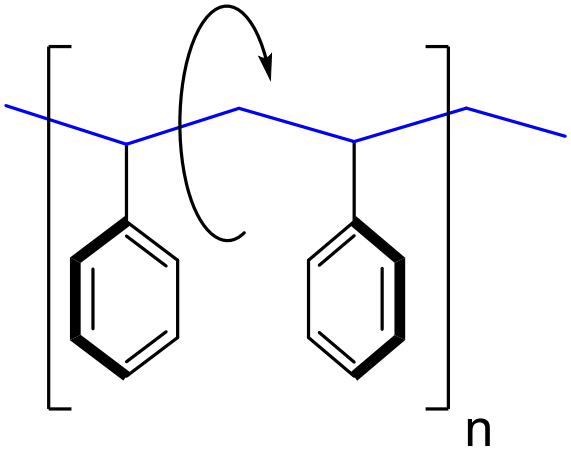

Single-Stranded Polymer

Figure 1.5. A rigid polystyrene ladder polymer and single-stranded polystyrene, illustrating its inherent torsional freedom.

Due to the rigid nature of the ladder polymer backbone, which prevents torsional freedom, they tend to have a host of unique and interesting properties. Like with many

polymers regardless of their architecture, their structure-property relationship is a key feature for scientists to investigate. More so, the ability to control the structure of generated polymers is highly important to then even better understand their structure-property relationship—ladder polymers have the benefit of having a rigid structure makes them top candidates for studying this relationship.

1.2.1 Conjugated Ladder Polymers

For conjugated ladder polymers containing an sp^2 carbon backbone, their rigid framework is exemplified, as the four linkages holding the polymer together no longer have the freedom of movement granted by sp^3 carbons. This type of ladder polymer is much more rigid and stiff, granting additional unique properties such as: inherent π-conjugation, strong π-π stacking, mechanical stability and fast intrachain charge transport[15]—but the challenges associated with ladder polymers are enhanced. Like with PAHs, solubility and structural determination is a major challenge facing the synthesis and analysis of conjugated ladder polymers.

Certain ladder polymers take advantage of the shape-persistency inherent in triptycene-like building blocks (**Scheme 1.2**).[16] While not fully conjugated (due to the presence of sp^3 carbon bridgehead units), significant conjugation exists despite remaining selectively flexible, allowing for a range of characteristics like improved stability, enhanced luminescent quantum yields, and a unique three-dimensional shape with high degrees of free internal volume.[16, 17] Given the coplanar nature of these conjugated systems, the length of conjugation is extended and reasonably allows for interesting

properties relating to luminescence, high carrier mobility, and other optical/electronic applications.

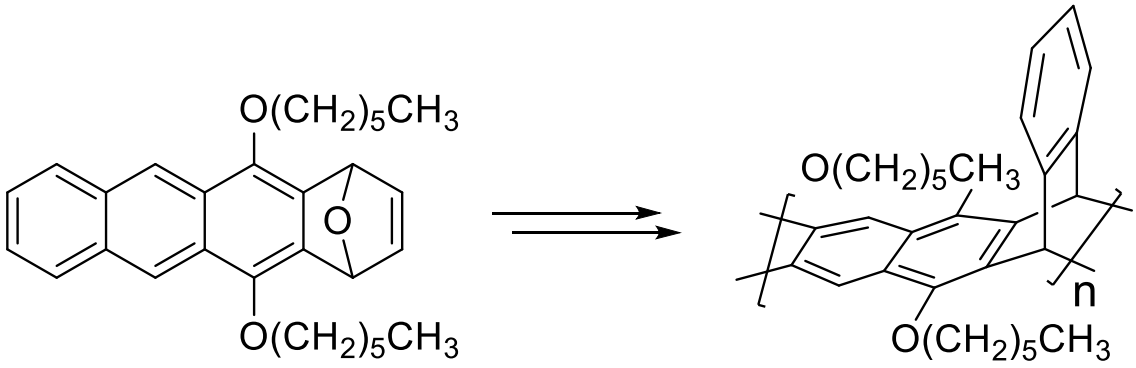

Scheme 1.2. Diels–Alder polymerization to form iptycene-based conjugated ladder polymers.

1.2.2 Polymerization Strategies

There are many strategies to achieve the multiple bond connectivity of ladder polymers—the most successful coupling strategies of course are those with high yields and high fidelity. In general, the following two synthetic methods are utilized to generate ladder polymers: (i) A two-step synthesis in which a linear polymer precursor is first generated followed by zipping up the ladder polymer in a second step, and (ii) a direct ladderization of the monomer units all in a one pot reaction.[12]

1.2.2.1 Cross Coupling/Imine Condensation

A common example of zipping up a polymer precursor is through having the second reactive step involve the deprotection of a Boc-protected aniline moiety to allow

it to then undergo an imine condensation with a ketone-containing partner.[12] In an early example by Tour, a Stille polymerization was utilized in forming the initial chain before TFA deprotection of *N*-Boc groups along the polymer backbone to form the polyphenylenethiophene ladder polymer,[18] and in another select example with an imine-bridged phenylenepyridine (**Scheme 1.3**).[19]

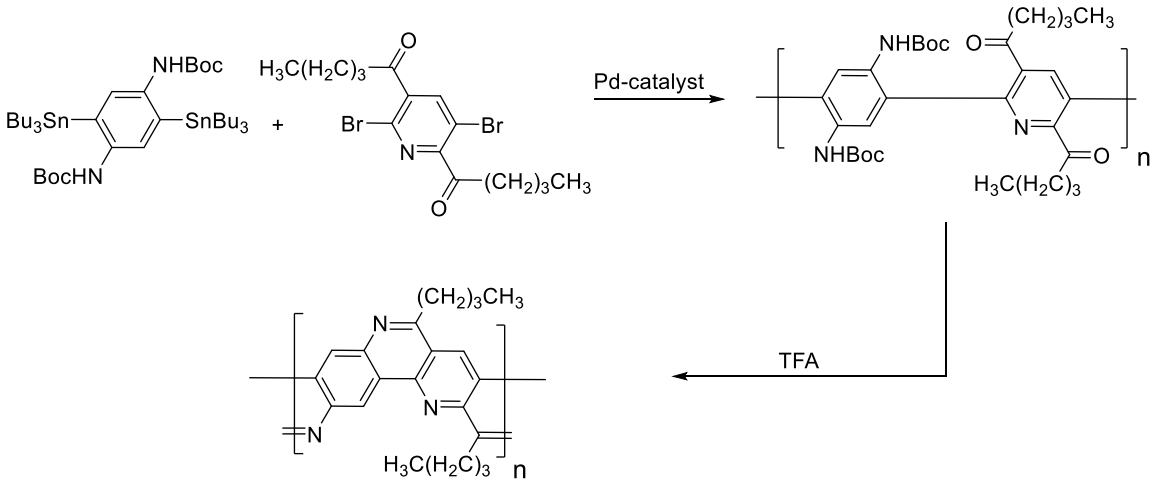

Scheme 1.3. Two-step ladder polymerization of polyphenylenepyridine.

In an example of a direct one-step ladderization, Wu and co-workers used a Suzuki coupling alongside an imine condensation (without protecting then deprotecting to zip up the polymer) along an aryl ketone (**Scheme 1.4**).[20] The dimeric species in test reactions showed excellent yields above 94%, and in the formation of the polymer, an overall yield of 85% was achieved. In comparison to many one-step procedures, utilizing a Suzuki coupling/Schiff base formation saves a synthetic/purification step along with being a very high yielding strategy.

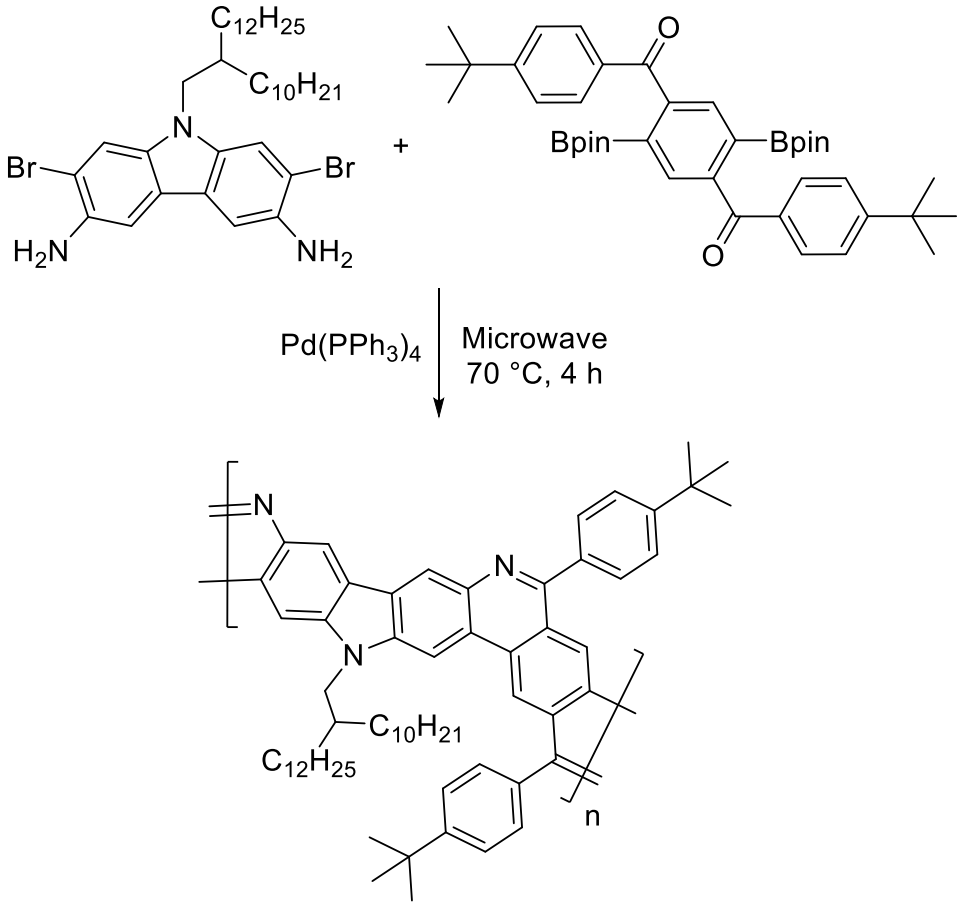

Scheme 1.4. Suzuki coupling/imine condensation to form conjugated ladder polymer.

1.3 Helical Polymers

From a structural standpoint, a helix has a fundamentally unique geometry. Helices are the product of a curve (i.e. a continuous flow of a line that is not straight) in three-dimensional space. Architectural spirals, drill bits, and coiled springs are everyday examples of helices. Much like molecules, helices also possess chirality as an inherent property. Depending on the turning or screwing motion of the helix, it is either right-handed (if clockwise motion moves the helix axis away from the observer) or left-handed (if the same motions moves it away). If chemists were able to synthesize a helix with

some rigidity, stability to a series of environments, and with an exact control of its helical sense, developing synthetic molecular helices to behave like classical Hookean springs would entirely be possible (**Figure 1.6**),[21] i.e. a helical polymer that could extend and compress again without losing significant elasticity while likewise storing mechanical energy.

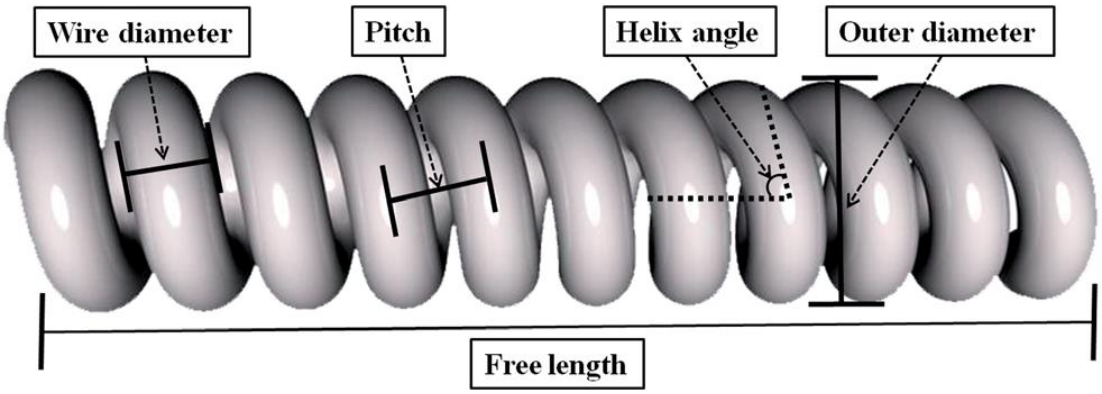

Figure 1.6. Various geometric properties of a helical coil (reproduced with permission.[22])

Chemists have thus sought after the generation of helical molecules because of the advanced repertoire of supramolecular systems that nature has created by utilizing helical structures, which in turn provide the fundamental basis for the processes of life. Helical polymeric systems have been anticipated to perform in a similar fashion, and therefore are of interest to polymer chemists because of their intriguing potential in materials chemistry like functional nanomachines, optical materials, asymmetric catalysis, chiral-resolution, and chemical sensors.[23-25] Many helical molecules of varying types have been synthesized, such as supramolecular assemblies,[26, 27] foldamers,[28-32] multi-stranded,[33-35] single-handed,[36-39] and ladder polymers.[40-42]

Previous work on synthesizing and investigating molecular helices shows their unique nature and their versatility for potential practical applications.[43-45] Because of the inherent chirality of helices, they may be used as a scaffold to help separate enantiomers or control optical properties.[44, 46-50] Controlling the helicity (right-handed *vs.* left-handed) of the structure has also been a topic of intrigue since a swap in configuration would change the properties of the system.[43, 51] Molecular helices have been synthesized previously with peptide couplings,[52] utilizing metals to induce the extending/contracting behavior of the helix,[53] or are they synthesized short (not on the nanoscale). Long freeform organic helices, however, still remain mostly undeveloped with very few existing examples and without efficient chemical synthesis.[42]

More so, coupled with the challenge of synthesizing helices, determining their exact helical nature (including handedness and pitch) is difficult and still unsolved for already-existing helical polymers.[25] As mentioned prior, a combination of effective qualities for molecular building blocks that ensures a particular geometry upon polymerization would make predictions of the exact "folding" nature of a synthesized helical polymer far simpler.

1.3.1 Helicenes

Helicenes are among the simplest molecular helices, with [6]helicene being the smallest possible helix with a handedness depending on how the terminal arene rings overlap (**Figure 1.7**).[54] The arene rings in a helicene system are annulated in subsequent *ortho* positions to produce its helical structure. The largest helicene produced to date was

is a 14-mer.[55] A few extended helicenes are suspected to behave like a molecular spring.[56, 57] As in general, such large PAHs are difficult to solubilize and thus work with. For this reason, helicenes are often functionalized to allow for more soluble products while retaining their unique charge-transfer properties.[58, 59] Nevertheless, there is no inherent control of handedness when growing out helicenes without the aid of a chiral catalyst.

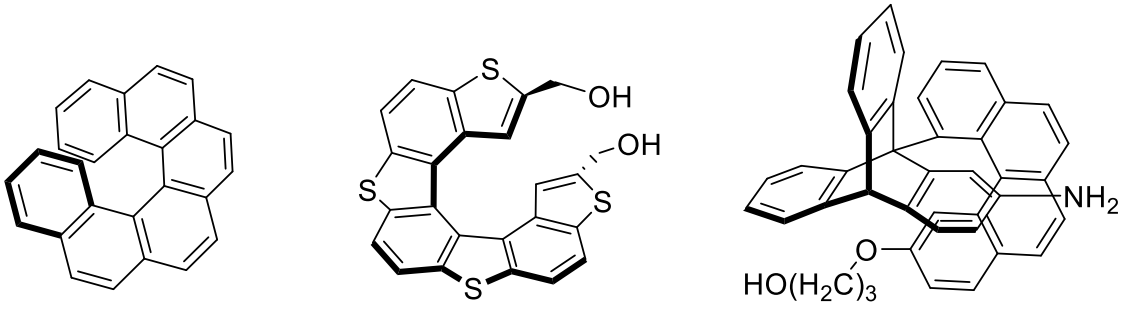

(M)-(-)-[6]helicene **(M)-(-)-thiahetero[7]helicene** **Molecular Ratchet**

Figure 1.7. [6]helicene, thiahetero[7]helicene,[60] and a [4]helicene-based ratchet.[61, 62]

1.3.2 Helical Ladder Polymers

When considering a helical ladder polymer, often what is discussed is the methodology behind the conjoining of the relevant building blocks to access the corresponding ladder polymer. Many conjugated helical polymers (such as helicenes) are, based on their linkages, technically ladder polymers, but are often not associated with such terminology. Accordingly, helical ladder polymers can be defined as a continuous network of unbroken bonds that turns along in a single direction. By virtue of their ladder-rung motif, these polymers are helical due to their architectural features alone and

not because of intra- or intermolecular binding. Very few examples of helical ladder polymers exist in the literature, and most are comprised primarily of PAHs (giving a helicene-type structure) or a thiophene-annulated backbone.[40, 41, 63] The difficulty in synthesizing helical ladder polymers arises for two primary reasons: first, a lack of a proper ladderization strategy to form the helical polymer, as zipping up the ladder polymer relies on a polymeric precursor, and structural defects are fundamentally difficult to overcome through this method along with the need for precise, high-efficiency reactions. Second, to generate a well-defined helical polymer, geometrically favorable building blocks are needed so when polymerization occurs the generated ladder polymer is inherently helical. These challenges presented are very much related and require a precise strategy to overcome.

A recent example of a helical ladder polymer which follows these guidelines is from the Swager group, where they utilized a two-step zipping strategy along with a triptycene-derivatized building block and helical-orienting spacer piece (**Scheme 1.4**).[42] By undergoing a Suzuki coupling to form the polymer precursor, a subsequent TFA addition then allows for an intramolecular cyclization by way of EAS to allow for a regioselective formation of the helical product of either right- or left-handedness depending on the starting triptycene building block. However, this zipping strategy, as made evident in the synthesis of the dimer and tetramer derivatives, does not afford an overall yield of higher than 50%, owing to the formation of structural defect byproducts. Additionally, the use of triptycene as an enantiomerically-pure building block requires chiral resolution, as well as a loss of product due to the unselective nature of

functionalizing triptycenes in general. My work in the Schneebeli group tackled both of these issues, and to address the general aforementioned challenges to generate single-handed helical ladder polymers with high fidelity and structural integrity.

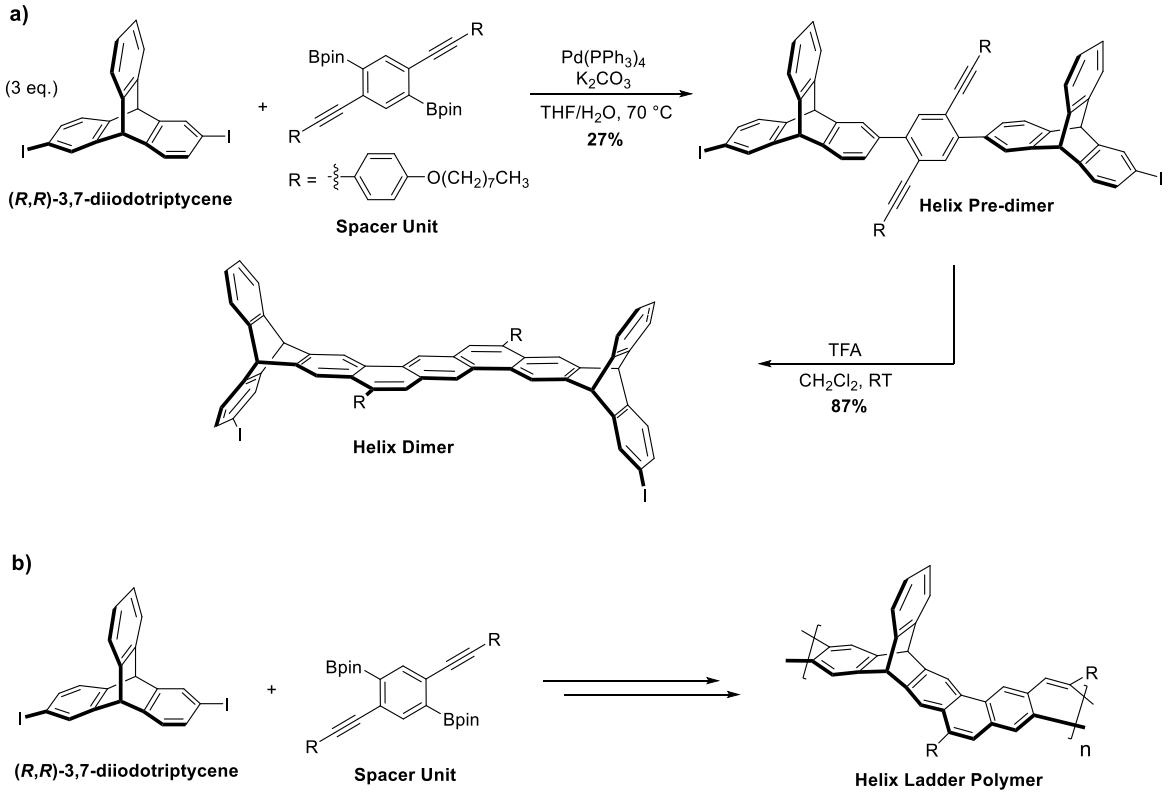

Scheme 1.4. Synthesis of a triptycene-based helical (**a**) dimer and (**b**) ladder polymer.

1.3.3 Spring-like Polymers

Polymeric molecular helical springs are much less understood in comparison to many of the mentioned molecular helices, but are still fundamentally interesting to scientists.[21, 24, 64, 65] Molecular springs in particular have received attention in their utility for a broad range of microsystems.[53, 66-68] For a helical object to appropriately behave like

a spring it must be elastic in its ability to return to its original shape within its tunable pitch, and twist in an anisotropic fashion, i.e. in a unidirectional, spring-like motion.[69-71] This ability for a helical molecular spring to do such work would lead to a host of potential applications, such as acting with a catalytic function, with compressions associated alongside a stimuli to bind a particular guest, and introduce another change to release it[69]—much like many biological processes such as muscle tissue in binding calcium which governs the key components myosin and actin in their motions.[72] Binding an ensemble of these molecular springs to surface (**Figure 1.10**) would see them acting concertedly to perform macroscopic scale feats with autonomous spring-like motion upon environmental changes.

DNA, while a biological helical polymer, does not have much capacity for behaving like a spring, as significant expansion of its backbone will cause it to permanently unfold, and not compress back to its original state.[73, 74] However, such spring-like polymers do exist in nature that allow for expansion and compression in true classical spring behavior. Titin, for example, is a very large protein (reaching up a micrometer) with spring-like properties and is known to be responsible for the passive elasticity in muscle,[75] as an adaptable spring it unfolds upon stretching and refolds upon removal of tension.[76] In another natural example, receptor-protein rhodopsin is responsible for converting stimuli from one form to another, effectively granting us vision. Similarly, rhodopsin compresses and expands as a molecular spring to release strain and thus adjust its surrounding environment in a selective manner that is vital to the visual phototransduction process.[77, 78]

While limited, examples of synthetic springs are more readily available, though their efficiency to perform as true classical springs is still a major field of study for many scientists.[79-85] Several examples of synthesized molecular springs have been reported but in general face problems with (i) unfolding under external stimuli, (ii) low selectivity in polymer synthesis, (iii) helical inversion, and (iv) retaining helicity only under specific chemical environments.[23, 24, 53, 67]

1.4 Investigations into Freeform Helices as Molecular Springs

Shape determines the properties of materials at all length-scales. We therefore need to learn how to create functional structures with well-defined shapes at the molecular level—helical springs and piezoelectric actuators[86, 87]—as components of next-generation materials. Hence, it comes to no surprise that the field of precise molecular shape control has grown remarkably in the recent past. A great variety of shape-defined structures have been created, ranging from hydrogen-bond-directed foldamers,[88] to completely shape-persistent spiroligozymes,[89] and large molecular strips.[4] These synthetic, precisely-defined entities have already found applications as protein-inspired, synthetic receptors,[45] selective catalysts,[90] and nanopores.[91]

With our CAS approach, we can (**Chapter 4**) create long freeform helices[66] using efficient chemical synthesis (**Scheme 1.5**). Such shape-persistent freeform helices[22] (**Figure 1.8**) inspire applications ranging all the way from molecular springs to actuators.[92] Due to their unique shape, we find (**Figure 1.9**) that our molecular springs can be stretched/compressed readily by at least a factor of three without bending and unfolding. This distinctive property, which is unique to freeform helices, makes our

molecular springs excellent shock absorbers.[93] Note that folded helices like DNA are not extended/contracted as easily, since the stabilizing interactions between the different parts of the helix hinder this type of movement. These helices have the capacity therefore to be integrated into strong and flexible next-generation materials needed[94] as shock absorbers for applications such as body armor (e.g. helmets, bullet-proof vests, etc.).

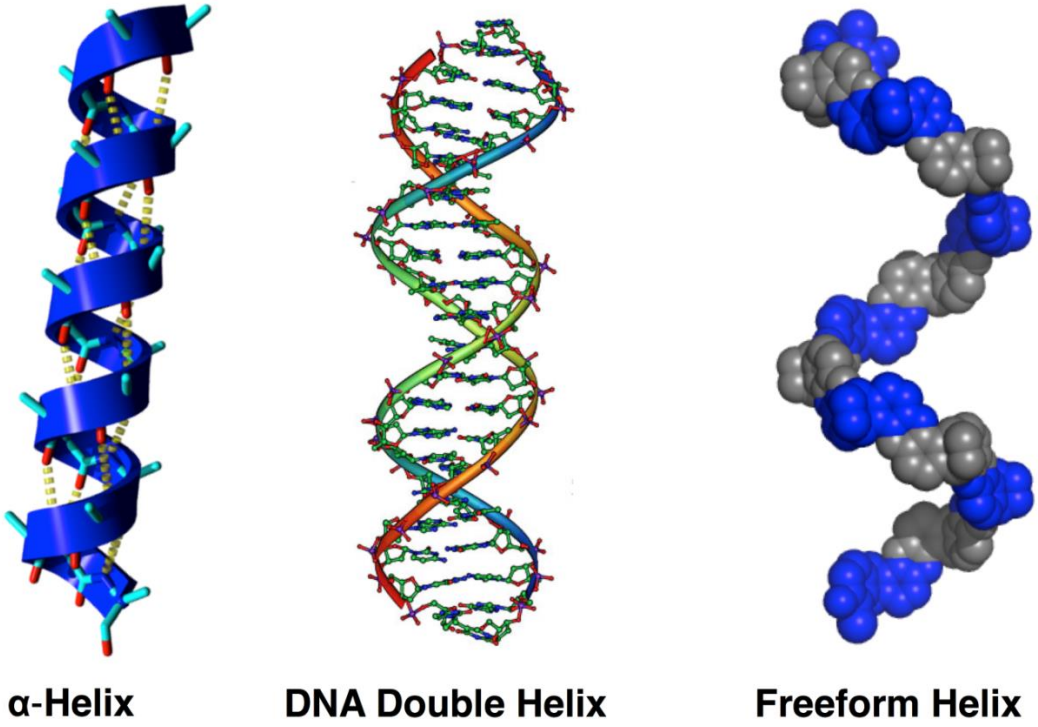

Figure 1.8. Comparison of helical structures in biology to a proposed freeform molecular helix.

In addition to functioning as tiny shock-absorbers, we will also be able to extend/contract the helices by applying a voltage difference. Given that the helices can be extended/contracted so easily (**Figure 1.9**), a small change in voltage might lead to a substantial extension/contraction of the materials along a specific direction, especially if

we attach oppositely charged groups to the ends of the helices. Such behavior could provide the basis for the creation of artificial molecular muscles[95, 96] and advanced impact sensors (e.g., for airbags). If processed appropriately, these molecules can likely act as molecular springs and change our future as parts of exceptionally strong and flexible materials.

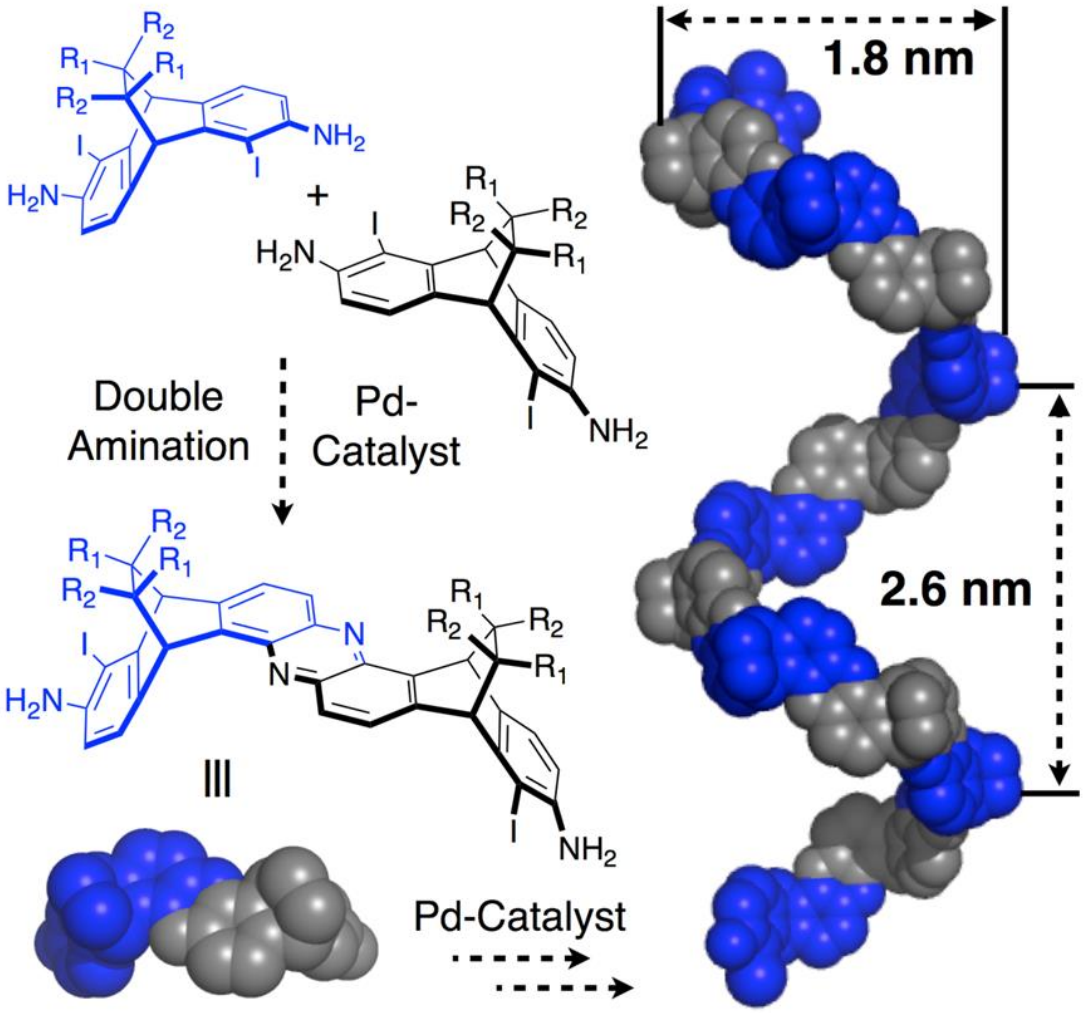

Scheme 1.5. Initial synthetic strategy to generate single-handed freeform helices with CAS, using Pd-catalyzed double-aminations on selectively iodinated building blocks.

We thus started our research in the realm of helical molecular springs by predicting the energy profile for extending and contracting CAS freeform helices with all-atom computer models. To calculate the energy profile for adiabatic extension and compression along the helical axis, a freeform helix with one turn was subjected to a minimum energy coordinate scan (**Figure 1.9**) at the molecular mechanics level (OPLS-2005 force field) with MacroModel (MacroModel, version 10.4, Schrödinger, LLC, New York, NY, 2014). For the coordinate scan, the distance between the two peripheral bridgehead carbons of the helix facing each other was constrained to a set of values in the interval [10.0, 35.0] Å with increments of 1.0 Å. The substituents R_1 and R_2 attached to the ethylene bridges of the helix were both set to hydrogens.

While we expected the nanoscale helices to display elastic behavior reminiscent of similar macroscopic structures, we found (**Figure 1.9**) a classical harmonic extension/contraction energy profile for our molecular system. Moreover, the calculated energy profile shows that the freeform molecular springs can be stretched/compressed by at least a factor of three without bending and unfolding. Also note how flexible the springs are, with a spring constant *k* of approximately 49 pN/Å. This fairly low spring constant manifests itself in the fact that, by changing the length of the helix from 10 to over 30 Å, the relative potential energy of the system increases by less than 25 kJ/mol.

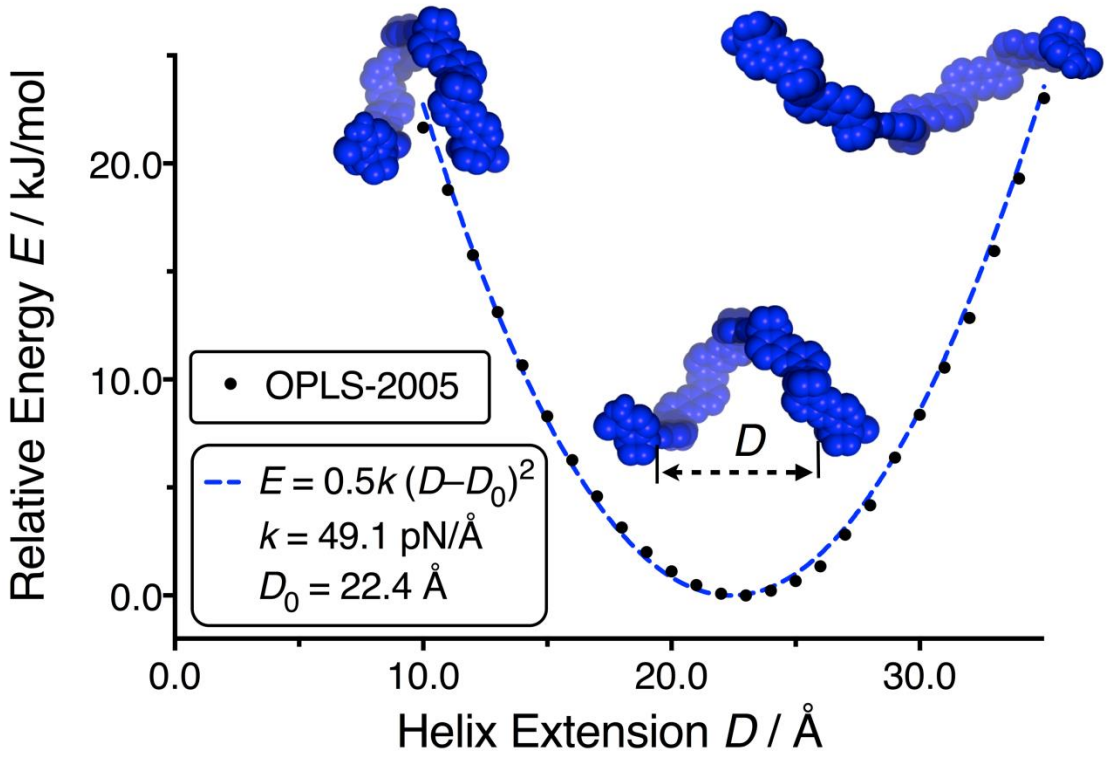

Figure 1.9. Calculated Energy Profile (OPLS-2005) for stretching/compressing a freeform helix with one turn ($R_1 = R_2 = H$). The blue, dashed line represents a least squares fit ($R^2 = 0.9986$) to the data, assuming an idealized Hookean spring.

In the future, we also plan to produce (**Figure 1.10**) an array of the helices attached to a substrate by a dip coating or spray coating process to analyze the bulk properties of our materials. By taking advantage of the exceptional elasticity and stability of these molecular springs, we envision a range of valuable potential applications for our new materials, including the creation of (i) next generation high impact springs and dampers[97] as well as (ii) anti-fouling water membrane filters.[98] We expect that large changes in the lengths of our springs (e.g., induced by a voltage) can help to minimize the

fouling behavior in water membrane filters,[99] therefore well-extending the filters' service lives.

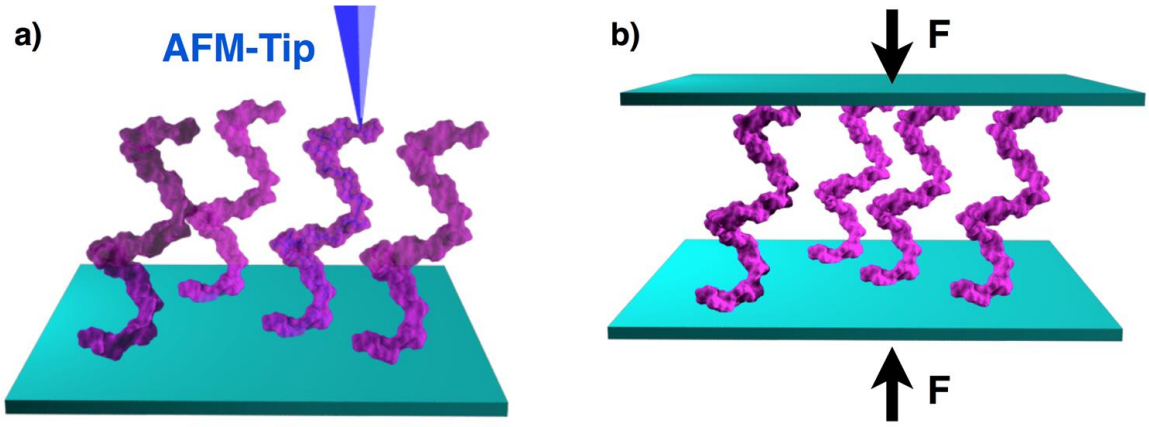

Figure 1.10. Proposed assemblies of freeform molecular helices on substrates.

1.5 Conclusions and Introductory Remarks

Macromolecules in general have provided scientists with a wide range of physical attributes to study in search for important applications. Most electronic visual displays utilize liquid crystals which, generally, make use of the change in optical properties of liquid crystalline compounds upon modification of an electric field. Scientists have been looking at chiral helical motifs in particular to elucidate such highly desired optical activity.[100, 101] Molecular actuators (a component of a machine that is responsible for moving a mechanism) have similarly been based on helical structures in response to the variety of dynamic helical mechanisms found in nature.[102] Stimuli-responsive polymers (smart polymers) are a relatively emergent field and in general have a wide variety of applications, as they are a unique class of materials where they respond to stimuli by changing their physical and/or chemical properties. Given their specific ability to respond

to a stimulus, they have found a variety of uses in actuators, sensors, and drug delivery systems.[103, 104] Stimuli-responsive molecular springs would be then an excellent example of a molecular system's ability to perform work as an actuator (i.e., perform work in a singular direction) in response to an environmental change, and then return to its original state without significant loss in elasticity to once again respond to a new stimulus.[103, 105-107]

While perhaps a far-reaching goal, it is difficult not to consider the aforementioned applications for macromolecules. To be able to specifically control a synthetic pathway, build precisely-defined structures in an exact fashion, and utilize those macromolecules to perform a particular function (e.g., display spring-like motion), are all goals that I have strived to complete during the course of my Ph.D. research. Thus, in the following chapters, I will explore the work I have done on: selective through-space directing nitration on a specific molecular site (**Chapter 2**), the synthesis of three-dimensional building blocks to function as the backbone of generated macromolecules (**Chapter 3**), and the synthesis of well-defined helical ladder polymers and subsequent investigations into their structure-property relationship (**Chapter 4**).

CHAPTER 2: ELECTROPHILIC AROMATIC NITRATION VIA THROUGH-SPACE DIRECTION

2.1 Introduction

Nature has evolved selective enzymes for the efficient biosynthesis of complex products. This exceptional ability stems from adapted enzymatic pockets, which geometrically constrain reactants and stabilize specific reactive intermediates by placing electron-donating/accepting residues nearby. Here we perform an abiotic EAS reaction, which is directed precisely through space. Chiral auxiliary ester arms—positioned above the planes of aromatic rings—enable it to distinguish between nearly identical, neighboring reactive positions. Quantum mechanical calculations show that, in two competing reaction pathways, both [C–H···O]–hydrogen bonding and electrophile preorganization by coordination to a carbonyl group likely play a role in controlling the reaction. These through-space directed mechanisms are inspired by dimethylallyl tryptophan synthases, which direct biological electrophilic aromatic substitutions by preorganizing dimethylallyl cations and by stabilizing reactive intermediates with [C–H···N]–hydrogen bonding. Our results demonstrate how the third dimension above and underneath arene subunits can be exploited to precisely control electrophilic aromatic nitrations.

2.2 Preexisting Synthetic Through-Space Nitration Methodologies

Very few examples of through-space electrophilic aromatic nitration methodologies exist, i.e. directing a nitro group to a specific locale on an aromatic ring.

Not dissimilar to mechanosynthesis[108, 109] (i.e. the ability of using molecular-mechanical restrictions to specifically guide a reactive molecule to a particular site), an auxiliary group acts to constrain the reactive process by selectively directing the reactive nitro group to a specific site. In an example by the Tsuzuki group, there is a through-space electronic interaction with an opposing benzene ring to decrease deactivation and (even under mild conditions) allow *ipso*-nitration process to readily occur to replace a *tert*-butyl group.[110] In another example by Corrie and co-workers, an *N*-acyl directing group on methoxyindoles was utilized to allow aromatic nitration proximal its location at the *7* positon as opposed to the father reaching *5* position, and with a regioselectivity of 12-to-1.[111]

Thomas Lectka showcased an elegant system in which a triptycene-like derivative with a fluoro group in close proximity to one of the arene subunits was exposed to EAS nitration conditions, from which only the aromatic ring proximal to the fluorine became nitrated (**Scheme 2.1.a**).[112-114] Opposed to traditional EAS reactions with fluorine by which it acts as an electron withdrawing group and impedes the rate, this unique nitration methodology dramatically improves the reaction rate. When compared to the control (with the fluorine pointing *away* from the top arene ring) there was no directing control over which aryl subunit became nitrated (**Scheme 2.1.b**). This interesting reactivity arises from the stabilizing effect of the lone pairs on the fluorine, donating into the π cloud of the nitroarenium ion intermediate formed during S_EAr reactions.

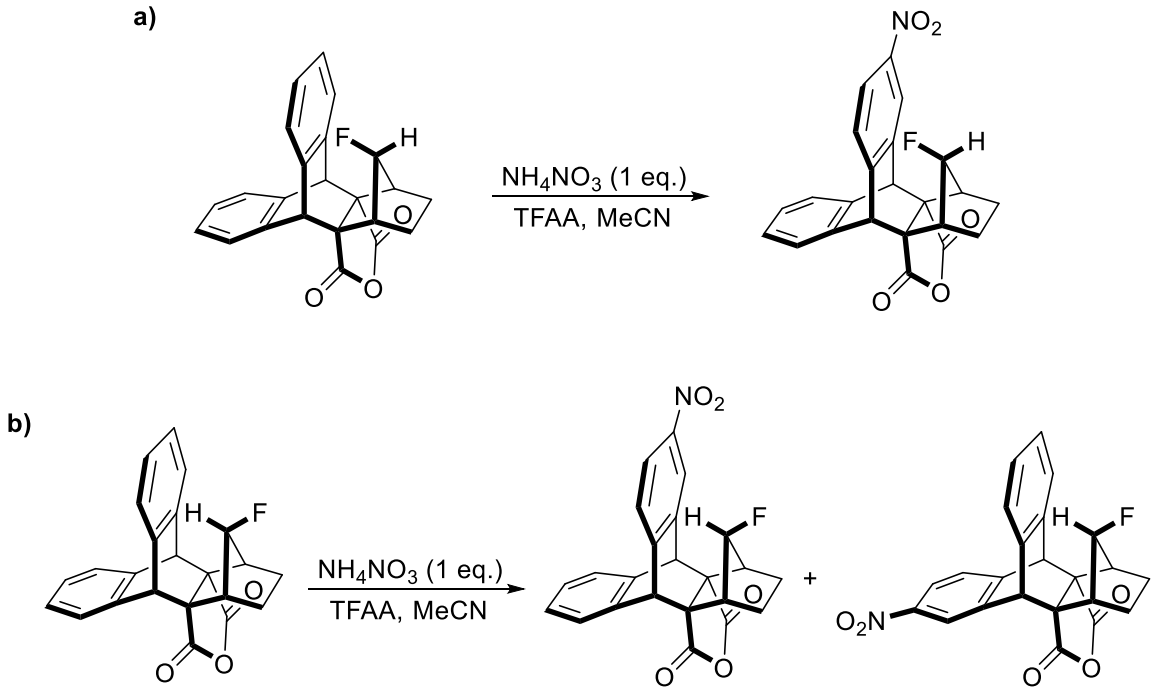

Scheme 2.1. (**a**) Through-space directed nitration of an arene ring proximal to a fluoro group. (**b**) No nitration control over the aryl subunit is found if the fluoro group is positioned distally.

During the formation of the Wheland intermediate[115, 116] of these fluorine-containing cycloadducts, the stabilizing effect can be thought of as more than just resonance or weak inductive activation via donation in the electron-deficient π-cloud of the arene ring—a "fluoronium" resonance form can be considered as a contributor for the Wheland intermediate (**Scheme 2.2**).[117] While the fluoronium ion may be not fully formed, σ-stabilization through the fluorine's lone pairs must still be acknowledged. Considering the "closed-cage" resonance form of the Wheland intermediate helps to

explain and visualize the unusual activation-directing nature of this electrophilic aromatic nitration.

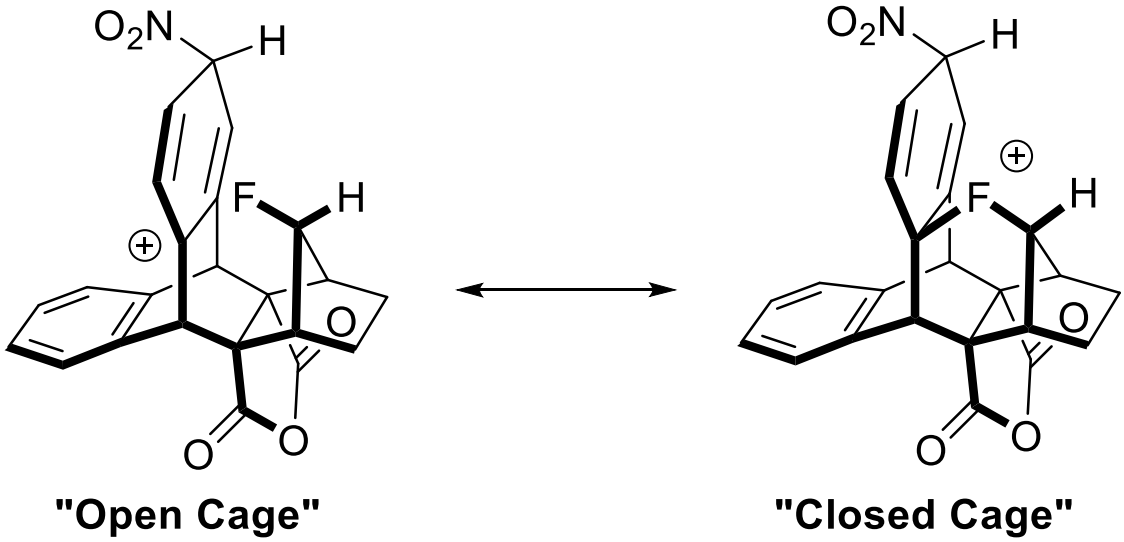

Scheme 2.2. Nitroarenium ion and fluoronium ion resonance forms.

Much like a Meisenheimer complex—where a reaction adduct containing a nitro withdrawing group is formed and stabilized in the presence a nucleophilic alkoxide[118]—if an oxygen-containing system where to be directed toward an electron withdrawn arene ring, the lone pair from the oxygen would stabilize the transition state in a Meisenheimer-like complex.[113] Furthermore, the work done by the Lectka group showed this case, in that even an electron deficient oxygen atom can meaningful contribute to selective EAS nitrations (**Scheme 2.3**), as the nitrate-ester moiety formed during the reaction occurred *prior* to the aromatic nitration of the bromoaryl subunit.[113]

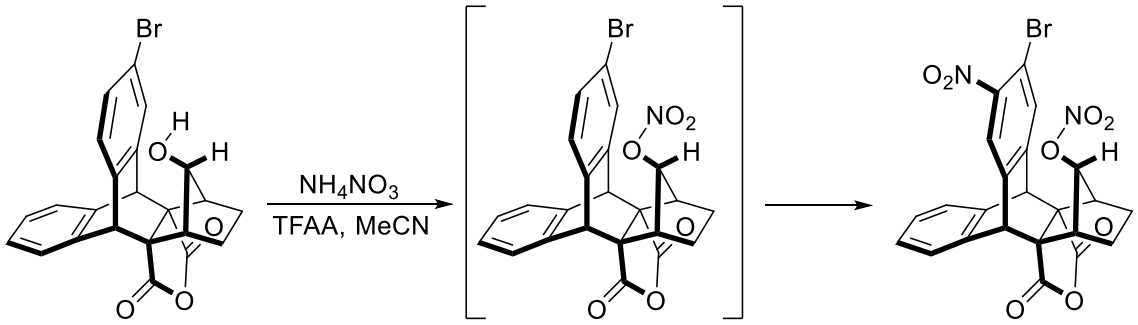

Scheme 2.3. Through-space directed nitration with an electron-deficient oxygen atom as the directing group.

2.3 Through-Space Nitrations in Nature

In this work, we investigate the fundamental question of how aromatic reactivity can be directed with high precision from above and below the planes of aromatic rings. By advancing towards this general goal, we aim to add a new dimension of control to the large class of S_EAr reactions. While synthetic chemists still rely largely on traditional covalent electron-donating and electron-withdrawing groups to direct S_EAr reactions,[119] nature has already mastered the third dimension in this regard. Enzymes, for instance, make heavy use of the areas above and underneath aromatic rings to (i) align electrophiles above/underneath a desired position of attack and (ii) stabilize reactive S_EAr intermediates through space with protein residues. This three-dimensional approach provides exquisite reaction selectivities and has enabled evolution to tailor enzymatic pockets to form different products selectively from the same starting materials. Different orthologs of dimethylallyl tryptophan synthase (DMATS) catalyse, for example, Friedel–Crafts alkylations of *L*-tryptophan with dimethylallyl diphosphate with varying regioselectivities.[120, 121] This family of enzymes is involved in the biosynthesis of ergot

alkaloids, which find use in a variety of pharmaceuticals currently on the market.[122] On the basis of high-resolution X-ray crystal structures, it was proposed[123, 124] that DMATS from *Aspergillus fumigatus* achieves (**Figure 2.1.a**) its regioselectivity owing to (i) preorganization of the dimethylallyl cation inside its active site as well as (ii) a key through-space [C–H···N] hydrogen bond. Such a non-classical hydrogen bond between Lys174 of the enzyme and the acidic proton being substituted likely stabilizes the cationic Wheland reaction intermediate of the S_EAr reaction selectively.

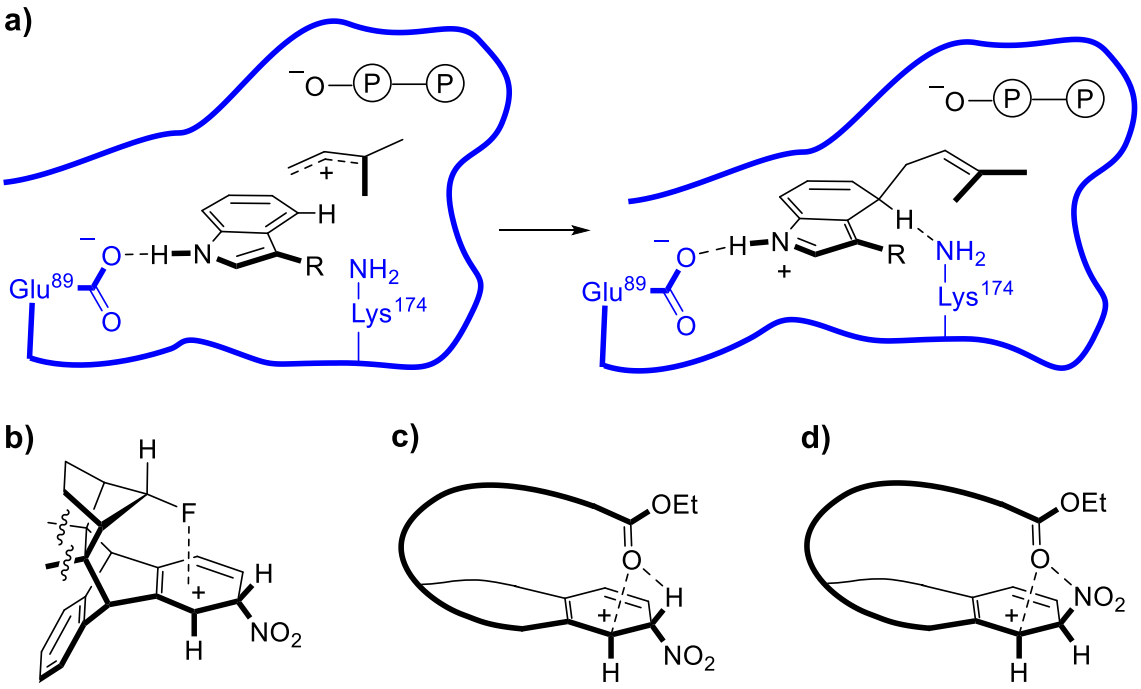

Figure 2.1. (**a**) Proposed[124] mechanism of through-space control in dimethylallyl tryptophan synthase (DMATS). The enzymatic pocket is illustrated schematically in blue. Note how (i) the precise positioning of the dimethylallyl cation inside the enzyme as well as (ii) a [C–H···N] hydrogen bond in the Wheland intermediate likely play a role in determining the selectivity of the reaction. (**b**) Placing a negatively polarized fluorine atom above the center of an aromatic ring activates[112] two symmetrically equivalent positions on the ring for S_EAr reactions. On the other hand, carbonyl groups located directly above two atoms of an aromatic ring (**c**/**d**, this work) can precisely direct the substitution to one specific location. Key stabilizing interactions involving electron donation from O/N lone pairs to carbocations and positively polarized H/N atoms are illustrated with dashed lines.

Nevertheless, little is known yet in the emerging field of precise, abiotic through-space control of S_EAr reactions. While directing groups installed on the side of aromatic rings have been used to successfully direct substitutions (for example, in *ortho*- and *meta*-metalations,[125, 126] few synthetic examples of S_EAr control from above or underneath arene subunits have been revealed to date. Only recently, it has been reported[112] that a fluorine substituent placed over the center of an aromatic ring (**Figure 2.1.b**) activates two symmetrically equivalent positions on the ring. Yet, it still remains mostly unexplored how to direct such substitutions to one specific location with an asymmetrically positioned through-space directing group. Furthermore, enzymes like DMATS achieve [120, 127, 128] their high selectivity with adaptable structures, while most synthetic examples[129-131] reported to date still involve architectures with limited conformational flexibility. Creating stiff structures often requires, however, substantial synthetic efforts. Thus, it is crucial to understand how to achieve through-space control of S_EAr reactions with more adaptable geometries in both a fundamental and practical sense.

Inspired by the way that DMATS from *A. fumigatus* directs S_EAr reactions by (i) constraining the orientation of a dimethylallyl cation with respect to the tryptophan substrate and (ii) stabilizing a specific Wheland intermediate with non-classical hydrogen bonding to a lysine residue (Lys174), we embarked on the discovery of synthetic, atomically precise S_EAr control in three dimensions. Our system operates with the carbonyl group of an ester functionality, positioned precisely in space with a partially flexible arm. Density functional theory (DFT) calculations show that, like Lys174 of DMATS, one electron pair of this carbonyl group participates (**Figure 2.1.c**) in a [C–

H···O] hydrogen bond, with the acidic proton being substituted. At the same time, the carbonyl oxygen of our system is also able to donate electron density directly into the empty orbital of the carbocation underneath to efficiently direct a S_EAr reaction to one specific location on a benzene ring. In a competing reaction mechanism (**Figure 2.1.d**) leading to the same major product, attack of the electrophile (NO_2^+) is controlled by coordination of a carbonyl lone pair to the electrophile. While this competing mode of through-space control leads to a less stable Wheland intermediate at the level of theory employed, it likely still contributes to the outcome of the S_EAr reaction. It operates by orienting the electrophile with O-to-electrophile coordination, akin to how DMATS's enzymatic pocket aligns a dimethylallyl cation with its tryptophan substrate.

2.4 Initial Synthetic Strategy on Molecular Building Blocks

First studies on three dimensional building blocks were done in the Schneebeli group by Dr. Liu whereby he discovered an efficient method of synthesizing large molecular strips.[4] A promising first generation of molecular shapes lead my own research to utilize the same building blocks for the initial stages of my studies. An acid catalyzed Diels–Alder cycloaddition with anthracene and electron-deficient tetraethyl ethylenetetracarboxylate lead to the formation of tetraester cycloadduct **2.1** (**Scheme 2.4**). This triptycene-like derivative is unique in its roof-shaped geometry and potential to functionalize its ester bridgehead to generate water-soluble molecular shapes for stronger binding affinities.[4, 8]

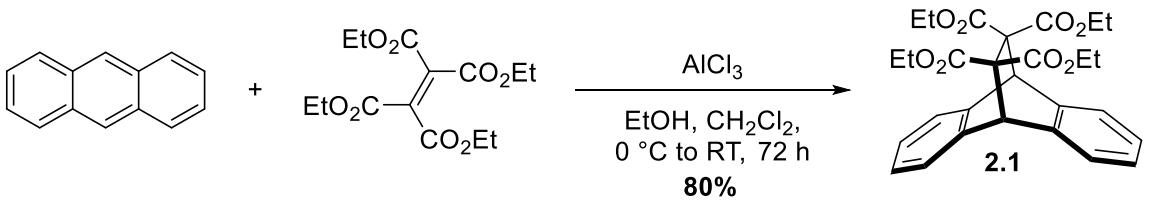

Scheme 2.4. Synthesis of achiral tetraester cycloadduct.

At the same time, I began to develop a second generation building block for molecular helices. In a similar fashion, following the formation of (−)-Bis[(*S*)-1-(ethoxycarbonyl)ethyl] fumarate **2.2**, the enantiomerically enriched diester underwent an uncatalyzed Diels–Alder cycloaddition with anthracene to form diastereomerically pure diester cycloadduct **2.3**[132] in good yields and high regioselectivity after recrystallization from EtOAc and hexanes (**Scheme 2.5**). As a note of interest, the diester cycloadduct appears to undergo a retro-Diels–Alder reaction over the course of the one week reaction time—monitoring by ^{1}H NMR shows the minor diastereomer chemical shifts decreasing over time where after a week the d.r. is 8-to-1. The reason for this may be because **2.3** has a proton attached to each chiral ester directed *into* the aromatic ring while the ester is pointing *away*, and for the diastereomer the methyl group must be pointed into the ring for the ester to be the farthest away, thus indicating that sterics are dictating the diastereomeric selectivity of the Diels–Alder cycloaddition.[133, 134] Similar to the tetraester cycloadduct, **2.3** has an inherent three-dimensional shape and functionalizable bridgeheads, while *also* containing chiral auxiliary arms to direct aromatic nitration reactions of its underlying aromatic ring in a stereoselective fashion for building well-defined CAS building blocks.

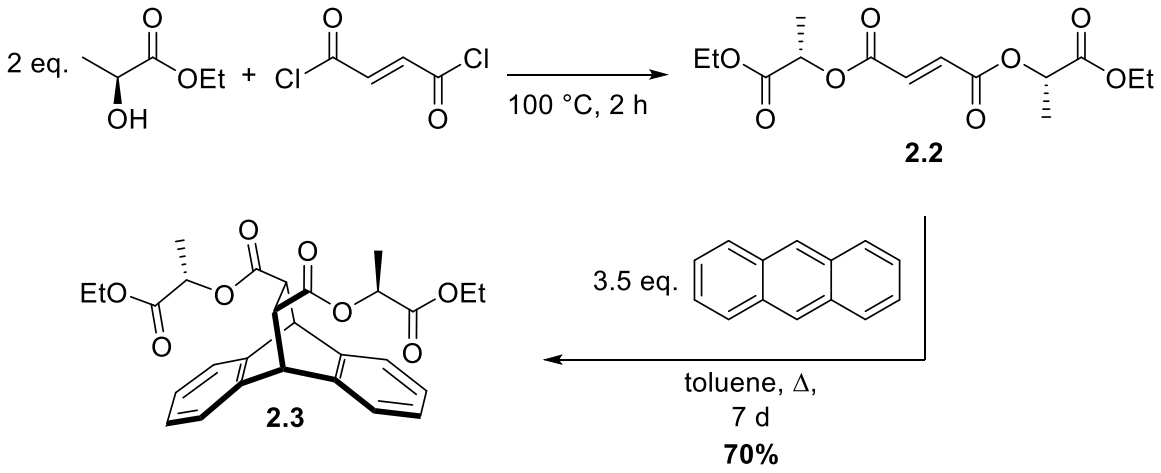

Scheme 2.5. Diastereoselective synthesis of the chiral diester cycloadduct.

2.5 Through-Space Direction with Ester Arms

To the best of our knowledge, most examples of through-space control in unsaturated systems to date have been utilizing stiff, bicyclic frameworks.[112, 135] Such arrangements have shown great promise in controlling the relative reaction rates of separate π-systems (for example, two different double bonds or benzene rings). Nevertheless, a structurally rigid approach renders it difficult to position a directing group precisely above or underneath one specific atom of an aromatic ring, especially if an optimal stabilizing effect is desired. With a more flexible, enzyme-inspired approach, however, enough wiggle-room likely remains to achieve effective through-space stabilization of a specific intermediate. Thus, we decided to attach our through-space directing groups to ester arms with some conformational freedom.

2.5.1 Nitration with Achiral Tetraester Arms

We found that the initial tetraester building block **2.1** developed by Dr. Liu with tetraester arms provided no selectivity upon nitration of **2.1** due to the inherently symmetrical nature of the tetraester cycloadduct. Thus, a racemic mixture of nitrated species (±)-**2.4** was produced alongside *meso* compound **2.4'** in a 1-to-1 mixture (**Scheme 2.6.a**), with the (*S,S*)-enantiomer separated out by chiral resolution in 96% *ee* later following reduction of the nitro groups to amines. In the case of mononitration of the tetraester building block, a racemic mixture of one (±)-**2.5** was produced (**Scheme 2.6.b**), but of course with no selectivity in the nitration substitution.

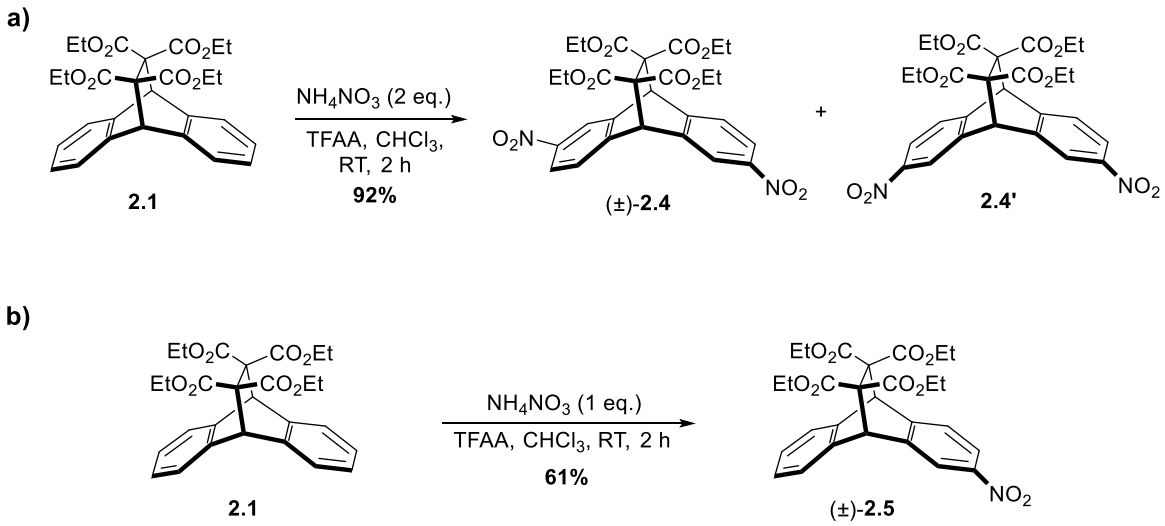

Scheme 2.6. (**a**) Dinitration of the tetraester cycloadduct, **2.1**. (**b**) Mononitration of the tetraester cycloadduct, **2.1**.

2.5.2 Nitrations Directed by Chiral Diester Arms

By virtue of having chiral ester arms—and only two unlike with the achiral tetraester arms—even if the added nitro groups were not selective for a single position on each aromatic ring, and we were afforded a mixture, the generated nitrated species would be regioisomers therefore separable by usual column chromatography. In the case of the tetraester cycloadduct, reduction to the aniline moiety was first necessary before utilizing chiral chromatography conditions to separate the two generated enantiomers.[4] This was in addition to separating off first the asymmetric dianiline enantiomers. In the case of using chiral diester **2.3**, we found selective nitration was occurring, but we first had to fully investigate whether the selective nitration process of the arene subunits was occurring due to (i) sterics (**Scheme 2.7**, steric-clashing sites illustrated in red), or (ii) if the process was electronically-driven, which we later confirmed was indeed the dominating nitration process (**Scheme 2.8**). This strategy then would allow us to bypass using chiral resolution, and thus it would improve the selectivity and yield by having a singularly major nitrated product rather than a mixture of *three* different nitrated species.

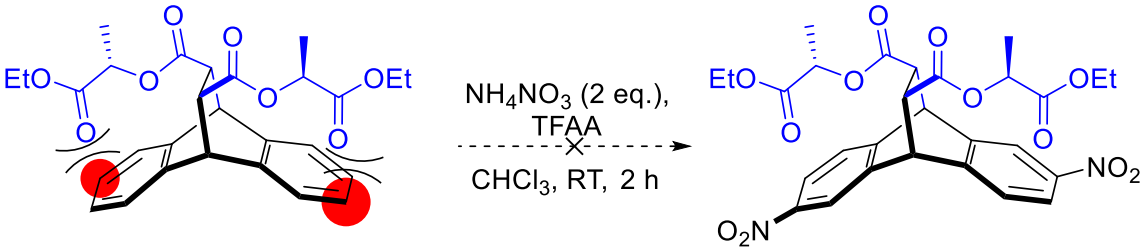

Scheme 2.7. Unfavorable chirality-transferred nitration directed by sterics of the diester arms.

With the strength of the chiral diester, (**Figure 2.2**) the two partially flexible auxiliary arms (illustrated in blue, **Scheme 2.8**) are located directly above positions *1* and *2* as well as *5* and *6*. While the presence of stereogenic centers in these ester arms reduces their conformational freedom, a non-trivial number of low-energy conformations are still readily available to both ester arms. A MacroModel (OPLS-2005 force field) conformational search of **2.3** (with the ethyl ester groups replaced by methyl) showed (**Figure 2.2**) that each lactate methyl ester arm contains approximately eight low energy ($E_{rel} < 1.4\,kcal\,mol^{-1}$) conformations, with the key ester-carbonyl groups pointing in distinct directions in all of them. First and foremost, however, the carbonyl-directing groups of the lactate esters are placed approximately in between the atom pairs *1–2* and *5–6*. This geometry is well suited to stabilize the intermediates of S_EAr reactions in positions *2* and *6* selectively with both [C–H···O] hydrogen bonding as well as direct electron donation from the carbonyl oxygens to the carbocation intermediates underneath.

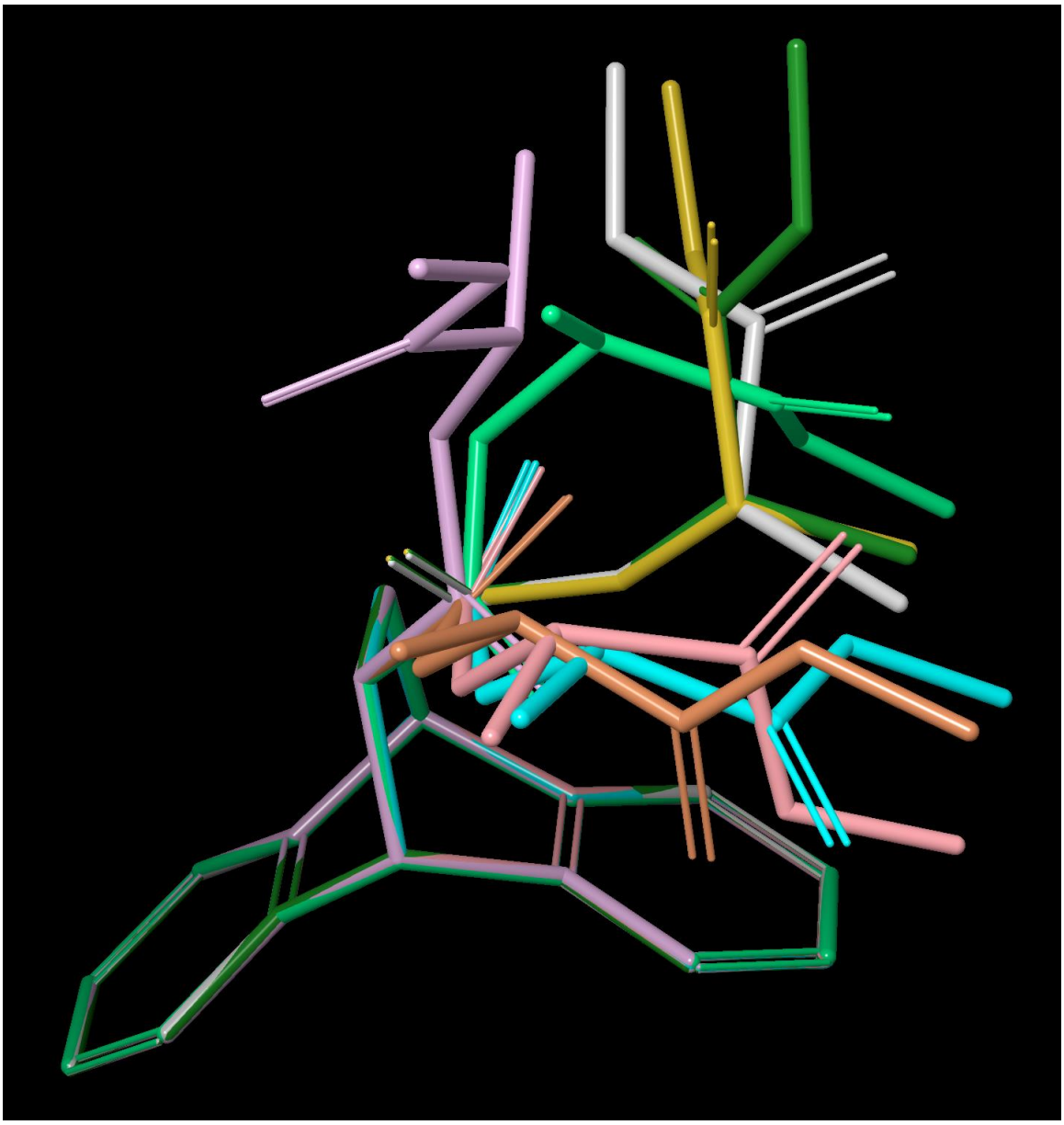

Figure 2.2. Estimation of compound **2.3**'s conformational flexibility—eight superimposed low energy conformations with relative energies < 1.4 kcal mol^{-1} are shown. All of these conformations were found with a conformational search of **2.3**. In order not to overestimate the conformational flexibility of **2.3**, only one ester arm was included for the calculation, with the terminal ethyl ester group replaced by methyl.

2.5.2.1 Di- and Mononitration

2.3 was thus subjected (**Scheme 2.8.b**) to standard S_EAr conditions with ammonium nitrate and TFAA in $CHCl_3$. We were pleased to find that double nitration of **2.3** afforded the 2,6-dinitro-substituted cycloadduct **2.7a** as the major product, 2,7-dinitro-substituted isomer **2.7b** as the minor product, and 3,7-dinitro-substituted isomer as a negligible minor product. In contrast, dinitration of the corresponding tetraester cycloadduct between anthracene and tetraethyl ethylenetetracarboxylate tetraester leads to a near statistical mixture of 2,6- and 2,7-dinitro-substituted isomers under almost identical reaction conditions (**Scheme 2.6.a**). The selective formation of the 2,6-dinitro derivative **2.7a**, therefore, indicates that the S_EAr reactions must indeed be directed by the chiral ester arms. We further corroborated this finding by mono-nitration of **2.3**, which led (**Scheme 2.8.a**) to a mostly inseparable mixture of the nitro derivatives **2.6a** and **2.6b** in a 5.3-to-1.0 molar ratio.

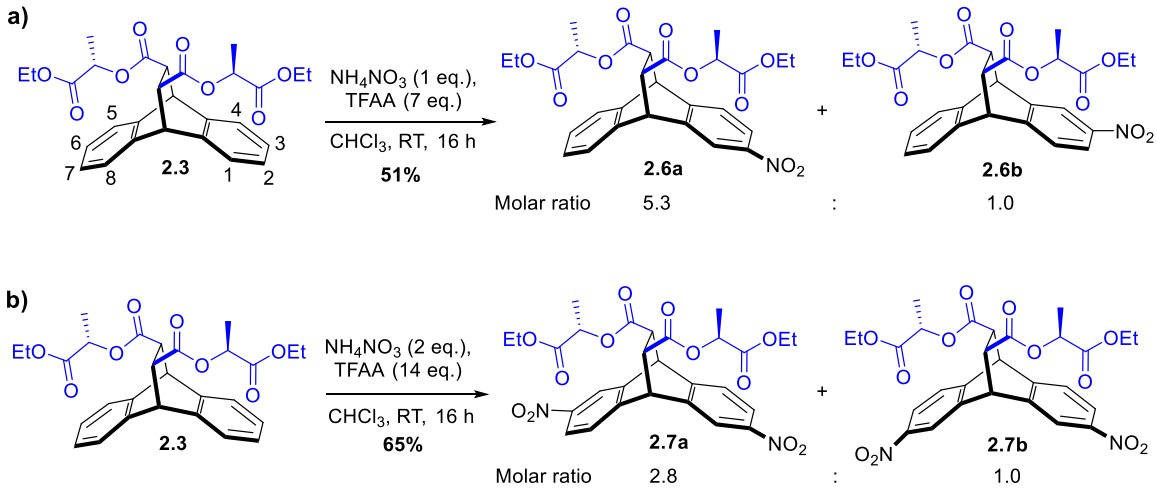

Scheme 2.8. Results for (**a**) mono- as well as (**b**) dinitration of **2.3** are shown. Both reactions are directed through space with remote chiral ester groups (illustrated in blue).

On the other hand, a mononitration of the cycloadduct between anthracene and dimethyl fumarate, in which both lactate ester arms have been replaced by methyl groups, was checked to see if any selectivity was present from overhanging ester arms, albeit shorter and achiral (**Scheme 2.9**). In the formation of cycloadduct **2.8**, the Diels–Alder reaction formed a racemic mixture of enantiomers unlike with the diester building block piece **2.3** where the Diels–Alder cycloaddition is diastereoselective. Subsequent nitration to form mononitro-substituted derivatives **2.9a** and **2.9b** formed an inseparable 1-to-1 mixture of isomers with nitro substituents in the *2* or *3* positions. Even with esters positioned above the arene subunit, due to their shorter and achiral nature, these methyl-esters are unable to direct through-space reactions to any degree of success.

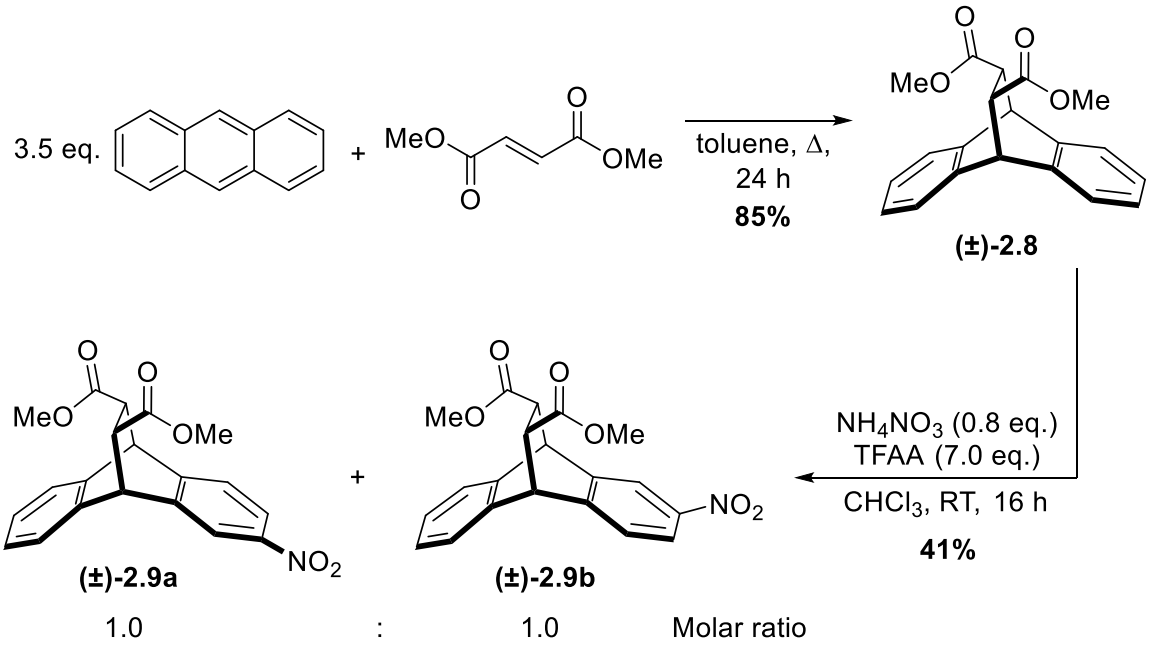

Scheme 2.9. Achiral Diels–Alder cycloaddition of dimethyl-diester **2.8** and subsequent unselective mononitration.

Moreover, when ethyl acetate was employed as the solvent for the mononitration reaction (**Scheme 2.10**), the selectivity dropped to a molar ratio of 1.8-to-1.0, though some selectivity still remained for the reactive site beneath the ester arm. When compared to the selectivity in chloroform, the mononitration selectivity had a molar ratio of 5.3-to-1.0 ratio observed in $CHCl_3$. This result is consistent with the lactate ester groups directing the nitrations to the preferred positions, since the ethyl ester groups of the ester solvent likely start to compete with the intramolecular ester-directing groups. Not unrelated, recent studies done in the Schneebeli group shows that the H-bonding character of the solvent and/or TFAA byproducts can reduce the selectivity of nitrations

byway of competing with the through-space directing prowess of the ester auxiliary groups.[136]

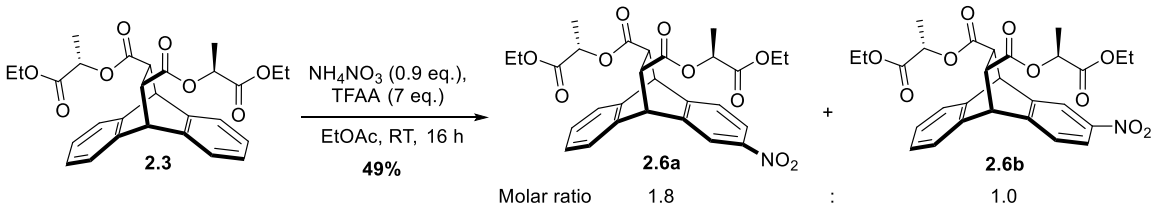

Scheme 2.10. A less selective mononitration of building block **2.3**.

2.5.2.2 ^{1}H NMR and 2D NOESY Analysis

To determine the relative reaction rates leading to the major and minor regioisomers of **2.6** and **2.7**, we integrated the representative aromatic peaks in ^{1}H NMR spectra (**Figure 2.3**) of the product mixtures. Note that the resonances corresponding to the 2- or 3-monosubstituted as well as to the 2,6- or 2,7-disubstituted isomers of **2.3** are clearly distinct for most aromatic ^{1}H NMR signals, allowing for accurate integrations of the relevant peaks. The data obtained (**Figure 2.3**) for the relative reaction rates of the consecutive nitration steps indicate that the selectivities for the second nitration are nearly independent of the first one. This finding manifests itself in mononitration affording the major product **2.6a** in a 5.3-to-1.0 molar ratio as compared to **2.6b**, while this number is approximately squared (expected ratio of **2.7a** to **2.7b**: 2.6-to-1.0, found: 2.8-to-1.0) for the formation of the 2,6-dinitro derivative **2.7a**.

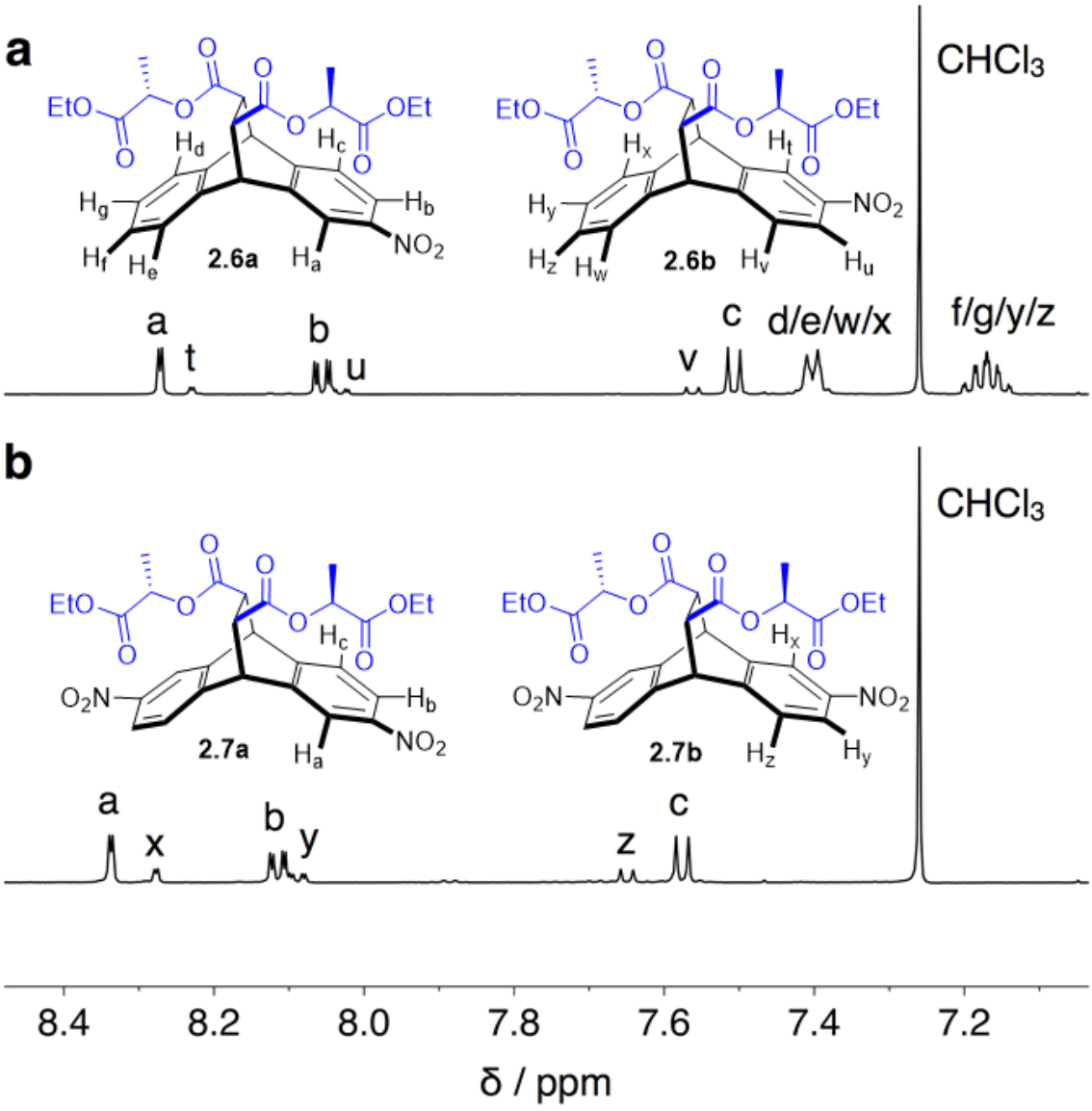

Figure 2.3. Partial ^{1}H NMR spectra illustrating the selectivity of through-space directed (**a**) mono- and (**b**) dinitration of **2.3**.

Elucidating the positions of the nitro groups relative to the ester chains in **2.6a** and **2.7a** was accomplished by 2D ^{1}H NMR spectroscopy. The ^{1}H–^{1}H nuclear Overhauser effect spectroscopy (NOESY) NMR spectrum (**Figure 2.4**) of the major product **2.7a** was recorded and analyzed, showing a through-space correlation between the protons H_h

(highlighted in red, attached directly to the ethylene bridges of **2.7a**) and the aromatic protons H_c (highlighted in red, located *meta* to the nitro groups). No such NOE cross-peaks are observed, however, between **2.7a**'s bridgehead protons H_h and the other aromatic protons H_a and H_b. These NOESY data thus prove that, in the major regioisomers **2.6a** and **2.7a**, nitration occurred directly below the auxiliary ester arms.

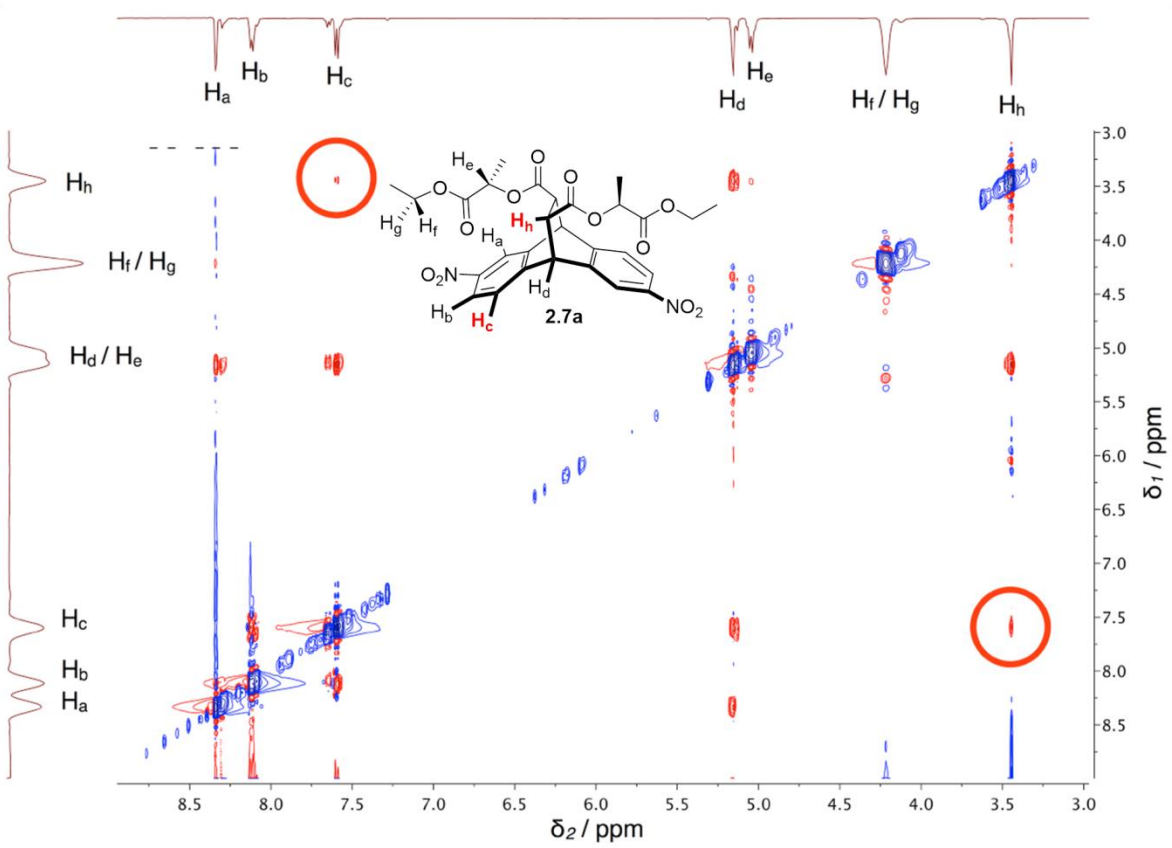

Figure 2.4. Annotated, partial ^{1}H–^{1}H NOESY NMR spectrum of **2.7a**. The key NOE cross-peaks and relevant hydrogens used to assign the compound's configuration are highlighted in red.

2.5.2.3 Quantum Mechanical Calculations

To understand our findings of selective, long-distance chirality transfer in the bicyclic ring system **2.3**, we analyzed the first nitration step with DFT calculations. The calculations were focused on the four key cationic Wheland intermediates (**Figure 2.5**)—with $[NO_2]^+$ attacking from either the *endo* or *exo* face of the aromatic rings at *C2* or *C3*. Note that the relative Gibbs free energies (G_{rel}) of these σ-complexes are anticipate[115] to govern the relative reaction rates, leading to the two observed products. The relative Gibbs free energies of the four Wheland intermediates revealed that *endo* $[NO_2]^+$ attack is favored for nitration at both the *C2* and *C3* positions of **2.3**. All four possible intermediates for mono-nitration of **2.3**—with $[NO_2]^+$ being attacked from either the top or bottom face at *C2* or *C3*—were thus optimized with DFT. For all of these optimizations, the Jaguar (Jaguar, version 8.4, Schrödinger, LLC, New York, NY, 2014.) software package was employed with default grids, the B3LYP[137, 138] exchange-correlation functional, and the 6-31G* basis set. Finally, the energies of the intermediates were refined by performing single point calculations with a larger basis set (6-311G**++) with the same functional.

Moreover, the calculations also predicted that nitration at *C2*, that is, the experimentally preferred position located directly below the ester arms, is indeed favored by an activation Gibbs free energy difference ($\Delta\Delta G^{\ddagger}$) of approximately $1.9\ \text{kcal mol}^{-1}$. This value is consistent with the experimentally observed product ratio of 5.3-to-1.0 for mononitration (**Scheme 2.8.a**) of **2.3**, which translates into a Gibbs free activation energy difference ($\Delta\Delta G^{\ddagger}$) of about $1.0\ \text{kcal mol}^{-1}$ at 298 K. The efficient long-distance chirality

transfer witnessed in our system can thus be explained quantitatively by the results of the DFT calculations.

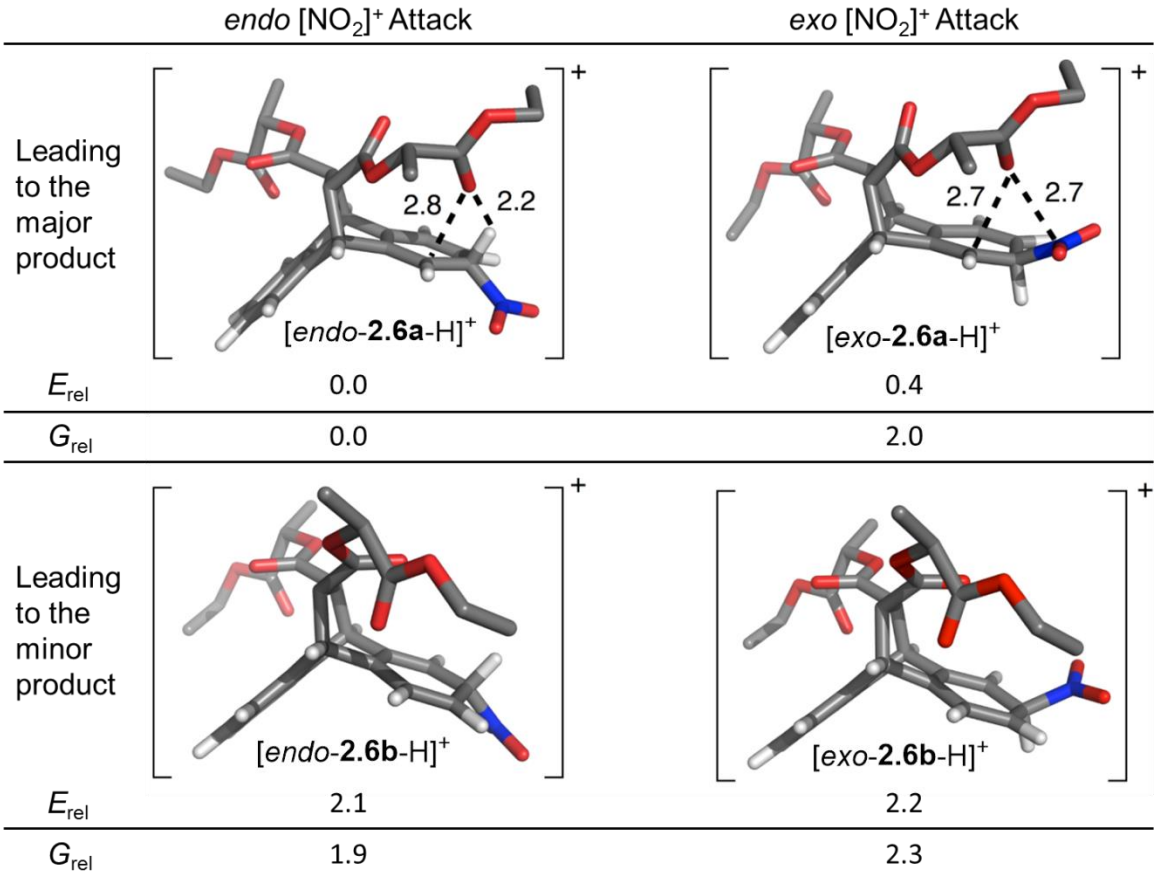

Figure 2.5. DFT-optimized structures of the four possible Wheland intermediates for mononitration of **2.3**. All values of G_{rel} and E_{rel} are reported at the B3LYP-MM/cc-pVDZ++ level of theory relative to the most stable intermediate [*endo*-**2.6a**-H]$^+$ in units of kcal mol^{-1}. The key stabilizing noncovalent interactions in the intermediates leading to the major products are highlighted with dashed lines. Corresponding distances are provided in Å.

The relative DFT energies of the intermediates revealed that, due to the significant steric bulk associated with the ester chains attached to the bridgehead carbons, attack from the bottom face is favored for nitration at the experimentally preferred *C2* position of **2.6a**. Moreover, the calculations also predicted, that nitration on *C2*, directly below the ester chains, is indeed favored by an activation energy difference ($\Delta\Delta E^{\ddagger}$) of approximately 1.8 kcal/mol. This number is consistent with the experimental product ratio of 5.3-to-1 for mononitration of **2.3**, which translates into a Gibbs free activation energy difference ($\Delta\Delta G^{\ddagger}$) of 1.0 kcal/mol at 298 K. As a note, for electrophilic aromatic substitution reactions the rate-determining transition states are usually very close in energy to the cationic tetrahedral intermediates. For this work, we therefore approximated the differences in activation Gibbs free energies for the different reaction pathways by the corresponding energy differences of the tetrahedral intermediates.

Yet, the DFT-optimized structures (**Figure 2.5**) of the lowest Gibbs free energy tetrahedral intermediates [*endo*-**2.6a**-H]$^+$ and [*endo*-**2.6b**-H]$^+$ for nitration in the *C2* and *C3* positions, respectively, also offer an intuitive explanation for the observed selectivity. Close contacts between the cationic *C1* and a carbonyl oxygen of the ester arm positioned directly above *C1* are observed in [*endo*-**2.6a**-H]$^+$. Furthermore, the lowest energy unoccupied molecular orbital of [*endo*-**2.6a**-H]$^+$ (**Figure 2.6**) clearly shows delocalization into one of the carbonyl oxygen's lone pairs. Both of these observations indicate through-space electron donation from an oxygen lone pair to stabilize the delocalized carbocation underneath.

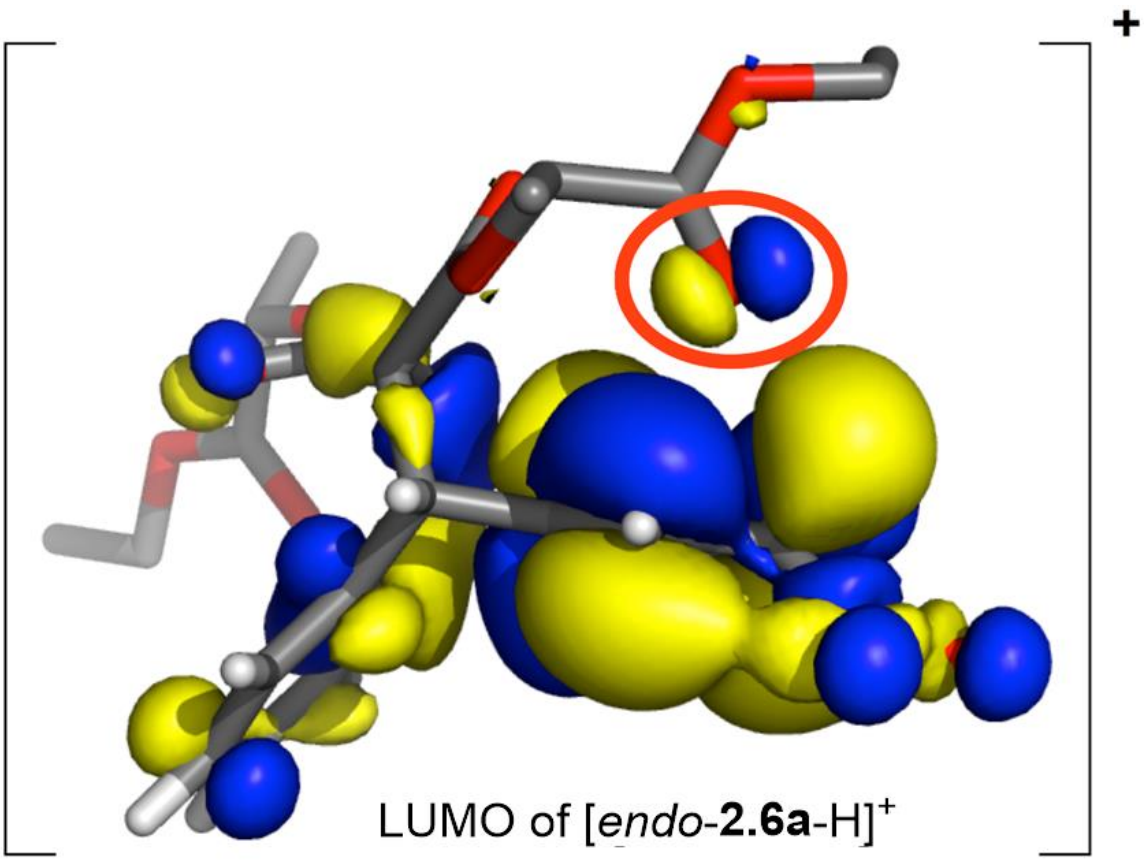

Figure 2.6. Isosurface plot of the lowest unoccupied molecular orbital (LUMO) belonging to the favored cationic intermediate [*endo*-**2.6a**-H]$^{+}$. Delocalization of the LUMO into the carbonyl group of the ester arm, which likely plays a crucial role in directing the electrophilic aromatic substitution reaction to the *C2* position, is circled in red.

An additional close contact is spotted between the same carbonyl oxygen and the positively polarized acidic hydrogen attached to *C2*, located α to the nitro group. This second close contact with an O–H distance of only 2.2 Å represents a typical [C–H···O]–hydrogen bond,[139] and likely also plays a key role in stabilizing the favored intermediate [*endo*-**2.6a**-H]$^{+}$. Further evidence that these observed close contacts represent indeed

significant, stabilizing non-covalent interactions (NCI), was obtained by analyzing the critical points of the calculated electron density, using NCI plots[140] acquired with Jaguar (Schrödinger Release 2016–3: Jaguar (Schrödinger, LLC, New York, NY, USA, 2016).[141] The NCI interaction strengths (E_{int}^{NCI}) showed that the strongest stabilizing noncovalent interaction (E_{int}^{NCI} = –0.016 a.u.) present in the Wheland intermediate [*endo*-**2.6a**-H]$^+$ is indeed the [C–H···O]-hydrogen bonding, followed by the slightly weaker (E_{int}^{NCI} = -0.013 a.u.) interaction caused by electron donation from an O–lone pair to the carbocation underneath.

Oxygen lone pair to carbocation electron donation (with E_{int}^{NCI} = -0.015 a.u.) is also observed for the Wheland intermediate [*exo*-**2.6a**-H]$^+$, which results from *exo* NO_2^+ attack in the favored *C2* position. Note that the stabilizing [C–H···O]–hydrogen bonding is replaced (**Figure 2.5**) by O-to-NO_2^+ coordination in this case. This weak (E_{int}^{NCI} = -0.012 a.u.) coordination interaction likely plays a fundamental role in controlling the relative orientations of the reactants for *exo* NO_2^+ attack in a manner not too far from how DMATS orients the dimethylallyl cation above its tryptophan substrate. While, at the level of theory employed, [*exo*-**2.6a**-H]$^+$ (G_{rel} = 2.0 kcal mol^{-1}) is less stable thermodynamically than [*endo*-**2.6a**-H]$^+$ (G_{rel} = 0.0 kcal mol^{-1}), the electronic energy gap (0.4 kcal mol^{-1}) between these two Wheland intermediates is much smaller than the corresponding Gibbs free energy difference (2.0 kcal mol^{-1}). Thus, considering that DFT-calculated relative entropies often carry[142] larger error bars than corresponding energies of about 1 kcal mol^{-1}, *exo* NO_2^+ attack could still be competing with *endo* attack in forming the major product.

The efficient long-distance chirality transfer witnessed in our system can thus be explained quantitatively by the results of the DFT calculations. The computed lowest energy structure of the tetrahedral intermediate for nitration (**Figure 2.7.b**) also offers, however, an intuitive explanation for the observed selectivity. Close contacts between the cationic *C1* and a carbonyl oxygen of the ester arm in **8**, positioned directly above *C1*, are observed in this structure. This observation can be explained by through space electron donation—illustrated with resonance structures in **Scheme 2.11**—from an oxygen lone-pair into the empty p_z-orbital of *C1*. An additional close contact is also spotted between the same carbonyl oxygen and the strongly positively polarized acidic hydrogen attached to *C2*, located α to the nitro group. This second close contact with a distance of only 2.1 Å resembles a typical [C–H···O]-hydrogen bond[139] and likely also plays a key role in stabilizing the favored intermediate **2.6a**.

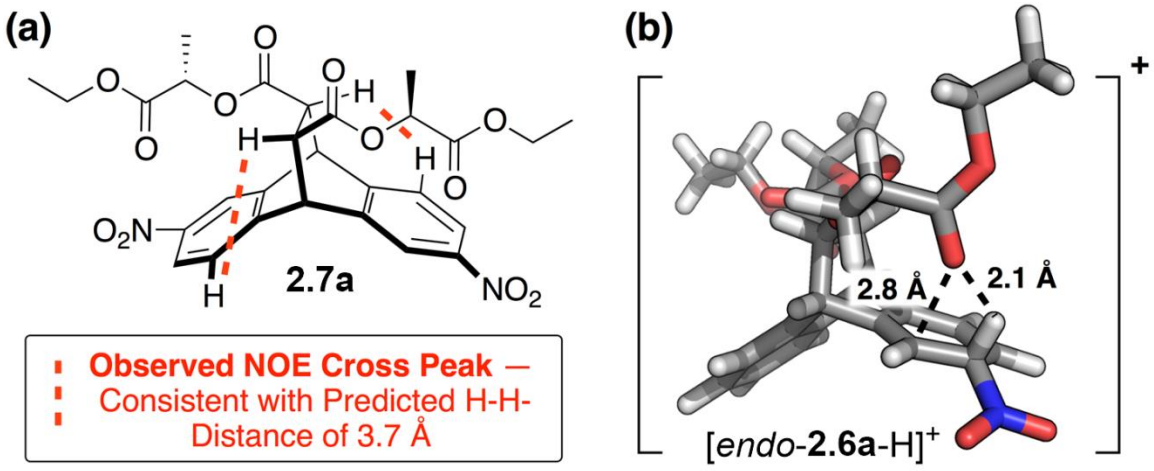

Figure 2.7. (**a**) Observed NOE cross peak (^{1}H–^{1}H NOESY NMR) used to assign the configuration of the favored stereoisomer of **2.7a**. (**b**) Structure of the lowest energy cationic intermediate for mononitration, optimized with DFT at the B3LYP/6-31G* level.

2.5.2.4. Proposed Mechanisms of Through-Space S_EAr Control

In general, our approach combines enzyme-inspired hydrogen bonding with electron donation from an oxygen lone pair to direct S_EArs through space. This combined tactic—designed to optimally stabilize carbocations—is best illustrated with resonance structures (**Scheme 2.11**), which also highlights the need to precisely position the key carbonyl group directly above carbons *1* and *2*.

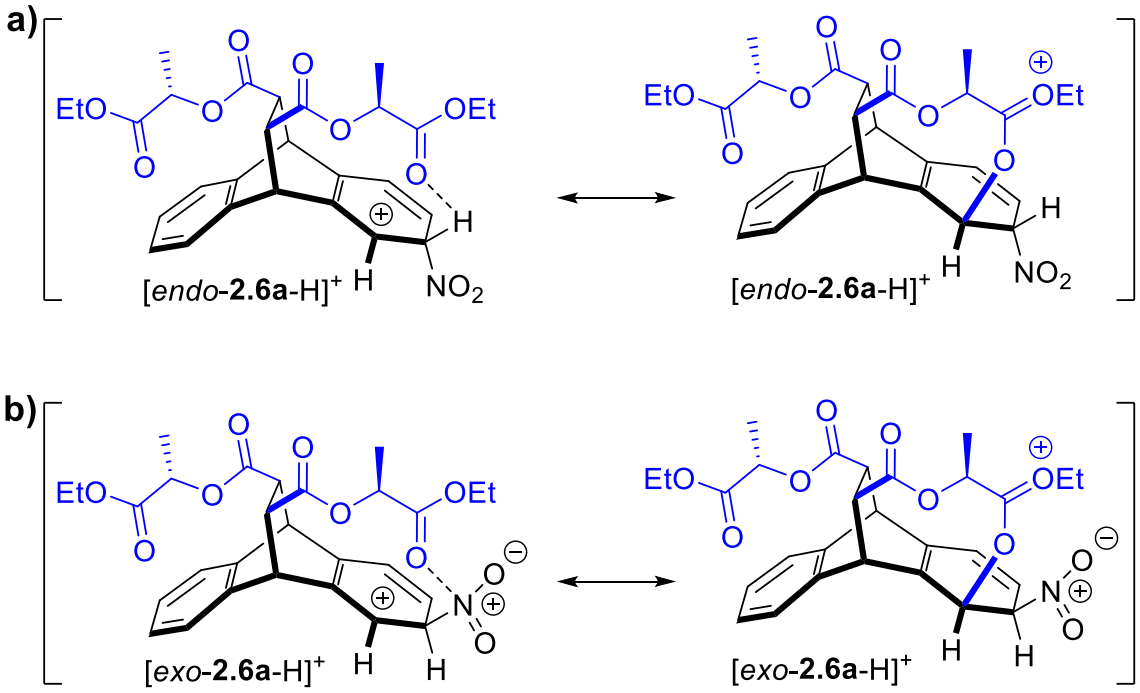

Scheme 2.11. Resonance structures of the cationic Wheland intermediates for favored mononitration of **2.3** in the *2* position, illustrating the key DMATS-inspired through-space directing effects observed in our system. (**a**) *Endo* and (**b**) *exo* $[NO_2]^+$ attack.

Owing to the off-centered positioning of this carbonyl group, our manner to direct S_EAr reactions through space is selective for specific positions on aromatic rings. On the basis of the results of the DFT calculations, we postulate that—like in the mechanism[123]

for DMATS—[C–H···O] hydrogen bonding (**Scheme 2.11.a**) and preorganization of the electrophile above the plane of an aromatic ring (**Scheme 2.11b**) are both important factors in achieving the observed selectivities.

We were thus pleased to find that nitration (**Scheme 2.12**) of **2.3** with ammonium nitrate and TFAA in $CHCl_3$ afforded the 2,6-dinitro-substituted stereoisomer of **2.7a** as the major product. This finding indicates, that nitration of **2.3** must be directed by the ester arms. Thus, there is long-distance chirality transfer occurring in the electrophilic aromatic nitration of **2.3**. In contrast, dinitration of the corresponding tetraester derivative leads to a near statistical mixture of 2,6- and 2,7-substituted regioisomers under almost identical reaction conditions. After elucidating the positions of the nitro groups relative to the ester chains by analyzing the major stereoisomer **2.7a** by ^{1}H–^{1}H NOESY NMR, we found that it matched our DFT results. This NOESY data thus proves that in the major isomer of **2.7a**, nitration occurred directly below the ester arms.

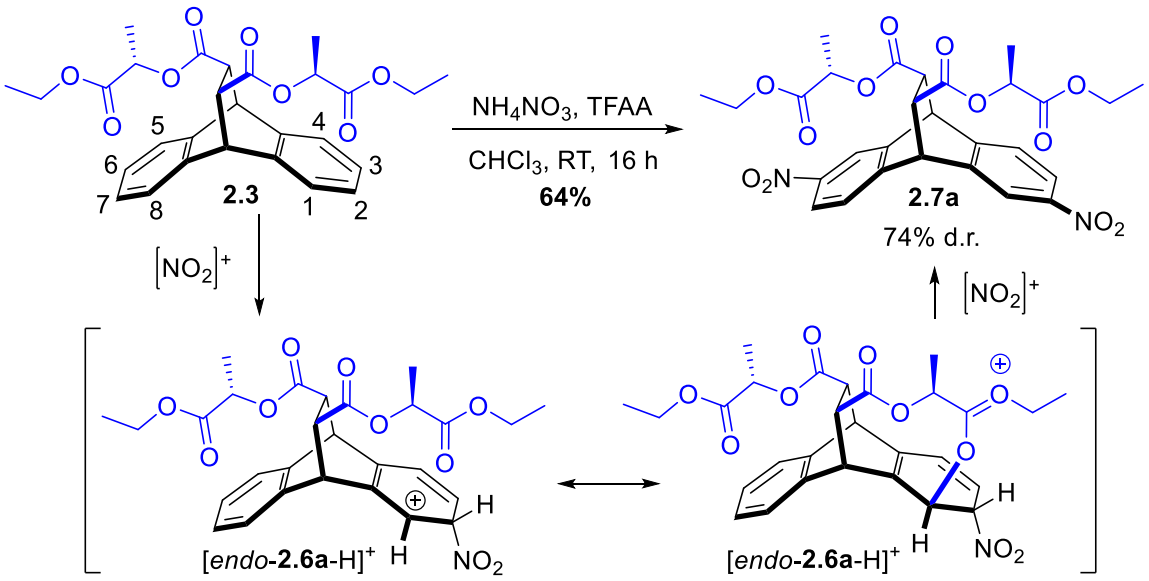

Scheme 2.12. Long-distance chirality transfer. Note how through-space electron donation from a precisely positioned ester group stabilizes the cationic intermediate, which—after a second nitration step—leads to the favored product **2.7a**.

2.5.3 Nitration with Other Functional Arms

To improve the selectivity of nitration onto our triptycene-like building blocks, we also investigated a host of various other auxiliary arms, much like in proof-of-concept nitration of methyl-diester **2.8** (**Scheme 2.13**). Thanks to the ease of functionalization of the ester arms, we were afforded a wide range of potential support groups to explore through-space directing effects of S_EAr nitrations. Starting from diester cycloadduct **2.3**, we followed a literature procedure to reduce the ester groups to form diol **2.10** (**Scheme 2.13**).[143] From there, **2.10** could be utilized to attach a variety of auxiliary groups. As a first example, hexyl chains were attached to diol **2.10** to form diether **2.11**, of which the 2,6-diamine derivative is a vital molecular building block which will be discussed in later

chapters. From there, **2.11** was exposed to typical EAS nitration conditions to form an inseparable mixture of the mononitrated species **2.12**, of which the diether chains provided no through-space directed selectivity.

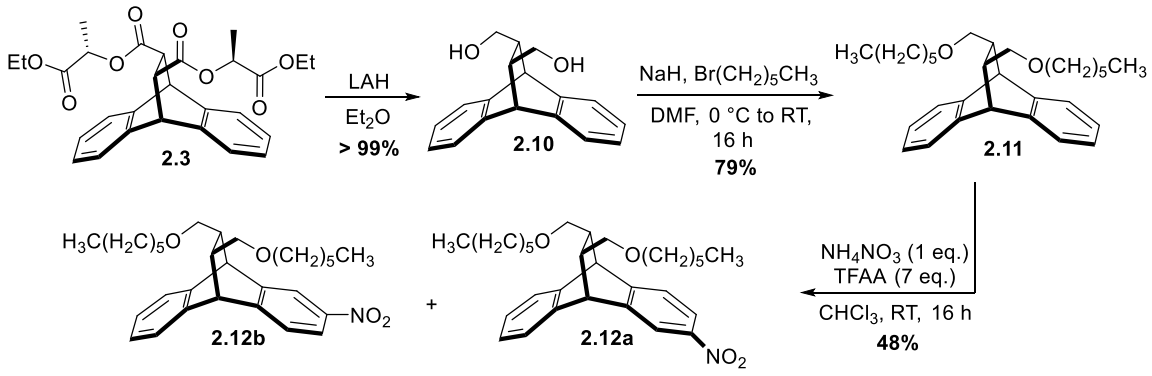

Scheme 2.13. Nitration of diether derivative **2.11**.

Next, in mimicking the original diester system, **2.10** was transformed into the resulting achiral diester species **2.13** (**Scheme 2.14**). The new diester derivative provides more flexibility due to the lack of the first carbonyl moiety as well as a lack of the following methyl, which we hypothesized might allow for the ester to stabilize the Wheland intermediate more readily. **2.13** was treated with the standard EAS nitration conditions which formed an inseparable mixture of the dinitrated species **2.14**. Based on ^{1}H NMR evidence, the more flexible ester arms provided no better through-space selectivity, with close to a 1-to-1-to-2 mole ratio of **2.14a** to **2.14b** to **2.14c**.

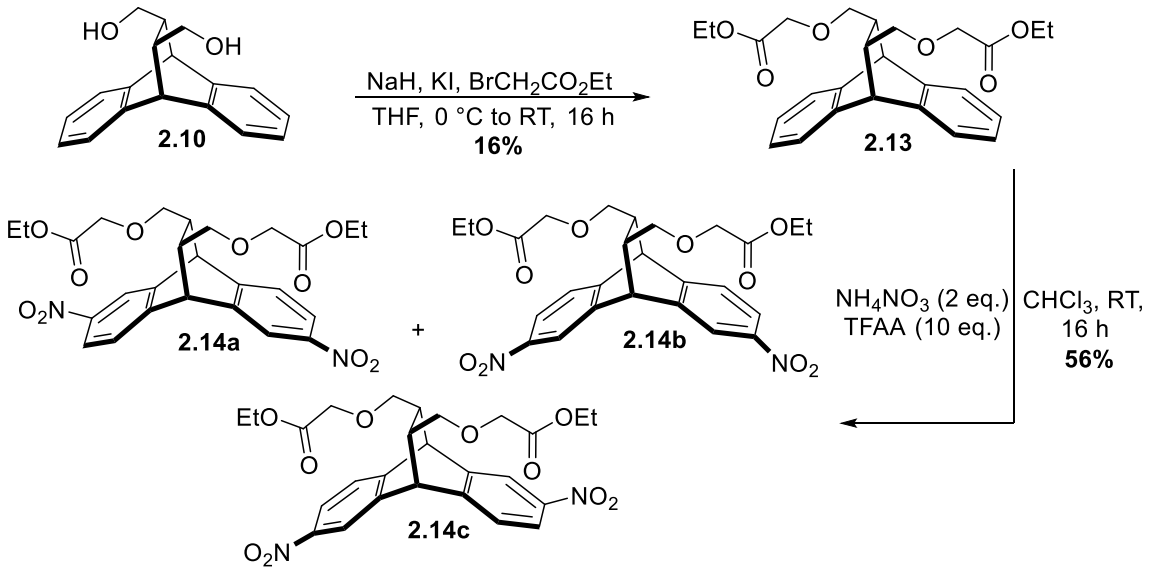

Scheme 2.14. Formation and nitration of achiral diester **2.13**.

To retain the chelating effects of the carbonyl functionality as present in cycloadduct **2.3**, we pursued a different system containing a tertiary amide. Starting from diester **2.3**, the ester groups were hydrolyzed off with an excess of potassium hydroxide (due to each ester arm containing two ester moieties) to form diacid **2.15** (**Scheme 2.15**). From there, **2.15** was treated with amide coupling conditions alongside reagent diethylamine to generate diamide **2.16**. Despite the shorter reach of the auxiliary arm, the *N*-diethyl moiety was hypothesized to have the capacity to much better donate into the nitroarenium ion intermediate to increase the stability of the system as compared to the initial diester arms. However, the ethyl chains may have been preventing appropriate reach to the arenium ion for stabilization, as when **2.16** was treated with typical EAS mononitration conditions, an inseparable 1-to-1 mixture formed of mononitro diamide species **2.17**.

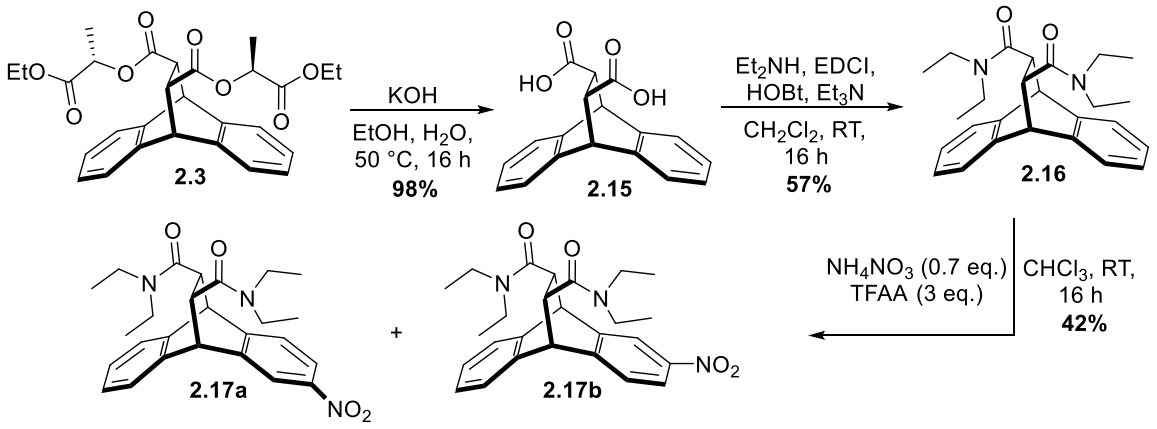

Scheme 2.15. Mononitration of diethyl-diamide **2.16**.

Next, a diamide with shorter methyl chains was synthesized to check for through-space selectivity. **2.15** was exposed to amide coupling conditions with dimethylamine to produce diamide **2.18** (**Scheme 2.16.a**). From there, **2.18** underwent S_EAr nitration conditions to form an inseparable mixture of dinitrated derivative **2.19**. However, excess TFAA had to be used (in comparison to typical aromatic nitration conditions thus far) due to the unreactive nature of **2.18**. Some selectivity was found with a 1.3-to-1.1-to-1 mixture of dinitrated species **2.19a**, **2.19b**, and **2.19c** respectively (based on the previously established reactive site due to through-space auxiliary directing groups). A potential issue was the excess of TFAA utilized to allow the reaction to progress, as noted previously the presence of H-bonding character in TFAA byproducts can reduce selectivity of nitration products. While not as great selectivity as the original chiral diester **2.3**, diamide **2.19** was carried forward to be utilized as a potential molecular building block, and as a proof-of-concept of the capacity for initial diester **2.3** to be easily functionalized and transformed into various species. **2.19** then had its nitro groups

reduced down to amines, and from there separation of minor diamine derivatives was much more easily performed to afford major product 2,6-diamine-substituted diamide **2.20** (**Scheme 2.16.b**).

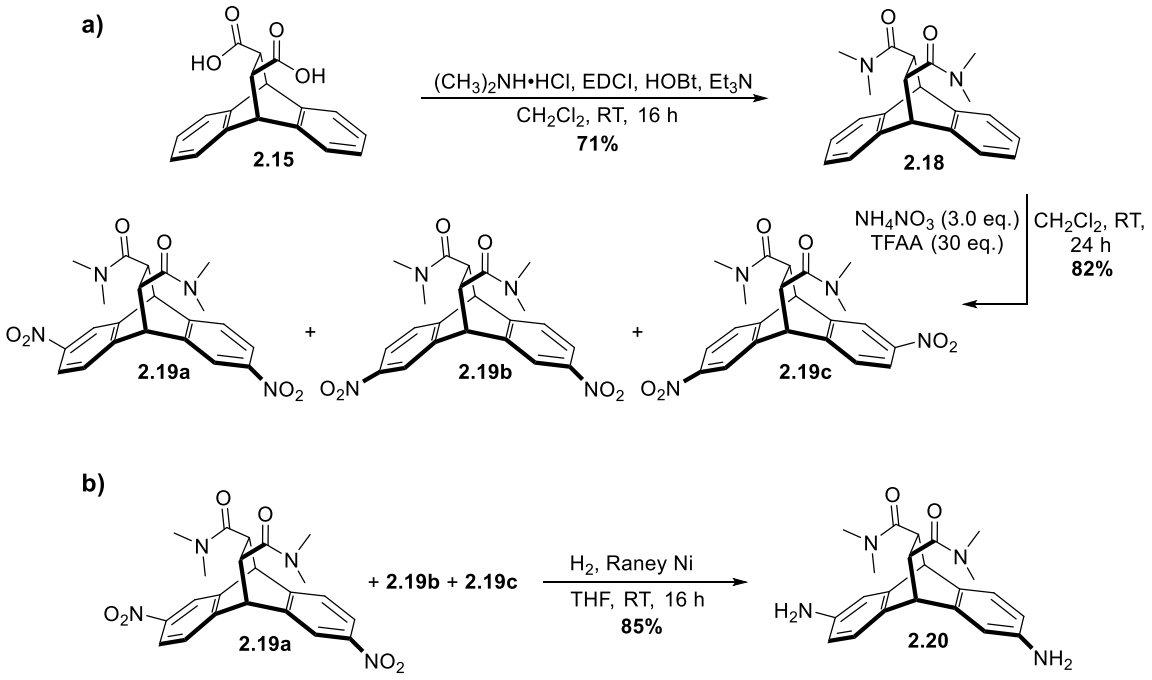

Scheme 2.16. (**a**) Dinitration and (**b**) subsequent reduction of dimethyl-diamide **2.18**.

Then, to further study through-space directing effects, the amide was moved to the end of a longer ether chain to investigate the effects of a much more flexible amide auxiliary arm with the capacity to better reach the nitration site for non-classic H-bonding stabilization. Diol **2.10** was alkylated to form diether-diamide **2.21** (**Scheme 2.17**). Upon exposure to standard EAS nitration condition, the result was an inseparable mixture of dinitrated species **2.22**, and with no meritable selectivity in nitro placement on the aryl rings. And, in general, it seemed as if some degradation occurred upon the nitration of these amide-based auxiliary systems. Despite the longer reach of the amide group,

unfortunately we were unable to improve upon the selectivity of diamide **2.18**. The first carbonyl moiety found in **2.3** may make for a more stabilized nitroarenium ion, as the much shorter diamide **2.18** was found to have some selectivity.

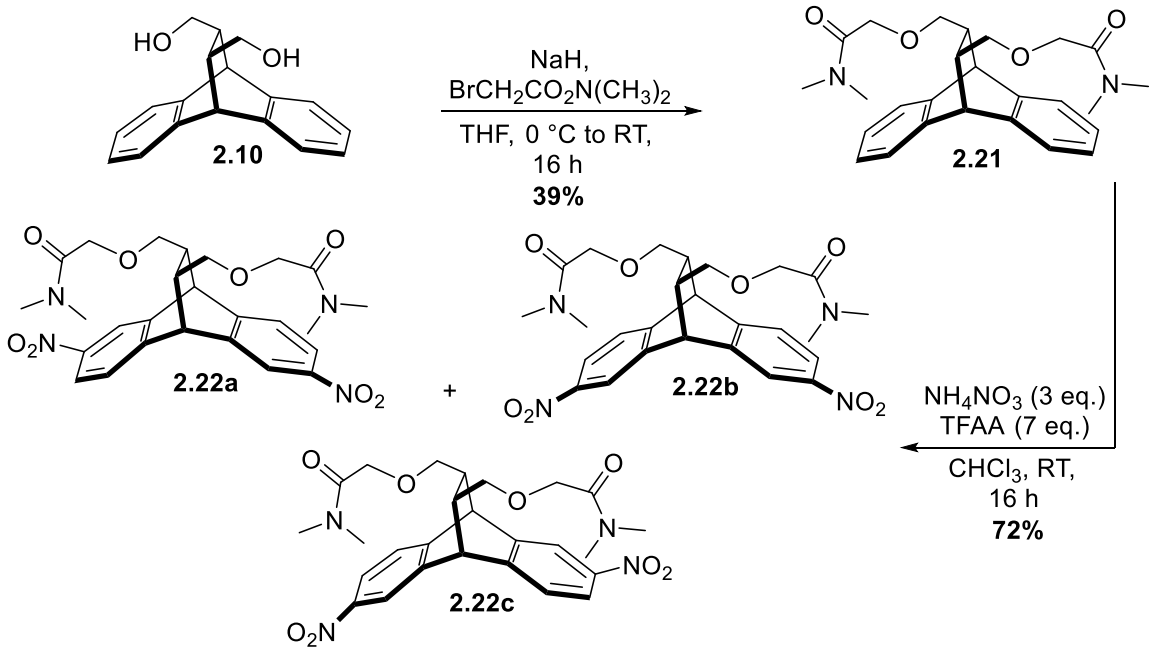

Scheme 2.17. Dinitration of longer chain diamide, **2.21**.

Initial studies of different auxiliary arms were met with some success. While a new system for selective through-space nitrations was not obtained, the capacity for diester **2.3** to be easily functionalized to a wide variety of different bridgehead arms was realized. Moreover, these studies of different support groups for EAS nitrations were carried forward to Dr. Joseph Campbell of the Schneebeli group who not only utilized the chiral lactate ester arm found in **2.3**, but further modified it to contain a bulkier isopropyl group, rather than a methyl group, to provide even greater S_EAr nitration selectivity on their respective arene subunits. While a more specific nitration methodology would be

ideal, screening for more efficient through-space auxiliary arms does stray from the purpose of my thesis objective in building helical ladder polymers, particularly when diester **2.3** provides good nitration selectivity already. Leaving further investigations into different support groups by other members of the Schneebeli lab helps to push this unique methodology forward nonetheless.

2.4 Other Nitration Work in the Schneebeli Group

Dr. Campbell was successfully able to utilize this chiral ester nitration methodology and applied it to his own molecular building blocks in development of an enantioselective electrophilic aromatic nitration.[144] Similar to my own system, the chiral ester arms on the tribenzotriquinacene (TBTQ) stabilized the generated Wheland intermediate through chelation of the two carbonyls (**Figure 2.8**). More so, $A^{1,3}$ strain prevented these chiral arms from directing the nitro group to the adjacent arene subunit, thus rendering each chiral auxiliary to only stabilize a single arenium ring on the system, and thus only direct one nitro group to one reactive site. Increasing the steric bulk of the chiral ester also provided even greater enantioselectivity because of greater $A^{1,3}$ strain.

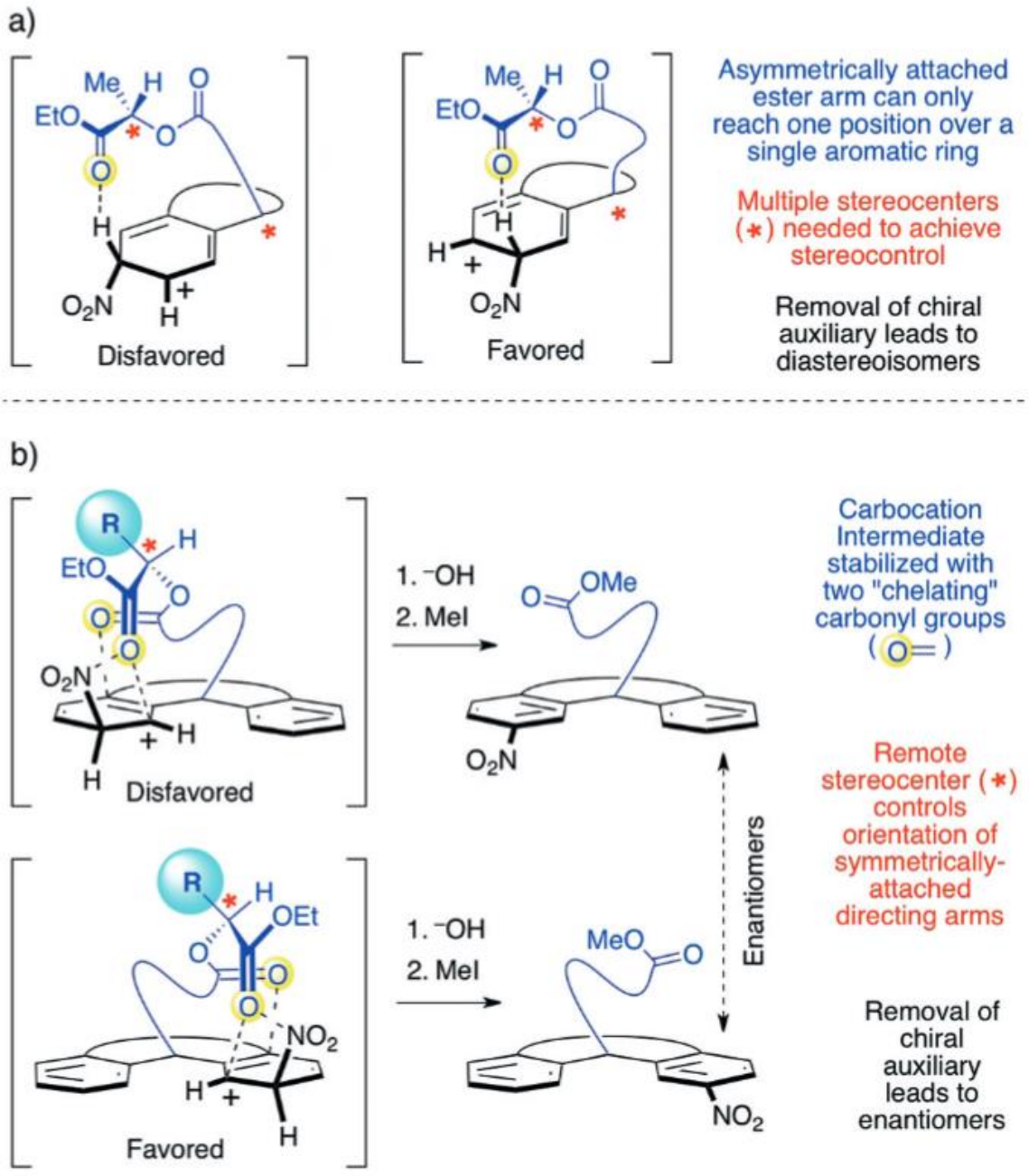

Figure 2.8. (**a**) My work on through-space nitrations and (**b**) Dr. Joseph Campbell's enantioselective nitration methodology.

Dr. Campbell's methodology is fundamentally distinct from the through-space directed S_EAr strategy reported by me. Particularly, in Dr. Campbell's approach the through-space directing groups were attached to the substrates in an asymmetric style, closer to the reactive site favoring nitration, thus ensuring that only this proximal site could be reached by the directing groups, and therefore lead to stereoselective nitrations. However, my nitration strategy was only able to provide diastereoselective product formation after removal (e.g., reduction) of the through-space directing groups as a direct result of the asymmetric linkage chemistry (**Figure 2.8.a**), whereas Dr. Campbell applied this methodology to a TBTQ building block composed of three arene subunits, thus increasing the number of disfavored nitrated byproducts and therefore the overall complexity of investigating this new strategy (**Figure 2.8.b**).

2.5 Conclusions and Outlook

In summary, we proposed and validated a simple, bioinspired strategy to control S_EAr through space by placing carbonyl substituents directly above the planes of aromatic rings. We demonstrated that the S_EAr reactions can be directed to specific locations on the aromatic rings, even if partially flexible linkers are employed to position these carbonyl groups. The mechanism of through-space activation was investigated with electronic structure theory calculations, the results of which agree quantitatively with the observed experimental selectivities. These calculations showed that—like in a related enzyme, which also catalyzes S_EAr reactions—through-space [C–H···X] hydrogen bonding and (in a competing mechanism) preorganization of the electrophile above the aromatic rings likely play a role in controlling the reactions. Our finding opens up the

third dimension above and underneath aromatic rings to control their reactivities with atomic precision. Furthermore, to be able to apply this through-space directing methodology to other 3D building blocks certainly shows its utility as a mechanosynthesis-type strategy. Selectively delivering nitro groups to specific reaction sites opens the door in generating molecular building blocks in high yields, and high stereospecificity—both crucial factors to consider when attempting to synthesize macromolecular structures.

CHAPTER 3: INITIAL STRATEGIES BASED ON CHIRALITY-ASSISTED SYNTHESIS TOWARD HELICAL POLYMERS

3.1. Introduction

Chirality-assisted synthesis (CAS) has emerged as a versatile method to control the shapes of π-conjugated macromolecules and supramolecular assemblies.[5] With CAS, the sequence and chirality of the monomeric building blocks dictates the shape and functions of the resulting macromolecules in a programmable fashion. Supramolecular materials with special functions, e.g. the ability to encapsulate macrocycles,[8] can be created with CAS. CAS has been utilized to synthesize a variety of shape-defined nanoscale structures, including polyaromatic strips,[4] molecular claws,[142] very large hydrogen-bonded closed-shell capsules,[145] and in the work presented in this chapter, helical strips.[146] Applications, challenges, and future directions of the growing CAS field are discussed in light of the unique shape-control abilities CAS has to offer.

3.2. En Route to Helical Polymers

While initial success was achieved in creating C-shaped strips with CAS in a "face-on" orientation, it has proven difficult to couple the aforementioned first generation CAS building blocks in a "side-on" orientation to afford helically shaped molecular structures. Obtaining the correct *o*-bromoaniline piece (or other halogen species) would allow for such side-on couplings to occur to generate phenazine-bridged helical macromolecules through Buchwald–Hartwig aminations (**Scheme 3.1**).[147-150] The initial

investigations into these side-on couplings was done so to generate helical-shaped strips, and eventually polymers, rather than molecular C-shaped strips.

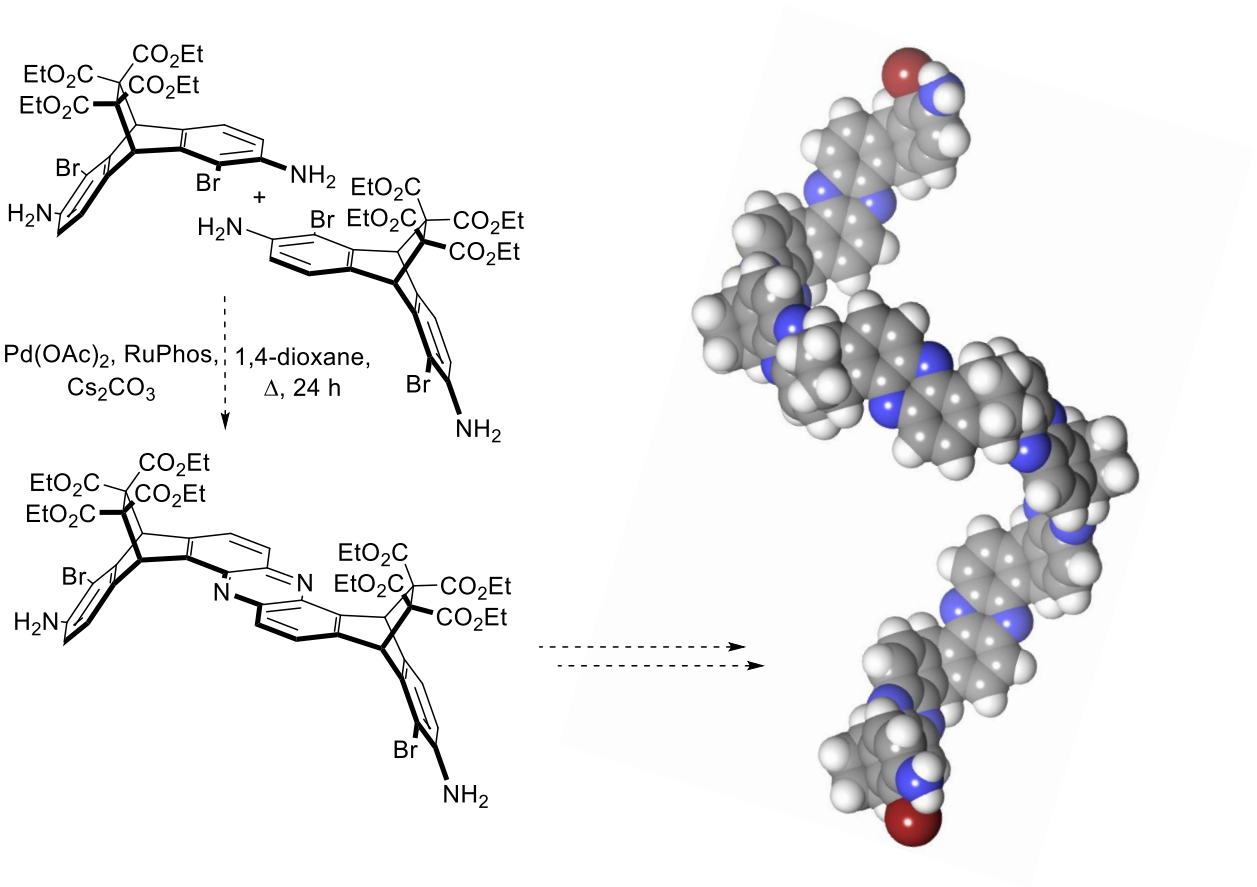

Scheme 3.1. Initial Pd-catalyzed double-amination strategy to afford molecular helices (helical representation has tetraester bridgeheads removed for clarity).

3.2.1. Tetraester Cycloadduct

The question was, first, how to arrange a halogen onto the aniline ring to promote side-on couplings? The nature of aromatic halogenation reactions with these cycloadduct systems has the halogen add *ortho* to the amine but *para* to the bridgehead carbon

(**Scheme 3.2**). First trials were done with the tetraester building block. Starting from the chiral resolved diamine **3.1**, initial attempts were done to alkylate the *para*-bridgehead-*ortho*-amine position, followed by bromination to enable side-on CAS coupling (**Scheme 3.1**). However, even the beginning steps of the synthesis proved difficult and low yielding, with little to no product obtained or inseparable mixtures of byproducts. Rather than alkylation, if a less active halogen species for Buchwald–Hartwig amination reactions were utilized (e.g. a chloro group) to block the first reactive halogenation position, *then* followed by a much more reactive halogen species (e.g. an iodo group), hypothetically a side-on coupling could occur. While this route was certainly considered, it would undoubtedly back the arene subunit much less active, and provide an opportunity for an additional amination site (with the chloro group)—even if a minor side reaction, this draws away from the intention of CAS where a coupling reaction can only happen in *one* entirely specific way.

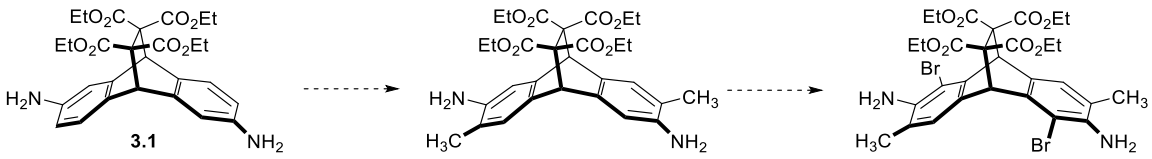

Scheme 3.2. Proposed methylation of most reactive halogenation site, followed by bromination.

Moving forward, a new route was proposed whereby a halogen species could be *exactly* placed in the desired side-on position. While flanking the amine group with two halogens proves unwieldly and likely unreactive for double-aminations, if one of the halogens were able to be removed selectively (e.g. the halogen *ortho* to the carbon

bridgehead) that would afford us exactly the desired building block. Even if the dehalogenation process were statistical, rather than selective, it would still provide an excellent starting point to at least determine if the coupling would happen side-on at all.

Starting from previously synthesized mononitro-tetraester **2.5**, the compound was reduced to the amine derivative **3.2** and kept as an enantiomeric mixture for the ease of checking its capabilities in selective dehalogenation (**Scheme 3.3**). From there, aniline **3.2** was over-iodinated to form diiodo-aniline **3.3**. Following this, **3.3** was exposed to Pd-catalyzed dehalogenation conditions where, to our surprise, selective deiodination occurred to form monoiodo-monoamine **3.4**. A mix of mono-deiodinated **3.4** and recovered starting material **3.3** was obtained from the reaction, even after letting the reaction progress as long as 16 hours. Initial trials included monitoring the reaction every ten minutes, but it became very apparent by ^{1}H NMR analysis that selective dehalogenation was occurring. Racemic monomer **3.4** was carried forward to check side-on coupling conditions.

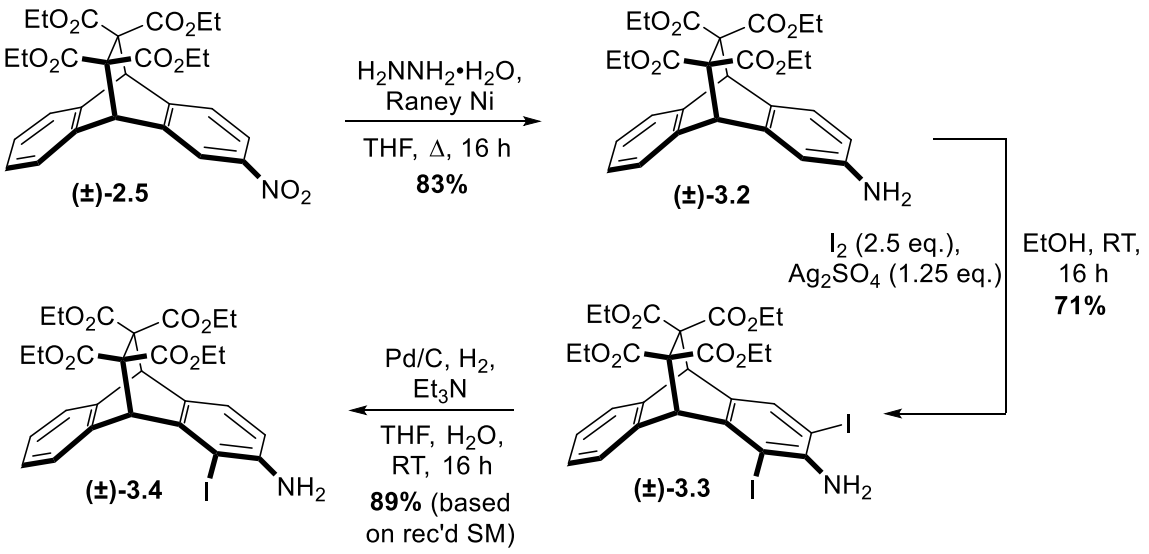

Scheme 3.3. Selective deiodination of tetraester diiodo-aniline **3.3** to form side-on coupling monomer.

When attempting to join the racemic mixture of **3.4** using the proven, Pd-catalyzed double-amination conditions[4] to form helical strip **3.5**, no coupled phenazine derivatives were observed (**Scheme 3.4**). This finding is most likely rooted in the densely functionalized ethylene bridges of **3.4**, which sterically obstruct the desired double-amination reactions. This, unluckily, is postulated as the same reason why selective deiodination is possible—the densely packed tetraester bridge obstructs Pd-insertion into the C–I bond. Whether by sterics exactly or a chelation effect is not yet investigated. As a note of interest, by ^{1}H NMR there seemed to be a minor byproduct that was the result of a retro Diels-Alder reaction on one of the teteraester moieties following some double-amination coupling, where anthracene-like aromatic chemical shifts were present.

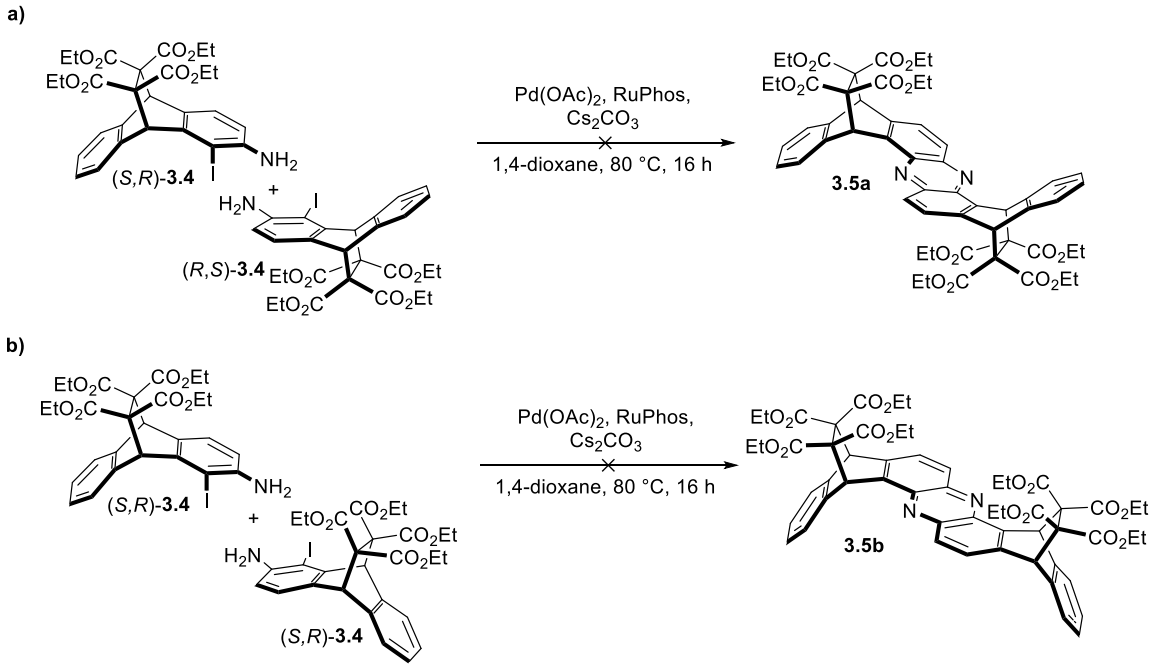

Scheme 3.4. Proposed double-amination coupling of racemic mixture with first generation CAS side-on monomers. (**a**) Coupling of (*R*,*S*)-**3.4** and (*S*,*R*)-**3.4** and (**b**) coupling of same enantiomer pair.

3.2.2. Chiral Diester Cycloadduct

After attempts with the first generation building block, efforts were moved to the diester cycloadduct **2.3**. For reasons previously elaborated on (**Chapter 2**), this second generation building block proved much more favorable in its abilities to form ideal CAS monomers. With a stereoselective nitration methodology to form (and easily purify) a well-defined building block, easily functionalized ester bridgehead, as well as being less sterically hindering, diester **2.3** seemed to be the best candidate for pursuing not only CAS side-on couplings, but for chirality-assisted couplings in general.

While the tetraester building block (**Chapter 1.3**) was known to couple in a double-amination to afford molecular strips, it was yet untested if the diester **2.3** was able to undergo such a reaction as well. As the new diester cycloadduct was the second generation of CAS building blocks, it was subjected to a manner of conditions to investigate it for its Pd-coupling capabilities before attempts into side-on coupling reactions to form helical strips.

To begin investigations into face-on CAS coupling, mononitro-substituted **2.6a** was subjected to reduction conditions with Raney nickel to form monoamine derivative **3.6** (**Scheme 3.5**). Separation of the other substituted isomer is typically done at the amine stage of the synthesis of the diester building block due to the easier separation conditions via column chromatography. Following this, mono-iodination was performed upon the amine derivative **3.6** to form CAS precursor **3.7**. Much like with the tetraester amine derivative, diiodination (or iodination in the side-on position over the face-on position) does not occur on the aryl ring unless extra equivalents of iodine monochlorine (ICl) are added to the reaction—with ICl the iodo group is much more electrophilic thanks to the electron withdrawing nature of the chlorine as opposed to elemental iodine (I_2), thus circumventing the need for a Lewis acid (e.g. Ag_2SO_4).

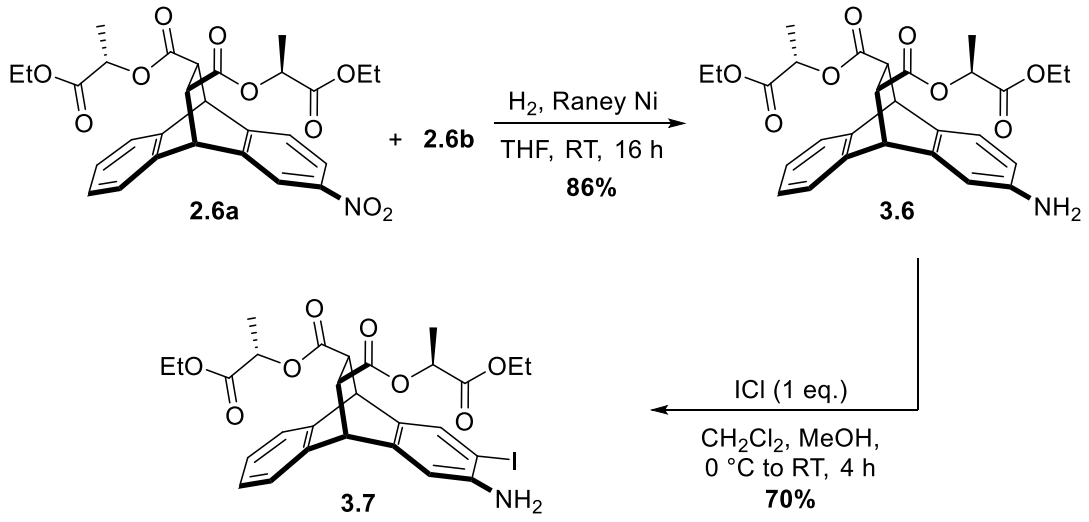

Scheme 3.5. Reduction and subsequent iodination of diester-mononitro **2.6a**.

With the CAS monomer **3.7** in hand, the next step was to probe it for its double-amination capabilities. **3.7** was exposed to CAS coupling conditions similar to those previously reported as successful, and we were afforded diester C-shaped strip **3.8**, albeit in low yields (**Scheme 3.7**). It seemed likely that the second carbonyl moiety on the ester auxiliary arm may have been obstructing Pd-insertion into the C–I bond to fully allow for the double-amination reaction to take place, hence the low yields of the reaction. It is well-documented that ester-containing substrates require harsh conditions to allow for Buchwald–Hartwig aminations to proceed.[151] Evidence for this could be found in the minor byproduct observed in purifying the reaction mixture by Preparative TLC was were of the dehalogenated starting material **3.6**. Nevertheless, to further expand upon the diester building blocks advantages over the generally unreactive tetraester's ethylene bridgehead, C-shaped strip **3.8** was treated with KOH to hydrolyze off the esters and form carboxylic acid derivative **3.9** (**Scheme 3.6**). By being able to functionalize these

diester compounds *after* forming CAS molecular shapes, the potential for adding on additional groups post-modification becomes very accessible. The diester cycloadduct and its coupled derivatives also possess large chiral cavities and hold shapes that match the contours of pillararene macrocycles. Previous studies with tetraester C-shaped strips showed that the strips bind to the outside of pillar[5]arene macrocycles in a 5-to-1 mixture of acetonitrile to water.[4] With these water soluble carboxylic acid strips acting as selective hosts for the pillararene macrocycles, we suspect binding studies can be done in only water and the interactions will therefore be stronger than in a mixture of acetonitrile and water. Nevertheless, despite low yields the success of the diester building block in forming dimer strip **3.8**, gave us confidence in the diester's capabilities in forming side-on helical strips through chirality-assisted coupling.

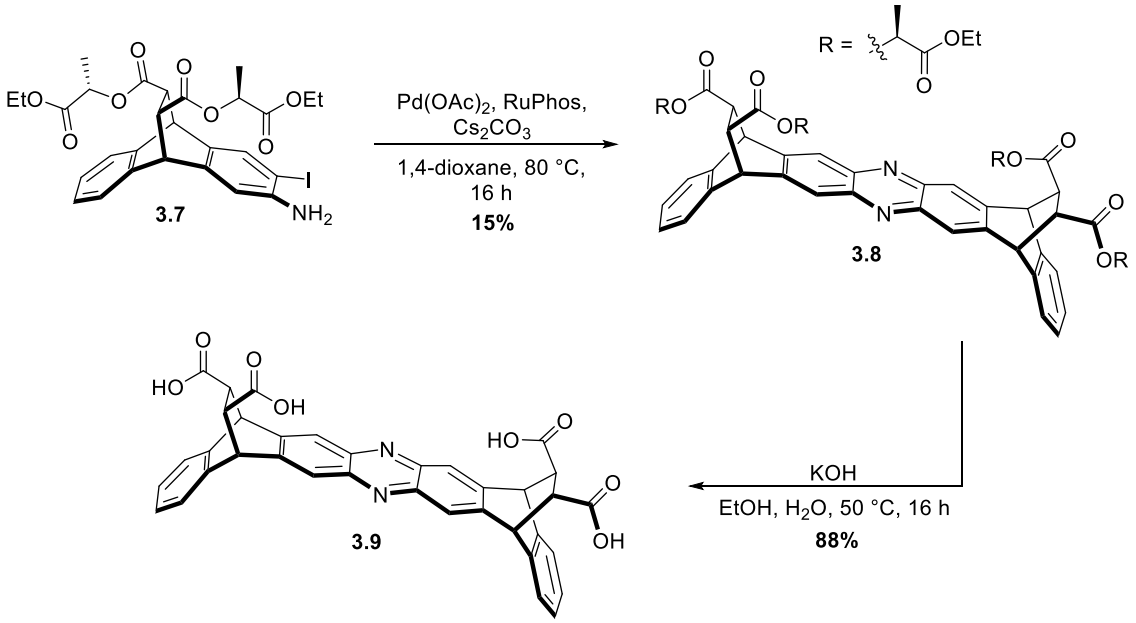

Scheme 3.6. CAS to form C-shaped dimer **3.8** and subsequent hydrolysis to form carboxylic acid derivative **3.9**.

With initial success, despite the low yield, we went ahead with our investigations into side-on couplings with the diester building block (**Scheme 3.7**). Starting from monoamine **3.6**, exposure to iodination conditions lead to the diiodo product **3.10**. As a note of interest, careful analysis by mass spec showed no chloro byproduct in the aromatic halogenation reaction—low yields seem likely to degradation, or partial iodination of the other arene subunit. Following this, attempts were done to promote selective deiodination to form side-on CAS monomer **3.11**. However, even after 16 hours with the typical conditions, only starting material, with some complete dehalogenation to reform **3.6**, remained. Similar to tetraester **3.3**, in **3.10** the carbonyl moiety above the side-on-iodo group prevented Pd-insertion into the C–I bond, but the same effect appeared to be occurring due to the *second* carbonyl on the same auxiliary arm obstructing Pd-insertion in the face-on-iodo group—not dissimilar to why forming C-shaped strip **3.8** occurred in such low yields. Even after extended periods of time, only starting material **3.10** or some slight total deiodinated **3.6** formed—by ^{1}H NMR analysis, not even the face-on monomer **3.7** was formed through dehalogenation.

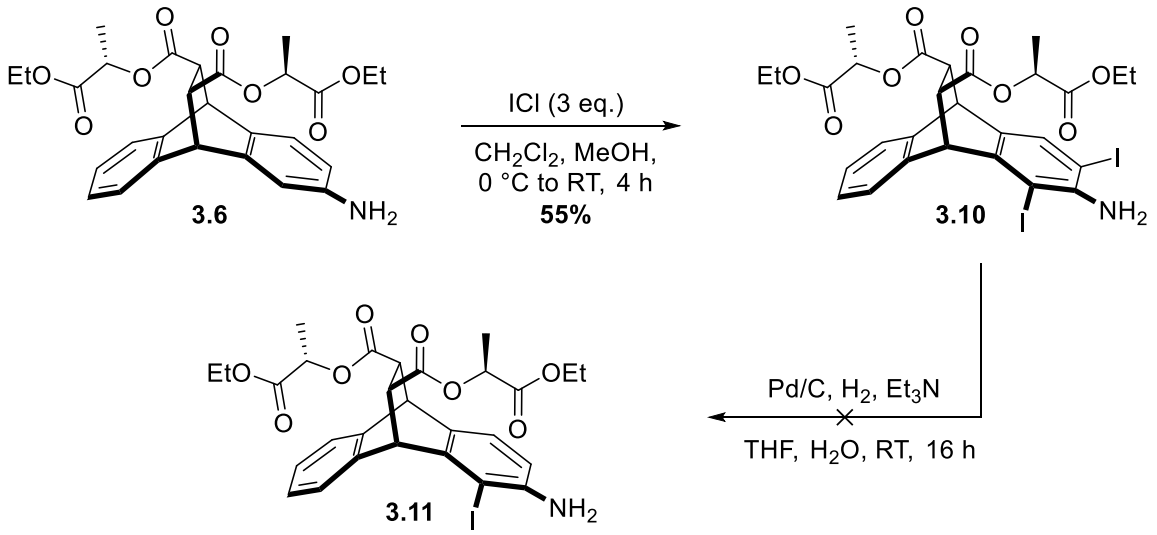

Scheme 3.7. Selective dehalogenation attempts on diiodo-monoamine derivative **3.10**.

Following the unsuccessful attempt at forming a less sterically-bulky side-on CAS monomer from the diester building block, we focused our efforts instead onto the diether derivative. As previously mentioned during discussions on nitrating diether cycloadduct **2.11** (**Chapter 2.3**), the diester compound can be easily functionalized to other derivatives to enhance its capabilities such as solubility, a decrease in steric bulk, or less electronic interactions into its arene subunits—all of these qualities are found in the diether derivative which was investigated for its chirality-assisted coupling capabilities, and to see if it could form the side-on CAS monomer through selective deiodination.

3.2.3. Diether Cycloadduct

To begin investigations with the diether, it also had to be probed for its ability to undergo face-on CAS coupling (**Scheme 3.8**). Similar to reduction of **2.3**, mononitro-substituted **2.6a** was subjected to reduction conditions to form diol derivative **3.12**—

again, much like with the diester, separation of the minor isomer byproduct is easiest after reduction to the amine derivative. Following this, a Williamson ether synthesis was performed on the crude material (identical to conditions done on **2.11**) on **3.12** to form mononitro-substituted diether **2.12** which was carried forward without further purification. Mononitro-substituted **2.12** was subjected to reduction conditions with Raney nickel to form monoamine derivative **3.13**, whereby separation of **3.13a** from isomer **3.13b** became possible.

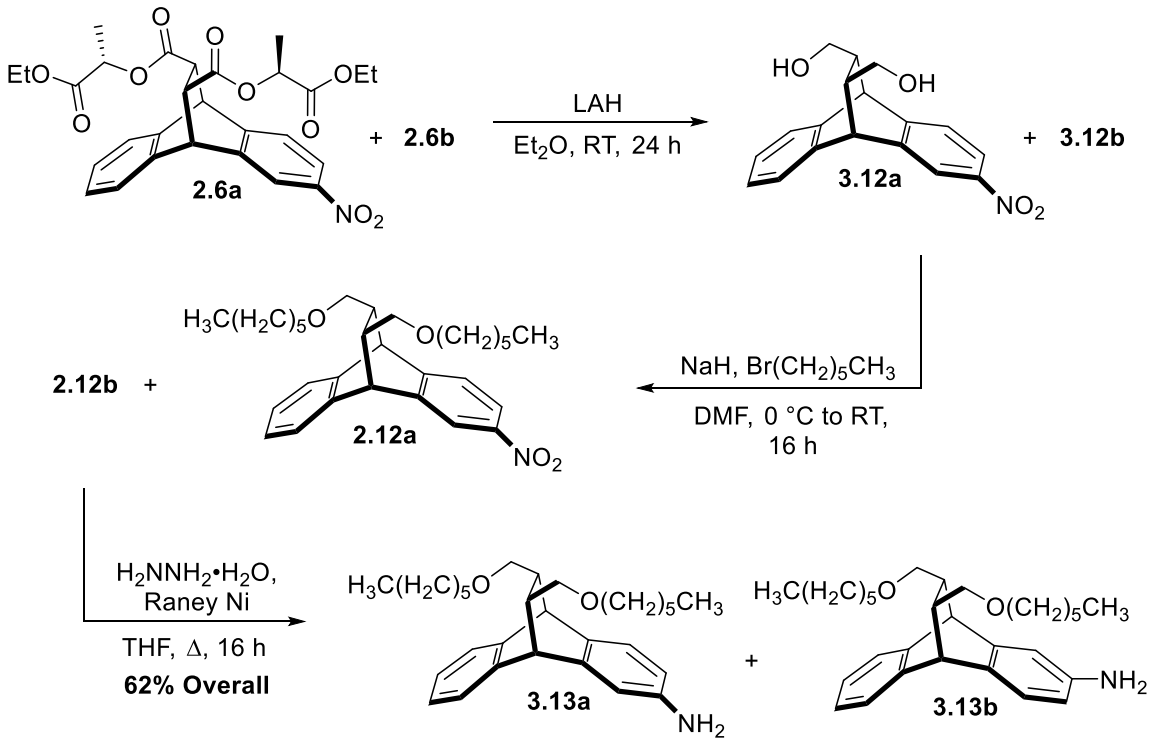

Scheme 3.8. Reaction pathway to form monoamine derivative **3.13** from mononitro-substituted diester **2.6**.

With building block **3.13a** prepared, it was treated with iodination conditions to form CAS monomer **3.14** in good yields (**Scheme 3.9**). With the appropriate piece to test

the diether cycloadduct for its chirality-assisted coupling capabilities, it was exposed to the typical double-amination conditions. Following treatment, C-shaped dimer strip **3.15** was produced, and in higher yields than with the diester CAS coupling reaction (**Scheme 3.7**). Not unlike the tetraester cycloadduct compared to the diester, the diether piece has less steric obstruction on its bridgehead and thus fewer opportunities to prevent Pd-insertion into the C–I bond during double-amination couplings. With another building block able to undergo CAS, the diether was then investigated for its ability to undergo side-on couplings.

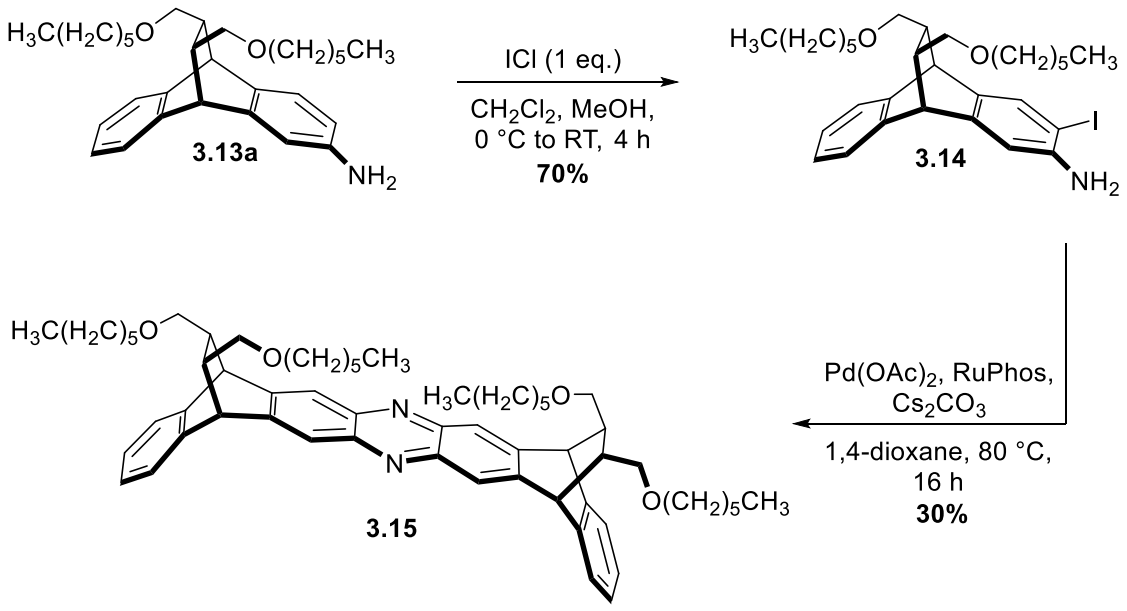

Scheme 3.9. Chirality-assisted coupling to form diether C-shaped dimer **3.15.**

Following the same strategy as with the other building block pieces, **3.13** was diiodinated with ICl to form diiodo-substituted **3.16**, then subsequent deselective halogenation conditions were utilized to yield the monoiodo derivative **3.17** (**Scheme 3.10**). With the ether chain directly above the relevant iodo group, the oxygen is proposed

to prevent Pd-insertion where, unlike in the case of the diester, there is no other oxygen-containing functional group further out in the hexyl chain to obstruct the dehalogenation of the less-hindered iodo group *para* to the bridgehead carbons. As a relevant note to further reactions, a small amount of minor isomer **3.13b** was moved forward in the synthesis to form the major side-on CAS monomer.

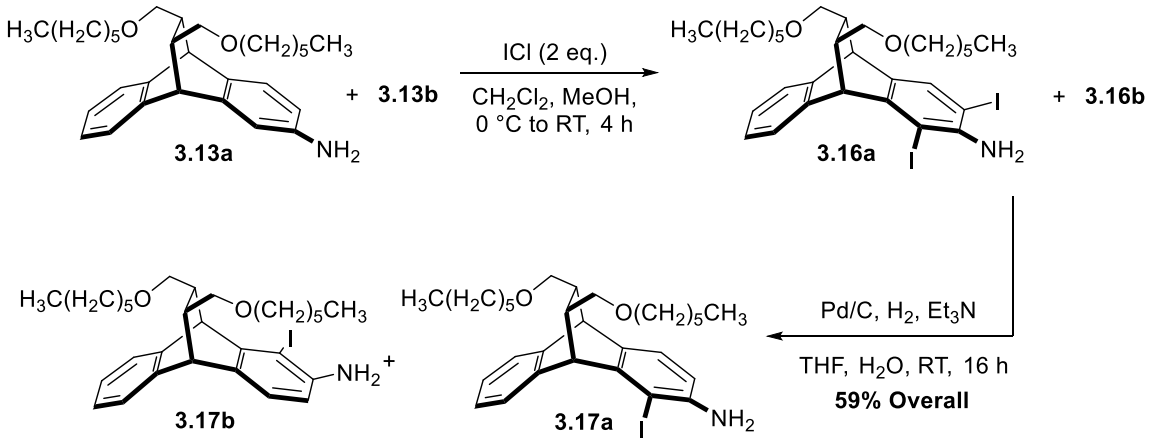

Scheme 3.10. Synthesis of side-on CAS monomer **3.17a** with 5-to-1 minor isomer **3.13b** carried forward through the reaction pathway.

Next, we embarked on the (intended) homocoupling of **3.17a** (**Scheme 3.11.a**) under standard double-amination conditions in the presence of palladium(II) acetate, RuPhos and Cs_2CO_3. The reaction did not progress as intended, and a significant portion of **3.17a** and dehalogenated precursor **3.13a** was recovered—once again, for the same reasons that the iodo group remained intact after exposure to dehalogenation conditions, the hexyl ether chain above the halogen appeared to prohibit the double-amination from occurring to form helical strip **3.18a**. However, the aforementioned minor isomer **3.17b** remained in the reaction mixture during the initial trial to homocouple **3.17a**, and instead

the side-on heterocoupling of **3.17b** with **3.17a** appeared to have occurred as the major product instead (**Scheme 3.11.b**). This particular side-on double-amination was successful, and the coupled phenazine derivative helical strip **3.18b** was isolated as a pure stereoisomer in approximately 78% yield (calculated based on **3.17b**). Interestingly, **3.17b** coupled selectively with **3.17a** leaving no starting compound behind, leading to a "zig-zag," β-sheet-like geometry of **3.18b**. Interestingly, there did not appear to be any homocoupled product of **3.17b**, which may have been due to the excess of available heterocoupling partner **3.17a** in comparison to **3.17b**.

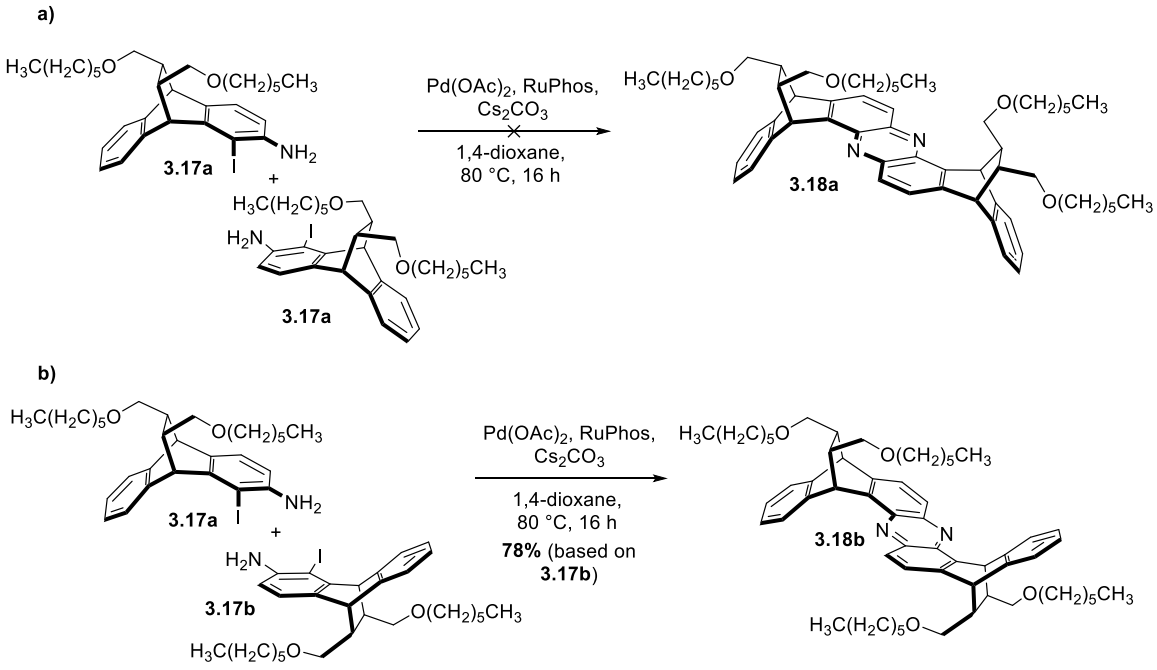

Scheme 3.11. In CAS side-on couplings, reaction prefers to proceed with minor isomer **3.17b** (**b**) rather than the major isomer (**a**) due to less obstruction from absence of ether group hanging over the amination site.

Thus, steric control of Pd-catalyzed phenazine formation was afforded. While the phenazine derivative resulting from the homocoupling of the major diastereoisomer of **3.17a** was not observed, the minor diastereoisomer **3.17b** (with the $-NH_2$ substituent attached to *C3* and –I attached to *C4*) coupled with the major diastereoisomer in approximately 78% yield (calculated, based on the minor diastereoisomer). These differences in reactivity likely arise from increased steric strain being present between the two central hexyl ether groups, if they are facing each other in the homocoupled product of the major diastereoisomer of **3.17a**.

Nonetheless, challenging side-on double-amination couplings have now become possible with building blocks synthesized by way of through-space directed nitrations. Although the intended helical strip **3.18a** could not be synthesized, side-on couplings appeared to be possible via less steric hindrance over the double-amination reactive site. This finding opens the door towards the creation of advanced shape-persistent molecules (for example, freeform molecular helices) with CAS.

3.3. Changing Position of the Aniline Moiety

The question now was how to best approach the next round of trials for side-on CAS couplings? With the ether auxiliaries hanging over the halogen as in the case of **3.17a**, the couplings appeared to be quite challenging, if not impossible. However, the case of **3.17b** coupling with **3.17a** led us to believe that homocoupling with **3.17b** should be even *more* readily accessible as long as the minor isomer was in fact the major species in the reaction solution. By utilizing **3.13b** through the halogenation/selective dehalogenation process, it seemed possible to obtain a side-on coupling candidate

(**Scheme 3.12**). Rather than focusing on isolating the minor isomer from the S_EAr selective nitrations of the diester, which would be very low yielding, we decided to develop a strategy to change the position of the aniline group on the arene subunit of the major isomer instead to generate the desired side-on CAS monomer.

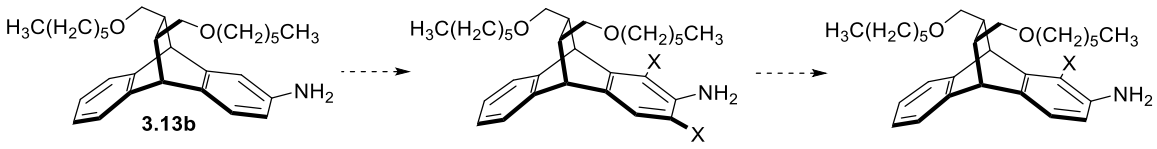

Scheme 3.12. Proposed selective dehalogenation strategy to form monomers for more-favorable side-on CAS couplings.

3.3.1. Chiral Diester Cycloadduct

Starting from crude mixture of dinitro-substituted diester **2.7a**, the compound was reduced to the stereomerically pure 2,6-diamine derivative **3.19** in modest yields before being exposed to Sandmeyer reaction conditions to convert the aniline functional groups to aryl iodides to receive **3.20** in quantitative yields (**Scheme 3.13**). Following this, EAS nitration was done again in the synthetic pathway, although in this case more ammonium nitrate and higher equivalents of TFAA had to be utilized to push the reaction forward—most likely due to the electron withdrawing nature of iodine. However, we were afforded a separable mixture of dinitro- and mononitro-substituted derivatives **3.21a** and **3.21b** respectively, again in quantitative yields. Heating the reaction mixture or utilizing TFAA as a solvent resulted in some degradation of product.

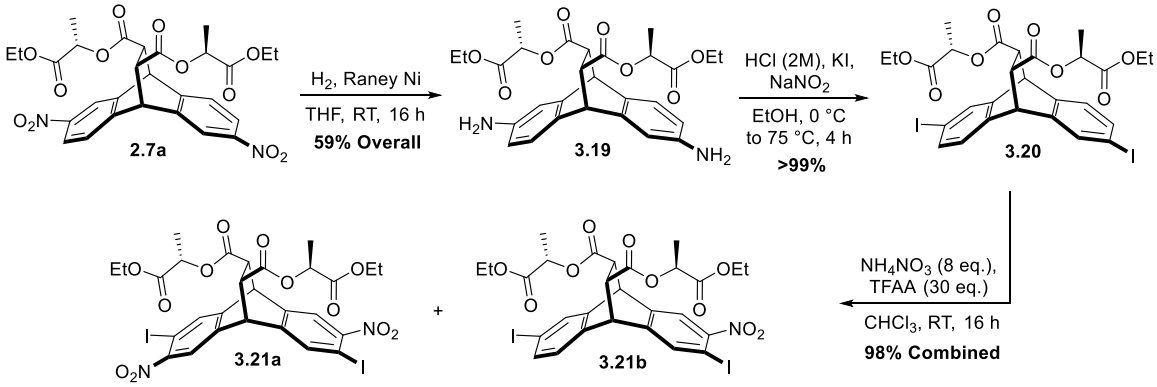

Scheme 3.13. Sandmeyer reaction and subsequent di- and mononitration of diamine-diester **3.19**.

Taking mononitro-diiodo species **3.21a**, it was exposed to a similar series of reaction conditions in the formation of **3.13** (**Scheme 3.8**). **3.21a** was reduced to mononitro-diol **3.12b** after treatment with LAH (**Scheme 3.14**). During the reductive process to the diol derivative, some minor byproduct present was due to full dehalogenation not occurring to form **3.12b**; this byproduct was carried through as Raney Ni reduction of the nitro group in a later step fully removes any present iodine on the aryl rings. Following this, hexyl groups were added onto the diol species to form mononitro-diether **2.12b**. Treatment with hydrazine monohydrate and Raney Ni afforded us the reduced monoamine derivative **3.13b**. With the *3*-substituted aniline in hand, we moved forward to attempt selective dehalogenation to generate the favored side-on CAS monomer.

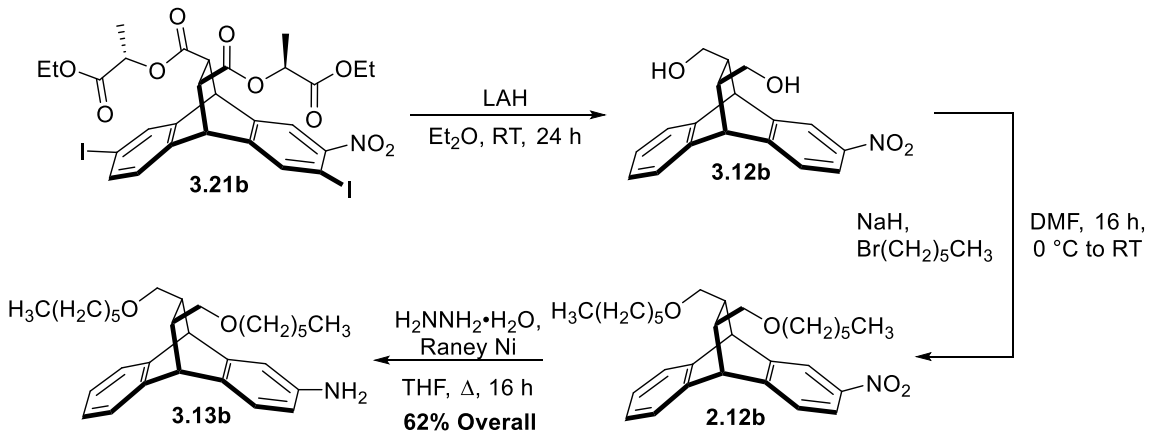

Scheme 3.14. Synthesis of side-on CAS coupling precursor **3.13b**.

3.3.2. Diether Cycloadduct

Similar to the other dehalogenation attempts, **3.13b** was treated with 2 equivalents of ICl to form the diiodo-monoamine derivative **3.16b** (**Scheme 3.15**). Then, the overhalogenated species was exposed to palladium on carbon, H_2, and basic conditions to deiodinate it. However, complete dehalogenation occurred to recover **3.13b**. Attempts to run the dehalogenation process in a shorter reaction time to instead afford statistical deiodination (rather than selective) only afforded starting material as well as the initial monoamine compound—presence of desired compound **3.17b** was not observed. Once again, very unluckily, it appeared that because the ether was not overhanging above either iodine, it was unable to obstruct C–I insertion of palladium. While product **3.17a** was able to be generated *due* to the ether directly above the iodo group, it could not couple in a side-on fashion for the very same reason as it obstructed palladium-catalyzed coupling from occurring. Additionally, while **3.17b** seemed like a better side-on coupling

candidate because the ethers would not block palladium-insertion, deselective iodination could not occur due to this very fact.

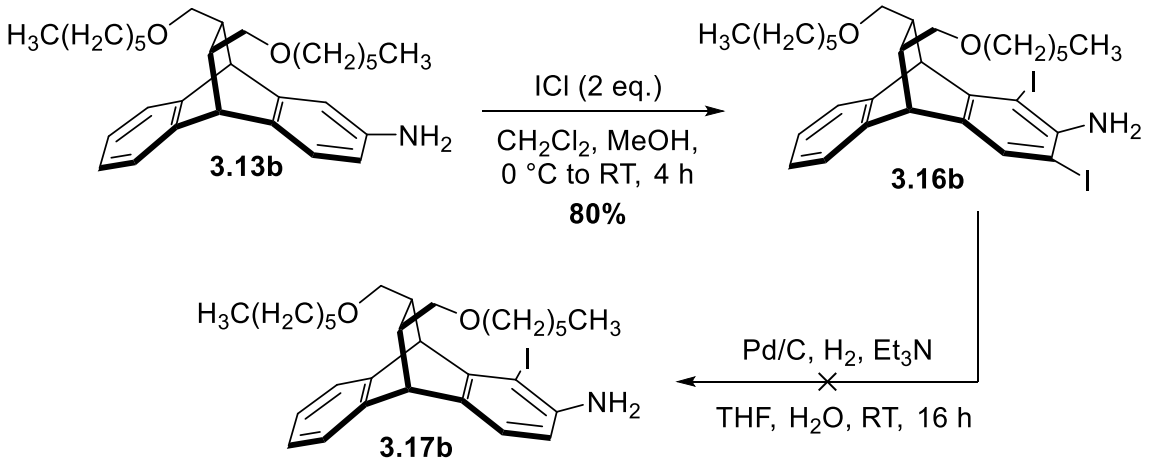

Scheme 3.15. Proposed selective deiodination to form favorable side-on coupling monomer **3.17b**, for favorable side-on couplings.

With **3.17b** seemingly very difficult to synthesize, we moved on to attempting to generate the same *o*-iodo-amine derivative with the chiral diester bridgeheads (**Scheme 3.16**). Starting once again with **3.21b**, the nitro group was reduced down to the amine to form **3.22** with complete dehalogenation occurring. Following this, over-iodinating the aniline was easily done to receive **3.23**. Once more, deselective iodination was attempting following the same reaction conditions in an attempt to form side-on coupling monomer **3.24**, but only starting material or complete dehalogenation initial reagent was obtained. Attempting to let the reaction run shorter to receive statistical dehalogenation did not afford any deiodination whatsoever. While in the case of **3.10** (**Scheme 3.7**), it was unable to undergo dehalogenation due to, we hypothesized, both carbonyl moieties obstructing palladium-insertion, the iodo group in the face-on position in **3.23** is in the *3*

position as opposed to the *2* position in **3.10**, which likely effects the capability of the ester to block the respective C–I bond.

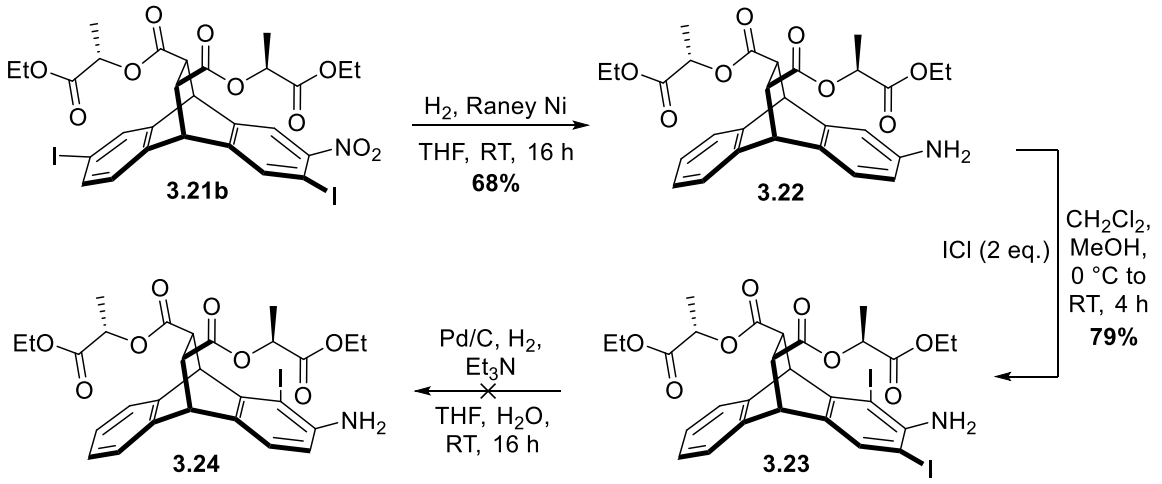

Scheme 3.16. Proposed selective dehalogenation to form diester-monomer **3.24** for favorable side-on couplings.

3.3.3. Diamine-Diether Cycloadduct

In yet another attempt to obtain the CAS monomer for favorable side-on couplings, a slightly different dehalogenation method was attempted (**Scheme 3.17**). Starting with **3.21a** (due to availability of material, and its potential of extra halogenation sites), a familiar synthetic pathway was followed starting with reduction of the ester moieties to achieve diol **3.25**, followed by ether synthesis to form diether-dinitro derivative **3.26**. The dinitro species was then reduced down to the diamine compound **3.27**, and subsequently exposed to two equivalents of ICl to afford selective iodination to each of the aryl subunits in forming **3.28**—over-iodination did not occur in this case due

to the electron withdrawing nature of the iodo group on the aniline rings. Then, rather than attaching additional iodo groups, bromo groups were added on instead in the side-on position through exposure to NBS to achieve **3.29**. Now, treatment with dehalogenation conditions were done once again in the hopes of selectively removing the iodo group while the stronger C–Br bond remained intact, even if as a statistical mixture. However, similar to the other trials, complete dehalogenation seemed to occur without any of the desired **3.30** product. Shorter reaction times also only produced starting material or total dehalogenation, despite the existence of two halogenated aniline rings per molecules.

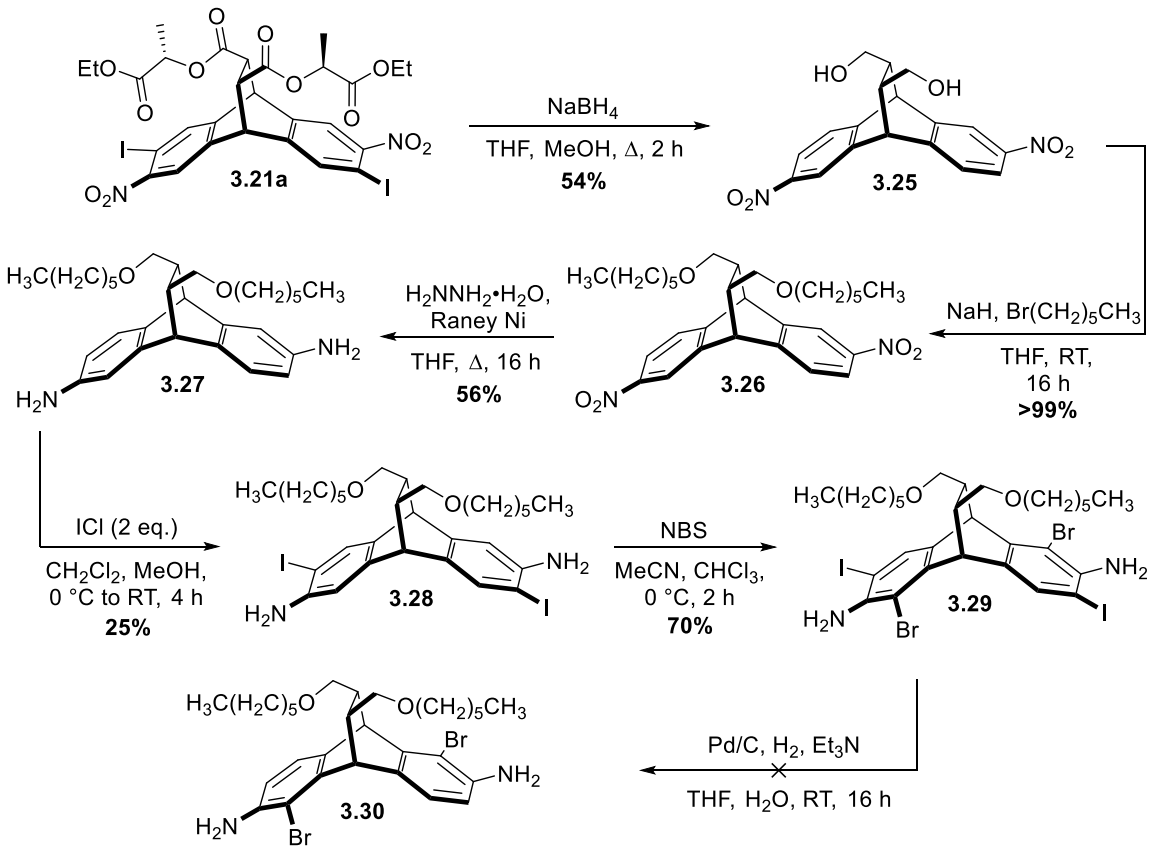

Scheme 3.17. Route to achieve side-on coupling monomer through dehalogenation.

Despite many attempts in forming a side-on coupling monomer through dehalogenation, it proved difficult to obtain one that was favorable for actually undergoing the palladium-catalyzed cross-coupling. In the cases of **3.17a** and **3.4**, homocoupling did not yield any helical strips. **3.17b** and **3.17a** were able to heterocouple to achieve a small amount of a β-sheet-like helical dimer **3.18b** (**Scheme 3.11.b**), however attempts to selectively synthesize **3.17b** or any of the other aforementioned monomers without the auxiliary arm hanging over the halogen and amine reactive sites were unable to be produced. Other CAS coupling strategies (**Chapter 3.4**) were surveyed during the investigations into selective dehalogenations of the previously mentioned building blocks. As will be explored in **Chapter 4**, we were able to find a CAS pathway that would allow us to synthesize helical strips and polymers.

3.4. Additional CAS Coupling Strategies

Many of the previously explored selective dehalogenation trials (particularly after the challenges encountered with the homocoupling of the original **3.17a**) were accomplished in tandem with other experiments to achieve our desired helical strips through CAS. While double-aminations to achieve side-on couplings were certainly a tempting pathway to pursue, especially after the success of Dr. Liu in building the C-shaped strips through face-on CAS,[4] limiting ourselves to only one style of forming ladder polymer-type molecules appeared to have restricted the success of my project. So, while also attempting the aforementioned dehalogenation attempts, a few other chirality-assisted coupling strategies were pursued in tandem.

Homocoupling of these building blocks in a face-on manner initially appeared to only form the aforementioned C-shaped strips, but through a clever strategy in how to connect the building blocks (see **Chapter 4.3**) were could eventually generate a kink in the bond connectivity between monomers which afford us a variety of tunable helical shapes.

3.4.1. Ladderization with Oxidative Ring Closures

As an alternate to forming 6-membered aromatic linkages (i.e. phenazine junctions) between monomers, we also elected to attempt to form *N*-H carbazole linkages instead, with the 5-membered nitrogen ring inducing the aforementioned kink in the chain of our potential polymers. However, rather than a one-pot reaction (as discussed in **Chapter 4.3**) to create ladder polymer-type connectivity, a two-step reaction strategy was employed initially, with the first step involving the creation of single-bond linkages between the monomer units, and the next step finally zipping up the polymer to form the carbazole backbone. A synthetic strategy was utilized whereby diphenylamine-like compounds can be oxidatively coupled in a Pd-catalyzed intramolecular biaryl formation under air (**Scheme 3.18**).[152] The end product is a carbazole, or biaryl molecule containing a carbazole motif. Following this unique oxidative coupling, we attempted to form our helical structures using CAS.

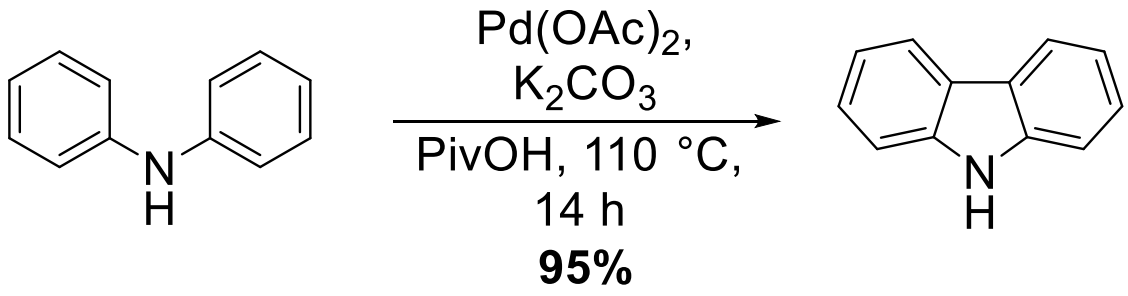

Scheme 3.18. Palladium-catalyzed oxidative ring closure.

To start, we performed a simple acyl protection of the diamine diester **3.19** with acetic anhydride to form methylamide-monoamine **3.31** (**Scheme 3.19.a**). The acyl-protected amine installed on the second arene ring was of particular importance, as we were concerned that with the oxidative ring closure we might see intermolecular C–C bond formation with the free aryl rings, rather than selective intramolecular carbazole formation. Next, after the previously discussed Sandmeyer reaction on **3.19** (**Scheme 3.13**) to generate diiodo **3.20**, the first step of the CAS coupling process was attempted. Taking two equivalents of **3.31** and one equivalent of **3.20**, they were treated with Buchwald–Hartwig conditions to form aminated trimer **3.32** (**Scheme 3.19.b**). The difference with our original CAS amination strategy is that the newly formed linkages still allows free rotation to occur between the building blocks. This in turn prevents the well-defined shape and structure-persistence CAS is known for and thus requires another oxidative ring closure step to complete ladderization and create a more rigid backbone.

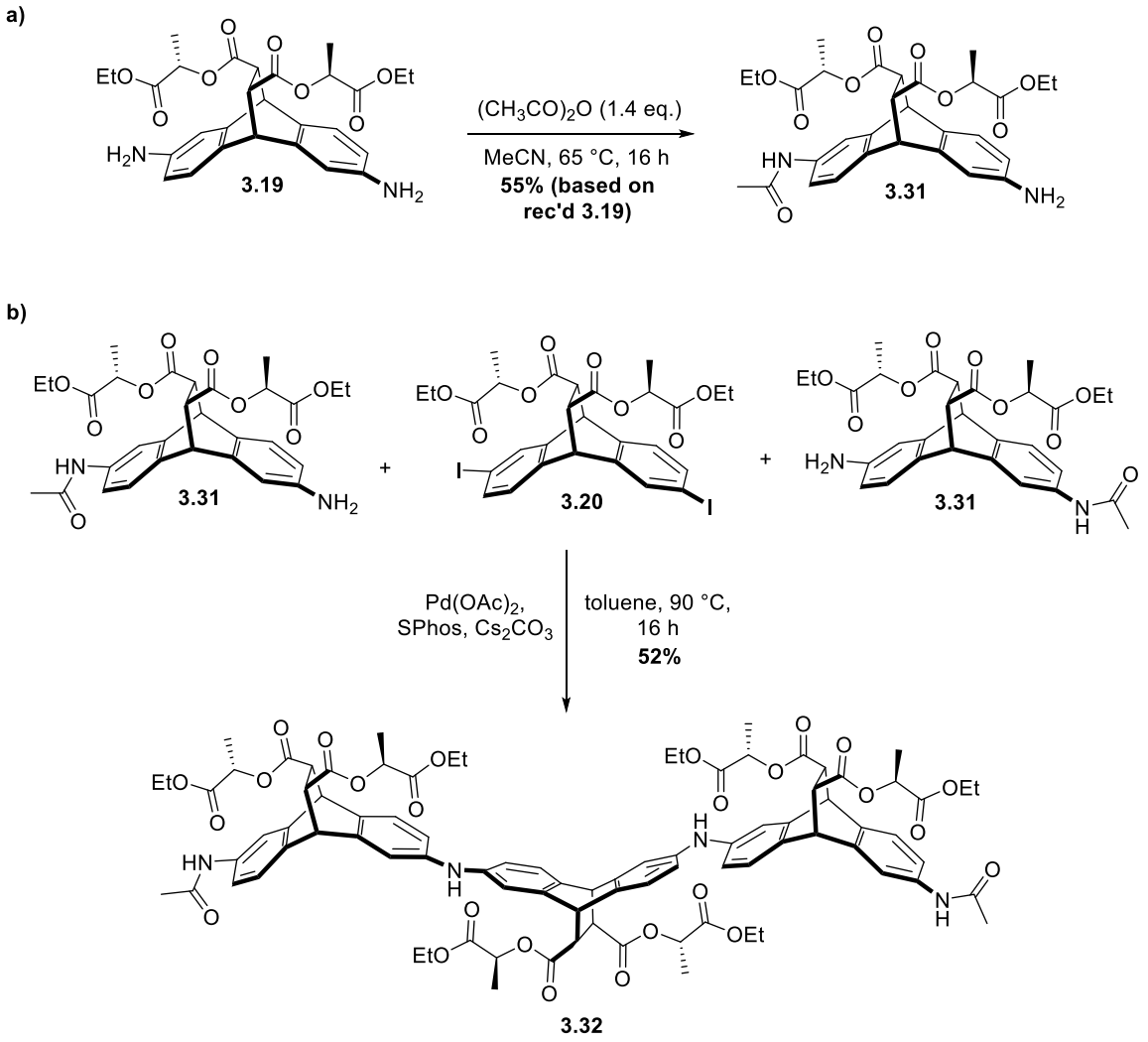

Scheme 3.19. (**a**) Monoacyl protection of diamine for the (**b**) cross-coupling reaction to generate linear trimer **3.32**.

The strategy in mind next was to close the rings to form carbazoles and thus garner a well-defined helical shape. Upon oxidative closure, the middle unit of the trimer would have to rotate downward (as shown in **3.32** above) to form face-on ring closures. Oxidative closure in a side-on orientation, or with the middle monomer flipped upward, would be very sterically hindering and appears much more unfavorable to form. The 5-

membered linkages between monomer units ensure a kink in the ladder polymer backbone and thus **3.33** possess a helical shape as illustrated in Scheme **3.20** (with a top-down view to best visualize the helical shape). With additional units, and thus a more three-dimensional structure, its helical nature will become even more evident.

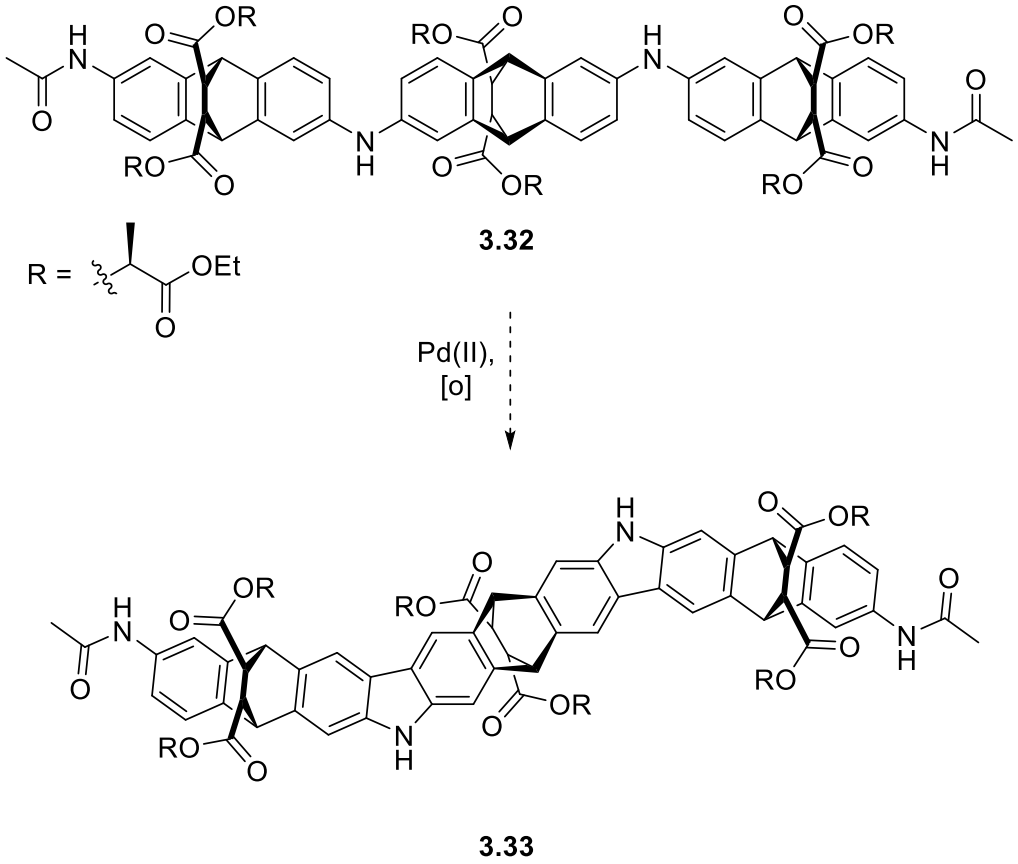

3.32

3.33

Scheme 3.20. Top-down illustration of proposed helical trimer **3.33**.

When linear trimer **3.32** was exposed to the standard oxidative closure conditions,[152] helical trimer **3.33** was not afforded (**Scheme 3.21**). A mix of starting material or degraded products was obtained upon harsher conditions such as higher heating with a pressure vessel. Therefore, the standard Pd-catalyzed ring closures best

operate with simple diphenylamines, with yields decreasing rapidly with added functional groups of both donating and withdrawing natures. With the complexity of the overhanging ester units, perhaps they once again obstructed Pd-insertion to facilitate C–C bond formation.

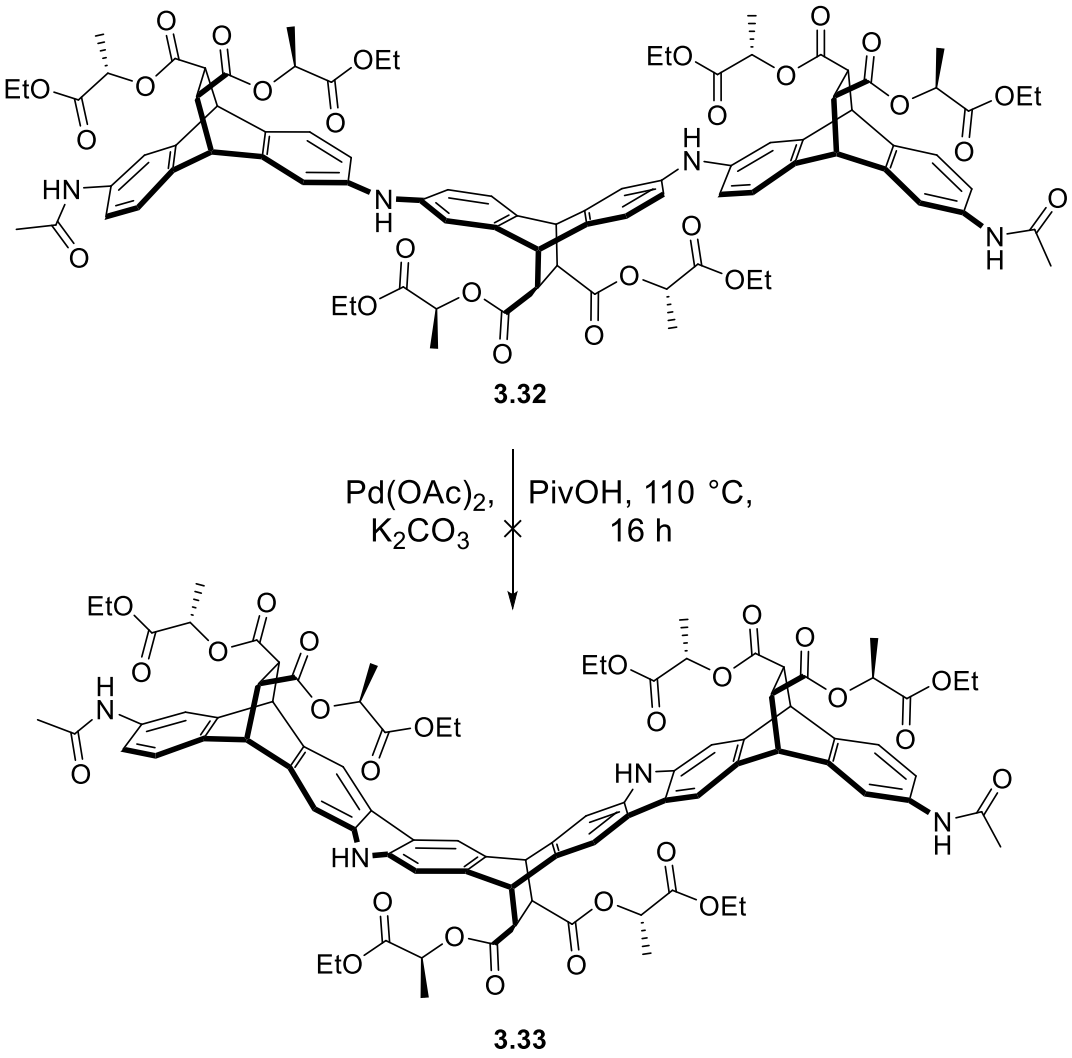

Scheme 3.21. Proposed CAS oxidative ring closure to form the helical strip **3.33**.

While utilizing Buchwald–Hartwig cross-coupling to form singular bonds between the diester building blocks was possible, closing up the units to form the

carbazole backbone did not yield the desired helical products. Certainly, other conditions could be attempted to zip up the ladder polymer backbone, but in the pursuit of a successful coupling strategy based on CAS, we decided to shelf the possibility of oxidative ring closures (as well as this tactic to be used for helical polymers in general) for the time being and moved on to investigate other coupling reaction.

3.4.2. Hydrogen-Bond Directed Helical Strips

In addition to utilizing only homocouplings to build our helical strips, we also began to pursue the possibility of adding a spacer piece via a heterocoupling strategy. With a careful design of a spacer unit between building block monomers, and a more mild set of Sonogashira cross-cross couplings conditions,[153, 154] we envisioned that we should also be able to create molecular helices. Utilizing a similar hydrogen-bonding induced coplanar conformation similar to the work done by Zhao and co-workers in synthesizing oligo(p-phenyleneethynylene)s,[155] (**Scheme 3.22**) we proposed to access the same H-bonding motif between the spacer unit and our CAS monomers to allow them to adopt helical structures.

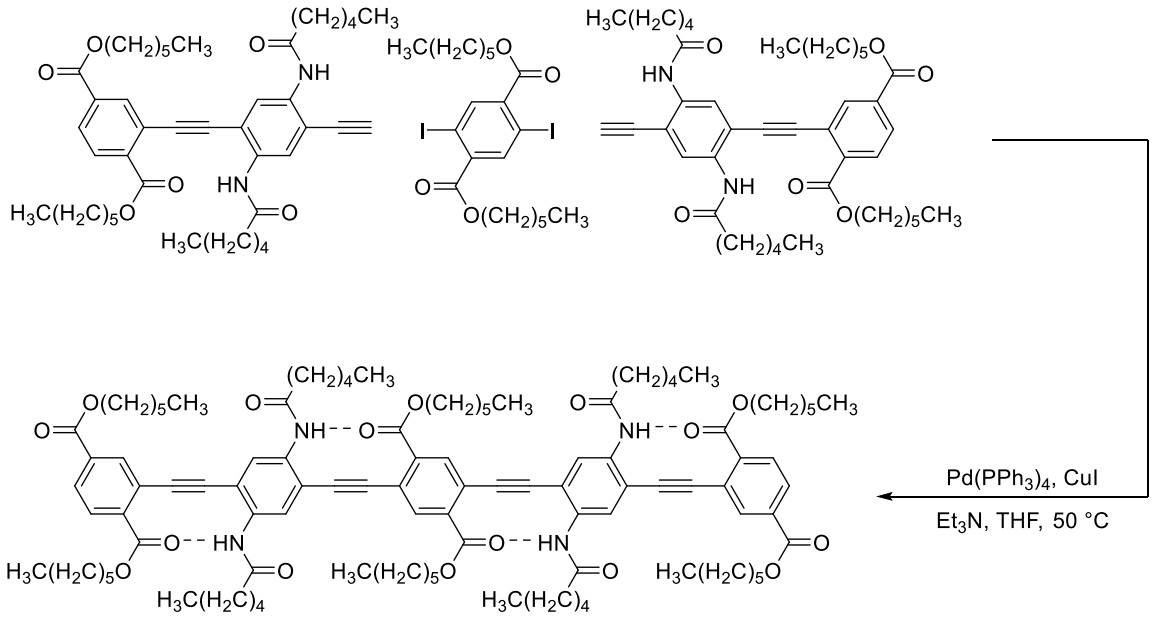

Scheme 3.22. Coplanar Conformation of a Phenyleneethynylene Trimer.

Nuclear Overhauser effect (NOE) correlations between amide protons and adjacent ethyl ester protons was determined to be the most helpful in determining the helical structure of our proposed polymers.[156] These end-to-end intramolecular NOE contacts are regarded as evidence for the formation of helical structures.[157] As long as there is observed H-bonding present between the alternately appended amide and ester side-chains, computational modeling shows that the polymers will adopt helical shapes. Much like in oligomeric phenyleneethynylenes, the helical nature could both be enhanced by the 10-membered intramolecular hydrogen bonding-induced ring, and display a rotational barrier high enough to maintain its spiral shape at room temperature.[155] Utilizing the chain-length dependence test, we can also further establish properties of these helices such as their helical conformation, binding, and enhanced reactivity, all properties that might change depending on the length of the polymer.[158]

To achieve a proper hydrogen bonding-induced coplanar conformation, we elected to install an amide functionality onto our building blocks. Utilizing monoiodo-monoamine **3.7**, we exposed the electron-withdrawn aniline to acetic anhydride at elevated temperatures to afford **3.34** in excellent yields (**Scheme 3.23.a**). With the cycloadduct **3.34** in hand, we then moved on to synthesize the spacer **3.37**, which was needed to place terminal *p*-alkynes to best facilitate the proposed helical structure (**Scheme 3.23.b**). Starting from commercially available 2,5-dibromoterephthalic acid, it was exposed to a catalytic amount of H_2SO_4 in ethanol to afford diester **3.35**. From there, **3.35** was treated with Sonogashira coupling conditions to afford TMS-protected **3.36**, followed by cleavage and transesterification utilizing methanol to achieve dialkyne-dimethylester spacer unit **3.37**.

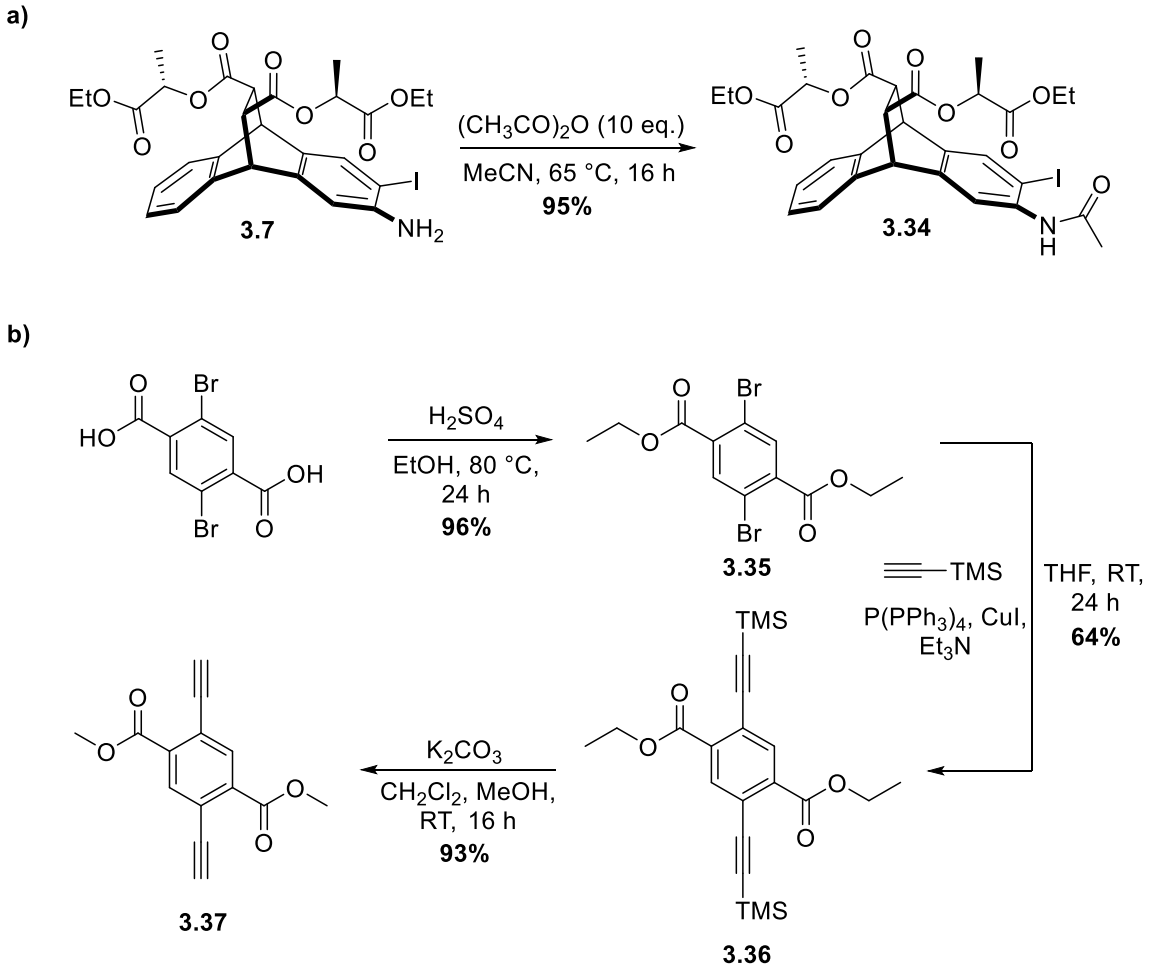

Scheme 3.24. (**a**) Synthesis of the monoamide-monoiodo monomer **3.34** for (**b**) the coupling with the dialkyne spacer unit **3.37**.

With the proper building blocks synthesized, Sonogashira cross-coupling was attempted on two equivalents of **3.34** and one equivalent of spacer piece **3.37** (**Scheme 3.24**). A successful coupling reaction occurred and we were afforded the dimer strip **3.38** in good yields. As illustrated in **Scheme 3.25**, we proposed that hydrogen bonding would be utilized in stabilizing the dimeric units to form a coplanar conformation that adopted a helical motif. One could imagine that, taking **3.34** to make the corresponding

macromonomer (with an iodo group an acyl-protected amide on the other arene subunit), a polymer born of these same units would allow for a long chain that, due to the three-dimensional roof-shape of the diester cycloadducts, would conform to an overall helical structure. This was the initial plan in synthesizing these Sonogashira cross-coupled polymers, and first successes in generating smaller dimeric units gave the project some credence.

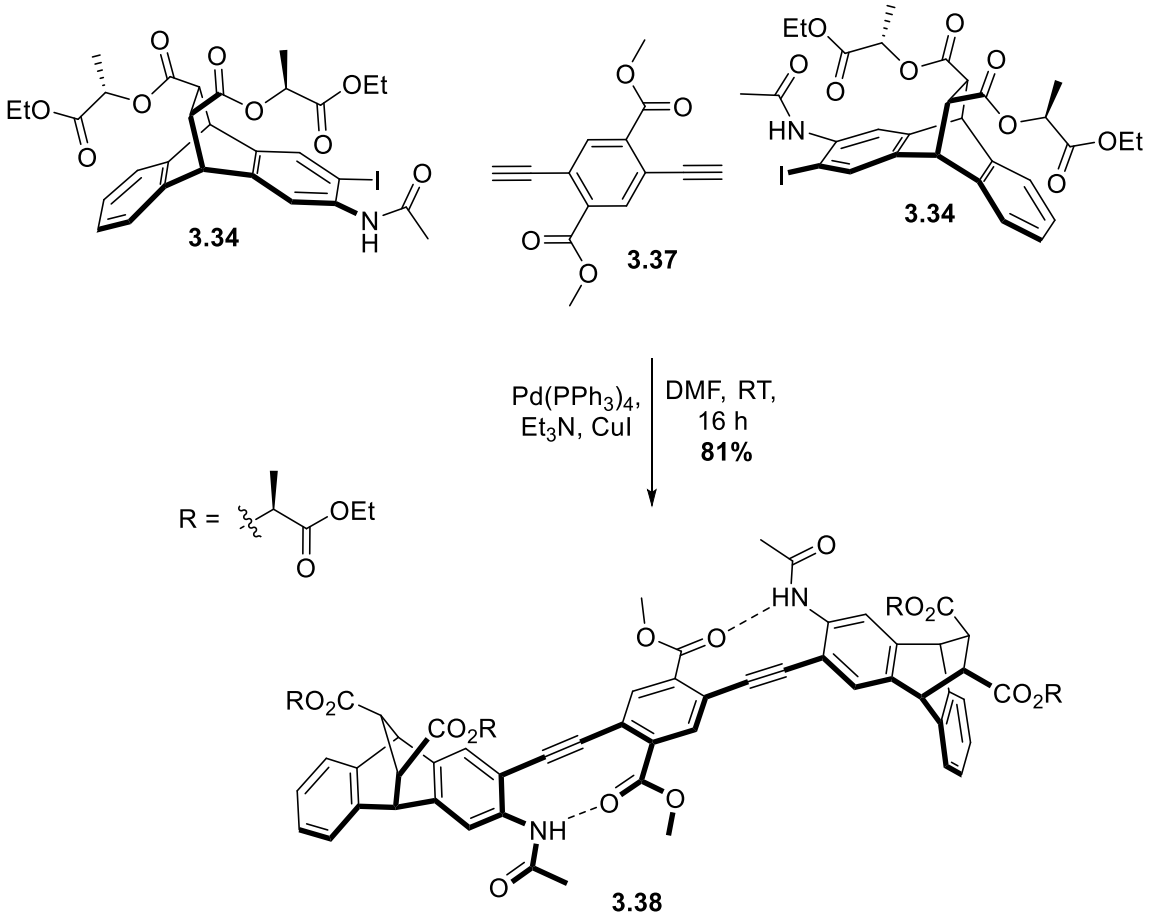

Scheme 3.24. Successful synthesis of Sonogashira-coupled dimer **3.38** with proposed H-bond-driven helicity.

Despite initial success in synthesizing the dimer, however, the strength of its hydrogen bonding to stabilize a helical motif was questioned. A structural downside to these foldamers is that they must be precisely designed to fold in a particular way with well-defined building blocks—their geometric shape is not inherent but consequential of the polymer's capacity for intramolecular H-bonding and/or its environment, often making a foldamer's helical structure quite limited. Thus, we initially proposed utilizing β-hairpins[30, 159] in lieu of simple methyl-ester or amide functional groups to strengthen the H-bonding capacity between monomer units. One could argue with a singular covalent bond between monomers, and a "second" bond orchestrated with several strong hydrogen-bonding groups, this could restrict the helical structure and essentially generate a ladder polymer whilst still following CAS principles. However, one of the main objectives of my research (and CAS in general) was to build sturdy ladder polymer materials with two covalent bonds connecting the monomer units, so as exposure to certain environmental conditions would not unfold our molecular helices. By utilizing H-bonding as a way to structurally stabilize the produced helices, this moves away from our initial aims, particularly as hydrogen bonding is much more easily disrupted than simple covalent bonds. While still an exciting result, and holding a lot of potential as another avenue of CAS (and helical polymers in general) to explore, we elected to focus our efforts on generating "true" ladder polymers with two linkages between monomers.

3.5. Conclusions and Outlook

While many of the coupling strategies proposed were not successful, the capabilities of these building blocks to be edited and adjusted for a particular pathway is undoubtedly useful—including in terms of the selective S_EAr nitrations to afford stereomerically pure products, the various functionalization options of the initial ester bridgeheads (**Chapter 2**), selective dehalogenation to afford different CAS options, and the wide range of coupling reactions that the building block pieces are able to undergo. Moreover, CAS in general offers a unique opportunity to program the shapes of linear and branched polyaromatic molecular strips in a fully predictable manner.[5] In the next chapter, I will fully explore a new, optimized, and successful coupling strategy in forming various helical strips as well as polymers. However, the attempts in this chapter are not without gain, as the opportunities in the future to incorporate these various approaches may prove particularly useful. Many of the failures, and successes, discussed here ultimately lead to the successful discovery of a unique strategy to generate helical ladder polymers.

CHAPTER 4: SYNTHESIS AND INVESTIGATIONS OF HELICAL STRIPS AND POLYMERS

4.1 Introduction

We have investigated different routes toward freeform molecular helices, built with CAS. These freeform helices are predicted (see **Chapter 1.6**) to behave similar to harmonic, macroscopic helical springs upon axial extension and compression. New synthetic methodology, comprising of long-distance chirality transfer during an electrophilic aromatic substitution reaction, was invented (see **Chapter 2**) to access the required CAS building blocks. Preliminary CAS coupling trials with the most advanced helical building blocks achieved initial success (**Chapter 3**, **Scheme 3.12.b**), paving the way for the synthesis of larger freeform CAS helices described in this chapter. Access to such unique, chiral molecular structures could help elucidate the fundamental laws governing the behavior of molecular springs connected either in series or in parallel, with potential uses for energy storage and actuation in mind. The methods described to create these stereospecific, Hookean, and helical ladder polymers can inspire a new class of robust spring-like shape-persistent molecular materials. Furthermore, since the freeform helices will emerge from CAS naturally in an enantiopure (i.e., single-handed) form, these miniature molecular springs could ultimately also find applications as enantioselective catalysts or chiral liquid crystals.

4.2 Background

As detailed in **Chapter 1.4**, in the case of many biologically relevant molecules, shape defines function. This too applies for biomimetic and synthetic organic polymers. It is then a general question, how one can investigate fundamental structure-property relationships in shape-defined polymers?[12] Progress in this realm has been slow, because most polymers are rather flexible, ladder polymers however, remain mostly rigid due to their continuous restrictive ring sequence and ladder-like connectivity.[15] Thus, polymers are of interest to chemists as their limited bond rotations along the uninterrupted ring-linked backbones bring out many unique properties.[14] Here, we now report a novel method to produce single-handed, shape-persistent, spring-like, helical ladder polymers with Hookean behavior owing to their flexibility in a uniquely unidirectional motion.

Chemists have long sought after the generation of helical molecules because of the advanced repertoire of supramolecular systems that nature has created by utilizing single-handed helical structures which in turn provide the fundamental basis for the processes of life.[24] While many natural and synthetic helices are known, most of these structures prevail as double helices or foldamers, stabilized by attractive supramolecular interactions. Thus, these molecules commonly unfold under tension, rather than retaining their helical shapes like macroscopic helical springs.[160] Proper freeform molecular helices, which keep their helical shapes regardless of temperature, solvent, extension, and compression are, however, still out of the ordinary. Nevertheless, since such freeform helices do not rely on supramolecular interactions to fold into their shapes, they represent better mimics of classical Hookean springs.

For the first time, we have developed helical ladder polymer regioisomers with a varying outer diameter (OD) that were investigated to determine their relative flexibility as classical Hookean springs.[21] A spring with a smaller OD requires more force to compress, as the overall mechanical structure is rigid as compared to a spring with a larger OD, which is more flexible. Our helical polymers have different ODs, which allows us to compare their spring-like nature using classic Hookean laws. Such chemical investigations have not yet been accomplished, but the spring-like nature of molecular helices has long been of interest to chemists.

While one-handed helical ladder polymers have previously been reported,[42] the ones described herein utilize: (i) stereoselective monomer synthesis instead of chiral-resolution, (ii) have stereospecific building blocks, (iii) perform a single efficient stereospecific coupling step (92% to make dimer) vs. two stereoselective steps (56% yield to make dimer, according to the SI), and thus (iv) are synthetically less defect-prone in general. In this work we show that by changing the location of the functional groups on linker pieces, we can change and investigate the structure-property relationship of the resulting polymers.

4.3. Chirality-Assisted Heterocoupling

In expanding the field of CAS,[5] we present a heterocoupling process to create smart shape-defined helical ladder polymers. Great strides by us have been made in completing this task due to (i) elegantly designed building blocks for stereospecific dictation, chiral-free resolution, high solubility, and limited flexible movement, (ii) CAS processes for low-defect and well-defined structures, and (iii) design of a partially rigid

helical architecture with π-conjugated pyridine-like junctions to probe compression/expansion in a single direction as a molecular spring. Previous discoveries in CAS by us allowed for the synthesis of powerful supramolecular binding and well-defined C-shaped molecular strips in a homocoupling process utilizing double-amination phenazine couplings,[4, 8] as well as a heterocoupling process in the generation of a "zig-zag," β-sheet-like phenazine derivative.[146] We also report stereoselective through-space-directed nitrations which exploit the third dimension beneath and above the planes of aromatic rings in construction of resolution-free and stereospecific building blocks for CAS.[144, 146] Using the previously described findings, we now present a heterocoupling process with one-pot Suzuki couplings/imine formations for the design and synthesis of well-defined, stereospecific, and high-performance helical ladder polymers.

The elegance of having both steps occur at once fully utilizes the dynamic covalent chemistry (DCC) behavior of imines—while imines are known to be in equilibrium during the process of their formation, by ensuring that following condensation they are a part of an aromatic system (as seen in **Figure 4.1** with the formed diaza-anthracene bridging unit) they no longer revert back to their original amine functionality but are fully stabilized as the desired product. Should an imine condensation occur disfavorably (e.g. with another molecule that has undergone its Suzuki coupling), it would thus revert back to the original aniline moiety before finally forming the aromatic connection piece when partner with adjacent Suzuki coupling. This utilization of CAS takes full advantage of the prowess of DCC and ensures high yields and full convergence to a singular product.

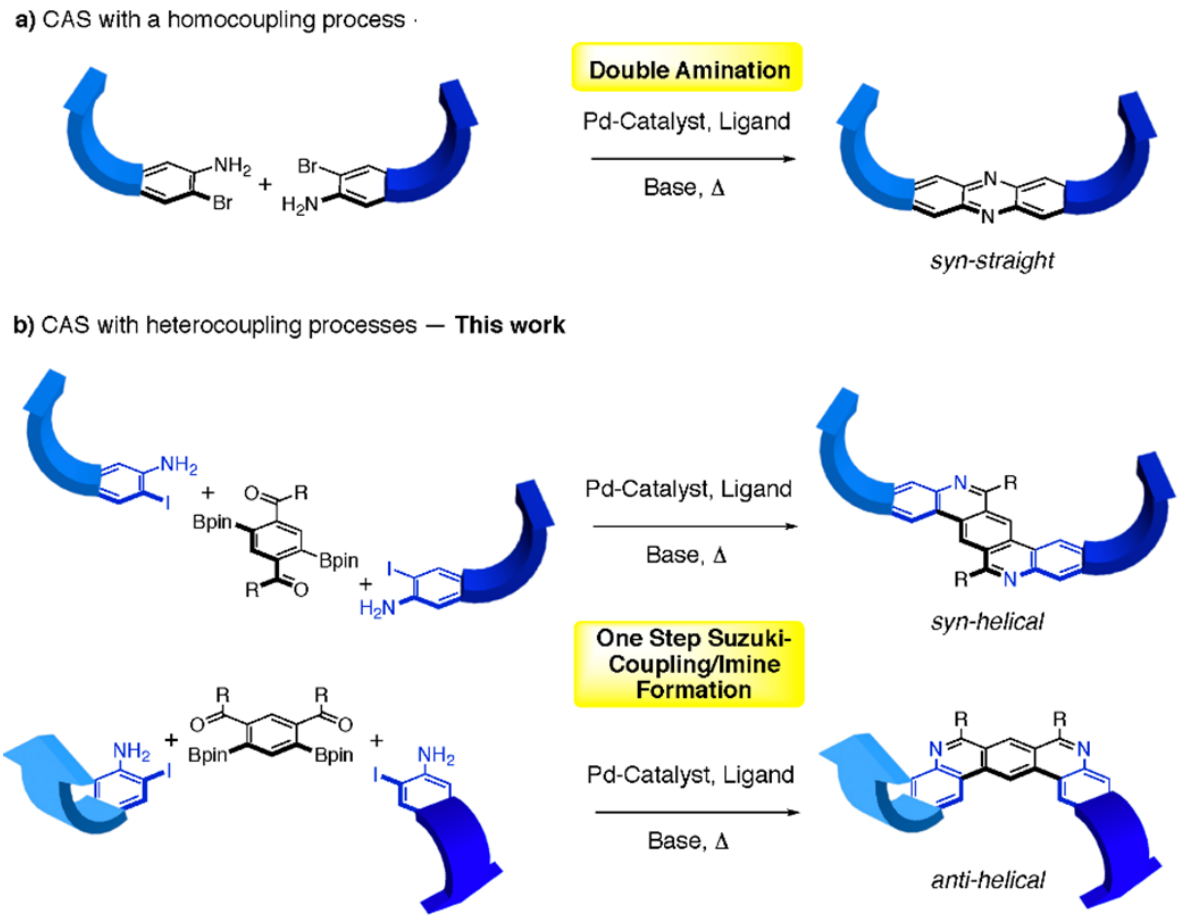

Figure 4.1. (**a**) A second generation CAS approach provides customizable products. (**b**) The same chiral building block can afford different helical shapes when combined with different achiral linkers.

4.3.1. Diester Building Block

While we were able to synthesize the aforementioned helical ladder polymers (see **Chapter 4.5**), the initial coupling strategy with Suzuki-coupling/imine condensation (see **Scheme 4.3**) was not as successful, but vital to understanding the behavior of the helices. To begin, we started from stereospecific dinitro-substituted cycloadduct **2.7**. In a

previously detailed synthesis (**Chapter 3**) we reduced down the nitro groups to amines and monoacyl protected the subsequent diamine to form **3.31**. In the final step to create the molecular building block, **3.31** was selectively iodinated *ortho* to the amine to produce diester **4.1**.

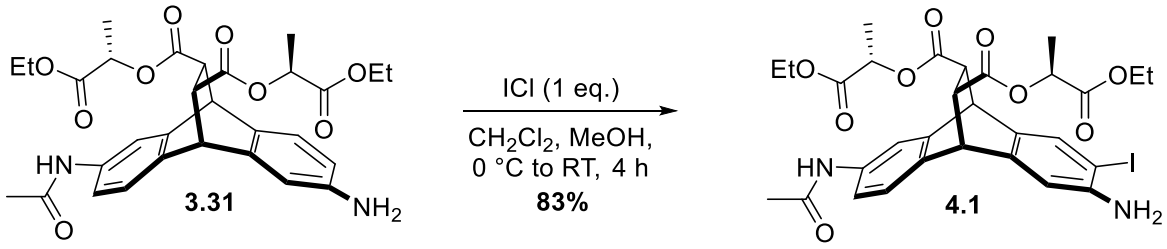

Scheme 4.1. Selective monoiodination to form the CAS monomer **4.1**.

Next, to create the first-utilized achiral linker in generating our *syn*-helix (**Scheme 4.2**), we began from commercially available 2,5-dibromoterephtalic acid. Following a literature procedure,[161] the acid chloride species was synthesized and subsequently exposed to Friedel–Crafts acylation to install amyl benzene moieties to produce **4.2**. The pentyl chain present on the spacer piece was hypothesized to assist in solubility of the generated helical polymers following Suzuki-coupling/imine formation. Next, B_2pin_2 was utilized in a Miyuara borylation to replace the bromo groups with Bpin units to generate the linker piece **4.3**.

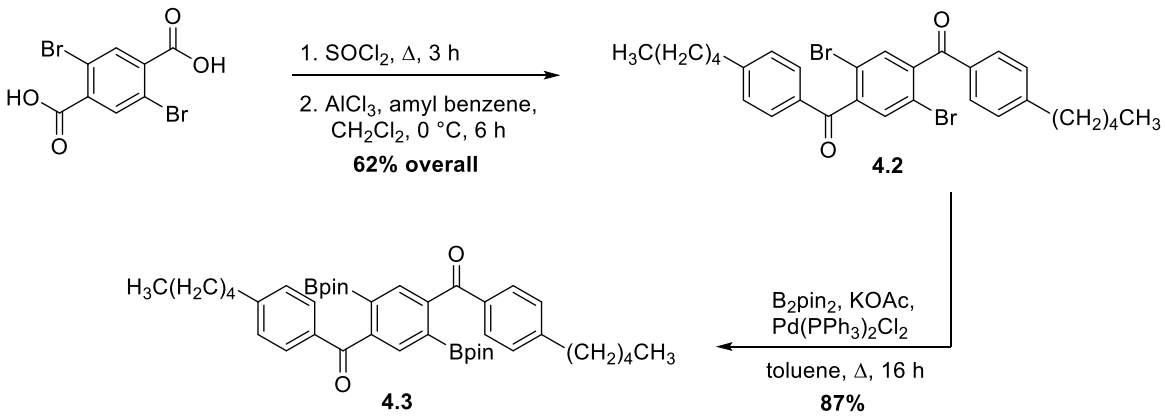

Scheme 4.2. Synthesis of the first generation *syn*-directing linker **4.3**.

In the first trials of creating *syn*-helical strips with CAS, we took two equivalents of monoiodo-monoamine **4.1** and a singular equivalent of spacer piece and exposed them to Suzuki coupling conditions (**Scheme 4.3**). In a one pot fashion, both the Suzuki coupling as well as the imine condensation occurred all within a single step—and we were afforded the helical dimer **4.4**. Even though the yield was not as high as expected, this synthesis proved to be better than previous attempts with the diester building block for CAS couplings (**Chapter 3**). Moreover, there were four consecutive reactive steps that occurred to form the helical strip, so even with a 55% overall yield, each step occurred at a modest 86%.

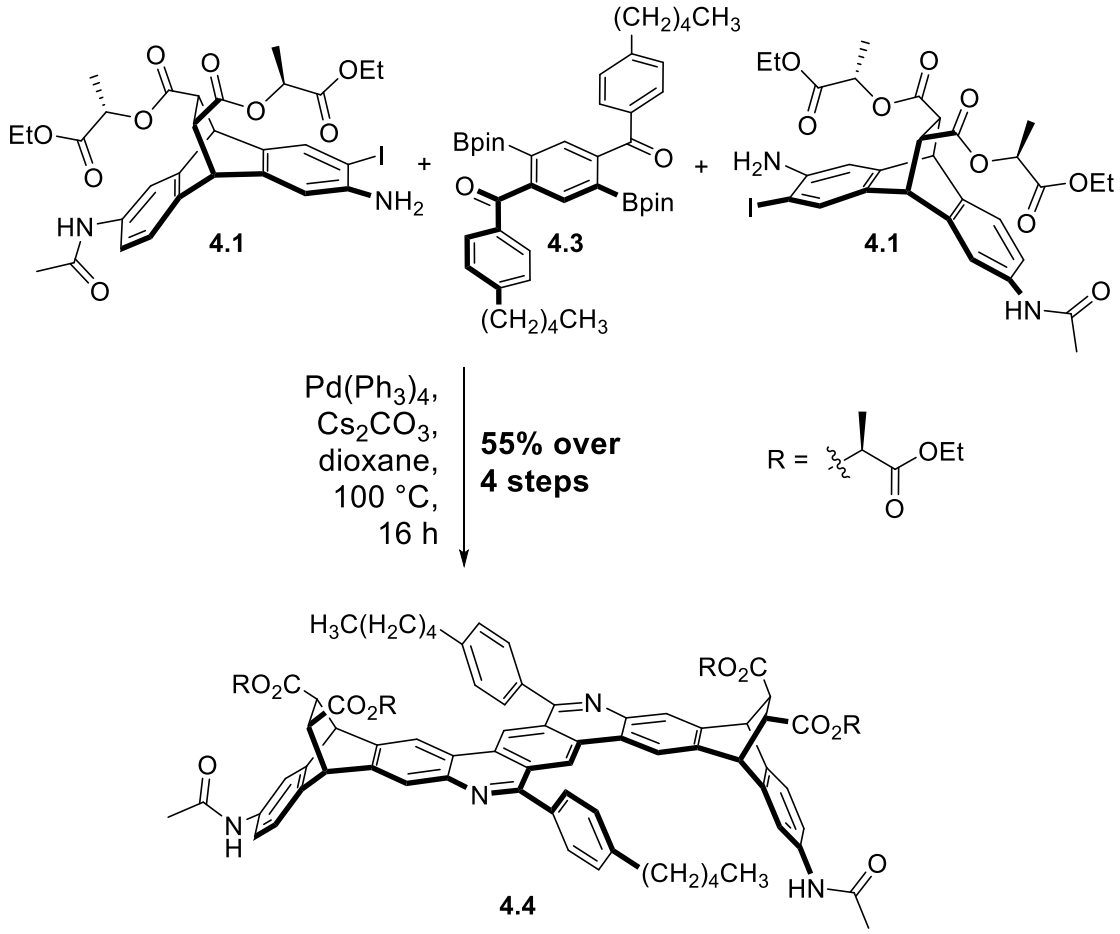

Scheme 4.3. CAS couplings of **4.1** with **4.3** to form *syn*-helical dimer **4.4**.

Not deterred by the low yields in the diester helix dimer, we attempted to form the helical polymer (**Scheme 4.4**). While generating the helix in an iterative, step-wise manner ensures an exactly known length (**Chapter 4.6**), it would involve a lengthy series of deprotection of the acyl groups, another monoprotection of one of the free amines, and a subsequent monoiodination before being able to undergo another Suzuki coupling to generate the hypothesized tetramer. Instead, we elected instead to see if forming the polymeric mixture was possible at all. Starting from diester-damine **3.19**, we selectively diiodinated both sides of the molecule in formation of diiodo-diamine **4.5**. With the linker

4.3 already in hand, we treated the 1-to-1 mixture with Suzuki-coupling conditions. By ^{1}H NMR analysis, there were a multitude of chemical shifts that indicated longer oligomers were formed, but no diagnostic broad peaks were found associated with polymers. It was apparent that in the formation of the polymer, the helix was unable to continue to grow and halted before a full turn was even completed, resulting in a mixture of inseparable, smaller, oligomers. By observing the structure of the helical polymer, we reasoned that, upon approaching a full turn of a helix, the pentyl chains present on the spacer piece **4.3** sterically obstructs its step-growth polymerization.

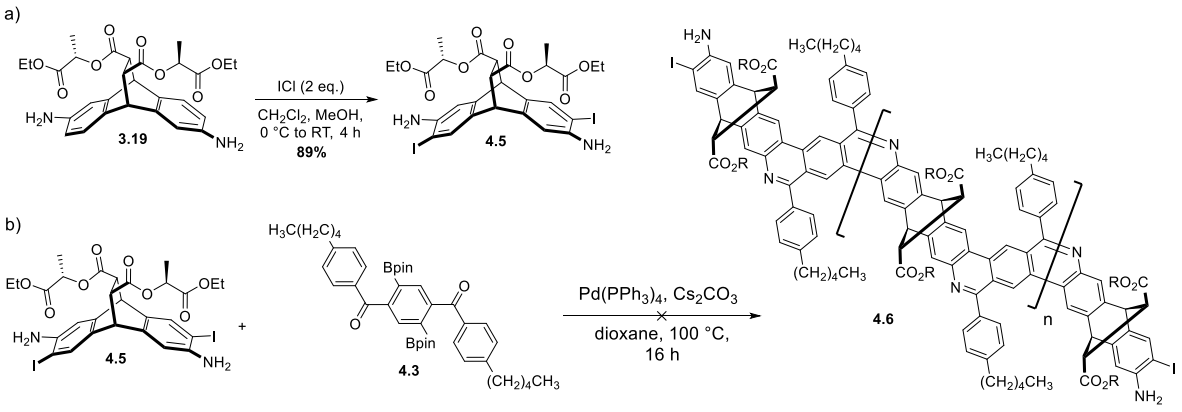

Scheme 4.4. (**a**) Diiodination of the diamine **3.19**, followed by (**b**) ladder polymerization with one-one pot Suzuki-coupling/imine condensations.

The issues that arose from the initial diester helical dimer and the attempt to form the *syn*-helix were quite clear. The low yield of forming **4.4** showed that it would be unreasonable to generate polymers in an appreciable amount, likely due to the ability of the various carbonyl moieties to obstruct Pd insertion into the C–I bond (as previously stated in **Chapter 3**), thus limiting the efficiency of Suzuki couplings. Moreover, the long

pentyl chains of the spacer units appeared to block the continued formation of the polymer due to the tightly wound nature of the *syn*-helix. And, with basic conditions utilized in the Suzuki couplings, we hypothesized that some hydrolysis would likely occur as well to generate random carboxylic acid moieties along the periphery of the proposed helical polymer. Thus, we elected to (once more) change up the CAS system, and alter the linker unit to possess a smaller alkyl chain on the phenyl groups, as well as to reduce the number of reactive auxiliary groups on the diester building block.

4.3.2. Diether Building Block

We started our investigations into these systems with the formation of the CAS building block that would be utilized to first generate the helical dimer strip as a test trial. Following a similar synthetic strategy as detailed in a previous study by us,[146] we began with the stereospecific dinitro-diester cycloadduct **2.7** with cleavage of the ester groups to the resulting diol **4.7** (**Scheme 4.5**), followed by S_N2 alkylation to form the hexyl-ether derivative **4.8**. Subsequently, the nitro groups are reduced in the formation of central building block piece diether-diamine **4.9**. As a note, if isomers of **4.9** have not been removed at this synthetic point, column purification via EtOAc/hexanes with a small percentage (~1%) of Et_3N has proved useful in separating major isomer **4.9**. From there, **4.9** was exposed to iodination conditions with just shy of 2 equivalents of ICl to form a mixture of monoiodo-diamine **4.10** and diiodo-diamine **4.11**. As another note, should minor isomers (particularly the diastereomer) still remain in the mixture after iodination, it becomes much simpler to coax out the minor isomers after halogenation due to a

significant decrease in H-bonding ability of the amine, requiring only a EtOAc/hexanes mixture to separate the isomers.

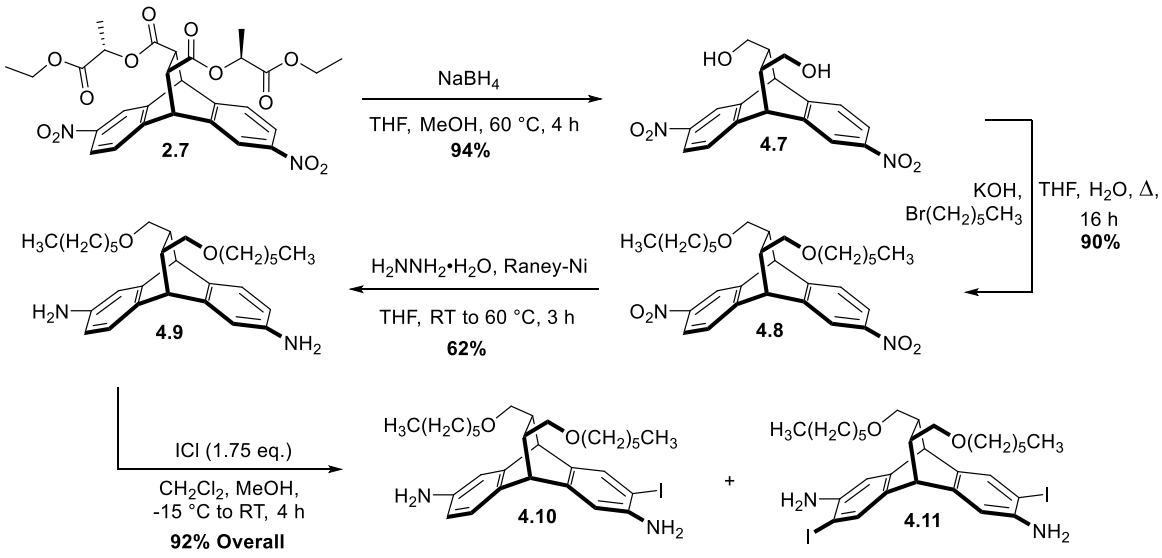

Scheme 4.5. Synthetic path to the central CAS building block diether-diamine, **4.9**, and subsequent iodination to form CAS monomers **4.10** and **4.11**.

Next, we looked at the formation of a shape-directed linker piece to generate our polymeric helices. To begin with a synthetic route towards the *syn*-helix, we once again started with commercially available 2,5-dibromoterephtalic acid. Following generation of the acid chloride derivative and subsequent Friedel–Crafts acylation, we were afforded spacer piece precursor **4.12** (**Scheme 4.6.a**). While *p*-addition of the toluene group was preferred, some minor byproduct for *o*-addition occurred as well. The more bulky amyl group from **4.2** prevented *o*-addition at that step. Nevertheless, the shape-directing linker piece **4.13** was then finally synthesized from the dibromo precursor by way of a Miyaura borylation. Likely due to the adjacent carbonyl near the Lewis acidic boron group,

degradation of the linker appeared to occur on regular silica, as well as residual B_2pin_2 co-eluting with the product, so recrystallizations in EtOAc/hexanes were mostly utilized to obtain pure product. Alongside the shape-directed linker, we also utilized monoiodo-diamine **4.10** for direct mono-Boc protection to produce CAS monomer monoiodo-monoamine-mono-Boc **4.14** in near quantitative yields (**Scheme 4.6.b**).

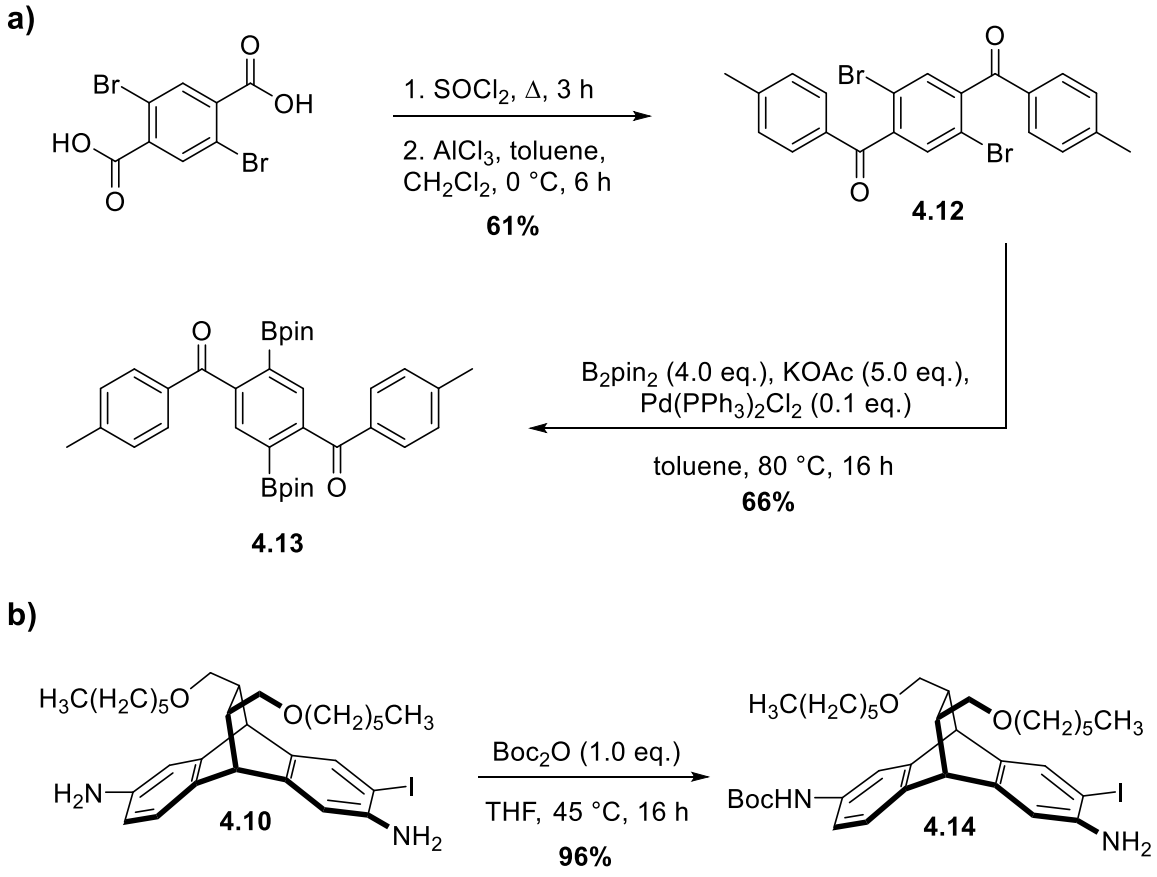

Scheme 4.6. Synthesis of (**a**) *syn*-directing linker **4.13** and (**b**) the CAS coupling partner, building block **4.14**.

4.3.3. *Syn*-Helix Dimer

With the second generation of materials in hand to attempt to form the *syn*-helix, we first attempted to synthesize the dimer strip. With two equivalents of monoiodo-monoamine CAS monomer **4.14** as well as one equivalent of the *syn*-linker piece **4.13**, we treated the reaction solution with Suzuki-coupling/imine condensation conditions (**Scheme 4.7**). We were afforded *syn*-helical strip **4.15** in excellent yields. The structure itself has a very evident helical-like geometry, owing to the shape-persistent nature of CAS. The yield itself was much better than the initial trials in forming the helical dimer with the diester and linker piece with the longer pentyl chains. The higher yields with the diether piece *vs.* diester is not dissimilar to the results found with face-on CAS couplings explored in **Chapter 3**, where the diester building block was proposed to block Pd insertion into the C–I bond. Again, with four reactive steps occurring to form the di-Boc dimer **4.15**, and at 92% yield, this meant that each step occurs nearly quantitatively. This gave us hope that the helical polymer would also be able to be generated in high enough yields and fidelity (due to the shorter methyl chains on the linker piece) which in hand would lead to the capability of the polymerization to continue to grow past a single helical turn. Not only this, but by changing the location of reactive groups on either of the building block pieces, we can change the overall shape of the resulting CAS product. Before delving into the development of freeform helical polymers, we wanted to probe the shape-directing nature of the linker unit to generate a dimer strip of a different geometry.

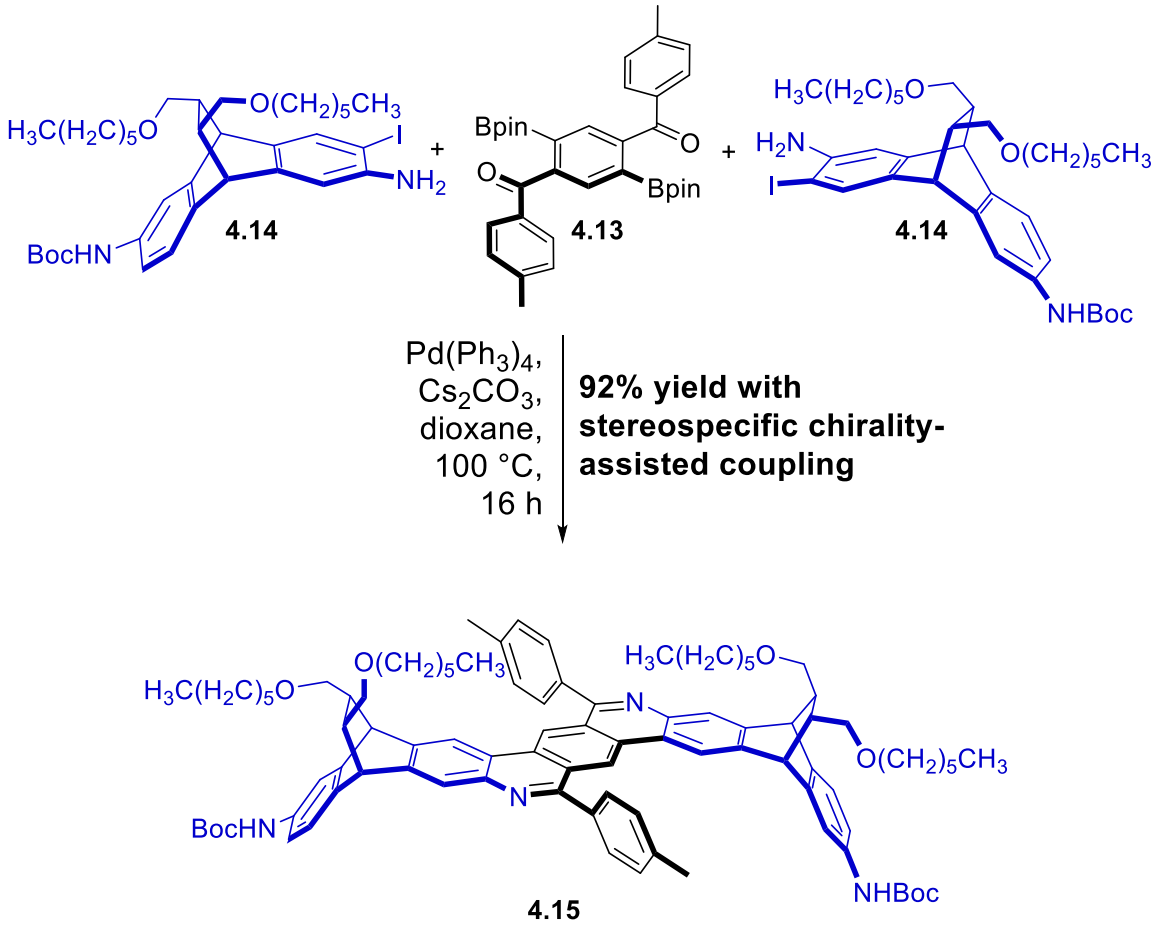

Scheme 4.7. Chirality-assisted coupling to form the di-Boc *syn*-helix dimer **4.15**.

One of the principles of CAS is the ability of building block pieces to join together in an unambiguous fashion. Thus, by changing the positions of reactive groups on a building block unit, we can completely change the shape of the generated molecule. With this in mind, we set out to change the *syn*-linker piece to orient the functional groups *meta* rather than *para* to their respective twin group, therefore creating an *anti*-linker piece which would dramatically increase the pitch of a generated helical polymer.

With that in mind, we set out to generate this new *anti*-directed spacer unit and utilize chirality-assisted coupling to generate a new shape-persistent material.

4.3.4. *Anti*-Helix Dimer

To begin synthesis of the *anti*-linker piece we first started from *m*-xylene, exposing it to aromatic bromination conditions to form dibromo compound **4.16** (**Scheme 4.8**). From there, it was treated with excess $KMnO_4$ to fully oxidize the methyl groups and produce carboxylic acid derivative **4.17**. Then, in a similar process to forming the *syn*-linker **4.12**, we treated it with thionyl chloride followed by subsequent treatment of Friedel-Crafts acylation conditions with toluene to afford precursor piece **4.18**. As note of interest, while starting from 1,4-dibromobenzene (as well as in the case of 1,3-dibromobenzene) *p*-toluoyl chloride was attempted to be utilized for a direct one-step acylation to produce the desired product and forgo the additional 3 steps of first creating the acid chloride before treating with Friedel–Crafts conditions—however this lead to low yields and degradation of product, so this potential shortcut was not utilized. Finally, dibromo compound **4.18** was reacted with Miyaura borylation conditions to afford the shape-directing linker piece **4.19**. Similar to the *syn*-linker, the *anti*-linker piece found difficulties in purification, so recrystallization in EtOAc/hexanes was mostly done to obtain pure product.

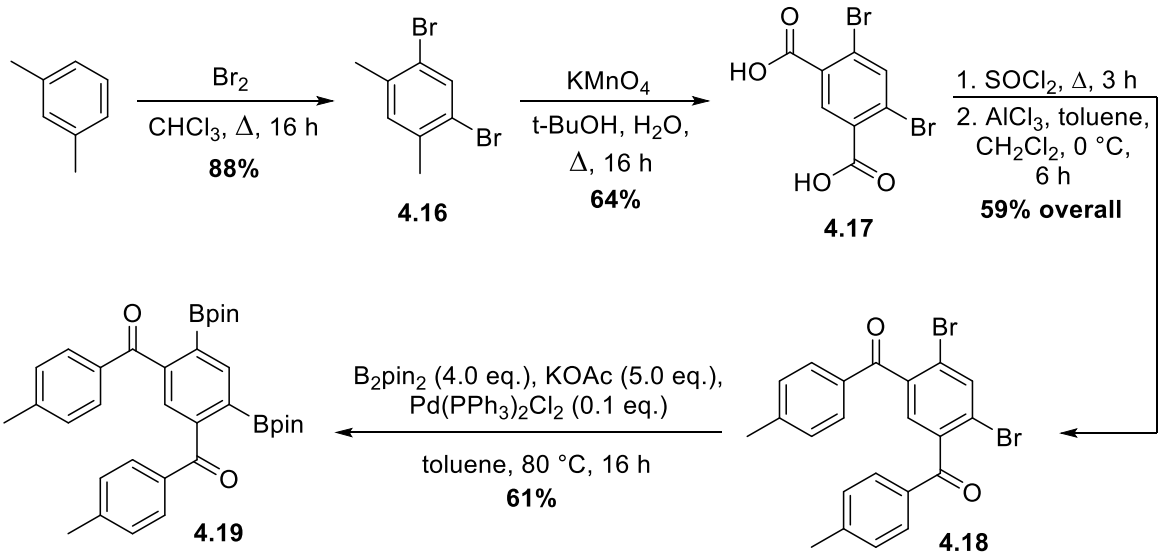

Scheme 4.8. Synthetic route to produce shape-directing piece, *anti*-linker **4.19**

Identical to the conditions used to form the *syn*-helix dimer **4.15**, we subjected two equivalents of CAS monomer **4.14** and one equivalent of *anti*-linker unit **4.19** to the aforementioned Suzuki-coupling/imine condensation conditions (**Scheme 4.9**). Thanks to the shape-directing capabilities of this new linker piece, we were afforded with *anti*-helix dimer di-Boc **4.20**. Upon first glance, it appears to have a "zig-zag," β-sheet-like conformation similar to CAS-coupled **3.18b**. This is due to the inherent geometrical fashion by which building block **4.14** reacts with the *anti*-linker, where one monomer must couple onto the linker upside down relative to the other. Again, this showcases the capabilities of CAS to force building blocks to couple in a single specific fashion, allowing us to generate a whole array of molecular shapes. Nevertheless, while **4.20** may not first appear to have any specific helicity, upon connecting on more units it attains a long, yet rigid, helical shape which will be investigated more later on.

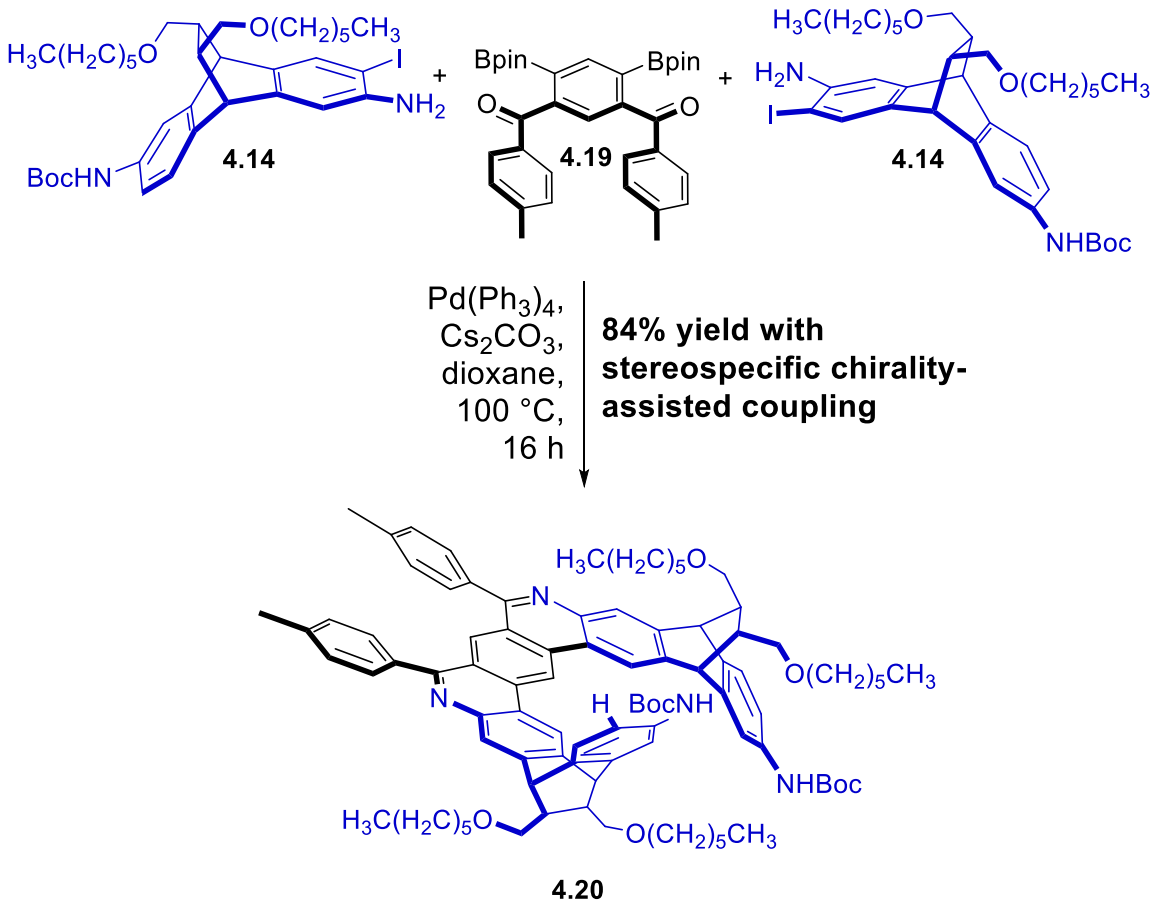

Scheme 4.9. Chirality-assisted coupling of CAS monomers and *anti*-directing linker to generate the *anti*-helical di-Boc dimer **4.20**.

4.3.5. DCC with Unprotected Building Blocks

After initial success with generating the helical dimer strips through the new CAS coupling conditions, we investigated the DCC nature of the imine condensation portion of the one-pot reaction. Because imines are in a dynamic equilibrium, depending on environmental conditions, we elected to Boc protect one of the aniline sites on the

diamine monomer **4.13** before attempting to use chirality-assisted coupling to generate our helical dimers. However, in principle, if **4.13** remained with one free amine during coupling which condensed to an imine, it would dynamically revert back to its original aniline form to allow for the much more favorable formation of the π-conjugated pyridine-like junctions. If one wanted to grow out the helical polymers step-wise by reacting two dimer units to form a tetramer, and two tetramers to form the octamer, and so on, several deprotection and protection steps would need to be done to achieve the highest possible yields. However, if the free amine reacting with the ketone of the linker piece were to dynamically revert back to its aniline state, we could forgo the Boc protection altogether, thus saving several synthetic steps from *N*-Boc protecting and deprotecting throughout the controlled iterative addition polymeric process.

We started this endeavor by first looking at forming the free amine *anti*-helix dimer. While keeping the *anti*-linker unit **4.19** the same, we had to forgo the mono-Boc protection used to generate **4.13** and use only its precursor **4.10** which has a free aniline. If one wished to garner a higher yield of monoiodo-diamine **4.10** (rather than with slight excess of ICl as in **Scheme 4.5**), starting from diamine **4.9** with treatment of the cycloadduct with only one equivalent of ICl would regioselectivity iodinate *ortho* to the amine to form **4.10**. In iodinating **4.9** (see **Scheme 4.6**), there is not much communication between the arene subunits, even though less than two equivalents of electrophilic iodine were utilized. Thus, a mixture of starting material, diiodo-diamine, and desired monoiodo product was formed—running the reaction at temperatures even when as low as -15 °C still afforded a mixture of products. Any resulting diiodo-diamine **4.11**—much like with

the selective dehalogenation experiments run on the building blocks (**Chapter 3**)—could be exposed to Pd-catalyzed conditions alongside H_2 to order to reobtain starting diamine **4.9** and carry forward the reclaimed starting material with another mono iodination attempt.

Next, two equivalents of the free amine monomer **4.10** and one equivalent of the shape-directing linker **4.19** were exposed to the Pd-catalyzed Suzuki-coupling/imine condensation conditions (**Scheme 4.10**). We obtained a mixture of the *anti*-helix diamine dimer **4.21** as well as the monomeric starting material **4.10**, which we propose had likely undergone DCC couplings and converted back to starting material. Based on this recovered starting material, we achieved a 90% yield, very comparable to the excellent yields attained for the *syn*-helix dimer **4.15** (**Scheme 4.7**).

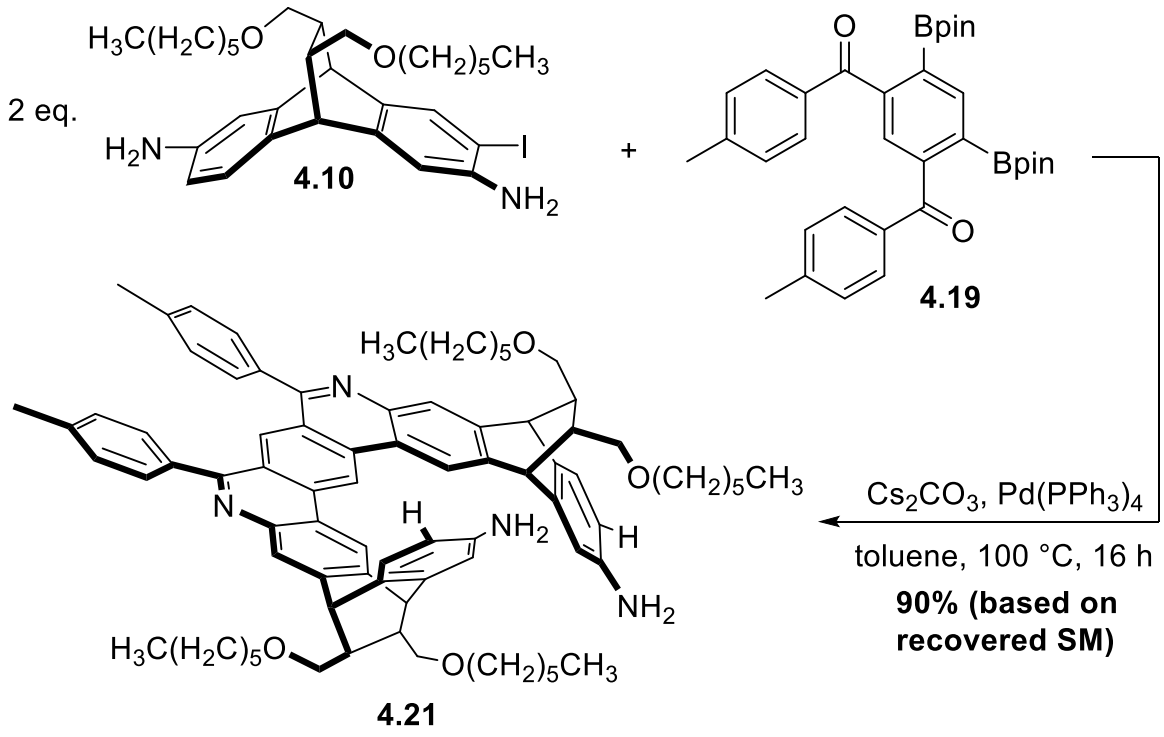

Scheme 4.10. CAS utilizing DCC to form *anti*-helix dimer **4.21** in excellent yields based on recovered **4.10**.

Next, we also tested the capability of the free aniline building block alongside the *syn*-linker unit for their capacity to utilize DCC in CAS couplings. Utilizing the same monoiodo-diamine **4.10**, two equivalents of it were reacted with one equivalent of shape-directing linker **4.13** in Pd-catalyzed Suzuki-coupling/imine formation (**Scheme 4.11**). Once again, we were afforded with another CAS-coupled helical strip, free amine *syn*-dimer **4.22**, in modest yields. It was found that the reaction progressed in approximately 77% yield, based again on recovered starting material. Certainly, further investigation into the ideal conditions for ensuring more product convergence is needed to improve yields to approach 90% as with dimer **4.21**, and enrich the viability of this methodology.

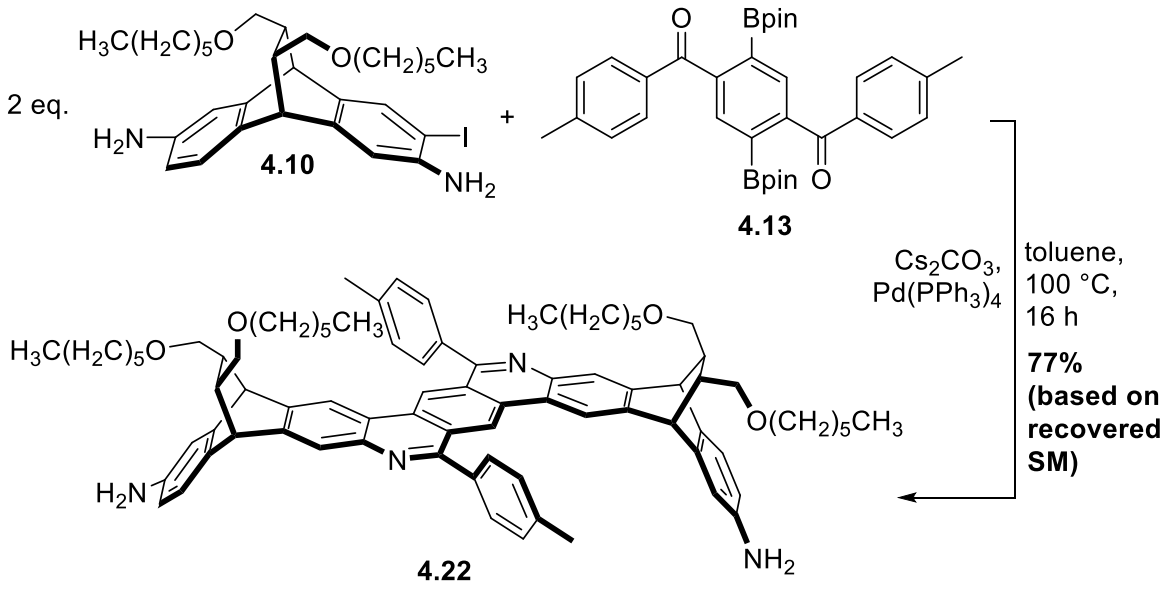

Scheme 4.11. CAS-coupled *syn*-helix dimer **4.22** formed in modest yields utilizing DCC.

While taking advantage of the DCC nature of free amines would save several synthetic steps when forming iteratively formed polymers, in practice there is a lower mass gain due to recovered starting material. *N*-Boc protecting the free amine in forming the CAS building block does yield a mixture of products from di-Boc protection, mono-Boc protection, and starting material, however the di-Boc product is easily deprotected via TFA to converge back to initial diamine starting compound to rerun a Boc protection (as will be showcased later on in the chapter). In principle this process would be similar to the protection-deprotection process of the mono-*N*-Boc strategy, whereby the free amine monomer **4.10** would be recovered from the reaction solution and re-exposed to the CAS coupling conditions, and subsequently any monomer **4.10** then remaining would once again have to be recollected until satisfactory convergence to the helical product was obtained. At this stage however, Boc protection ensures a greater yield with less

unrecoverable side products, of which seems to be a mix of monocoupled compounds based on ^{1}H NMR analysis. Fine-tuning conditions to achieve greater yields from reacting free amine monomers with the shape-directing linkers would make this a highly useable strategy and save many synthetic steps over the course of making controlled iterative sequence-defined polymers.

Thus, to showcase the efficiency of these heterocoupling reactions, and as a proof of principle to utilize CAS in making molecular helices, we generated both *syn*- and *anti*-helical dimers by using two equivalents of the building block with only one active *ortho*-iodo aniline site for regioselective Pd-catalyzed Suzuki-coupling/imine condensation, and one equivalent of the respective linker piece, both resulting in excellent yields in this one-pot four-reactive-step synthesis. With the formation of the diaza-anthracene junctions, there is no appreciable reversibility with the generated imines which would undo formed dimers and polymers, and thus unfold the helices.

The products of these CAS coupling reactions are naturally stereomerically pure, as shown by CD analysis (**Figure 4.2**), thus, there is no need for further chiral resolution. Moreover, in a comparison of the *syn*-helix dimer **4.22** with the *anti*-helix dimer **4.21**, we see a positive Cotton effect just after 300 nm, indicating that both molecules are indeed of a right-handed helical geometry.[80, 162] Both molecules have a similar emission spectrum though with different intensities owing to their structural differences and self-interactions in solution. And, both compounds contain extra (yet smaller) bands around 400 nm, consistent with $\pi \rightarrow \pi^*$ transitions associated with aromatic rings bearing amino groups.[163]

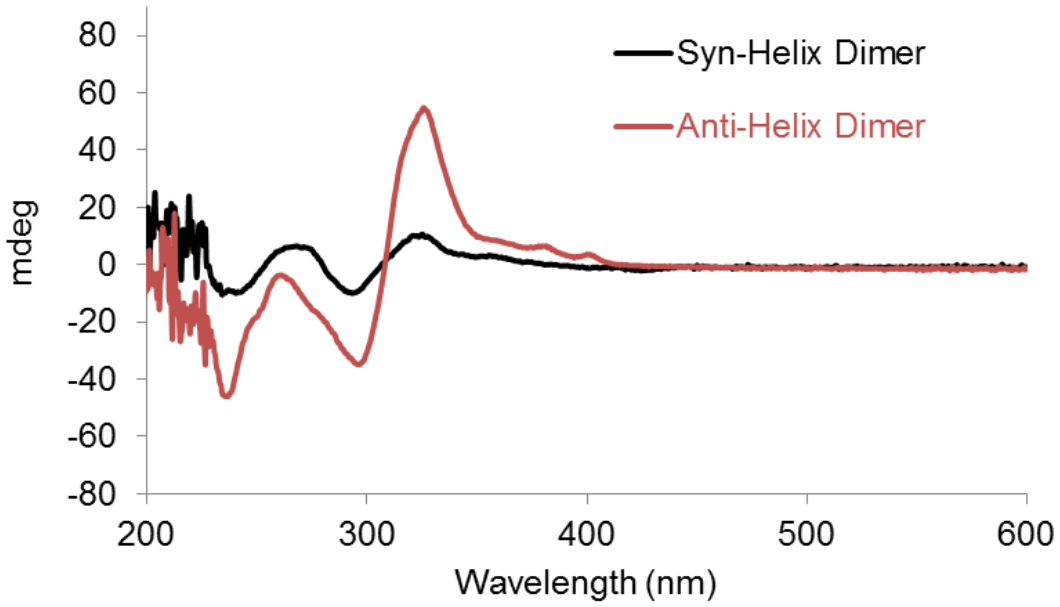

Figure 4.2. CD spectra of the *syn*-dimer **4.22** and *anti*-dimer **4.21** recorded in $CHCl_3$ at RT.

4.4. Ring Formation via Suzuki-Coupling/Imine Condensation

Straying away from the normal cycloadduct building block piece, we briefly investigated another potential system that would allow for interesting molecular shapes byway of Suzuki-coupling/imine condensations. Given the unique pyridine-type junction associated with forming the helical dimers, it would seem impossible to form ring-like structures with them. However, by utilizing a carbazole-based building block with a simple dihalogen-diamine benzene linker piece, we could potentially generate a flat, fully conjugated, π system in the form of a ring. The most stable ring structure was found to be a "pentamer" containing five carbazole units conjoined with five linkers. (**Figure 4.3**). Alternatively, should the coupling process be unfavorable to form a planar ring system,

the coupling ends may “miss” and instead form right- and left-handed helicenes in the form of a fully conjugated ladder polymer.

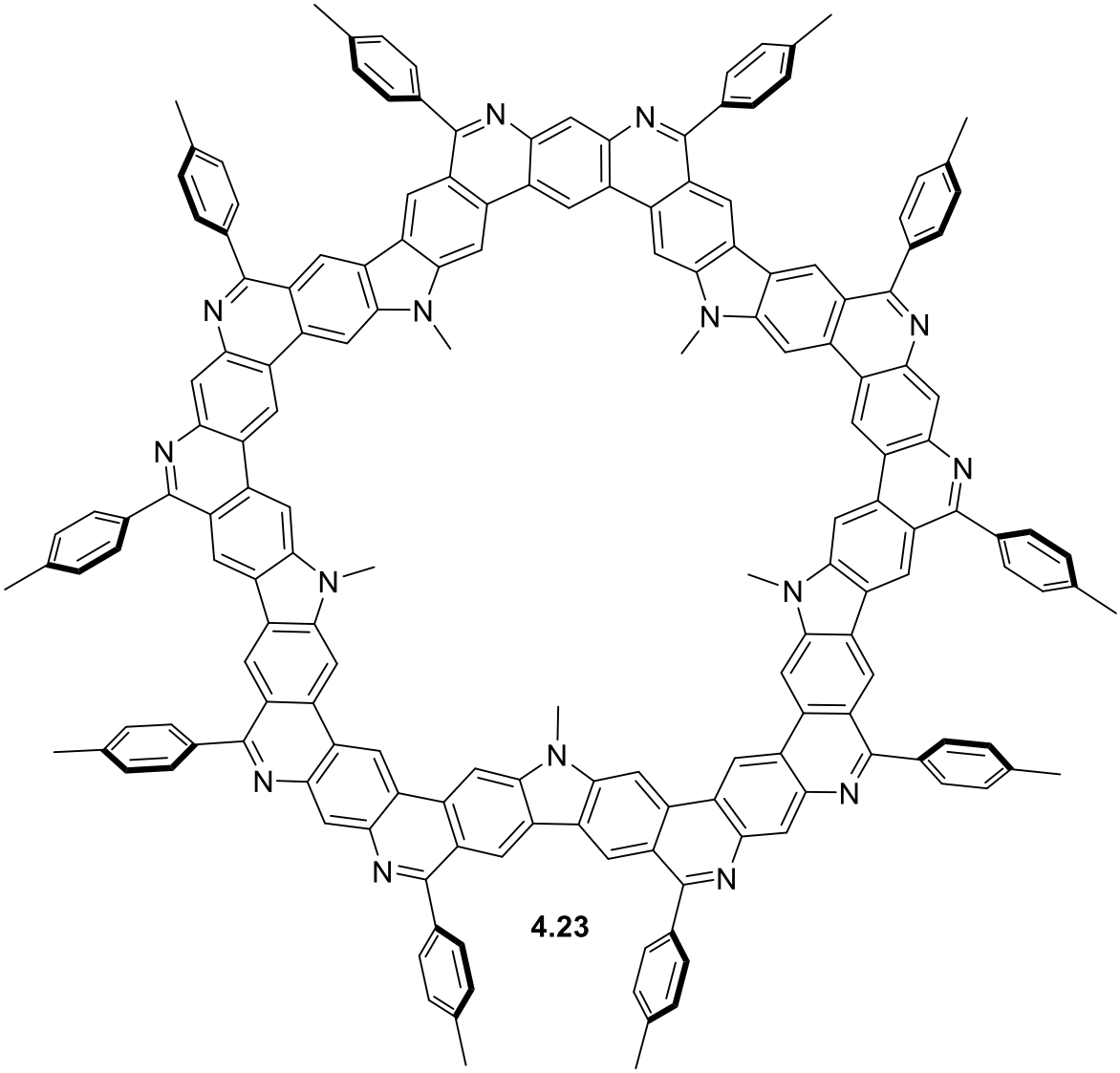

Figure 4.3. Proposed planar, fully conjugated, Suzuki-coupled/imine-condensed pentamer ring.

Starting from commercially available *m*-phenylenediamine, the shape-directing linker **4.24** was formed by simple aromatic bromination, we found that the process was regioselective for the *4* and *6* positions with very little tribrominated product formed (**Scheme 4.12.a**). As a note of interest, the diiodo derivative was not utilized as it had a decomposition point lower than the temperature that would be utilized for Suzuki couplings. Next, the carbazole monomer was built from commercially available starting compound 2,7-dibromo-9H-carbazole. Starting from the *N*-H carbazole, it was treated with excess iodomethane to methylate the nitrogen to form *N*-methyl **4.25**, thus preventing any unwanted side reactions during future imine condensations (**Scheme 4.12.b**). Following this, **4.25** was exposed to Friedel–Crafts acylation conditions utilizing *p*-toluoyl chloride which gave addition of aryl ketones *ortho* to the bromo groups to form monomer precursor **4.26**. Finally, **4.26** was treated with pre-established Miyaura borylation conditions to form monomer building block unit **4.27** in modest yields.

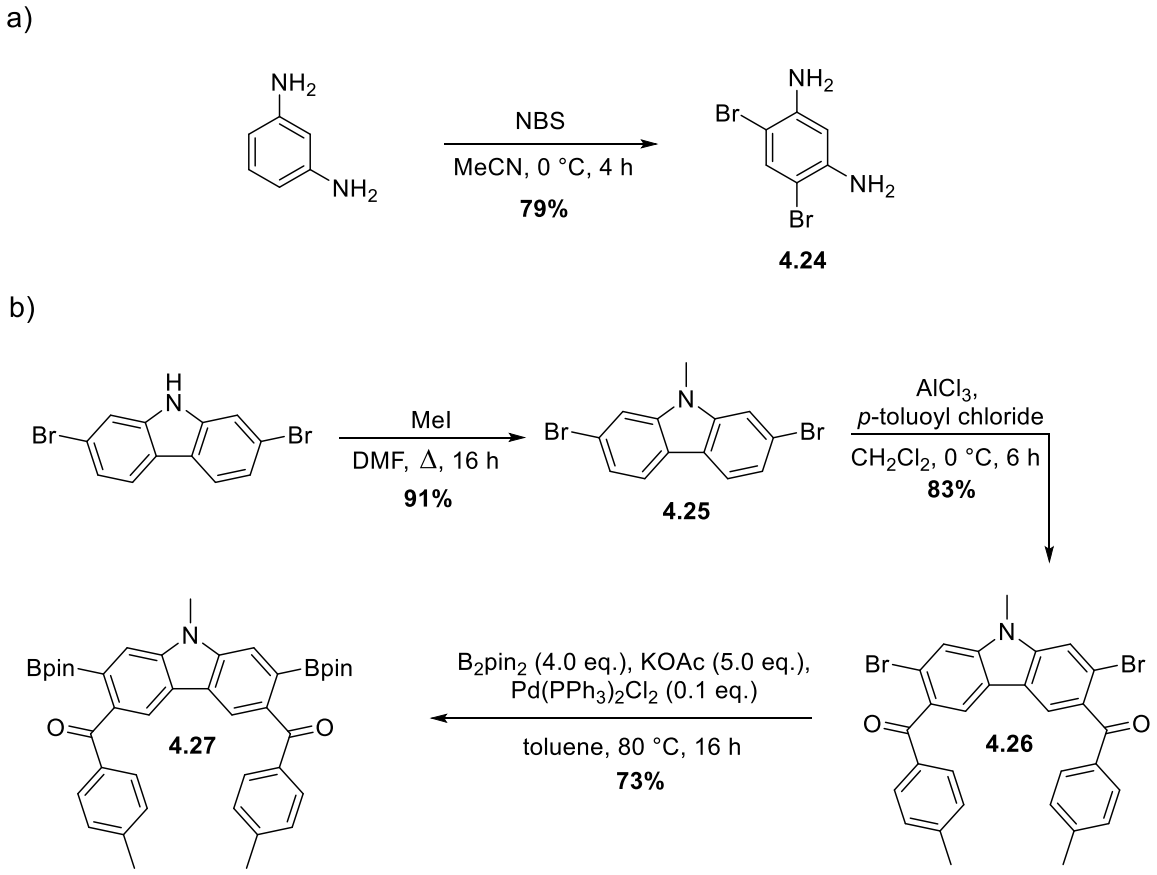

Scheme 4.12. Synthesis of shape-directed linker **4.24** and building block monomer carbazole **4.27**.

As a note of interest, the dibromo-*N*-methyl-carbazole **4.25** was found to have incredibly low yields upon initial attempts to undergo Miyaura borylations. It seemed likely—and this was found the case in both *syn*-linker **4.13** and *anti*-linker **4.19**—that Suzuki couplings were occurring alongside Miyaura borylations to form homocoupled oligomer side products.[164] With only two equivalents of B_2pin_2 leading to slow formation of borylated product, it appeared that there was excess aryl bromide in solution that would homocouple with mono- and diborylated species that would form *in situ*. It was

found that a partial excess of B_2pin_2 to help fasten the formation of borylated product, along with lower heat gave a much greater yield (**Scheme 4.13**). In case the case of the *syn*- and *anti*-linker units, the product was found to co-elute with remaining B_2pin_2 in solution, however the yields were still much more favorable than the lower (>20%) yields found by using stoichiometric amounts of B_2pin_2.

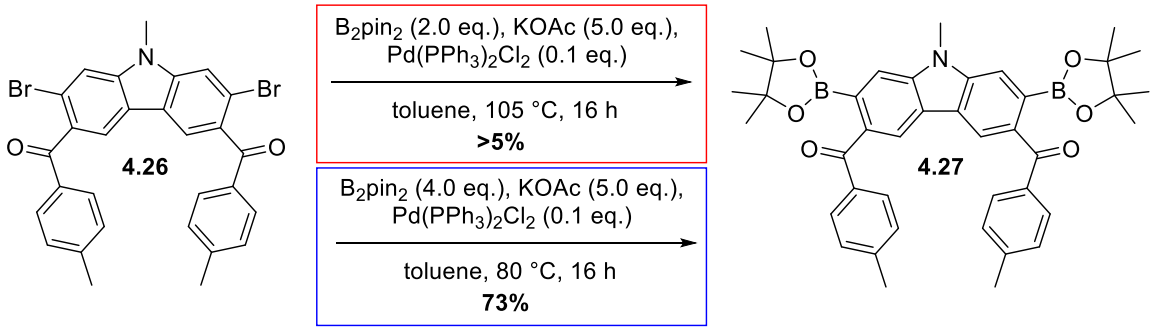

Scheme 4.13. Extra equivalents of B_2pin_2 and lower heat found higher yields for forming borylated monomer building block **4.27**.

In an attempt to form the proposed Suzuki-coupled/imine condensed conjugated ring **4.23**, we exposed a one-to-one reaction mixture of carbazole **4.27** and diamine **4.24** to Suzuki coupling conditions (**Scheme 4.14**). Unfortunately, analysis of the crude reaction mixture appeared to only show a mixture of degraded byproducts and unreacted starting material. Moreover, there seemed to be a loss of crude mass that we attributed to some polymerization occurring, but the resulting mix of oligomers was likely too insoluble, as previously mentioned conjugated ladder polymers can be, for characterization. A potential solution to this challenge would be to attach on longer alkyl chains to the aryl ketone of **4.26**—a pentyl chain rather than a methyl chain, for instance,

would insure potent solubility upon coupling. Attaching a longer alkyl chain to the nitrogen of the carbazole **4.25** would likely cause extreme steric clashing in the process of forming the planar ring, potentially preventing its formation at all.

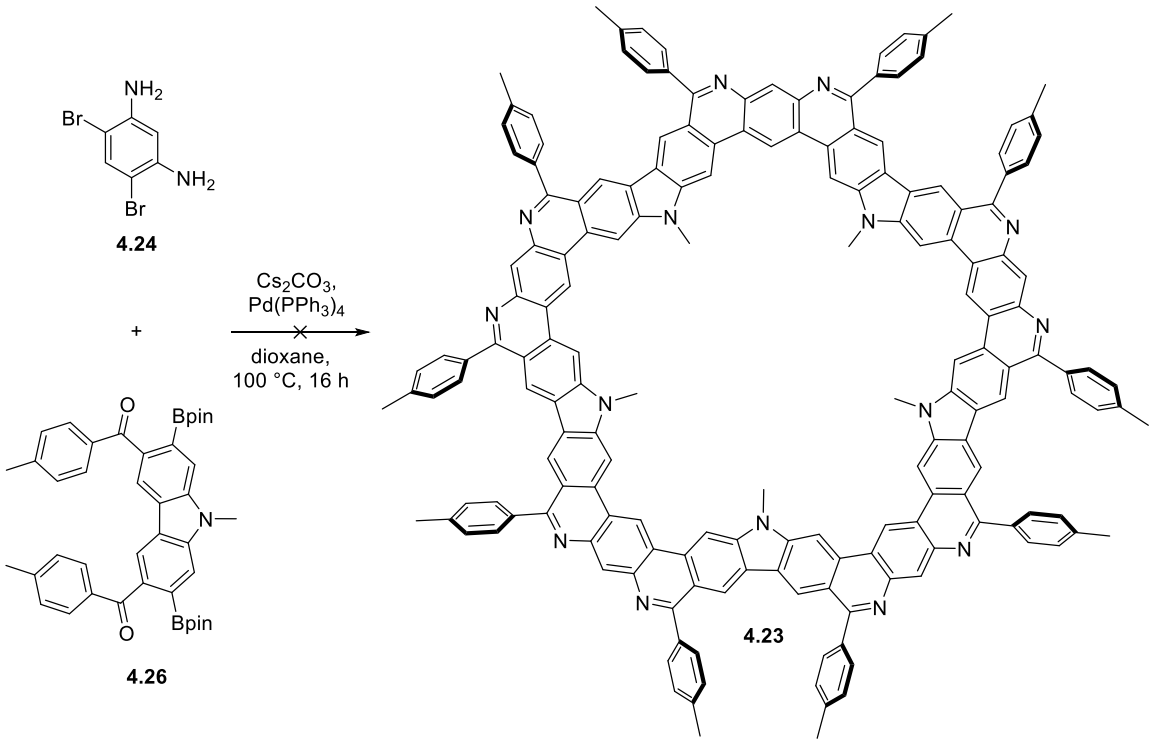

Scheme 4.14. Suzuki-coupling/imine condensation attempt to form pentamer-ring, **4.23**.

However, a concern was that the carbazole system (as it is unique from the diether building block, which has sp^3 carbons as bridgeheads between arene rings) may be unfit for the Suzuki-coupling/imine condensation process. As a trial we exposed one equivalent of carbazole building block **4.27** to two equivalents of commercially available 2-iodoaniline (**Scheme 4.15**). By only attaching two arene systems we would ensure at least some solubility of the resulting proposed coupled product **4.28**. Upon exposing the aforementioned substrates to coupling conditions, we found that the desired product was

not formed to any appreciable extent. Instead, there appeared to have been only monocoupled side-product **4.29** acquired in 36% yields. Other degradation occurred likely the result of other monocoupled byproducts, as well as recovered starting material. It is likely that solubility issues still occurred, or the uniquely conjugated linkages that formed within the carbazole backbone prevents a second coupling from occurring due electronic interactions with the Pd species, thus leaving the Bpin moiety inactive, which may have been why majority cleavage of the Bpin group occurred rather than sufficient Suzuki coupling reactivity to form a new C–C bond. It has been shown in catalytic-transfer polymerizations,[165] that deboronation of Bpin can occur with base.[166]

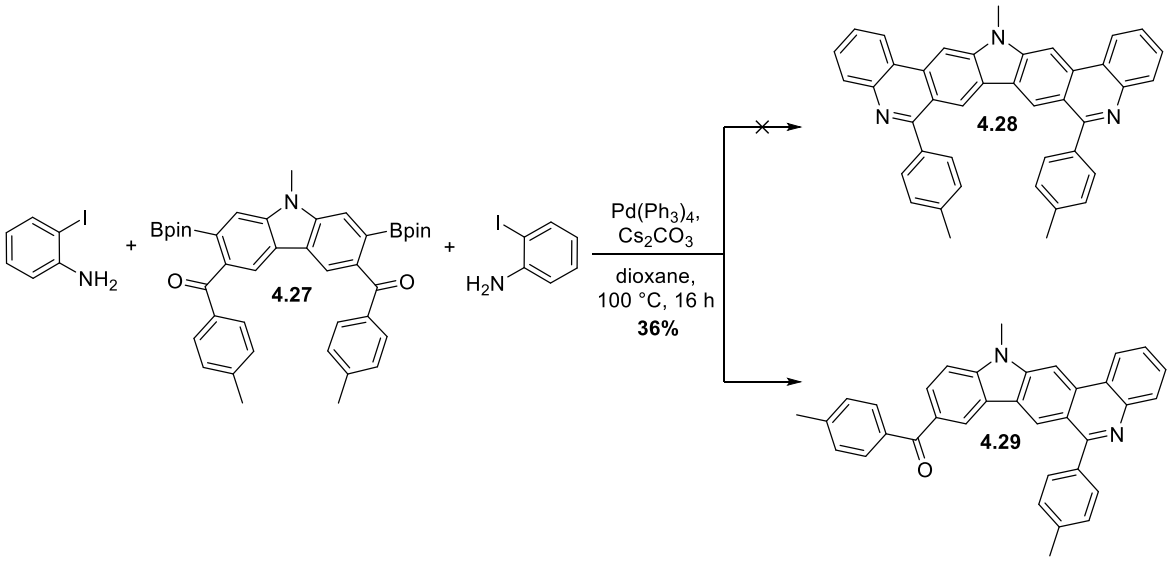

Scheme 4.15. Attempted Suzuki-coupling/imine condensation to form dimer **4.28**.

Further testing must certainly be done on this system to form resulting planar rings or fully conjugated helicene polymers. Attaching longer alkyl chains to the aryl groups of building block carbazole **4.27** may help with solubility and thus reactivity; or a

change in the palladium catalyst utilized. Totally planar, fully conjugated PAH molecules and ladder polymers are of great interest to materials chemists due to the unique electronic effects born of having such a long uninterrupted π network. Moreover, with the *N*-methyl functionality present in the conjugated ring (regardless of if longer alkyl chains are attached to the outer aryl groups), these nitrogens could be protonated to allow for these fully aromatic rings to be at least somewhat water soluble.

4.5. Shape-Directed Helical Ladder Polymers

While the prospect of growing out the polymers in a step-wise manner had been laid out (and previously afforded with forming tetramer C-shaped strips), we first wanted to first investigate the ability of our building blocks to polymerize directly with the shape-directing units to generate helical polymers directly. Moreover, while running the reaction as a one-pot Suzuki-coupling/imine condensation we would ensure direct ladderization of our polymer rather than having to "zip" the polymer up in a subsequent second step. The ultimate goal of this process, and my own research, is to generate freeform helical ladder polymers. By ensuring this process is functional and with high fidelity and good yields, we could assure that a method for producing shape persistent and well-defined helical polymers was indeed a possibility.

4.5.1. *Syn*-Helix

With the already established CAS monomer diiodo-diamine **4.11** and *syn*-linker **4.13**, we attempted to couple **4.11** in a one-to-one molar equivalence with **4.13** utilizing

the well-established Pd-catalyzed conditions (**Scheme 4.16**). From the resulting Suzuki-coupling/imine formation, we were successfully afforded *syn*-helix **4.30**. Due to the polymeric mixture that resulted from the polymerization, size-exclusion chromatography was used to retrieve the largest polymer units from the reaction mixture. By GPC analysis, it was found that the *syn*-helix had an average of 20 units with a PDI of 1.18—utilizing the number average molecular mass retrieved (M_n = 14,6128 g/mol), it was also found *syn*-helix generation occurred at 41% yield. Considering (on average) 80 reactions have to take place to form a polymer of 20 units, each individual reaction must have taken place at yields over 99%.

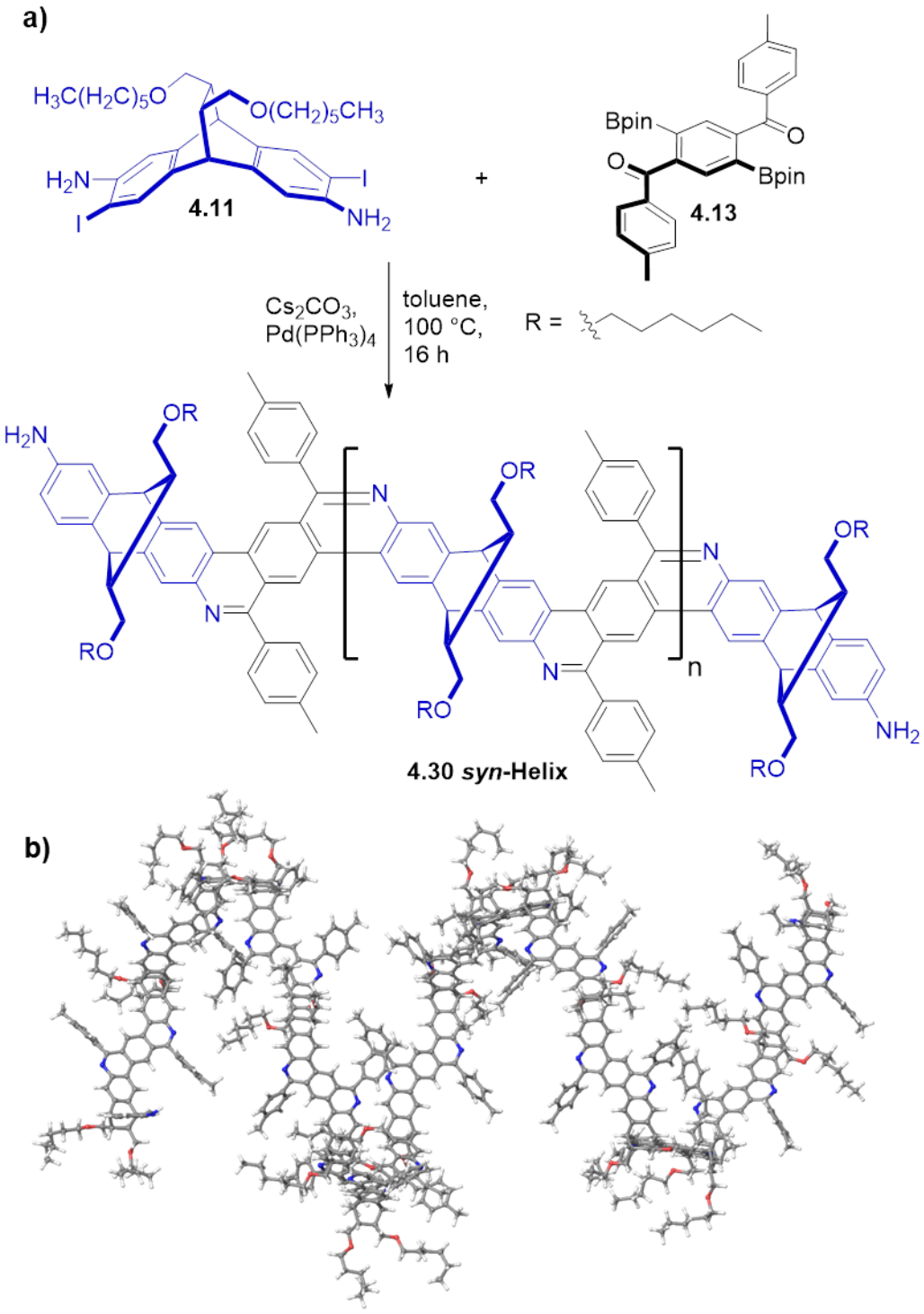

Scheme 4.16. (**a**) Ladder polymerization of in generation of *syn*-helix ladder polymer **4.30**. (**b**) Minimized structure of hexadecamer *syn*-helix.

The process for forming the *syn*-helix polymer **4.30** was a great first success, with good yields and a high fidelity of coupling. The achievement of generating a freeform helical polymer with CAS was a long-sought goal of the Schneebeli group. However, to truly prove the flexibility and adjustability of these Suzuki-coupling/imine condensation reactions, we elected to next try a polymerization with the *anti*-directing linker to generate a helical ladder polymer of a different structure.

4.5.2. *Anti*-Helix

Utilizing the same CAS monomer **4.11**, we looked next at shape-directing linker **4.19**. Again, we exposed a one-to-one molar equivalent ratio of **4.11** and **4.19** to Pd-catalyzed Suzuki coupling conditions (**Scheme 4.17**). Once more, we were successfully afforded with a helical ladder polymer; *anti*-helix polymer **4.31**. Size-exclusion chromatography was again used to obtain the longest polymeric units from the crude mixture. With GPC analysis, the *anti*-helix was found to have an average of 16 units, with a PDI of 1.09—looking again at the number average molecular mass (M_n = 11,081 g/mol), the *anti*-helix synthesis was established at a 40% yield. While the yield was not as high as *syn*-helix **4.30**, with 64 reactions occurring to form a polymer of a hexadecamer average length, each singular reaction still occurred at near 99% efficiency. With long chains of building blocks coupling together, minor differences in % yield (even near 99%) become increasingly evident upon multiple reactions to form polymers.

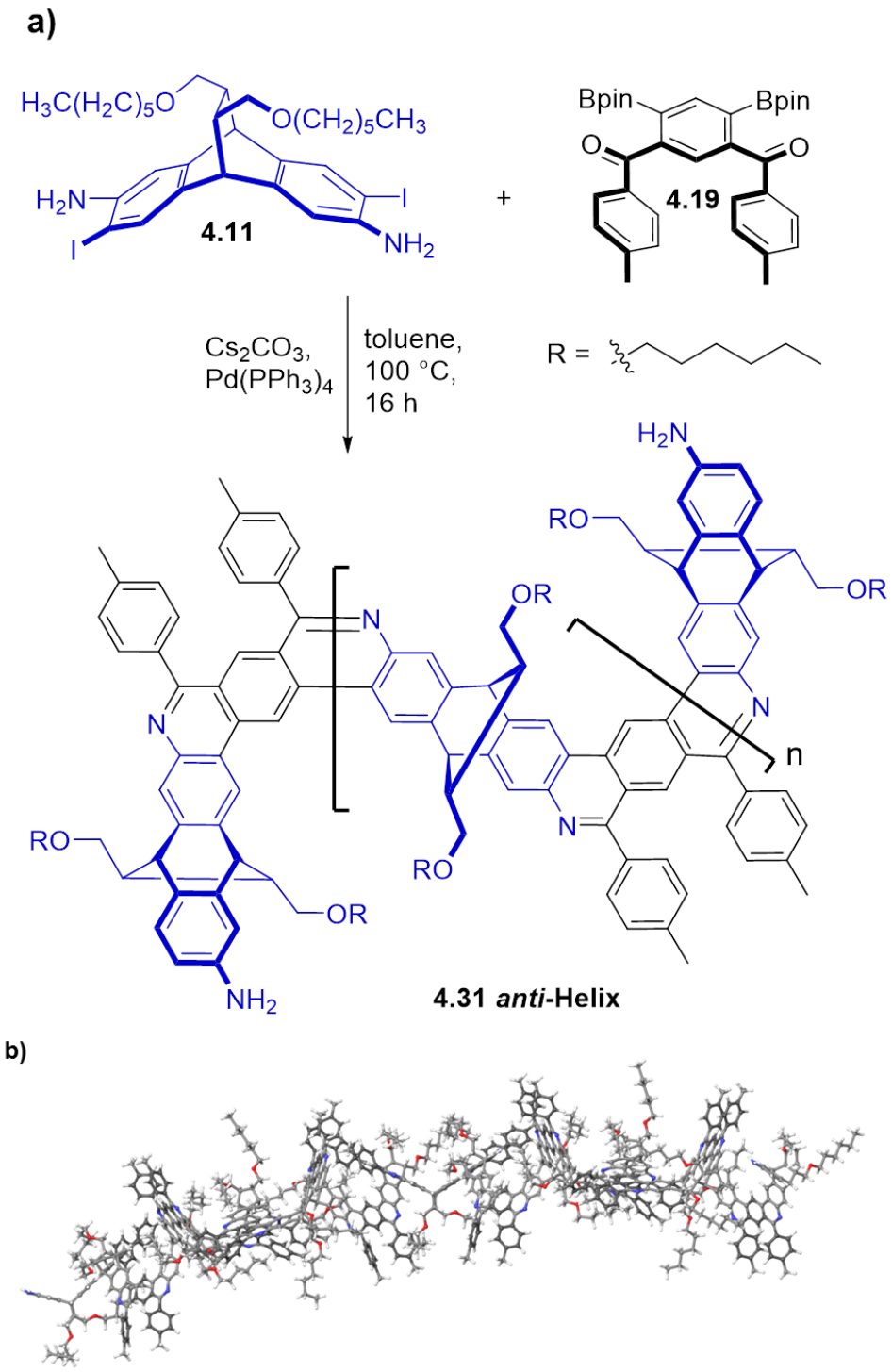

Scheme 4.17. (**a**) Direct ladderization in generation of *anti*-helix ladder polymer **4.31**. (**b**) Minimized structure of hexadecamer *anti*-helix.

With two successful chirality-assisted coupling polymerizations, we thus showcased the powerful capabilities of CAS building blocks married with Suzuki-coupling/imine condensations to form well-defined and shape persistent macromolecular structures. By simply changing the location of reactive groups on the shape-directing linkers, we are afforded with helical polymers of a completely different overall structure. While both helical in nature, the *syn*-helix **4.30** noticeably has a geometry more akin to a spring, while the *anti*-helix **4.31** can be observed as a rigid rod. These clear differences in structure would also lead to differences in their properties. By being able to study the structure-property relationship of these polymers, we can gain valuable insight into how the overall shape of helical ladder polymers affects their behavior. If shape is to define function, then thusly so too must sequence define shape.

Aside from the differences observed by ^{1}H NMR, we looked again to CD spectroscopy to detect what different inherent properties the helices had due to their variance in structure. The concentration of chromophores (the diaza-anthracene junctions) was kept consistent between the two helices (at 0.4 mg per mL in CH_3Cl) to garner the most comparable resultant CD data. In a direct comparison of the polymers (**Figure 4.4.a**) we find that the overall motif of the observed positive cotton effect are somewhat similar with only slight differences in smaller absorbance band peaks and location of the subsequent trough—moreover this positive cotton effect is consistent with a right-handed helical structure.[80, 167, 168] With a very intense bisignate couplet with a negative band at around 300 nm and a positive peak around 330 nm, this is also reminiscent of a helical motif.[163] Then, by comparing each polymer with their respective

dimer unit, we can see that the general absorbance bands are very similar with a red shift of the initial positive band of the bisignate couplet for the polymer spectra—red-shifting is an indicator of aggregation which, in a general sense, is essentially what the polymers are structurally in relation to their dimer components. Interestingly, the *syn*-helix displays more of a red shift than the *anti*-helix which, given the more coiled structure of the polymer, makes sense as this compressed state would lead to more $\pi \rightarrow \pi^*$ transitions (**Figure 4.4.b**). The presence of small bands around 400 nm indicates the presence of amine groups on aromatic rings, which seem to be far reduced for the *syn*-helix yet interestingly not the *anti*-helix. In a general sense, this structural association with each helical polymer to their respective dimer is not unimportant, as it aids us in identifying the polymers specific geometry and allows us to make justifiable comparisons to the well-defined dimers. By introducing chiral amide groups to the periphery of our helices, whose conformation could be readily changed by the polarity/donor character of a solvent, we could perhaps see an extension/compression upon solvent change through CD spectroscopy alone.[80]

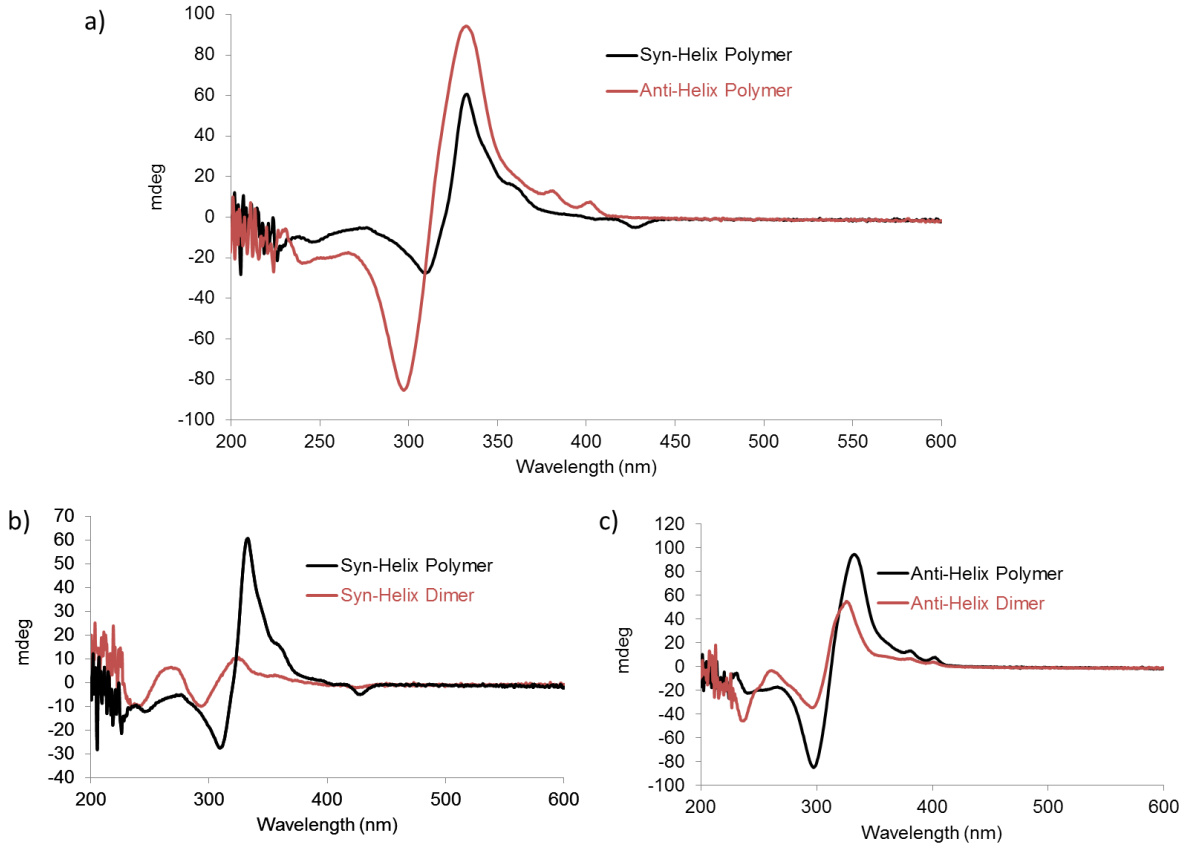

Figure 4.4. CD spectra comparison of (**a**) the *syn*- and *anti*-helices, (**b**) the *syn*-helical polymer **4.30** and dimer **4.22**, and (**c**) the *anti*-helical polymer **4.31** and dimer **4.21**.

4.5.3. DOSY Analysis

Diffusion-ordered NMR spectroscopy (DOSY) is an strategic tool for chemists to analyze polymers, both synthetic and biological.[169-171] With some geometric assumptions of sphere-like particles, the diffusion coefficients of polymers can be plugged into the Stokes–Einstein equation for determining their approximate length through solving for their radius (**Figure 4.5**). The diffusion coefficient (D) is inversely related to the hydrodynamic radius (r) and solvent viscosity (η). However, this equation does not hold

up well when dealing with particles that are over five times the radius of the solvent molecules (e.g. $CDCl_3$).[171] Instead, we elected to examine acquired DOSY data by way of the modified Stokes–Einstein equation developed by Torre and co-workers,[172] which assumes that the polymer in question is a rigid rod with a length-to-width ratio (*p*) no less than two. While this is true more so for the longer rod-like structure of the *anti*-helix based on computational predications, the *syn*-helix falls just over this *p* value lower limit. Utilizing two different equations (assuming a sphere-like particle for one, and a rigid rod for another) would also be problematic, so for the sake of consistency we utilized the better performing equation modified by Torre.

$$D = \frac{k_B \cdot T}{6\pi \cdot} \qquad\qquad D_t = \frac{1}{3} \cdot \frac{k_B \cdot T \cdot (\ln p + C_t)}{\pi \cdot}$$

Figure 4.5. Stokes–Einstein equation for determination of the hydrodynamic radius of a sphere (*r*) and modified equation by Torre and co-workers for determination of the length of a rod (*L*), respectively.

Due to worries of self-aggregation, a common property of polymers,[173, 174] we elected to analyze each polymer by DOSY ^{1}H NMR at relatively dilute amounts (0.4 mg / 0.75 mL $CDCl_3$) so as not to have longer observed lengths due to the formation of helical bundles. A *p* of 2 for the *syn*-helix as well as 2 for the *anti*-helix was assumed, which we anticipated to be a reasonable assumption given their predicted structures—while certainly the *anti*-helix would be have a larger length-to-width ratio, we did not want to change too many variables between polymers which would arbitrarily create differences between them. Based then on their diffusion coefficients (D), the *syn*-helix (D = 2.55 x

10^{-10} m^2s^{-1}) was found to have a length of 4.08 nm and the *anti*-helix (D = 2.30 x 10^{-10} m^2s^{-1}) a length of 4.50 nm.

In a similar fashion, utilizing well-established standards of polystyrene, one can also approximate the corresponding molecular weight of a polymer by placing its resulting diffusion-ordered peaks onto the produced polystyrene calibration curve (**Figure 4.6**).[170] While the protocol set is for determining average molecular weight, in reality the measurements obtained from the calibration are more so for the length of a polymer—we can compare a polystyrene molecule of a particular molecular weight to our own polymers and, from the length of the polystyrene, we can determine how long our polymers should be. This, married with GPC analysis, and polymer length observed via the Stokes–Einstein equation, we can obtain a more accurate representation of how many units exist within our helical polymers.

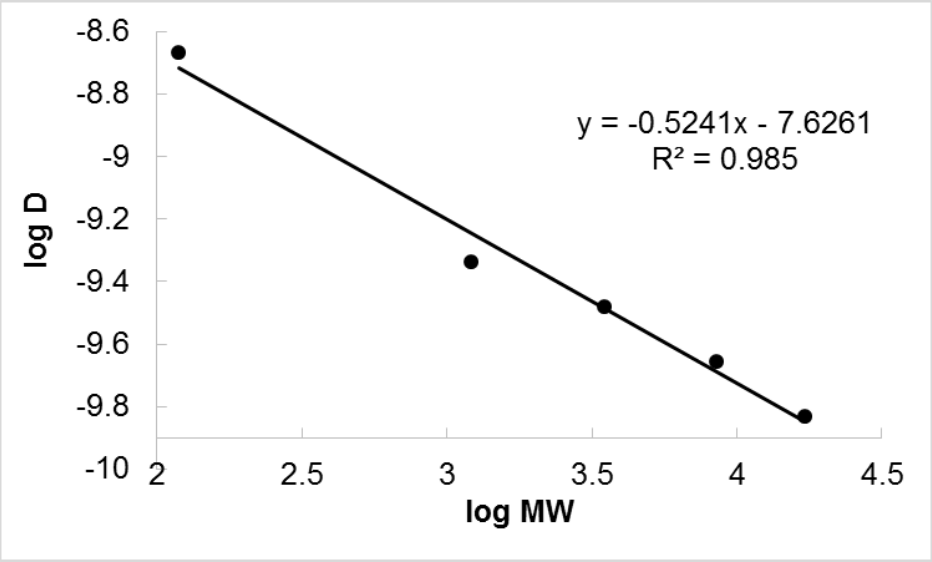

Figure 4.6. Polystyrene calibration curve in $CDCl_3$ for M_w prediction. Polystyrene standards used were of molecular weights 1220, 3510, 8560, and 17 300 g/mol.

Extrapolating the calibration curve, the M_w for $CHCl_3$ was found to be 98 g/mol, with about a 12% difference from its calculated value—this shows the power of a polystyrene calibration tool even for small molecular weight molecules. As compared to the *syn*- and *anti*-helices upon inputting their diffusion coefficients, the calibration curve showed a molecular weight of 5673 and 7518 g/mol respectively. When compared to the length of the closest styrene polymer match through computational predications, the *syn*-helix was found to be of 21 units long, and the *anti*-helix of 17 units long.

An interesting observation from the lengths calculated by the Stokes–Einstein equation is that the *syn*-helix is much shorter than the *anti*-helix. What makes this difference in length so interesting is that the *syn*-helix was experimentally determined to be 4 units longer than the *anti*-helix. This dramatic difference between the two polymers can be explained by their structural differences which accounts for the intriguing shorter nature of the *syn*-helix. The *syn*-helix has a much smaller helical pitch and larger outer diameter, resulting in it being more wound than its regioisomer *anti*-helix which has a larger helical pitch and smaller outer diameter and thus is comparatively longer due to these geometric constraints alone. This gives credence to not only the computationally predicted helical shape of these polymers, but also the potential of the *syn*-helix to have behavior much like a spring, and conversely the *anti*-helix to have performance akin to a rigid rod.

4.6. Iterative Sequence-Defined Polymers

To fully showcase the potential of these chirality-assisted coupling reactions in building helical ladder polymers, we attempted to generate helical strips of different

lengths. By starting from monomer **4.9**, we can synthesize the *syn*-dimer **4.16**, and following a similar deprotection, monoprotection and iodination strategy that lead to the formation of **4.14**, we can form the tetramer. Potentially, one can continue this process of iterative coupling to generate longer and longer helical macrostructures. The advantage of utilizing an iterative step-wise procedure over step-growth is that that number of units within the helix generated is exactly known. This can lead to a host of investigations into the properties of these helices, provided they are of a singularly size rather than a multitude of varying units. In particular, single-molecule pulling experiments utilizing AFM[174-177] can be accurately done to determine mechanical strength, retention of elasticity, and overall spring-like nature of these well-defined helical polymers.

4.6.1. Helical Tetramer

To begin, we started from *N*,*N'*-di-Boc protected *syn*-dimer **4.15**, exposing the helical strip to TFA to induce full deprotection and form diamine *syn*-dimer **4.22** (**Scheme 4.18**). From there, **4.22** was treated with one equivalent of Boc anhydride to give a statistical mixture of di- and mono-Boc protected products, and recovered starting material, of which mono-Boc dimer **4.32** was obtained in 73% yield. With one active aniline site, **4.32** was exposed to electrophilic iodine in the form of ICl to afford monoiodo-monoamine-mono-Boc **4.33**. Again, while several synthetic steps are required to afford the reactive precursor to the next coupling step, it is advantageous over attempts to monoiodinate at the diamine stage because there are no side-product-inducing imines that can form from free amines during the subsequent coupling phase, thus granting a

higher yield. Moreover, di-Boc side product can be easily deprotected with TFA to converge with the recovered diamine starting material to ensure no potential product is wasted.

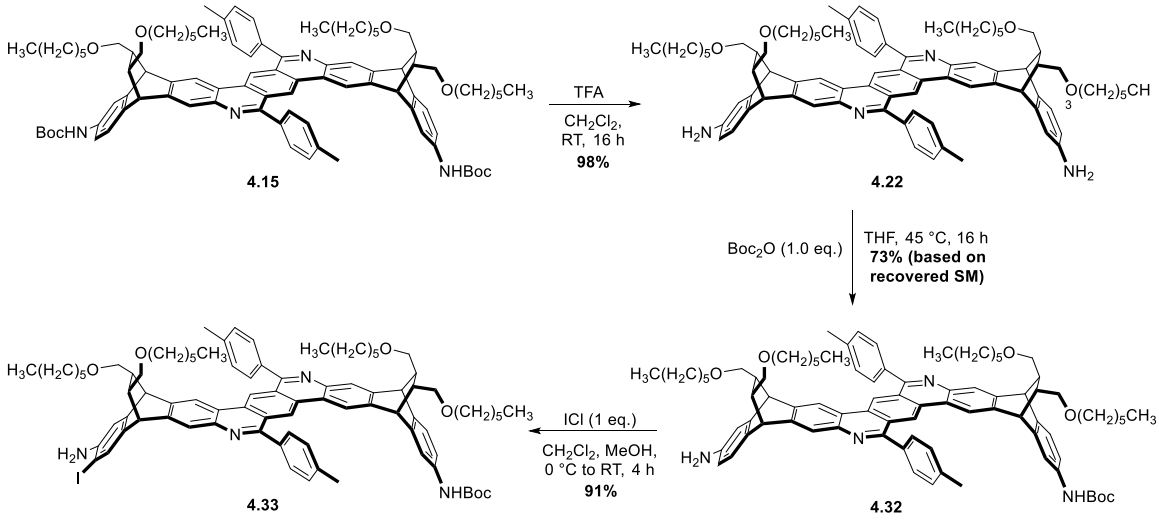

Scheme 4.18. Synthesis of *syn*-helix dimer CAS building block, **4.33**.

With the CAS-reactive dimer in hand, we next attempted to generate the *syn*-helical tetramer following the same Suzuki-coupling/imine condensation strategy (**Scheme 4.19**). Monoamine-monoiodo dimer **4.33** was thus treated with pre-established Pd-catalyzed conditions alongside *syn*-linker **4.13** to successfully afford *N,N'*-di-Boc protected *syn*-helical strip tetramer **4.34**. Based on simple MD simulations, the *syn*-tetramer is just over half a helical turn, though still with ample space between the terminal ends to allow for continued growth. With the goal in mind of producing a well-defined molecular helix of a singular turn to pursue single-molecule pulling experiments and probe for spring-like characteristics, we next set out to synthesize the *syn*-helical octamer.

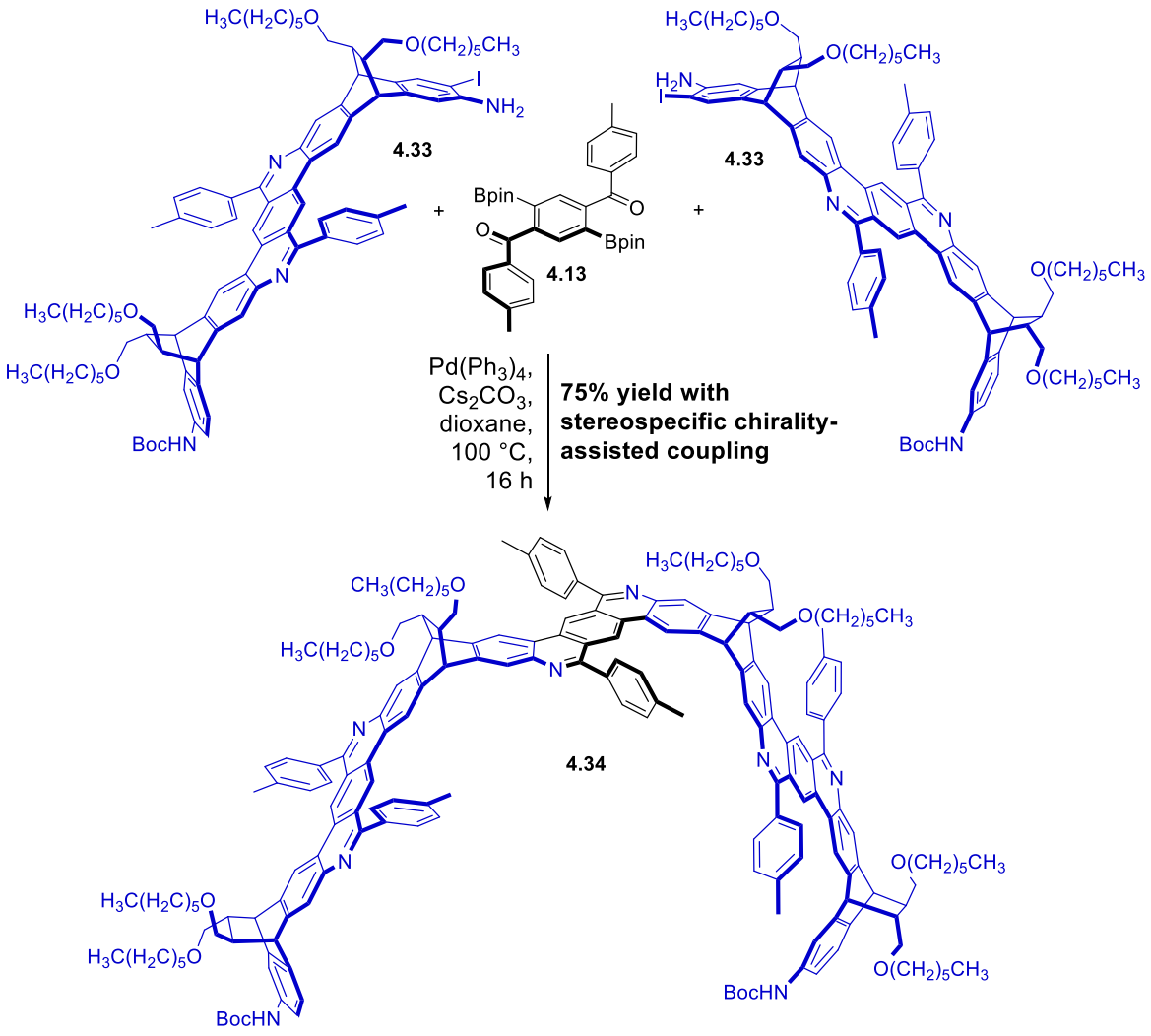

Scheme 4.19. Chirality-assisted coupling of *syn*-helical CAS dimer **4.33** to form *syn*-helix tetramer **4.34.**

4.6.2. Helical Octamer

For the next round of synthetic preparation, we started from *syn*-tetramer **4.34**, exposing the helical strip yet again to TFA to thus fully deprotect it and form dianiline *syn*-helical tetramer **4.35** (**Scheme 4.20**). From there, **4.35** was treated with just over one equivalent of Boc anhydride to give a statistical mixture of di- and mono-Boc protected

products, and recovered starting material, of which mono-Boc dimer **4.36** was obtained in 75% yield. As a note of interest, several rounds of gathering the di-Boc side product, deprotecting, and combined with recovered (unprotected) diamine to yet again mono-Boc protect the tetramer were done in order afford enough material to carry through to the final halogenation and subsequent coupling step. Now with only one free amine site, mono-Boc-protected **4.36** was exposed to ICl to regioselectively iodinate *ortho* to the aniline and afford reactive precursor monoiodo-monoamine **4.37**.

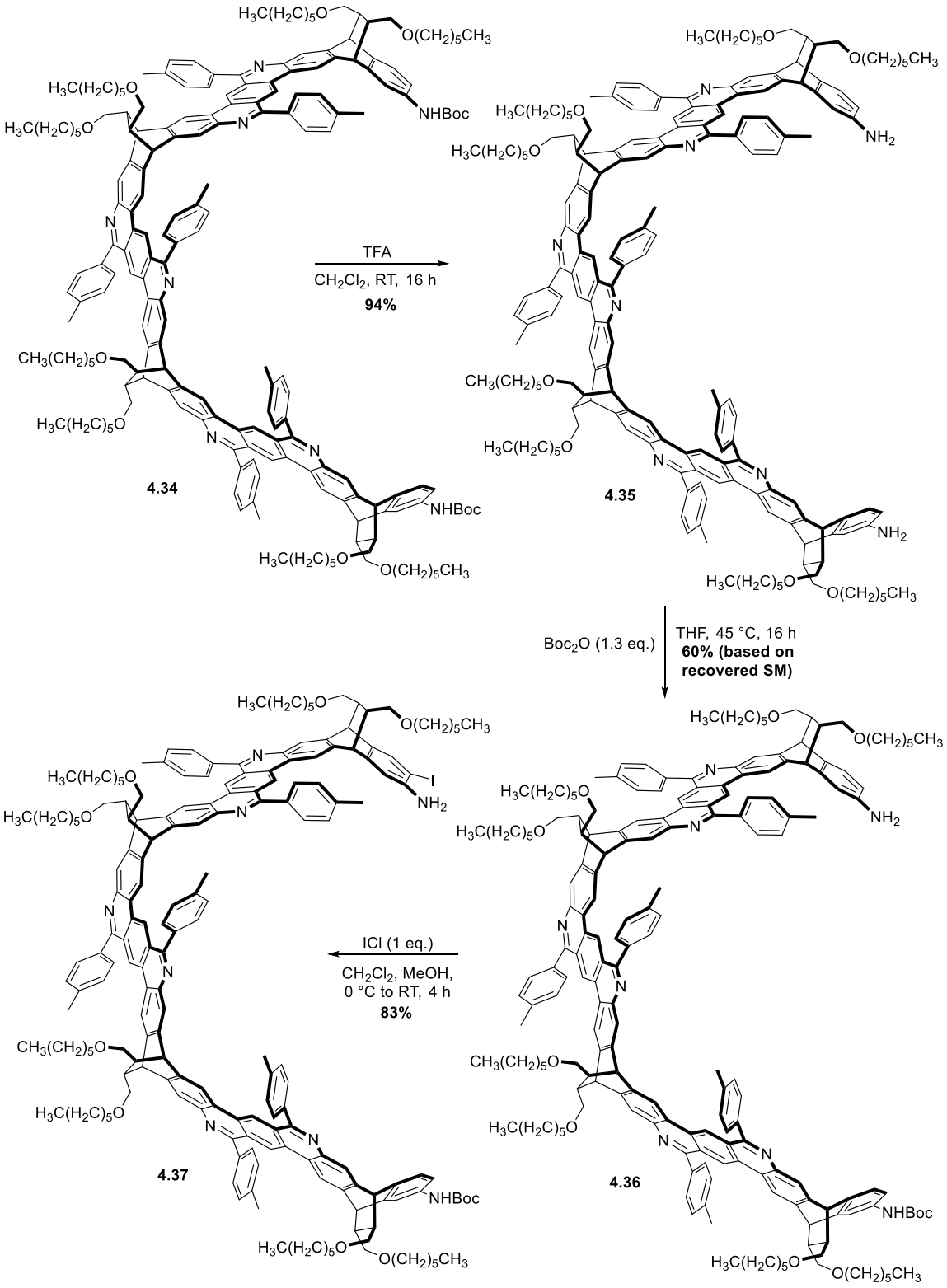

Scheme 4.20. Synthesis of *syn*-helix tetramer CAS building block, **4.37**.

Now with the CAS tetramer in hand with only one active *ortho*-iodo aniline site, we optimistically approached the next coupling attempt to form the single-helical-turn *syn*-octamer (**Scheme 4.21**). Two equivalents of tetramer **4.37** along with one equivalent of shape-directing unit **4.37** were treated with the well-established Suzuki-coupling/imine formation conditions in an attempt to generate *syn*-helix octamer **4.38**. First trials in generating the octameric species were not successful due to the minimal amount of starting material **4.37** (< 3 mg) available to work with, whereby any present impurities may have hindered CAS couplings. Nonetheless, with the octamer helix pushing past a single helical turn, it is suspected to be a great candidate of first single-molecule pulling studies. The *syn*-octamer could be investigated in this fashion for a deeper understanding of the spring-like properties that these helical strips and polymers possess. Moreover, we suspect that utilizing the *anti*-linker unit would provide similar success in synthesizing well-defined *anti*-helical molecules of an exactly known length utilizing a step-wise procedure.

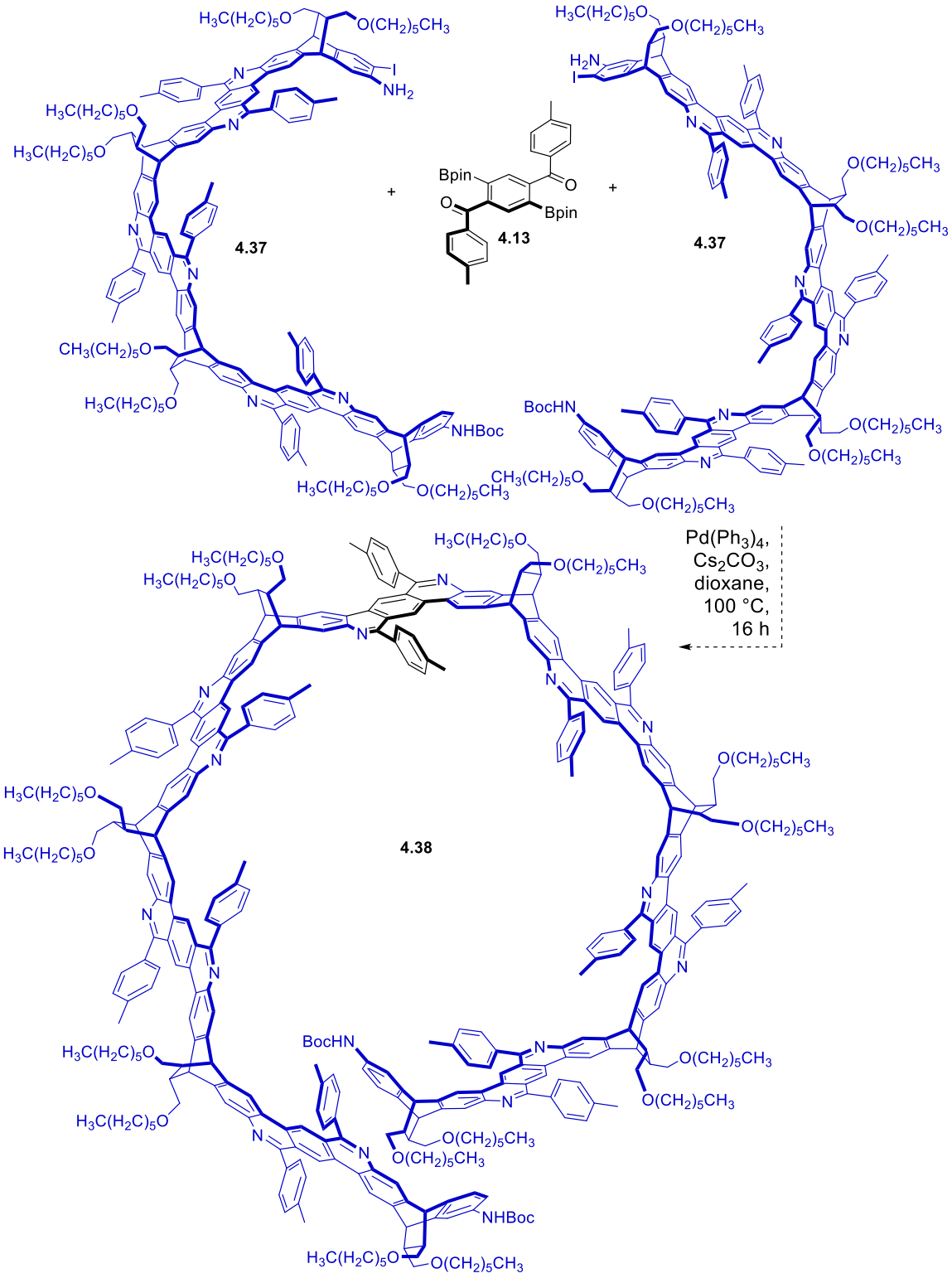

Scheme 4.21. Proposed chirality-assisted coupling to generate *syn*-helix octamer **4.38**.

We were able to generate *syn*-helical tetramer **4.34** utilizing an iterative growth strategy, as well as showcase a synthetic pathway toward the syn-helix octamer **4.38**, all while retaining a shape-persistent structure that CAS inherently provides as a highly efficient coupling tactic. It appeared, upon first trials, that coupling together larger pieces (rather than just CAS monomers) saw a slight decrease in yields. A larger scale-up of the building blocks would be required to generate longer, yet longer ladder polymer helices. A hexadecamer helix in particular would be of a similar average unit length observed for the polymeric mixture **4.30** by GPC (around 20 units), and with over two turns of a helical backbone it would be a great synthetic pursuit for subsequent aforementioned single-molecule investigations. Moreover, while polymerization saw a 20-mer helix has the average length, we may be able to mitigate terminal length issues or eventual catalyst failing by selectively coupling large, exactly known, helical units together to continue to grow the helical polymers to a size we so choose.

4.7. Investigations into Spring-like Motion

Unlike other ladder polymers,[12, 15] ours exhibit semi-flexible spring-like behavior. We employ a helical platform where the pitch can readily be adjusted by external stimuli without unfolding, (unlike most biomimetic polymers). Nitrogen sites allow us to now explore such effects for the first time experimentally. These ladder polymers are programmable, as during the coupling process using different achiral linkers with the same chiral building block piece affords helices with different average pitches and diameters. Depending on the exact geometry of the helix, we observe different stiffness.

The structure of our polymer also affects its mechanical properties. In the case of the *syn*-helix **4.30**, the backbone compresses and expands, resulting in unidirectional motion like a spring. Our *anti*-helix **4.31** remains mostly stiff, and while it does exhibit some unidirectional movement, it does not undergo the same degree of motion as with the *syn*-helix, which we observe in relaxation data and computational analysis.

4.7.1. Environmental Stimuli to Induce Spring-like Behavior

Introducing an external stimuli (diacid) causes the ladder polymer to compress, while removing the stimuli via quenching allows the helix to relax back to its original state. The nitrogen sites on our helical platform allow us to investigate these unique properties for the first time. The structure of our polymer also affects its mechanical properties. In the case of the *syn*-helix, the backbone compresses upon diacid addition and expands upon quenching, resulting in unidirectional motion. Our *anti*-helix remains mostly stiff and does not undergo the same degree of motion upon addition and removal of the stimuli. Thus, the specific geometry of our ladder polymers determines their smart mechanical behavior.

Initial thoughts on providing evidence for this smart behavior was utilizing TFA to induce compression/extension. With diaza-anthracene junctions connecting the monomer units, the nitrogen atoms with lone pairs orthogonal to the conjugated system were predicted to become protonated upon addition of TFA and cause repulsive behavior between the helical turns of the *syn*-helix backbone, extending it. The *anti*-helix, however, would remain mostly stiff and remain unaffected. We could then quench the

protonated helices, and observe that the *syn*-helix had returned to its original length, showcasing its spring-like properties, while the *anti*-helix still more or less remained the same length.

The initial plan was to use the aforementioned strategy on determining length by DOSY ^{1}H NMR analysis through extension/compression via TFA addition and subsequent quenching. First trials proved difficult to analysis, as it was unclear whether TFA addition was causing the helices to extend or aggregate which would cause a change in viscosity—DOSY analysis is often done on polymers to investigation their propensity for self-aggregation.[178] Instead, we turned again to CD analysis, this time to determine if, after TFA quenching, the helical polymer would return to its original state (**Figure 4.7**). Once again, difficulties emerged due to potential for self-aggregation. While the general motif across the CD spectra remained the same, a significant increase in positive cotton effect at around 350 nm occurred for both helices after TFA addition, but subsequent quenching and analysis revealed no change. Induced aggregation may have occurred that was unable to disaggregate following quenching without other means of separation. Moreover, there was a clear red-shift of this bisignate couplet, indicating (as aforementioned) strong aromatic stacking; substantially more evident for the *anti*-helix where (given its rod-like structure) it has more surface area to undergo aggregation. While certainly we could force the polymers apart, this would not prove the *syn*-helix's spring-like behavior as aggregation seemed to be the result of the environmental stimuli, not compression/extension.

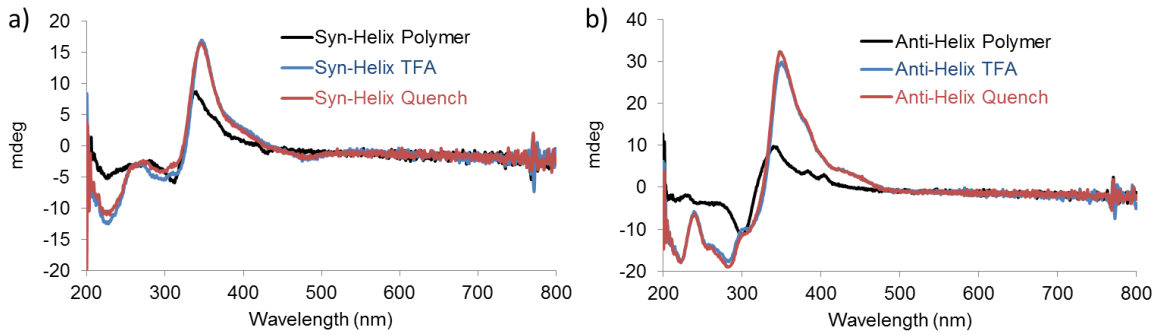

Figure 4.7. CD spectral analysis of (**a**) *syn*-helix and (**b**) *anti*-helix before and after TFA addition.

Next, we attempted to restrict the protonation sites that would occur from acid addition. With TFA, it would be impossible to control which nitrogen sites were affected, however by introducing a rigid diacid system (e.g. 4,4'-biphenyldisulfonic acid) we could more accurately probe the inner helical turns and create a link between parallel aza-anthracene nitrogens and force the overall helical structure of the *syn*-helix to compress (**Scheme 4.8**). Subsequent quenching with an organic base (e.g. Et_3N) would hypothetically revert the system back to its original length, thus showcasing our helix's spring-like behavior while with the *anti*-helix, without a small enough helical pitch to have the addition of the rigid diacid effect it, would remain largely unchanged.

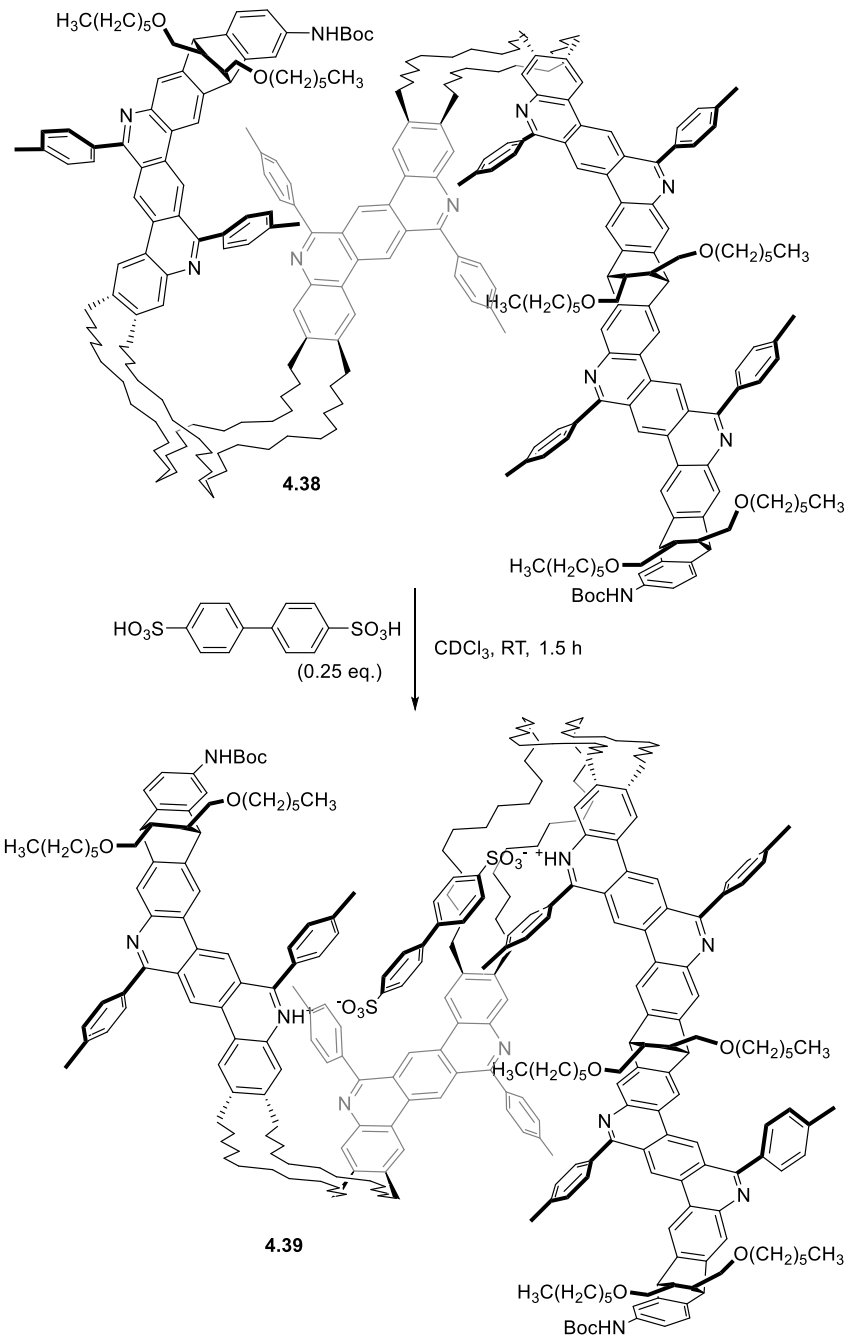

Figure 4.8. Proposed addition of rigid 4,4'-biphenyldisulfonic acid would induce compression along the helical backbone of the *syn*-helix. Model is octamer *syn*-helix **4.38**, and has some periphery groups removed.

Molecular dynamic simulations were run to first analysis the effects of introducing the rigid diacid to each polymer (**Figure 4.9**). It was found that for a hexadecamer *syn*-helix (**Figure 4.9.A**) the stiff diacid introduced (**Figure 4.9.B**) severely restricted its ambient spring-like motions based on end-to-end distance analysis.(**Figure 4.9.C**) When compared directly to the octamer *anti*-helix (**Figure 4.9.D**), addition of diacid (**Figure 4.9.E**) was found to have essentially no effect on the overall motions of the structure (**Figure 4.9.F**). With this information in hand, we attempted to run similar DOSY experiments with diacid addition (equivalents based on the number of chromophore units in a mass amount of both polymers) and subsequent quenching to show the compression/extension of the *syn*-helix. Unfortunately, we found that there was little to no change in the system for both the *syn*- and *anti*-helix. By adding extra equivalents of the diacid, we feared we would face similar problems of being unable to tell whether aggregation (or a change in viscosity) was occurring rather than compression/extension.

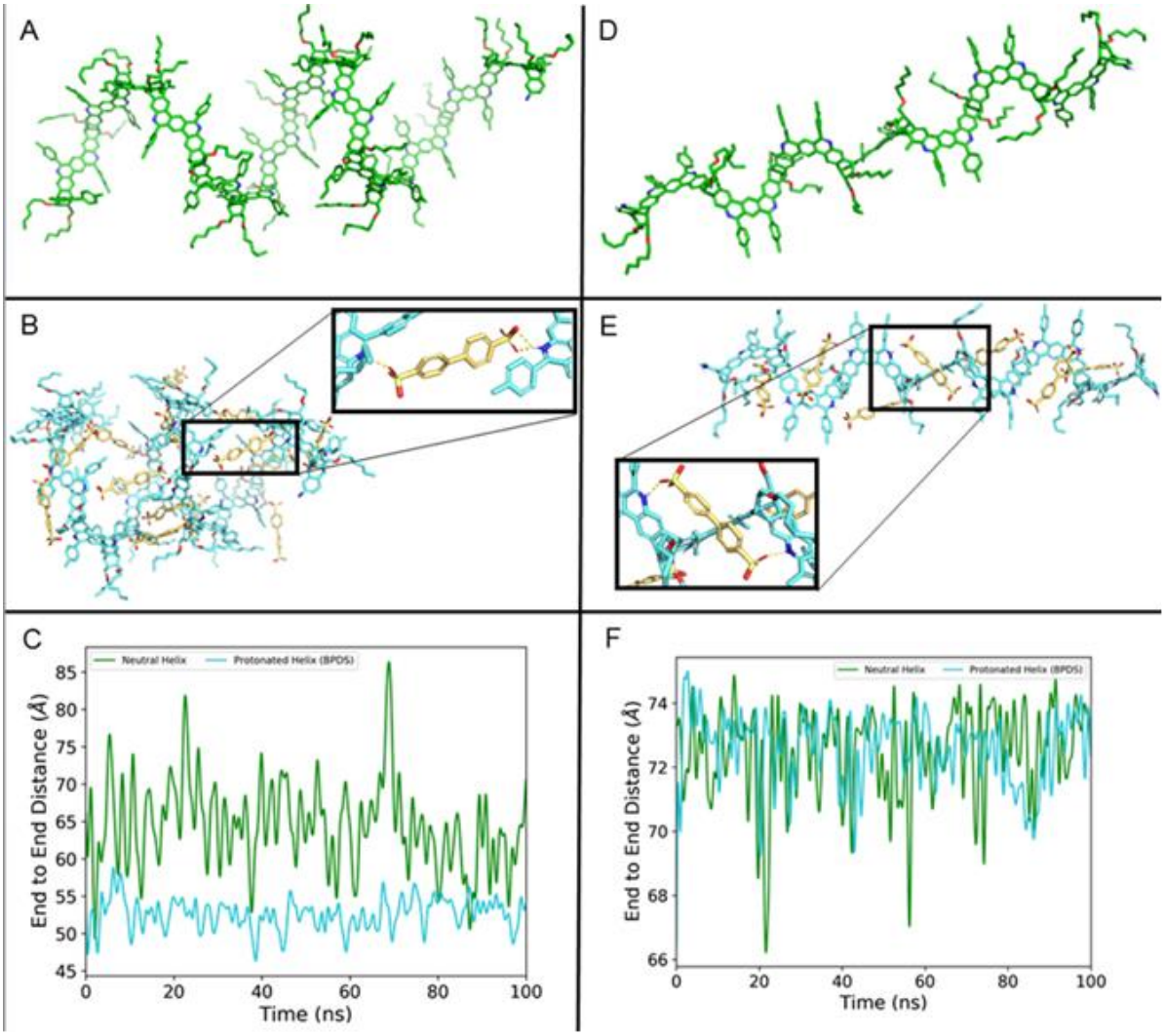

Figure 4.9. MD simulation of (**A**) hexadecamer *syn*-helix and (**D**) octamer *anti*-helix with subsequent (**B**,**E**) addition of 4,4'-biphenyldisulfonic acid with a (**C**,**F**) comparison of their respective end-to-end distances.

4.7.2. MD Analysis of Helical Polymers

With the unfortunate, inconclusive results from probing the *syn*-helix for its behavior under different environmental stimuli, we found that the resulting MD

simulations were particularly helpful in observing the structure-property relationship of both *syn*- and *anti*-helices. While, certainly, it appeared that a rigid diacid introduced would decrease the overall pitch of the *syn*-helix and leave the *anti*-helix mostly unchanged, we were interested instead at comparing the ambient motions of both helices without any introduced stimuli. This would allow us to run experimental investigations without utilizing external stimuli that may cause self-aggregation to occur with the polymers while still directly comparing the results to MD simulations.

Indeed, it was found that the *syn*-helix participated in more flexible spring-like motions than the *anti*-helix. In a comparison of the two hexadecamer helices, the end-to-end distances[179] of the *syn*-helix fluctuated much more readily than the *anti*-helix, which was found to stay relatively rigid on a scale of 200 nanoseconds (**Figure 4.10**). This seemingly small difference in molecular motions are not unimportant, as even without provocation by an external stimuli, our *syn*-helix underwent behavior not unlike a spring and the *anti*-helix was found to behave much like a rigid rod.

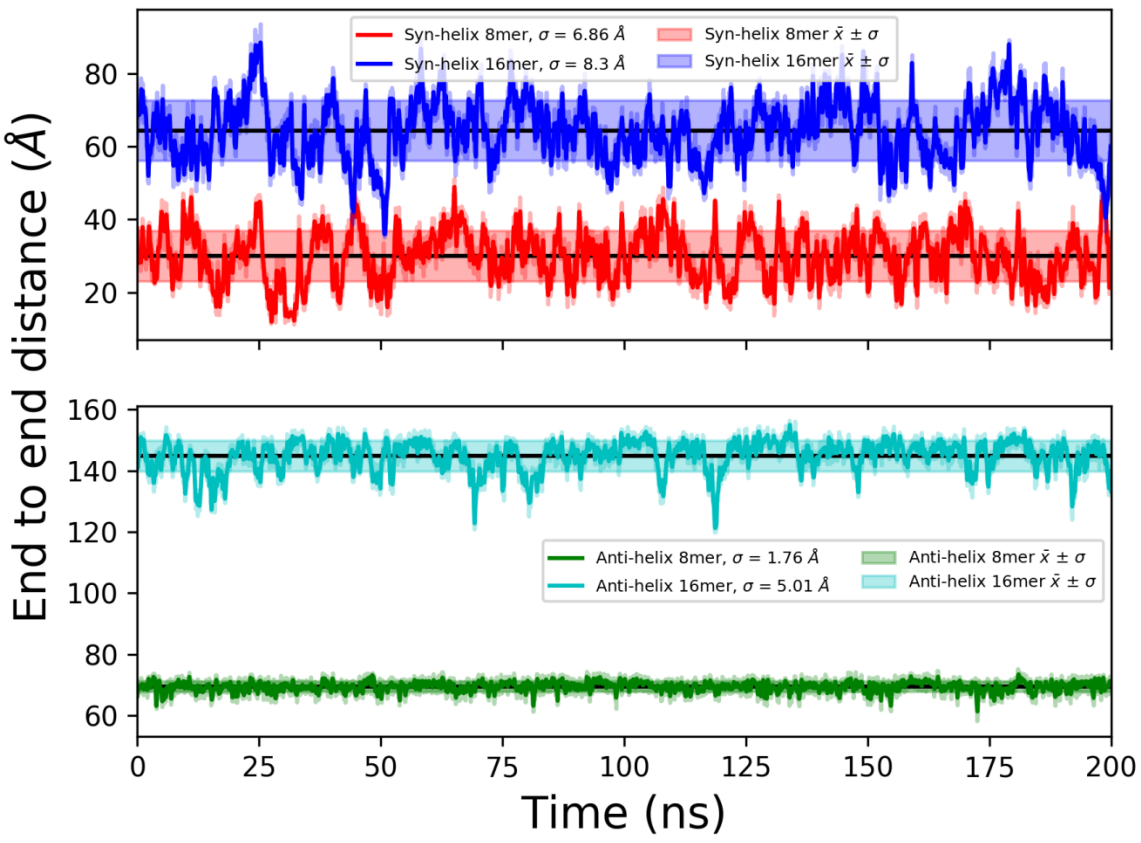

Figure 4.10. End-to-end distance fluctuations of both octamer and hexadecamer *syn*- and *anti*-helices.

Next, the persistence length of both polymers were analyzed through similar MD simulation work (**Figure 4.11**).[180, 181] Persistence length (L) is polymer stiffness and can be readily estimated by measuring the angles between the vectors of each residue-to-residue distance. The persistence length graph shown below displays average angle vs "residue step" along the helical backbone. The residue step is equivalent to which vector that is being projecting, so at step = 0 the same vector is being projected onto itself (e.g. this value always equals 1), at step = 1 then the angles between all vectors created by

measuring the first residue's residue-length from each other is being measured, and so on. For reference, the *L* value for double stranded DNA is around 390 Å,[182] meaning it is quite flexible in comparison to the *syn*-helix which has an *L* several times larger, however the *anti*-helix is several times larger than this. Thus, through several MD simulations, it is shown that the *anti*-helix has much more inherent rigidness based on its structure in compassion to the *syn*-helix which has a flexible structure-property relationship.

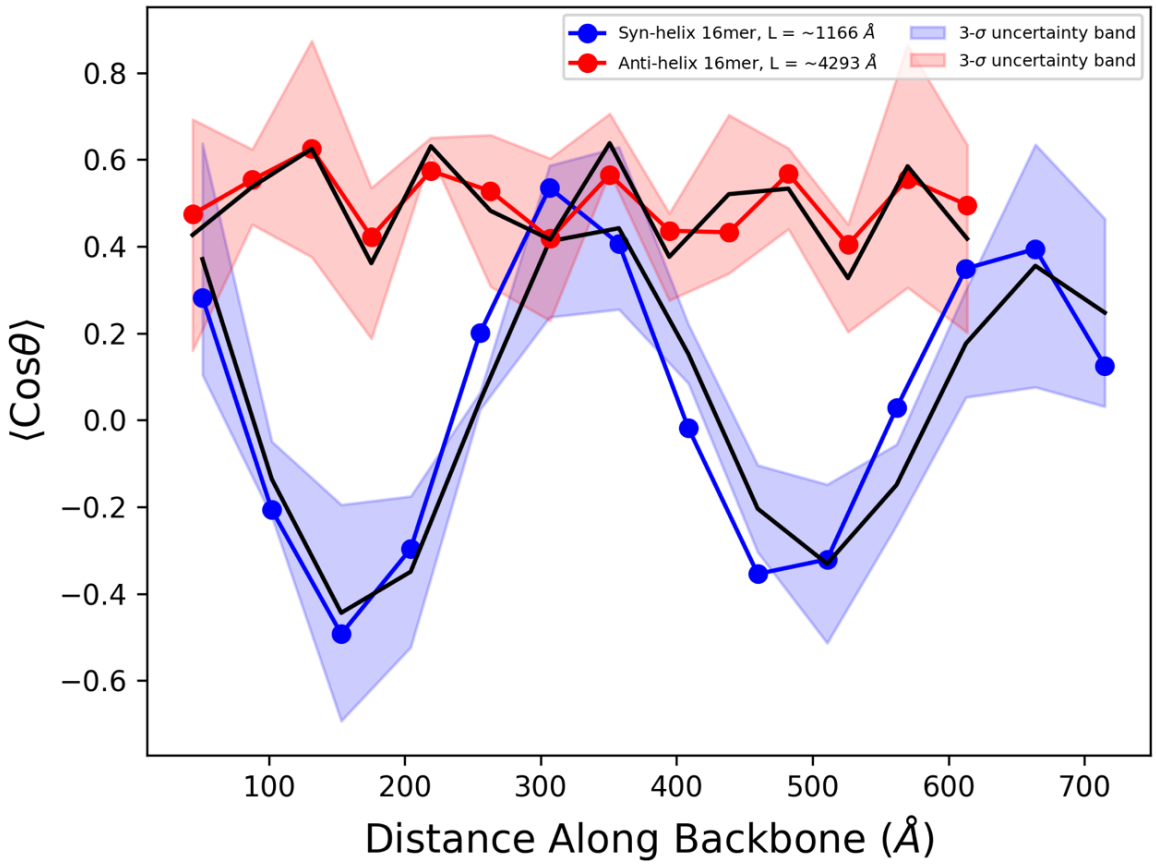

Figure 4.11. Persistence length (*L*) of hexadecamer *syn*- and *anti*-helix.

4.7.3. Fluorescence Lifetime

Both *syn*- and *anti*-helical polymers were investigated for their fluorescence lifetime, i.e. how long each particular polymer remained in their excited state before returning back to their ground state. In general, more rigid molecules tend to fluoresce more intensely due to a lack of non-radiative decay processes they can go through,[183] thus most reference dyes used for fluorescence lifetime and imaging used are non-flexible and conjugated molecules, such as rhodamine. With this in mind, we expected to find that *anti*-helix polymer fluoresced more due to its rigid rod-like structure as compared to the spring-like *syn*-helix polymer. Rigid conjugated polymers have shown great promise in the field of chemical sensing due to their superior performance in producing observable optical or electronic effects from a chemical signal as compared to non-rigid polymer systems.[184] Persistent fluorescent materials in general are very sought after in the field of biological imaging—molecular probes with consistent and well-defined lifetime decay can be greatly utilized in receiving diagnostic information (e.g. treatment-response monitoring, functional imaging for cancer, etc.) from specific biological events that perturb the luminescent material. Diffuse optical imaging in particular is a newer method with lifetime-based devices available,[184] though fluorescence decay technology is not still without its own challenges.[185]

Following excitement with a 375 nm laser at RT, both the *syn*- and *anti*-helix were compared in a solution of $CHCl_3$ for their resulting emission spectrum (**Figure 4.12**). While the exact molarity of the polymeric mixtures were unknown, similar to CD experiments the mass of each polymer in solution was kept identical to keep the number

of fluorophores (the conjugated diaza-anthracene-type junctions) the same. It was found that, indeed, the *anti*-helix polymer fluoresced more intensely than the *syn*-helix. As expected, the more rigidified backbone of the *anti*-helix proved to marginalize the number of non-radiative pathways and result in an increase of subsequent fluorescence.

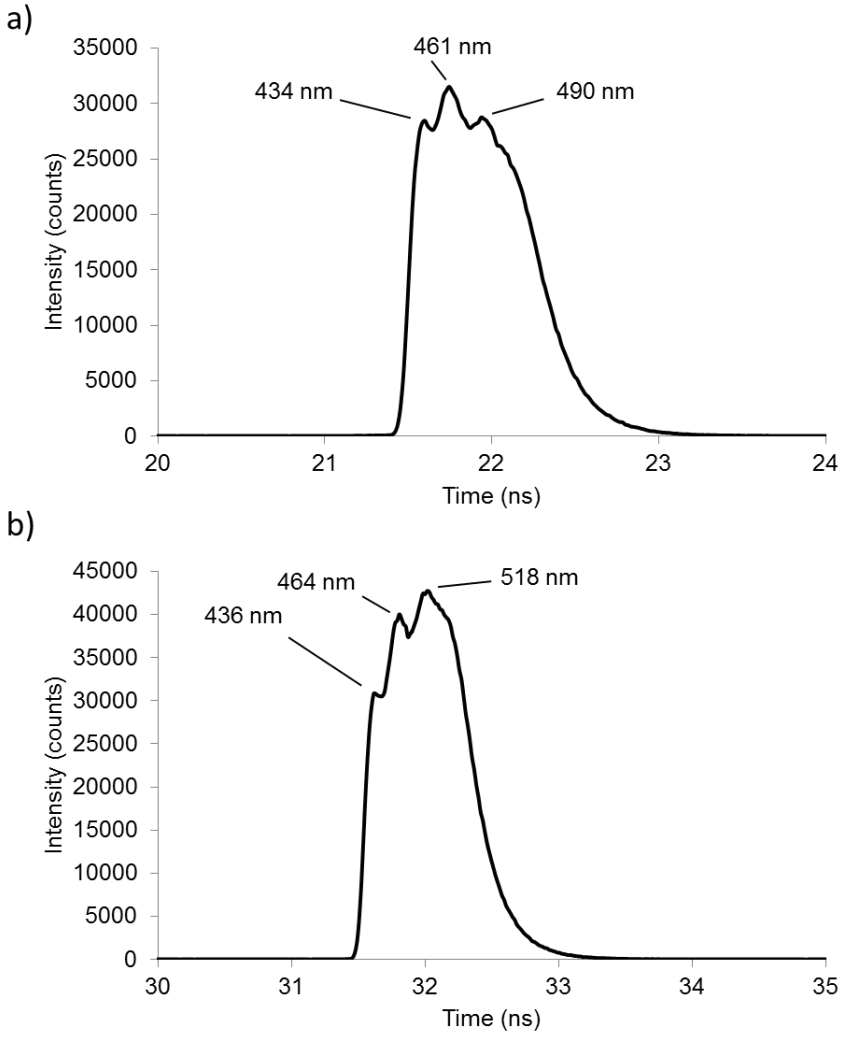

Figure 4.12. Fluorescence emission spectrum at 375 nm excitation of (**a**) *syn*-helix **3.30** and (**b**) *anti*-helix **3.31** polymers at RT in $CHCl_3$, with about 0.042 mM concentration (0.05 mg / mL) based on diaza-anthracene junction fluorophores.

Moreover, the fluorescence lifetime (lifetime decay) of the most intense emission spectrum for each polymer was monitored as well (**Figure 4.13**). After an initial excitement by the 375 nm laser, each polymer gave a resulting emission spectrum. We were able to observe each most pronounced emission wavelength specifically to see what their respective lifetime was. For the most intense emission wavelength for each polymer (518 nm for the *anti*-helix, and 461 nm for the *syn*-helix) we found that the *anti*-helix had a much longer lifetime decay of 52 ns versus the *syn*-helix's decay of 13 ns (**Figure 4.13**). This too corroborates well with more rigid molecules, which have often been found to give a much longer fluorescence lifetime than with flexible polymers.[186, 187] Long-lived lifetimes of 20 to 90 ns are desirable in organic dyes, moreover naturally occurring fluorescent proteins have a lifetime of 4 ns,[186] therefore fluorescent imaging techniques seek organic dyes that have a longer lifetime than competing proteins which produce an autofluorescence background.[188]

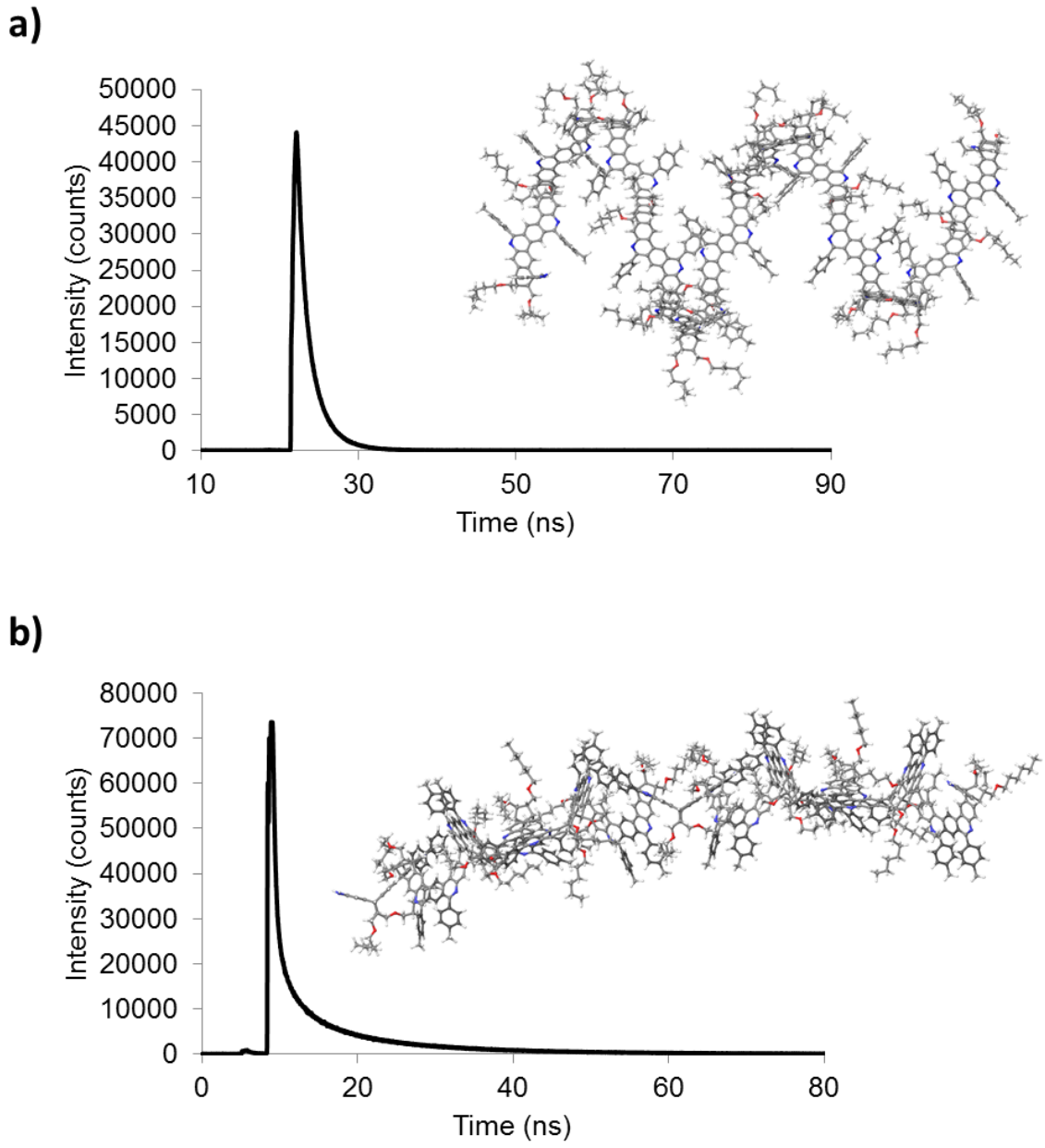

Figure 4.13. Fluorescence lifetime of (**a**) *syn*-helix **3.30** at 460 nm and (**b**) *anti*-helix **3.31** at 518 nm with lifetimes of 13 and 52 ns respectively.

Thus, we have shown an interesting aspect of the *anti*-helix's structure-property relationship in its more rigid backbone providing long-lived lifetime decay akin to

quantum dots and organic dyes which hold an average fluorescence decay of 20-30 ns.[186] The *syn*-helix, comparatively, has an inherently more flexible backbone owing to its larger outer diameter yet smaller helical pitch. While certainly not direct proof on its own of the *syn*-helix's spring-like nature, this investigation clearly shows the *anti*-helix's more rigid rod-type structure and its resulting properties.

4.7.4. Spin-Lattice Relaxation Studies

Generally, in ^{1}H NMR, protons directly aid in the quick relaxation of neighboring nuclei after a 90 degree pulse, as well as the tumbling and movement of the overall molecule. Utilizing this phenomenon, we attempted to observe that the *syn*-helix has protons that were quicker to relax as compared to the *anti*-helix, thus showing that the *syn*-helix has more flexible, fast motions than its more unmoving counterpart. This observation would be born from the *syn*-helix's more readily available spring-like movement as opposed to the *anti*-helix's more stiff and rigid behavior, thus allowing the protons within the *syn*-helix to relax more quickly. Using different frequency NMR to obtain spin-lattice relaxation time (T_1) data, which is dependent on magnetic field strength, we were able to provide evidence to support this claim.[189]

The dynamic information on fast internal motions of macromolecules in NMR relaxation experiments can be described with: (i) a generalized order parameter δ, (ii) as well as an effective correlation time τ_e. δ is a description of spatial restriction of motion, while τ_e is a measure of the time scale or rate of that motion. T_1 relaxation times were used to achieve this information and fit iteratively to obtain these parameters by least

squares fitting, utilizing Szabo's "model-free" approach[190] and assuming a system of anisotropic (i.e., isotropic rigid rotor) motion.[191] Due to the magnetic field dependence of T_1, we can thus utilize varying magnetic field strengths in measuring ^{1}H T_1 times to gain information regarding the proton motions of our polymers. For a proton absolutely rigidly attached to the backbone of an anisotropic macromolecular backbone, $\delta^2 = 1$. Following this, τ_e and δ^2 must be treated as adjustable parameters with the constraint on δ^2 that it must assume a value between 0 and 1 and that τ_e must be positive. Our relaxation results (assuming relaxation is mostly dipolar) can be related to the motional spectral density function ($J(\omega)$) (**Figure 4.14.**)[167]—and because motion is anisotropic, the model-free approach can next be utilized, where $1/\tau = (1/\tau_c) + (1/\tau_e)$, and $J(\omega)$ is described as seen in **Figure 4.14**.[190]

$$\frac{1}{T_1} = \frac{3}{10}\gamma^4\hbar^2 \sum_{j \neq i} \left(r_{ij}^{-6}\right)\{J(\omega) + 4J(2\omega)\}$$

$$J(\omega) = \frac{2}{5}\left(\frac{\delta^2\tau_c}{1+\tau_c^2\omega^2} + \frac{(1-\delta^2)\tau}{1+\tau^2\omega^2}\right)$$

Figure 4.14. Relationship of T_1 to the motional spectral density function $J(\omega)$, and the model-free approach, respectively. γ is the gyromagnetic ratio, $\hbar$ is the reduced Planck's constant, and r_{ij} is the distance between nuclei *i* and *j*. The entirety of the term $\frac{3}{10}\gamma^4\hbar^2 \sum_{j \neq i}\left(r_{ij}^{-6}\right)$ was treated as another adjustable parameter, using simple assumptions to start with an initial value for the iterative least squares fitting procedure.

Every major resonance available in both polymers was analyzed for its T_1 measurement, including more minor chemical-shifts that were well-assumed to be from

end groups. The proton's location on each polymer was assumed based on the very closely related *syn*- and *anti*-dimer respectively. However, not every resulting T_1 value was able to be fit with a high level of confidence—generally $R^2 > 0.99$ for at least one proton of both polymers, when $\delta^2 > 0.01$, and using reasonable assumptions.[190] The protons that were successfully fit well were analyzed for their δ^2 value, of which a value closer to 1 meant the proton was more rigidly attached to the backbone of the macromolecule, and a value closer to 0 meant the proton was more flexible. Each proton that could be fit from the *syn*-helix was compared to the proton "counterpart" of the *anti*-helix in an analysis of the overall flexible motions of those protons. Due to the large number of parameters to be fit, we found we were able mitigate some parameter fitting by constraining rotational correlation time τ_c (i.e. the time it takes the particle to rotate by one radian) based on the lengths of each polymer found from DOSY analysis.[192] By approximating the effective hydrodynamic radius (r) as their found length, we were easily afforded their respective τ_c values as seen in **Figure 4.14**.

$$\tau_c = \frac{4\pi\eta r^3}{3k_B T}$$

Figure 4.14. Rotational correlation time (τ_c) of a particle as related to its hydrodynamic radius (r).

It was found, quite successfully, that the *anti*-helix had the majority of its protons more rigidly attached (a higher δ^2 value) than the *syn*-helix (**Figure 4.15**). It is important to note that no protons were omitted that had met the parameter fitting procedure standards. Interestingly, both protons H_f and an end group H_f (labeled H_f_end) had

significant differences in their δ^2 value—these sp^3 carbons provide the most flexibility along the backbone of the polymers, so the *syn*-helix's less rigid H_f protons is indicative of the *anti*-helix's less flexible structure. Overall, the difference in rigidity was 11 ± 2%, a very noticeable variance in mechanical behavior between the two polymers. An exception to this was of proton H_d, however, the error bar indicates they may be of the same rigidity. Nevertheless, the *syn*-helix may have had its phenyl group with no more freedom than the *anti*-helix due to proton H_a (H_p in the *anti*-helix) located in an inflexible bay region of an aromatic ring sequence. Of course, the data fitting can be improved by additional magnetic field strengths, investigation of T_2 relation times, or introducing more variable parameters such as a weighting coefficient or another correlation time τ.[167]

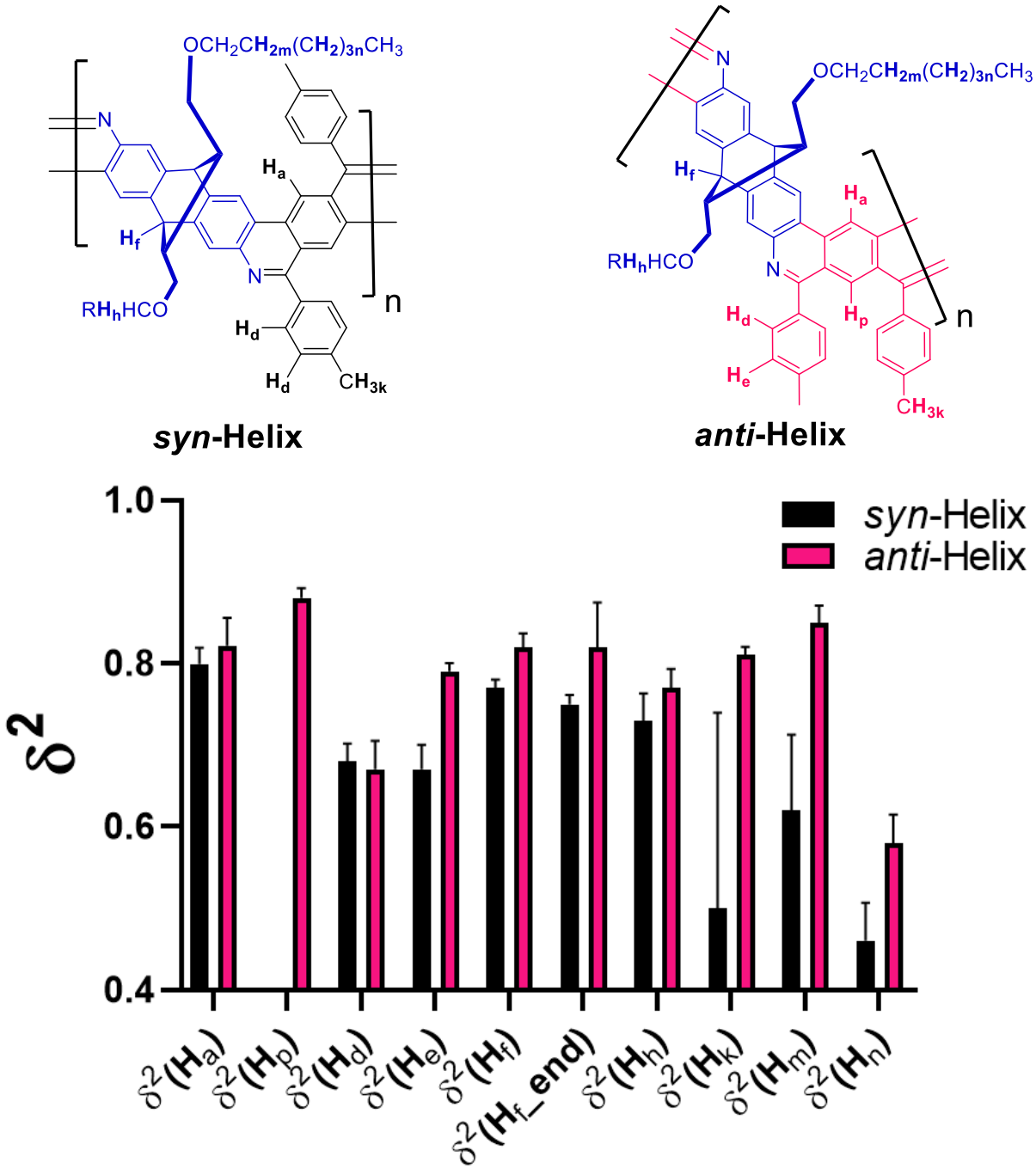

Figure 4.15. Generalized order parameter (δ^2) analysis from iterative least square fitting utilizing T_1 values found for both *syn*- and *anti*-helix polymers across 300, 400, 500, 600, and 800 MHz ^{1}H NMR experiments. Relevant protons are labeled alphabetically from the order they were generally assigned in ^{1}H NMR.

Despite being several units longer and thus heavier (as supported by GPC results and ^{1}H NMR end group analysis) but more compressed than its *anti* regioisomer (as evidenced by size-analysis from previously mentioned DOSY data as well as computational results), the *syn*-helix still observes more flexible protons overall, owing to its more spring-promoted performance. This is unsurprising, given the aforementioned (**Chapter 1**) fundamental nature of Hookean classical springs. A smaller spring outer diameter requires more force to compress its overall organization, as is the case with our more rigid *anti*-helix which has a rod-like structure. The *syn*-helix, however, needs less force to undergo ambient spring-like motion. Thus, the specific geometry of our ladder polymers determines their general mechanical behavior.

4.8. Conclusions and Future Directions

In general, the *syn*-helix polymer has a much higher capacity to move in a single unidirectional fashion while the *anti*-helix behaves without flexibility in a singular direction. This makes the *syn*-helix a very viable candidate for materials that can pulled or pushed without bending or taking up any substantial volume upon compression/expansion—a sought after property of flexible smart materials,[103, 193, 194] being able to stretch to great extents and then revert to their original shape without any structural failure induced by strain.[69, 195] Most materials expand in all directions upon addition of heat, but our *syn*-helix would only experience thermal expansion in a singular direction—these sort of reversible expansion properties, may make them suitable for thermal-responsive materials and luminescent thermometers.[196] Moreover, such low

density polymeric springs is a desired material property for thermal protection systems in spacecraft design.[197]

With the advent of polymeric ladderization of helical polymers as well as an efficient strategy to build iteratively grown polymers, certainly it would be a courageous yet more accurate pursuit to grow exactly known lengths of both the *syn*- and *anti*-helices in comparison for their material properties. While the investigations performed to probe the *syn*-helix polymer for its spring-like character and the *anti*-helix polymer for its rigid-rod structure were experimentally sound, a direct comparison by the same unit length would undoubtedly be a more entirely accurate assessment of their respective structure-property relationship.

Moreover, having shown we can couple not only monomeric species in a well-defined manner, but continue to grow out these generated dimers into the tetrameric and then octameric species, we demonstrate this reaction pathway to have great promise for building larger shape-persistent species. By changing the linker piece between couplings, we can also develop a programmable strategy in generating unique molecular shapes with inherently different characteristics. These high efficiency Suzuki-coupling/imine condensation reactions alongside CAS building blocks certainly lends itself well to the research done in the Schneebeli group in pursuit of building precise and structurally interesting molecules.

CHAPTER 5: EXPERIMENTAL PROCEDURES AND CHARACTERIZATION DATA

5.1. General Methods and Materials

All commercially available starting materials were purchased from *Sigma Aldrich*, *Fisher Scientific*, *CombiBlocks* or *Oakwood Chemical*. Phosphorous ligands for Buchwald–Hartwig aminations were purchased from *Strem Chemical*. All reagents were used as received without further purification. Known compounds were synthesized according to published literature procedures and any modifications are noted. When needed, tetrahydrofuran (THF), diethyl ether, dichloromethane (DCM), dimethylformamide (DMF), and toluene were dried using a Glass Contour solvent purification system by SG Water USA, *LLC*. HPLC grade acetonitrile (MeCN) and anhydrous 1,4-dioxane were used as received from *Fisher Scientific*. If necessary, air or moisture sensitive reactions were carried out under an inert atmosphere of nitrogen or argon. Removal of solvents was accomplished on a Büchi R-210 rotary evaporator and further concentration was done under a *Fisher Scientific* Maxima C-Plus vacuum line. Column chromatography was preformed manually with *Sorbent* grade 60 silica with a mesh size between 230–400 using a forced flow of indicated solvents, or automatically with a Teledyne *CombiFlash*® chromatography system. Analytical thin layer chromatography (TLC) plates were purchased from *Fisher Scientific* (EMD Millipore TLC Silica Gel 60 F254). Visualization was accomplished by irradiation under UV light (254 nm) or staining with iodine vapor. All ^{1}H NMR spectra were recorded at 298K on a Varian Unity Inova 500 (500 MHz) or a Bruker Ascend 500 (500 MHz) spectrometer. All

^{13}C NMR spectra were recorded on a Bruker ARX 500 (125 MHz) spectrometer. Samples were dissolved in $CDCl_3$ unless stated otherwise. The spectra were referenced to the residual solvent peak (chloroform-*d*: 7.26 ppm for ^{1}H NMR and 77.16 ppm for ^{13}C NMR), or tetramethylsilane (TMS) as the internal standard. Chemical shift values were recorded in parts per million (ppm). Data are reported as follows: chemical shift, multiplicity (s = singlet, d = doublet, t = triplet, q = quartet, m = multiplet, br = broad peak), coupling constants (Hz), and number of protons. High resolution mass spectrometry data were obtained on Waters XEVO G2-XS QT in positive ESI mode. Low resolution mass spectra were recorded on a Bruker Daltonics UltrafleXtreme MALDI-TOF-MS. Room temperature Circular Dichroism (CD) spectra were obtained on a Jasco J-815 CD spectropolarimeter (scanning range: 900–200 nm, Data pitch: 1.0 nm, bandwidth: 1.0 nm, scan speed: 100 nm/min, CD detector: PMT).

General Procedure for Regioselective Electrophilic Aromatic Iodination: Into a round-bottom flask cooled to -15 °C were added sequentially (i) 1-to-1 mixture of DCM and MeOH, (ii) aniline species (1 eq.), (iii) 1 M concentration of ICl (eq. depending on desired number of added iodo groups) in DCM stored at -15 °C. Reaction was let slowly warmed to RT over 4 hours with monitoring by TLC until reaction was determined complete. Reaction solution was quenched with aqueous sodium thiosulfate followed by extraction by DCM (3 × 20 mL) with final brine wash (1 × 20 mL). The organic layer was then dried over anhydrous $MgSO_4$, filtered, and concentrated under reduced pressure to afford crude material. The crude product obtained was purified by flash column chromatography (EtOAc in hexanes) to afford product. Degradation of material was

observed during monitoring of reaction due to exposure of dilute acid by ^{1}H NMR without (i) proper work up and (ii) dry $CDCl_3$ solvent.

General Procedure for Buchwald–Hartwig amination: Into a flame-dried, argon-purged, Schlenk tube were sequentially (i) aryl halide building block (2 eq.), (ii) RuPhos ligand (0.2 eq.), (iii) cesium carbonate (4.0 eq.), (iv) palladium(II) acetate (0.1 eq.), (v) as well as dry, degassed 1,4-dioxane followed by ten minutes of bubbling argon through the reaction mixture. The mixture was then heated to 100 °C under argon for 16 hours. After completion, the solution was cooled to room temperature, filtered through a pad of Celite, and rinsed with DCM. The solution was then washed with water (1 × 20 mL), the aqueous layer was extracted with DCM (3 × 20 mL) and the combined organic layers were then washed with brine (1 × 20 mL). The organic layer was then dried over anhydrous $MgSO_4$, filtered, and concentrated under reduced pressure to afford crude material. The crude product obtained was purified by flash column chromatography (EtOAc in hexanes) to afford product.

General Procedure for Miyaura Borylation: Into a flame-dried, argon-purged, Schlenk tube were sequentially added (i) aryl dibromo shape-directing precursor (1 eq.), (ii) bis(pinacolato)diboron (B_2pin_2) (4.0 eq.), (iii) potassium acetate (6.0 eq.), (iv) bis(triphenylphosphine)palladium(II) dichloride (0.1 eq.), (v) as well as dry, degassed toluene followed by ten minutes of bubbling argon through the reaction mixture. The mixture was then heated to 80 °C under argon for 16 hours. (4 equivalents of bis(pinacolato)diboron and lower than reflux temperatures were used to disfavor homocoupling byproducts.) After completion, the solution was cooled to room

temperature, filtered through a pad of Celite, and rinsed with DCM. The solution was then washed with water (1 × 20 mL), the aqueous layer was extracted with DCM (3 × 20 mL) and the combined organic layers were then washed with brine (1 × 20 mL). The organic layer was then dried over anhydrous $MgSO_4$, filtered, and concentrated under reduced pressure to afford crude material. The crude product obtained was purified by recrystallization (due to observed slow degradation on silica) with EtOAc/hexanes to afford product as a white powder. Final flash column chromatography with EtOAc and hexanes were done on remaining product in crude mixture filtrate.

General Procedure for Suzuki Coupling/Imine Condensation: Into a flame-dried, argon-purged, Schlenk tube were sequentially (i) aryl iodide building block (2 or 1 eq. depending), (ii) shape-directing di-Bpin piece (1 eq.), (iii) cesium carbonate (4.5 eq.), (iv) palladium(0) tetrakis(triphenylphosphine) (0.1 eq.), (v) as well as dry, degassed 1,4-dioxane (ensuring a concentration no more dilute than of 0.10 M as compared to the aryl halide) followed by ten minutes of bubbling argon through the reaction mixture. The mixture was then heated to 100 °C under argon for 16 hours. After completion, the solution was cooled to room temperature, filtered through a pad of Celite, and rinsed with DCM. The solution was then washed with water (1 × 20 mL), the aqueous layer was extracted with DCM (3 × 20 mL) and the combined organic layers were then washed with brine (1 × 20 mL). The organic layer was then dried over anhydrous $MgSO_4$, filtered, and concentrated under reduced pressure to afford crude material. The crude product obtained was purified by flash column chromatography (EtOAc in hexanes) to afford product.

5.2. Experimental Procedures and Characterization for Chapter 2

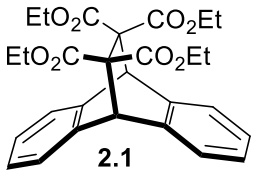

2.1

Tetraester cycloadduct (2.1): $AlCl_3$ (11.33 g, 84.9 mmol) was added in portions to 70 mL of anhydrous DCM at 0 °C, followed by the addition of 4.95 mL anhydrous EtOH. The resulting mixture was stirred for 5 minutes. Then, anthracene (7.58 g, 42.5 mmol) and tetraethyl ethylenetetracarboxylate (12.75 g, 40.3 mmol) were added to the solution in one portion. The reaction mixture was then warmed to room temperature, and stirred under N_2. After 2 days, the reaction was quenched by adding 70 mL of a 2M aqueous HCl solution at 0 °C, followed by the addition of 70 mL water and 50 mL DCM. The organic layer was then separated and the aqueous layer was washed with more DCM (3×50 mL). Finally, the combined organic extracts were washed with brine, dried over anhydrous $MgSO_4$, filtered, and evaporated under reduced pressure. The crude product was further purified by trituration from (i) DCM (to remove residual anthracene), and (ii) 100% EtOH. The product was isolated as a pale yellow solid in 80% yield. Spectral characterization matched reported literature values.[198]

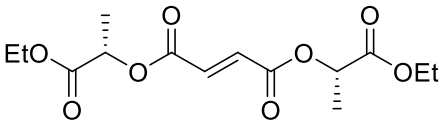

2.2

(−)-Bis[(*S*)-1-(ethoxycarbonyl)ethyl] fumarate (2.2): To a round-bottom with fumaryl chloride (25 mL, 230 mmol) was added ethyl (–)-L-lactate (50.3 mL, 439.0 mmol) and let

stir neat at 100 °C for 24 h. The reaction was quenched with slow addition of 100 mL $NaHCO_3$ (aq) at 0 °C, followed by extraction with DCM, with the aqueous layer washed with DCM (2×50 mL). Finally, the combined organic extracts were washed with brine (1×50 mL), dried over anhydrous $MgSO_4$, filtered, and evaporated under reduced pressure. The product **2.2** was obtained (57.1 g, 180.6 mmol) as a pale yellow oil without further purification in 79% yield, and carried forward in the generation of **2.3**. The reaction was run in a 1-to-1.9 ratio to prevent observed polymerization from occurring, and any acid chloride remaining (from monocoupled side product) is pulled into the aqueous layer during workup. Spectral characterization matched reported literature values.[143]

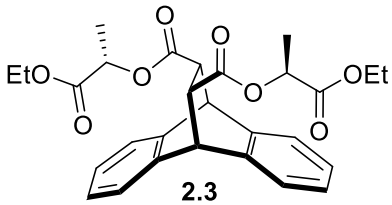

2.3

Diester cycloadduct (2.3): To a solution of anthracene (19.7 g, 110.7 mmol) in 150 mL toluene, **2.2** (10.0 g, 31.6 mmol) was added. The reaction was left to stir at reflux for 8 days. Once cooled to room temperature, the crude mixture was filtered to removal residual anthracene. The reaction mixture was then quenched by addition of 100 mL of water and 50 mL DCM. The organic layer was then separated and the aqueous layer was washed with more DCM (3×50 mL). Finally, the combined organic extracts were washed with brine, dried over anhydrous $MgSO_4$, filtered, and evaporated under reduced pressure. The crude product was further purified by trituration from DCM (to

remove residual anthracene) three times, followed by recrystallization in EtOAc and hexanes. Under these conditions, diastereomerically pure **2.3** (10.8 g, 21.9 mmol) was obtained in 70% yield as a light grey powder. Leaving the reaction to run for less than 7 days generally lead to lower diastereomeric ratios (rather than the 8-to-1 seen by ^{1}H NMR analysis). Spectral characterization matched reported literature values.[143]

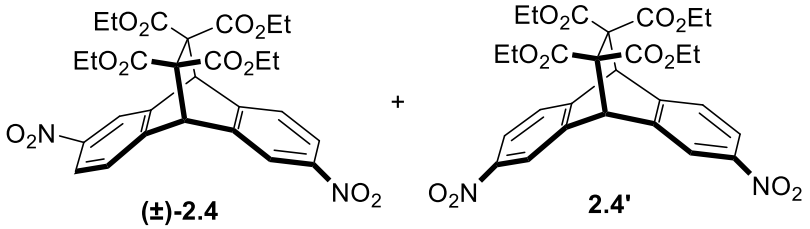

2,6-dinitro tetraester (2.4) and 2,7-dinitro tetraester (2.4'): To a stirred solution of trifluoroacetic anhydride (1.2 mL, 8.5 mmol) in 3 mL $CHCl_3$ was added ammonium nitrate (0.2 g, 2.5 mmol). Then, **2.1** (0.49 g, 1.0 mmol) was added into the reaction mixture in portions. After stirring at room temperature under N_2 for 3 h, 15 mL of H_2O were added to quench the reaction. The aqueous layer was extracted with DCM (2×30 mL) and the combined organic layers were dried over anhydrous Na_2SO_4, filtered, and evaporated under reduced pressure to afford crude material. The crude product was purified by trituration with 66% EtOH in H_2O (10 mL) to afford a 1-to-1mixture (0.54g) of **2.4** and **2.4'** as a white solid in 92% combined yield. Spectral characterization matched our reported literature values.[4]

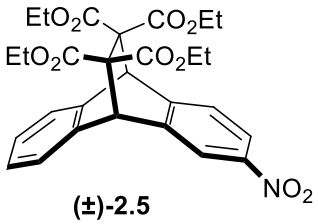

(±)-2.5

2-mononitro tetraester (2.5): To a stirred solution of trifluoroacetic anhydride (4.7 mL, 13.8 mmol) in 30 mL $CHCl_3$ was added ammonium nitrate (0.554 g, 6.92 mmol). Then, **2.1** (3.42 g, 6.92 mmol) was added into the reaction mixture in portions. After stirring at room temperature under N_2 for 3 h, 15 mL of H_2O were added to quench the reaction. The aqueous layer was extracted with DCM (2×30 mL) and the combined organic layers were dried over anhydrous Na_2SO_4, filtered, and evaporated under reduced pressure to afford crude material. The crude product was purified by trituration with 66% EtOH in H_2O (10 mL) to afford racemic **2.5** (3.1 g, 5.75 mmol) as a pale yellow solid in 83% yield. Spectral characterization matched our reported literature values.[4]

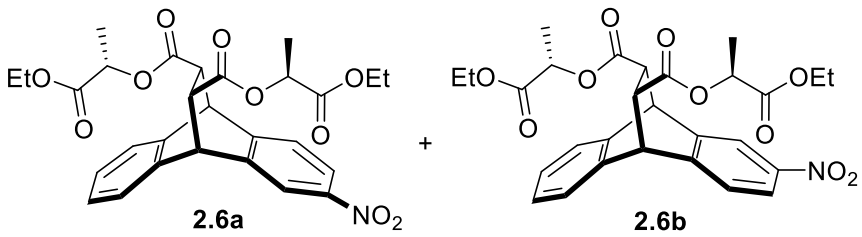

2.6a **2.6b**

2-mononitro diester (2.6a) and 3-mononitro diester (2.6b): Diastereomerically pure diester **2.3** (1.34 g, 2.71 mmol) was dissolved in 30 mL of $CHCl_3$, followed by the addition of ammonium nitrate (217 mg, 2.71 mmol). To the stirred solution, trifluoroacetic anhydride (1.9 mL, 13.7 mmol) in 30 mL $CHCl_3$ was added. After stirring under N_2 at room temperature for 16 hours, 30 mL of H_2O were added to quench

the reaction. The aqueous layer was extracted with DCM (2×30 mL) and the combined organic layers were washed with brine (1x50 mL), dried over $MgSO_4$, filtered, and evaporated under reduced pressure to afford crude material. The crude product was purified by flash column chromatography (0% to 15% EtOAc in hexanes) to afford 2.99 g of an inseparable mixture of **2.6a** and **2.6b** in a 5.3-to-1.0 molar ratio and 51% combined yield. Spectral characterization matched our reported literature values.[146]

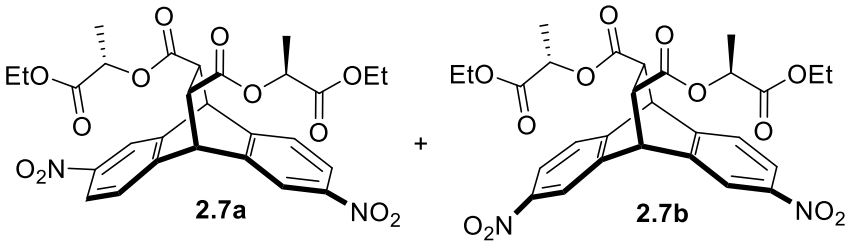

2,6-dinitro diester (2.7a) and 2,7-dinitro diester (2.7b): Diastereomerically pure diester **2.3** (2.45 g, 4.95 mmol) was dissolved in 70 mL of $CHCl_3$, followed by the addition of ammonium nitrate (792 mg, 9.90 mmol). To the stirred solution, trifluoroacetic anhydride (3.8 mL, 74.2 mmol) in 70 mL $CHCl_3$ was added. After stirring under N_2 at room temperature for 16 hours, 70 mL of H_2O were added to quench the reaction. The aqueous layer was extracted with DCM (2×50 mL) and the combined organic layers were washed with brine (1×100 mL), dried over $MgSO_4$, filtered, and evaporated under reduced pressure to afford crude material. The crude product was purified by flash column chromatography (0% to 15% EtOAc in hexanes) to afford 1.89 g of an inseparable mixture of **2.7a** and **2.7b** in a 2.8-to-1.0 molar

ratio and 65% combined yield. Spectral characterization matched our reported literature values.[146]

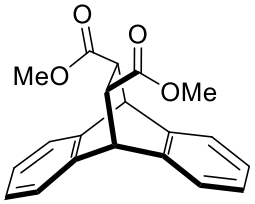

(±)-2.8

Dimethyl-diester cycloadduct (2.8): To a solution of anthracene (1.0 g, 5.62 mmol) in 10 mL toluene, dimethyl fumarate (230 mg, 1.59 mmol) was added. The reaction was left to stir at reflux for 8 days. Once cooled to room temperature, the crude mixture was filtered to removal residual anthracene. The reaction mixture was then quenched by addition of 100 mL of water . The organic layer was then separated and the aqueous layer was washed with more DCM (3×50 mL). Finally, the combined organic extracts were washed with brine, dried over anhydrous $MgSO_4$, filtered, and evaporated under reduced pressure. The crude product was further purified by trituration from DCM (to remove residual anthracene) three times and was purified by flash column chromatography (0% to 10% EtOAc in hexanes) to afford racemic **2.8** (439.3 mg, 1.37 mmol) in 86% yield. Spectral characterization matched reported literature values.[199]

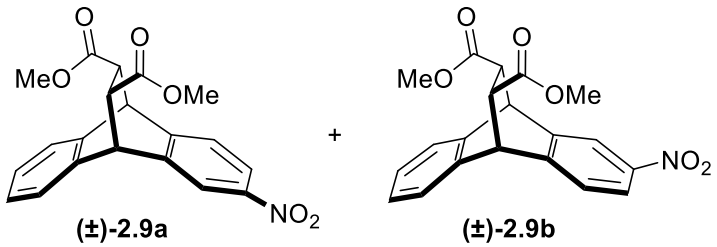

2-mononitro dimethyl-diester (2.9a) and 3-mononitro dimethyl-diester (2.9b): A racemic mixture of **2.8** (116.4 mg, 0.361 mmol) was dissolved in 5 mL of $CHCl_3$, followed by the addition of ammonium nitrate (23.1 mg, 0.289 mmol).Next, trifluoroacetic anhydride (0.370 mL, 2.66 mmol) in 30 mL $CHCl_3$ was added to the solution. After stirring under N2at room temperature for 16 hours, 20 mL of H_2O were added to quench the reaction. The aqueous layer was extracted with DCM (2×20 mL) and the combined organic layers were washed with brine (1×20 mL), dried over $MgSO_4$, filtered, and evaporated under reduced pressure to afford crude material. The crude product was purified by Preparative TLC (25% EtOAc in hexanes) to afford 54.4 mg of an inseparable 1-to-1 mixture of **(±)-2.9a** and **(±)-2.9b** in 41% overall yield. Spectral characterization matched our reported literature values.[146]

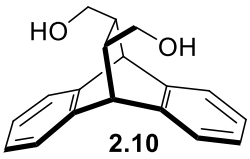

Diol cycloadduct (2.10): **2.3** (547.3 mg, 1.11 mmol) dissolved in 10 mL diethyl ether was added dropwise to a vigorously stirred (1000 rpm) suspension of $LiAlH_4$ (250 mg, 6.64 mmol) in 70 mL diethyl ether at room temperature under a N_2 atmosphere. After stirring for 24 hours, the solution was cooled to 0 °C and water (40 mL) was

added dropwise with vigorous stirring until quenching of the reaction was complete. Next, after acidifying the reaction mixture with a 1M aqueous HCl solution, the aqueous layer was extracted with diethyl ether (3×30 mL) and the combined organic layers were washed with brine (1×50 mL), dried over $MgSO_4$, filtered, evaporated under reduced pressure, and washed through a plug of silica with 5% MeOH in DCM to afford 269 mg (1.01 mmol) of **2.10** in 91% yield which was carried forward without further purification. As a note, this process works for the diester cycloadduct with one or zero nitro groups on the arene subunits, but following dinitration, reduction by LAH leads to drastically minimized yields, and $NaBH_4$ is used in its stead. Spectral characterization matched reported literature values.[199]

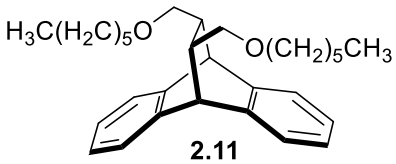

2.11

Dihexyl-diether cycloadduct (2.11): To a flame-dried round-bottom, diol **2.10** (269 mg, 1.01 mmol) in 5 mL DMF was added dropwise to a suspension of NaH (60% suspension in oil) (192 mg, 4.0 mmol) in 10 mL DMF with vigorous stirring (1000 rpm) under N_2 at 0 °C. Subsequently, bromohexane (0.425 mL, 3.0 mmol) was added dropwise, and the reaction mixture was allowed to warm to room temperature and stirred for 16 hours. Afterwards, the reaction was quenched with 30 mL of water and the aqueous layer was extracted with DCM (3×30 mL). Finally, the organic layers were combined and washed with brine (1×30 mL), dried over $MgSO_4$, and concentrated under vacuum. The crude product was purified by flash column

chromatography (0% to 30% EtOAc in hexanes) to afford 420 mg (0.965 mmol) of **2.11** in 96% yield. ^{1}H NMR (500 MHz, $CDCl_3$): δ 7.31 – 7.20 (m, 4H), 7.12 – 7.04 (m, 4H), 4.34 (d, *J* = 2.3 Hz, 2H), 3.36 (dt, *J* = 9.5, 6.5 Hz, 2H), 3.28 (dt, *J* = 9.5, 6.7 Hz, 2H), 3.14 (dd, *J* = 9.3, 4.9 Hz, 2H), 2.73 (t, *J* = 9.4 Hz, 2H), 1.54 (tdd, *J* = 13.3, 6.7, 3.9 Hz, 6H), 1.42 – 1.23 (m, 12H), 0.91 (t, *J* = 7.0 Hz, 6H). ^{13}C NMR (125 MHz, $CDCl_3$): δ 143.72, 141.26, 125.90, 125.54, 125.46, 123.54, 73.49, 71.19, 45.85, 43.33, 31.79, 29.75, 26.00, 22.76, 14.18. LRMS calcd. for $[C_{30}H_{43}O_2]^+$: 435.3; found: 435.5.

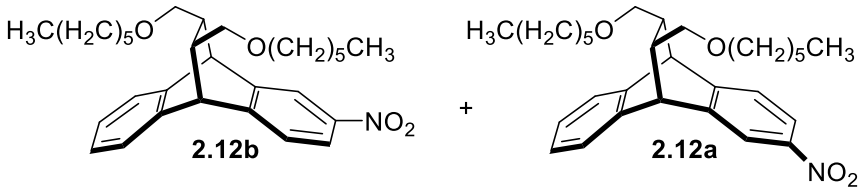

2-mononitro diether (2.12a) and 3-mononitro diether (2.12b): A 5-to-1 mixture of diol **3.12a** and **3.12b** (679 mg, 2.18 mmol) in 5 mL DMF was added dropwise to a suspension of NaH (60% suspension in oil) (418 mg, 8.72 mmol) in 10 mL DMF with vigorous stirring (1000 rpm) under N_2 at 0 °C. Subsequently, bromohexane (1.54 mL, 10.9 mmol) was added dropwise, and the reaction mixture was allowed to warm to room temperature and stirred for 16 hours. Afterwards, the reaction was quenched with 30 mL of water and the aqueous layer was extracted with DCM (3×30 mL). Finally, the organic layers were combined and washed with brine (1×30 mL), dried over $MgSO_4$, and concentrated under vacuum. The crude product was purified by flash column chromatography (0% to 30% EtOAc in hexanes) to afford 727.7 mg of **2.12a** and **2.12b** in a 5-to-1 inseparable mixture in a 70% combined yield. Spectral characterization matched our reported literature values.[146]

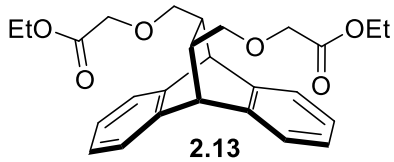

2.13

Diether-diester cycloadduct (2.13): To a flame-dried round-bottom, diol **2.10** (27.3 mg, 0.102 mmol) in 2 mL THF was added dropwise to a suspension of NaH (60% suspension in oil) (192 mg, 4.0 mmol), KI (7.0 mg, 0.04 mmol) in 5 mL THF with vigorous stirring (1000 rpm) under N_2 at 0 °C. Subsequently, ethyl bromoacetate (70 μL, 0.61 mmol) was added dropwise, and the reaction mixture was allowed to warm to room temperature and stirred for 16 hours. Afterwards, the reaction was quenched with 30 mL of water and the aqueous layer was extracted with DCM (3×30 mL). Finally, the organic layers were combined and washed with brine (1×30 mL), dried over $MgSO_4$, and concentrated under vacuum. The crude product was purified by Preparative TLC 25% EtOAc in hexanes to afford 10.8 mg (0.025 mmol) of **2.11** in 24% yield. ^{1}H NMR (500 MHz, $CDCl_3$): δ 7.34 – 7.27 (m, 4H), 7.13 – 7.08 (m, 4H), 4.39 (d, *J* = 2.3 Hz, 2H), 4.20 (q, *J* = 7.2 Hz, 4H), 4.01 (d, *J* = 1.1 Hz, 4H), 3.29 (dd, *J* = 8.9, 4.9 Hz, 2H), 2.92 (t, *J* = 9.2 Hz, 2H), 1.65 – 1.59 (m, 2H), 1.27 (t, *J* = 7.1 Hz, 6H). ^{13}C NMR (125 MHz, $CDCl_3$): δ 170.40, 143.47, 140.81, 126.02, 125.62, 125.60, 123.53, 74.45, 68.61, 60.80, 45.49, 43.10, 14.22. LRMS calcd. for $[C_{26}H_{31}O_6]^+$: 439.2; found: 439.4.

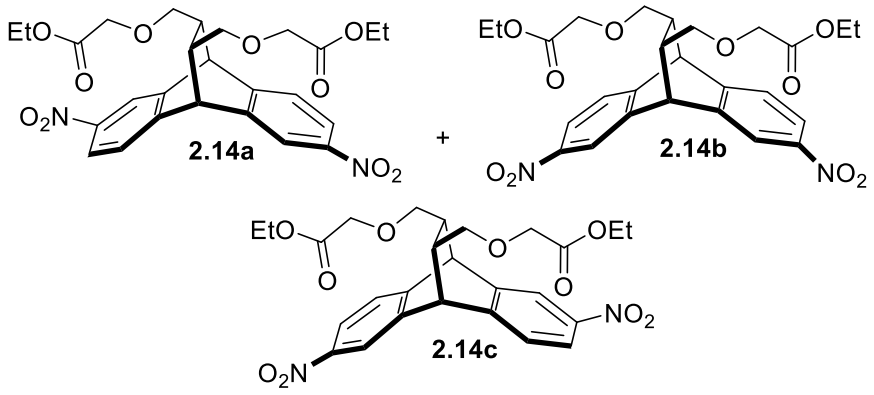

2,6-dinitro (2.14a), 2,7-dinitro (2.14b), and 3,7-dinitro (2.14c): Diastereomerically pure cycloadduct **2.13** (3.8 mg, 0.0087 mmol) was dissolved in 2 mL of $CHCl_3$, followed by the addition of ammonium nitrate (1.9 mg, 0.025 mmol). To the stirred solution, trifluoroacetic anhydride (11 µL, 0.087 mmol) was added. After stirring under N_2 at room temperature for 16 hours, 10 mL of H_2O were added to quench the reaction. The aqueous layer was extracted with DCM (2×10 mL) and the combined organic layers were washed with brine (1×20 mL), dried over $MgSO_4$, filtered, and evaporated under reduced pressure to afford crude material. The resulting dinitrated derivatives of **2.13** were dissolved in 10% EtOAc in hexanes, filtered through a pad of silica gel, and concentrated under vacuum to afford 2.6 mg of an inseparable mixture of **2.14a**, **2.14b**, and **2.14c** in a 56% combined yield. ^{1}H NMR (500 MHz, $CDCl_3$) was very complex due to the mixture of regioisomers and diastereomers, and thus values are not reported.

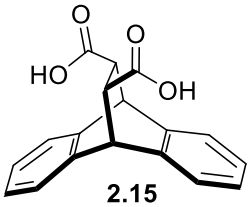

2.15

Diacid cycloadduct (2.10): Diastereomerically pure cycloadduct **2.3** (215 mg, 0.435 mmol) was dissolved in 3 mL of EtOH and 50 µL of H_2O, followed by the addition of KOH (243 mg, 4.35 mmol) and the stirred solution was heated to 50 °C. After 16 hours, 10 mL of H_2O were added to quench the reaction. The aqueous layer was extracted with DCM (3×10 mL) and the combined organic layers were washed with brine (1×20 mL), extracted again with DCM (2×10 mL) dried over $MgSO_4$, filtered, and evaporated under reduced pressure to afford crude material which was washed through a plug of silica with 5% MeOH in DCM to afford 125 mg (0.425 mmol) of **2.15** in 98% yield which was carried forward without further purification. Spectral characterization matched reported literature values.[143] HRMS calcd. for $[C_{18}H_{13}O_4]^-$: 293.0814; found: 293.0812.

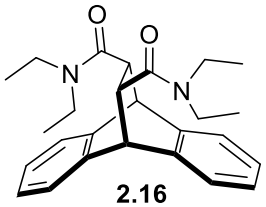

2.16

Diethylamide cycloadduct (2.16): Diastereomerically pure cycloadduct **2.15** (54 mg, 0.183 mmol) was dissolved in 5 mL of DCM, followed by the sequential addition of (i) hydroxybenzotriazole (89.3 mg, 0.661 mmol), (ii) 1-ethyl-3-(3-dimethylaminopropyl)carbodiimide (102 mg, 0.661 mmol), (iii) Et_3N (15 µL, 0.10

mmol), and (iv) diethyl amine (68.4 µL, 0.661 mmol). After stirring under N_2 at room temperature for 16 hours, 10 mL of H_2O were added to quench the reaction. The aqueous layer was extracted with DCM (2×10 mL) and the combined organic layers were washed with brine (1×20 mL), dried over $MgSO_4$, filtered, and evaporated under reduced pressure to afford crude material. The crude product obtained was purified by flash column chromatography (0 to 5% MeOH in DCM) to afford 42.3 mg of **2.16** in 57% yield. DCC was used as a coupling agent prior to EDCI, and it was found that DCC co-eluted with product by column chromatography. Spectral characterization matched reported literature values.[200] LRMS calcd. for $[C_{26}H_{33}N_2O_2]^+$: 405.3; found: 405.4.

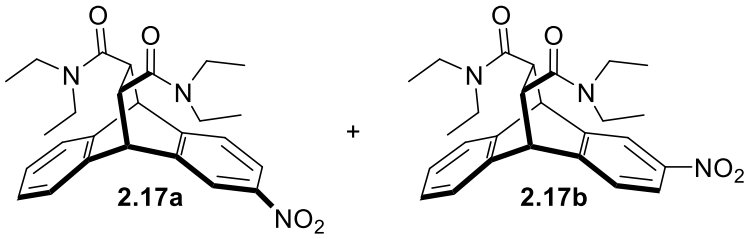

2-mononitro (2.17a) and 3-mononitro (2.17b): Diastereomerically pure cycloadduct **2.13** (21.2 mg, 0.052 mmol) was dissolved in 2 mL of $CHCl_3$, followed by the addition of ammonium nitrate (3.0 mg, 0.037 mmol). To the stirred solution, trifluoroacetic anhydride (50 µL, 0.157 mmol) was added. After stirring under N_2 at room temperature for 16 hours, 10 mL of H_2O were added to quench the reaction. The aqueous layer was extracted with DCM (2×10 mL) and the combined organic layers were washed with brine (1×20 mL), dried over $MgSO_4$, filtered, and evaporated under reduced pressure to afford crude material. The resulting dinitrated derivatives of **2.16**

were further purified by Preparative TLC (5% MeOH in DCM) to afford 9.8 mg of an inseparable mixture of **2.17a** and **2.17b** in a 59% combined yield. ^{1}H NMR (500 MHz, $CDCl_3$) was complex due to the mixture of isomers, and thus values are not reported. LRMS calcd. for $[C_{26}H_{32}N_3O_4]^+$: 450.2393; found: 450.2388.

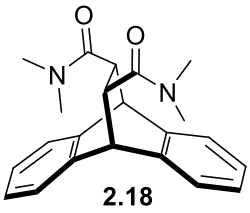

2.18

Dimethylamide cycloadduct (2.18): Diastereomerically pure cycloadduct **2.15** (24.4 mg, 0.083 mmol) was dissolved in 5 mL of DCM, followed by the sequential addition of (i) hydroxybenzotriazole (33.6 mg, 0.249 mmol), (ii) 1-ethyl-3-(3-dimethylaminopropyl)carbodiimide (54 µL, 0.249 mmol), (iii) Et_3N (119 µL, 0.83 mmol), and (iv) dimethylamine hydrochloride (91 mg, 0.498 mmol). After stirring under N_2 at room temperature for 16 hours, 10 mL of H_2O were added to quench the reaction. The aqueous layer was extracted with DCM (2×10 mL) and the combined organic layers were washed with brine (1×20 mL), dried over $MgSO_4$, filtered, and evaporated under reduced pressure to afford crude material. The crude product obtained was purified by Preparative TLC (5% MeOH in DCM) to afford 20.7 mg of **2.18** in 71% yield. Spectral characterization matched reported literature values.[200] LRMS calcd. For $[C_{22}H_{25}N_2O_2]^+$: 349.2; found: 349.4.

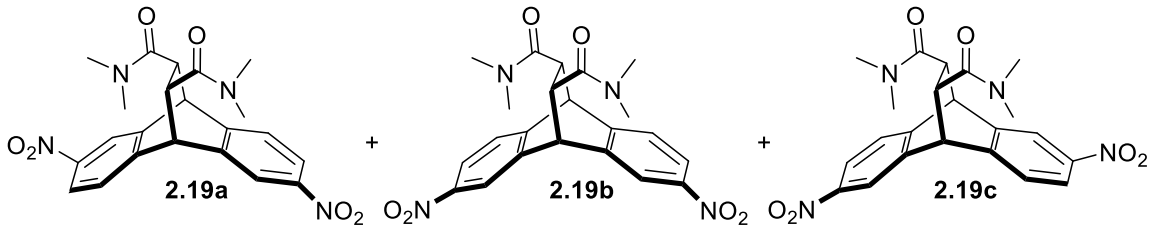

2,6-dinitro (2.19a), 2,7-dinitro (2.19b), and 3,7-dinitro (2.19c): Diastereomerically pure cycloadduct **2.18** (8.8 mg, 0.025 mmol) was dissolved in 2 mL of $CHCl_3$, followed by the addition of ammonium nitrate (6.0 mg, 0.075 mmol). To the stirred solution, trifluoroacetic anhydride (120 µL, 0.75 mmol) was added in three portions over 24 hours. After stirring under N_2 at room temperature for 48 hours, 10 mL of H_2O were added to quench the reaction. The aqueous layer was extracted with DCM (2×10 mL) and the combined organic layers were washed with brine (1×20 mL), dried over $MgSO_4$, filtered, and evaporated under reduced pressure to afford crude material. The resulting dinitrated derivatives of **2.18** were further purified by Preparative TLC (30% EtOAc in DCM) to afford 8.9 mg of an inseparable mixture of **2.19a**, **2.19b**, and **2.19c** in an 82% combined yield. ^{1}H NMR (500 MHz, $CDCl_3$) was very complex due to the mixture of regioisomers and diastereomers, and thus values are not reported. HRMS calcd. for $[C_{22}H_{23}N_4O_6]^+$: 439.1618; found: 439.1629.

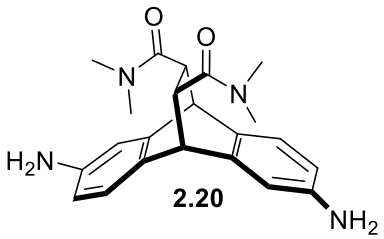

2.20

2,6-diamine dimethylamide (2.20): To a mixture of **2.19a**, **2.19b**, and **2.19c** (8.9 mg) in THF (5 mL) was added a spatula tip of Raney-nickel before the solution was purged under vacuum and backfilled with H_2 five times which was then stirred vigorously (1150 rpm) under H_2. After 16 h the solution was filtered through a pad of Celite, which was then rinsed with DCM. The crude product was taken up in DCM, washed with H_2O (1×20 mL) and then the aqueous layer extracted with DCM (2×20 mL). The combined organic layers were washed with brine (1×20 mL), dried over anhydrous $MgSO_4$, filtered, and evaporated under reduced pressure to afford crude material. The crude product obtained was purified by Preparative TLC (20% MeOH in DCM) to afford 2.4 mg of **2.20** in 85% yield based on reacted **2.19a**. ^{1}H NMR (500 MHz, $CDCl_3$): δ 6.88 (d, *J* = 7.9 Hz, 2H), 6.53 (d, *J* = 2.3 Hz, 2H), 6.25 (dd, *J* = 8.0, 2.4 Hz, 2H), 4.01 (d, *J* = 6.1 Hz, 2H), 3.66 – 3.58 (m, 2H), 3.56 (s, 2H), 3.12 (s, 6H), 3.06 – 3.02 (m, 3H), 2.82 (s, Hz, 6H). LRMS calcd. for $[C_{26}H_{35}N_4O_2]^+$: 435.3; found: 435.5.

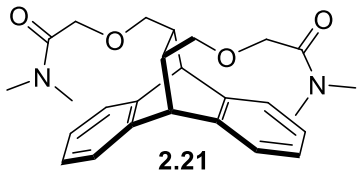

2.21

Diether-dimethylamide cycloadduct (2.21): To a flame-dried round-bottom, diol **2.10** (64 mg, .240 mmol) in 2 mL THF was added dropwise to a suspension of NaH

(60% suspension in oil) (50 mg, .961 mmol), in 5 mL THF with vigorous stirring (1000 rpm) under N_2 at 0 °C. Subsequently, 2-bromo-*N*,*N*-dimethyl acetamide (78 μL, 0.721 mmol) was added dropwise, and the reaction mixture was allowed to warm to room temperature and stirred for 16 hours. Afterwards, the reaction was quenched with 30 mL of water and the aqueous layer was extracted with DCM (3×30 mL). Finally, the organic layers were combined and washed with brine (1×30 mL), dried over $MgSO_4$, and concentrated under vacuum. The crude product was purified by flash column chromatography (0% to 30% EtOAc in DCM) to afford 43.6 mg (0.0929 mmol) of **2.11** in 39% yield. ^{1}H NMR (500 MHz, $CDCl_3$): δ 7.19 (ddd, *J* = 7.2, 4.1, 1.8 Hz, 4H), 7.07 – 6.97 (m, 4H), 4.28 (d, *J* = 2.1 Hz, 2H), 3.99 (s, 4H), 3.18 (dd, *J* = 9.1, 5.1 Hz, 2H), 2.94 (s, 6H), 2.87 (s, 6H), 1.84 (s, 2H), 1.55 (ddd, *J* = 6.3, 5.0, 2.4 Hz, 2H). ^{13}C NMR (125 MHz, $CDCl_3$): δ ppm. HRMS calcd. for $[C_{28}H_{36}N_2O_4Na]^+$: 487.2572; found: 487.2560.

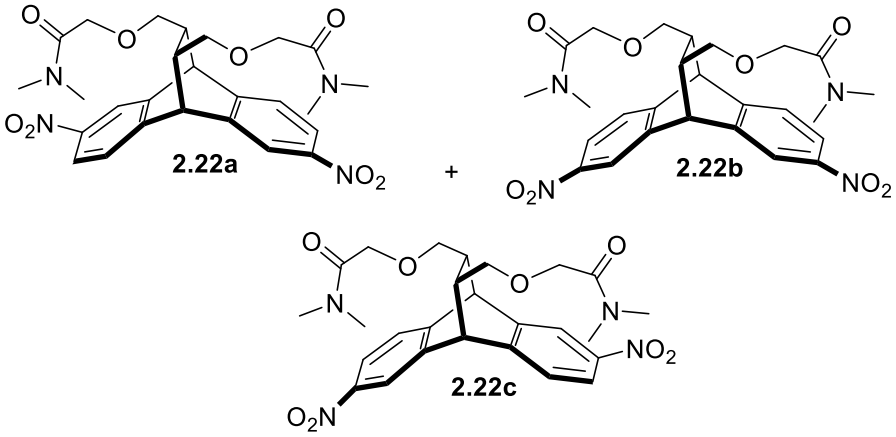

2,6-dinitro (2.22a), 2,7-dinitro (2.22b), and 3,7-dinitro (2.22c): Diastereomerically pure cycloadduct **2.21** (21.9 mg, 0.04645 mmol) was dissolved in 5 mL of $CHCl_3$, followed by the addition of ammonium nitrate (11.1 mg, 0.140 mmol). To the stirred solution, trifluoroacetic anhydride (45 µL, 0.65 mmol) was added. After stirring under N_2 at room temperature for 16 hours, 10 mL of H_2O were added to quench the reaction. The aqueous layer was extracted with DCM (2×10 mL) and the combined organic layers were washed with brine (1×20 mL), dried over $MgSO_4$, filtered, and evaporated under reduced pressure to afford crude material. The resulting dinitrated derivatives of **2.18** were further purified by Preparative TLC (15% MeOH in DCM) to afford 15.5 mg of an inseparable mixture of **2.21a**, **2.21b**, and **2.21c** in a 72% combined yield. ^1H NMR (500 MHz, $CDCl_3$) was very complex due to the mixture of regioisomers and diastereomers, and thus values are not reported. HRMS: calcd. for $[C_{27}H_{38}N_5O_8]^+$: 572.2720. Found: 572.2722.

5.3. Experimental Procedures and Characterization for Chapter 3

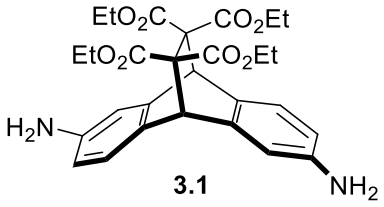

3.1

2,6-diamine tetraester (3.1): To a stirred solution of **2.4** and **2.4'** (27.66 g, 47.35 mmol) in 185 mL THF was added hydrazine monohydrate (73.49 mL, 1.5 mol) in portions.

Then, a spatula tip of Raney-Ni was added. The reaction was stirred at room temperature for 1 hour before being warmed to 60 °C. After stirring overnight at that temperature, the reaction mixture was allowed to cool to room temperature and filtered through a pad of Celite, which was then rinsed with DCM. The combined filtrates were then concentrated under reduced pressure. The crude oil obtained was re-dissolved in 185mL of DCM and washed with saturated aqueous sodium bicarbonate solution (2×178 mL). Finally, the combined aqueous layers were extracted with DCM (4×100 mL) and the combined organic layers washed with brine (1×300 mL), dried over anhydrous $MgSO_4$, filtered, and evaporated under reduced pressure to afford the crude product, as a 1-to-1 mixture of the regioisomers. To separate the two regioisomers, a 1-to-1 v/v mixture of $CHCl_3$ and diethyl ether (194 mL) was added to the crude material. This mixture was heated at 45 °C for 5 minutes under swirling, then removed from heat and cooled to room temperature. The precipitate formed was collected using vacuum filtration to afford mostly **3.1** as a light yellow solid. For further purification, this solid was triturated again from a warm 1:1 v/v mixture of chloroform and diethyl ether (96 mL), leading to 9.7 g of pure (±)-**3.1** as a white solid in 78% yield. As a note, (±)-**3.1** can be resolved kinetically to separate out pure (*S*,*S*)-3.1 as a singular enantiomer in high *ee*—spectral characterization matched our reported literature values.[4]

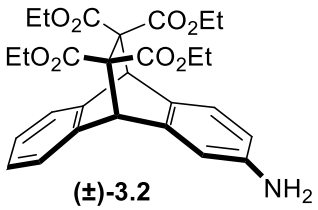

(±)-3.2

2-monoamine tetraester (3.2): To a stirred solution of **2.5** (3.1 g, 5.75 mmol) in 30 mL THF was added hydrazine monohydrate (5 mL, 101 mmol) in portions. Then, a spatula tip of Raney-Ni was added. The reaction was stirred at room temperature for 1 hour before being warmed to 60 °C. After stirring overnight at that temperature, the reaction mixture was allowed to cool to room temperature and filtered through a pad of Celite, which was then rinsed with 40 mL DCM and washed with saturated $NaHCO_3$ (aq) (1×25 mL). Finally, the combined aqueous layers were extracted with DCM (2×25 mL) and the combined organic layers washed with brine (1×25 mL), dried over anhydrous MgSO4, filtered, and evaporated under reduced pressure to afford the crude product before running flash column chromatography (0% to 50% EtOAc in hexanes) and obtaining racemic **3.2** (2.46 g, 4.8 mmol) in 83% yield. Spectral characterization matched our reported literature values.[146]

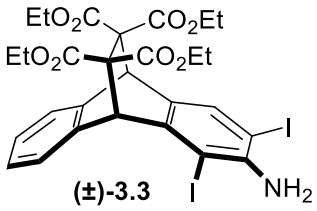

(±)-3.3

2-monoamine-diiodo tetraester (3.3): Racemic monoamine **3.2** (1.95 g, 3.82 mmol) was dissolved in 40 mL of EtOH. Then, Ag_2SO_4 (1.49 g, 4.78 mmol) and I_2 (2.42 g, 9.55 mmol) were added to the solution sequentially. After stirring at room temperature for 16 hours under N_2, the reaction mixture was filtered through a pad of Celite, which was rinsed with DCM. The combined filtrates were concentrated under reduced pressure and the crude oil obtained was re-dissolved in 50 mL of DCM and washed with H_2O (1×50 mL). Finally, the aqueous layer was washed with DCM (2×30 mL), the

combined organic layers were washed with a saturated aqueous sodium thiosulfate solution (1×50mL) and brine (1×60mL), dried over anhydrous $MgSO_4$, filtered, and evaporated under reduced pressure to afford the crude product. The crude product obtained was purified by flash column chromatography (0 to 40% EtOAc in hexanes) to afford 2.06 g of (±)-**3.3** in 71% yield. As a note, this EAS iodination strategy was used before ICl procedures were established in the group. Spectral characterization matched our reported literature values.[146]

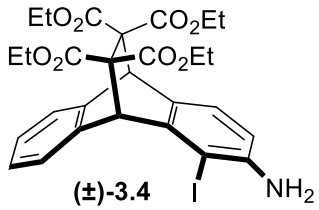

(±)-3.4

2-monoamine-*o*-iodo tetraester (3.4): The diiodo derivative(±)-**3.3** (900 mg, 1.18 mmol) was dissolved in 5 mL of THF. Next, three equivalents of Et_3N (495 μL, 3.55 mmol), six equivalents of H_2O (128 μL, 7.09 mmol), as well as a spatula tip of palladium on carbon were added to the solution and the reaction mixture was stirred vigorously (1150 rpm) under H_2 (1 atm). After 16 hours, the reaction mixture was filtered through a pad of Celite, which was then rinsed with DCM. The crude product was washed with H_2O (1×50 mL) and then the aqueous layer was extracted with DCM (2×30 mL). Finally, the combined organic layers were washed with brine (50 mL), dried over anhydrous $MgSO_4$, filtered, and evaporated under reduced pressure to afford crude material. The crude product obtained was purified by flash column chromatography (20% to 30% EtOAc in hexanes) to afford 585 mg of (±)-**3.4** in 89% yield (calculated,

based on recovered unreacted **3.3**). Spectral characterization matched our reported literature values.[146]

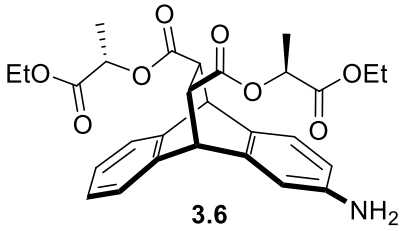

3.6

2-monoamine-diester (3.6): Nitro derivative **2.6a** (771.5 mg, 1.43 mmol) was dissolved in THF (5 mL) Next, a spatula tip of Raney-nickel was added to the solution before the reaction mixture was purged under vacuum and backfilled with H_2 five times and then stirred vigorously (1150 rpm) under H_2. After 16 h the solution was filtered through a pad of Celite, which was then rinsed with DCM. The crude product was taken up in DCM, washed with H_2O (1×20 mL) and then the aqueous layer extracted with DCM (2×20 mL). The combined organic layers were washed with brine (1×20 mL), dried over anhydrous $MgSO_4$, filtered, and evaporated under reduced pressure to afford crude material. The crude product obtained was purified by flash column chromatography (0 to 15% EtOAc in hexanes) to afford 567.2 mg of **3.6** in 78% yield. Spectral characterization matched our reported literature values.[146] LRMS calcd. for $[C_{28}H_{32}NO_8]^+$: 510.2; found: 510.4.

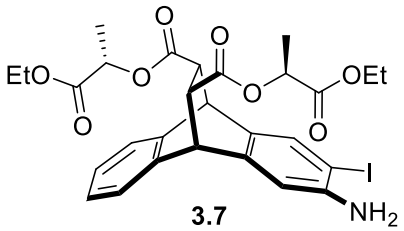

3.7

2-monoamine-*o*-iodo-diester (3.7): Following the general procedure for regioselective electrophilic iodination, monoamine **3.6** (33.5 mg, 0.0687 mmol) was dissolved in a blend of DCM (5 mL) and MeOH (5 mL) with slow addition of iodine monochloride (11.8 mg, 0.0723 mmol) at -15 °C, afforded 16.1 mg of **4.1** in 70% yield based on recovered **3.6**. The crude product obtained was purified by flash column chromatography (0 to 15% EtOAc in hexanes). ^{1}H NMR (500 MHz, $CDCl_3$): δ 7.62 (s, 1H), 7.33 (ddd, *J* = 6.9, 5.3, 2.3 Hz, 1H), 7.16 – 7.09 (m, 1H), 6.85 (s, 1H), 5.06 (q, *J* = 7.1 Hz, 1H), 5.01 (q, *J* = 7.0 Hz, 1H), 4.69 (d, *J* = 2.3 Hz, 2H), 4.32 – 4.17 (m, 5H), 4.15 (q, *J* = 7.2 Hz, 1H), 3.47 – 3.35 (m, 2H), 1.49 (d, *J* = 7.0 Hz, 3H), 1.46 (d, *J* = 7.0 Hz, 3H), 1.32 – 1.23 (m, 6H). ^{13}C NMR (125 MHz, $CDCl_3$): δ 171.57, 171.53, 170.52, 170.38, 144.91, 141.83, 141.45, 139.88, 134.32, 133.12, 126.40, 126.34, 125.29, 123.37, 112.84, 80.68, 68.97, 68.95, 61.37, 61.30, 47.90, 47.27, 46.45, 45.36, 17.03, 17.00, 14.12, 14.10.

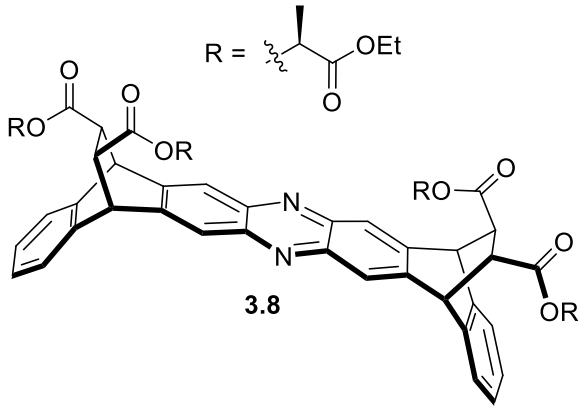

3.8

Diester C-shaped strip (3.8): Following the general procedure for Buchwald–Hartwig amination, monoiodo **3.7** (26.5 mg, 0.0417 mmol) in 1,4-dioxane (1 mL) afforded 4.4 mg dimer strip **3.8** in 15% yield. The crude product obtained was purified by Preparative TLC (60% EtOAc in hexanes). ^{1}H NMR (500 MHz, $CDCl_3$): δ 8.10 (d, *J* = 14.6 Hz, 4H),

7.54 – 7.36 (m, 4H), 7.22 – 7.08 (m, 4H), 5.15 – 4.88 (m, 8H), 4.20 (td, *J* = 7.1, 4.8 Hz, 8H), 3.60 (td, *J* = 5.7, 2.4 Hz, 2H), 3.54 (dd, *J* = 5.5, 2.3 Hz, 2H), 1.55 – 1.42 (m, 12H), 1.31 – 1.17 (m, 12H). ^{13}C NMR (125 MHz, $CDCl_3$): δ 171.23, 171.18, 170.22, 170.13, 142.58, 138.28, 127.16, 127.14, 126.92, 125.98, 125.69, 125.01, 123.81, 122.64, 69.14, 69.12, 61.40, 61.28, 47.23, 46.67, 46.48, 46.31, 16.91, 16.89, 14.01, 14.00. LRMS calcd. for $[C_{56}H_{57}N_2O_{16}]^+$: 1013.4; found: 1013.8.

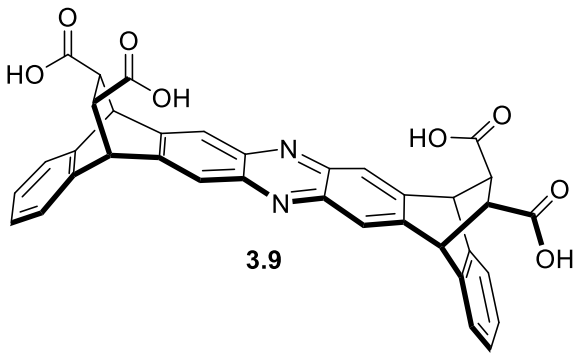

3.9

Diacid C-shaped strip (3.9): Dimer strip **3.8** (4.4 mg, 0.00434 mmol) was dissolved in 5 mL of EtOH and 50 µL of H_2O, followed by the addition of KOH (80 mg, 1.4 mmol) and the stirred solution was heated to 50 °C. After 16 hours, 10 mL of H_2O were added to quench the reaction. The aqueous layer was extracted with EtOAc (3×10 mL) and the combined organic layers were washed with brine (1×20 mL), extracted again with EtOAc (2×10 mL) dried over $MgSO_4$, filtered, and evaporated under reduced pressure to afford crude material which was washed through a plug of silica with 10% MeOH in DCM to afford 2.6 mg of **3.9** in quantitative yields. ^{1}H NMR (500 MHz, DMSO) δ 12.70 (br, 4H), 8.15 (d, *J* = 6.7 Hz, 2H), 8.00 (d, *J* = 4.4 Hz, 2H), 7.47 (dd, *J* = 9.9, 5.6 Hz, 2H), 7.38 (dt, *J* = 8.9, 4.2 Hz, 2H), 7.16 (dt, *J* = 12.1, 3.9 Hz, 4H),

4.99 (d, *J* = 19.7 Hz, 4H), 4.30 (d, *J* = 5.5 Hz, 2H), 3.66 – 3.56 (m, 2H). LRMS calcd. for $[C_{36}H_{25}N_2O_8]^+$: 613.2; found: 613.3.

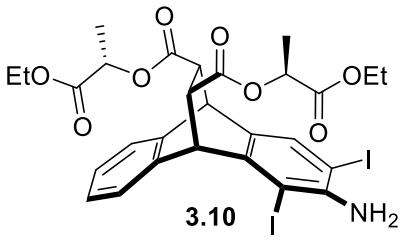

3.10

2-monoamine-diiodo diester (3.10): Following the general procedure for regioselective electrophilic iodination, monoamine **3.6** (93.5 mg, 0.183 mmol) was dissolved in a blend of DCM (2 mL) and MeOH (2 mL) with slow addition of iodine monochloride (89.4 mg, 0.550 mmol) at -15 °C, afforded 76.1 mg of **3.10** in 55% yield. The crude product obtained was purified by flash column chromatography (0 to 10% EtOAc in hexanes). ^{1}H NMR (500 MHz, $CDCl_3$): δ 7.61 (s, 1H), 7.39 – 7.35 (m, 1H), 7.33 – 7.30 (m, 1H), 7.13 – 7.09 (m, 2H), 5.06 (d, *J* = 2.4 Hz, 1H), 5.03 – 4.94 (m, 2H), 4.68 (d, *J* = 2.6 Hz, 1H), 4.60 (s, 2H), 4.26 – 4.09 (m, 4H), 3.46 – 3.37 (m, 2H), 1.45 (d, *J* = 3.2 Hz, 2H), 1.43 (d, *J* = 3.1 Hz, 2H), 1.24 (t, *J* = 7.2 Hz, 3H), 1.14 (t, *J* = 7.2 Hz, 3H). ^{13}C NMR (125 MHz, $CDCl_3$): δ 171.69, 171.54, 170.75, 170.52, 144.69, 141.59, 134.00, 126.98, 126.94, 125.67, 124.03, 108.27, 98.74, 85.40, 78.49, 68.89, 67.98, 67.71, 45.89, 33.60, 29.56, 28.16, 24.31, 23.78, 22.53, 17.35, 14.46. LRMS calcd. for $[C_{28}H_{29}I_2NO_8]^+$: 762.0; found: 762.2.

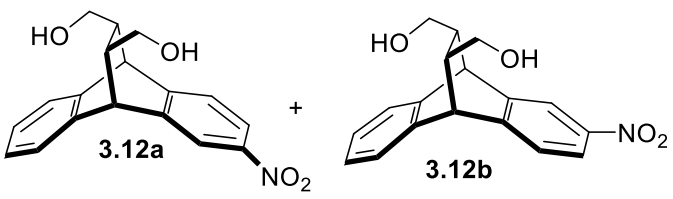

3.12a + **3.12b**

2-mononitro diol (3.12a) and 3-mononitro diol (3.12b): A 5-to-1 mixture (965 mg, 1.74 mmol) of **2.6a** and **2.6b**—dissolved in 10 mL diethyl ether—was added dropwise to a stirred (1500 rpm) suspension of $LiAlH_4$ (965 mg, 10.7 mmol) in 40mL diethyl ether at room temperature under a N_2 atmosphere. After stirring for 24 hours, the solution was cooled to 0 °C and water (40 mL) was added dropwise with vigorous stirring until quenching of the reaction was complete. Next, after acidifying the reaction mixture with a 1M aqueous HCl solution, the aqueous layer was extracted with diethyl ether (3x30 mL) and the combined organic layers were washed with brine (1x50 mL), dried over MgSO4, filtered, evaporated under reduced pressure, and washed through a plug of silica with 5% MeOH in DCM to afford 519.9 mg (1.67 mmol) of an inseparable mixture of **3.12a** and **3.12b** in a combined 96% yield. As a note, this process works for the diester cycloadduct with one or zero nitro groups on the arene subunits, but following dinitration, reduction by LAH leads to drastically minimized yields, and $NaBH_4$ is used in its stead. Spectral characterization matched our reported literature values.[146]

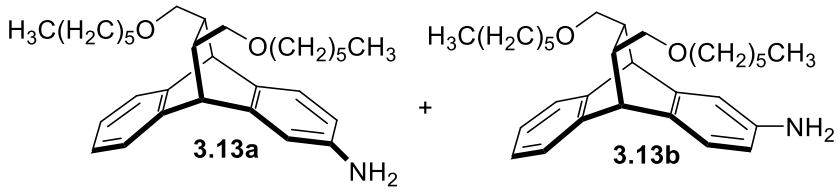

2-monoamine dieither (3.13a) and 3-monoamine diether (3.13b): For the reduction to the amines, hydrazine monohydrate (1.8 mL, 3.7 mmol) was added dropwise to a stirred solution of a 5-to-1 mixture of mononitro derivatives **2.12a** and **2.12b** (567 mg, 1.14 mmol) in 20 mL THF. Then, a spatula tip of Raney-Ni was added and the reaction

mixture was stirred at room temperature for 1 h before being warmed to 60 °C. After stirring overnight at that temperature, the reaction mixture was allowed to cool to room temperature and filtered through a pad of Celite, which was then rinsed with DCM. Thereafter, the combined filtrates were concentrated under reduced pressure and the crude oil obtained was re-dissolved in 40 mL of DCM. Finally, after washing with water (1×40 mL), the aqueous layer was extracted with DCM (3×20 mL), the combined organic layers washed with brine (1×30 mL), dried over anhydrous $MgSO_4$, filtered, and evaporated under reduced pressure to yield a mixture of crude **3.13a** and **3.13b**. The crude material was further purified using flash column chromatography (0% to 10% EtOAc in hexanes) to afford 480 mg (1.07 mmol) of **8a** and **8b** in a 5-to-1 molar ratio and a 93% combined yield. Spectral characterization matched our reported literature values.[146]

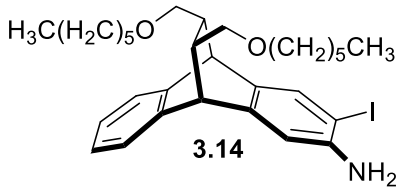

3.14

2-monoamine-*o*-iodo-diether (3.14): Following the general procedure for regioselective electrophilic iodination, monoamine **3.13a** (64.9 mg, 0.149 mmol) was dissolved in a blend of DCM (5 mL) and MeOH (5 mL) with slow addition of iodine monochloride (25.8 mg, 0.159 mmol) at -15 °C, afforded 59.6 mg of **3.14** in 70% yield. The crude product obtained was purified by flash column chromatography (0 to 5% EtOAc in hexanes). ^{1}H NMR (500 MHz, $CDCl_3$): δ 7.52 (s, 1H), 7.25 – 7.17 (m, 2H), 7.11 – 7.05 (m, 2H), 6.72 (s, 1H), 4.18 (d, *J* = 2.3 Hz, 2H), 3.93 (s, 2H), 3.44 – 3.23 (m, 4H), 3.18

(dd, *J* = 9.2, 5.1 Hz, 1H), 3.11 (dd, *J* = 9.2, 5.1 Hz, 1H), 2.83 (t, *J* = 9.5 Hz, 1H), 2.69 (t, *J* = 9.5 Hz, 1H), 1.42 – 1.25 (m, 12H), 0.92 (t, *J* = 6.9 Hz, 6H). ^{13}C NMR (125 MHz, $CDCl_3$): δ 144.28, 143.13, 143.01, 141.28, 136.03, 133.24, 125.85, 125.69, 125.22, 123.46, 112.72, 80.21, 77.29, 77.03, 76.78, 73.35, 73.24, 71.14, 71.12, 45.56, 44.31, 43.52, 42.92, 31.72, 31.72, 29.68, 25.93, 22.68, 14.12. LRMS calcd. for $[C_{30}H_{43}INO_2]^+$: 576.3; found: 576.5.

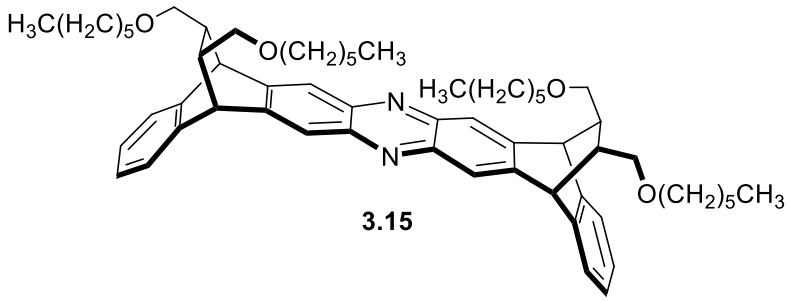

3.15

Diether C-shaped strip (3.15): Following the general procedure for Buchwald–Hartwig amination, monoiodo **3.14** (25.9 mg, 0.045 mmol) in 1,4-dioxane (1 mL) afforded 11.6 mg dimer strip **3.15** in 30% yield. The crude product obtained was purified by Preparative TLC (10% EtOAc in hexanes). ^{1}H NMR (500 MHz, $CDCl_3$): 8.01 (d, *J* = 3.5 Hz, 4H), 7.35 (dtd, *J* = 8.7, 4.8, 2.7 Hz, 4H), 7.17 (tt, *J* = 5.2, 2.7 Hz, 4H), 4.58 (t, *J* = 2.0 Hz, 4H), 3.50 – 3.37 (m, 2H), 3.38 – 3.26 (m, 4H), 3.21 (ddd, *J* = 14.0, 9.3, 5.3 Hz, 4H), 2.90 – 2.80 (m, 4H), 1.73 (ddp, *J* = 7.6, 5.3, 2.4 Hz, 4H), 1.62 – 1.49 (m, 8H), 1.42 – 1.27 (m, 24H), 0.99 – 0.87 (m, 12H). ^{13}C NMR (125 MHz, $CDCl_3$): δ 146.27, 144.01, 142.86, 142.64, 142.32, 139.98, 126.84, 126.53, 126.01, 124.52, 124.20, 122.35, 73.27, 72.91, 71.57, 71.41, 45.87, 42.93, 31.88, 31.85, 29.83, 29.79, 26.06, 26.04, 22.83, 22.80, 14.26, 14.25. LRMS calcd. for $[C_{60}H_{81}N_2O_4]^+$: 893.6; found: 893.8.

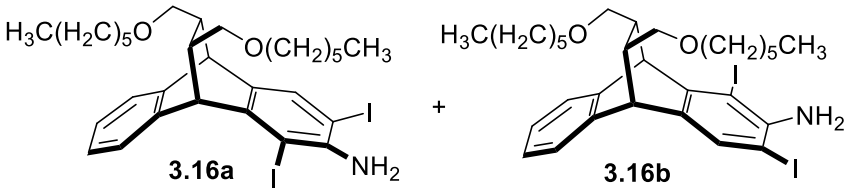

2-monoamine-diiodo dieither (3.16a) and 3-monoamine-diiodo diether (3.16b): 11 (68.2 mg, 0.152 mmol) of a 5-to-1 mixture of **3.13a** and **3.13b** were dissolved in 5 mL of DCM and 5 mL of MeOH at -15 °C and under N_2. ICl (98.5 mg, 0.61 mmol) was added dropwise with stirring. The reaction mixture was left to warm back to room temperature. After 4 hours, the reaction was quenched with saturated sodium thiosulfate and the resulting organic layer was then diluted with 30 mL DCM. The organic layer was separated, washed with brine, and dried over anhydrous $MgSO_4$, filtered, and concentrated under reduced pressure. The crude material was further purified using flash column chromatography (0% to 3% EtOAc in hexanes) to afford 72 mg of diiodinated **3.16a** and **3.16b** as an inseparable mixture in 68% combined yield. Spectral characterization matched our reported literature values.[146]

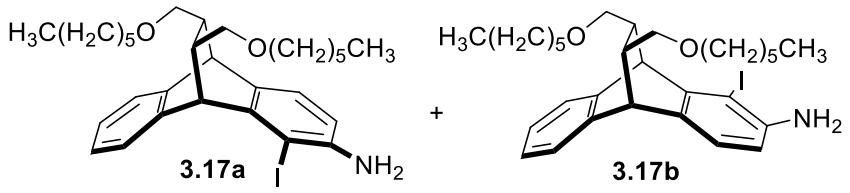

2-monoamine-*o*-iodo dieither (3.17a) and 3-monoamine-*o*-iodo diether (3.17b): **3.16a** and **3.16b** in a 5-to-1 mixture (40 mg, 0.057 mmol) were dissolved in 5 mL of THF. Next, three equivalents of Et_3N (15 μL, 0.1053 mmol), six equivalents of H_2O (5 μL, 0.211 mmol), as well as a spatula tip of palladium on carbon were added to the

reaction mixture, which was then stirred vigorously (1150 rpm) under H_2. After 16 h the solution was filtered through a pad of Celite, which was then rinsed with DCM. The crude product was taken up in DCM, washed with H_2O (1×50 mL) and then the aqueous layer extracted with DCM (2×30 mL). The combined organic layers were washed with brine (1×50 mL), dried over anhydrous $MgSO_4$, filtered, and evaporated under reduced pressure to afford crude material. The crude product obtained was purified by flash column chromatography (0 to 3% EtOAc in hexanes) to afford 18 mg (0.032 mmol) of a 5-to-1 mixture of **3.17a** and **3.17b** in 56% yield. Spectral characterization matched our reported literature values.[146]

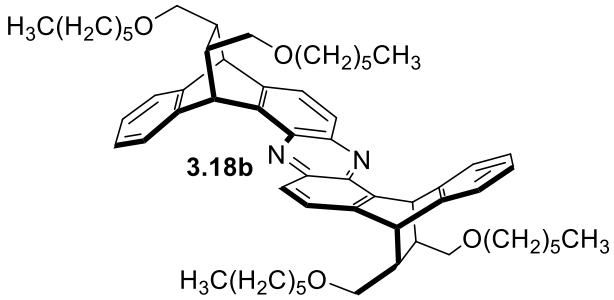

Diether helical strip (3.18b): Following the general procedure for Buchwald–Hartwig amination, a 5-to-1 mixture of **3.17a**-to-**3.17b** (18 mg, 0.032 mmol) in dioxane afforded 1.8 mg of helical strip **3.18b** in 78% yield (calculated based on **3.17b** as the limiting reagent). Purified by Preparative TLC (10% EtOAc in hexanes). Spectral characterization matched our reported literature values.[146]

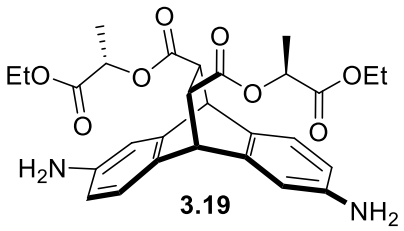

3.19

2,6-diamine diester (3.19): Nitro derivative **2.7a** (1.68 g, 2.44 mmol) was dissolved in THF (20 mL) Next, a scoop of Raney-nickel was added to the solution before the reaction mixture was purged under vacuum and backfilled with H_2 five times and then stirred vigorously (1150 rpm) under H_2. After 16 h the solution was filtered through a pad of Celite, which was then rinsed with DCM. The crude product was taken up in DCM, washed with H_2O (1×20 mL) and then the aqueous layer extracted with DCM (2×20 mL). The combined organic layers were washed with brine (1×20 mL), dried over anhydrous $MgSO_4$, filtered, and evaporated under reduced pressure to afford crude material. The crude product obtained was purified by flash column chromatography (0 to 40% EtOAc in hexanes) to afford 1.14 g of **3.19** in 76% yield. Several scoops of Raney-nickel (bordering stoichiometric addition rather than catalytic) was found most effective when more than one nitro group is found on the arene subunits of the cycloadduct due to coordination of formed amine moieties to the Raney-Ni catalyst. A very slow gradient from 30 to 37.5% EtOAc in hexanes was best found to separate any remaining isomers in the diamine reaction mixture; a 1% Et_3N mixture in a lower % EtOAc in hexanes can next be used should an isomeric mixture of diamine derivatives still remain. ^{1}H NMR (500 MHz, $CDCl_3$): δ 7.07 (d, *J* = 7.9 Hz, 2H), 6.69 (s, 2H), 6.39 (d, *J* = 7.8, 2H), 5.01 (q, *J* = 7.1 Hz, 2H), 4.56 (s, 2H), 4.32 – 4.08 (m, 4H), 3.51 (s, 4H), 3.35 (s, 2H), 1.44 (d, *J* = 7.0 Hz, 6H), 1.25 (t, *J* = 7.2 Hz, 6H). ^{13}C NMR (125 MHz, $CDCl_3$): δ 171.81, 170.58,

144.02, 141.67, 132.89, 123.89, 113.27, 112.59, 68.85, 61.30, 47.99, 46.11, 17.05, 14.12. HRMS calcd. for $[C_{28}H_{33}N_2O_8]^+$: 525.2237; found: 525.2243.

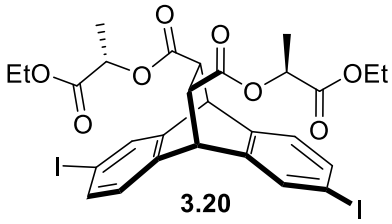

3.20

2,6-diiodo diester (3.20): To a round-bottom with 2 M HCl (40 mL) chilled to 0 °C was added **3.19** (772 mg, 1.47 mmol) in a dissolved solution of EtOH (10 mL). A solution of sodium nitrite (609 mg, 8.83 mmol) in H_2O (2 mL) was slowly added to the reaction. After 15 minutes, a solution of KI (2.0 g, 12.0 mmol) in H_2O was slowly added to the mixture. After 15 minutes, the reaction was let to heat at 70 °C. After 3 hours, the reaction solution was quenched with 50 mL of aqueous sodium thiosulfate followed by extraction by DCM (3 × 20 mL) with final brine wash (1 × 50 mL). The organic layer was then dried over anhydrous $MgSO_4$, filtered, and concentrated under reduced pressure to afford crude material. The crude product obtained was purified by flash column chromatography (0 to 5% EtOAc in hexanes) to afford 1.09 g of **3.20** in quantitative yields. ^{1}H NMR (500 MHz, $CDCl_3$): 7.73 (d, J = 1.8 Hz, 2H), 7.50 (dd, J = 7.8, 1.8 Hz, 2H), 7.12 (d, J = 7.8 Hz, 2H), 5.04 (q, J = 7.0 Hz, 2H), 4.76 (s, 2H), 4.26 (q, J = 7.1 Hz, 4H), 3.39 (s, 2H), 1.50 (d, J = 7.2 Hz, 6H), 1.29 (t, J = 7.1 Hz, 6H). ^{13}C NMR (125 MHz, $CDCl_3$): δ ppm. HRMS calcd. for $[C_{28}H_{28}I_2O_8Na]^+$: 768.9771; found: 768.9779.

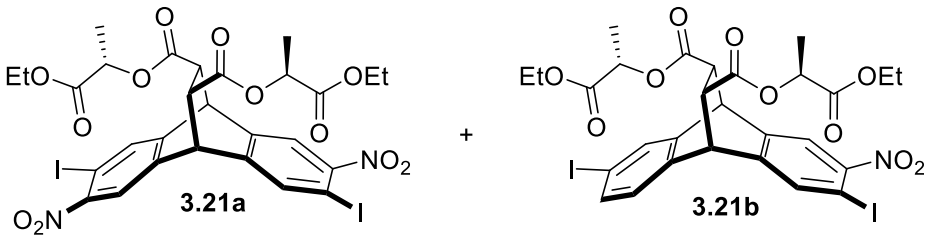

2,6-diiodo-dinitro diester (3.21a) and 2,6-diiodo-mononitro diester (3.21b): Diiodo diester **3.20** (660 mg, 0.884 mmol) was dissolved in 10 mL of $CHCl_3$, followed by the addition of ammonium nitrate (283 mg, 3.54 mmol). To the stirred solution, trifluoroacetic anhydride (1.0 mL, 7.07 mmol) was added. After stirring under N_2 at room temperature for 16 hours, 300 mg of ammonium nitrate (3.8 mmol) and 1.2 mL of trifluoroacetic anhydride (8.5 mmol) were sequentially added. After stirring under N_2 for an additional 16 hours, 10 mL of H_2O were added to quench the reaction. The aqueous layer was extracted with DCM (2×10 mL) and the combined organic layers were washed with brine (1×20 mL), dried over $MgSO_4$, filtered, and evaporated under reduced pressure to afford crude material. The crude product was purified by flash column chromatography (0 to 20% EtOAc in hexanes) to afford 380 mg of **3.21a** and 338.3 mg of **321b** in a 98% combined yield. It was found that attempting to push the reaction forward to only **3.21a** with more equivalents of ammonium nitrate and TFAA afforded large amounts of degradation. **(3.21a)**: ^{1}H NMR (500 MHz, $CDCl_3$): δ 8.09 (s, 2H), 7.85 (s, 2H), 4.97 (q, *J* = 7.0 Hz, 2H), 4.91 (s, 2H), 4.18 (q, *J* = 7.2 Hz, 4H), 3.38 (s, 2H), 1.46 (d, *J* = 7.2 Hz, 6H), 1.22 (t, *J* = 7.1 Hz, 6H). ^{13}C NMR (125 MHz, $CDCl_3$): δ 170.34, 170.20, 151.30, 144.36, 141.62, 139.71, 120.96, 84.74, 69.49, 61.81, 46.14, 45.42, 16.84, 14.23. LRMS calcd. for $[C_{28}H_{26}I_2N_2O_{12}Na]^+$: 859.0; found: 859.0. **(3.21b)**:

^{1}H NMR (500 MHz, $CDCl_3$): δ 8.12 (s, 1H), 7.92 (s, 1H), 7.79 (d, *J* = 1.8 Hz, 1H), 7.55 (dd, *J* = 7.9, 1.8 Hz, 1H), 7.15 (d, *J* = 7.9 Hz, 1H), 5.09 – 5.02 (m, 2H), 4.88 (dd, *J* = 9.3, 2.4 Hz, 2H), 4.27 (q, *J* = 7.1 Hz, 4H), 3.48 – 3.43 (m, 1H), 3.43 – 3.38 (m, 1H), 1.56 – 1.49 (m, 6H), 1.34 – 1.26 (m, 6H). ^{13}C NMR (125 MHz, $CDCl_3$): δ 170.70, 170.51, 170.30, 170.21, 151.06, 145.06, 142.78, 141.91, 139.39, 138.35, 137.67, 136.96, 124.70, 120.71, 95.87, 84.32, 69.43, 69.37, 61.76, 61.73, 46.45, 46.29, 45.44, 45.07, 16.91, 16.85, 14.23, 14.13, 14.09.

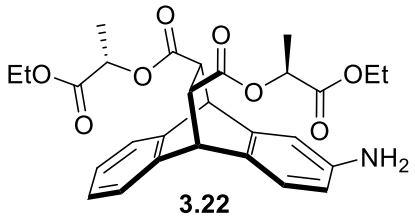

3.22

3-monoamine-diester (3.22): Nitro derivative **3.21b** (66.6 mg, 0.0842 mmol) was dissolved in THF (15 mL). Next, several spatula tips of Raney-nickel were added to the solution before the reaction mixture was purged under vacuum and backfilled with H_2 five times and then stirred vigorously (1500 rpm) under H_2. After 16 h the solution was filtered through a pad of Celite, which was then rinsed with DCM. The crude product was taken up in DCM, washed with H_2O (1×20 mL) and then the aqueous layer extracted with DCM (2×20 mL). The combined organic layers were washed with brine (1×20 mL), dried over anhydrous $MgSO_4$, filtered, and evaporated under reduced pressure to afford crude material. The crude product obtained was purified by flash column chromatography (0 to 50% EtOAc in hexanes) to afford 29.2 mg of **3.22** in 68% yield. ^{1}H NMR (500 MHz, $CDCl_3$): δ 7.35 – 7.29 (m, 2H), 7.16 – 7.03 (m, 3H), 6.73 (d, *J* = 2.3

Hz, 1H), 6.39 (dd, *J* = 7.9, 2.4 Hz, 1H), 5.11 – 4.94 (m, 2H), 4.69 (dd, *J* = 15.8, 2.4 Hz, 2H), 4.31 – 4.15 (m, 4H), 3.56 (s, 2H), 3.39 (dd, *J* = 5.4, 2.4 Hz, 1H), 3.34 (dd, *J* = 5.4, 2.4 Hz, 1H), 1.46 (d, *J* = 7.0 Hz, 3H), 1.43 (d, *J* = 7.0 Hz, 3H), 1.29 – 1.20 (m, 6H). ^{13}C NMR (125 MHz, $CDCl_3$): δ 172.07, 171.86, 170.83, 170.79, 145.50, 145.30, 143.56, 138.63, 132.22, 129.31, 127.08, 126.68, 126.24, 123.79, 112.89, 111.30, 69.34, 69.29, 61.70, 60.76, 48.09, 47.65, 46.74, 46.15, 17.39, 17.34, 14.49, 14.47. LRMS calcd. for $[C_{28}H_{31}N_1O_8Na]^+$: 532.2; found: 532.4.

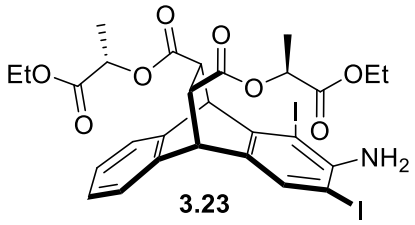

3.23

3-monoamine-diiodo-diester (3.23): Following the general procedure for regioselective electrophilic iodination, monoamine **3.22** (37.7 mg, 0.074 mmol) was dissolved in a blend of DCM (5 mL) and MeOH (5 mL) with slow addition of iodine monochloride (52.1 mg, 0.321 mmol) at -15 °C to afford 44.5 mg of **3.23** in 79% yield. The crude product obtained was purified by flash column chromatography (0 to 10% EtOAc in hexanes). ^{1}H NMR (500 MHz, $CDCl_3$): δ 7.62 (d, *J* = 3.2 Hz, 2H), 7.35 – 7.31 (m, 2H), 7.09 (dd, *J* = 7.9, 2.1 Hz, 1H), 5.12 (d, *J* = 2.1 Hz, 1H), 5.07 – 4.97 (m, 3H), 4.73 – 4.60 (m, 2H), 4.28 – 4.15 (m, 4H), 3.39 – 3.28 (m, 2H), 1.49 (t, *J* = 7.1 Hz, 6H), 1.32 – 1.22 (m, 6H).^{13}C NMR (125 MHz, $CDCl_3$): δ 171.65, 171.45, 170.80, 170.61, 147.13, 144.91, 144.53, 137.75, 136.23, 132.82, 131.72, 127.57, 126.71, 123.89, 82.80, 78.84, 69.58,

69.57, 61.94, 61.76, 51.79, 47.52, 46.73, 46.58, 17.35, 17.32, 14.63, 14.53. LRMS calcd. for $[C_{28}H_{29}I_2NNaO_8]^+$: 784.0; found: 784.1.

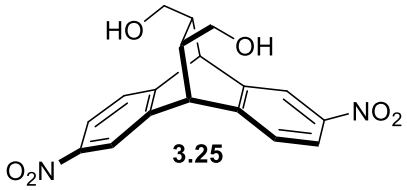

3.25

3,7-dinitro diol (3.25): **3.21a** (118 mg, 0.141 mmol) was dissolved in THF (5 mL) and then added dropwise to a stirring suspension of sodium borohydride (64.3 mg, 1.42 mmol) in THF (10 mL) at room temperature, and then heated to 60 °C for 15 minutes. Following this, MeOH (5 mL) was added dropwise to the stirring, heated solution, stopping addition briefly when vigorous bubbling occurred. The solution was then left to heat and stir for 2 hours. After, the reaction mixture was allowed to cool to room temperature and diluted with DCM (20 mL) and washed with water (1×20 mL). The aqueous layer was then extracted with a blend of 5-to-1, DCM to MeOH (5×10 mL) and the combined organic layers were dried over anhydrous $MgSO_4$, filtered, and evaporated under reduced pressure to obtain crude product which was then filtered through a plug of silica with 5% MeOH and DCM to afford 50.2 mg of nitro-diol **3.25** in quantitative yields and was carried forward without further purification. ^{1}H NMR is complex due to presence of minor remaining iodo groups on arene rings, however during Raney-Ni reduction to produce **3.27**, these persisting iodo groups are reduced, and thus these minor impurities are carried forward in this synthesis. ^{1}H NMR (500 MHz, MeOD): δ 8.18 (d, *J* = 2.4 Hz, 2H), 8.07 (dd, *J* = 8.1, 2.3 Hz, 2H), 7.58 (d, *J* = 8.1 Hz, 2H), 4.74 (dd, *J* = 4.3, 2.0 Hz, 2H), 3.77 – 3.69 (m, 2H), 3.40 – 3.30 (m, 2H), 1.91 – 1.83 (m, 2H). ^{13}C NMR

(125 MHz, $CDCl_3$): δ 149.07, 148.06, 127.69, 126.11, 122.73, 119.71, 68.83, 30.88, 26.46. LRMS calcd. for $[C_{18}H_{15}N_2O_6]^-$: 355.1; found: 354.9.

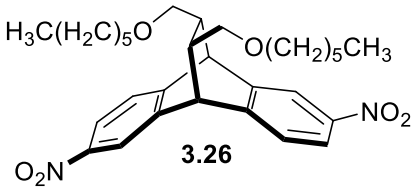

3.26

3,7-dinitro diether (3.26): A solution of **3.25** (50.2 mg, 0.096 mmol) in a blend of THF (48 mL) and water (2 mL) was heated to reflux upon addition of KOH (17.8 mg, 0.317 mmol). This solution was left to heat and stir for 1 hour. Then, bromohexane (45 µL, 0.317 mmol) was added dropwise to the solution. After 16 hours, more KOH (17.8 mg, 0.317 mmol) was added to the solution and left to heat and stir for 1 hour. Then, another portion of bromohexane (45 µL, 0.317 mmol) was added dropwise to the solution. After 4 hours the solution was allowed to cool to room temperature and concentrated under reduced pressure, and the crude oil obtained was re-dissolved in 20 mL of DCM. After washing with water (1×20 mL), the aqueous layer was extracted with DCM (3×10 mL), the combined organic layers washed with brine (1×20 mL), dried over anhydrous MgSO4, filtered, and evaporated under reduced pressure to afford crude material. The crude product was further purified using flash column chromatography (0 to 30% EtOAc in hexanes) to afford 44.4 mg of **3.26** in near quantitative yields. By ^{1}H NMR analysis, if the product 4.8 had not fully converted, more aliquots of KOH and bromohexane can be added to the mixture.^{1}H NMR (500 MHz, $CDCl_3$): δ 8.19 (d, *J* = 2.3 Hz, 2H), 8.09 (dd, *J* = 8.2, 2.2 Hz, 2H), 7.49 (d, *J* = 8.1 Hz, 2H), 4.60 (s, 2H), 4.12 (q, *J* = 7.2 Hz, 2H), 3.35

(s, 2H), 3.33 – 3.14 (m, 1H), 2.05 (s, 2 H), 1.76 (t, *J* = 4.3 Hz, 4H), 1.38 – 1.24 (m, 12H), 0.96 – 0.83 (m, 2H). ^{13}C NMR (125 MHz, $CDCl_3$): δ 147.08, 146.81, 143.35, 126.20, 122.16, 119.02, 65.15, 60.43, 55.99, 53.43, 45.98, 44.89, 29.70, 21.06, 14.19.

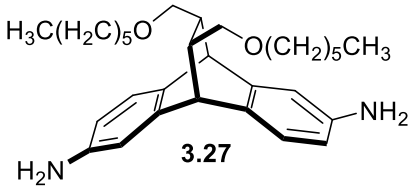

3.27

3,7-diamine diether (3.27): A spatula tip of Raney-Ni was added to dinitro **3.26** (29.7 mg, 0.057 mmol) in 20 mL of THF. The reaction mixture was stirred at room temperature and hydrazine monohydrate (2 mL, 41.2 mmol) was added dropwise to the solution and then warmed to 60 °C. After stirring for 3 hours, the reaction mixture was allowed to cool to room temperature and filtered through a pad of Celite, which was then rinsed with DCM. Thereafter, the filtrate was concentrated under reduced pressure and the crude oil obtained was re-dissolved in 40 mL of DCM. Finally, after washing with water (1×40 mL), the aqueous layer was extracted with DCM (3×20 mL), the combined organic layers washed with brine (1×30 mL), dried over anhydrous $MgSO_4$, filtered, and evaporated under reduced pressure to afford crude material. The crude product was further purified using flash column chromatography (0 to 20% EtOAc in hexanes) to afford diamine **3.27** in 14.7 mg and at a 56% yield. ^{1}H NMR (500 MHz, $CDCl_3$): δ 6.91 (d, *J* = 7.8 Hz, 2H), 6.57 (d, *J* = 2.3 Hz, 2H), 6.32 (dd, *J* = 7.8, 2.3 Hz, 2H), 4.00 (d, *J* = 1.5 Hz, 2H), 3.44 (s, 4H), 3.30 (dt, *J* = 9.5, 6.6 Hz, 2H), 3.21 (dt, *J* = 9.6, 6.7 Hz, 2H), 3.07 (dd, *J* = 9.1, 4.7 Hz, 2H), 2.71 (t, *J* = 9.4 Hz, 2H), 1.40 – 1.35 (m, 2H), 1.34 – 1.19 (m, 12H), 0.84 (t, *J* = 7.0 Hz, 6H).

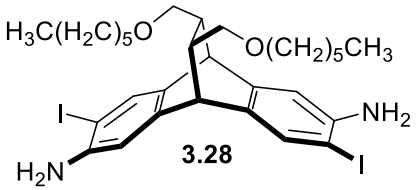

3.28

3,7-diamine-diiodo diether (3.28): Following the general procedure for regioselective electrophilic iodination, diamine **3.27** (2.9 mg, 0.0062 mmol) dissolved in a blend of DCM (10 mL) and MeOH (10 mL) with slow addition of iodine monochloride (2 eq.) at -15 °C, afforded 3.7 mg of **4.5** in 83% yield. The crude product obtained was purified by flash column chromatography (0 to 10% EtOAc in hexanes). ^{1}H NMR (500 MHz, $CDCl_3$): δ 7.46 (s, 2H), 6.70 (s, 2H), 4.03 (d, *J* = 1.5 Hz, 2H), 3.97 (s, 4H), 3.48 – 3.26 (m, 6H), 3.16 (dd, *J* = 9.3, 4.3 Hz, 2H), 2.80 (t, *J* = 9.3 Hz, 2H), 1.46 (s, 2H), 1.42 – 1.32 (m, 12H), 0.95 – 0.92 (m, 6H). ^{13}C NMR (125 MHz, $CDCl_3$): δ 145.51, 144.77, 135.02, 132.73, 110.56, 79.75, 73.05, 71.15, 44.18, 42.98, 31.71, 29.61, 25.93, 22.71, 14.13, 14.09. LRMS calcd. for $[C_{30}H_{43}I_2N_2O_2]^+$: 717.2; found: 717.4.

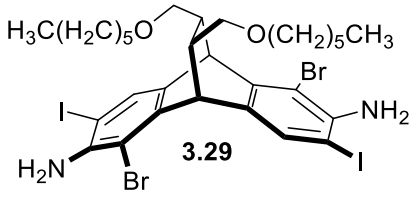

3.29

3,7-diamine-diiodo-dibromo diether (3.28): Following the general procedure for regioselective electrophilic iodination, diamine **3.27** (3.7 mg, 0.0052 mmol) dissolved in MeCN at -15 °C with slow addition of NBS (2 eq.) dissolved in MeCN at -15 °C, afforded 1.7 mg of **4.5** in 38% yield. The crude product obtained was purified by Preparative TLC with 10% EtOAc in hexanes. ^{1}H NMR (500 MHz, $CDCl_3$): 7.30 (s, 2H),

4.64 – 4.58 (m, 2H), 4.50 (s, 4H), 3.47 – 3.38 (m, 2H), 3.34 – 3.26 (m, 2H), 3.19 – 3.11 (m, 2H), 2.85 (t, *J* = 9.3 Hz, 2H), 1.66 – 1.46 (m, 8H), 1.36 (dd, *J* = 25.9, 6.0 Hz, 12H), 0.92 (t, *J* = 6.9 Hz, 6H). ^{13}C NMR (125 MHz, $CDCl_3$): δ 143.21, 140.10, 131.47, 128.30, 106.33, 105.13, 72.90, 71.00, 45.12, 41.75, 31.72, 29.70, 25.97, 22.70, 14.11.

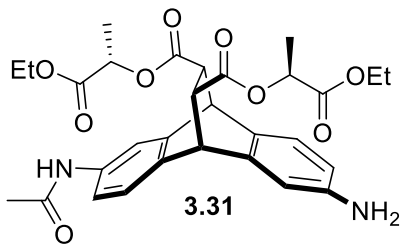

3.31

2-amine-6-methylamide diester (3.31): Diamine **3.19** (1.08 g, 2.205 mmol) was dissolved in MeCN (5 mL) and heated to 65 °C under N_2. A solution of acetic anhydride (288 µL, 3.05 mmol) in MeCN (2 mL) was added dropwise to the stirring solution. After 16 hours, the solution was concentrated under vacuum to remove solvent and then re-dissolved in 20 mL of DCM washed with H_2O (1×20 mL). Thereafter the aqueous layer was extracted with DCM (3×20 mL) and the combined organic layers were then washed with brine (1×20 mL) and the organic layer was dried over anhydrous $MgSO_4$, filtered, and concentrated under reduced pressure to afford crude material. The crude product obtained was purified by flash column chromatography (0 to 30% EtOAc in hexanes) to afford 562 mg of *N*-actyl-**3.31** in 55% yield based on recovered **3.19**. ^{1}H NMR (500 MHz, $CDCl_3$): δ 7.69 (s, 1H), 7.44 (d, *J* = 2.3 Hz, 1H), 7.19 (dd, *J* = 8.0, 2.2 Hz, 1H), 7.12 (d, *J* = 8.1 Hz, 1H), 7.02 (d, *J* = 7.9 Hz, 1H), 6.68 (d, *J* = 2.4 Hz, 1H), 6.36 (dd, *J* = 7.9, 2.4 Hz, 1H), 4.98 (dq, *J* = 20.6, 7.0 Hz, 2H), 4.61 (t, *J* = 2.4 Hz, 2H), 4.24 – 4.06 (m, 4H), 3.56 (s, 2H), 3.35 (dd, *J* = 5.3, 2.4 Hz, 1H), 3.31 (dd, *J* = 5.3, 2.4 Hz, 1H), 2.01 (s,

3H), 1.46 – 1.39 (m, 6H), 1.27 – 1.15 (m, 6H). ^{13}C NMR (125 MHz, $CDCl_3$): δ 171.85, 171.67, 170.58, 170.57, 168.33, 144.88, 141.36, 140.91, 138.13, 136.23, 132.20, 124.04, 123.58, 117.39, 117.13, 113.13, 112.47, 69.06, 68.99, 61.37, 48.01, 47.80, 46.31, 45.99, 24.40, 17.05, 17.00, 14.22, 14.12, 14.08. HRMS calcd. for $C_{30}H_{35}N_2O_9$: 567.2343; found: 567.2356.

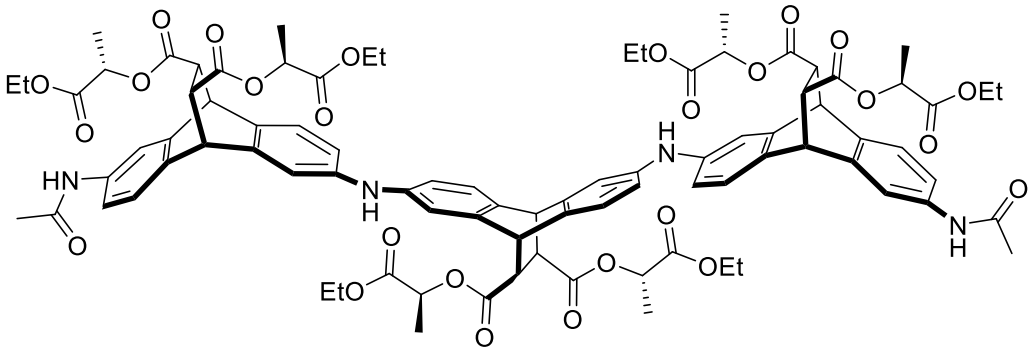

3.32

***N,N*'-diacyl trimer diester strip (3.32)**: Following the general procedure for Buchwald–Hartwig amination, diiodo **3.20** (67.2 mg, 0.090 mmol), monoamine **3.31** (102 mg, 0.180 mmol) and SPhos (29.6 mg, 0.072 mmol) in toluene (3 mL) afforded 76.4 mg trimer strip **3.32** in 52% yield. The crude product obtained was purified by flash column chromatography (0 to 40% EtOAc in hexanes). ^{1}H NMR (500 MHz, $CDCl_3$): δ 7.37 (d, *J* = 14.2 Hz, 4H), 7.25 – 7.13 (m, 4H), 7.07 (dd, *J* = 8.0, 3.7 Hz, 4H), 6.93 (d, *J* = 5.6 Hz, 4H), 6.69 (dd, *J* = 8.0, 1.8 Hz, 4H), 4.97 – 4.87 (m, 6H), 4.60 (dd, *J* = 6.9, 2.1 Hz, 4H), 4.55 (s, 2H), 4.10 (t, *J* = 6.9 Hz, 2H), 4.08 – 4.01 (m, 12H), 3.34 – 3.24 (m, 6H), 2.01 (s, 6H), 1.39 – 1.34 (m, 18H), 1.21 – 1.16 (m, 18H). ^{13}C NMR (125 MHz, $CDCl_3$): 172.04, 171.88, 171.50, 170.85, 170.78, 170.74, 168.44, 142.02, 141.80, 141.72, 141.45, 141.23, 138.46, 136.52, 134.97, 134.61, 124.33, 124.25, 124.03, 117.75, 117.49, 115.66, 115.18,

69.37, 69.34, 69.27, 61.68, 61.65, 60.73, 48.21, 48.17, 48.07, 46.66, 46.55, 46.40, 21.37, 17.34, 17.31, 14.52, 14.40, 14.35, 14.32. HRMS calcd. for $[C_{88}H_{95}N_4O_{26}]^+$: 1739.7072; found: 1739.7092.

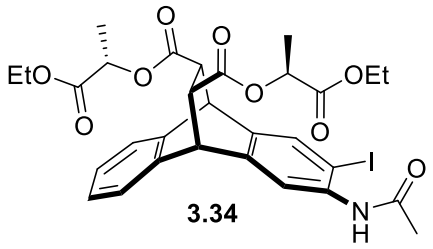

3.34

2-methylamide-*o*-iodo diester (3.34): Monoamine **3.7** (42.8 mg, 0.0674 mmol) was dissolved in MeCN (5 mL) and heated to 65 °C under N_2. A solution of acetic anhydride (120 µL, 1.09 mmol) in MeCN (1 mL) was added dropwise to the stirring solution. After 16 hours, the solution was concentrated under vacuum to remove solvent and then re-dissolved in 20 mL of DCM washed with H_2O (1×20 mL). Thereafter the aqueous layer was extracted with DCM (3×20 mL) and the combined organic layers were then washed with brine (1×20 mL) and the organic layer was dried over anhydrous $MgSO_4$, filtered, and concentrated under reduced pressure to afford crude material. The crude product obtained was purified by flash column chromatography (0 to 30% EtOAc in hexanes) to afford 43.4 mg of *N*-actyl-**3.34** in 95% yield. LRMS calcd. for $[C_{30}H_{32}INO_9Na]^+$: 677.1; found: 677.3.

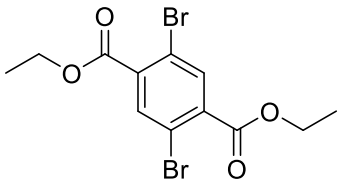

3.35

***p*-dibromo-*o*-diethylester (3.35)**: To a round-bottom with 2,5-dibromoterephthalic acid (1.0 g, 3.09 mmol) was added EtOH (30 mL) and concentrated H_2SO_4 (100 µL, catalytic) and heated to reflux. After 24 hours, an additional portion of 100 µL H_2SO_4 was added. After an additional 24 hours, the reaction was quenched with 40 mL of H_2O. The aqueous layer was extracted with DCM (2×40 mL) and the combined organic layers were washed with saturated $NaHCO_3$ (1×25 mL), dried over $MgSO_4$, filtered, and evaporated under reduced pressure to afford 1.13 g of **3.35** in 96% yield which was carried forward without further purification. Spectral characterization matched reported literature values.[201]

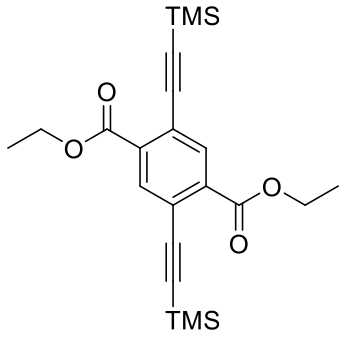

3.36

***p*-(trimethylsilyl)ethynyl-*o*-diethylester (3.36)**: Into a flame-dried, argon-purged, Schlenk tube were sequentially (i) aryl halide building block **3.34** (1.13 mg, 2.97 mmol), (ii) palladium(0) tetrakis (68.6 mg, 0.0594 mmol), (iii) Et_3N (2.5 mL, 17.8 mmol), (iv) Copper(I) iodide (28.3 mg, 0.141 mmol), (v) as well as dry, degassed THF (50 mL) followed by ten minutes of bubbling N_2 through the reaction mixture whereby (vi) trimethylactylene (4.24 mL, 29.7 mmol) was added followed by an additional two minutes of bubbling N_2 through the solution (being careful not to evaporate

trimethylactylene). The mixture was let stir at room temperature under N_2 for 24 hours. After completion, the solution was cooled to room temperature, filtered through a pad of Celite, and rinsed with DCM. The solution was then washed with water (1×20 mL), the aqueous layer was extracted with DCM (3×20 mL) and the combined organic layers were then washed with brine (1×20 mL). The organic layer was then dried over anhydrous $MgSO_4$, filtered, and concentrated under reduced pressure to afford crude material. The crude product obtained was purified by flash column chromatography (0 to 5% EtOAc in hexanes) to afford 0.790 g of **3.36** in 64% yield. Spectral characterization matched reported literature values.[202]

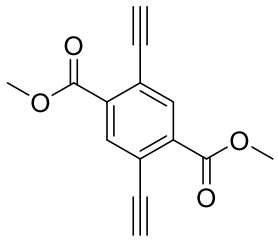

3.37

***p*-ethynyl-*o*-dimethylester (3.37)**: To a round-bottom with **3.36** (0.79 g, 1.91 mmol) was added MeOH (30 mL) and K_2CO_3 (1.05 g, 7.62 mmol) and stirred at room temperature. After 16 hours, the reaction was quenched with 40 mL of H_2O. The aqueous layer was extracted with DCM (2×40 mL) and the combined organic layers were washed with saturated $NaHCO_3$ (1×25 mL), dried over $MgSO_4$, filtered, and evaporated under reduced pressure to afford crude material. The crude product obtained was purified by flash column chromatography (0 to 25% EtOAc in hexanes) to afford 430 mg of **3.37** in 93% yield. ^{1}H NMR (500 MHz, $CDCl_3$): δ 8.17 (s, 2H), 3.96 (s, 6H), 3.52 (s,

2H). ^{13}C NMR (125 MHz, $CDCl_3$): δ 165.34, 137.07, 135.34, 123.03, 85.33, 81.08, 53.04. LRMS calcd. for $[C_{14}H_{11}O_4]^+$: 243.1. Found: 243.3.

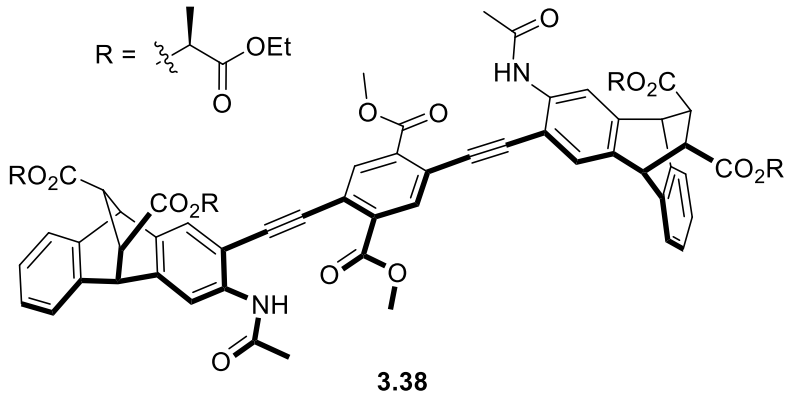

3.38

Sonogashira-coupled diester strip (3.38): Into a flame-dried, argon-purged, Schlenk tube were sequentially (i) aryl halide building block **3.34** (43.4 mg, 0.06403 mmol), (ii) linker piece **3.37** (6.0 mg, 0.0248 mmol), (iii) palladium(0) tetrakis (1.5 mg, 0.0013 mmol), (iv) Et_3N (21 µL, 0.286 mmol), (v) Copper(I) iodide (0.5 mg, 0.00262 mmol), (vi) as well as dry, degassed DMF followed by ten minutes of bubbling N_2 through the reaction mixture. The mixture was let stir at room temperature under N_2 for 16 hours. After completion, the solution was cooled to room temperature, filtered through a pad of Celite, and rinsed with DCM. The solution was then washed with water (1 × 20 mL), the aqueous layer was extracted with DCM (3 × 20 mL) and the combined organic layers were then washed with brine (1 × 20 mL). The organic layer was then dried over anhydrous $MgSO_4$, filtered, and concentrated under reduced pressure to afford crude material. The crude product was purified by Preparative TLC (60% EtOAc in hexanes) to afford 27.6 mg of **3.38** in 81% yield. ^{1}H NMR (500 MHz, $CDCl_3$): δ 9.10 (s, 2H), 8.64 (s, 2H), 8.31 (s, 2H), 7.54 (s, 2H), 7.44 – 7.32 (m, 4H), 7.21 – 7.09 (m, 4H), 5.02 (dq, *J* =

11.4, 7.0 Hz, 4H), 4.85 (d, *J* = 2.3 Hz, 2H), 4.78 (d, *J* = 2.1 Hz, 2H), 4.32 – 4.13 (m, 8H), 3.99 (s, 6H), 3.47 – 3.37 (m, 4H), 2.39 (s, 6H), 1.45 (dd, *J* = 9.6, 7.0 Hz, 12H), 1.25 (td, *J* = 7.1, 2.0 Hz, 12H). ^{13}C NMR (125 MHz, $CDCl_3$): δ 171.81, 170.82, 170.65, 169.76, 165.27, 143.47, 142.09, 140.60, 140.26, 139.69, 137.48, 136.30, 132.71, 130.76, 127.01, 126.78, 125.79, 124.14, 123.72, 108.73, 94.71, 94.06, 69.80, 69.38, 61.87, 61.74, 53.29, 48.14, 47.80, 47.46, 46.34, 24.95, 17.39, 17.39, 14.52, 14.50. LRMS calcd. for $[C_{77}H_{84}N_2O_{22}]^+$: 1341.6. Found: 1341.6.

5.4. Experimental Procedures and Characterization for Chapter 4

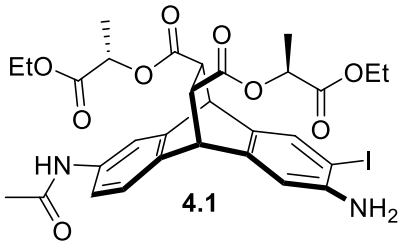

4.1

2-amine-3-iodo-6-methylamide diester (4.1): Following the general procedure for regioselective electrophilic iodination, monoamine **3.31** (562 mg, 0.992 mmol) dissolved in a blend of DCM (10 mL) and MeOH (10 mL) with slow addition of iodine monochloride (161 mg, 0.992 mmol) at -15 °C, afforded 497.3 mg of **4.1** in 73% overall yield. The crude product obtained was purified by flash column chromatography (0 to 15% EtOAc in hexanes). ^{1}H NMR (500 MHz, $CDCl_3$): δ 7.57 (s, 1H), 7.37 (d, *J* = 2.3 Hz, 2H), 7.24 (d, *J* = 8.5 Hz, 1H), 7.16 (s, 1H), 6.80 (s, 1H), 5.01 (dq, *J* = 21.1, 7.1 Hz, 2H), 4.63 (dd, *J* = 8.1, 2.4 Hz, 2H), 4.28 – 4.15 (m, 4H), 3.96 (s, 2H), 3.37 (dd, *J* = 5.5, 2.4

Hz, 1H), 3.33 (dd, *J* = 5.3, 2.4 Hz, 1H), 2.11 (s, 3H), 1.46 (dd, *J* = 11.7, 7.1 Hz, 6H), 1.26 (t, *J* = 7.1 Hz, 6H). HRMS calcd. for $[C_{30}H_{34}IN_2O_9]^+$: 693.1309; found: 693.1298.

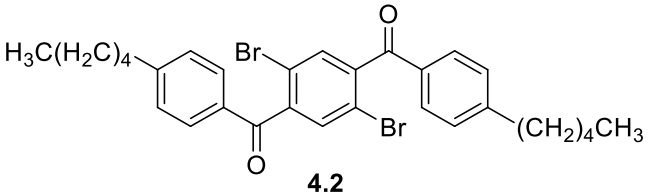

4.2

***p*-dibromo-*o*-dipentylbenzoyl benzene (4.2)**: To a round-bottom with thionyl chloride (10 mL) was added 2,5-dibromoterephtalic acid (2.16 g, 6.67 mmol) and heated to reflux under N_2. The reaction was concentrated to remove $SOCl_2$, and dissolved in DCM at 0 °C before slowly adding the crude reaction mixture to a stirred solution of $AlCl_3$ (1.3g, 10.0 mmol) and amylbenzene (3.4 mL, 20.0 mmol) in DCM (20 mL) at -15 °C, letting warm to room temperature. After 16 h the solution was filtered through a pad of Celite, which was then rinsed with DCM. The crude product was taken up in DCM, washed with 0 °C $NaHCO_3$ (aq) (1×50 mL) and then the aqueous layer extracted with DCM (2×30 mL). The combined organic layers were washed with brine (1×50 mL), dried over anhydrous $MgSO_4$, filtered, and evaporated under reduced pressure to afford crude material. The crude product obtained was purified by flash column chromatography (0 to 10% EtOAc in hexanes) to afford 1.07 g of **4.2** in 28% overall yield. Spectral characterization matched reported literature values.[203] LRMS calcd. for $[C_{30}H_{33}Br_2O_2]^+$: 583.1; found: 583.3.

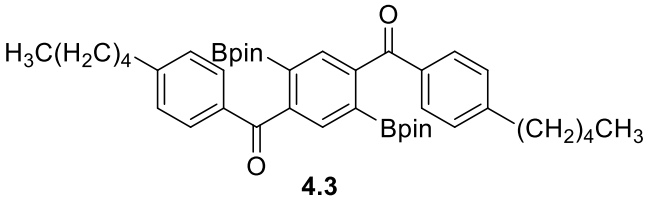

4.3

***p*-diBpin-*o*-dipentylbenzoyl benzene linker (4.3)**: Following the general procedure for Miyaura borylation, *p*-dibromo **4.2** (1.07 g, 1.83 mmol) was dissolved in 1,4-dioxane along with bis(pinacolato)diboron (930 mg, 3.66 mmol) to afford 1.13 g of *syn*-linker **4.3** in 91% yield. The crude product obtained was purified by flash column chromatography (0 to 10% EtOAc in hexanes). ^{1}H NMR (500 MHz, $CDCl_3$): δ 7.88 (s, 2H), 7.71 (d, *J* = 8.2 Hz, 4H), 7.24 (d, *J* = 8.4 Hz, 4H), 2.66 (t, *J* = 7.7 Hz, 4H), 1.67 – 1.59 (m, 4H), 1.37 – 1.30 (m, 8H), 1.09 (s, 24H), 0.89 (t, *J* = 7.0 Hz, 6H). ^{13}C NMR (125 MHz, $CDCl_3$): *δ* ppm. LRMS calcd. for $[C_{42}H_{57}B_2O_6]^+$: 679.4; found: 679.7.

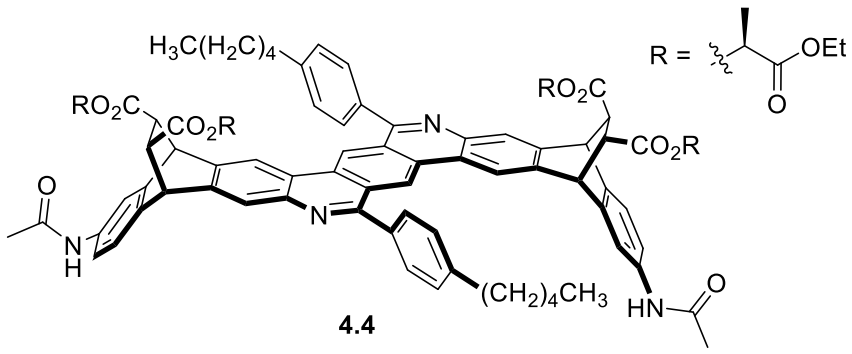

4.4

***N,N*'-diacyl diester *syn*-helical strip (4.4)**: Following the general procedure for Suzuki coupling/imine condensation, *N*-methylamide-**4.1** (41.0 mg, 0.059 mmol) and *syn*-linker **4.3** (20.1 mg, 0.030 mmol) in 1,4-dioxane (1.5 mL) afforded 26.0 mg (0.0164 mmol) of *syn*-helical dimer **4.4** in 55% yield. The crude product obtained was purified by flash column chromatography (0 to 40% EtOAc in hexanes). ^{1}H NMR (500 MHz, $CDCl_3$): 9.50 (s, 2H), 8.41 (s, 2H), 8.21 (s, 2H), 7.85 (d, *J* = 8.1 Hz, 4H), 7.72 (s, 2H), 7.59 (d, *J* = 8.2 Hz, 4H), 7.39 (d, *J* = 8.1 Hz, 2H), 7.26 (d, *J* = 7.9 Hz, 2H), 7.10 (s, 2H), 5.10 – 5.01 (m, 6H), 4.29 – 4.21 (m, 6H), 3.55 (dd, *J* = 5.4, 2.5 Hz, 2H), 3.51 (dd, *J* = 5.5, 2.4 Hz, 2H), 2.92 (td, *J* = 7.3, 2.6 Hz, 4H), 2.16 (s, 6H), 1.85 (p, *J* = 7.5 Hz, 4H), 1.49 (d, *J* = 6.9 Hz, 6H), 1.46 (d, *J* = 7.0 Hz, 6H), 1.30 (t, *J* = 7.1 Hz, 6H), 1.19 (t, *J* = 7.1 Hz, 6H), 1.01 (t, *J* = 7.1 Hz, 6H). ^{13}C NMR (125 MHz, $CDCl_3$): δ 171.50, 171.48, 170.49, 170.43, 170.34, 168.09, 144.21, 142.38, 141.18, 140.90, 137.72, 137.06, 136.42, 133.16, 131.12, 129.93, 129.02, 126.95, 125.65, 124.08, 123.76, 122.93, 121.99, 117.81, 117.57, 116.84, 112.71, 69.25, 68.98, 61.51, 61.43, 60.41, 47.82, 47.38, 46.69, 46.16, 35.97, 31.65, 31.09, 24.85, 22.62, 17.01, 16.94, 14.11, 14.09. HRMS calcd. for $[C_{94}H_{112}N_4O_{18}]^{2+}$: 760.3360; found: 760.3376.

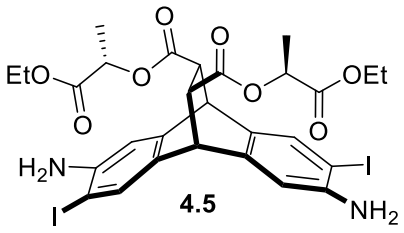

4.5

2,6-diamine-diiodo diester (4.5): Following the general procedure for regioselective electrophilic iodination, diamine **3.19** (1.04 g, 1.977 mmol) dissolved in a blend of DCM

(10 mL) and MeOH (10 mL) with slow addition of iodine monochloride (642.1 mg, 3.96 mmol) at -15 °C, afforded 1.16 g of **4.5** in 77% overall yield. The crude product obtained was purified by flash column chromatography (0 to 10% EtOAc in hexanes). ^{1}H NMR (500 MHz, $CDCl_3$): δ 7.55 (s, 2H), 6.79 (s, 2H), 5.02 (q, *J* = 7.1 Hz, 2H), 4.52 (s, 2H), 4.30 – 4.11 (m, 4H), 3.34 (s, 2H), 1.46 (d, *J* = 7.1 Hz, 6H), 1.24 (t, *J* = 7.1 Hz, 6H). ^{13}C NMR (125 MHz, $CDCl_3$): δ 171.43, 170.45, 145.06, 141.53, 133.68, 133.13, 112.58, 80.59, 68.94, 61.36, 47.55, 45.07, 17.03, 14.11. LRMS calcd. for $C_{28}H_{31}I_2N_2O_8$: 777.0; found: 777.1.

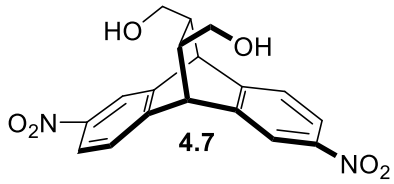

4.7

2,6-dinitro diol (4.7): **2.7a** (2.41 g, 4.12 mmol) was dissolved in THF (20 mL) and then added dropwise to a stirring suspension of sodium borohydride (3.90 g, 103.1 mmol) in THF (30 mL) at room temperature, and then heated to 60 °C for 15 minutes. Following this, MeOH (10 mL) was added dropwise to the stirring, heated solution, stopping addition briefly when vigorous bubbling occurred. The solution was then left to heat and stir for 2 hours. After, the reaction mixture was allowed to cool to room temperature and diluted with DCM (100 mL) and washed with water (1×100 mL). The aqueous layer was then extracted with a blend of 5-to-1, DCM to MeOH (5×30 mL) and the combined organic layers were dried over anhydrous $MgSO_4$, filtered, and evaporated under reduced pressure to obtain crude product which was then filtered through a plug of silica with 5% MeOH and DCM to afford 1.44 g (4.04 mmol) of crude nitro-diol **4.7** in 98% yield. ^{1}H

NMR (500 MHz, MeOD) δ 8.22 (d, *J* = 2.4 Hz, 2H), 8.08 (dd, *J* = 8.2, 2.3 Hz, 2H), 7.56 (d, *J* = 8.1 Hz, 2H), 4.73 (d, *J* = 2.0 Hz, 2H), 3.36 (s, 2H), 3.36 – 3.30 (m, 2H), 2.95 (dd, *J* = 10.9, 9.1 Hz, 2H), 1.50 (td, *J* = 5.5, 2.3 Hz, 2H). ^{13}C NMR (125 MHz, MeOD) δ 151.57, 147.84, 142.84, 125.59, 123.41, 121.84, 65.21, 46.82, 46.06. HRMS calcd. for $[C_{18}H_{16}N_2O_6]^{COOH-}$: 401.0985; found: 401.0986.

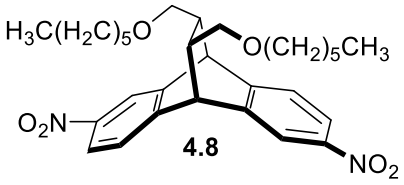

4.8

2,6-dinitro diether (4.8): A solution of **4.7** in a blend of THF (48 mL) and water (2 mL) was heated to reflux upon addition of KOH (907 mg, 16.2 mmol). This solution was left to heat and stir for 1 hour. Then, bromohexane (1.56 mL, 11.0 mmol) was added dropwise to the solution. After 16 hours, more KOH (907 mg, 16.2 mmol) was added to the solution and left to heat and stir for 1 hour. Then, another portion of bromohexane (1.56 mL, 11.0 mmol) was added dropwise to the solution. After 4 hours the solution was allowed to cool to room temperature and concentrated under reduced pressure, and the crude oil obtained was re-dissolved in 40 mL of DCM. After washing with water (1×40 mL), the aqueous layer was extracted with DCM (3×20 mL), the combined organic layers washed with brine (1×30 mL), dried over anhydrous MgSO4, filtered, and evaporated under reduced pressure to afford crude material. The crude product was further purified using flash column chromatography (0 to 15% EtOAc in hexanes) to afford 1.77 g of **4.8** in an 82% yield. By ^{1}H NMR analysis, if the product 4.8 had not fully converted, more aliquots of KOH and bromohexane can be added to the mixture. Should an inseparable

mixture of isomers still be present, they can be carried forward to be fully separated after reduction to the dianiline derivative. ^{1}H NMR (500 MHz, $CDCl_3$): δ 8.15 (s, J = 2.2 Hz, 2H), 8.10 (d, J = 8.1 Hz, 2H), 7.48 (d, J = 8.2 Hz, 2H), 4.64 (d, J = 1.0 Hz, 2H), 3.40 – 3.34 (m, 2H), 3.32 – 3.26 (m, 2H), 3.22 (dd, J = 9.3, 4.7 Hz, 2H), 2.72 (t, J = 9.3 Hz, 2H), 1.65 – 1.60 (m, 2H), 1.59 – 1.52 (m, 4H), 1.40 – 1.27 (m, 12H), 0.92 (t, J = 7.0 Hz, 6H); ^{13}C NMR (125 MHz, $CDCl_3$): δ 149.77, 146.65, 141.39, 124.68, 122.58, 120.83, 72.63, 71.59, 46.04, 42.41, 31.79, 29.72, 26.03, 22.77, 14.20. HRMS (ESI): calcd. for $[C_{30}H_{40}N_2O_6]^+$: 525.2965. Found: 525.2971.

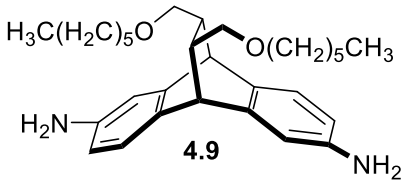

4.9

2,6-diamine diether (4.9): A spatula tip of Raney-Ni was added to dinitro **4.8** (863 mg, 1.64 mmol) in 20 mL of THF. The reaction mixture was stirred at room temperature and hydrazine monohydrate (2 mL, 41.2 mmol) was added dropwise to the solution and then warmed to 60 °C. After stirring for 3 hours, the reaction mixture was allowed to cool to room temperature and filtered through a pad of Celite, which was then rinsed with DCM. Thereafter, the filtrate was concentrated under reduced pressure and the crude oil obtained was re-dissolved in 40 mL of DCM. Finally, after washing with water (1×40 mL), the aqueous layer was extracted with DCM (3×20 mL), the combined organic layers washed with brine (1×30 mL), dried over anhydrous $MgSO_4$, filtered, and evaporated under reduced pressure to afford crude material. The crude product was further purified using flash column chromatography (0 to 20% EtOAc in hexanes) to fully separate 2,6-

diamine **4.9** and afford 562.0 mg in 92% yield (based on removal of preexisting isomers). Should separating the isomers prove difficult, a lower % of EtOAc to hexanes ratio can be utilized with ~1% Et_3N to assist in full separation—if isomers still remain, after Boc protection and/or iodination, separation of isomers should become more feasible. ^1H NMR (500 MHz, $CDCl_3$): δ 6.99 (d, *J* = 7.8 Hz, 2H), 6.61 (s, 2H), 6.38 (d, *J* = 7.8 Hz, 2H), 4.08 (d, *J* = 1.3 Hz, 2H), 3.45 (br, 4H), 3.41 – 3.35 (m, 2H), 3.34 – 3.28 (m, 2H), 3.15 (dd, *J* = 9.2, 4.8 Hz, 2H), 2.81 (t, *J* = 9.4 Hz, 2H), 1.60 – 1.53 (m, 4H), 1.51 – 1.45 (m, 2H), 1.43 – 1.29 (m, 12H), 0.93 (t, *J* = 7.0 Hz, 6H); ^{13}C NMR (125 MHz, $CDCl_3$): δ 144.10, 143.15, 134.13, 123.90, 113.05, 111.82, 73.66, 71.09, 53.50, 45.06, 43.77, 31.77, 29.74, 25.97, 22.73, 14.15. HRMS (ESI): calcd. for $[C_{30}H_{44}N_2O_2]^+$: 465.3481. Found: 465.3481.

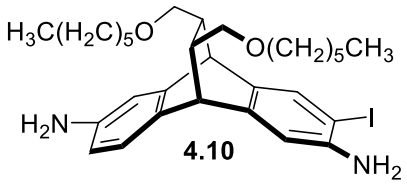

4.10

2,6-diamine-monoiodo diether (4.10): Following the general procedure for regioselective electrophilic iodination, diamine **4.9** (1.08 g, 2.33 mmol) dissolved in a blend of DCM (10 mL) and MeOH (10 mL) with slow addition of iodine monochloride (662 mg, 4.08 mmol) at -15 °C, afforded 240 mg of building block **4.10** and 1.21 g of **4.11** in 90% overall yield. The crude product obtained was purified by flash column chromatography (0 to 15% EtOAc in hexanes). ^1H NMR (500 MHz, $CDCl_3$): δ 7.48 (s, 1H), 6.99 (d, *J* = 7.8 Hz, 1H), 6.68 (s, 1H), 6.60 (s, *J* = 1H), 6.40 (d, *J* = 7.8 Hz, 1H), 4.06 (d, *J* = 1.8 Hz, 1H), 4.04 (d, *J* = 1.7 Hz, 1H), 3.91 (s, 2H), 3.51 (s, 2H), 3.40 – 3.33 (m,

2H), 3.32 – 3.25 (m, 2H), 3.15 (dd, *J* = 9.0, 4.4 Hz, 1H), 3.13 (dd, *J* = 8.8, 4.3 Hz, 1H), 2.80 (t, *J* = 9.6 Hz, 1H), 2.78 (t, *J* = 9.5 Hz, 1H), 1.58 – 1.52 (m, 4H), 1.50 – 1.45 (m, 2H), 1.40 – 1.28 (m, 12H), 0.92 (t, *J* = 7.0, 3H), 0.91 (t, *J* = 7.0 Hz, 3H); ^{13}C NMR (125 MHz, $CDCl_3$): δ 144.37, 144.34, 143.87, 142.56, 136.10, 133.71, 133.20, 124.14, 113.15, 112.62, 112.14, 80.03, 73.54, 73.48, 71.21, 71.17, 44.77, 44.59, 43.61, 43.53, 31.84, 31.83, 29.82, 29.79, 26.04, 26.03, 22.80, 22.80, 14.24, 14.23. HRMS (ESI): calcd. for $[C_{30}H_{43}IN_2O_2]^+$: 591.2447. Found: 591.2438.

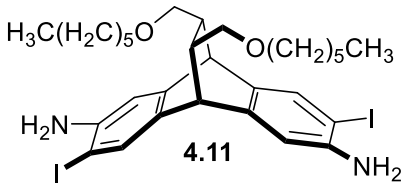

4.11

2,6-diamine-diiodo diether (4.11): Following the general procedure for regioselective electrophilic iodination, diamine **4.9** (403.9 mg, 0.8692 mmol) dissolved in a blend of DCM (10 mL) and MeOH (10 mL) with slow addition of iodine monochloride (282.2mg, 1.738 mmol) at -15 °C, afforded 0.532 mg of building block **4.11** in 85% yield. The crude product obtained was purified by flash column chromatography (0 to 5% EtOAc in hexanes). ^{1}H NMR (500 MHz, $CDCl_3$): δ 7.48 (s, 2H), 6.67 (s, 2H), 4.03 (d, *J* = 1.2 Hz, 2H), 3.93 (s, 4H), 3.40 – 3.33 (m, 2H), 3.32 – 3.25 (m, 2H), 3.14 (dd, *J* = 9.3, 4.7 Hz, 2H), 2.78 (t, *J* = 9.5 Hz, 2H), 1.59 – 1.51 (m, 4H), 1.50 – 1.43 (m, 2H), 1.40 – 1.27 (m, 12H), 0.92 (t, *J* = 7.0 Hz, 6H); ^{13}C NMR (125 MHz, $CDCl_3$): δ 144.52, 143.08, 135.36, 133.22, 112.51, 80.18, 73.28, 71.10, 44.15, 43.25, 31.76, 29.75, 25.97, 22.75, 14.23. HRMS (ESI): calcd. for $[C_{30}H_{42}I_2N_2O_2]^+$: 717.1414. Found: 717.1408.

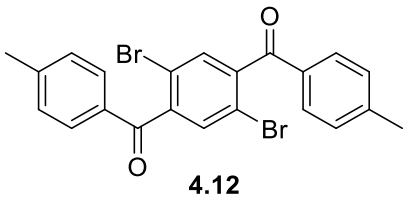

4.12

***p*-dibromo-*o*-dimethylbenzoyl benzene (4.12)**: To a round-bottom with thionyl chloride (10 mL, excess) was added 2,5-dibromoterephtalic acid (2.66 g, 8.22 mmol) and heated to reflux under N_2. Additional $SOCl_2$ (1 mL aliquots) was added if the reaction remained a cloudy beige color, reaction is assumed complete when the solution turns opaque (usually after 4 h). The reaction was concentrated to remove $SOCl_2$, and dissolved in DCM at 0 °C before slowly adding the crude reaction mixture to a stirred solution of $AlCl_3$ (1.64 g, 8.22 mmol) and toluene (2 mL, 18.7 mmol) in DCM (10 mL) at -15 °C, letting warm to room temperature. After 16 h the solution was filtered through a pad of Celite, which was then rinsed with DCM. The crude product was taken up in DCM, washed with 0 °C $NaHCO_3$ (aq) (1×50 mL) and then the aqueous layer extracted with DCM (2×30 mL). The combined organic layers were washed with brine (1×50 mL), dried over anhydrous $MgSO_4$, filtered, and evaporated under reduced pressure to afford crude material. The crude product obtained was purified by flash column chromatography (0 to 10% EtOAc in hexanes) to afford 1.01 g of **4.12** in 27% overall yield. Spectral characterization matched reported literature values.[204]

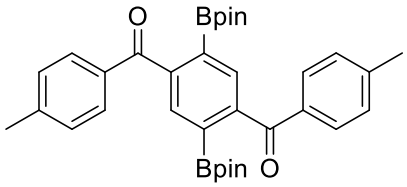

4.13

***syn*-linker (4.13)**: Following the general procedure for Miyaura borylation, *p*-dibromo **4.12** (402 mg, 0.851 mmol) was dissolved in toluene along with bis(pinacolato)diboron (864 mg, 3.40 mmol) to afford 290 mg of *syn*-linker **4.13** in 61% yield by way of recrystallization. ^{1}H NMR (500 MHz, $CDCl_3$): δ 7.86 (s, 2H), 7.70 (d, *J* = 8.0 Hz, 2H), 7.24 (d, *J* = 8.0 Hz, 2H), 2.42 (s, 6H), 1.11 (s, 24H). ^{13}C NMR (125 MHz, $CDCl_3$): δ 197.79, 145.66, 143.68, 135.50, 133.45, 130.45, 129.09, 84.36, 24.68, 24.59, 21.81. HRMS (ESI): calcd. for $[C_{34}H_{40}B_2O_6]^+$: 567.3089. Found: 567.3105.

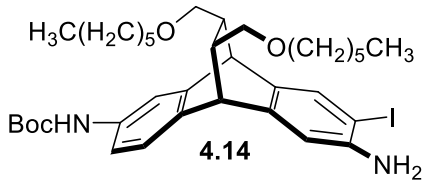

4.14

2-amine-*o*-iodo-6-*N*-Boc diether (4.14): Monoiodo-diamine **4.10** (134.5 mg, 0.228 mmol) was dissolved in THF (5 mL) and heated to 45 °C under N_2. A solution of boc anhydride (54.8 mg, 0.251 mmol) in THF (5 mL) was added dropwise to the stirring solution. After 16 hours, the solution was concentrated under vacuum to remove THF and then re-dissolved in 20 mL of DCM washed with a saturated, aqueous sodium bicarbonate solution (1×20 mL). Thereafter the aqueous layer was extracted with DCM (2×20 mL) and the combined organic layers were then dried over anhydrous $MgSO_4$, filtered, and concentrated under reduced pressure to afford crude material. The crude product obtained was purified by flash column chromatography (0 to 15% EtOAc in hexanes) to afford 154.3 mg of *N*-Boc-**4.14** in 98% yield. At temperatures below reflux, it was found efficient to add a slight excess of Boc_2O, as the amine *ortho* to the iodine is too deactivated to form the resulting carbamate species. ^{1}H NMR (500 MHz, $CDCl_3$): δ

7.48 (s, 1H), 7.24 (s, 1H), 7.13 (d, *J* = 7.9 Hz, 1H), 7.06 (d, *J* = 7.6 Hz, 1H), 6.69 (s, 1H), 6.34 (s, 1H), 4.13 (d, *J* = 1.7 Hz, 1H), 4.12 (d, *J* = 1.7 Hz, 1H), 3.92 (s, 2H), 3.41 – 3.26 (m, 4H), 3.18 (dd, *J* = 9.2, 4.8 Hz, 1H), 3.09 (dd, *J* = 9.3, 5.2 Hz, 1H), 2.80 (t, *J* = 9.5 Hz, 1H), 2.79 (t, *J* = 9.2 Hz, 1H), 1.59 – 1.52 (m, 4H), 1.50 (s, 9H), 1.50 – 1.46 (m, 2H), 1.41 – 1.25 (m, 12H), 0.92 (t, *J* = 7.0 Hz, 3H), 0.91 (t, *J* = 7.0 Hz, 3H). ^{13}C NMR (125 MHz, $CDCl_3$): δ 152.90, 146.85, 144.41, 143.22, 142.25, 138.11, 136.14, 135.85, 133.30, 123.83, 116.21, 115.94, 112.67, 85.26, 80.15, 73.52, 73.38, 71.22, 71.20, 44.98, 44.63, 43.53, 43.29, 31.81, 29.77, 29.76, 28.46, 27.51, 26.01, 25.97, 22.78, 22.76, 14.21. HRMS (ESI): calcd. for $[C_{35}H_{51}IN_2O_4]^+$: 691.2972. Found: 691.2975.

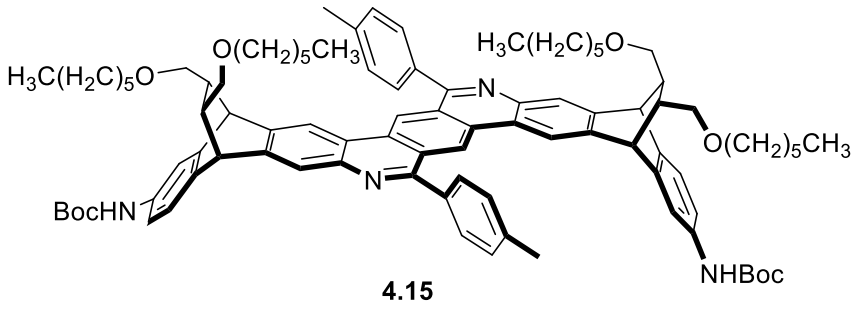

4.15

***N,N*'-diBoc-*syn*-helical dimer strip (4.15)**: Following the general procedure for Suzuki coupling/imine condensation, *N*-Boc-**4.14** (180.4 mg, 0.2612 mmol) and *syn*-linker **4.13** (74.0 mg, 0.1306 mmol) in 1,4-dioxane (2 mL) afforded 143 mg of *syn*-helix dimer **4.15** in 92% yield. The crude product obtained was purified by flash column chromatography (0 to 30% EtOAc in hexanes). ^{1}H NMR (500 MHz, 4:1 CD_3CN:$CDCl_3$ v/v): δ 9.47 (s, 2H), 8.33 (s, 2H), 7.95 (s, 2H), 7.81 (d, *J* = 7.9 Hz, 4H), 7.53 (d, *J* = 6.3 Hz, 4H), 7.49 (s,

2H), 7.36 (s, 2H), 7.23 (d, *J* = 8.0 Hz, 2H), 7.06 (d, *J* = 8.0 Hz, 2H), 4.53 (d, *J* = 1.4 Hz, 2H), 4.49 (d, *J* = 1.5 Hz, 2H), 3.41 – 3.23 (m, 8H), 3.16 (dd, *J* = 8.8, 5.4 Hz, 2H), 3.11 (dd, *J* = 9.3, 5.7 Hz, 2H), 2.84 (t, *J* = 8.9 Hz, 2H), 2.83 (t, *J* = 9.2 Hz, 2H), 2.59 (s, 6H), 1.65 – 1.49 (m, 12H), 1.48 (s, 18H), 1.43 – 1.23 (m, 24H), 0.92 (dd, *J* = 8.8, 5.0 Hz, 6H), 0.87 (t, *J* = 6.9 Hz, 6H); ^{1}H NMR (500 MHz, $CDCl_3$): δ 9.43 (s, 2H), 8.30 (s, 2H), 8.08 (s, 2H), 7.80 (d, *J* = 8.0 Hz, 4H), 7.56 (d, *J* = 7.9 Hz, 4H), 7.24 (d, *J* = 8.0 Hz, 2H), 6.95 (d, *J* = 8.0 Hz, 2H), 6.40 (s, 2H), 4.56 (d, *J* = 1.7 Hz, 2H), 4.51 (d, *J* = 1.7 Hz, 2H), 3.46 – 3.35 (m, 8H), 3.32 (t, *J* = 6.8 Hz, 2H), 3.24 (dd, *J* = 8.9, 4.9 Hz, 2H), 3.17 (dd, *J* = 9.2, 5.2 Hz, 2H), 2.87 (t, *J* = 8.9 Hz, 2H), 2.63 (s, 6H), 1.68 – 1.60 (m, 8H), 1.57 – 1.52 (m, 4H), 1.50 (s, 18H), 1.42 – 1.25 (m, 24H), 0.93 (t, *J* = 6.9 Hz, 6H), 0.89 (t, *J* = 6.9 Hz, 6H). ^{13}C NMR (125 MHz, $CDCl_3$): δ 160.86, 152.87, 143.03, 142.76, 142.03, 141.49, 138.98, 138.97, 137.95, 136.92, 136.32, 131.01, 129.81, 129.65, 126.55, 125.63, 123.98, 122.74, 122.73, 121.65, 116.52, 80.17, 73.41, 73.30, 71.36, 71.32, 53.42, 46.10, 45.14, 43.47, 43.29, 31.71, 29.66, 29.57, 28.33, 25.84, 24.78, 22.64, 22.60, 21.55, 14.09, 14.05. HRMS (ESI): calcd. for $[C_{92}H_{114}N_4O_8]^{2+}$: 702.4397. Found: 702.4391. In $CDCl_3$, the *N*-H carbamate shift is not apparent in the ^{1}H spectrum, but in a 4-to-1 mixture of CD_3CN-to-$CDCl_3$, said carbamate shift is visible.

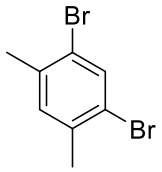

4.16

***m*-dibromo-*o*-dimethyl benzene (4.16)**: To a round-bottom protected from light with *m*-xylene (3 mL, 24.3 mmol) was added $CHCl_3$ (50 mL) and I_2 (14.0 g, 60.8 mmol). Then, Br_2 (2.8 mL, 55.0 mmol) was slowly added to the solution. After 16 hours, the reaction was quenched with aqueous sodium thiosulfate (1×50 mL) and 2 M NaOH (1×50 mL) and the aqueous layer was washed with DCM (3×50 mL). The combined organic layers were washed with brine (1×50 mL), dried over anhydrous $MgSO_4$, filtered, and evaporated under reduced pressure to afford crude material. The crude product was then recrystallized from EtOH to afford 2.081 g of **4.16** in 33% yield. Spectral characterization matched reported literature values.[205]

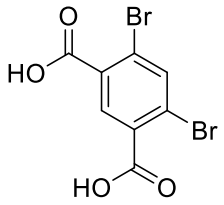

4.17

2,4-dibromoterephtalic acid (4.17): To a round-bottom with dibromo **4.16** (2.08 g, 7.89 mmol) was added t-BuOH (25 mL) and H_2O (25 mL) along with NaOH (1.26 g, 31.6 mmol) before the solution was heated to reflux. $KMnO_4$ (9.98 g, 63.12 mmol) was added in spatula tips over the course of an hour. After 16 hours, the reaction was filtered hot over Celite, and washed with 400 mL hot H_2O, then to the purple filtrate was added 10 mL 2 M HCl, the solution turning clear and diacid crashing out of solution as a cream colored solid. The Celite pad was then washed with DCM to extract insoluble, unreacted starting compound **4.16**. The solution wash filtered and afford 651.8 mg of **4.17** in 44%

yield based on recovered **4.16**. Spectral characterization matched reported literature values.[206]

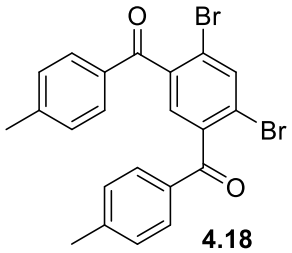

4.18

***m*-dibromo-*o*-dimethylbenzoyl benzene (4.18)**: To a round-bottom with thionyl chloride (5 mL, excess) was added 2,4-dibromoterephtalic acid **4.17** (651.8 mg, 2.01 mmol) and heated to reflux under N_2. Additional $SOCl_2$ (1 mL aliquots) was added if the reaction remained a cloudy beige color, reaction is assumed complete when the solution turns opaque (usually after 4 h). The reaction was concentrated to remove $SOCl_2$, and dissolved in DCM at 0 °C before slowly adding the crude reaction mixture to a stirred solution of $AlCl_3$ (540 mg, 4.02 mmol) and toluene (2 mL, 18.7 mmol) in DCM (8 mL) at -15 °C, letting warm to room temperature. After 16 h the solution was filtered through a pad of Celite, which was then rinsed with DCM. The crude product was taken up in DCM, washed with 0 °C $NaHCO_3$ (aq) (1×50 mL) and then the aqueous layer extracted with DCM (2×30 mL). The combined organic layers were washed with brine (1×50 mL), dried over anhydrous $MgSO_4$, filtered, and evaporated under reduced pressure to afford crude material. The crude product obtained was purified by flash column chromatography (0 to 10% EtOAc in hexanes) to afford 697.9 mg of **4.18** in 73% overall yield. Spectral characterization matched reported literature values.[207]

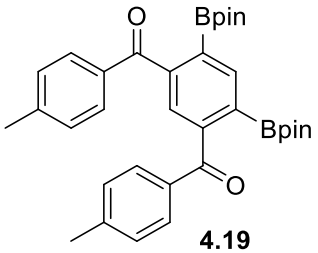

4.19

***anti*-linker (4.19)**: Following the general procedure for Miyaura borylation, *m*-dibromo **4.18** (299.9 mg, 0.635 mmol) was dissolved in toluene along with bis(pinacolato)diboron (642.7 mg, 2.54 mmol) to afford 197 mg of *anti*-linker **4.19** in 66% yield by way of recrystallization. ^{1}H NMR (500 MHz, $CDCl_3$): δ 8.13 (s, 1H), 7.65 (d, *J* = 8.0 Hz, 4H), 7.60 (s, 1H), 2.39 (s, 7H), 1.17 (s, *J* = 14.4 Hz, 24H); ^{13}C NMR (125 MHz, $CDCl_3$) δ 197.26, 145.74, 143.57, 139.37, 135.18, 130.23, 128.97, 127.65, 84.24, 24.57, 21.64. HRMS (ESI): calcd. for $[C_{34}H_{40}B_2O_6]^+$: 567.3089. Found: 567.3102.

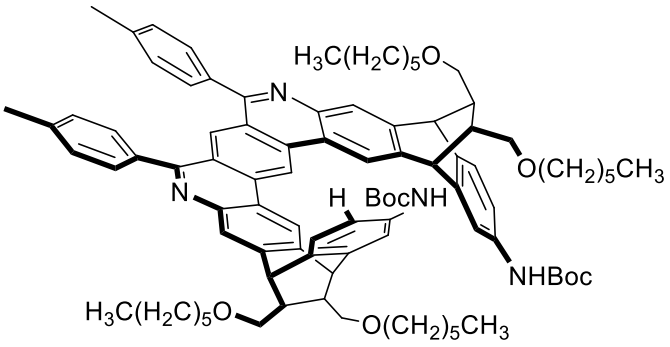

4.20

***N,N*'-diBoc *anti*-helical dimer strip (4.20)**: Following the general procedure for Suzuki coupling/imine condensation, monoiodo-diamine-**4.10** (12.8 mg, 0.0185 mmol) and *anti*-linker **4.19** (5.2 mg, 0.0092 mmol) in 1,4-dioxane (400 μL) afforded 10.9 mg (0.0078 mmol) of *anti*-helical dimer **4.20** in 84% yield. The crude product obtained was purified by flash column chromatography (0 to 30% EtOAc in hexanes). ^{1}H NMR (500 MHz,

$CDCl_3$): δ 9.91 (s, 1H), 8.94 (s, 1H), 8.87 (s, 2H), 8.14 (s, 2H), 7.65 (d, *J* = 8.1 Hz, 4H), 7.55 (d, *J* = 2.0 Hz, 2H), 7.31 (dd, *J* = 8.0, 2.4 Hz, 4H), 7.14 (dd, *J* = 8.1, 2.3 Hz, 2H), 6.45 (s, 2H), 4.79 (d, *J* = 2.3 Hz, 2H), 4.60 (d, *J* = 2.3 Hz, 2H), 3.56 – 3.42 (m, 4H), 3.36 (t, *J* = 6.8 Hz, 4H), 3.29 (ddd, *J* = 18.5, 9.1, 5.2 Hz, 2H), 3.04 (t, *J* = 9.2 Hz, 2H), 2.93 (t, *J* = 9.5 Hz, 2H), 2.47 (s, 6H), 1.81 – 1.67 (m, 6H), 1.63 – 1.55 (m, 12H), 1.55 (s, 18H), 1.51 – 1.27 (m, 16H), 0.99 (t, *J* = 7.0 Hz, 6H), 0.91 (t, *J* = 6.9 Hz, 6H). ^{13}C NMR (125 MHz, $CDCl_3$): δ 161.06, 152.70, 143.44, 143.01, 142.75, 141.54, 138.51, 138.09, 136.33, 136.11, 133.56, 131.07, 129.68, 128.83, 126.57, 124.08, 123.31, 121.21, 116.83, 116.20, 73.34, 71.32, 71.22, 46.30, 45.14, 43.43, 43.25, 31.65, 31.64, 29.63, 29.59, 28.25, 25.80, 25.76, 22.63, 22.53, 21.23, 14.07, 13.97. HRMS calcd. for $[C_{92}H_{115}N_4O_8]^+$: 1403.8715; found: 1403.8694.

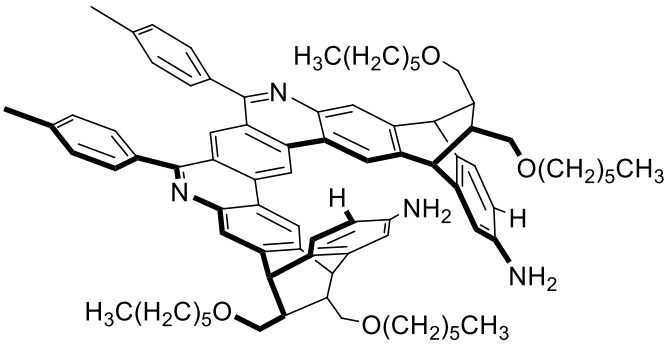

4.21

diamine *anti*-helical dimer strip (4.21): Following the general procedure for Suzuki coupling/imine condensation, monoiodo-diamine-**4.10** (59.7 mg, 0.101 mmol) and *anti*-linker **4.19** (28.6 mg, 0.0510 mmol) in 1,4-dioxane (1 mL) afforded 13.4 mg of *anti*-helical dimer **4.21** in 90% yield based on recovered **4.10**. The crude product obtained was purified by flash column chromatography (0 to 30% EtOAc in hexanes). ^{1}H NMR (500

MHz, $CDCl_3$): δ 9.89 (s, 2H), 8.92 (s, 2H), 8.84 (s, 2H), 8.10 (s, 2H), 7.62 (d, *J* = 7.9 Hz, 4H), 7.28 (d, *J* = 7.9 Hz, 4H), 7.15 (d, *J* = 7.9 Hz, 2H), 6.84 (s, *J* = 2.1 Hz, 2H), 6.49 (d, *J* = 7.8 Hz, 2H), 4.69 (d, *J* = 1.9 Hz, 2H), 4.49 (d, *J* = 1.9 Hz, 2H), 3.61 (br, 4H), 3.55 – 3.48 (m, 2H), 3.47 – 3.41 (m, 2H), 3.37 – 3.29 (m, 6H), 3.20 (dd, *J* = 9.2, 5.5 Hz, 2H), 2.97 (t, *J* = 9.6 Hz, 2H), 2.91 (t, *J* = 9.4 Hz, 2H), 2.44 (s, 6H), 1.78 – 1.64 (m, 6H), 1.59 – 1.49 (m, 8H), 1.46 – 1.38 (m, 8H), 1.38 – 1.22 (m, 16H), 0.99 (t, *J* = 6.9 Hz, 6H), 0.88 (t, *J* = 6.8 Hz, 6H). ^{13}C NMR (125 MHz, $CDCl_3$): δ 161.09, 144.45, 144.14, 143.29, 142.88, 141.85, 138.59, 136.50, 133.78, 129.80, 128.94, 126.47, 124.99, 124.47, 123.36, 121.24, 116.75, 114.76, 113.39, 113.25, 112.53, 73.68, 73.27, 71.43, 71.27, 46.32, 45.04, 43.93, 43.57, 31.80, 31.75, 29.79, 29.71, 25.97, 25.87, 22.78, 22.64, 21.35, 14.22, 14.08. HRMS (ESI): calcd. for $[C_{82}H_{98}N_4O_4]^{2+}$: 602.3872. Found: 602.3861.

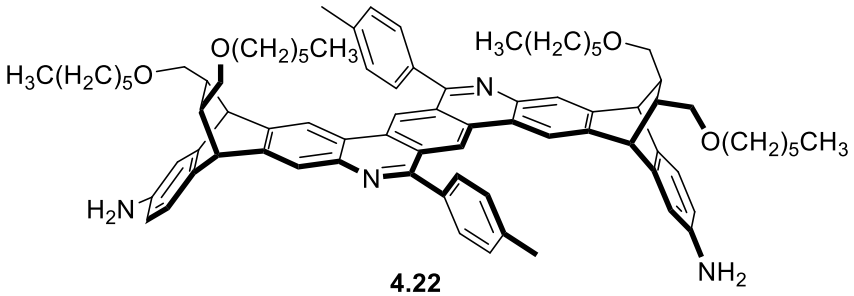

4.22

diamine *syn*-helical dimer strip (4.22): Following the general procedure for Suzuki coupling/imine condensation, monoiodo-diamine **4.10** (54.8 mg, 0.0928 mmol) and *syn*-linker **4.13** (19.8 mg, 0.0351 mmol) in 1,4-dioxane (700 μL) afforded 15.1 mg of *syn*-helical dimer **4.22** in 77% yield based on recovered **4.10**. The crude product obtained was purified by flash column chromatography (0 to 30% EtOAc in hexanes). ^{1}H NMR (500 MHz, $CDCl_3$): δ 9.42 (s, 1H), 8.30 (s, 1H), 8.08 (s, 1H), 7.80 (d, *J* = 7.7 Hz, 1H), 7.53 (d,

J = 7.8 Hz, 2H), 7.10 (d, *J* = 8.2 Hz, 1H), 6.73 (d, *J* = 1.7 Hz, 1H), 6.44 (d, *J* = 6.0 Hz, 1H), 4.49 (s, 2H), 4.43 (s, 2H), 3.54 (s, 4H), 3.50 – 3.36 (m, 6H), 3.34 – 3.27 (m, 4H), 3.14 (d, *J* = 5.5 Hz, 2H), 2.88 (q, *J* = 10.4, 9.8 Hz, 4H), 2.61 (s, 6H), 1.72 – 1.58 (m, 8H), 1.46 – 1.17 (m, 24H), 0.94 (t, *J* = 6.8 Hz, 6H), 0.89 (t, *J* = 7.0 Hz, 6H). ^{13}C NMR (125 MHz, $CDCl_3$): δ 160.57, 144.24, 143.34, 143.11, 141.91, 141.55, 138.76, 136.94, 133.49, 130.90, 129.75, 129.47, 126.26, 125.42, 124.26, 122.55, 121.41, 116.23, 113.08, 112.28, 73.48, 73.10, 71.26, 71.15, 45.82, 44.79, 43.53, 43.21, 31.59, 29.55, 29.46, 25.78, 25.71, 22.57, 22.49, 21.41, 14.00, 13.93. HRMS calcd. for $[C_{82}H_{100}N_4O_4]^{2+}$: 602.3872; found: 602.3869.

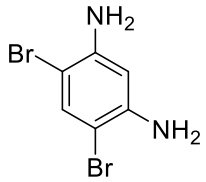

4.24

***m*-dibromo dianiline (4.24)**: To a solution of *m*-phenyldiamine (1.001g, 9.27 mmol) in DMF (10 mL) at -15 °C was added NBS (3.298 g, 18.53 mmol) in DMF (10 mL). The reaction was let warm to room temperature. Quenched the reaction after 16 hours with 50 mL of H_2O, whereby grey crystals crashed out from the reaction solution and was filtered and washed with an additional 50 mL of H_2O. Tribromo impurity appeared present in the reaction mixture, and was further purified by flash column chromatography (50% hexanes in DCM to remove tribromo impurity, followed by 5% MeOH in DCM) to afford 1.650 g of dibromo **4.24** in 68% yield. Spectral characterization matched reported literature values.[208]

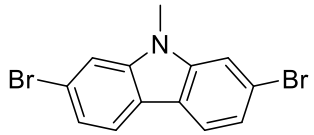

4.25

dibromo-N-methyl-carbazole (4.25): A solution of 2,7-dibromo-9H-carbazole (3.00 g, 9.23 mmol) in DMF (20 mL) was added NaOH (1.11 g, 27.7 mmol) and a spatula tip of 18-crown-6 and let stir at room temperature for 20 minutes before CH_3I (1.15 mL, 18.5 mmol) was added dropwise. After 24 hours, 200 mL of H_2O was added whereby a white solid crashed out of solution and was filtered and washed with H_2O (50 mL) to afford 3.06 g of **4.25** in quantitative yields. Spectral characterization matched reported literature values.[209]

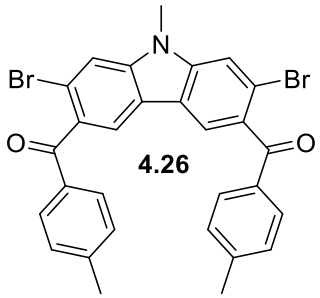

4.26

dibromo-N-methyl-dimethylbenzoyl-carbazole (4.26): To a round-bottom with carbazole **4.25** (3.056 g, 9.012 mmol) cooled to 0 °C was sequentially added (i) $CHCl_3$ (50 mL), (ii) $AlCl_3$ (2.7 g, 20.3 mmol), (iii) *p*-toluoyl chloride (4.5 mL, 33.8 mmol), and was heated to reflux under N_2. The solution turned green upon $AlCl_3$ addition, turning dark yellow upon *p*-toluoyl chloride addition. After 16 h the solution was filtered through a pad of Celite, which was then rinsed with EtOAc. The crude product was taken up in EtOAc, washed with 0 °C $NaHCO_3$ (aq) (1×50 mL) and then the aqueous layer extracted

with EtOAc (2×30 mL). The combined organic layers were washed with brine (1×50 mL), dried over anhydrous $MgSO_4$, filtered, and evaporated under reduced pressure to afford crude material. The crude product obtained was purified by recrystallization with hexanes and EtOAc to afford 4.28 g of **4.26** as a beige powder in 83% yield. Spectral characterization matched reported literature values.[210]

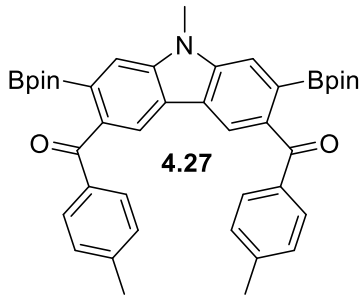

4.27

diBpin-N-methyl-dimethylbenzoyl-carbazole (4.27): Following the general procedure for Miyaura borylation, dibromo **4.26** (316.5 mg, 0.550 mmol) was dissolved in toluene (5 mL) along with bis(pinacolato)diboron (556.7 mg, 2.20 mmol) to afford 305.9 mg of carbazole **4.27** in 83% yield by way of recrystallization with EtOAc and hexanes. ^{1}H NMR (500 MHz, $CDCl_3$): 8.32 (s, 2H), 7.77 (d, J = 7.9 Hz, 4H), 7.73 (s, 2H), 7.28 (d, J = 8.1 Hz, 4H), 4.01 (s, 3H), 2.43 (s, 6H), 1.36 (s, 10H). ^{13}C NMR (125 MHz, $CDCl_3$): δ 197.42, 143.52, 142.89, 135.55, 134.41, 130.38, 129.13, 123.68, 123.12, 113.98, 83.89, 60.50, 29.78, 24.97, 21.76. HRMS calcd. for $[C_{41}H_{46}B_2NO_6]^+$: 670.3511; found: 670.3508.

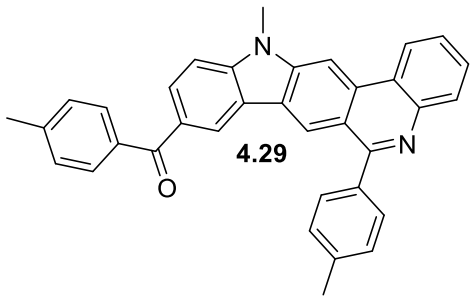

Monocoupled carbazole dimer (4.29): Following the general procedure for Suzuki coupling/imine condensation, carbazole **4.27** (38.8 mg, 0.058 mmol) and 2-iodoaniline (25.4 mg, 0.116 mmol) in 1,4-dioxane (800 μL) afforded 10.0 mg of mono-coupled dimer **4.29** in 36% yield. The crude product obtained was purified by flash column chromatography (0 to 20% EtOAc in hexanes). ^{1}H NMR (500 MHz, $CDCl_3$): δ 8.84 (s, 1H), 8.79 – 8.73 (m, 1H), 8.66 (d, *J* = 1.8 Hz, 1H), 8.57 (s, 1H), 8.26 (dd, *J* = 8.2, 1.6 Hz, 1H), 8.04 (dd, *J* = 8.4, 1.8 Hz, 1H), 7.79 – 7.74 (m, 3H), 7.73 – 7.69 (m, 3H), 7.49 (d, *J* = 8.5 Hz, 1H), 7.43 (d, *J* = 7.9 Hz, 1H), 7.32 (d, *J* = 8.2 Hz, 1H), 4.10 (s, 3H), 2.53 (s, 3H), 2.48 (s, 3H). ^{13}C NMR (125 MHz, $CDCl_3$): δ 196.18, 162.19, 145.61, 143.50, 142.71, 138.64, 137.56, 135.93, 132.73, 130.45, 130.34, 130.25, 129.92, 129.70, 129.36, 129.01, 128.66, 126.34, 124.14, 124.03, 123.77, 122.76, 121.96, 121.74, 120.20, 107.84, 99.78, 29.77, 21.66, 21.45. LRMS calcd. for $[C_{35}H_{27}N_2O]^+$: 491.2; found: 491.3.

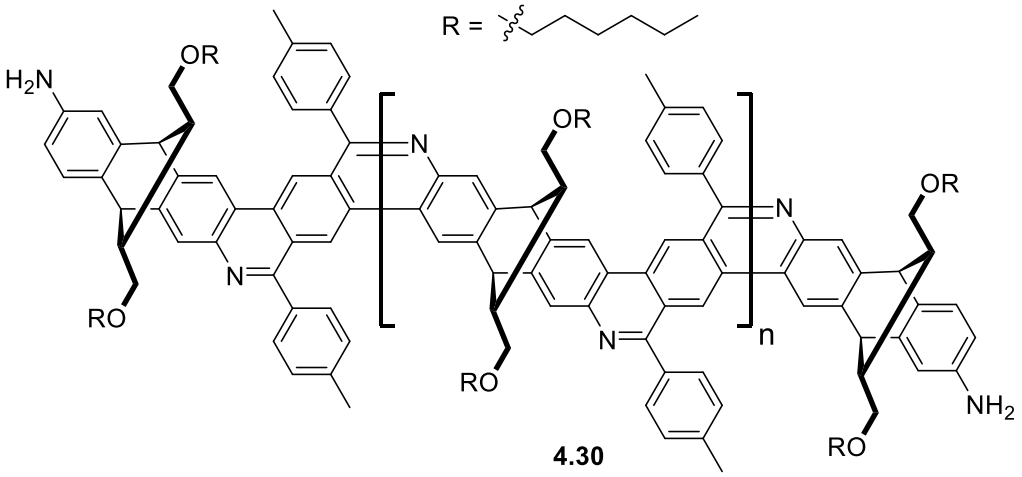

4.30

***Syn*-helix polymer (4.30)**: Following the general procedure for Suzuki coupling/imine condensation, diiodo-diamine **4.11** (36.7 mg, 0.0512 mmol) and *syn*-linker **4.13** (29.0 mg, 0.0512 mmol) in 1,4-dioxane (3 mL) afforded 57.8 mg of crude polymeric mixture. The crude product obtained was purified by size exclusion chromatography to afford 15.4 mg of *syn*-helix **4.30** in 41% overall yield (based on 20-mer). ^{1}H NMR (500 MHz, $CDCl_3$): δ 9.44 (br, 2H), 8.39 (br, 2H), 8.20 (br, 2H), 7.78 (br, 4H), 7.54 (br, 4H), 4.83 (br, 2H), 3.38 (br, 2H), 3.29 (br, 2H), 2.93 (br, 2H), 2.64 (br, 6H), 2.45 (br, 2H), 1.78 (br, 2H), 1.60 (br, 4H), 1.34 (br, 12H), 0.90 (br, 6H).

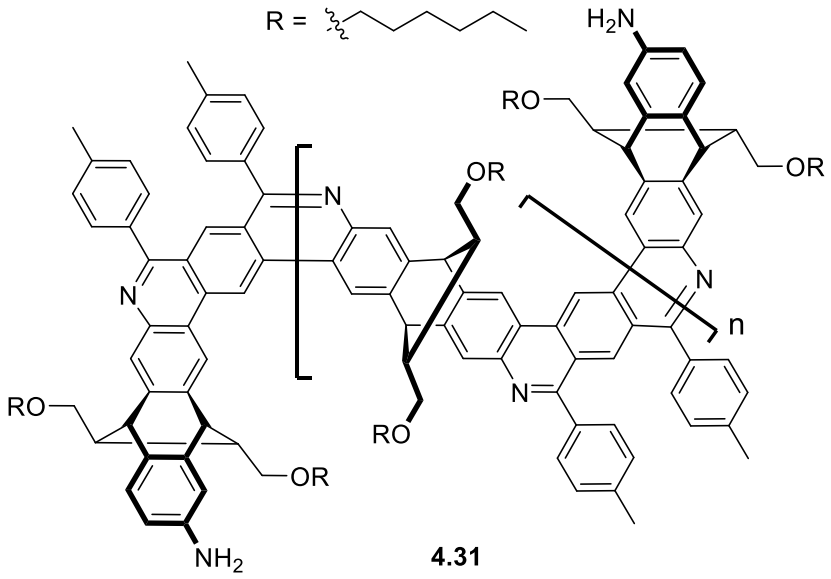

4.31

***Anti*-helix polymer (4.31)**: Following the general procedure for Suzuki coupling/imine condensation, diiodo-diamine **4.11** (37.4 mg, 0.0522 mmol) and *anti*-linker **4.19** (29.6 mg, 0.0522 mmol) in 1,4-dioxane (3 mL) afforded 49.2 mg of crude polymeric mixture. The crude product obtained was purified by size exclusion chromatography to afford 14.7 mg of *syn*-helix **4.31** in 40% overall yield (based on 16-mer). ^{1}H NMR (500 MHz, $CDCl_3$): δ 10.03 (br, 1H), 9.06 (br, 1H), 8.96 (br, 2H), 8.37 (br, 2H), 7.65 (br, 4H), 7.30 (br, 4H), 5.17 (br, 2H), 3.46 (br, 2H), 3.39 (br, 2H), 3.34 – 3.13 (br, 2H), 3.07 (br, 2H), 2.43 (br, 6H), 1.95 (br, 2H), 1.70 (br, 4H), 1.50 – 1.20 (br, 12H), 1.00 – 0.80 (br, 6H).

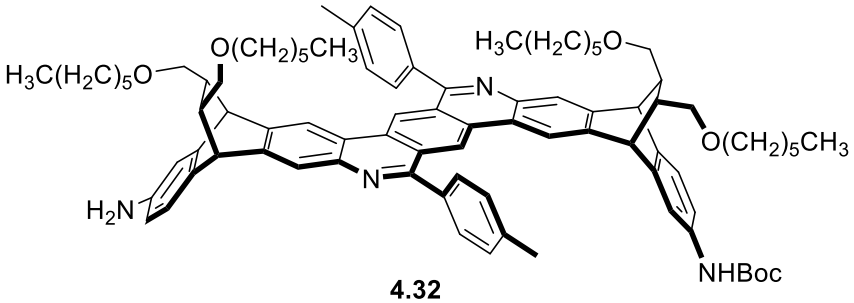

4.32

***N*-Boc *syn*-helical dimer strip (4.32)**: Diamine **4.22** (32.7 mg, 0.0272 mmol) was dissolved in THF (5 mL) and heated to 45 °C under N_2. A solution of boc anhydride (6.6 mg, 0.0299 mmol) in THF (5 mL) was added dropwise to the stirring solution. After 16 hours, the solution was concentrated under vacuum to remove THF and then re-dissolved in 20 mL of DCM washed with H_2O (1×20 mL). Thereafter the aqueous layer was extracted with DCM (3×20 mL) and the combined organic layers were then washed with brine (1×20 mL) and the organic layer was dried over anhydrous $MgSO_4$, filtered, and concentrated under reduced pressure to afford crude material. The crude product obtained was purified by flash column chromatography (0 to 30% EtOAc in hexanes) to afford 22.7 mg of *N*-Boc-**4.32** in 76% yield based on recovered **4.22**. ^{1}H NMR (500 MHz, $CDCl_3$): δ 9.35 (d, *J* = 1.9 Hz, 2H), 8.23 (d, *J* = 4.1 Hz, 2H), 8.02 (d, *J* = 5.2 Hz, 2H), 7.73 (d, *J* = 7.8 Hz, 4H), 7.48 (dd, *J* = 13.3, 8.1 Hz, 4H), 7.17 (d, *J* = 8.0 Hz, 1H), 7.04 (d, *J* = 7.8 Hz, 1H), 6.88 (dd, *J* = 8.0, 2.2 Hz, 1H), 6.67 (d, *J* = 2.4 Hz, 1H), 6.37 (d, *J* = 9.9 Hz, 1H), 6.33 (s, 1H), 4.49 (s, 1H), 4.44 (s, 1H), 4.42 (s, 1H), 4.37 (s, 1H), 3.44 – 3.16 (m, 14H), 3.09 (s, 4H), 2.80 (t, *J* = 9.7 Hz, 4H), 2.56 (s, 3H), 2.54 (s, 3H), 1.62 – 1.52 (m, 8H), 1.43 (s, 9H), 1.35 – 1.22 (m, 24H), 0.96 – 0.77 (m, 12H). ^{13}C NMR (125 MHz, $CDCl_3$): δ 160.97, 152.95, 143.80, 143.56, 142.89, 142.24, 142.17, 141.72, 140.85, 139.77, 139.06, 138.25, 137.47, 137.12, 136.30, 131.23, 131.15, 131.05, 130.43, 130.04, 129.97, 129.84, 129.76, 129.30, 126.77, 126.54, 126.50, 125.80, 125.70, 125.62, 124.88, 124.20, 123.27, 122.85, 121.95, 121.72, 116.70, 116.53, 113.39, 112.60, 88.25, 73.77, 73.58, 73.45, 72.98, 71.58, 71.58, 71.53, 71.46, 46.25, 45.80, 45.31, 45.09, 44.13, 43.64, 43.45, 43.14, 33.35, 31.89, 30.76, 29.85, 29.85, 29.76, 29.74, 29.51, 28.49, 26.08, 26.01,

24.88, 22.87, 22.83, 22.78, 22.78, 21.74, 21.71, 14.29, 14.27, 14.23, 14.23. HRMS calcd. for $[C_{87}H_{108}N_4O_6]^{2+}$: 652.4134; found: 652.4137.

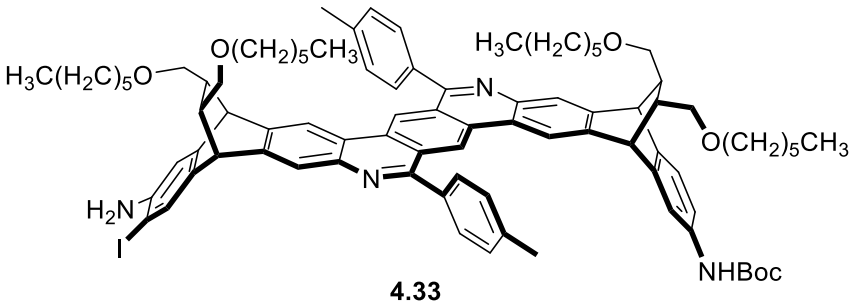

4.33

***N*-Boc-monoiodo *syn*-helical dimer strip (4.33)**: Following the general procedure for regioselective electrophilic iodination, *N*-Boc **4.32** (22.7 g, 0.0174 mmol) dissolved in a blend of DCM (10 mL) and MeOH (10 mL) with slow addition of iodine monochloride (4.2 mg, 0.0261 mmol) at -15 °C afforded 21.3 mg of monoiodo **4.33** in 86% overall yield. The crude product obtained was purified by flash column chromatography (0 to 15% EtOAc in hexanes). ^{1}H NMR (500 MHz, $CDCl_3$): δ 9.35 (d, *J* = 8.7 Hz, 2H), 8.22 (d, *J* = 2.0 Hz, 2H), 8.02 (d, *J* = 7.6 Hz, 2H), 7.73 (dd, *J* = 8.0, 1.1 Hz, 4H), 7.52 (s, 1H), 7.48 (dd, *J* = 16.8, 8.1 Hz, 4H), 7.16 (s, 1H), 6.88 (dd, *J* = 8.0, 2.2 Hz, 1H), 6.72 (s, 1H), 6.34 (s, 1H), 4.49 (d, *J* = 2.3 Hz, 1H), 4.44 (d, *J* = 2.3 Hz, 1H), 4.40 (d, *J* = 2.4 Hz, 1H), 4.33 (d, *J* = 2.4 Hz, 1H), 3.90 (br, 2H), 3.57 (t, *J* = 6.6 Hz, 1H), 3.43 – 3.20 (m, 12H), 3.20 – 3.14 (m, 1H), 3.08 (ddd, *J* = 18.9, 9.3, 5.5 Hz, 2H), 2.80 (t, *J* = 9.3 Hz, 4H), 2.56 (s, 3H), 2.54 (s, 3H), 1.66 – 1.45 (m, 8H), 1.43 (s, 9H), 1.39 – 1.22 (m, 24H), 0.90 – 0.77 (m, 12H). ^{13}C NMR (125 MHz, $CDCl_3$): δ 171.30, 161.16, 160.91, 152.96, 144.74, 144.71, 143.24, 143.22, 142.96, 142.85, 142.78, 142.48, 142.31, 142.19, 142.16, 141.70, 139.20, 139.07, 138.23, 137.21, 137.04, 136.30, 135.56, 133.76, 131.23, 131.13, 130.05,

129.97, 129.87, 129.76, 126.77, 125.82, 125.74, 124.21, 122.98, 122.84, 121.88, 121.80, 117.15, 116.67, 112.85, 80.68, 73.57, 73.51, 73.44, 73.25, 71.58, 71.55, 71.53, 71.49, 63.25, 60.54, 46.25, 45.75, 45.31, 44.51, 43.64, 43.44, 43.22, 32.93, 31.89, 31.78, 29.86, 29.84, 29.81, 29.74, 29.51, 28.49, 26.08, 26.02, 25.56, 22.86, 22.84, 22.83, 22.78, 21.75, 21.71, 21.20, 14.35, 14.32, 14.29, 14.27, 14.24, 14.23, 14.17.

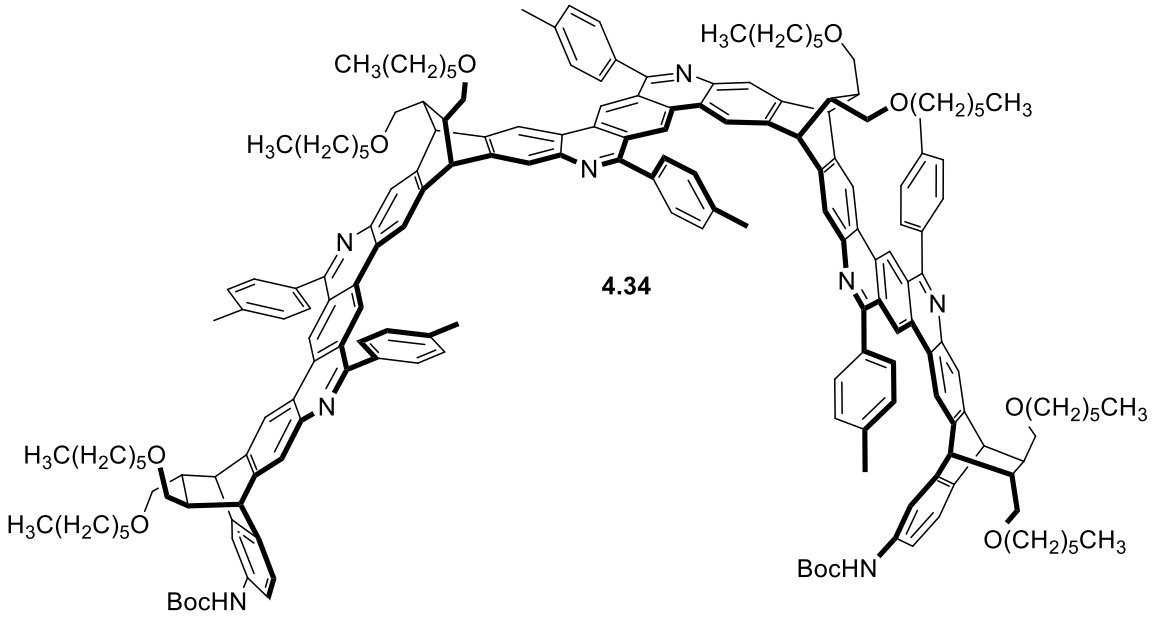

***N,N*'-diBoc *syn*-helical tetramer strip (4.34)**: Following the general procedure for Suzuki coupling/imine condensation, monoiodo-diamine **4.33** (9.5 mg, 0.0066 mmol) and *anti*-linker **4.19** (1.9 mg, 0.0033 mmol) in 1,4-dioxane (200 μL) afforded 7.2 mg (0.0025 mmol) of *syn*-helical tetramer **4.34** in 75% yield. The crude product obtained was purified by flash column chromatography (0 to 30% EtOAc in hexanes). ^{1}H NMR (500 MHz, $CDCl_3$): δ 9.44 (s, 2H), 9.43 (s, 2H), 9.40 (s, 2H), 8.39 (s, 4H), 8.27 (s, 2H), 8.21 (d, J = 7.3 Hz, 4H), 8.08 (s, 2H), 7.89 – 7.69 (m, 12H), 7.61 – 7.44 (m, 12H), 7.22 (d, J = 7.9 Hz, 2H), 6.92 (d, J = 7.8 Hz, 2H), 6.35 (s, 2H), 4.84 (s, 4H), 4.54 (s, 2H), 4.49 (s,

2H), 3.39 (t, J = 7.3 Hz, 12H), 3.30 (d, J = 6.2 Hz, 8H), 3.24 (d, J = 14.6 Hz, 2H), 3.21 – 3.13 (m, 2H), 3.01 – 2.92 (m, 4H), 2.90 – 2.81 (m, 4H), 2.63 (s, 12H), 2.61 (s, 6H), 1.79 (s, 4H), 1.69 – 1.55 (m, 12H), 1.46 (s, 18H), 1.37 (d, J = 23.8 Hz, 48H), 0.97 – 0.84 (m, 24H). ^{13}C NMR (125 MHz, $CDCl_3$): δ 161.10, 160.84, 160.84, 158.82, 152.77, 143.03, 142.82, 142.57, 142.19, 142.06, 141.53, 139.54, 139.11, 138.59, 138.06, 136.94, 136.85, 136.13, 134.90, 131.16, 130.94, 130.40, 130.18, 129.88, 129.80, 129.70, 129.62, 129.49, 129.21, 127.07, 126.62, 125.66, 124.08, 122.87, 122.05, 121.60, 119.59, 119.06, 116.97, 116.56, 116.06, 73.44, 73.30, 72.68, 71.64, 71.43, 71.39, 53.42, 46.09, 45.85, 45.16, 43.48, 43.29, 31.93, 31.77, 31.75, 29.69, 29.67, 29.62, 29.60, 29.37, 28.34, 28.32, 25.87, 22.70, 22.68, 22.66, 22.64, 21.61, 21.41, 14.12, 14.09. HRMS calcd. for $[C_{196}H_{224}N_8O_{12}]^{2+}$: 1441.8614; found: 1441.8616.

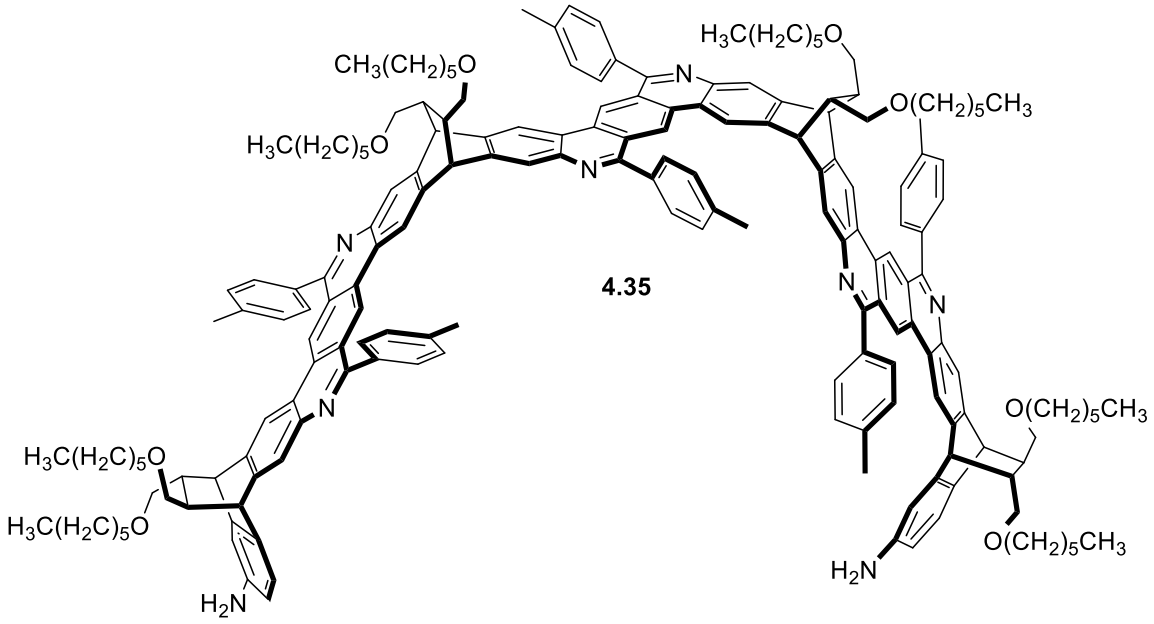

diamine *syn*-helical tetramer strip (4.35): DiBoc **4.34** (7.20 mg, (0.0025 mmol) was dissolved in DCM (2 mL) and trifluoroacetic acid (0.250 mL, excess) was added dropwise to the stirring solution. After 16 hours, the solution was poured over ice and diluted with 20 mL DCM before washing with a 2 M aqueous NaOH (1×20 mL) solution. Then the aqueous layer was further washed with DCM (2×20 mL) and the combined organic layers were then washed with brine (1×20 mL) and finally dried over anhydrous $MgSO_4$, filtered, and concentrated under reduced pressure to afford 6.3 mg of diamine **4.35** in 94% yield without further purification. As a note, despite excess TFA, if the reaction is not let run sufficiently long, unreacted diBoc persists in the reaction mixture. ^{1}H NMR (500 MHz, $CDCl_3$): δ 9.53 – 9.36 (m, 6H), 8.39 (s, 4H), 8.28 (s, 2H), 8.21 (d, *J* = 7.8 Hz, 4H), 8.07 (s, 2H), 7.87 – 7.74 (m, 12H), 7.58 – 7.50 (m, 12H), 7.08 (d, *J* = 7.8 Hz, 2H), 6.70 (s, 2H), 6.41 (d, *J* = 9.9 Hz, 2H), 4.83 (s, 4H), 4.51 – 4.41 (m, 4H), 3.55 – 3.12 (m, 32H), 2.99 – 2.80 (m, 8H), 2.64 (s, 12H), 2.59 (s, 6H), 1.78 (s, 4H), 1.60 (d, *J* =

7.0 Hz, 12H), 1.32 (d, *J* = 19.8 Hz, 48H), 0.99 – 0.82 (m, 24H). ^{13}C NMR (125 MHz, $CDCl_3$): δ 161.00, 161.00, 160.73, 160.73, 160.32, 145.98, 144.35, 144.15, 143.53, 143.23, 142.58, 142.17, 141.69, 139.08, 138.98, 136.99, 133.65, 131.21, 131.09, 130.88, 130.66, 130.40, 130.18, 129.89, 129.88, 129.70, 129.69, 129.65, 129.62, 129.62, 129.48, 129.23, 129.20, 127.08, 126.44, 125.63, 125.11, 124.44, 124.43, 122.85, 122.05, 121.48, 119.05, 116.95, 116.37, 115.32, 113.23, 112.43, 73.63, 73.25, 71.64, 71.42, 71.31, 45.97, 45.85, 44.94, 43.67, 43.37, 43.26, 37.40, 31.93, 31.76, 31.75, 29.71, 29.67, 29.62, 29.37, 25.94, 25.86, 22.71, 22.70, 22.66, 22.64, 21.61, 21.56, 21.40, 14.14, 14.11, 14.08. HRMS calcd. for $[C_{186}H_{208}N_8O_8]^{2+}$: 1340.8058; found: 1340.8054.

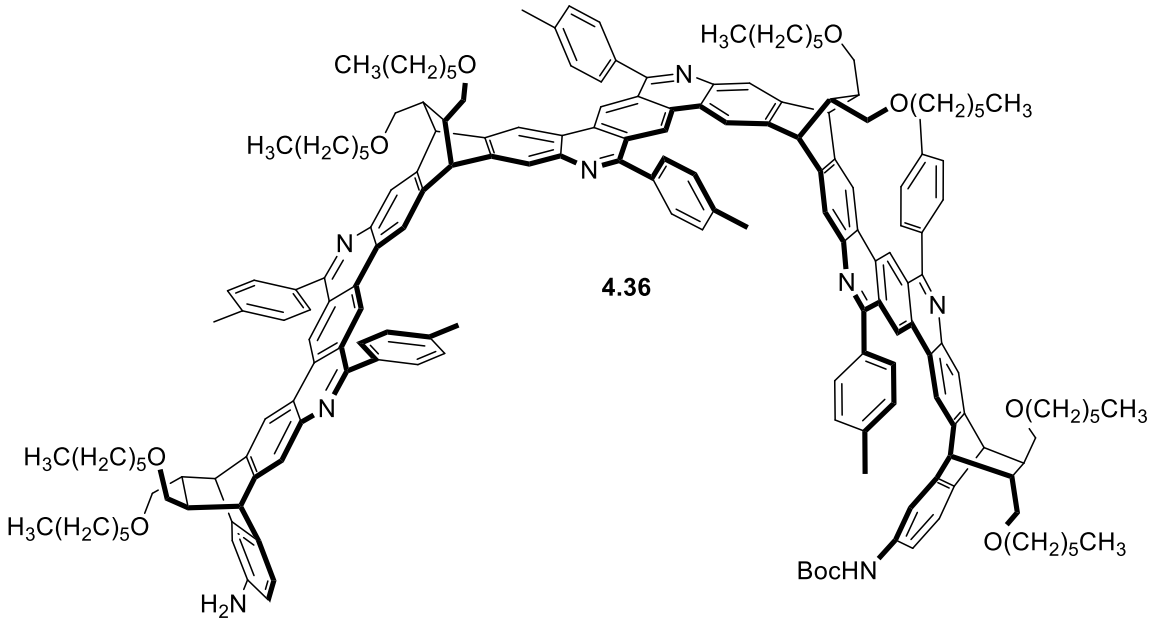

***N*-Boc *syn*-helical tetramer strip (4.36)**: Diamine **4.35** (23.4 mg, 8.73 μmol) was dissolved in THF (5 mL) and heated to 45 °C under N_2. A solution of boc anhydride (2.43 mg, 11.1 μmol) in THF (5 mL) was added dropwise to the stirring solution. After

16 hours, the solution was concentrated under vacuum to remove THF and then re-dissolved in 20 mL of DCM washed with H_2O (1×20 mL). Thereafter the aqueous layer was extracted with DCM (3×20 mL) and the combined organic layers were then washed with brine (1×20 mL) and the organic layer was dried over anhydrous $MgSO_4$, filtered, and concentrated under reduced pressure to afford crude material. The crude product obtained was purified by flash column chromatography (0 to 30% EtOAc in hexanes) to afford 6.9 mg of *N*-Boc-**4.36** in 60% yield based on recovered **4.35**. The ^{13}C resonances are overlapped and complex, but the general chemical shifts are reported nonetheless. Note the presence of the hexyl chains on the ether auxiliary. ^{1}H NMR (500 MHz, $CDCl_3$): 9.54 – 9.41 (m, 6H), 8.42 (s, 6H), 8.32 – 8.08 (m, 6H), 7.85 – 7.76 (m, 12H), 7.62 – 7.52 (m, 12H), 7.24 (d, *J* = 8.1 Hz, 1H), 7.11 (d, *J* = 7.9 Hz, 1H), 6.94 (d, *J* = 6.1 Hz, 1H), 6.72 (s, 1H), 6.44 (d, *J* = 8.1 Hz, 1H), 6.38 (s, 1H), 4.86 (s, 4H), 4.49 – 4.39 (m, 4H), 3.46 – 3.16 (m, 20H), 3.02 – 2.87 (m, 8H), 2.71 – 2.58 (m, 18H), 1.84 – 1.79 (m, 4H), 1.63 (d, *J* = 6.0 Hz, 12H), 1.49 (s, 9H), 1.39 – 1.33 (m, 48H), 0.99 – 0.86 (m, 24H). ^{13}C NMR (125 MHz, $CDCl_3$): 160.04, 141.58, 141.20, 138.07, 135.89, 130.20, 128.86, 128.67, 126.07, 124.61, 121.87, 120.96, 115.94, 72.22, 70.62, 70.40, 63.07, 59.38, 44.82, 43.91, 42.24, 36.54, 32.69, 30.91, 30.74, 30.72, 29.14, 28.68, 28.64, 28.60, 28.34, 28.23, 27.29, 25.69, 24.84, 21.67, 21.64, 21.62, 20.58, 20.03, 13.18, 13.10, 13.06. HRMS calcd. for $[C_{191}H_{217}N_8O_{10}]^{3+}$: 927.5573; found: 927.5571.

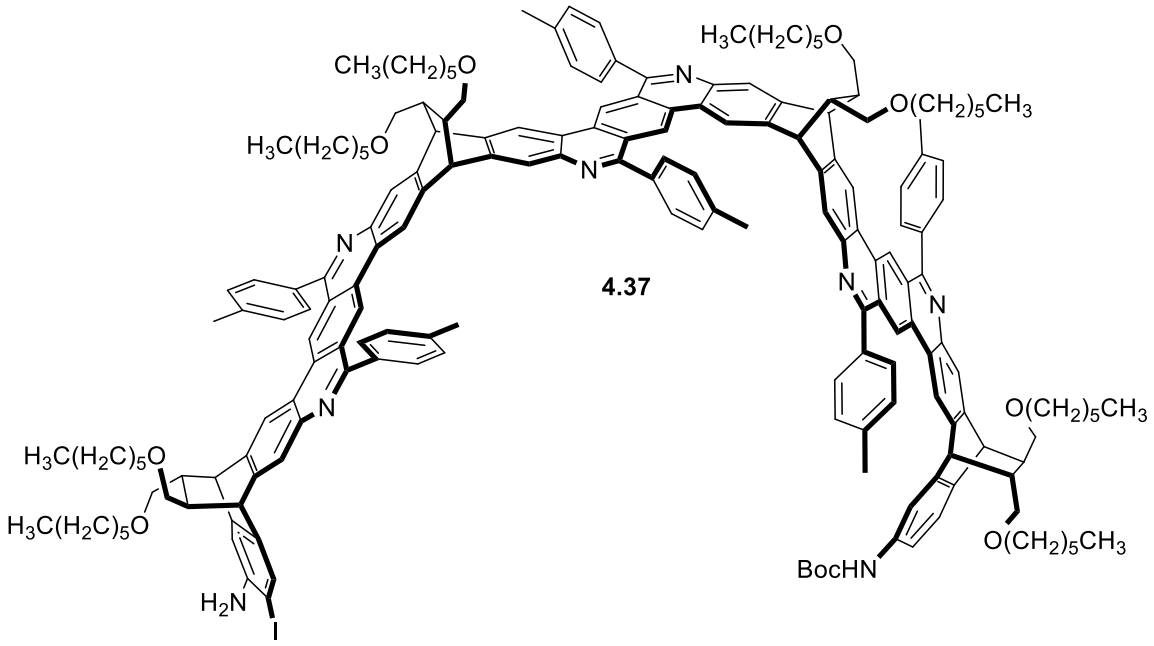

***N*-Boc-monoiodo *syn*-helical tetramer strip (4.37)**: Following the general procedure for regioselective electrophilic iodination, *N*-Boc **4.36** (2.0 mg, 0.72 μmol) dissolved in a blend of DCM (10 mL) and MeOH (10 mL) with slow addition of iodine monochloride (0.24 mg, 1.5 μmol) at -15 °C, afforded 1.5 mg of monoiodo **4.37** in 83% yield based on recovered **4.36**. The crude product obtained was purified by flash column chromatography (0 to 10% EtOAc in hexanes). The ^{13}C resonances are overlapped and complex, but the general chemical shifts are reported nonetheless. Note the presence of the hexyl chains on the ether auxiliary. ^{1}H NMR (500 MHz, $CDCl_3$): δ 9.51 – 9.41 (m, 6H), 8.42 (s, 4H), 8.33 – 8.13 (m, 8H), 7.86 – 7.75 (m, 12H), 7.65 – 7.52 (m, 13H), 7.24 (d, *J* = 8.1 Hz, 1H), 6.95 (d, *J* = 6.3 Hz, 1H), 6.79 (s, 1H), 6.38 (s, 1H), 4.94 – 4.82 (m, 4H), 4.61 – 4.41 (m, 4H), 3.46 – 3.27 (m, 20H), 2.93 (d, *J* = 40.6 Hz, 8H), 2.71 – 2.58 (m, 18H), 1.81 (s, 4H), 1.61 (s, 12H), 1.49 (s, 9H), 1.36 (s, 48H), 0.99 – 0.86 (m, 24H).

^{13}C NMR (125 MHz, $CDCl_3$): δ 169.13, 160.03, 147.23, 146.65, 141.15, 138.98, 138.07, 135.88, 128.86, 128.68, 128.47, 127.94, 126.98, 126.75, 126.07, 125.84, 124.63, 121.86, 120.97, 120.58, 115.92, 111.97, 109.13, 105.48, 100.15, 80.96, 72.22, 70.62, 70.38, 66.76, 65.18, 55.52, 52.39, 44.83, 42.23, 37.90, 36.08, 31.74, 30.91, 30.74, 30.72, 29.56, 29.02, 28.68, 28.64, 28.60, 28.57, 28.43, 28.34, 28.07, 27.97, 27.29, 25.36, 24.84, 23.90, 22.97, 21.95, 21.67, 21.64, 21.61, 20.58, 17.62, 13.09, 13.06, 13.02, 10.23, 10.07, 7.09.

COMPREHENSIVE LIST OF REFERENCES

1. Anfinsen, C. B., Principles that govern the folding of protein chains. *Science* **1973,** *181* (4096), 223-30.

2. Mathias, J. P.; Stoddart, J. F., Constructing a molecular LEGO set. *Chemical Society Reviews* **1992,** *21* (4), 215.

3. Schmidt, B. V.; Fechler, N.; Falkenhagen, J.; Lutz, J. F., Controlled folding of synthetic polymer chains through the formation of positionable covalent bridges. *Nat Chem* **2011,** *3* (3), 234-38.

4. Liu, X.; Weinert, Z. J.; Sharafi, M.; Liao, C.; Li, J.; Schneebeli, S. T., Regulating Molecular Recognition with C-Shaped Strips Attained by Chirality-Assisted Synthesis. *Angew Chem Int Ed Engl* **2015,** *54* (43), 12772-6.

5. Campbell, J. P.; Sharafi, M.; Murphy, K. E.; Bocanegra, J. L.; Schneebeli, S. T., Precise molecular shape control of linear and branched strips with chirality-assisted synthesis. *Supramolecular Chemistry* **2019,** *31* (8), 565-574.

6. Ashton, P. R.; Brown, G. R.; Isaacs, N. S.; Giuffrida, D.; Kohnke, F. H.; Mathias, J. P.; Slawin, A. M. Z.; Smith, D. R.; Stoddart, J. F.; Williams, D. J., Molecular LEGO. 1. Substrate-directed synthesis via stereoregular Diels-Alder oligomerizations. *Journal of the American Chemical Society* **1992,** *114* (16), 6330-6353.

7. Chong, J. H.; MacLachlan, M. J., Synthesis and structural investigation of new triptycene-based ligands: en route to shape-persistent dendrimers and macrocycles with large free volume. *J Org Chem* **2007,** *72* (23), 8683-90.

8. Schneebeli, S.; Li, J.; Sharafi, M.; Weinert, Z.; Cohen, I.; Liao, C.; Ivancic, M., Controlled Self-Assembly inside C-Shaped Polyaromatic Strips. *Synlett* **2016,** *27* (14), 2145-2149.

9. Furrow, M. E.; Schaus, S. E.; Jacobsen, E. N., Practical Access to Highly Enantioenriched C-3 Building Blocks via Hydrolytic Kinetic Resolution. *J Org Chem* **1998,** *63* (20), 6776-6777.

10. Staudinger, H., Über Polymerisation. *Berichte der deutschen chemischen Gesellschaft (A and B Series)* **1920,** *53* (6), 1073-1085.

11. Qiu, L. Y.; Bae, Y. H., Polymer architecture and drug delivery. *Pharm Res* **2006,** *23* (1), 1-30.

12. Teo, Y. C.; Lai, H. W. H.; Xia, Y., Synthesis of Ladder Polymers: Developments, Challenges, and Opportunities. *Chemistry* **2017,** *23* (57), 14101-14112.

13. Takagi, K.; Tanaka, H.; Mikami, K., Ladderization of polystyrene derivatives by palladium-catalyzed polymer direct arylation. *Polymer Chemistry* **2019,** *10* (21), 2647-2652.

14. Scherf, U., Ladder-type materials. *Journal of Materials Chemistry* **1999,** *9* (9), 1853-1864.

15. Lee, J.; Kalin, A. J.; Yuan, T.; Al-Hashimi, M.; Fang, L., Fully conjugated ladder polymers. *Chem Sci* **2017,** *8* (4), 2503-2521.

16. Chen, Z.; Amara, J. P.; Thomas, S. W.; Swager, T. M., Synthesis of a Novel Poly(iptycene) Ladder Polymer. *Macromolecules* **2006,** *39* (9), 3202-3209.

17. Swager, T. M., Iptycenes in the design of high performance polymers. *Acc Chem Res* **2008,** *41* (9), 1181-9.

18. Zhang, Q. T.; Tour, J. M., Imine-Bridged Planar Poly(phenylenethiophene)s and Polythiophenes. *Journal of the American Chemical Society* **1997,** *119* (41), 9624-9631.

19. Yao, Y.; Tour, J. M., Synthesis of Imine-Bridged Phenylenepyridine Ladder Polymers. Optical Band Gap Widening through Intramolecular Charge Transfer in Planar Polymers. *Macromolecules* **1999,** *32* (8), 2455-2461.

20. Ren, X.; Zhang, H.; Song, M.; Cheng, C.; Zhao, H.; Wu, Y., One-Step Route to Ladder-Type C–N Linked Conjugated Polymers. *Macromolecular Chemistry and Physics* **2019,** *220* (9), 1900044.

21. Ushiba, S.; Masui, K.; Taguchi, N.; Hamano, T.; Kawata, S.; Shoji, S., Size dependent nanomechanics of coil spring shaped polymer nanowires. *Sci Rep* **2015,** *5*, 17152.

22. Liu, L.; Zhang, L.; Kim, S. M.; Park, S., Helical metallic micro- and nanostructures: fabrication and application. *Nanoscale* **2014,** *6* (16), 9355-65.

23. Yashima, E.; Maeda, K.; Iida, H.; Furusho, Y.; Nagai, K., Helical polymers: synthesis, structures, and functions. *Chem Rev* **2009,** *109* (11), 6102-211.

24. Yashima, E.; Ousaka, N.; Taura, D.; Shimomura, K.; Ikai, T.; Maeda, K., Supramolecular Helical Systems: Helical Assemblies of Small Molecules, Foldamers, and Polymers with Chiral Amplification and Their Functions. *Chem Rev* **2016,** *116* (22), 13752-13990.

25. Yashima, E., Synthesis and structure determination of helical polymers. *Polymer Journal* **2010,** *42* (1), 3-16.

26. Vacogne, C. D.; Wei, C.; Tauer, K.; Schlaad, H., Self-Assembly of alpha-Helical Polypeptides into Microscopic and Enantiomorphic Spirals. *J Am Chem Soc* **2018,** *140* (36), 11387-11394.

27. De Greef, T. F.; Smulders, M. M.; Wolffs, M.; Schenning, A. P.; Sijbesma, R. P.; Meijer, E. W., Supramolecular polymerization. *Chem Rev* **2009,** *109* (11), 5687-754.

28. De, S.; Chi, B.; Granier, T.; Qi, T.; Maurizot, V.; Huc, I., Designing cooperatively folded abiotic uni- and multimolecular helix bundles. *Nat Chem* **2018,** *10* (1), 51-57.

29. Ziach, K.; Chollet, C.; Parissi, V.; Prabhakaran, P.; Marchivie, M.; Corvaglia, V.; Bose, P. P.; Laxmi-Reddy, K.; Godde, F.; Schmitter, J. M.; Chaignepain, S.; Pourquier, P.; Huc, I., Single helically folded aromatic oligoamides that mimic the charge surface of double-stranded B-DNA. *Nat Chem* **2018,** *10* (5), 511-518.

30. Appella, D. H.; Christianson, L. A.; Karle, I. L.; Powell, D. R.; Gellman, S. H., β-Peptide Foldamers: Robust Helix Formation in a New Family of β-Amino Acid Oligomers. *Journal of the American Chemical Society* **1996,** *118* (51), 13071-13072.

31. Saha, S.; Kauffmann, B.; Ferrand, Y.; Huc, I., Selective Encapsulation of Disaccharide Xylobiose by an Aromatic Foldamer Helical Capsule. *Angew Chem Int Ed Engl* **2018,** *57* (41), 13542-13546.

32. Wechsel, R.; Zabka, M.; Ward, J. W.; Clayden, J., Competing Hydrogen-Bond Polarities in a Dynamic Oligourea Foldamer: A Molecular Spring Torsion Balance. *J Am Chem Soc* **2018,** *140* (10), 3528-3531.

33. Zaccai, N. R.; Chi, B.; Thomson, A. R.; Boyle, A. L.; Bartlett, G. J.; Bruning, M.; Linden, N.; Sessions, R. B.; Booth, P. J.; Brady, R. L.; Woolfson, D. N., A de novo peptide hexamer with a mutable channel. *Nat Chem Biol* **2011,** *7* (12), 935-41.

34. Furusho, Y.; Yashima, E., Development of synthetic double helical polymers and oligomers. *Journal of Polymer Science Part A: Polymer Chemistry* **2009,** *47* (20), 5195-5207.

35. Furusho, Y.; Yashima, E., Synthesis and function of double-stranded helical polymers and oligomers. *Macromol Rapid Commun* **2011,** *32* (2), 136-46.

36. Yamamoto, T.; Murakami, R.; Komatsu, S.; Suginome, M., Chirality-Amplifying, Dynamic Induction of Single-Handed Helix by Chiral Guests to Macromolecular Chiral Catalysts Bearing Boronyl Pendants as Receptor Sites. *J Am Chem Soc* **2018,** *140* (11), 3867-3870.

37. Ke, Y. Z.; Nagata, Y.; Yamada, T.; Suginome, M., Majority-Rules-Type Helical Poly(quinoxaline-2,3-diyl)s as Highly Efficient Chirality-Amplification Systems for Asymmetric Catalysis. *Angew Chem Int Ed Engl* **2015,** *54* (32), 9333-7.

38. Ishiwari, F.; Nakazono, K.; Koyama, Y.; Takata, T., Induction of Single-Handed Helicity of Polyacetylenes Using Mechanically Chiral Rotaxanes as Chiral Sources. *Angewandte Chemie* **2017,** *129* (47), 15054-15058.

39. Wu, Z. Q.; Nagai, K.; Banno, M.; Okoshi, K.; Onitsuka, K.; Yashima, E., Enantiomer-selective and helix-sense-selective living block copolymerization of isocyanide enantiomers initiated by single-handed helical poly(phenyl isocyanide)s. *J Am Chem Soc* **2009,** *131* (19), 6708-18.

40. Daigle, M.; Morin, J.-F., Helical Conjugated Ladder Polymers: Tuning the Conformation and Properties through Edge Design. *Macromolecules* **2017,** *50* (23), 9257-9264.

41. Iwasaki, T.; Katayose, K.; Kohinata, Y.; Nishide, H., A Helical Ladder Polymer: Synthesis and Magnetic Circular Dichroism of Poly[phenylene-4,6-bis(methylsulfonio)-1,3-diyl triflate]. *Polymer Journal* **2005,** *37* (8), 592-598.

42. Ikai, T.; Yoshida, T.; Shinohara, K. I.; Taniguchi, T.; Wada, Y.; Swager, T. M., Triptycene-Based Ladder Polymers with One-Handed Helical Geometry. *J Am Chem Soc* **2019,** *141* (11), 4696-4703.

43. Park, K. H.; Noh, T. H.; Shim, Y. B.; Jung, O. S., Construction of right-handed-, left-handed-, and racemic helical coordination polymers. Enantioselective recognition using chiral helical crystals. *Chem Commun (Camb)* **2013,** *49* (38), 4000-2.

44. Ohta, E.; Sato, H.; Ando, S.; Kosaka, A.; Fukushima, T.; Hashizume, D.; Yamasaki, M.; Hasegawa, K.; Muraoka, A.; Ushiyama, H.; Yamashita, K.; Aida, T., Redox-responsive molecular helices with highly condensed pi-clouds. *Nat Chem* **2011,** *3* (1), 68-73.

45. Chandramouli, N.; Ferrand, Y.; Lautrette, G.; Kauffmann, B.; Mackereth, C. D.; Laguerre, M.; Dubreuil, D.; Huc, I., Iterative design of a helically folded aromatic oligoamide sequence for the selective encapsulation of fructose. *Nat Chem* **2015,** *7* (4), 334-41.

46. Wang, P.; Jeon, I.; Lin, Z.; Peeks, M. D.; Savagatrup, S.; Kooi, S. E.; Van Voorhis, T.; Swager, T. M., Insights into Magneto-Optics of Helical Conjugated Polymers. *J Am Chem Soc* **2018,** *140* (20), 6501-6508.

47. Tamura, K.; Miyabe, T.; Iida, H.; Yashima, E., Separation of enantiomers on diastereomeric right- and left-handed helical poly(phenyl isocyanide)s bearing l-alanine pendants immobilized on silica gel by HPLC. *Polym. Chem.* **2011,** *2* (1), 91-98.

48. Shen, J.; Okamoto, Y., Efficient Separation of Enantiomers Using Stereoregular Chiral Polymers. *Chem Rev* **2016,** *116* (3), 1094-138.

49. Li, H.; Zheng, X.; Su, H.; Lam, J. W.; Sing Wong, K.; Xue, S.; Huang, X.; Huang, X.; Li, B. S.; Tang, B. Z., Synthesis, optical properties, and helical self-assembly of a bivaline-containing tetraphenylethene. *Sci Rep* **2016,** *6*, 19277.

50. Zhong, Y.; Trinh, M. T.; Chen, R.; Purdum, G. E.; Khlyabich, P. P.; Sezen, M.; Oh, S.; Zhu, H.; Fowler, B.; Zhang, B.; Wang, W.; Nam, C. Y.; Sfeir, M. Y.; Black, C. T.; Steigerwald, M. L.; Loo, Y. L.; Ng, F.; Zhu, X. Y.; Nuckolls, C., Molecular helices as electron acceptors in high-performance bulk heterojunction solar cells. *Nat Commun* **2015,** *6*, 8242.

51. Berl, V.; Huc, I.; Khoury, R. G.; Krische, M. J.; Lehn, J. M., Interconversion of single and double helices formed from synthetic molecular strands. *Nature* **2000,** *407* (6805), 720-3.

52. Asher, S. A.; Mikhonin, A. V.; Bykov, S., UV Raman demonstrates that alpha-helical polyalanine peptides melt to polyproline II conformations. *J Am Chem Soc* **2004,** *126* (27), 8433-40.

53. Jung, O.-S.; Kim, Y. J.; Lee, Y.-A.; Park, J. K.; Chae, H. K., Smart Molecular Helical Springs as Tunable Receptors. *Journal of the American Chemical Society* **2000,** *122* (41), 9921-9925.

54. Newman, M. S.; Lednicer, D., The Synthesis and Resolution of Hexahelicene1. *Journal of the American Chemical Society* **1956,** *78* (18), 4765-4770.

55. Martin, R. H.; Baes, M., Helicenes. *Tetrahedron* **1975,** *31* (17), 2135-2137.

56. Nakakuki, Y.; Hirose, T.; Sotome, H.; Miyasaka, H.; Matsuda, K., Hexa- peri-hexabenzo[7]helicene: Homogeneously pi-Extended Helicene as a Primary Substructure of Helically Twisted Chiral Graphenes. *J Am Chem Soc* **2018,** *140* (12), 4317-4326.

57. Nakakuki, Y.; Hirose, T.; Matsuda, K., Synthesis of a Helical Analogue of Kekulene: A Flexible pi-Expanded Helicene with Large Helical Diameter Acting as a Soft Molecular Spring. *J Am Chem Soc* **2018,** *140* (45), 15461-15469.

58. Schuster, N. J.; Hernandez Sanchez, R.; Bukharina, D.; Kotov, N. A.; Berova, N.; Ng, F.; Steigerwald, M. L.; Nuckolls, C., A Helicene Nanoribbon with Greatly Amplified Chirality. *J Am Chem Soc* **2018,** *140* (20), 6235-6239.

59. Shen, Y.; Chen, C. F., Helicenes: synthesis and applications. *Chem Rev* **2012,** *112* (3), 1463-535.

60. Tanaka, K.; Osuga, H.; Kitahara, Y., Elongation and contraction of molecular springs. Synthesis, structures, and properties of bridged [7]thiaheterohelicenes. *J Org Chem* **2002,** *67* (6), 1795-801.

61. Kelly, T. R.; Cai, X.; Damkaci, F.; Panicker, S. B.; Tu, B.; Bushell, S. M.; Cornella, I.; Piggott, M. J.; Salives, R.; Cavero, M.; Zhao, Y.; Jasmin, S., Progress toward a rationally designed, chemically powered rotary molecular motor. *J Am Chem Soc* **2007,** *129* (2), 376-86.

62. Kelly, T. R.; Sestelo, J. P.; Tellitu, I., New Molecular Devices: In Search of a Molecular Ratchet. *The Journal of Organic Chemistry* **1998,** *63* (11), 3655-3665.

63. Dai, Y.; Katz, T. J.; Nichols, D. A., Synthesis of a Helical Conjugated Ladder Polymer. *Angewandte Chemie International Edition in English* **1996,** *35* (18), 2109-2111.

64. Jin, Y. J.; Aoki, T.; Kwak, G., Control of Intramolecular Hydrogen Bonding in a Conformation-switchable Helical Spring Polymer by Solvent and Temperature. *Angew Chem Int Ed Engl* **2019**.

65. Dong, H.; Shu, J. Y.; Dube, N.; Ma, Y.; Tirrell, M. V.; Downing, K. H.; Xu, T., 3-Helix micelles stabilized by polymer springs. *J Am Chem Soc* **2012,** *134* (28), 11807-14.

66. Farahani, R. D.; Chizari, K.; Therriault, D., Three-dimensional printing of freeform helical microstructures: a review. *Nanoscale* **2014,** *6* (18), 10470-85.

67. Kim, H. J.; Lee, E.; Park, H. S.; Lee, M., Dynamic extension-contraction motion in supramolecular springs. *J Am Chem Soc* **2007,** *129* (36), 10994-5.

68. Marsella, M. J.; Rahbarnia, S.; Wilmot, N., Molecular springs, muscles, rheostats, and precessing gyroscopes: from review to preview. *Org Biomol Chem* **2007,** *5* (3), 391-400.

69. Miwa, K.; Furusho, Y.; Yashima, E., Ion-triggered spring-like motion of a double helicate accompanied by anisotropic twisting. *Nat Chem* **2010,** *2* (6), 444-9.

70. Suzuki, Y.; Nakamura, T.; Iida, H.; Ousaka, N.; Yashima, E., Allosteric Regulation of Unidirectional Spring-like Motion of Double-Stranded Helicates. *J Am Chem Soc* **2016,** *138* (14), 4852-9.

71. Chen, X.; Gerger, T. M.; Rauber, C.; Raabe, G.; Gob, C.; Oppel, I. M.; Albrecht, M., A Helicate-Based Three-State Molecular Switch. *Angew Chem Int Ed Engl* **2018,** *57* (36), 11817-11820.

72. Schoenauer, R.; Bertoncini, P.; Machaidze, G.; Aebi, U.; Perriard, J. C.; Hegner, M.; Agarkova, I., Myomesin is a molecular spring with adaptable elasticity. *J Mol Biol* **2005,** *349* (2), 367-79.

73. Engel, M. C.; Smith, D. M.; Jobst, M. A.; Sajfutdinow, M.; Liedl, T.; Romano, F.; Rovigatti, L.; Louis, A. A.; Doye, J. P. K., Force-Induced Unravelling of DNA Origami. *ACS Nano* **2018,** *12* (7), 6734-6747.

74. Bustamante, C.; Bryant, Z.; Smith, S. B., Ten years of tension: single-molecule DNA mechanics. *Nature* **2003,** *421* (6921), 423-7.

75. Granzier, H.; Labeit, S., Cardiac titin: an adjustable multi-functional spring. *J Physiol* **2002,** *541* (Pt 2), 335-42.

76. Herzog, W., The multiple roles of titin in muscle contraction and force production. *Biophys Rev* **2018,** *10* (4), 1187-1199.

77. Rohrig, U. F.; Guidoni, L.; Laio, A.; Frank, I.; Rothlisberger, U., A molecular spring for vision. *J Am Chem Soc* **2004,** *126* (47), 15328-9.

78. Kawamura, S.; Gerstung, M.; Colozo, A. T.; Helenius, J.; Maeda, A.; Beerenwinkel, N.; Park, P. S.; Muller, D. J., Kinetic, energetic, and mechanical differences between dark-state rhodopsin and opsin. *Structure* **2013,** *21* (3), 426-37.

79. Maeda, K.; Mochizuki, H.; Watanabe, M.; Yashima, E., Switching of macromolecular helicity of optically active poly(phenylacetylene)s bearing cyclodextrin pendants induced by various external stimuli. *J Am Chem Soc* **2006,** *128* (23), 7639-50.

80. Leiras, S.; Freire, F.; Seco, J. M.; Quiñoá, E.; Riguera, R., Controlled modulation of the helical sense and the elongation of poly(phenylacetylene)s by polar and donor effects. *Chemical Science* **2013,** *4* (7), 2735.

81. Sakai, R.; Okade, S.; Barasa, E. B.; Kakuchi, R.; Ziabka, M.; Umeda, S.; Tsuda, K.; Satoh, T.; Kakuchi, T., Efficient Colorimetric Anion Detection Based on Positive Allosteric System of Urea-Functionalized Poly(phenylacetylene) Receptor. *Macromolecules* **2010,** *43* (18), 7406-7411.

82. Motoshige, A.; Mawatari, Y.; Yoshida, Y.; Motoshige, R.; Tabata, M., Synthesis and solid state helix to helix rearrangement of poly(phenylacetylene) bearing n-octyl alkyl side chains. *Polym. Chem.* **2014,** *5* (3), 971-978.

83. Motoshige, R.; Mawatari, Y.; Motoshige, A.; Yoshida, Y.; Sasaki, T.; Yoshimizu, H.; Suzuki, T.; Tsujita, Y.; Tabata, M., Mutual conversion between stretched and contracted helices accompanied by a drastic change in color and spatial structure of poly(phenylacetylene) prepared with a [Rh(nbd)Cl]2-amine catalyst. *Journal of Polymer Science Part A: Polymer Chemistry* **2014,** *52* (6), 752-759.

84. Percec, V.; Rudick, J. G.; Peterca, M.; Heiney, P. A., Nanomechanical function from self-organizable dendronized helical polyphenylacetylenes. *J Am Chem Soc* **2008,** *130* (23), 7503-8.

85. Iamsaard, S.; Asshoff, S. J.; Matt, B.; Kudernac, T.; Cornelissen, J. J.; Fletcher, S. P.; Katsonis, N., Conversion of light into macroscopic helical motion. *Nat Chem* **2014,** *6* (3), 229-35.

86. Quan, X.; Marvin, C. W.; Seebald, L.; Hutchison, G. R., Single-Molecule Piezoelectric Deformation: Rational Design from First-Principles Calculations. *The Journal of Physical Chemistry C* **2013,** *117* (33), 16783-16790.

87. Werling, K. A.; Griffin, M.; Hutchison, G. R.; Lambrecht, D. S., Piezoelectric hydrogen bonding: computational screening for a design rationale. *J Phys Chem A* **2014,** *118* (35), 7404-10.

88. Connor, A. L.; Hu, T.; Detchou, C. S.; Liu, R.; Pulavarti, S. V.; Szyperski, T.; Lu, Z.; Gong, B., Aromatic oligureas as hosts for anions and cations. *Chem Commun (Camb)* **2016,** *52* (64), 9905-8.

89. Bird, G. H.; Pornsuwan, S.; Saxena, S.; Schafmeister, C. E., Distance distributions of end-labeled curved bispeptide oligomers by electron spin resonance. *ACS Nano* **2008,** *2* (9), 1857-64.

90. Parker, M. F.; Osuna, S.; Bollot, G.; Vaddypally, S.; Zdilla, M. J.; Houk, K. N.; Schafmeister, C. E., Acceleration of an aromatic Claisen rearrangement via a designed spiroligozyme catalyst that mimics the ketosteroid isomerase catalytic dyad. *J Am Chem Soc* **2014,** *136* (10), 3817-27.

91. Wei, X.; Zhang, G.; Shen, Y.; Zhong, Y.; Liu, R.; Yang, N.; Al-Mkhaizim, F. Y.; Kline, M. A.; He, L.; Li, M.; Lu, Z. L.; Shao, Z.; Gong, B., Persistent Organic Nanopores Amenable to Structural and Functional Tuning. *J Am Chem Soc* **2016,** *138* (8), 2749-54.

92. Fu, H.; Cohen, R. E., Polarization rotation mechanism for ultrahigh electromechanical response in single-crystal piezoelectrics. *Nature* **2000,** *403* (6767), 281-3.

93. McGough, A., Membrane skeleton: How to build a molecular shock absorber. *Current Biology* **1999,** *9* (23), R887-R889.

94. Yang, W.; Quan, H.; Meyers, M. A.; Ritchie, R. O., Arapaima Fish Scale: One of the Toughest Flexible Biological Materials. *SSRN Electronic Journal* **2019**.

95. Kay, E. R.; Leigh, D. A.; Zerbetto, F., Synthetic molecular motors and mechanical machines. *Angew Chem Int Ed Engl* **2007,** *46* (1-2), 72-191.

96. Shepherd, H. J.; Gural'skiy, I. A.; Quintero, C. M.; Tricard, S.; Salmon, L.; Molnar, G.; Bousseksou, A., Molecular actuators driven by cooperative spin-state switching. *Nat Commun* **2013,** *4*, 2607.

97. Shang, Y.; He, X.; Li, Y.; Zhang, L.; Li, Z.; Ji, C.; Shi, E.; Li, P.; Zhu, K.; Peng, Q.; Wang, C.; Zhang, X.; Wang, R.; Wei, J.; Wang, K.; Zhu, H.; Wu, D.; Cao, A., Super-stretchable spring-like carbon nanotube ropes. *Adv Mater* **2012,** *24* (21), 2896-900.

98. Liu, L.; Xu, X.; Zhao, C.; Yang, F., A new helical membrane module for increasing permeate flux. *Journal of Membrane Science* **2010,** *360* (1-2), 142-148.

99. Formoso, P.; Pantuso, E.; De Filpo, G.; Nicoletta, F. P., Electro-Conductive Membranes for Permeation Enhancement and Fouling Mitigation: A Short Review. *Membranes (Basel)* **2017,** *7* (3).

100. Kim, D.-Y.; Lee, K. M.; White, T. J.; Jeong, K.-U., Cholesteric liquid crystal paints: in situ photopolymerization of helicoidally stacked multilayer nanostructures for flexible broadband mirrors. *NPG Asia Materials* **2018,** *10* (11), 1061-1068.

101. Mandle, R. J.; Goodby, J. W., A Nanohelicoidal Nematic Liquid Crystal Formed by a Non-Linear Duplexed Hexamer. *Angew Chem Int Ed Engl* **2018,** *57* (24), 7096-7100.

102. Forterre, Y.; Dumais, J., Materials science. Generating helices in nature. *Science* **2011,** *333* (6050), 1715-6.

103. Asshoff, S. J.; Lancia, F.; Iamsaard, S.; Matt, B.; Kudernac, T.; Fletcher, S. P.; Katsonis, N., High-Power Actuation from Molecular Photoswitches in Enantiomerically Paired Soft Springs. *Angew Chem Int Ed Engl* **2017,** *56* (12), 3261-3265.

104. Wei, M.; Gao, Y.; Li, X.; Serpe, M. J., Stimuli-responsive polymers and their applications. *Polymer Chemistry* **2017,** *8* (1), 127-143.

105. Alzubi, M.; Arias, S.; Rodriguez, R.; Quinoa, E.; Riguera, R.; Freire, F., Chiral Conflict as a Method to Create Stimuli-Responsive Materials Based on Dynamic Helical Polymers. *Angew Chem Int Ed Engl* **2019,** *58* (38), 13365-13369.

106. Li, W.; Huang, G.; Yan, H.; Wang, J.; Yu, Y.; Hu, X.; Wu, X.; Mei, Y., Fabrication and stimuli-responsive behavior of flexible micro-scrolls. *Soft Matter* **2012,** *8* (27), 7103.

107. Yoshida, K.; Nakajima, S.; Kawano, R.; Onoe, H., Spring-shaped stimuli-responsive hydrogel actuator with large deformation. *Sensors and Actuators B: Chemical* **2018,** *272*, 361-368.

108. Kassem, S.; Lee, A. T. L.; Leigh, D. A.; Marcos, V.; Palmer, L. I.; Pisano, S., Stereodivergent synthesis with a programmable molecular machine. *Nature* **2017,** *549* (7672), 374-378.

109. Kelly, T. R.; Snapper, M. L., Nanotechnology: A molecular assembler. *Nature* **2017,** *549* (7672), 336-337.

110. Yamato, T.; Tsuchihashi, K.; Nakamura, N.; Hirahara, M.; Tsuzuki, H., Medium-sized cyclophanes, part 59:1 Nitration of [3.3]- and [3.3.3]metacyclophanes — Through-space electronic interactions between two or three benzene rings. *Canadian Journal of Chemistry* **2002,** *80* (2), 207-215.

111. Papageorgiou, G.; Corrie, J. E. T., REGIOSELECTIVE NITRATION OF 1-ACYL-4-METHOXYINDOLINES LEADS TO EFFICIENT SYNTHESIS OF A PHOTOLABILEl-GLUTAMATE PRECURSOR. *Synthetic Communications* **2002,** *32* (10), 1571-1577.

112. Holl, M. G.; Struble, M. D.; Singal, P.; Siegler, M. A.; Lectka, T., Positioning a Carbon-Fluorine Bond over the pi Cloud of an Aromatic Ring: A Different Type of Arene Activation. *Angew Chem Int Ed Engl* **2016,** *55* (29), 8266-9.

113. Guan, L.; Holl, M. G.; Pitts, C. R.; Struble, M. D.; Siegler, M. A.; Lectka, T., Through-Space Activation Can Override Substituent Effects in Electrophilic Aromatic Substitution. *J Am Chem Soc* **2017,** *139* (42), 14913-14916.

114. Holl, M. G.; Pitts, C. R.; Lectka, T., Fluorine in a C-F Bond as the Key to Cage Formation. *Angew Chem Int Ed Engl* **2018,** *57* (11), 2758-2766.

115. Wheland, G. W., A Quantum Mechanical Investigation of the Orientation of Substituents in Aromatic Molecules. *Journal of the American Chemical Society* **1942,** *64* (4), 900-908.

116. Reed, C. A.; Kim, K. C.; Stoyanov, E. S.; Stasko, D.; Tham, F. S.; Mueller, L. J.; Boyd, P. D., Isolating benzenium ion salts. *J Am Chem Soc* **2003,** *125* (7), 1796-804.

117. Pitts, C. R.; Holl, M. G.; Lectka, T., Spectroscopic Characterization of a [C-F-C](+) Fluoronium Ion in Solution. *Angew Chem Int Ed Engl* **2018,** *57* (7), 1924-1927.

118. Terrier, F., Rate and equilibrium studies in Jackson-Meisenheimer complexes. *Chemical Reviews* **1982,** *82* (2), 77-152.

119. Allemann, O.; Duttwyler, S.; Romanato, P.; Baldridge, K. K.; Siegel, J. S., Proton-catalyzed, silane-fueled Friedel-Crafts coupling of fluoroarenes. *Science* **2011,** *332* (6029), 574-7.

120. Jost, M.; Zocher, G.; Tarcz, S.; Matuschek, M.; Xie, X.; Li, S. M.; Stehle, T., Structure-function analysis of an enzymatic prenyl transfer reaction identifies a reaction chamber with modifiable specificity. *J Am Chem Soc* **2010,** *132* (50), 17849-58.

121. Mori, T.; Zhang, L.; Awakawa, T.; Hoshino, S.; Okada, M.; Morita, H.; Abe, I., Manipulation of prenylation reactions by structure-based engineering of bacterial indolactam prenyltransferases. *Nat Commun* **2016,** *7*, 10849.

122. Srivastava, V., **2019**.

123. Metzger, U.; Schall, C.; Zocher, G.; Unsold, I.; Stec, E.; Li, S. M.; Heide, L.; Stehle, T., The structure of dimethylallyl tryptophan synthase reveals a common architecture of aromatic prenyltransferases in fungi and bacteria. *Proc Natl Acad Sci U S A* **2009,** *106* (34), 14309-14.

124. Tanner, M. E., Mechanistic studies on the indole prenyltransferases. *Nat Prod Rep* **2015,** *32* (1), 88-101.

125. Snieckus, V., Directed ortho metalation. Tertiary amide and O-carbamate directors in synthetic strategies for polysubstituted aromatics. *Chemical Reviews* **1990,** *90* (6), 879-933.

126. Leow, D.; Li, G.; Mei, T. S.; Yu, J. Q., Activation of remote meta-C-H bonds assisted by an end-on template. *Nature* **2012,** *486* (7404), 518-22.

127. Schwarzer, D. D.; Gritsch, P. J.; Gaich, T., Mimicking dimethylallyltryptophan synthase: experimental evidence for a biosynthetic cope rearrangement process. *Angew Chem Int Ed Engl* **2012,** *51* (46), 11514-6.

128. Muller, J. M.; Stark, C. B., Diastereodivergent Reverse Prenylation of Indole and Tryptophan Derivatives: Total Synthesis of Amauromine, Novoamauromine, and epi-Amauromine. *Angew Chem Int Ed Engl* **2016,** *55* (15), 4798-802.

129. Struble, M. D.; Scerba, M. T.; Siegler, M.; Lectka, T., Evidence for a symmetrical fluoronium ion in solution. *Science* **2013,** *340* (6128), 57-60.

130. Struble, M. D.; Holl, M. G.; Scerba, M. T.; Siegler, M. A.; Lectka, T., Search for a Symmetrical C-F-C Fluoronium Ion in Solution: Kinetic Isotope Effects, Synthetic Labeling, and Computational, Solvent, and Rate Studies. *J Am Chem Soc* **2015,** *137* (35), 11476-90.

131. Struble, M. D.; Guan, L.; Siegler, M. A.; Lectka, T., A C-F Bond Directed Diels-Alder Reaction. *J Org Chem* **2016,** *81* (17), 8087-90.

132. Hartmann, H.; Hady, A. F. A.; Sartor, K.; Weetman, J.; Helmchen, G., High Stereoselectivity in Lewis-Acid-Catalyzed and Uncatalyzed Diels–Alder Reactions of the

Fumarate of(S)-Ethyl Lactate. *Angewandte Chemie International Edition in English* **1987,** *26* (11), 1143-1145.

133. Boul, P. J.; Reutenauer, P.; Lehn, J. M., Reversible Diels-Alder reactions for the generation of dynamic combinatorial libraries. *Org Lett* **2005,** *7* (1), 15-8.

134. Widstrom, A. L.; Lear, B. J., Structural and solvent control over activation parameters for a pair of retro Diels-Alder reactions. *Scientific Reports* **2019,** *9* (1).

135. Halton, B.; Russell, S. G. G., .pi.-Selective dichlorocyclopropanation and epoxidation of 9-chloro-1,4,5,8-tetrahydro-4a,6a-methanonaphthalene. Controlled synthesis of the C-9 epimers of (1a.alpha.,2a.alpha.,6a.alpha.,7a.alpha.)-1,8,8-trichloro-1a,2,3,6,7,7a-hexahydro-2a,6a-methanocyclopropa[b]naphthalene. *The Journal of Organic Chemistry* **1991,** *56* (19), 5553-5556.

136. Campbell, J. P.; Rajappan, S. C.; Jaynes, T. J.; Sharafi, M.; Ma, Y. T.; Li, J.; Schneebeli, S. T., Enantioselective Electrophilic Aromatic Nitration: A Chiral Auxiliary Approach. *Angewandte Chemie* **2018,** *131* (4), 1047-1052.

137. Lee, C.; Yang, W.; Parr, R. G., Development of the Colle-Salvetti correlation-energy formula into a functional of the electron density. *Phys Rev B Condens Matter* **1988,** *37* (2), 785-789.

138. Stephens, P. J.; Devlin, F. J.; Chabalowski, C. F.; Frisch, M. J., Ab Initio Calculation of Vibrational Absorption and Circular Dichroism Spectra Using Density Functional Force Fields. *The Journal of Physical Chemistry* **1994,** *98* (45), 11623-11627.

139. Desiraju, G. R., The C-h...o hydrogen bond: structural implications and supramolecular design. *Acc Chem Res* **1996,** *29* (9), 441-9.

140. Johnson, E. R.; Keinan, S.; Mori-Sanchez, P.; Contreras-Garcia, J.; Cohen, A. J.; Yang, W., Revealing noncovalent interactions. *J Am Chem Soc* **2010,** *132* (18), 6498-506.

141. Bochevarov, A. D.; Harder, E.; Hughes, T. F.; Greenwood, J. R.; Braden, D. A.; Philipp, D. M.; Rinaldo, D.; Halls, M. D.; Zhang, J.; Friesner, R. A., Jaguar: A high-performance quantum chemistry software program with strengths in life and materials sciences. *International Journal of Quantum Chemistry* **2013,** *113* (18), 2110-2142.

142. Plata, R. E.; Singleton, D. A., A case study of the mechanism of alcohol-mediated Morita Baylis-Hillman reactions. The importance of experimental observations. *J Am Chem Soc* **2015,** *137* (11), 3811-26.

143. Zacconi, F. C.; Koll, L. C.; Podestá, J. C., Synthesis of optically active derivatives of bicyclic chiral diols with C2 symmetry. *Tetrahedron: Asymmetry* **2011,** *22* (1), 40-46.

144. Campbell, J. P.; Rajappan, S. C.; Jaynes, T. J.; Sharafi, M.; Ma, Y. T.; Li, J.; Schneebeli, S. T., Enantioselective Electrophilic Aromatic Nitration: A Chiral Auxiliary Approach. *Angew Chem Int Ed Engl* **2019,** *58* (4), 1035-1040.

145. Beaudoin, D.; Rominger, F.; Mastalerz, M., Chirality-Assisted Synthesis of a Very Large Octameric Hydrogen-Bonded Capsule. *Angew Chem Int Ed Engl* **2016,** *55* (50), 15599-15603.

146. Murphy, K. E.; Bocanegra, J. L.; Liu, X.; Chau, H. Y. K.; Lee, P. C.; Li, J.; Schneebeli, S. T., Precise through-space control of an abiotic electrophilic aromatic substitution reaction. *Nature Communications* **2017,** *8* (1).

147. Guram, A. S.; Rennels, R. A.; Buchwald, S. L., A Simple Catalytic Method for the Conversion of Aryl Bromides to Arylamines. *Angewandte Chemie International Edition in English* **1995,** *34* (12), 1348-1350.

148. Louie, J.; Hartwig, J. F., Palladium-catalyzed synthesis of arylamines from aryl halides. Mechanistic studies lead to coupling in the absence of tin reagents. *Tetrahedron Letters* **1995,** *36* (21), 3609-3612.

149. Hamann, B. C.; Hartwig, J. F., Sterically Hindered Chelating Alkyl Phosphines Provide Large Rate Accelerations in Palladium-Catalyzed Amination of Aryl Iodides, Bromides, and Chlorides, and the First Amination of Aryl Tosylates. *Journal of the American Chemical Society* **1998,** *120* (29), 7369-7370.

150. Forero-Cortés, P. A.; Haydl, A. M., The 25th Anniversary of the Buchwald–Hartwig Amination: Development, Applications, and Outlook. *Organic Process Research & Development* **2019,** *23* (8), 1478-1483.

151. Takise, R.; Muto, K.; Yamaguchi, J., Cross-coupling of aromatic esters and amides. *Chem Soc Rev* **2017,** *46* (19), 5864-5888.

152. Liegault, B.; Lee, D.; Huestis, M. P.; Stuart, D. R.; Fagnou, K., Intramolecular Pd(II)-catalyzed oxidative biaryl synthesis under air: reaction development and scope. *J Org Chem* **2008,** *73* (13), 5022-8.

153. Sonogashira, K.; Tohda, Y.; Hagihara, N., A convenient synthesis of acetylenes: catalytic substitutions of acetylenic hydrogen with bromoalkenes, iodoarenes and bromopyridines. *Tetrahedron Letters* **1975,** *16* (50), 4467-4470.

154. Sonogashira, K., Development of Pd–Cu catalyzed cross-coupling of terminal acetylenes with sp2-carbon halides. *Journal of Organometallic Chemistry* **2002,** *653* (1-2), 46-49.

155. Hu, W.; Zhu, N.; Tang, W.; Zhao, D., Oligo(p-phenyleneethynylene)s with hydrogen-bonded coplanar conformation. *Org Lett* **2008,** *10* (13), 2669-72.

156. Dolain, C.; Grelard, A.; Laguerre, M.; Jiang, H.; Maurizot, V.; Huc, I., Solution structure of quinoline- and pyridine-derived oligoamide foldamers. *Chemistry* **2005,** *11* (21), 6135-44.

157. Zhang, D. W.; Zhao, X.; Hou, J. L.; Li, Z. T., Aromatic amide foldamers: structures, properties, and functions. *Chem Rev* **2012,** *112* (10), 5271-316.

158. Stone, M. T.; Heemstra, J. M.; Moore, J. S., The chain-length dependence test. *Acc Chem Res* **2006,** *39* (1), 11-20.

159. Nair, R. V.; Kotmale, A. S.; Dhokale, S. A.; Gawade, R. L.; Puranik, V. G.; Rajamohanan, P. R.; Sanjayan, G. J., Formation of a pseudo-beta-hairpin motif utilizing the Ant-Pro reverse turn: consequences of stereochemical reordering. *Org Biomol Chem* **2014,** *12* (5), 774-82.

160. Barboiu, M.; Stadler, A. M.; Lehn, J. M., Controlled Folding, Motional, and Constitutional Dynamic Processes of Polyheterocyclic Molecular Strands. *Angew Chem Int Ed Engl* **2016,** *55* (13), 4130-54.

161. Jiang, Y.; Fang, M.; Chang, S. J.; Huang, J. J.; Chu, S. Q.; Hu, S. M.; Liu, C. F.; Lai, W. Y.; Huang, W., Towards Monodisperse Star-Shaped Ladder-Type Conjugated Systems: Design, Synthesis, Stabilized Blue Electroluminescence, and Amplified Spontaneous Emission. *Chemistry* **2017,** *23* (23), 5448-5458.

162. Arias, S.; Freire, F.; Quiñoá, E.; Riguera, R., The leading role of cation–π interactions in polymer chemistry: the control of the helical sense in solution. *Polymer Chemistry* **2015,** *6* (26), 4725-4733.

163. Zhong, Y.; Yang, Y.; Shen, Y.; Xu, W.; Wang, Q.; Connor, A. L.; Zhou, X.; He, L.; Zeng, X. C.; Shao, Z.; Lu, Z. L.; Gong, B., Enforced Tubular Assembly of Electronically Different Hexakis(m-Phenylene Ethynylene) Macrocycles: Persistent Columnar Stacking Driven by Multiple Hydrogen-Bonding Interactions. *J Am Chem Soc* **2017,** *139* (44), 15950-15957.

164. Ishiyama, T.; Murata, M.; Miyaura, N., Palladium(0)-Catalyzed Cross-Coupling Reaction of Alkoxydiboron with Haloarenes: A Direct Procedure for Arylboronic Esters. *The Journal of Organic Chemistry* **1995,** *60* (23), 7508-7510.

165. Leone, A. K.; Goldberg, P. K.; McNeil, A. J., Ring-Walking in Catalyst-Transfer Polymerization. *J Am Chem Soc* **2018,** *140* (25), 7846-7850.

166. Nojima, M.; Kosaka, K.; Kato, M.; Ohta, Y.; Yokozawa, T., Alternating Intramolecular and Intermolecular Catalyst-Transfer Suzuki-Miyaura Condensation Polymerization: Synthesis of Boronate-Terminated pi-Conjugated Polymers Using Excess Dibromo Monomers. *Macromol Rapid Commun* **2016,** *37* (1), 79-85.

167. Torda, A. E.; Norton, R. S., Proton nmr relaxation study of the dynamics of anthopleurin-A in solution. *Biopolymers* **1989,** *28* (3), 703-16.

168. Watanabe, K.; Akagi, K., Helically assembled pi-conjugated polymers with circularly polarized luminescence. *Sci Technol Adv Mater* **2014,** *15* (4), 044203.

169. Groves, P., Diffusion ordered spectroscopy (DOSY) as applied to polymers. *Polymer Chemistry* **2017,** *8* (44), 6700-6708.

170. Li, W.; Chung, H.; Daeffler, C.; Johnson, J. A.; Grubbs, R. H., Application of (1)H DOSY for Facile Measurement of Polymer Molecular Weights. *Macromolecules* **2012,** *45* (24), 9595-9603.

171. Cohen, Y.; Avram, L.; Frish, L., Diffusion NMR spectroscopy in supramolecular and combinatorial chemistry: an old parameter--new insights. *Angew Chem Int Ed Engl* **2005,** *44* (4), 520-54.

172. Ortega, A.; García de la Torre, J., Hydrodynamic properties of rodlike and disklike particles in dilute solution. *The Journal of Chemical Physics* **2003,** *119* (18), 9914-9919.

173. Gilbert, M., States of Aggregation in Polymers. **2017**, 39-57.

174. Kong, S. M.; Liu, H.; Xue, Y. H.; Liu, X. L.; Jia, X. X.; Cui, F. C., Polymerization-induced polymer aggregation or polymer aggregation-enhanced polymerization? A computer simulation study. *Phys Chem Chem Phys* **2018,** *20* (37), 24379-24388.

175. Farrance, O. E.; Paci, E.; Radford, S. E.; Brockwell, D. J., Extraction of accurate biomolecular parameters from single-molecule force spectroscopy experiments. *ACS Nano* **2015,** *9* (2), 1315-24.

176. Colizzi, F.; Perozzo, R.; Scapozza, L.; Recanatini, M.; Cavalli, A., Single-molecule pulling simulations can discern active from inactive enzyme inhibitors. *J Am Chem Soc* **2010,** *132* (21), 7361-71.

177. Linke, W. A.; Grutzner, A., Pulling single molecules of titin by AFM--recent advances and physiological implications. *Pflugers Arch* **2008,** *456* (1), 101-15.

178. Zayed, J. M.; Biedermann, F.; Rauwald, U.; Scherman, O. A., Probing cucurbit[8]uril-mediated supramolecular block copolymer assembly in water using diffusion NMR. *Polymer Chemistry* **2010,** *1* (9), 1434.

179. Stirnemann, G.; Giganti, D.; Fernandez, J. M.; Berne, B. J., Elasticity, structure, and relaxation of extended proteins under force. *Proc Natl Acad Sci U S A* **2013,** *110* (10), 3847-52.

180. Zhang, J. Z.; Peng, X. Y.; Liu, S.; Jiang, B. P.; Ji, S. C.; Shen, X. C., The Persistence Length of Semiflexible Polymers in Lattice Monte Carlo Simulations. *Polymers (Basel)* **2019,** *11* (2).

181. Kroon-Batenburg, L. M. J.; Kruiskamp, P. H.; Vliegenthart, J. F. G.; Kroon, J., Estimation of the Persistence Length of Polymers by MD Simulations on Small Fragments in Solution. Application to Cellulose. *The Journal of Physical Chemistry B* **1997,** *101* (42), 8454-8459.

182. Gross, P.; Laurens, N.; Oddershede, L. B.; Bockelmann, U.; Peterman, E. J. G.; Wuite, G. J. L., Quantifying how DNA stretches, melts and changes twist under tension. *Nature Physics* **2011,** *7* (9), 731-736.

183. Lakowicz, J. R., **2006**.

184. Thomas, S. W., 3rd; Joly, G. D.; Swager, T. M., Chemical sensors based on amplifying fluorescent conjugated polymers. *Chem Rev* **2007,** *107* (4), 1339-86.

185. Zhang, X., Instrumentation in Diffuse Optical Imaging. *Photonics* **2014,** *1* (1), 9-32.

186. Berezin, M. Y.; Achilefu, S., Fluorescence lifetime measurements and biological imaging. *Chem Rev* **2010,** *110* (5), 2641-84.

187. Kong, L.; Huang, Z.; Chen, P.; Wang, H.; Zhu, S.; Yang, J., Enhanced intersystem crossing to achieve long-lived excitons based on inhibited molecular motion and rigid structure. *Dyes and Pigments* **2020,** *173*, 107886.

188. Cordina, N. M.; Sayyadi, N.; Parker, L. M.; Everest-Dass, A.; Brown, L. J.; Packer, N. H., Reduced background autofluorescence for cell imaging using nanodiamonds and lanthanide chelates. *Sci Rep* **2018,** *8* (1), 4521.

189. Allerhand, A.; Doddrell, D.; Komoroski, R., Natural Abundance Carbon-13 Partially Relaxed Fourier Transform Nuclear Magnetic Resonance Spectra of Complex Molecules. *The Journal of Chemical Physics* **1971,** *55* (1), 189-198.

190. Lipari, G.; Szabo, A., Model-free approach to the interpretation of nuclear magnetic resonance relaxation in macromolecules. 2. Analysis of experimental results. *Journal of the American Chemical Society* **1982,** *104* (17), 4559-4570.

191. Wilbur, D. J.; Norton, R. S.; Clouse, A. O.; Addleman, R.; Allerhand, A., Determination of rotational correlation times of proteins in solution from carbon-13 spin-lattice relaxation measurements. Effect of magnetic field strength and anisotropic rotation. *J Am Chem Soc* **1976,** *98* (25), 8250-4.

192. **2007**.

193. Koo, J. H.; Kim, D. C.; Shim, H. J.; Kim, T.-H.; Kim, D.-H., Flexible and Stretchable Smart Display: Materials, Fabrication, Device Design, and System Integration. *Advanced Functional Materials* **2018,** *28* (35), 1801834.

194. Rong, Q.; Lei, W.; Liu, M., Conductive Hydrogels as Smart Materials for Flexible Electronic Devices. *Chemistry* **2018,** *24* (64), 16930-16943.

195. Yun, G.; Tang, S. Y.; Sun, S.; Yuan, D.; Zhao, Q.; Deng, L.; Yan, S.; Du, H.; Dickey, M. D.; Li, W., Liquid metal-filled magnetorheological elastomer with positive piezoconductivity. *Nat Commun* **2019,** *10* (1), 1300.

196. Liu, Z.; Liu, C.; Li, Q.; Chen, J.; Xing, X., Spring-like motion caused large anisotropic thermal expansion in nonporous M(eim)2 (M = Zn, Cd). *Phys Chem Chem Phys* **2017,** *19* (36), 24436-24439.

197. Kulkarni, A. D.; Truhlar, D. G.; Goverapet Srinivasan, S.; van Duin, A. C. T.; Norman, P.; Schwartzentruber, T. E., Oxygen Interactions with Silica Surfaces: Coupled

Cluster and Density Functional Investigation and the Development of a New ReaxFF Potential. *The Journal of Physical Chemistry C* **2012,** *117* (1), 258-269.

198. Ripoll, J.-L., *Bull. Soc. Chimique France* **1974,** *11*, 2567–2571.

199. Phutdhawong, W.; Eksinitkun, G.; Pyne, S. G.; Willis, A. C.; Phutdhawong, W. S., Stereoselective synthesis of α-methylenecyclopentenones via a Diels–Alder/retro-Diels–Alder protocol. *Tetrahedron* **2013,** *69* (44), 9270-9276.

200. McNamara, Y. M.; Bright, S. A.; Byrne, A. J.; Cloonan, S. M.; McCabe, T.; Williams, D. C.; Meegan, M. J., Synthesis and antiproliferative action of a novel series of maprotiline analogues. *Eur J Med Chem* **2014,** *71*, 333-53.

201. Cai, L.; Moehl, T.; Moon, S. J.; Decoppet, J. D.; Humphry-Baker, R.; Xue, Z.; Bin, L.; Zakeeruddin, S. M.; Gratzel, M., 4,9-Dihydro-4,4,9,9-tetrahexyl-s-indaceno[1,2-b:5,6-b']dithiophene as a pi-spacer of donor-pi-acceptor dye and its photovoltaic performance with liquid and solid-state dye-sensitized solar cells. *Org Lett* **2014,** *16* (1), 106-9.

202. Sorensen, J. K.; Vestergaard, M.; Kadziola, A.; Kilsa, K.; Nielsen, M. B., Synthesis of oligo(phenyleneethynylene)-tetrathiafulvalene cruciforms for molecular electronics. *Org Lett* **2006,** *8* (6), 1173-6.

203. Fang, M.; Huang, J.; Chang, S.-J.; Jiang, Y.; Lai, W.-Y.; Huang, W., Ladder-type oligo(p-phenylene)s with D–π–A architectures: design, synthesis, optical gain properties, and stabilized amplified spontaneous emission. *Journal of Materials Chemistry C* **2017,** *5* (23), 5797-5809.

204. Lee, S. Y.; Yasuda, T.; Park, I. S.; Adachi, C., X-shaped benzoylbenzophenone derivatives with crossed donors and acceptors for highly efficient thermally activated delayed fluorescence. *Dalton Trans* **2015,** *44* (18), 8356-9.

205. Malytskyi, V.; da Silva, V. D.; Siri, O.; Giorgi, M.; Raimundo, J.-M., Versatile synthesis of tunable N,S-bridged-[1.1.1.1]-cyclophanes promoted by ester functions. *Tetrahedron* **2016,** *72* (41), 6363-6367.

206. Wei, Y.; Zheng, X.; Lin, D.; Yuan, H.; Yin, Z.; Yang, L.; Yu, Y.; Wang, S.; Xie, L. H.; Huang, W., Superelectrophilic-Initiated C-H Functionalization at the beta-Position of Thiophenes: A One-Pot Synthesis of trans-Stereospecific Saddle-Shaped Cyclic Compounds. *J Org Chem* **2019,** *84* (17), 10701-10709.

207. Chardonneus, L. *Helvetica Chimica Acta* **1956,** *39* (7), 1981-1985.

208. Wilson, D.; Djukic, B.; Lemaire, M. T., Synthesis of bromine- or aryl-substituted ditopic Schiff base ligands and their bimetallic iron(II) complexes: electronic and magnetic properties. *Transition Metal Chemistry* **2013,** *39* (1), 17-24.

209. Kawabata, K.; Goto, H., Electrosynthesis of 2,7-linked polycarbazole derivatives to realize low-bandgap electroactive polymers. *Synthetic Metals* **2010,** *160* (21-22), 2290-2298.

210. Müllen, K.; Dierschke, F.; Grimsdale, A. C., Efficient Synthesis of 2,7-Dibromocarbazoles as Components for Electroactive Materials. *Synthesis* **2003,** (16), 2470-2472.

APPENDIX

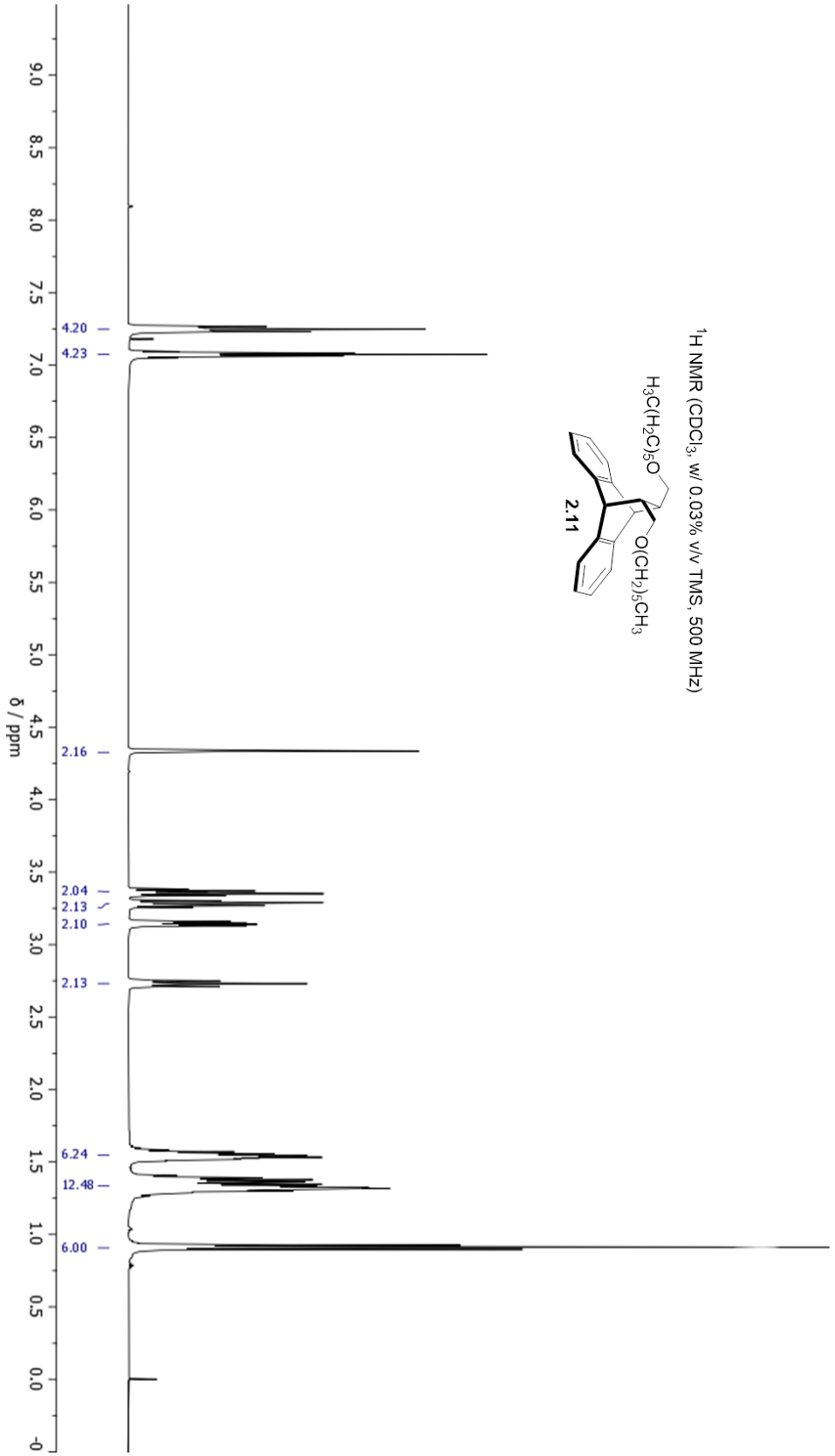
^{1}H NMR ($CDCl_3$, w/ 0.03% v/v TMS, 500 MHz)
$H_3C(H_2C)_5O$
$O(CH_2)_5CH_3$
2.11
δ / ppm
9.0
8.5
8.0
7.5
7.0
6.5
6.0
5.5
5.0
4.5
4.0
3.5
3.0
2.5
2.0
1.5
1.0
0.5
0.0
-0
4.20
4.23
2.16
2.04
2.13
2.10
2.13
6.24
12.48
6.00

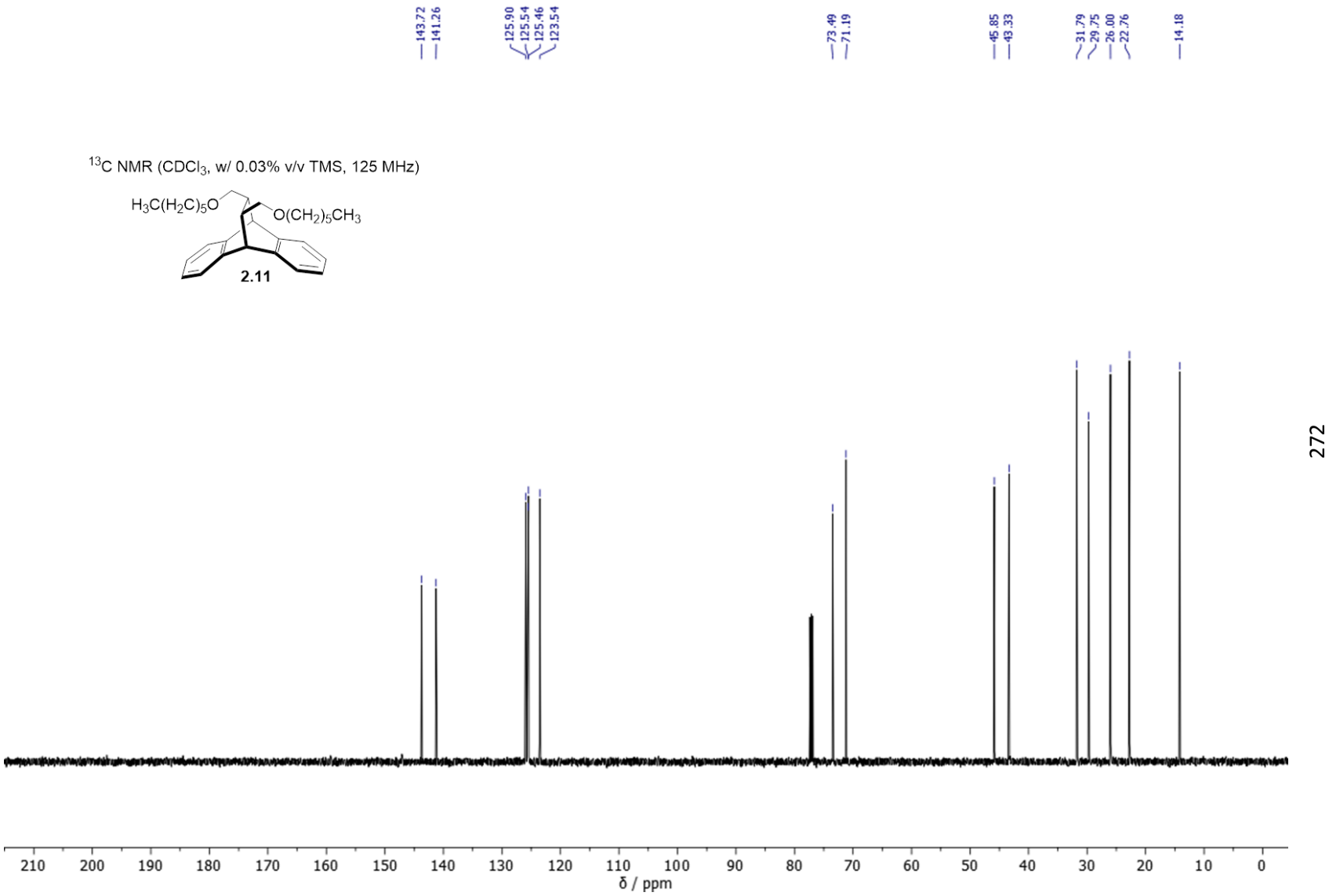
143.72
141.26
125.90
125.54
125.46
123.54
73.49
71.19
45.85
43.33
31.79
29.75
26.00
22.76
14.18
^{13}C NMR ($CDCl_3$, w/ 0.03% v/v TMS, 125 MHz)
$H_3C(H_2C)_5O$
$O(CH_2)_5CH_3$
2.11
272
210 200 190 180 170 160 150 140 130 120 110 100 90 80 70 60 50 40 30 20 10 0
δ / ppm

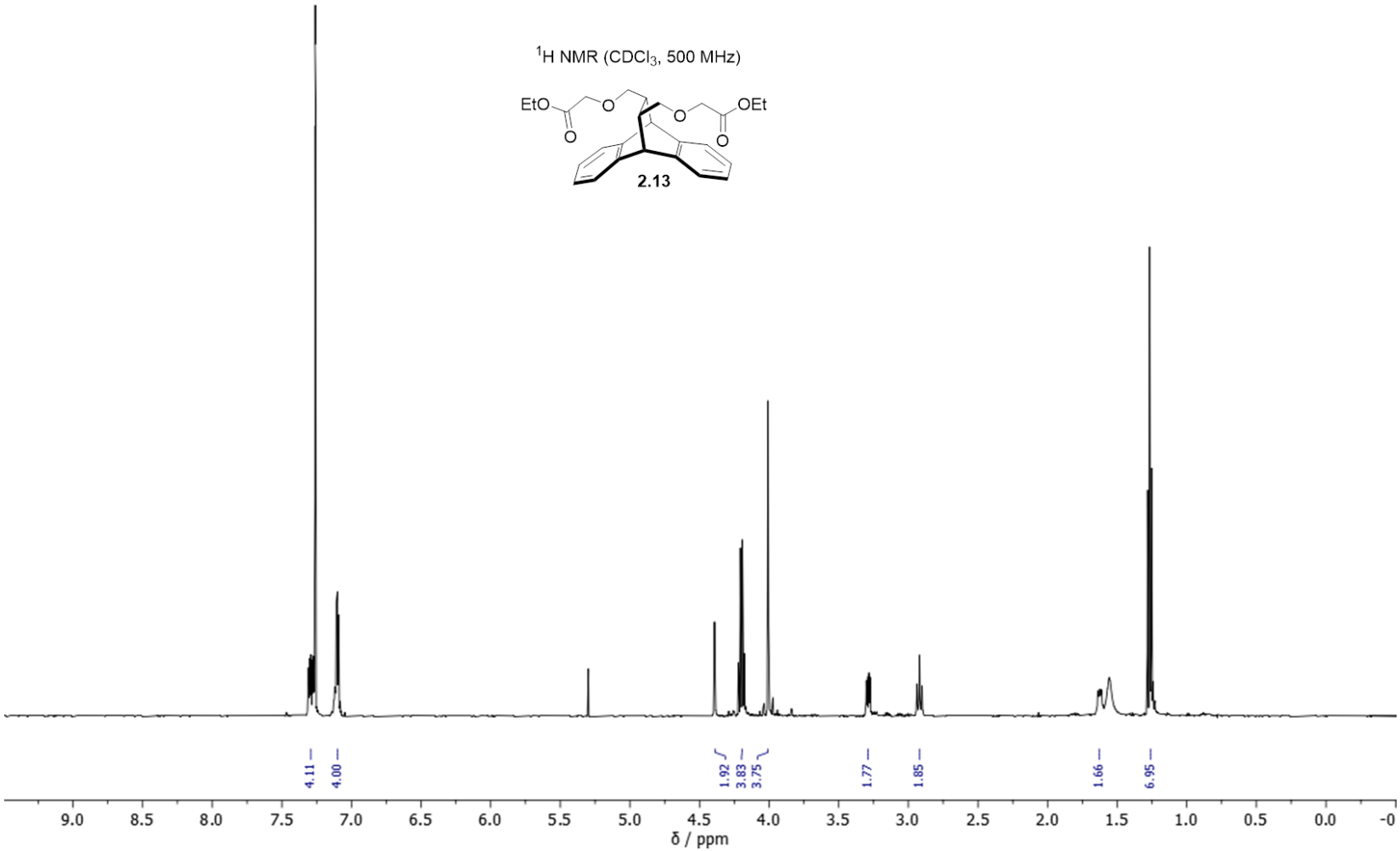
^{1}H NMR ($CDCl_3$, 500 MHz)
EtO
O
O
O
O
OEt
2.13
4.11
4.00
1.92
3.83
3.75
1.77
1.85
1.66
6.95
9.0
8.5
8.0
7.5
7.0
6.5
6.0
5.5
5.0
4.5
4.0
3.5
3.0
2.5
2.0
1.5
1.0
0.5
0.0
-0
δ / ppm

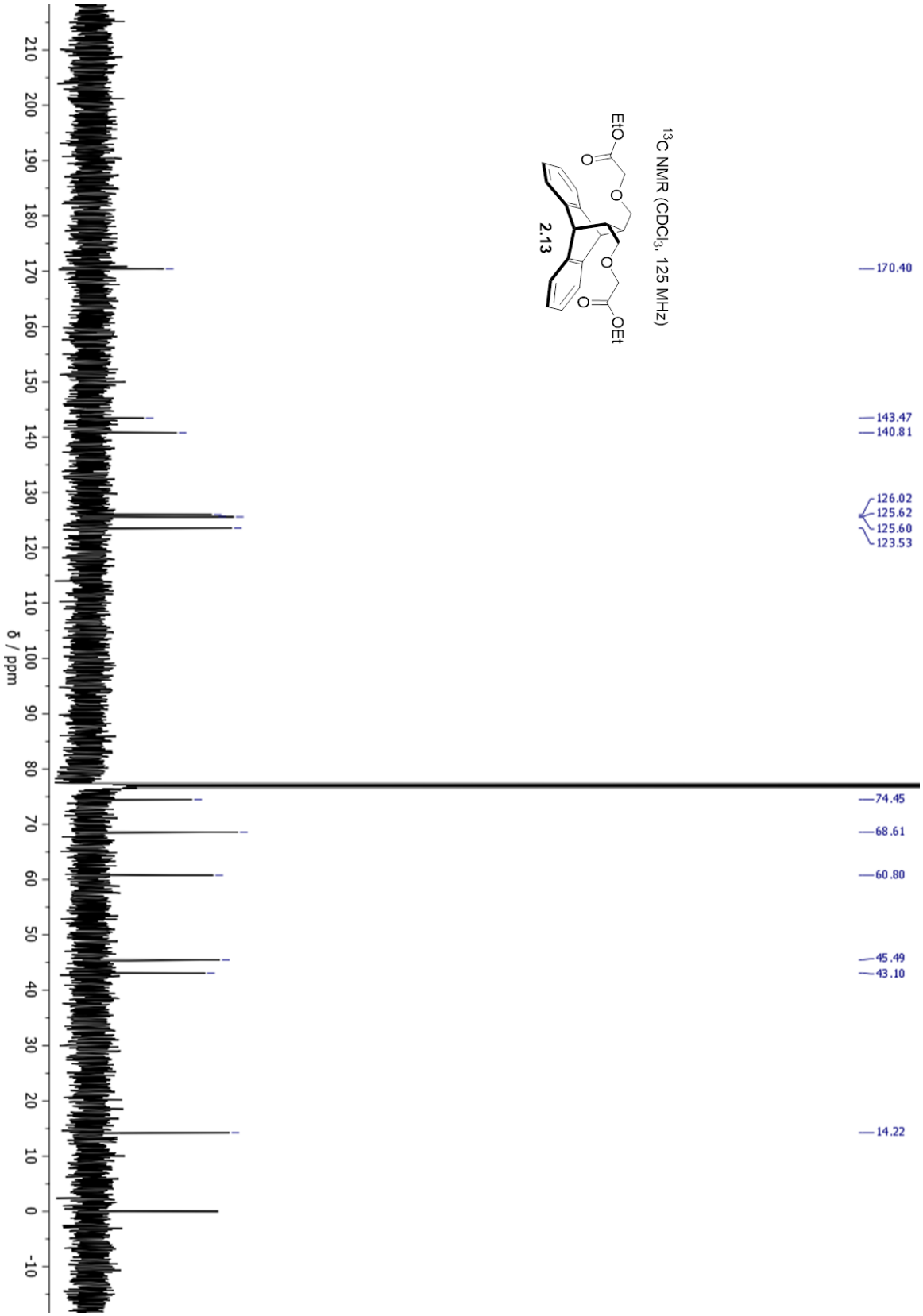
^{13}C NMR (CDCl$_3$, 125 MHz)
2.13
EtO
OEt
δ / ppm
170.40
143.47
140.81
126.02
125.62
125.60
123.53
74.45
68.61
60.80
45.49
43.10
14.22

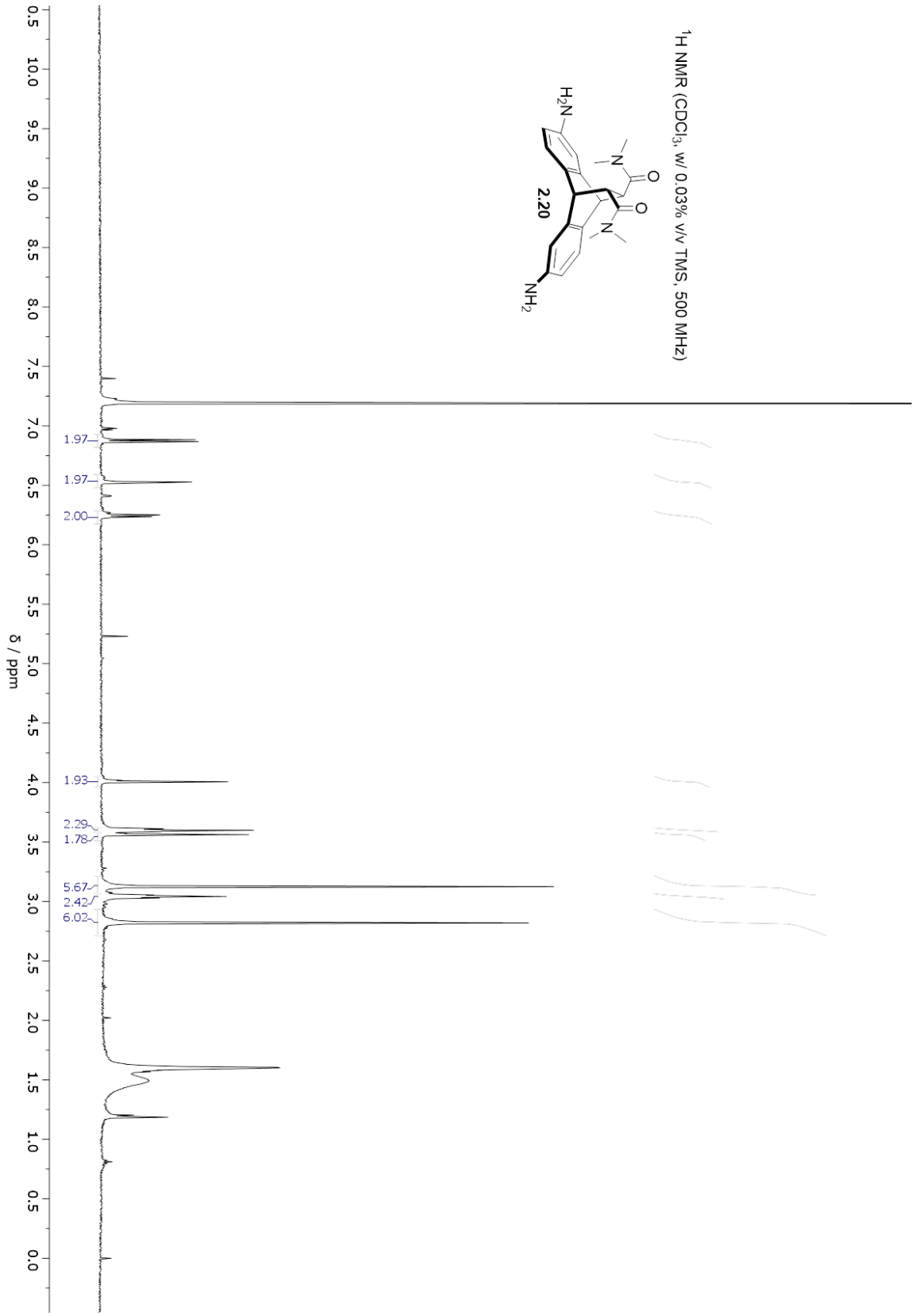
^{1}H NMR ($CDCl_3$, w/ 0.03% v/v TMS, 500 MHz)
H_2N
NH_2
2.20
δ / ppm
1.97
1.97
2.00
1.93
2.29
1.78
5.67
2.42
6.02

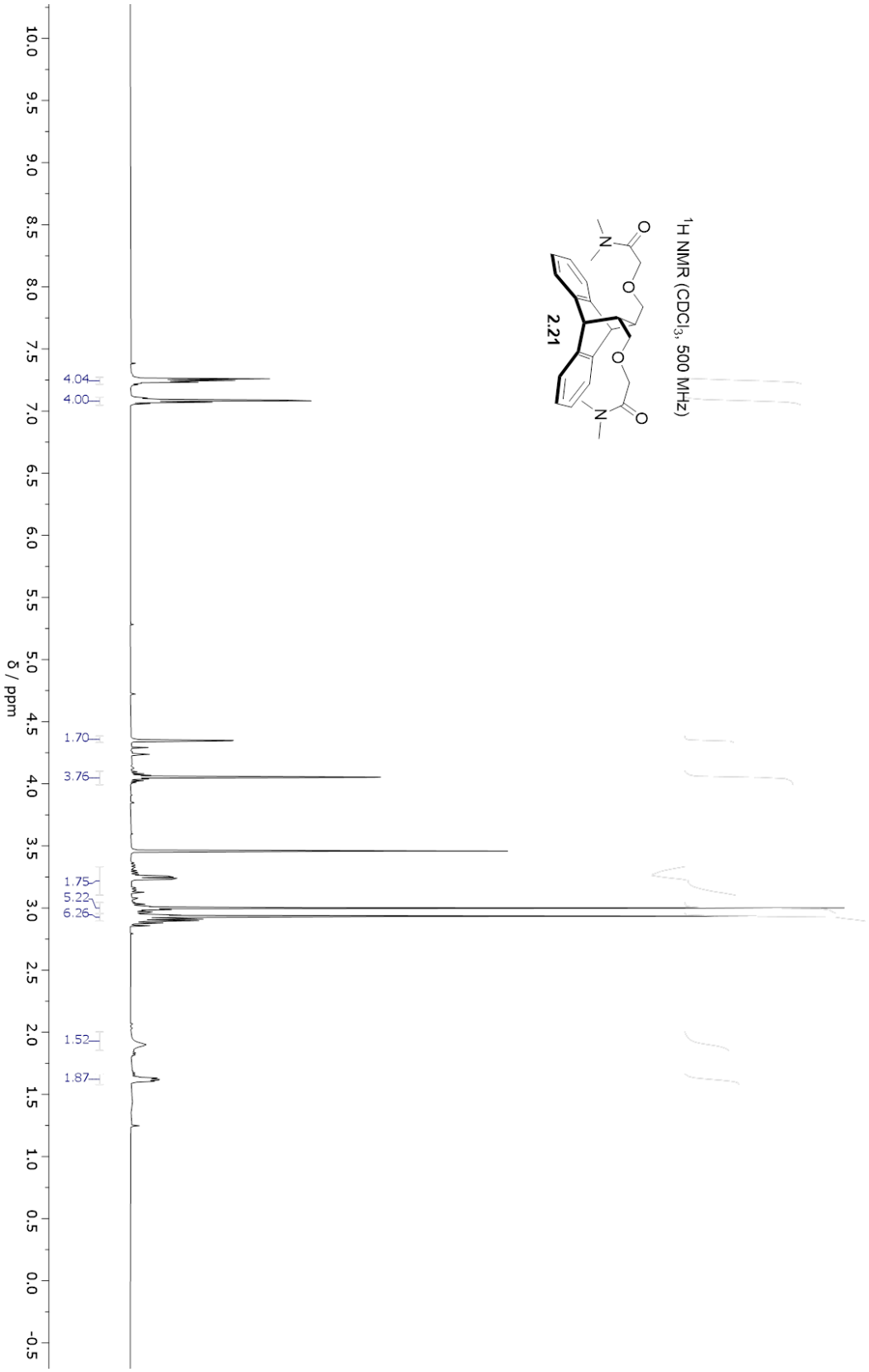
^{1}H NMR ($CDCl_3$, 500 MHz)
2.21
δ / ppm
10.0
9.5
9.0
8.5
8.0
7.5
7.0
6.5
6.0
5.5
5.0
4.5
4.0
3.5
3.0
2.5
2.0
1.5
1.0
0.5
0.0
-0.5
4.04
4.00
1.70
3.76
1.75
5.22
6.26
1.52
1.87

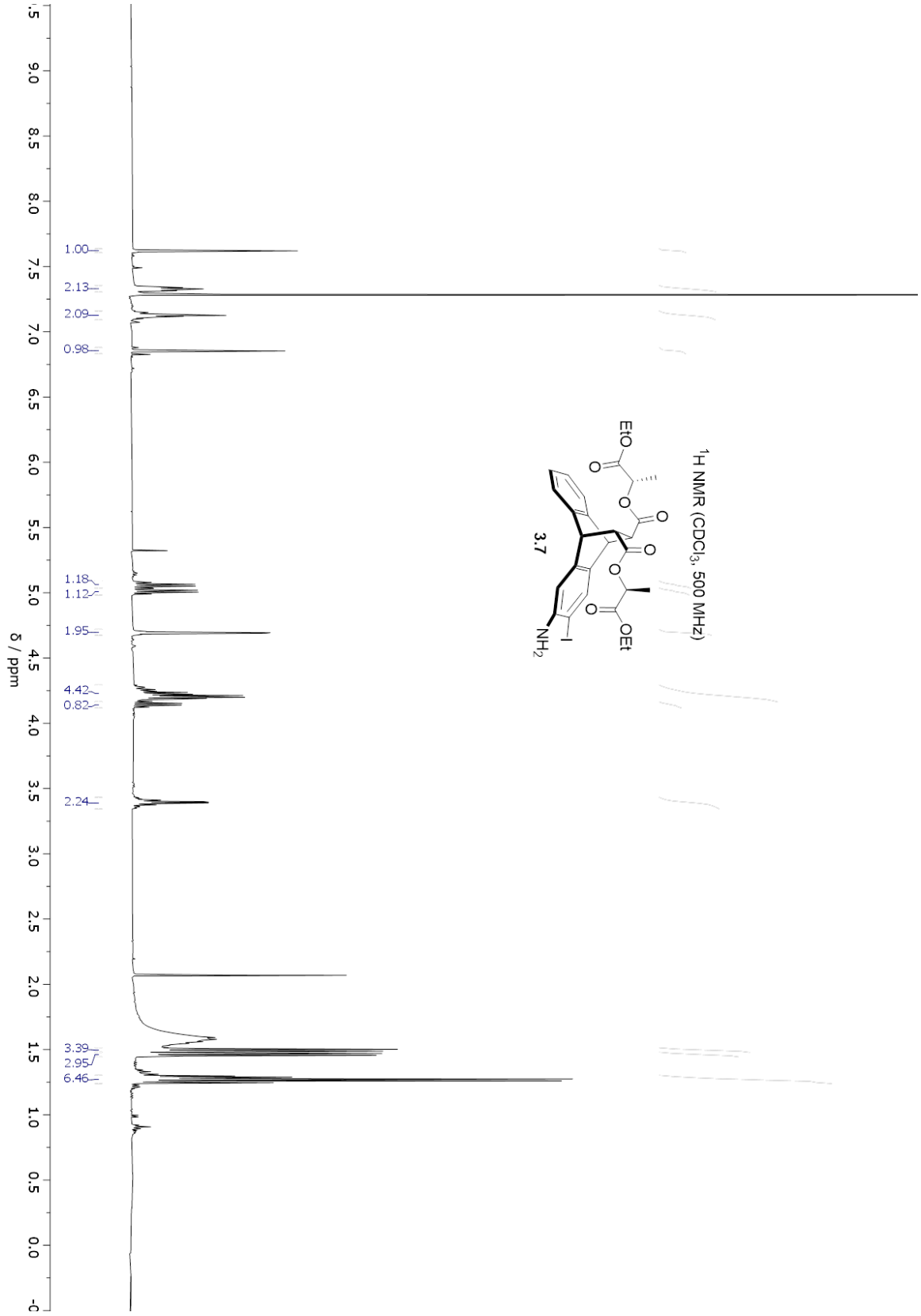
^{1}H NMR ($CDCl_3$, 500 MHz)
3.7
EtO
OEt
NH_2
I
δ / ppm
1.00
2.13
2.09
0.98
1.18
1.12
1.95
4.42
0.82
2.24
3.39
2.95
6.46

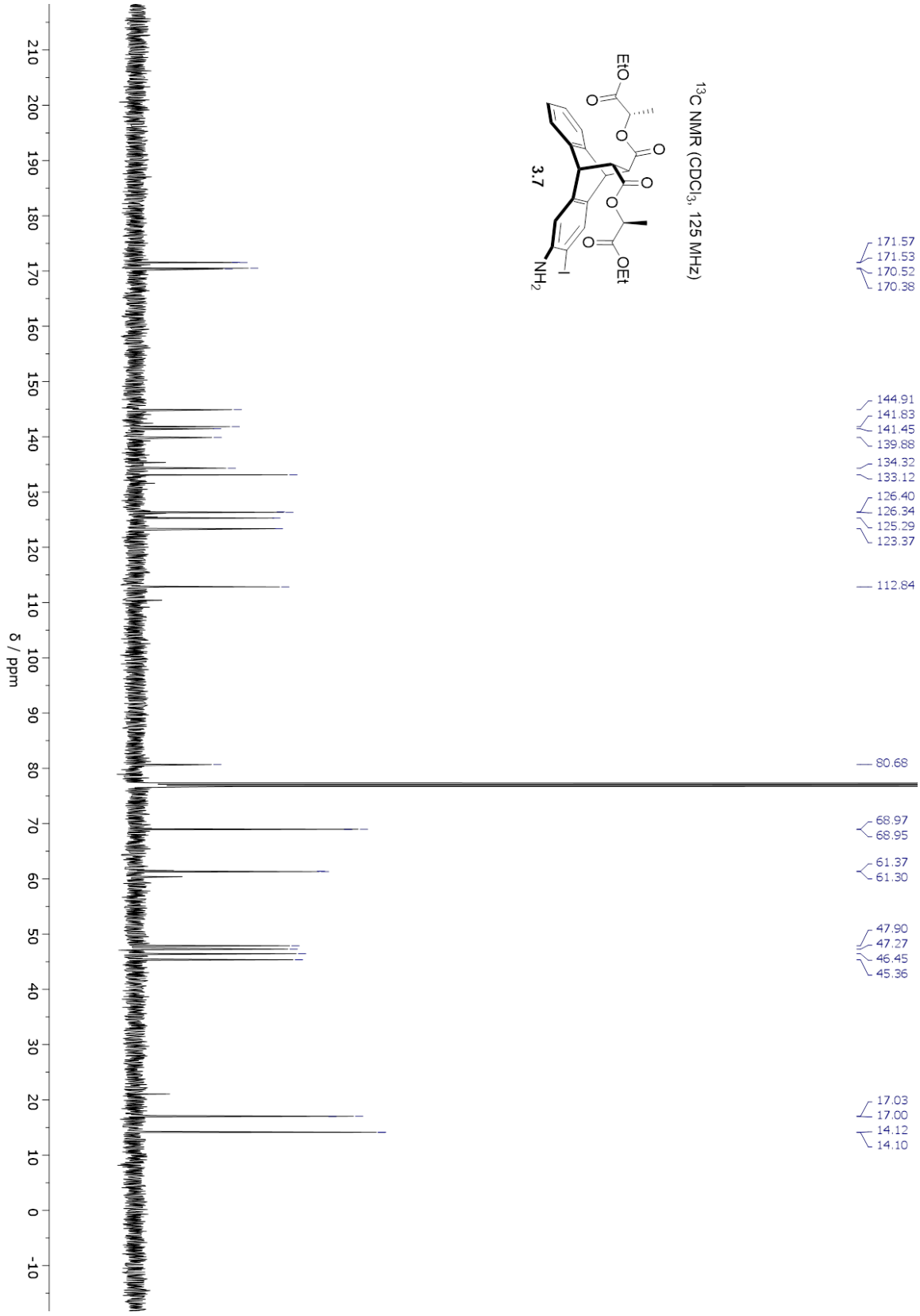
^{13}C NMR (CDCl$_3$, 125 MHz)
3.7
EtO
OEt
NH$_2$
I
171.57
171.53
170.52
170.38
144.91
141.83
141.45
139.88
134.32
133.12
126.40
126.34
125.29
123.37
112.84
80.68
68.97
68.95
61.37
61.30
47.90
47.27
46.45
45.36
17.03
17.00
14.12
14.10
δ / ppm

^{1}H NMR (CDCl$_3$, 500 MHz)
3.8
R =
OEt
RO
OR
δ / ppm
4.01
4.34
4.05
8.49
8.06
2.01
1.89
12.76
12.34

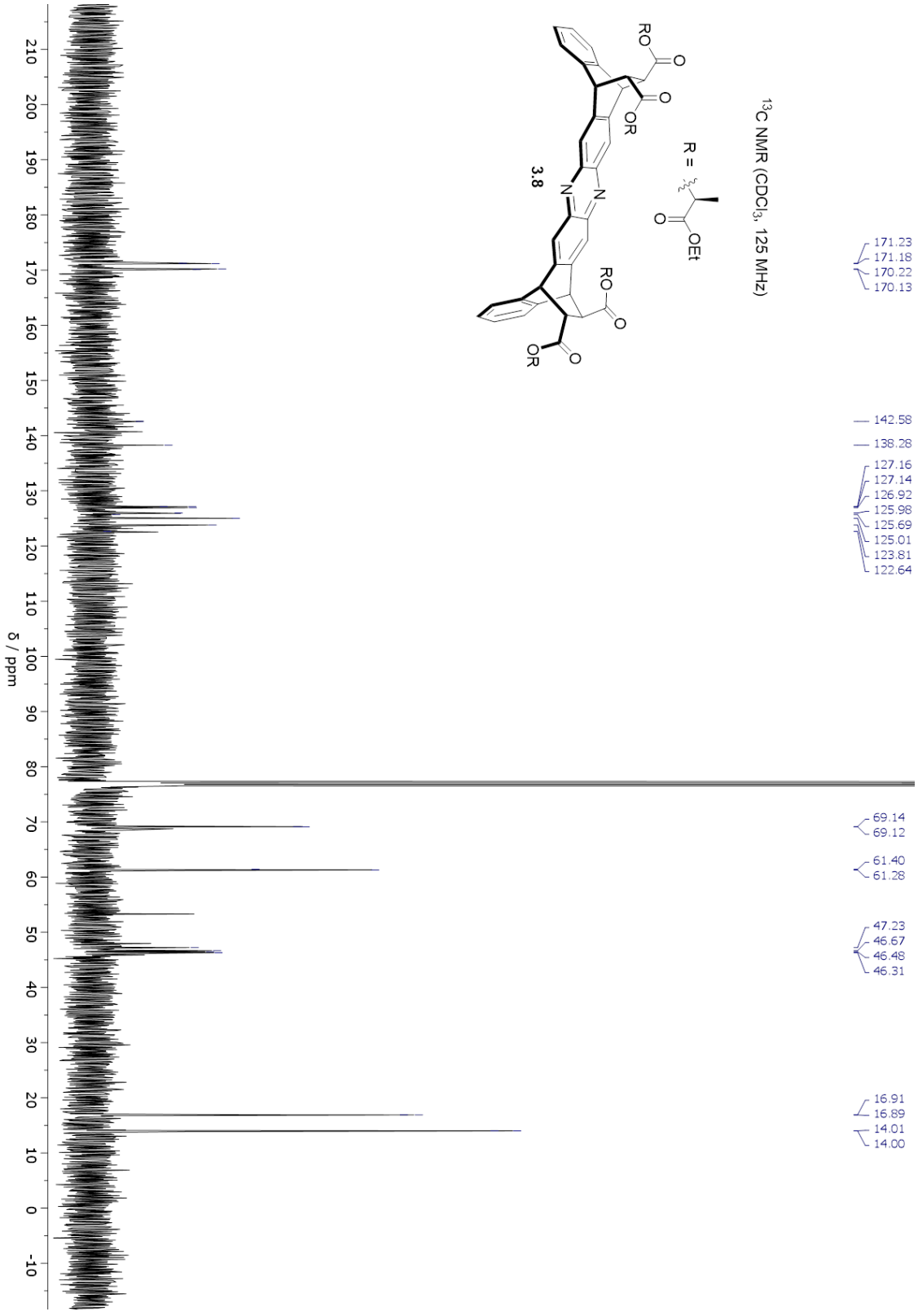
^{13}C NMR (CDCl$_3$, 125 MHz)
3.8
R =
OEt
171.23
171.18
170.22
170.13
142.58
138.28
127.16
127.14
126.92
125.98
125.69
125.01
123.81
122.64
69.14
69.12
61.40
61.28
47.23
46.67
46.48
46.31
16.91
16.89
14.01
14.00
δ / ppm

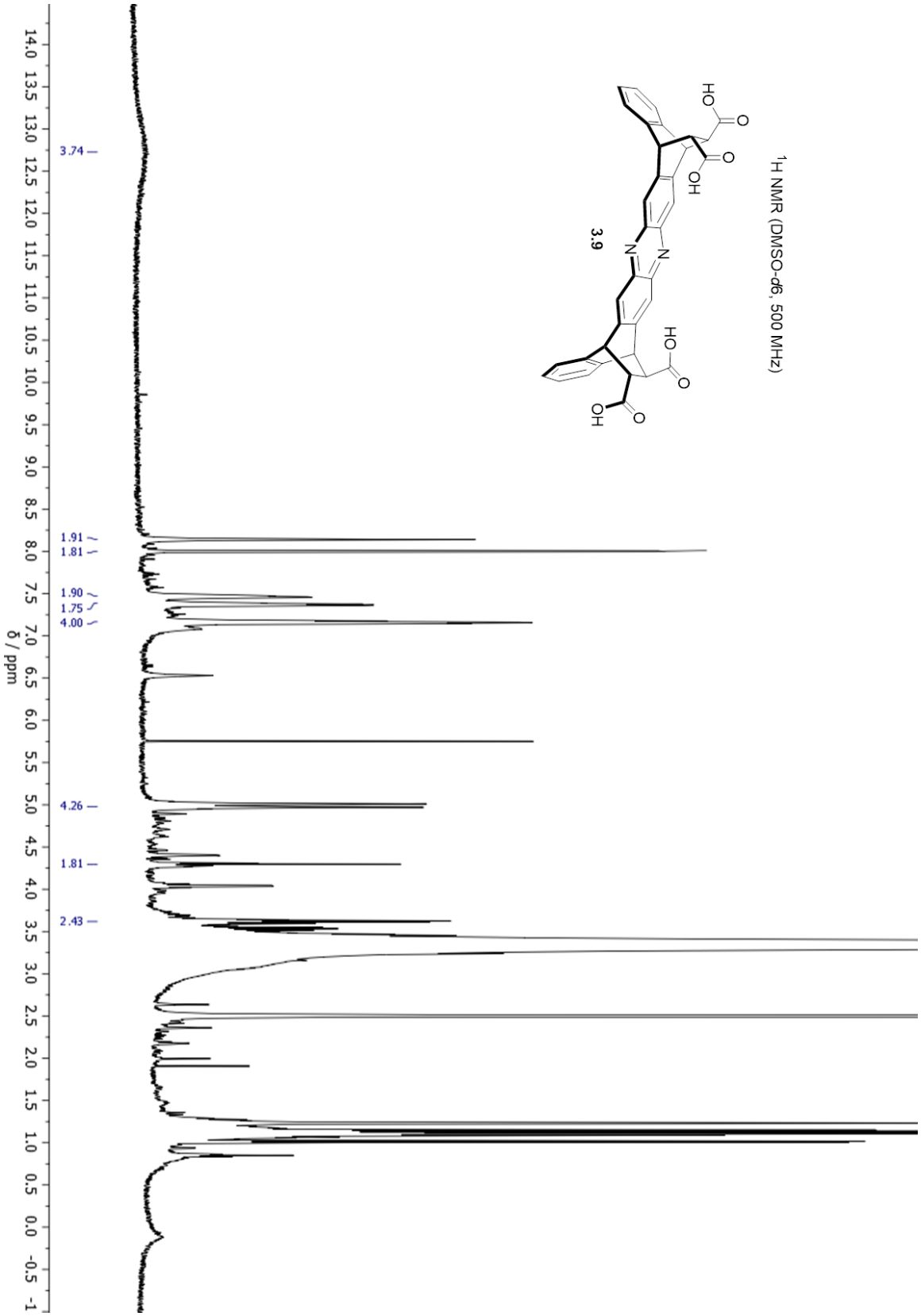
3.74
1.91
1.81
1.90
1.75
4.00
4.26
1.81
2.43
δ / ppm
14.0 13.5 13.0 12.5 12.0 11.5 11.0 10.5 10.0 9.5 9.0 8.5 8.0 7.5 7.0 6.5 6.0 5.5 5.0 4.5 4.0 3.5 3.0 2.5 2.0 1.5 1.0 0.5 0.0 -0.5 -1
HO
O
OH
O
N
N
HO
O
OH
O
3.9
^{1}H NMR (DMSO-d6, 500 MHz)

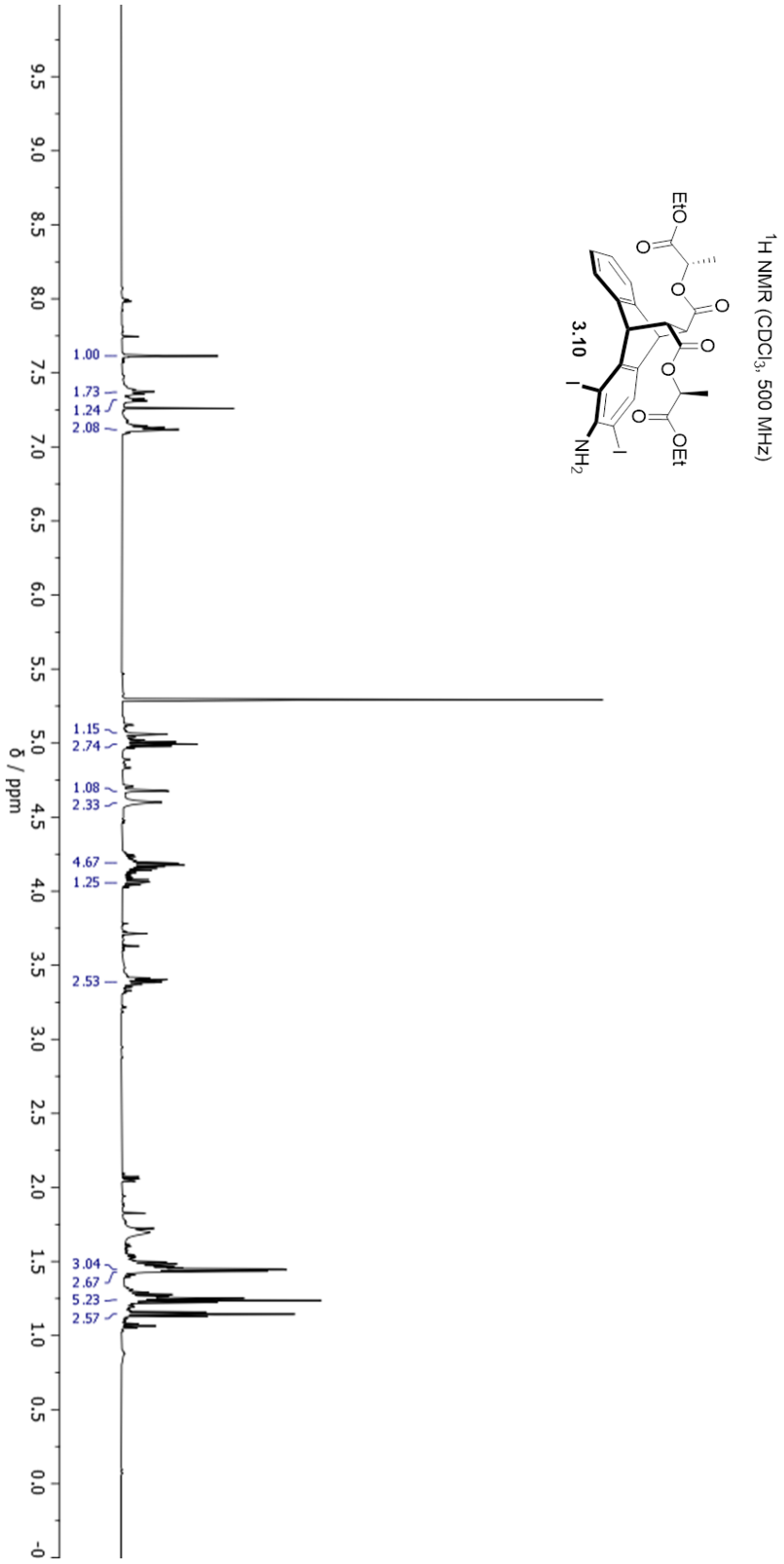
^{1}H NMR (CDCl$_3$, 500 MHz)
3.10
EtO
OEt
NH$_2$
I
I
δ / ppm
1.00
1.73
1.24
2.08
1.15
2.74
1.08
2.33
4.67
1.25
2.53
3.04
2.67
5.23
2.57

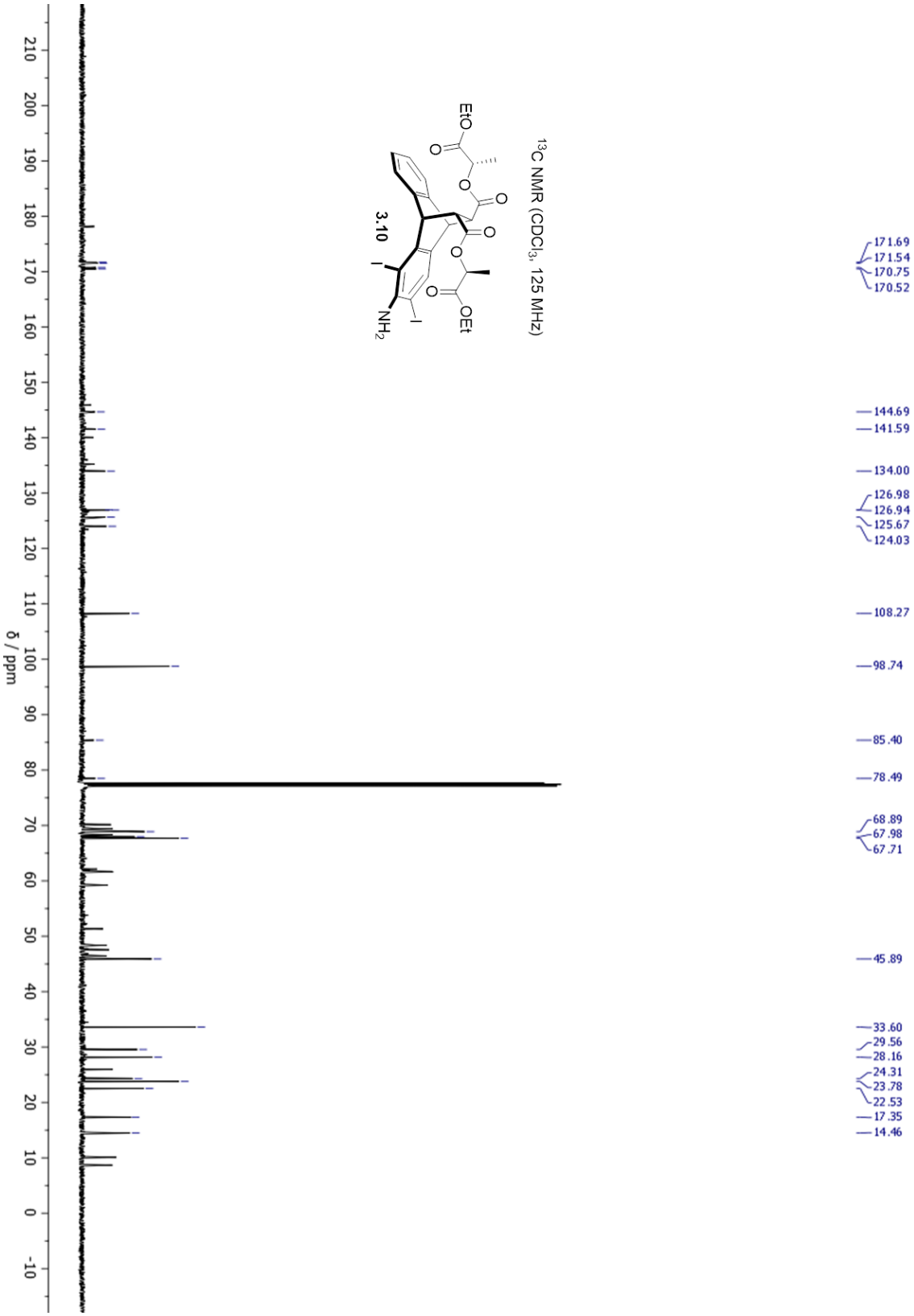
^{13}C NMR ($CDCl_3$, 125 MHz)
3.10
EtO
OEt
NH_2
I
I
δ / ppm
171.69
171.54
170.75
170.52
144.69
141.59
134.00
126.98
126.94
125.67
124.03
108.27
98.74
85.40
78.49
68.89
67.98
67.71
45.89
33.60
29.56
28.16
24.31
23.78
22.53
17.35
14.46

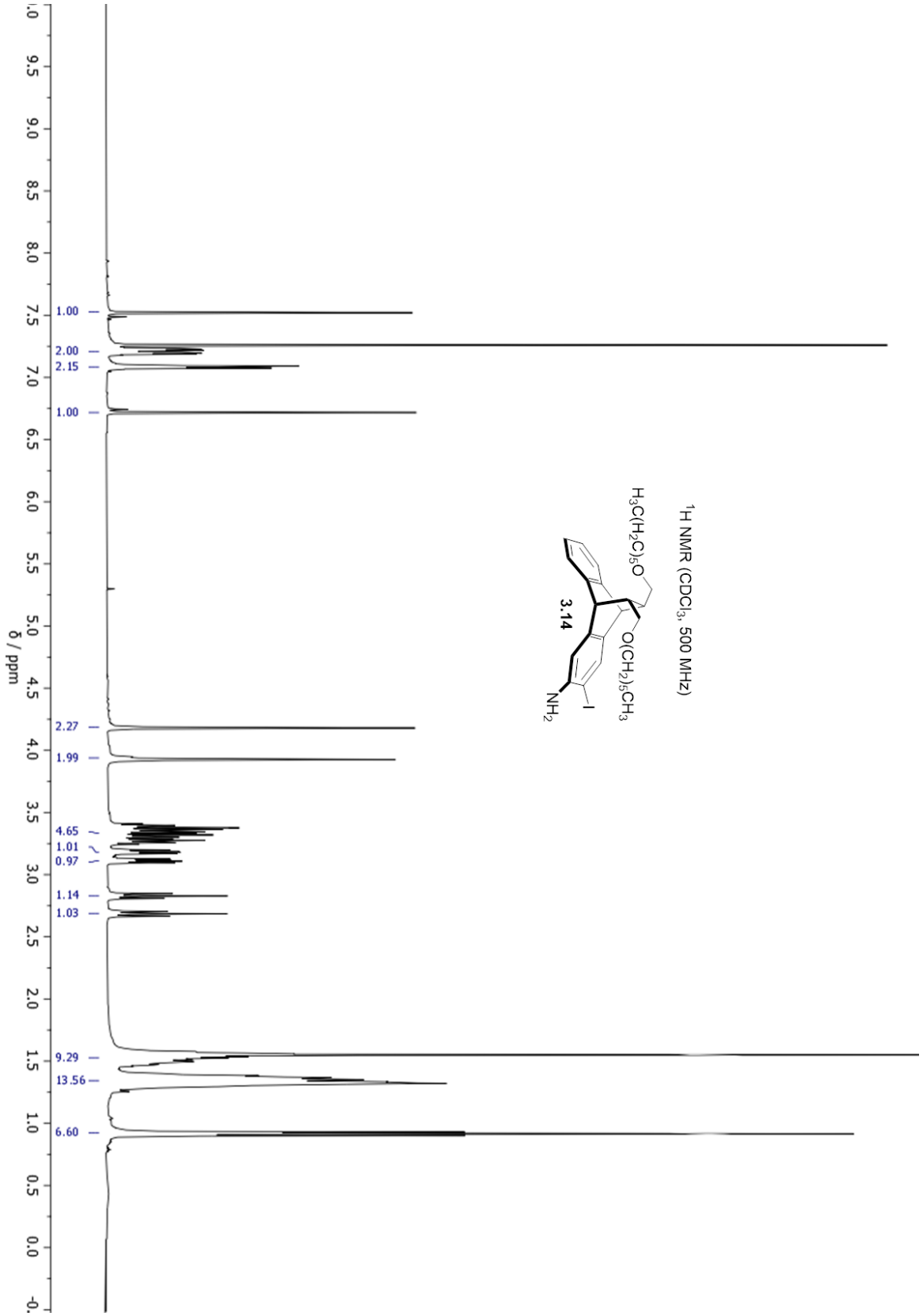
^{1}H NMR ($CDCl_3$, 500 MHz)
$H_3C(H_2C)_5O$
$O(CH_2)_5CH_3$
3.14
I
NH_2
δ / ppm
1.00
2.00
2.15
1.00
2.27
1.99
4.65
1.01
0.97
1.14
1.03
9.29
13.56
6.60

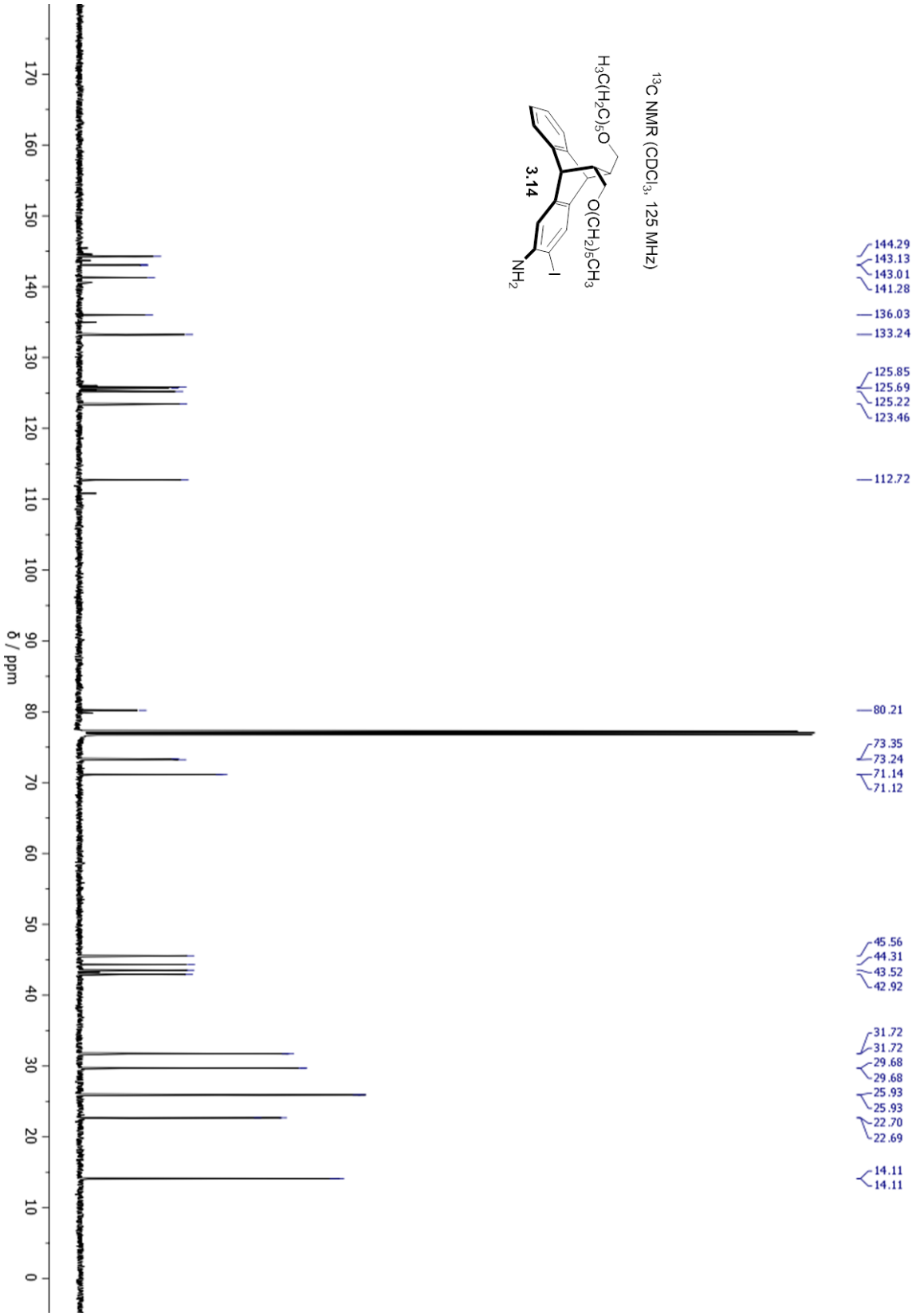
^{13}C NMR ($CDCl_3$, 125 MHz)
$H_3C(H_2C)_5O$
$O(CH_2)_5CH_3$
3.14
NH_2
I
144.29
143.13
143.01
141.28
136.03
133.24
125.85
125.69
125.22
123.46
112.72
80.21
73.35
73.24
71.14
71.12
45.56
44.31
43.52
42.92
31.72
31.72
29.68
29.68
25.93
25.93
22.70
22.69
14.11
14.11
δ / ppm

^{1}H NMR ($CDCl_3$, 500 MHz)

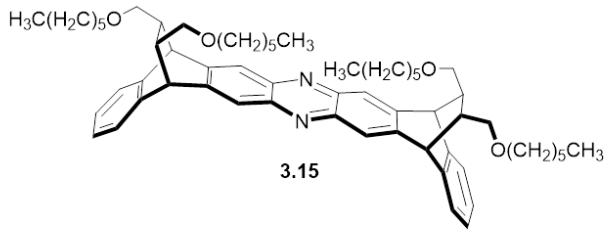

3.15

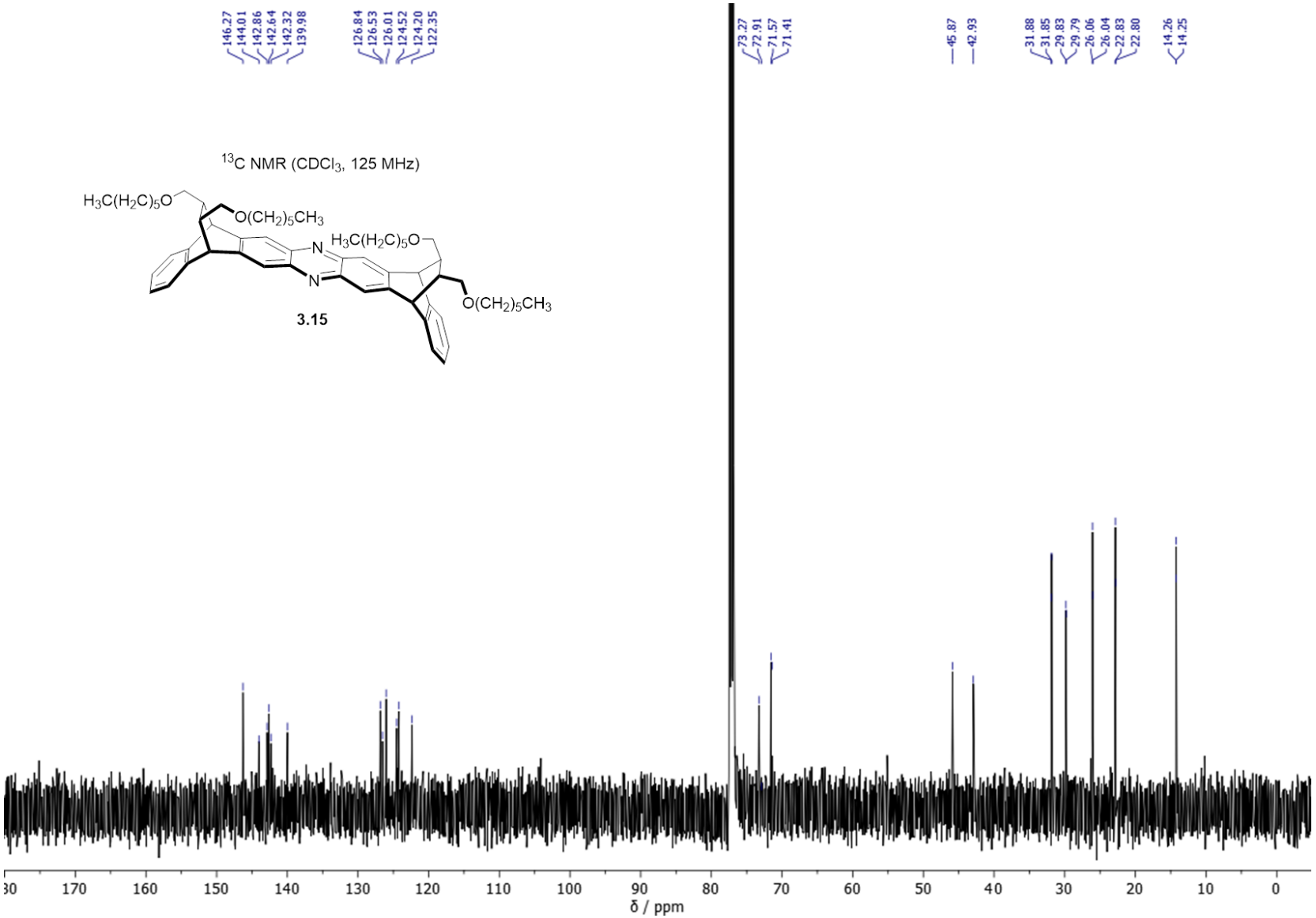
146.27
144.01
142.86
142.64
142.32
139.98
126.84
126.53
126.01
124.52
124.20
122.35
73.27
72.91
71.57
71.41
45.87
42.93
31.88
31.85
29.83
29.79
26.06
26.04
22.83
22.80
14.26
14.25
13C NMR (CDCl3, 125 MHz)
H3C(H2C)5O
O(CH2)5CH3
N
N
H3C(H2C)5O
O(CH2)5CH3
3.15
δ / ppm

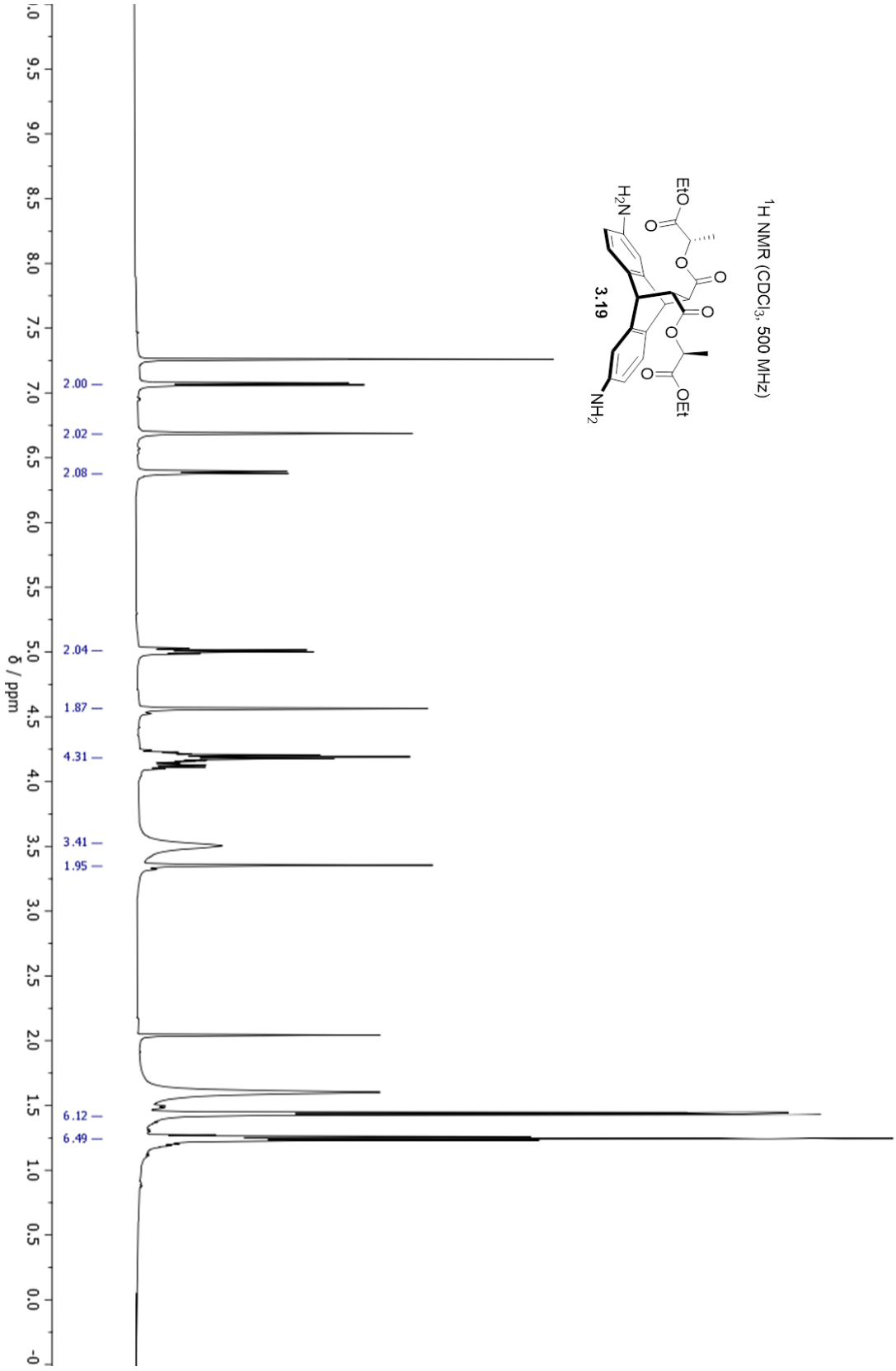
^{1}H NMR ($CDCl_3$, 500 MHz)
3.19
H_2N
NH_2
EtO
OEt
δ / ppm
2.00
2.02
2.08
2.04
1.87
4.31
3.41
1.95
6.12
6.49

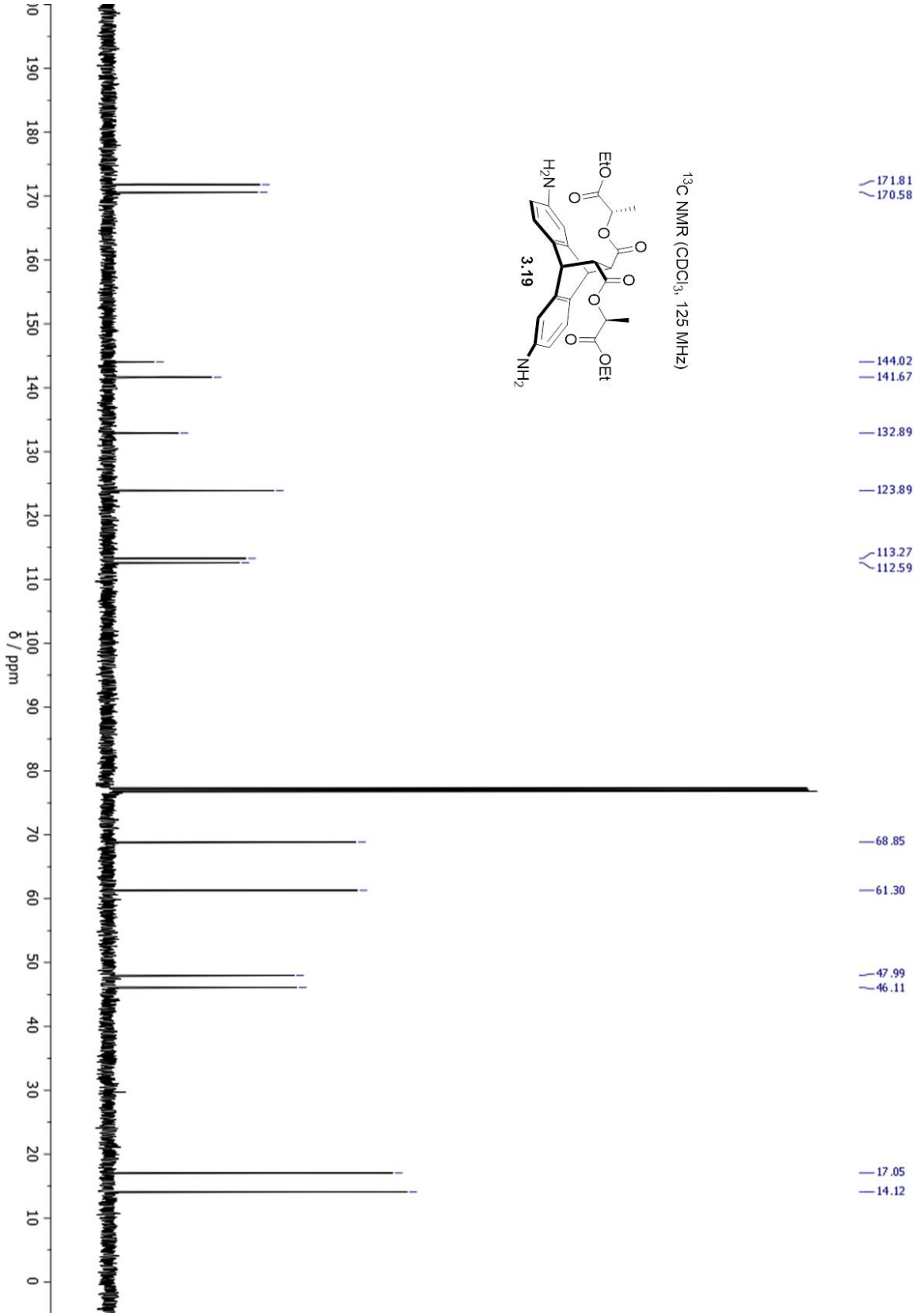
^{13}C NMR (CDCl$_3$, 125 MHz)
3.19
171.81
170.58
144.02
141.67
132.89
123.89
113.27
112.59
68.85
61.30
47.99
46.11
17.05
14.12
δ / ppm

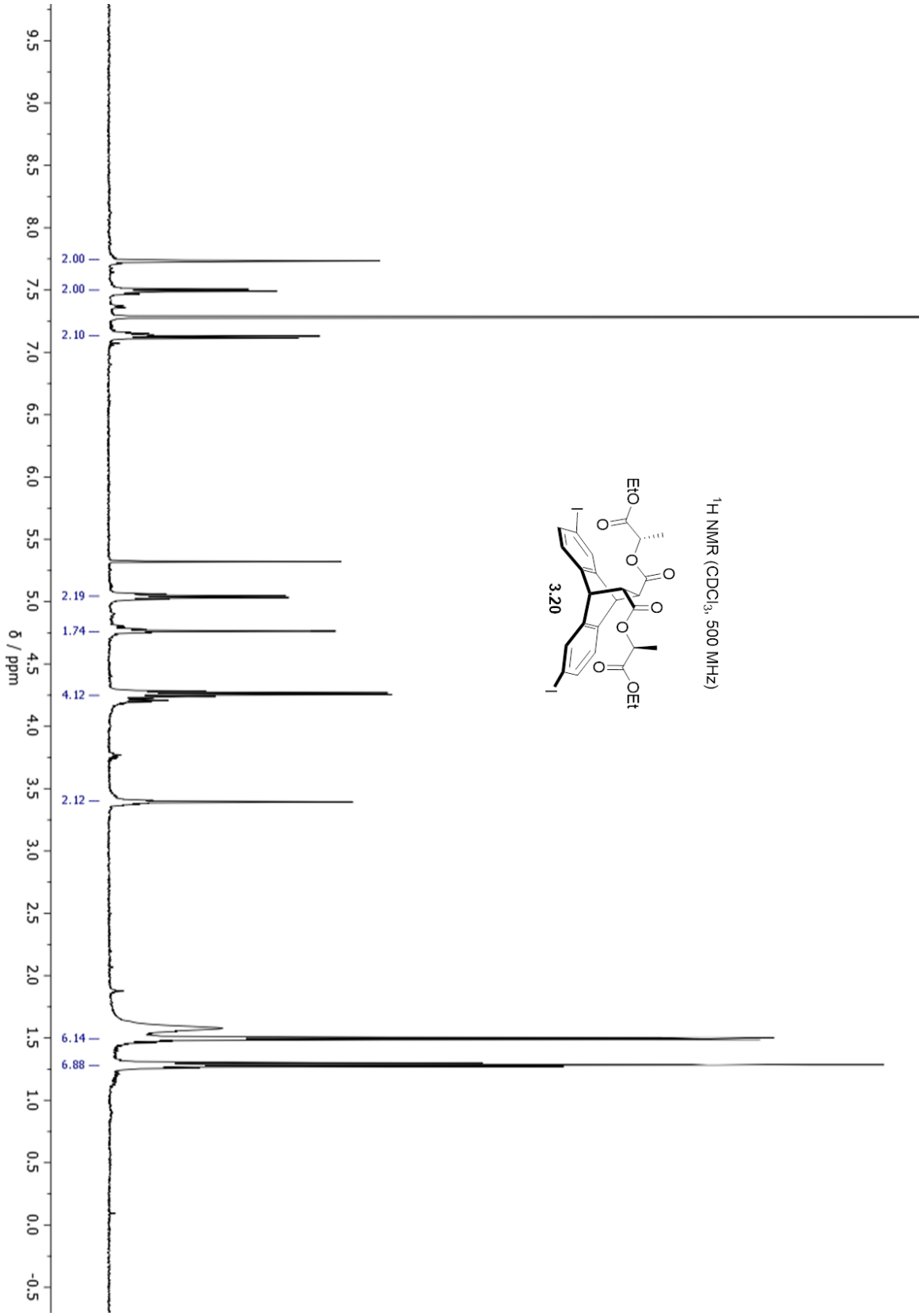
^{1}H NMR (CDCl$_3$, 500 MHz)
3.20
EtO
OEt
I
I
O
O
O
O
O
O
O
O
2.00
2.00
2.10
2.19
1.74
4.12
2.12
6.14
6.88
δ / ppm
9.5
9.0
8.5
8.0
7.5
7.0
6.5
6.0
5.5
5.0
4.5
4.0
3.5
3.0
2.5
2.0
1.5
1.0
0.5
0.0
-0.5

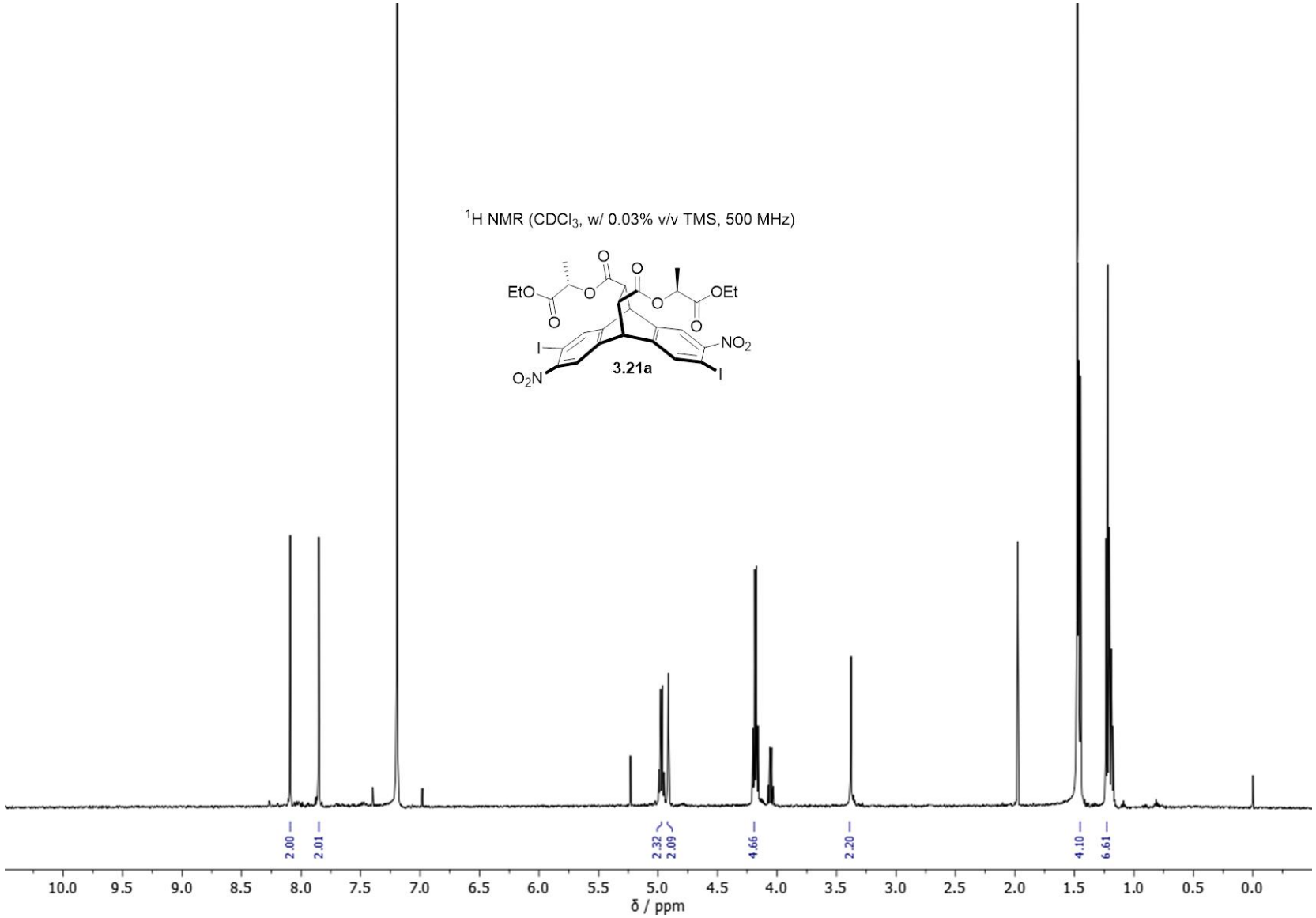
^{1}H NMR ($CDCl_3$, w/ 0.03% v/v TMS, 500 MHz)
EtO
OEt
I
NO_2
O_2N
I
3.21a
2.00
2.01
2.32
2.09
4.66
2.20
4.10
6.61
10.0 9.5 9.0 8.5 8.0 7.5 7.0 6.5 6.0 5.5 5.0 4.5 4.0 3.5 3.0 2.5 2.0 1.5 1.0 0.5 0.0
δ / ppm

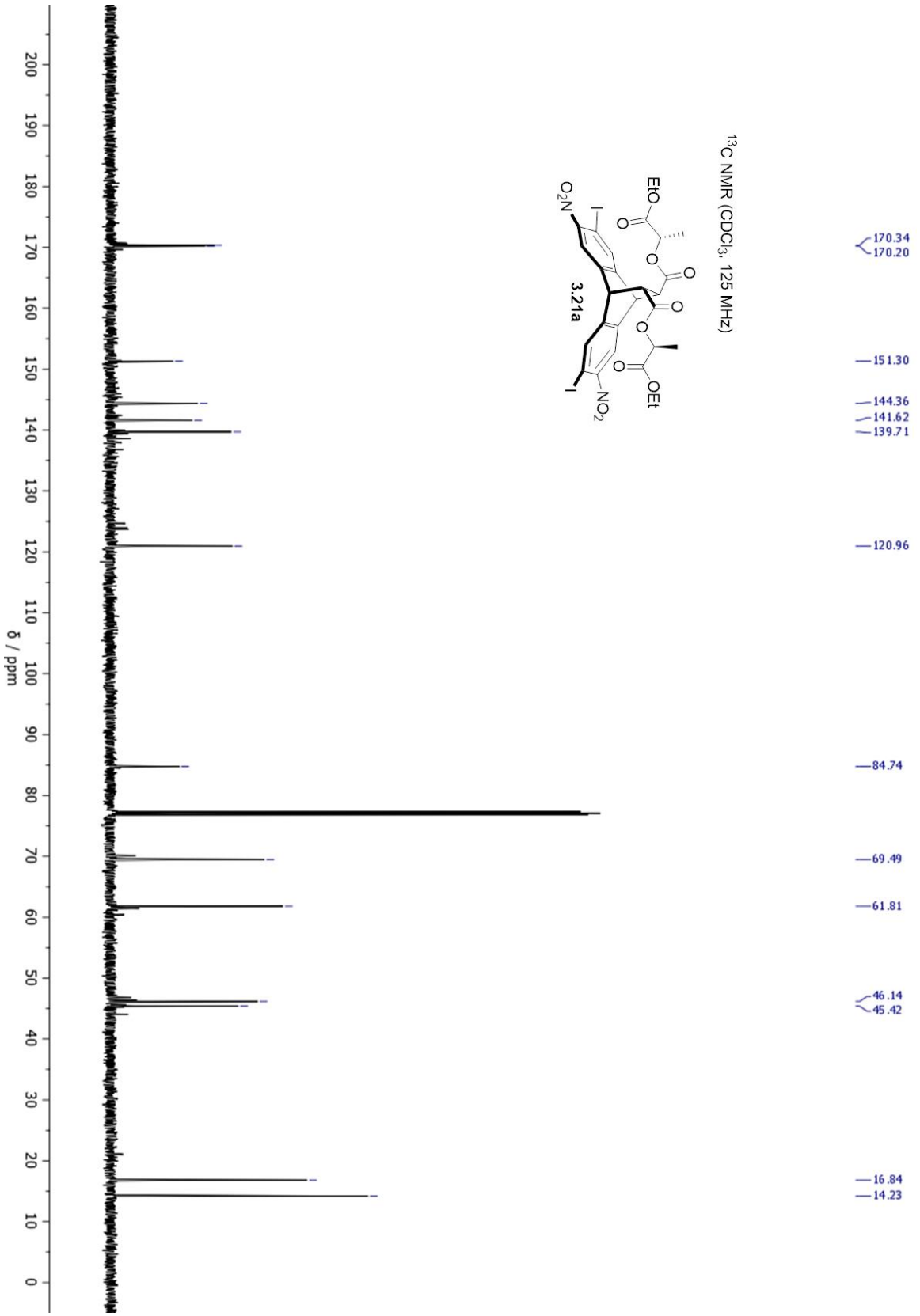
^{13}C NMR ($CDCl_3$, 125 MHz)
3.21a
170.34
170.20
151.30
144.36
141.62
139.71
120.96
84.74
69.49
61.81
46.14
45.42
16.84
14.23
δ / ppm

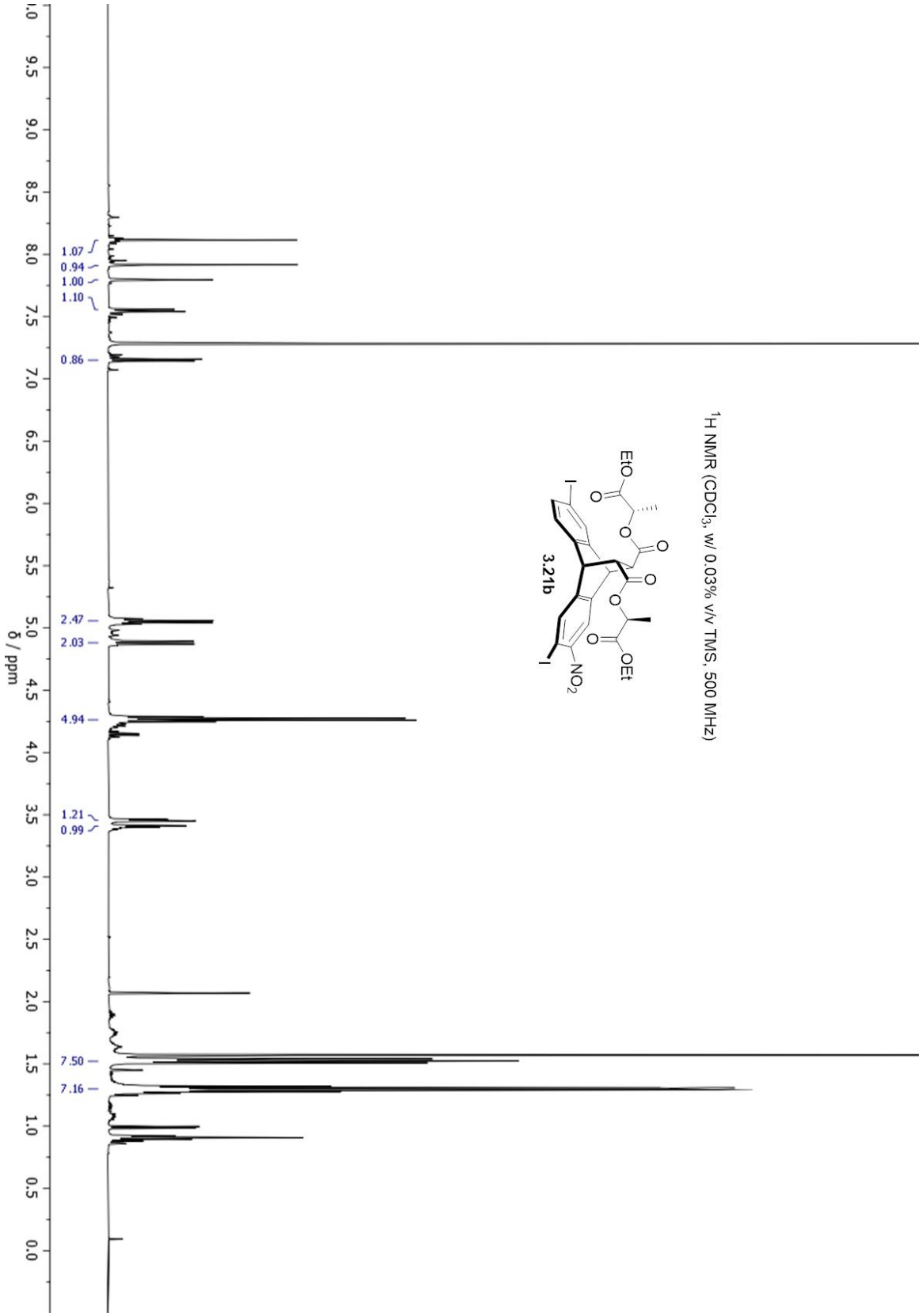
^{1}H NMR ($CDCl_3$, w/ 0.03% v/v TMS, 500 MHz)
3.21b
EtO
OEt
NO_2
δ / ppm
1.07
0.94
1.00
1.10
0.86
2.47
2.03
4.94
1.21
0.99
7.50
7.16

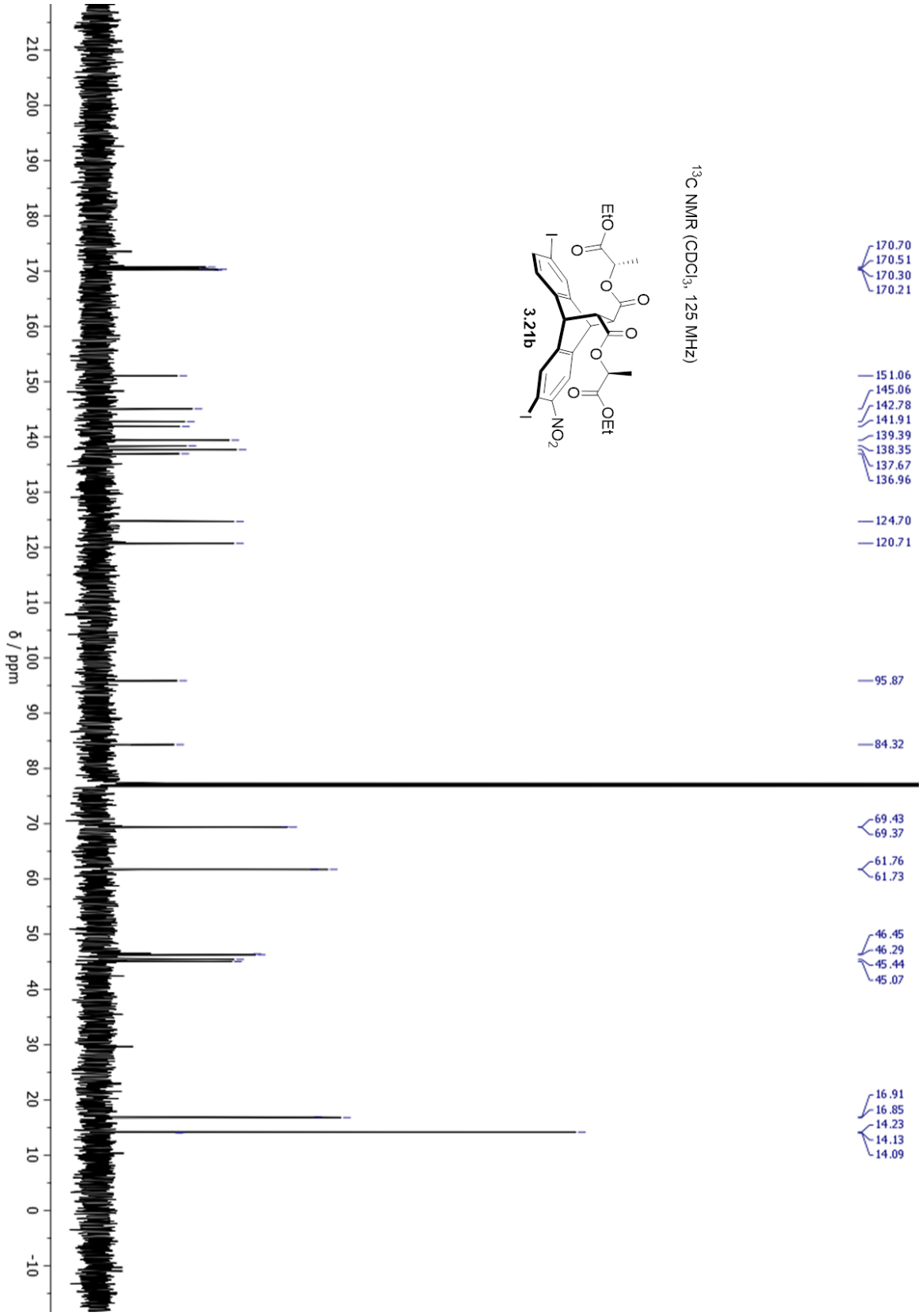
^{13}C NMR ($CDCl_3$, 125 MHz)
3.21b
EtO
OEt
I
I
NO_2
O
δ / ppm
210
200
190
180
170
160
150
140
130
120
110
100
90
80
70
60
50
40
30
20
10
0
-10
170.70
170.51
170.30
170.21
151.06
145.06
142.78
141.91
139.39
138.35
137.67
136.96
124.70
120.71
95.87
84.32
69.43
69.37
61.76
61.73
46.45
46.29
45.44
45.07
16.91
16.85
14.23
14.13
14.09

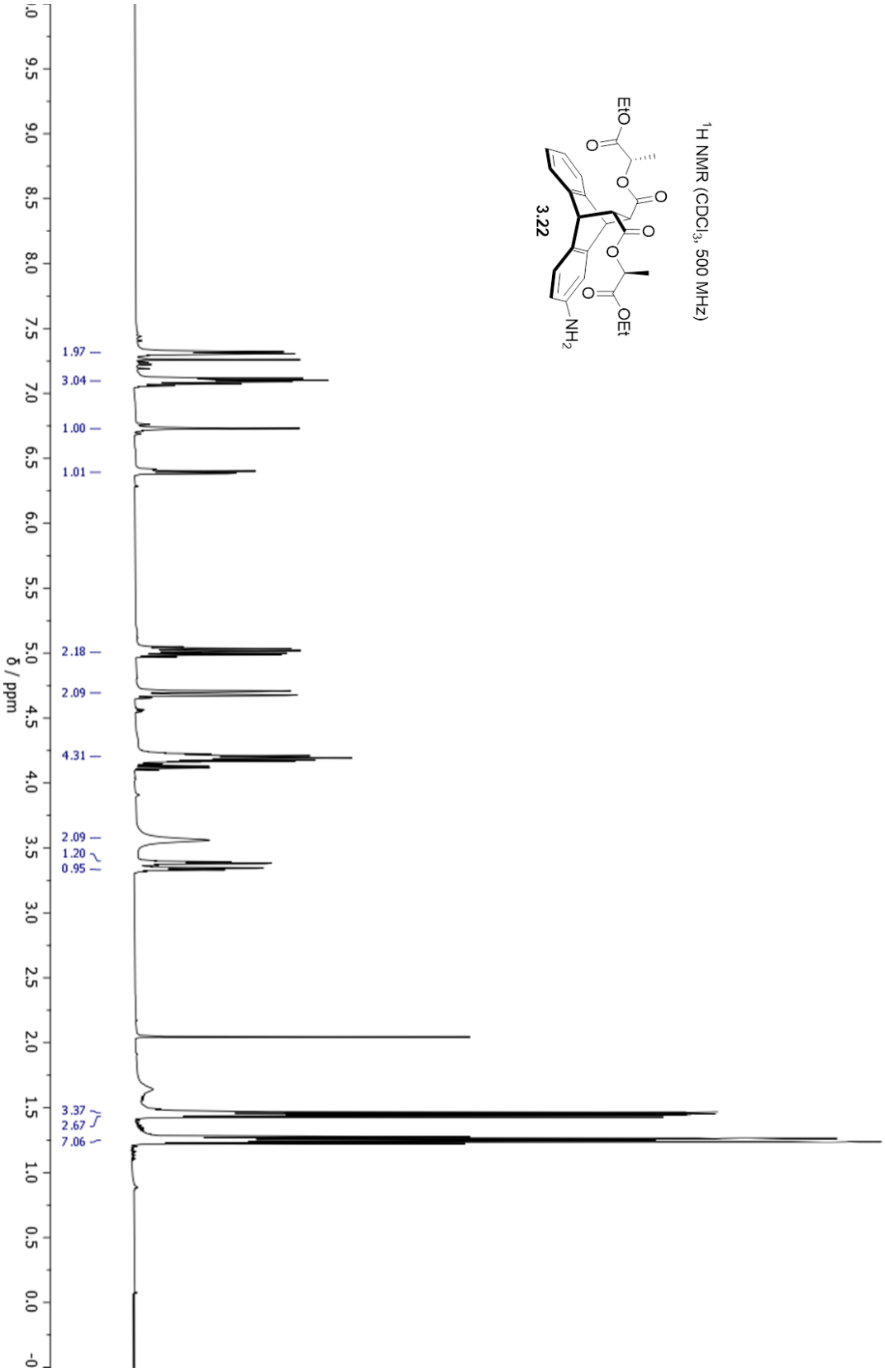
^{1}H NMR ($CDCl_3$, 500 MHz)
3.22
EtO
OEt
NH_2
δ / ppm
1.97
3.04
1.00
1.01
2.18
2.09
4.31
2.09
1.20
0.95
3.37
2.67
7.06

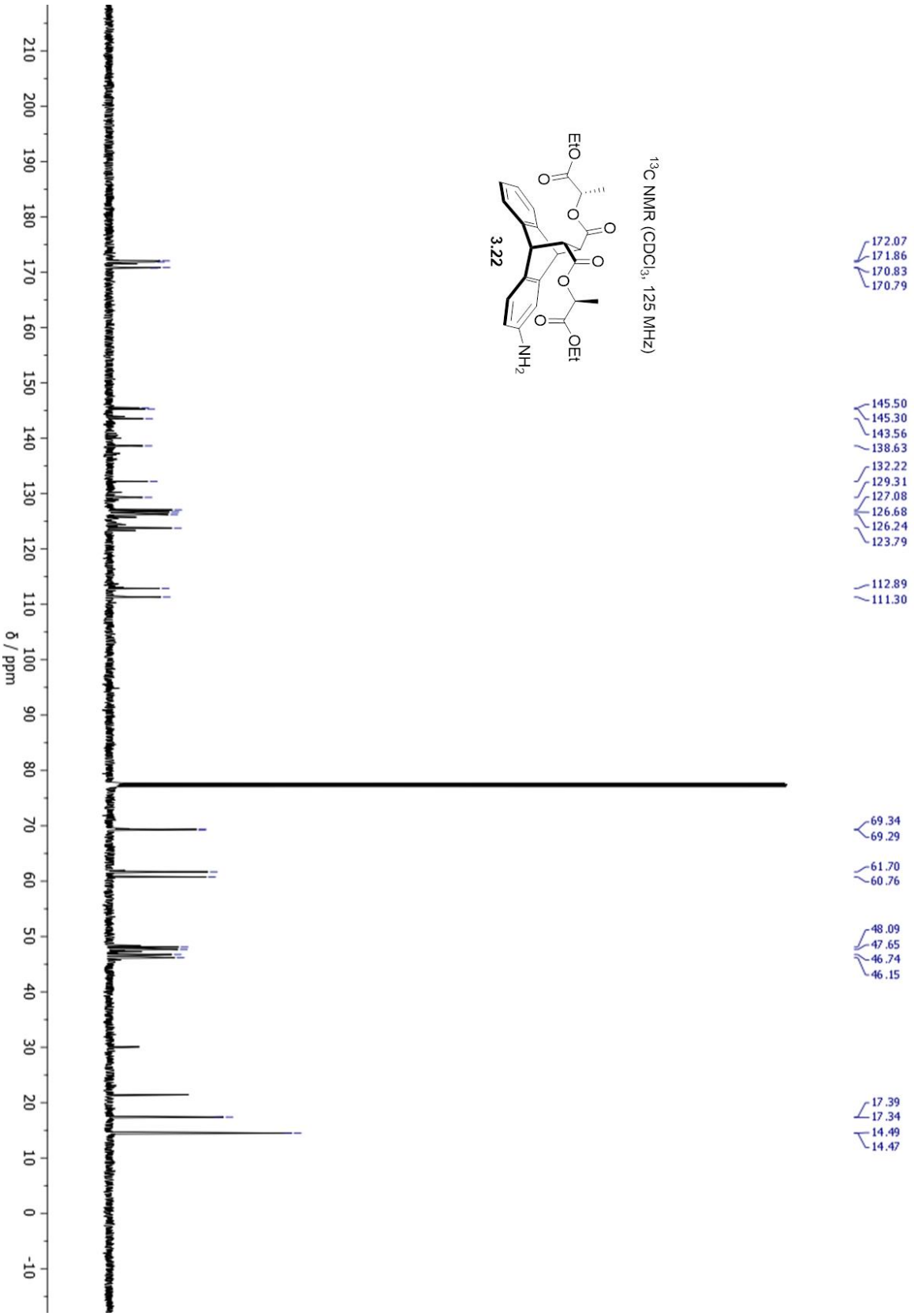
^{13}C NMR ($CDCl_3$, 125 MHz)
3.22
EtO
OEt
NH_2
δ / ppm
172.07
171.86
170.83
170.79
145.50
145.30
143.56
138.63
132.22
129.31
127.08
126.68
126.24
123.79
112.89
111.30
69.34
69.29
61.70
60.76
48.09
47.65
46.74
46.15
17.39
17.34
14.49
14.47

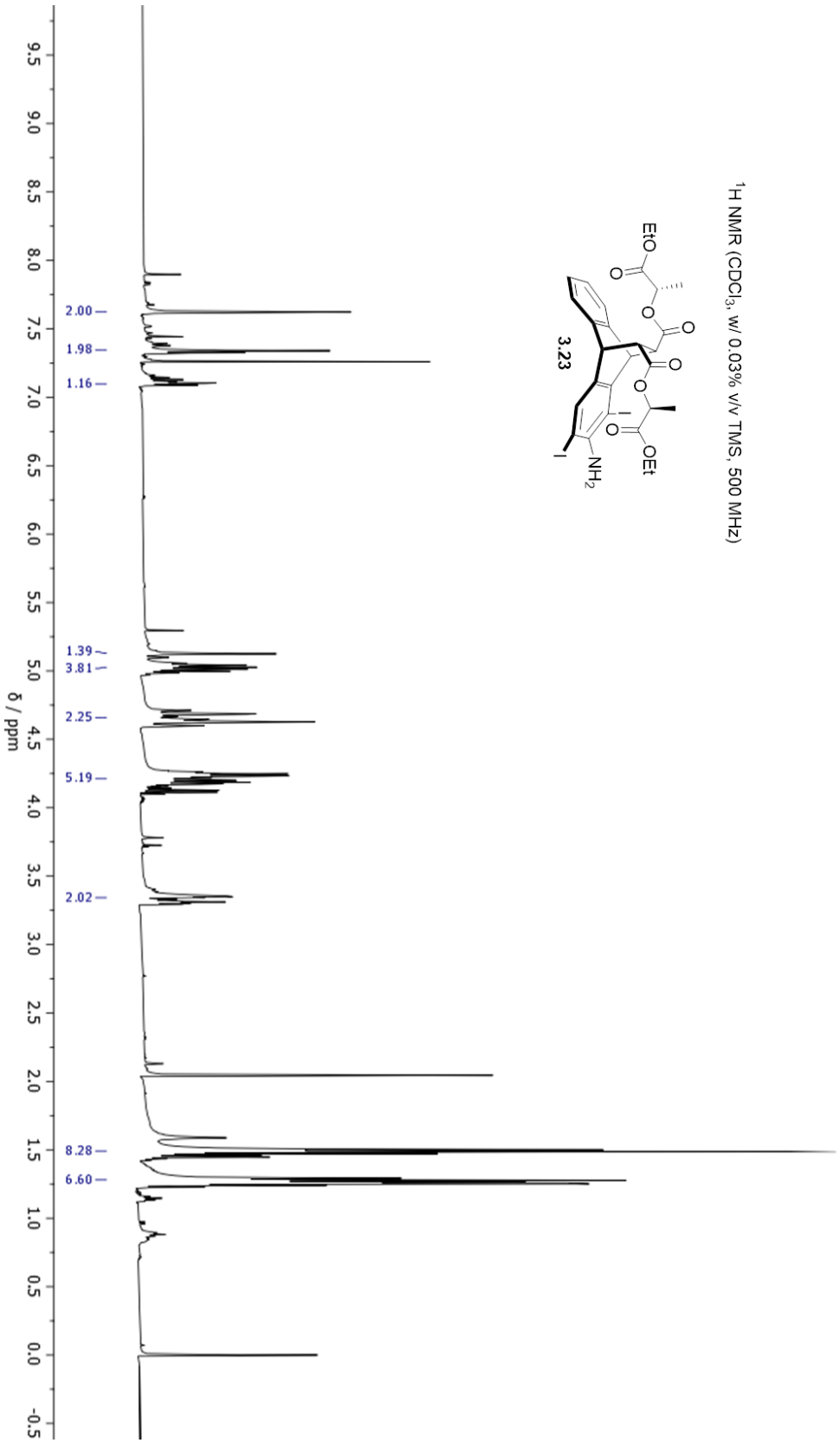
^{1}H NMR ($CDCl_3$, w/ 0.03% v/v TMS, 500 MHz)
3.23
EtO
OEt
NH_2
δ / ppm
2.00
1.98
1.16
1.39
3.81
2.25
5.19
2.02
8.28
6.60

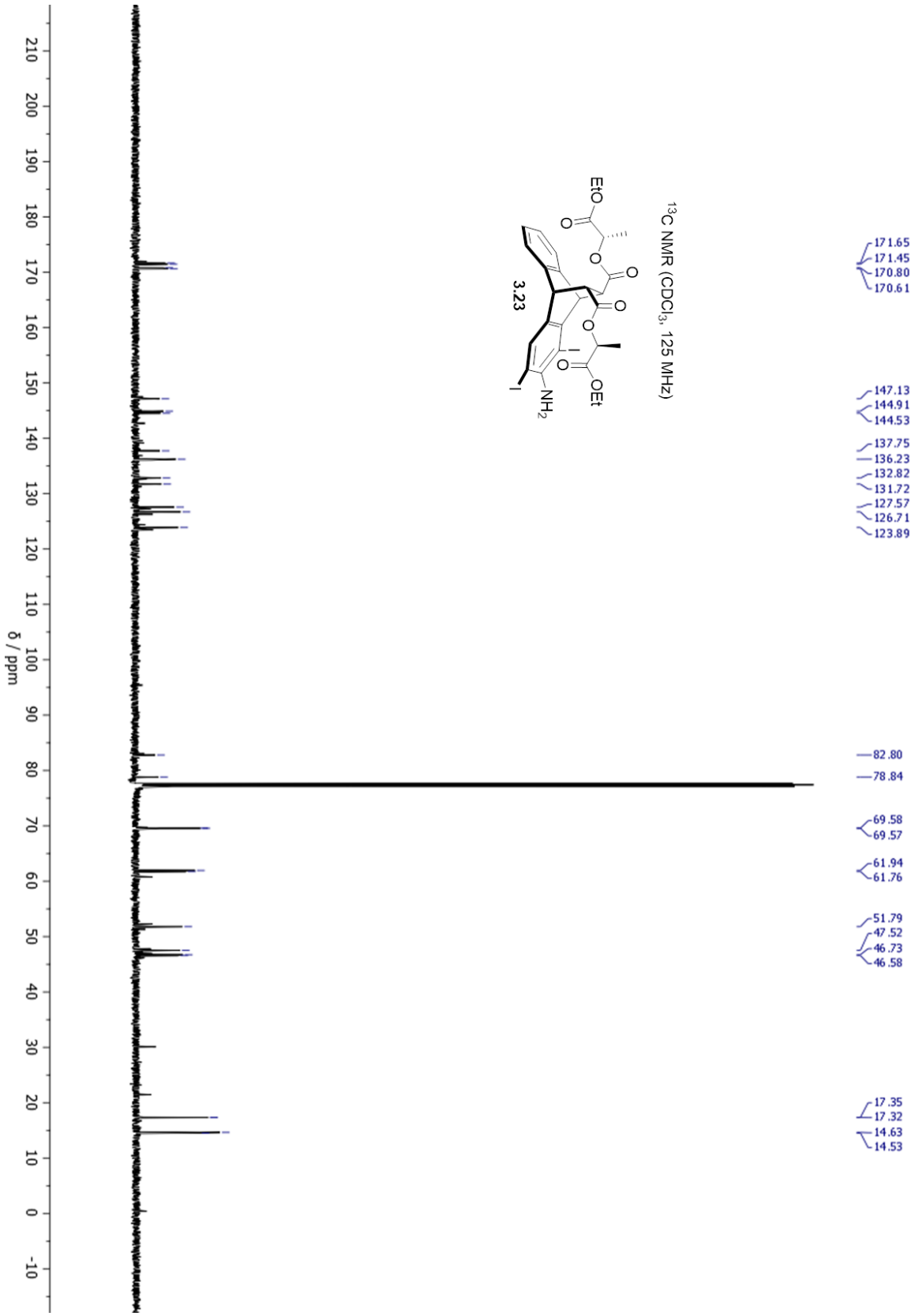
^{13}C NMR ($CDCl_3$, 125 MHz)
3.23
EtO
OEt
NH_2
171.65
171.45
170.80
170.61
147.13
144.91
144.53
137.75
136.23
132.82
131.72
127.57
126.71
123.89
82.80
78.84
69.58
69.57
61.94
61.76
51.79
47.52
46.73
46.58
17.35
17.32
14.63
14.53
δ / ppm

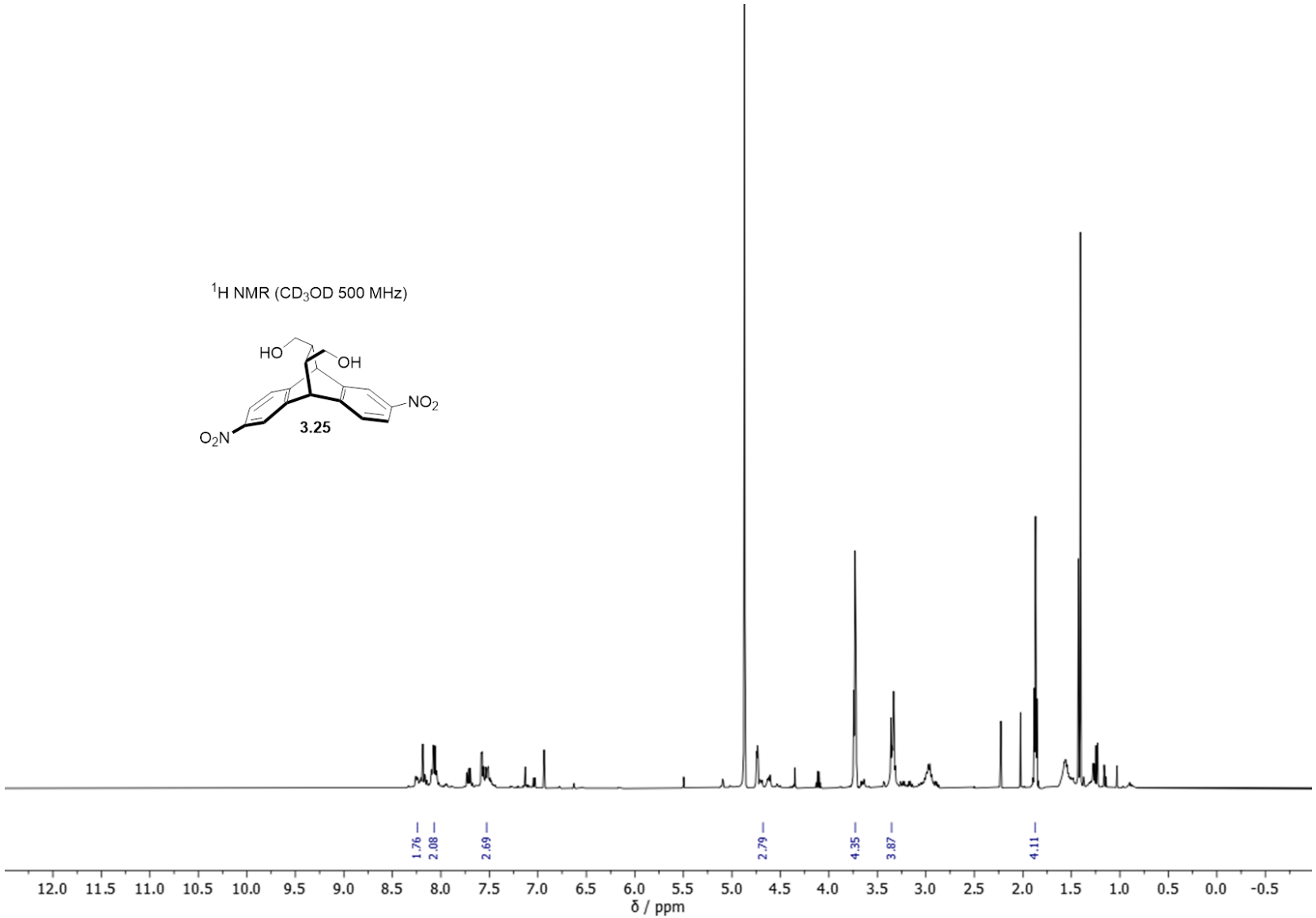
^{1}H NMR (CD_3OD 500 MHz)
HO
OH
NO_2
O_2N
3.25
1.76
2.08
2.69
2.79
4.35
3.87
4.11
12.0 11.5 11.0 10.5 10.0 9.5 9.0 8.5 8.0 7.5 7.0 6.5 6.0 5.5 5.0 4.5 4.0 3.5 3.0 2.5 2.0 1.5 1.0 0.5 0.0 -0.5
δ / ppm

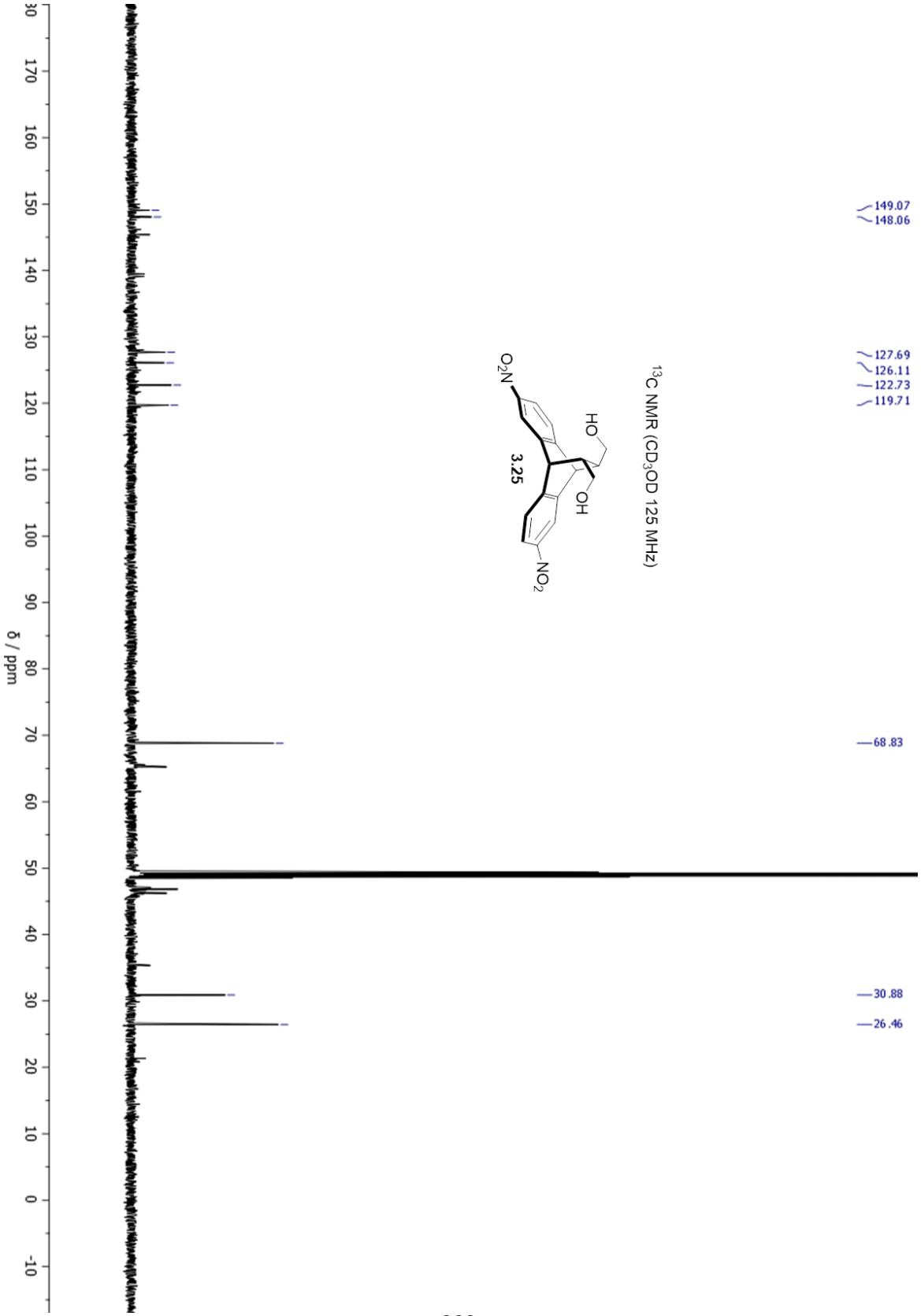
149.07
148.06
127.69
126.11
122.73
119.71
68.83
30.88
26.46
^{13}C NMR (CD_3OD 125 MHz)
O_2N
HO
OH
NO_2
3.25
δ / ppm

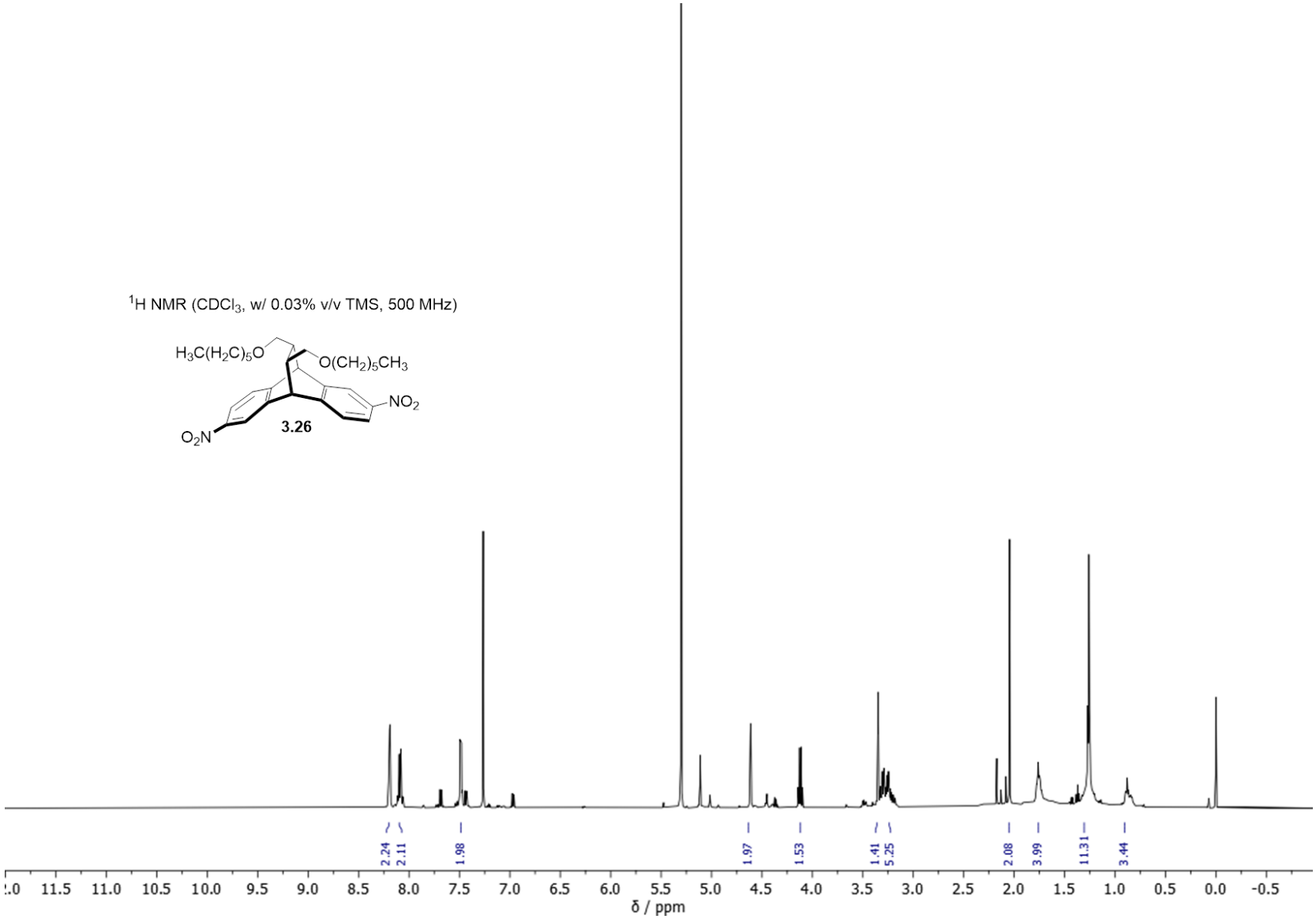
^{1}H NMR ($CDCl_3$, w/ 0.03% v/v TMS, 500 MHz)
$H_3C(H_2C)_5O$
$O(CH_2)_5CH_3$
NO_2
O_2N
3.26
2.24
2.11
1.98
1.97
1.53
1.41
5.25
2.08
3.99
11.31
3.44
δ / ppm

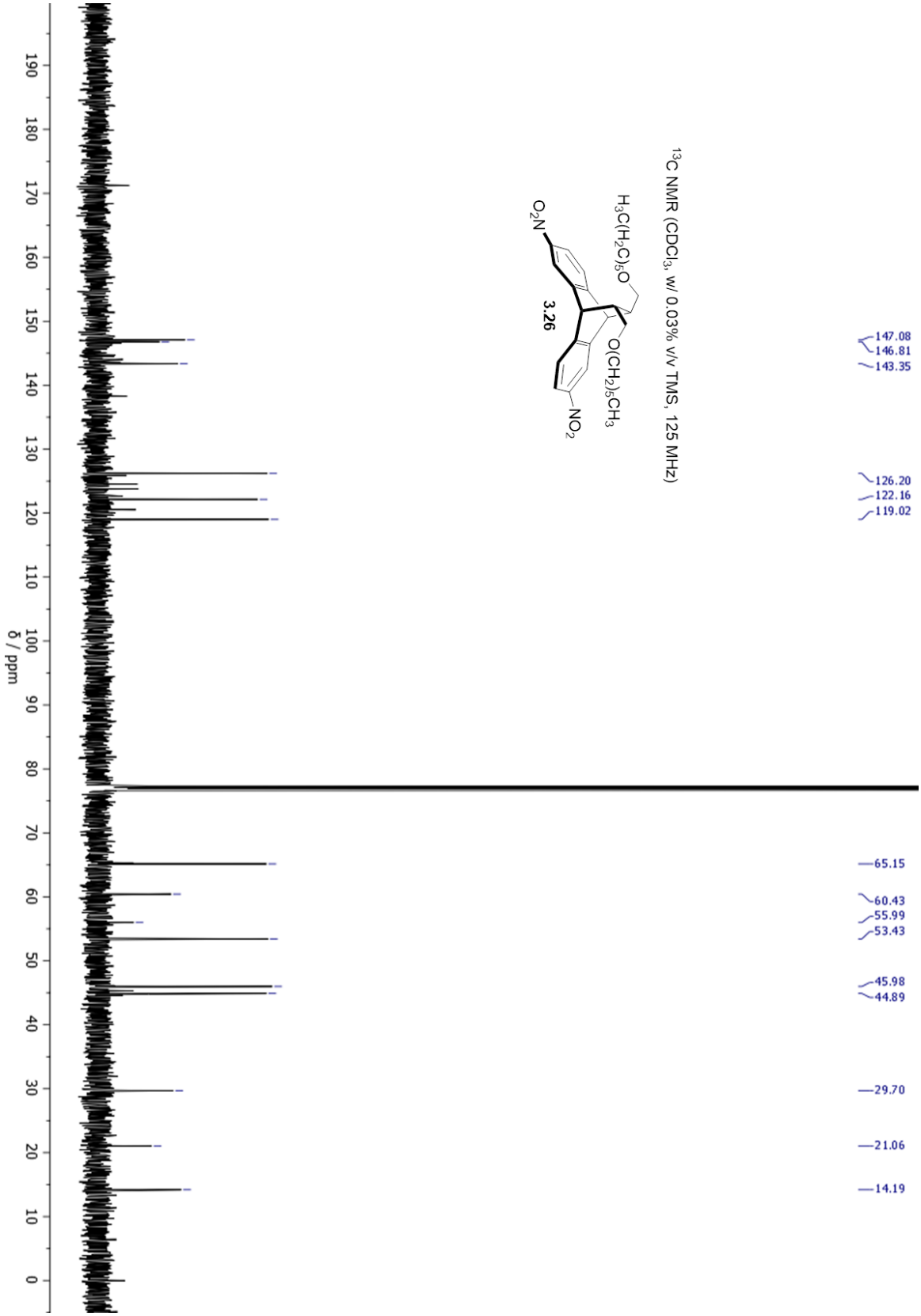
^{13}C NMR (CDCl$_3$, w/ 0.03% v/v TMS, 125 MHz)
$H_3C(H_2C)_5O$
O_2N
3.26
$O(CH_2)_5CH_3$
NO_2
147.08
146.81
143.35
126.20
122.16
119.02
65.15
60.43
55.99
53.43
45.98
44.89
29.70
21.06
14.19
δ / ppm

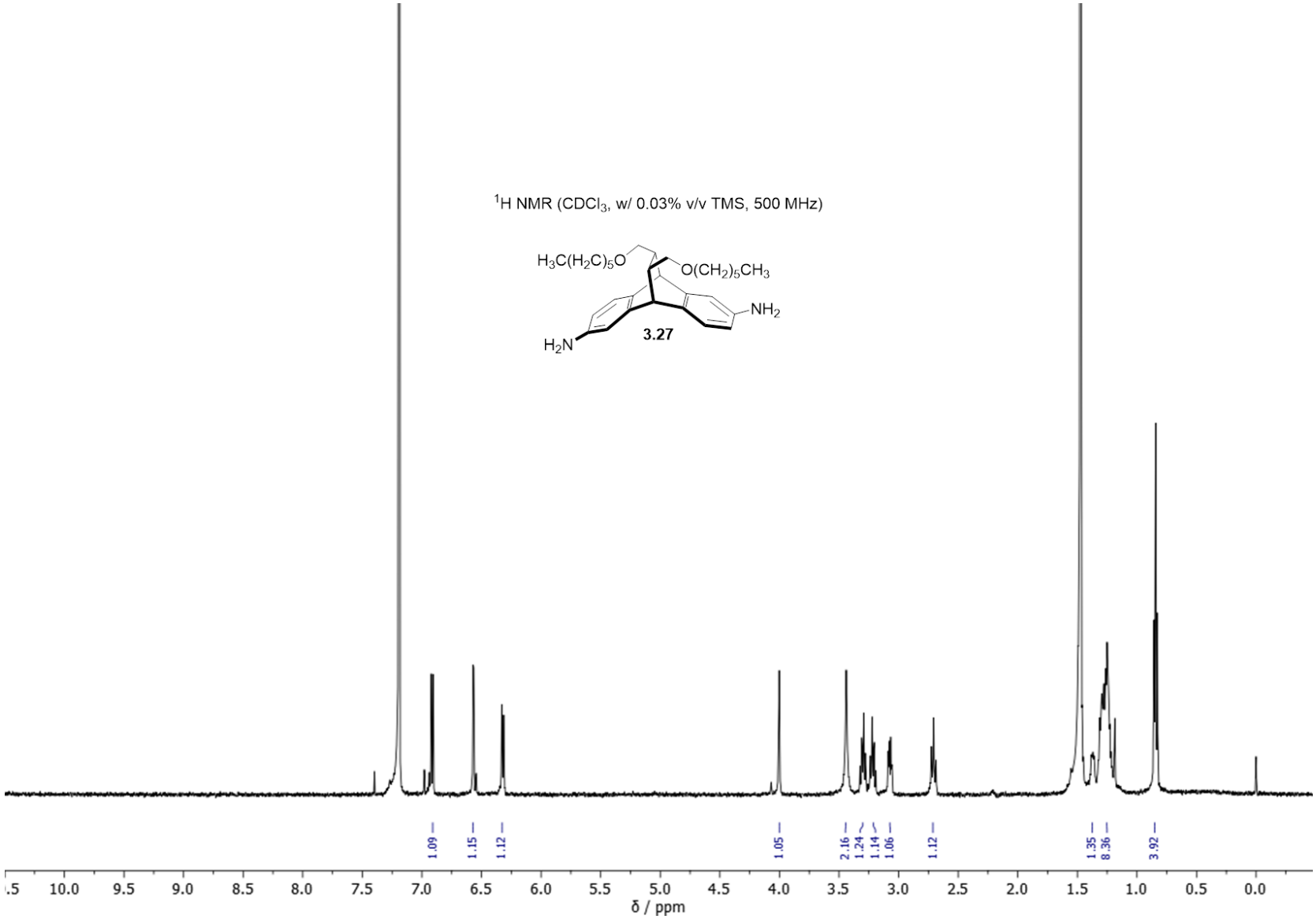
^{1}H NMR ($CDCl_3$, w/ 0.03% v/v TMS, 500 MHz)
$H_3C(H_2C)_5O$
$O(CH_2)_5CH_3$
NH_2
H_2N
3.27
1.09
1.15
1.12
1.05
2.16
1.24
1.14
1.06
1.12
1.35
8.36
3.92
δ / ppm

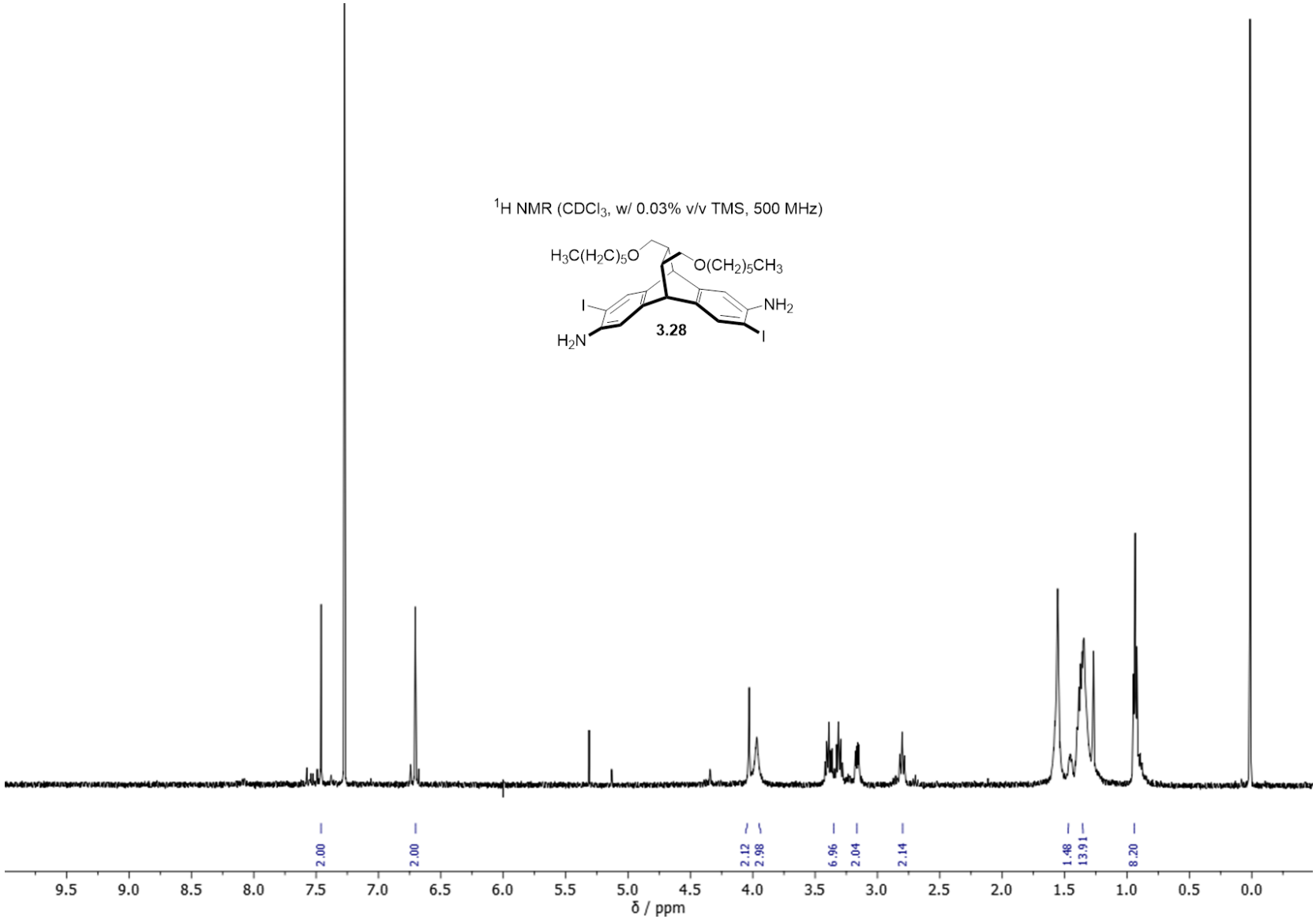
^{1}H NMR ($CDCl_3$, w/ 0.03% v/v TMS, 500 MHz)
$H_3C(H_2C)_5O$
$O(CH_2)_5CH_3$
I
NH_2
H_2N
I
3.28
2.00
2.00
2.12
2.98
6.96
2.04
2.14
1.48
13.91
8.20
9.5 9.0 8.5 8.0 7.5 7.0 6.5 6.0 5.5 5.0 4.5 4.0 3.5 3.0 2.5 2.0 1.5 1.0 0.5 0.0
δ / ppm

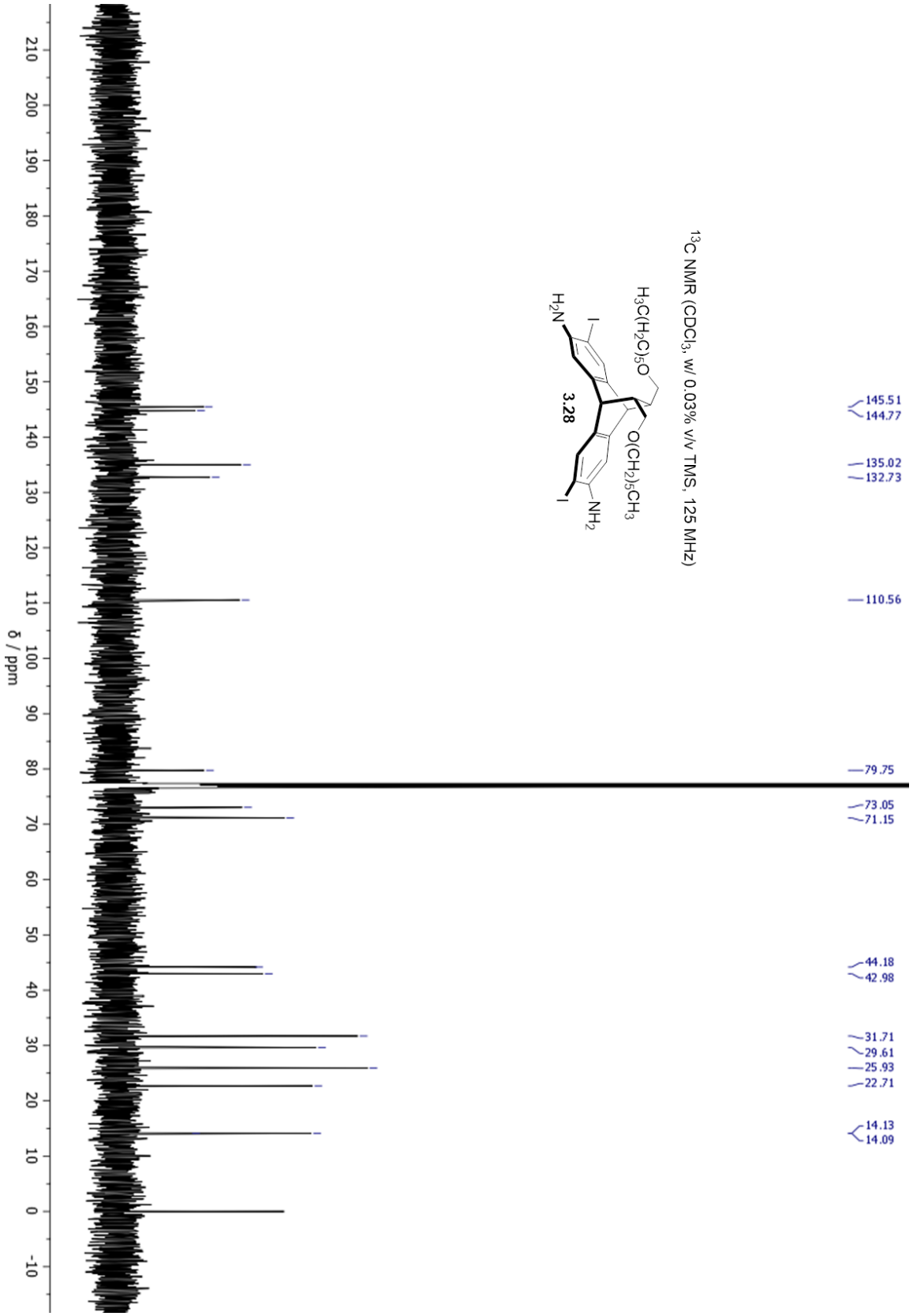
^{13}C NMR (CDCl$_3$, w/ 0.03% v/v TMS, 125 MHz)
3.28
δ / ppm
145.51
144.77
135.02
132.73
110.56
79.75
73.05
71.15
44.18
42.98
31.71
29.61
25.93
22.71
14.13
14.09

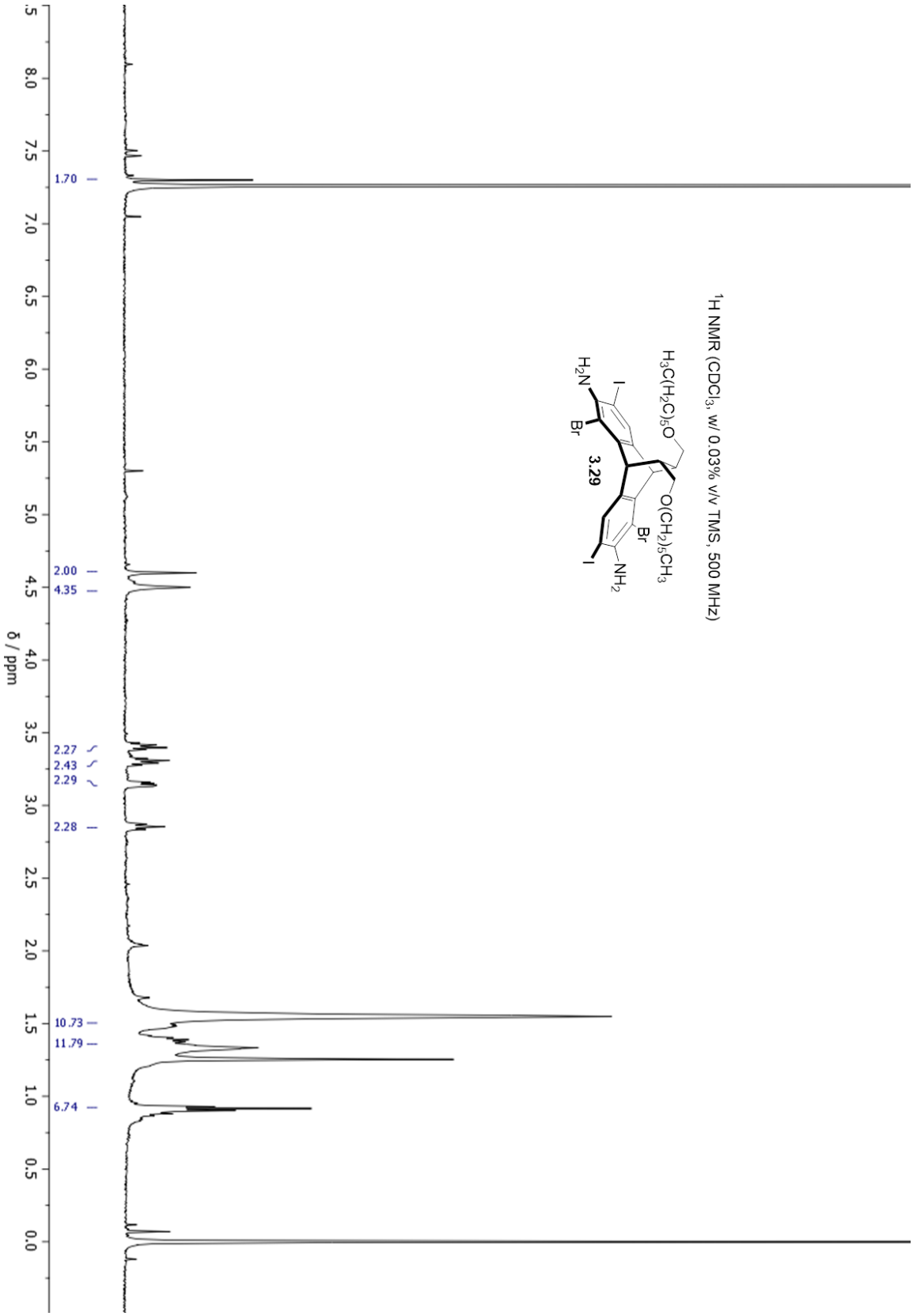
^{1}H NMR ($CDCl_3$, w/ 0.03% v/v TMS, 500 MHz)
$H_3C(H_2C)_5O$
$O(CH_2)_5CH_3$
H_2N
Br
I
Br
I
NH_2
3.29
δ / ppm
1.70
2.00
4.35
2.27
2.43
2.29
2.28
10.73
11.79
6.74

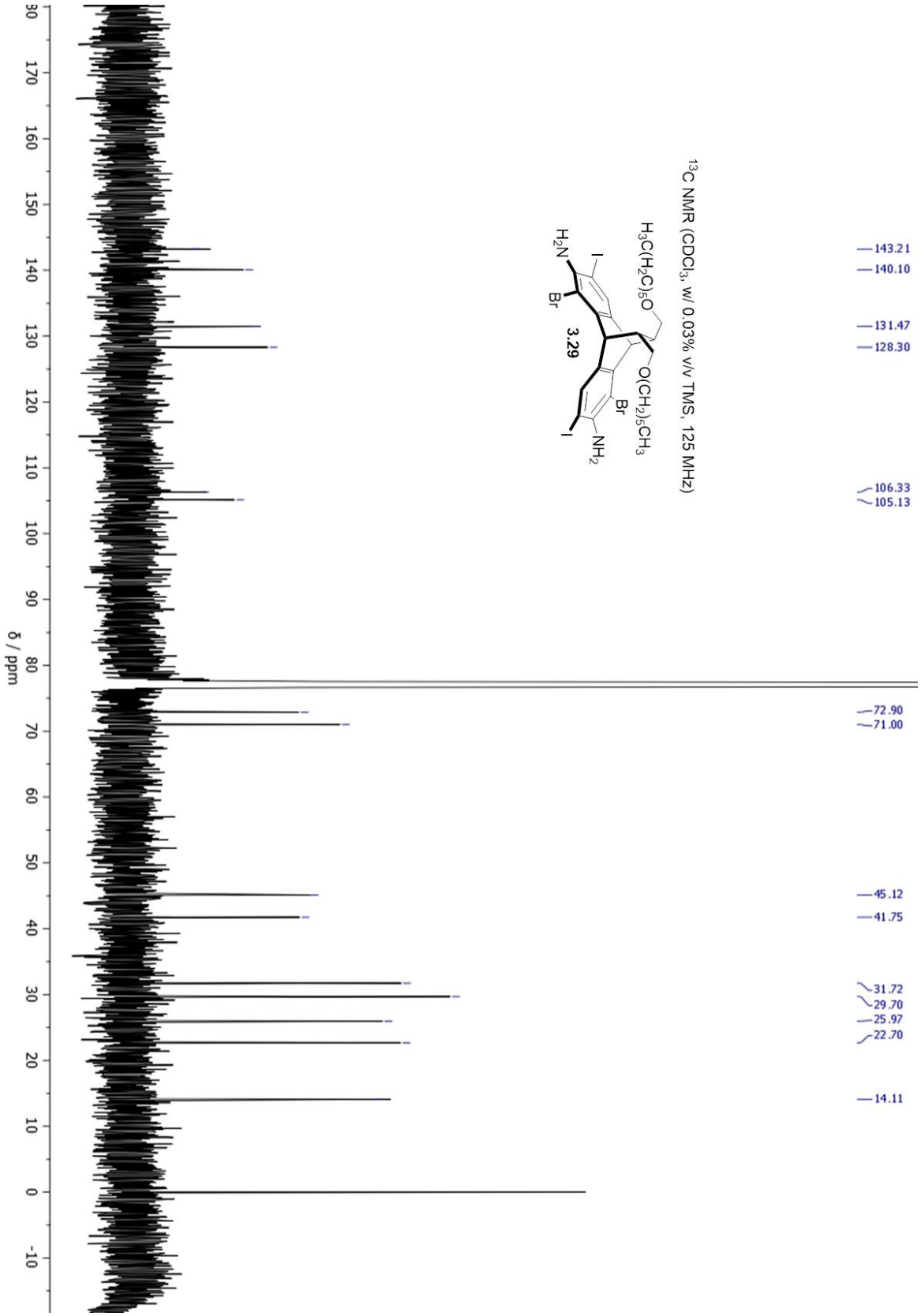
^{13}C NMR (CDCl$_3$, w/ 0.03% v/v TMS, 125 MHz)
H$_3$C(H$_2$C)$_5$O
O(CH$_2$)$_5$CH$_3$
H$_2$N
Br
I
Br
NH$_2$
I
3.29
δ / ppm
143.21
140.10
131.47
128.30
106.33
105.13
72.90
71.00
45.12
41.75
31.72
29.70
25.97
22.70
14.11

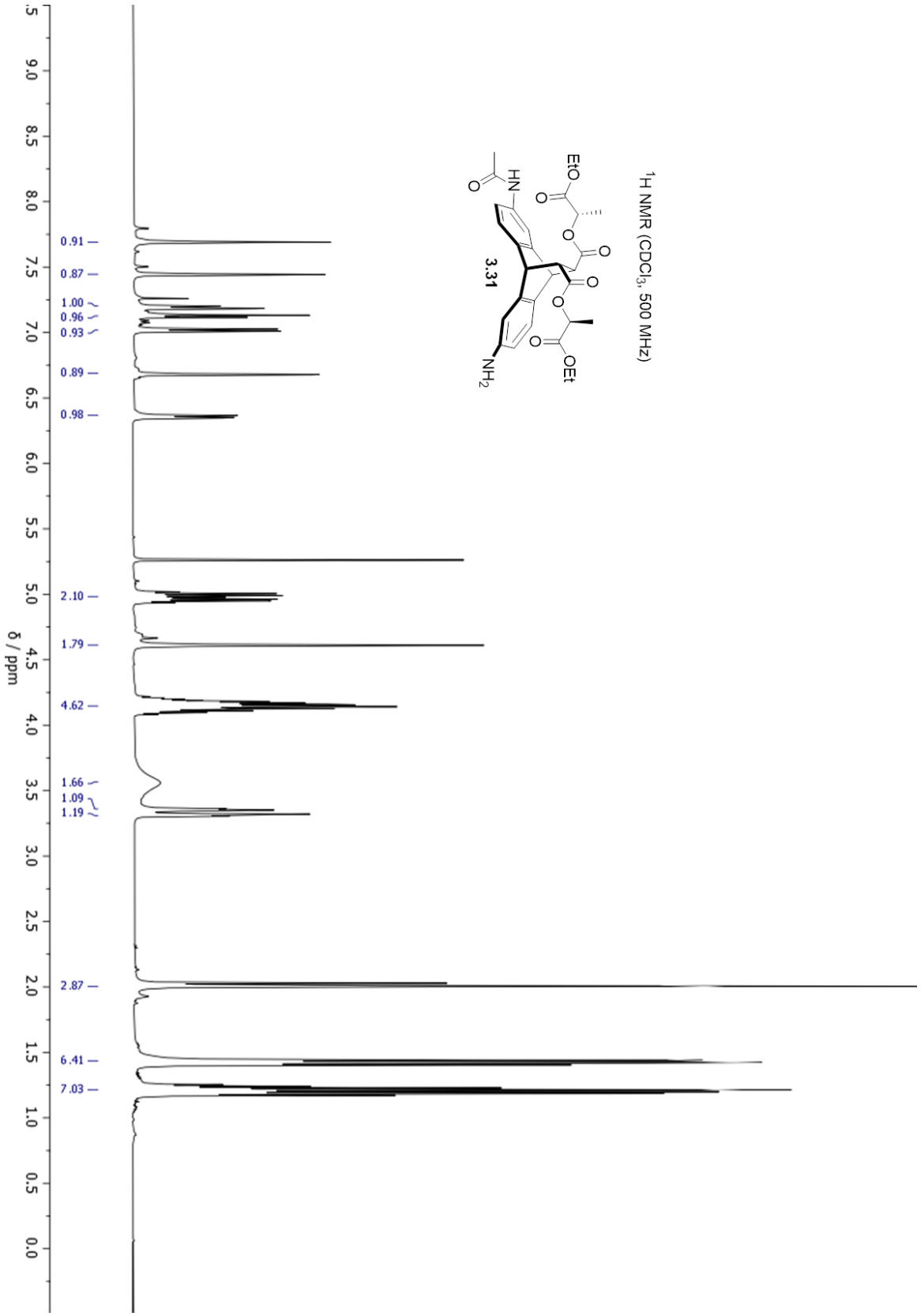
^{1}H NMR ($CDCl_3$, 500 MHz)
3.31
HN
EtO
OEt
NH_2
δ / ppm
0.91
0.87
1.00
0.96
0.93
0.89
0.98
2.10
1.79
4.62
1.66
1.09
1.19
2.87
6.41
7.03

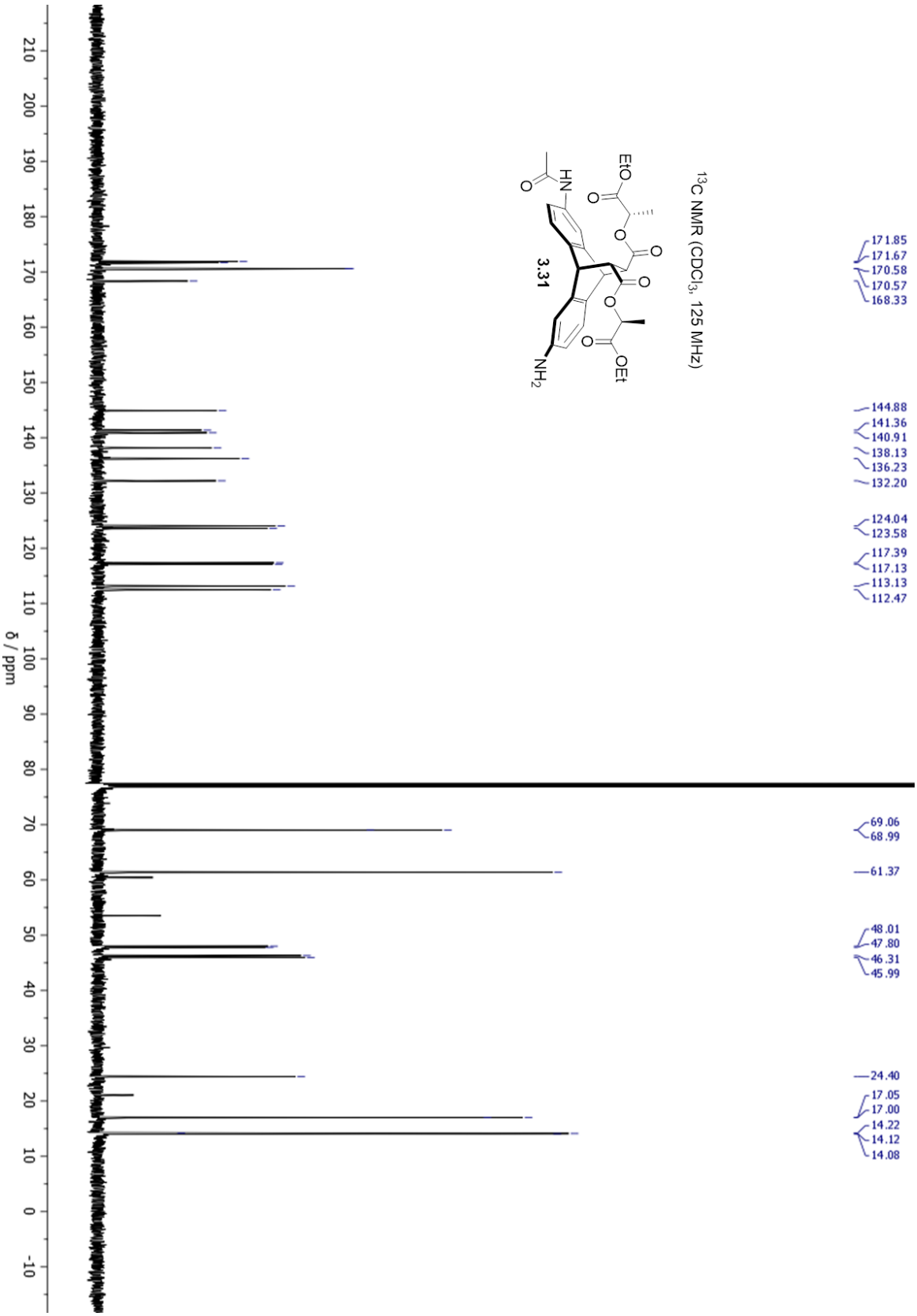
^{13}C NMR (CDCl$_3$, 125 MHz)
3.31
171.85
171.67
170.58
170.57
168.33
144.88
141.36
140.91
138.13
136.23
132.20
124.04
123.58
117.39
117.13
113.13
112.47
69.06
68.99
61.37
48.01
47.80
46.31
45.99
24.40
17.05
17.00
14.22
14.12
14.08
δ / ppm

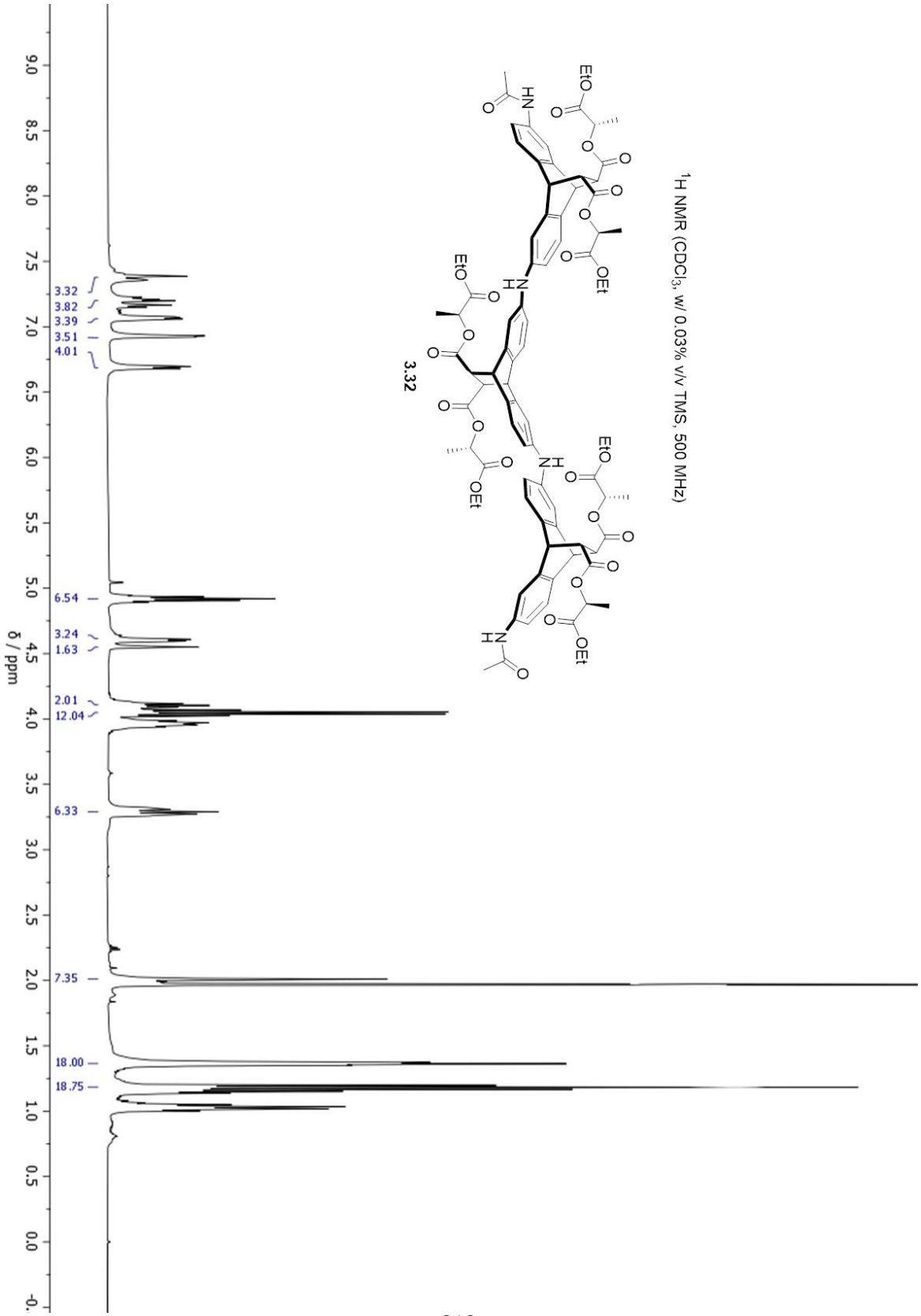

^{1}H NMR ($CDCl_3$, w/ 0.03% v/v TMS, 500 MHz)

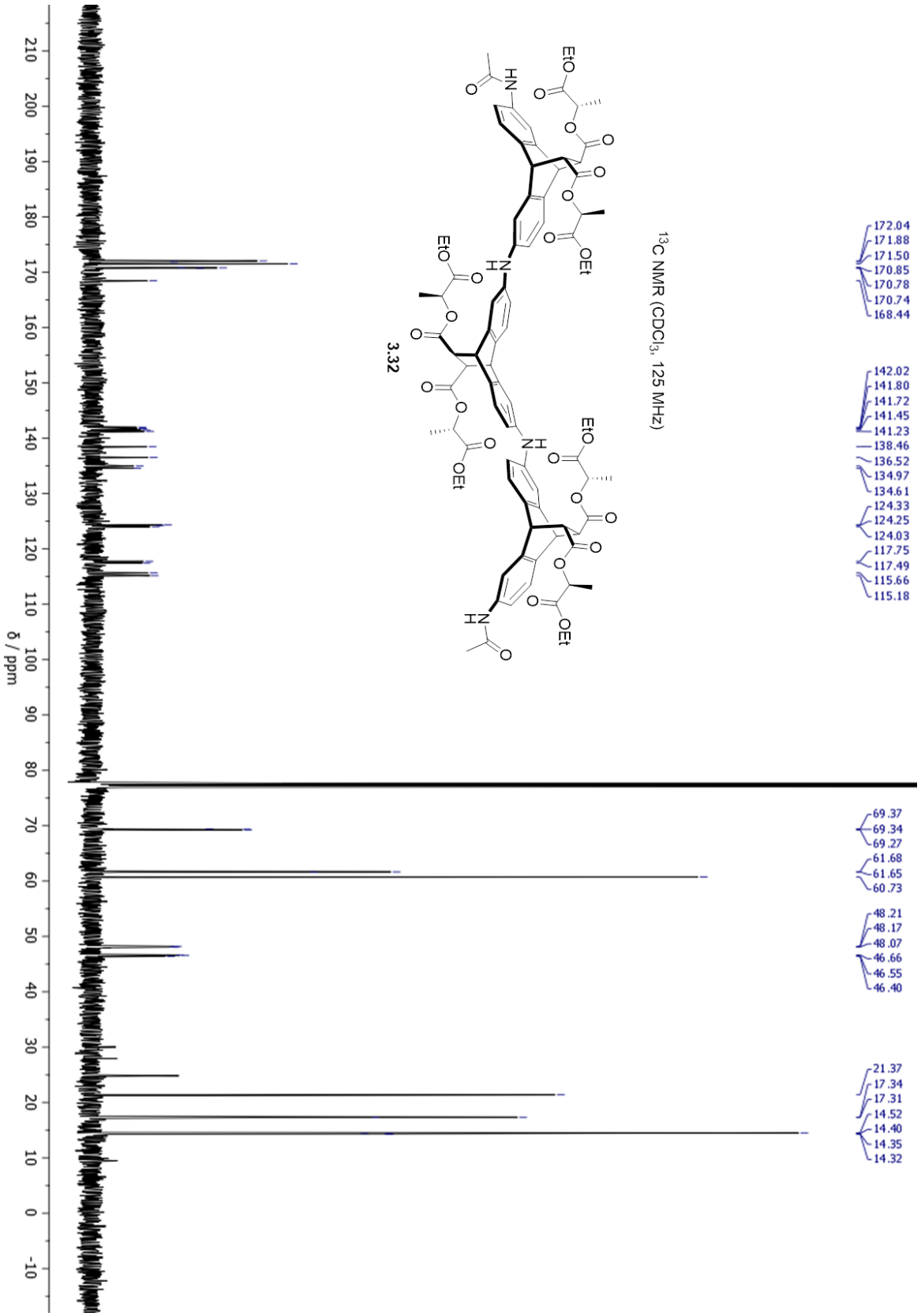
3.32
^{13}C NMR ($CDCl_3$, 125 MHz)
δ / ppm
172.04
171.88
171.50
170.85
170.78
170.74
168.44
142.02
141.80
141.72
141.45
141.23
138.46
136.52
134.97
134.61
124.33
124.25
124.03
117.75
117.49
115.66
115.18
69.37
69.34
69.27
61.68
61.65
60.73
48.21
48.17
48.07
46.66
46.55
46.40
21.37
17.34
17.31
14.52
14.40
14.35
14.32

^{1}H NMR ($CDCl_3$, 500 MHz)

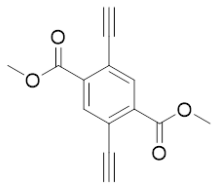

3.37

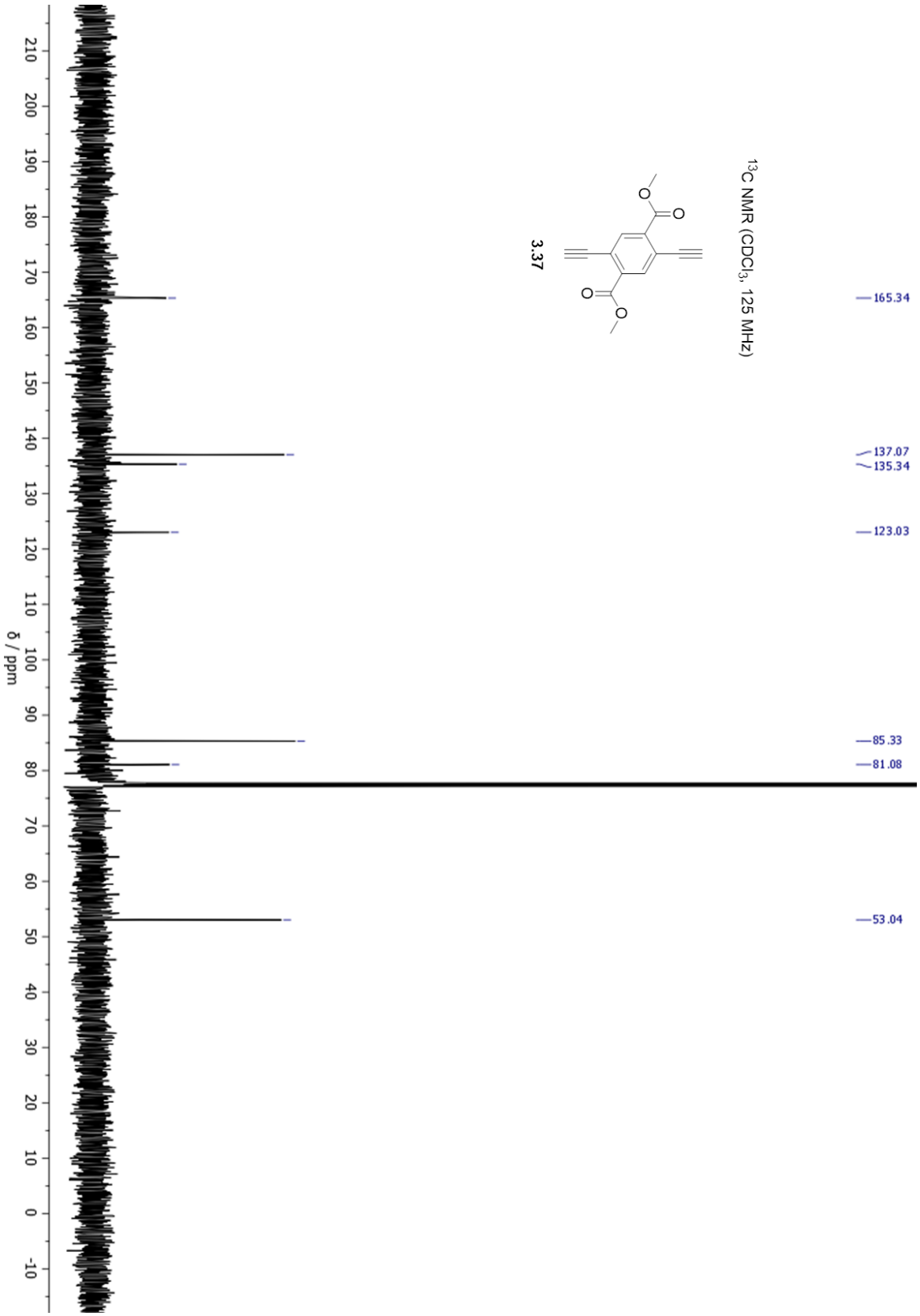
3.37
^{13}C NMR (CDCl$_3$, 125 MHz)
165.34
137.07
135.34
123.03
85.33
81.08
53.04
δ / ppm

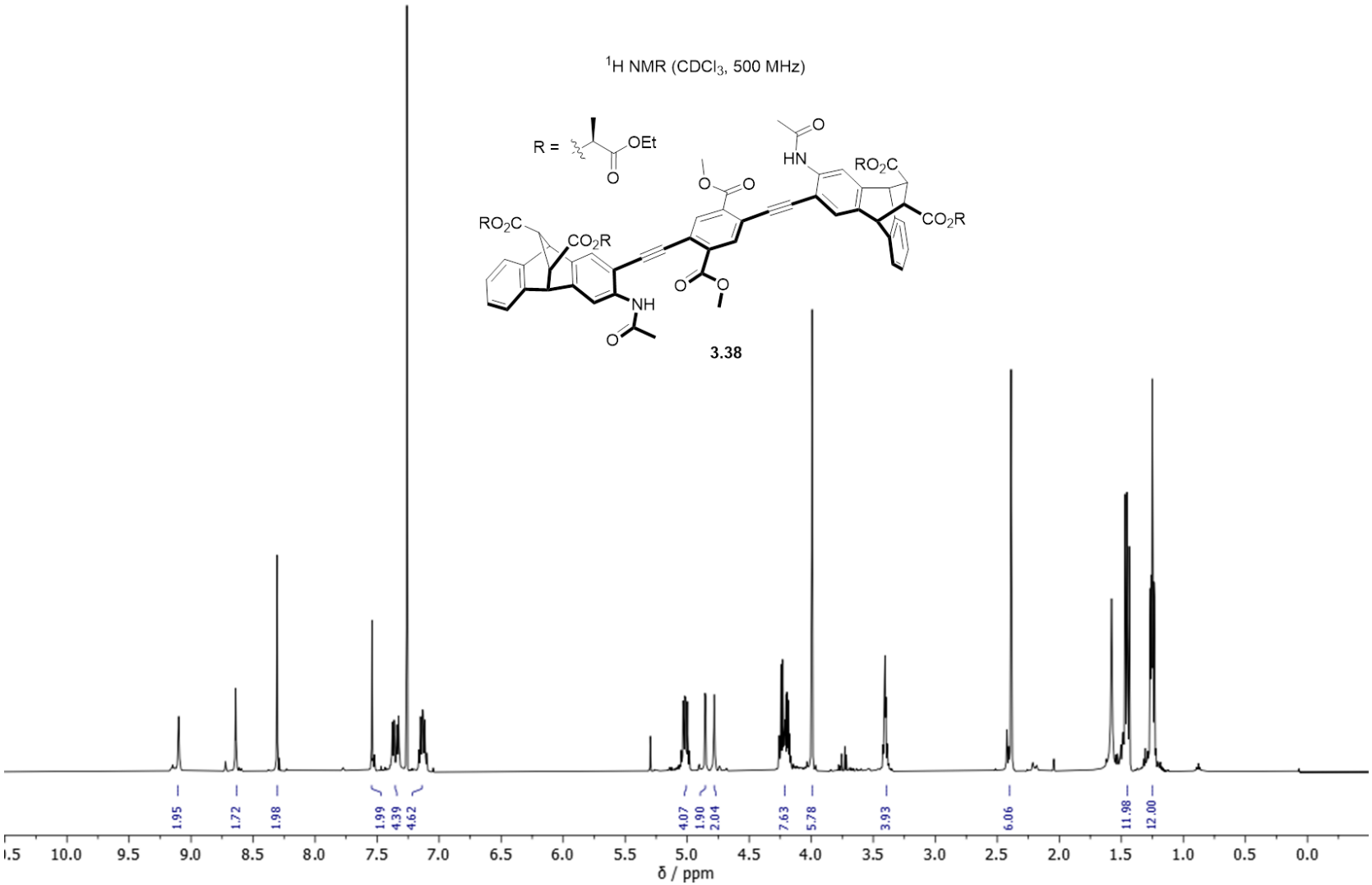
1H NMR (CDCl3, 500 MHz)
R =
OEt
O
HN
O
RO2C
CO2R
O
O
RO2C
CO2R
NH
O
O
O
3.38
1.95
1.72
1.98
1.99
4.39
4.62
4.07
1.90
2.04
7.63
5.78
3.93
6.06
11.98
12.00
10.0
9.5
9.0
8.5
8.0
7.5
7.0
6.5
6.0
5.5
5.0
4.5
4.0
3.5
3.0
2.5
2.0
1.5
1.0
0.5
0.0
δ / ppm

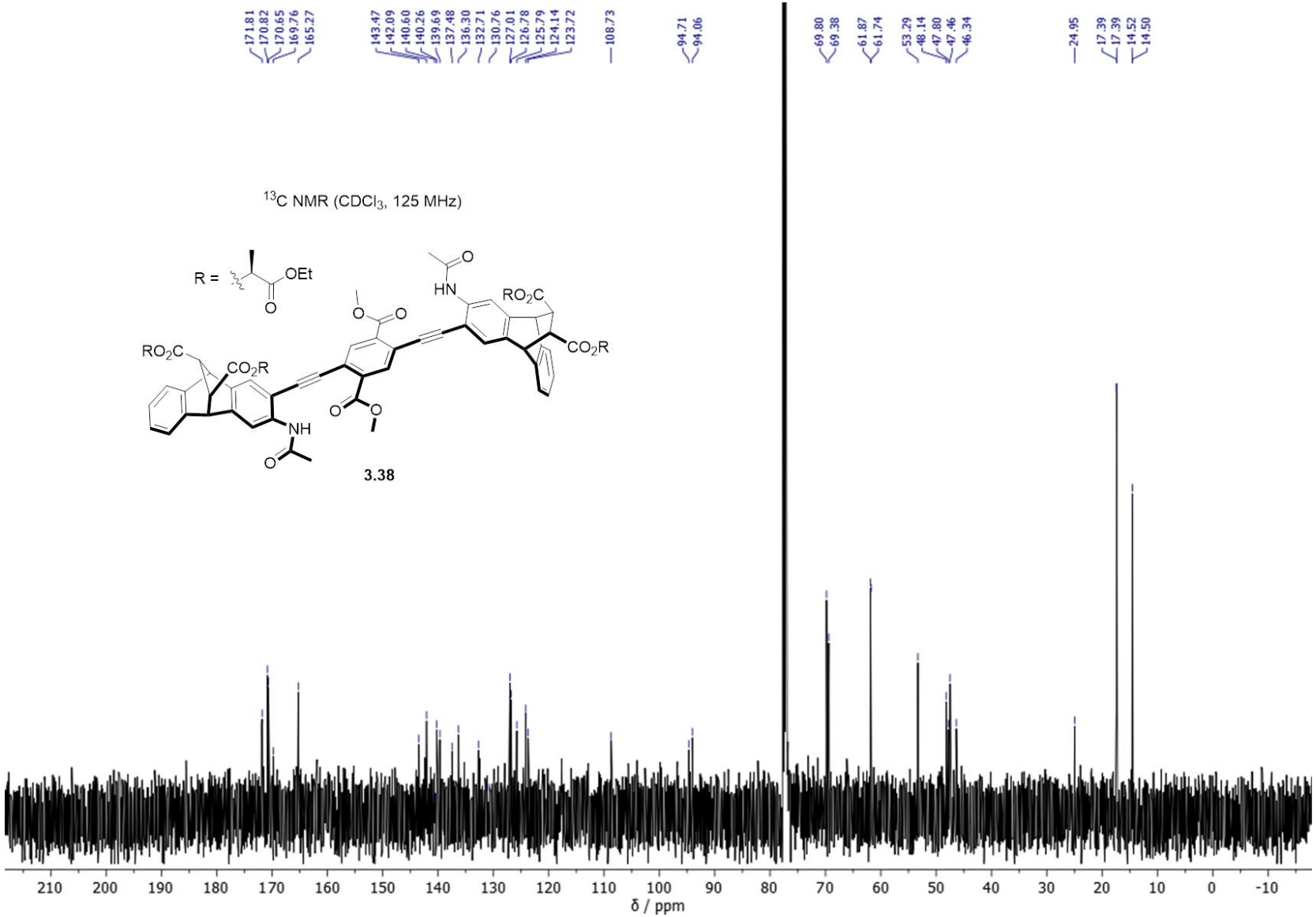
171.81
170.82
170.65
169.76
165.27
143.47
142.09
140.60
140.26
139.69
137.48
136.30
132.71
130.76
127.01
126.78
125.79
124.14
123.72
108.73
94.71
94.06
69.80
69.38
61.87
61.74
53.29
48.14
47.80
47.46
46.34
24.95
17.39
17.39
14.52
14.50
^{13}C NMR ($CDCl_3$, 125 MHz)
R =
OEt
O
HN
O
RO_2C
CO_2R
CO_2R
RO_2C
NH
O
O
O
O
O
3.38
210
200
190
180
170
160
150
140
130
120
110
100
90
80
70
60
50
40
30
20
10
0
-10
δ / ppm

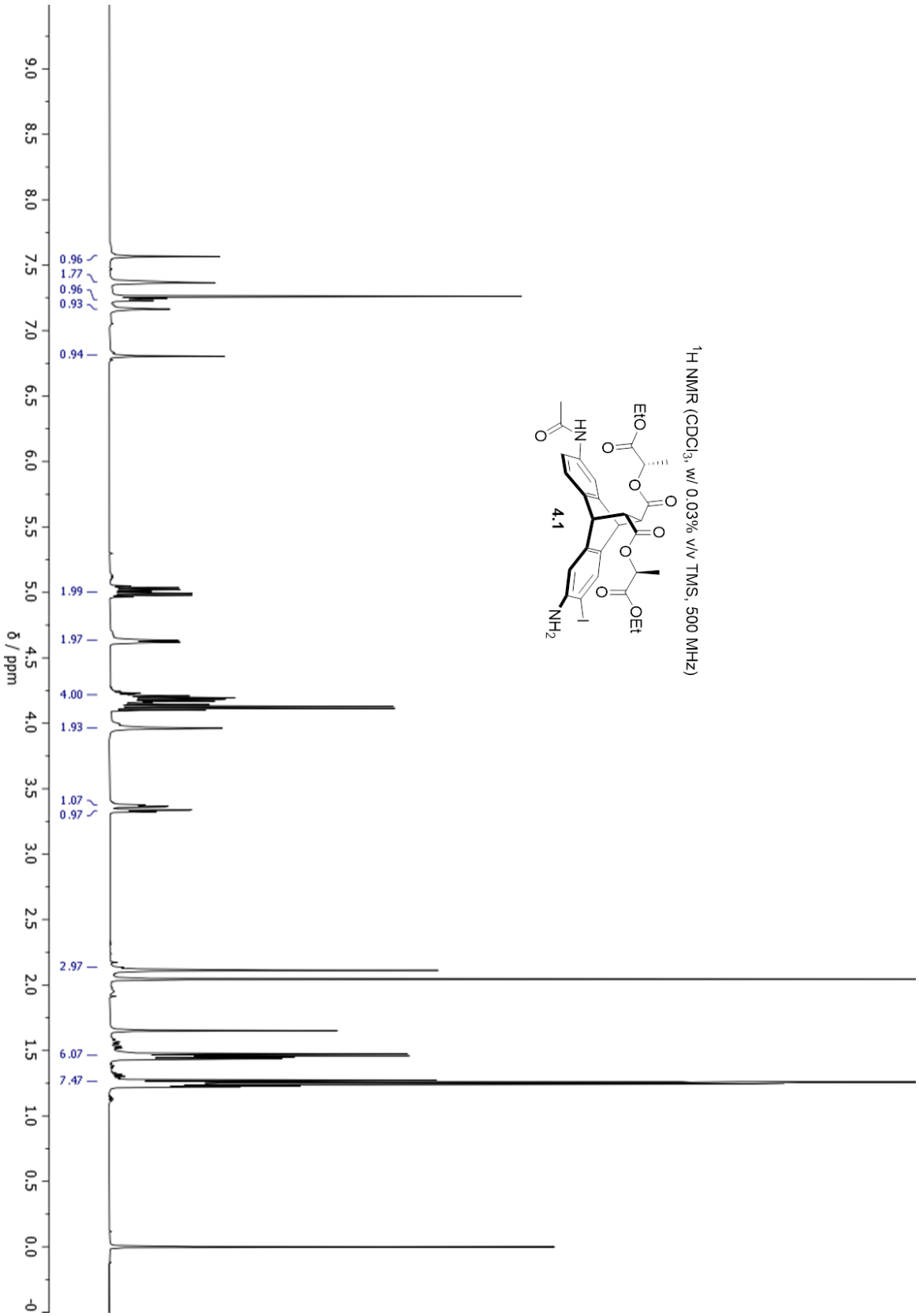
^{1}H NMR ($CDCl_3$, w/ 0.03% v/v TMS, 500 MHz)
4.1
δ / ppm
0.96
1.77
0.96
0.93
0.94
1.99
1.97
4.00
1.93
1.07
0.97
2.97
6.07
7.47

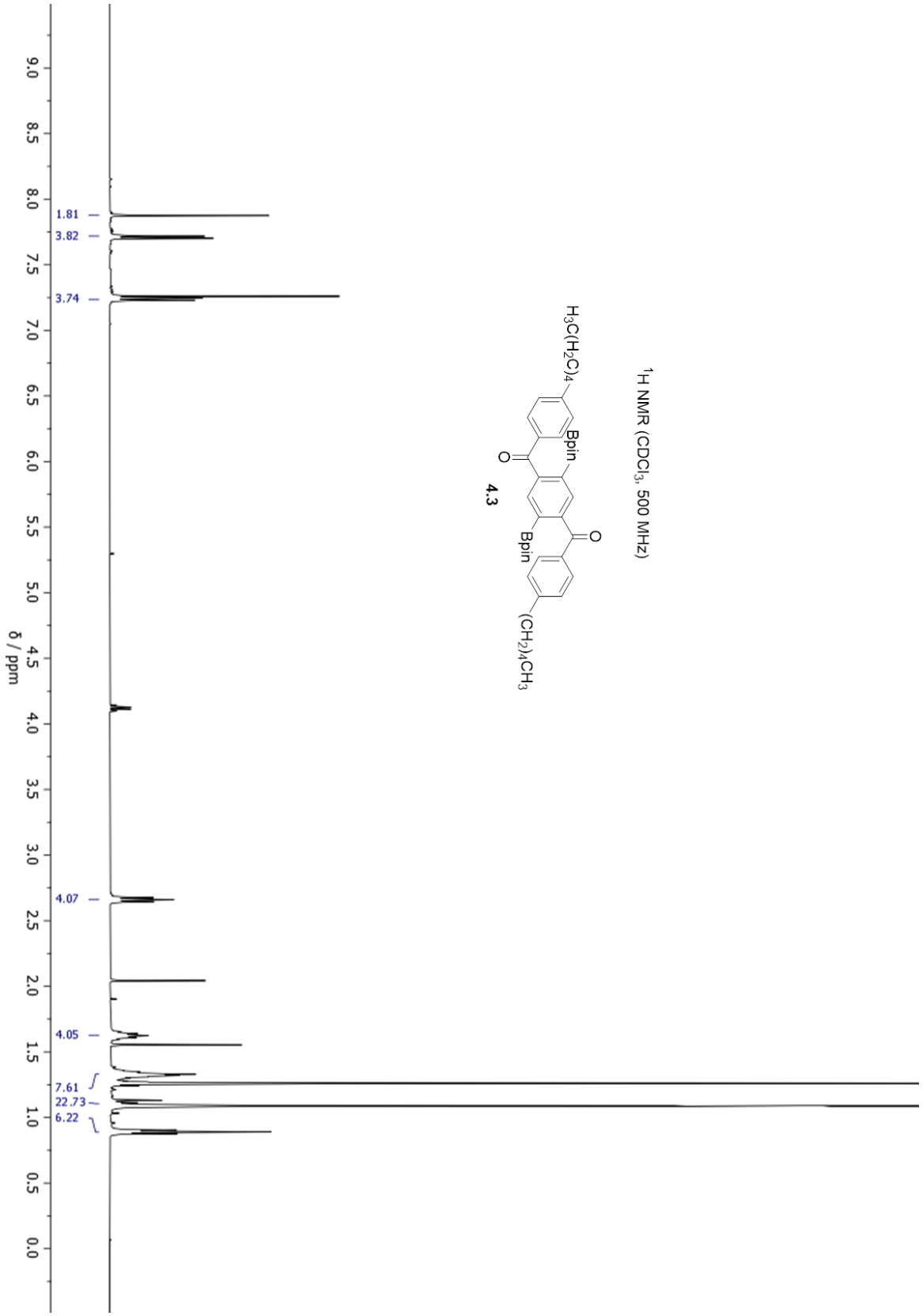
^{1}H NMR ($CDCl_3$, 500 MHz)
$H_3C(H_2C)_4$
Bpin
O
O
Bpin
$(CH_2)_4CH_3$
4.3
δ / ppm
9.0
8.5
8.0
7.5
7.0
6.5
6.0
5.5
5.0
4.5
4.0
3.5
3.0
2.5
2.0
1.5
1.0
0.5
0.0
1.81
3.82
3.74
4.07
4.05
7.61
22.73
6.22

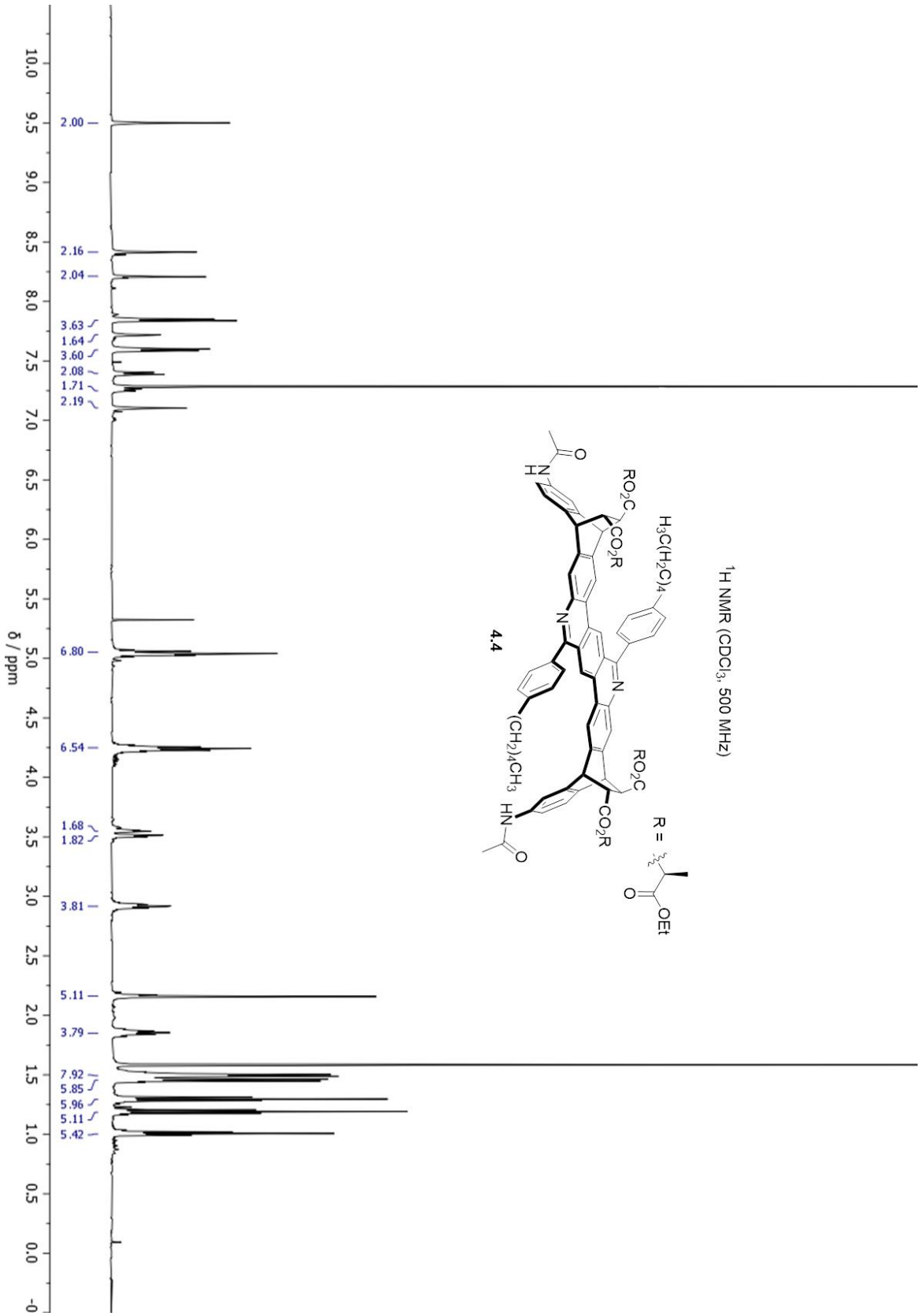
^{1}H NMR (CDCl$_3$, 500 MHz)
4.4
R =
δ / ppm
2.00
2.16
2.04
3.63
1.64
3.60
2.08
1.71
2.19
6.80
6.54
1.68
1.82
3.81
5.11
3.79
7.92
5.85
5.96
5.11
5.42

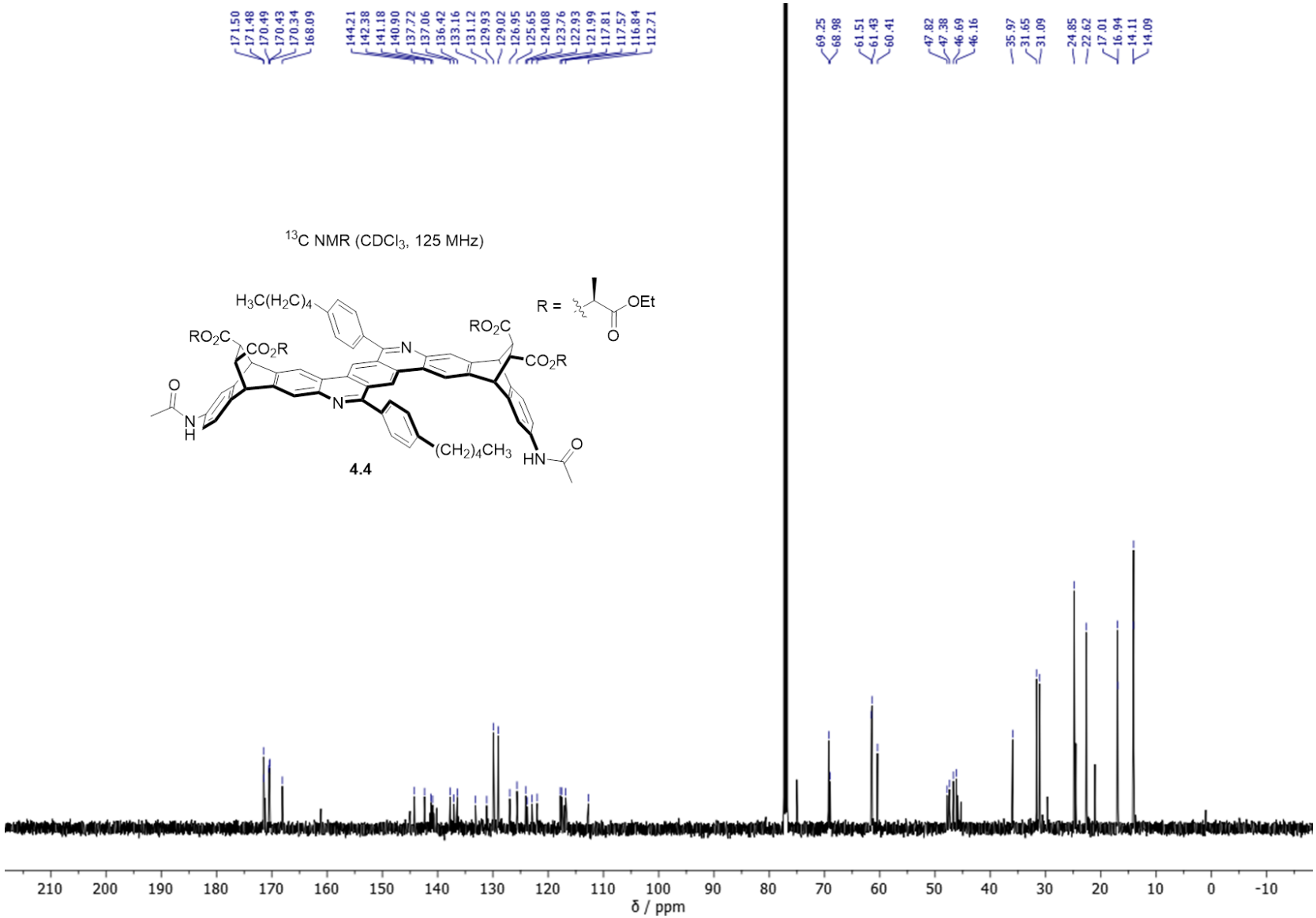

^{13}C NMR ($CDCl_3$, 125 MHz)

4.4

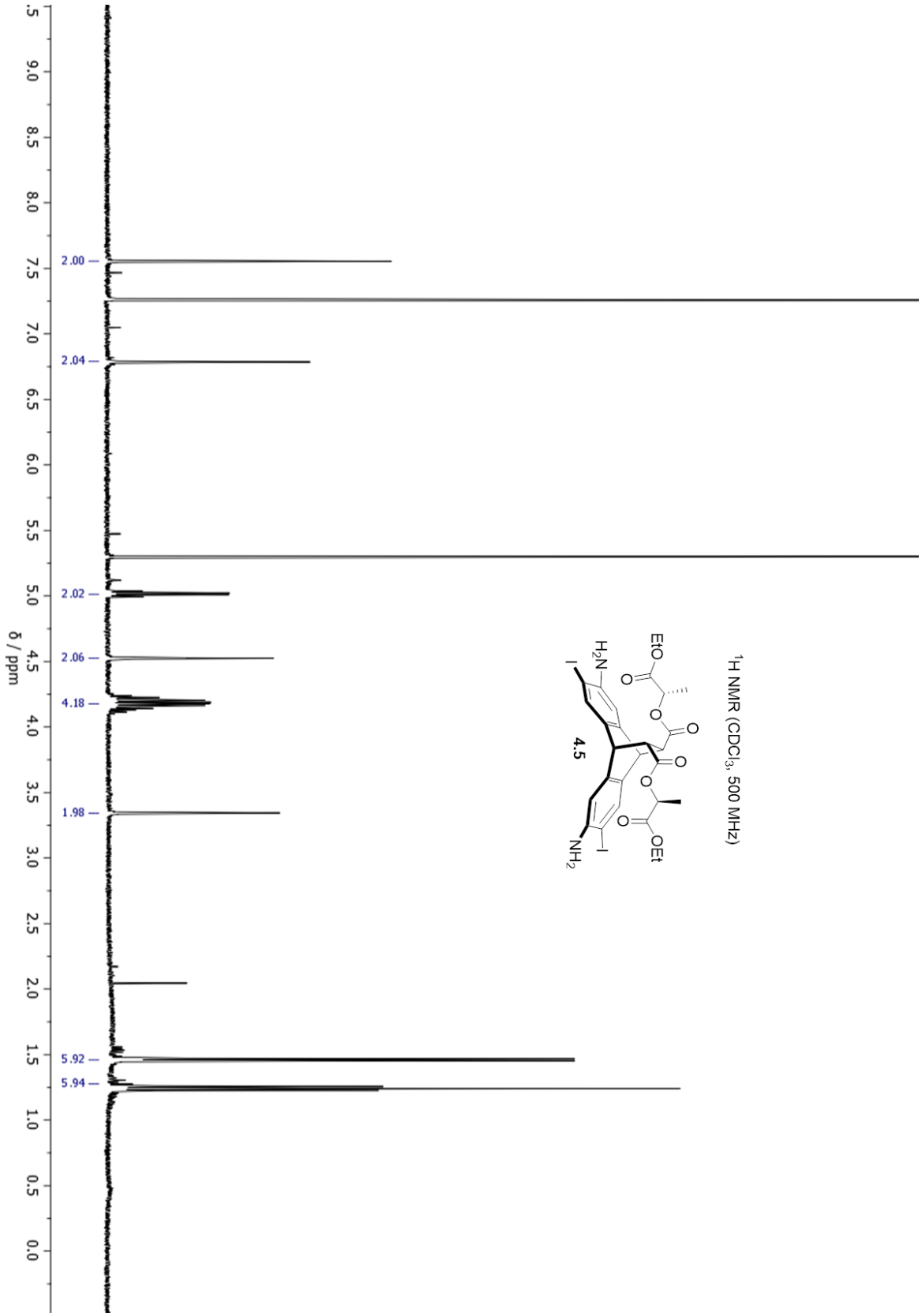
δ / ppm
2.00
2.04
2.02
2.06
4.18
1.98
5.92
5.94
4.5
^{1}H NMR (CDCl$_3$, 500 MHz)

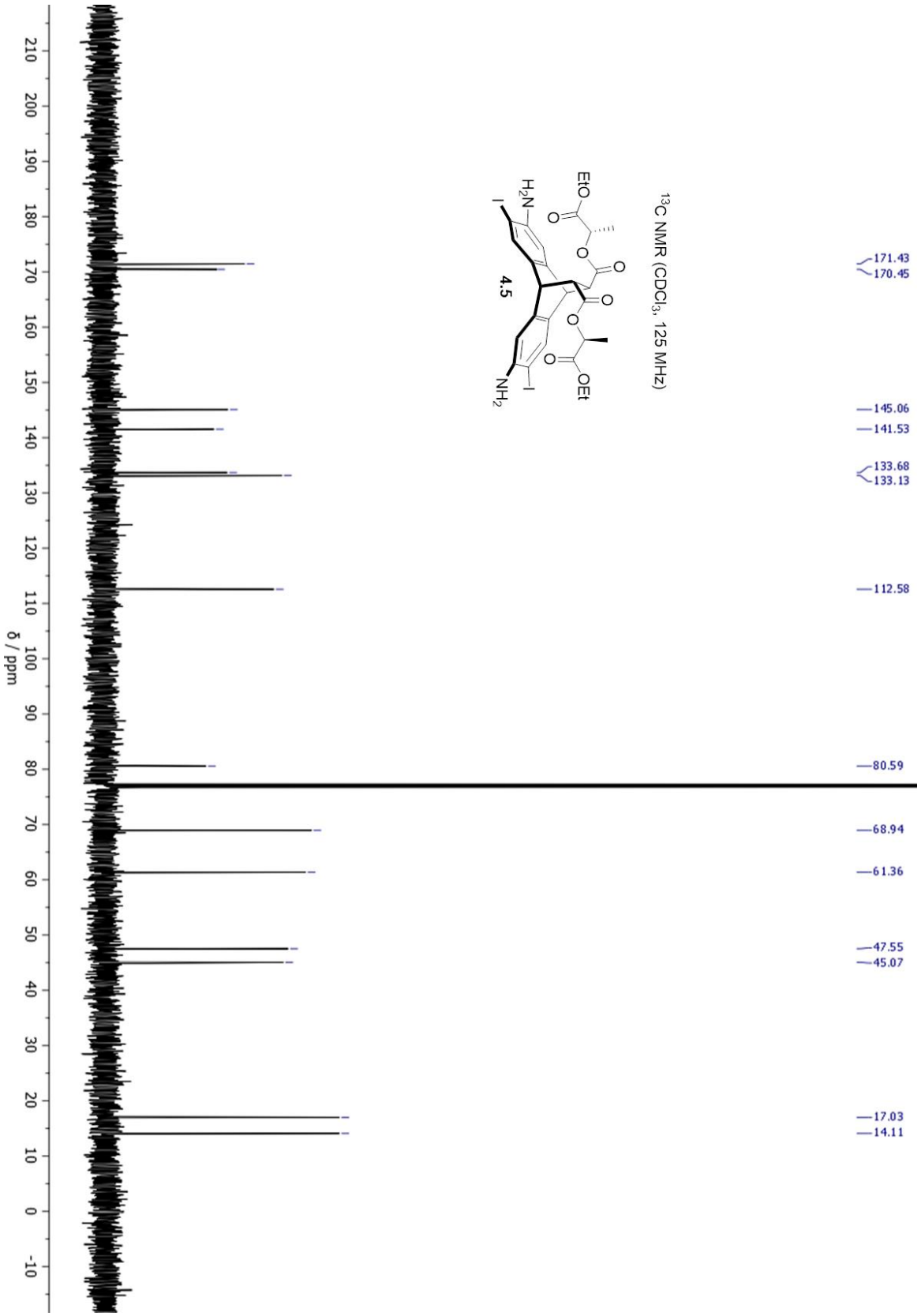
^{13}C NMR (CDCl$_3$, 125 MHz)
4.5
171.43
170.45
145.06
141.53
133.68
133.13
112.58
80.59
68.94
61.36
47.55
45.07
17.03
14.11
δ / ppm

^{1}H NMR (CD_3OD, w/ 0.03% v/v TMS, 500 MHz)

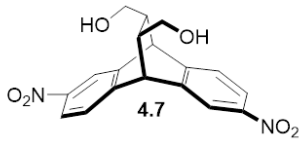

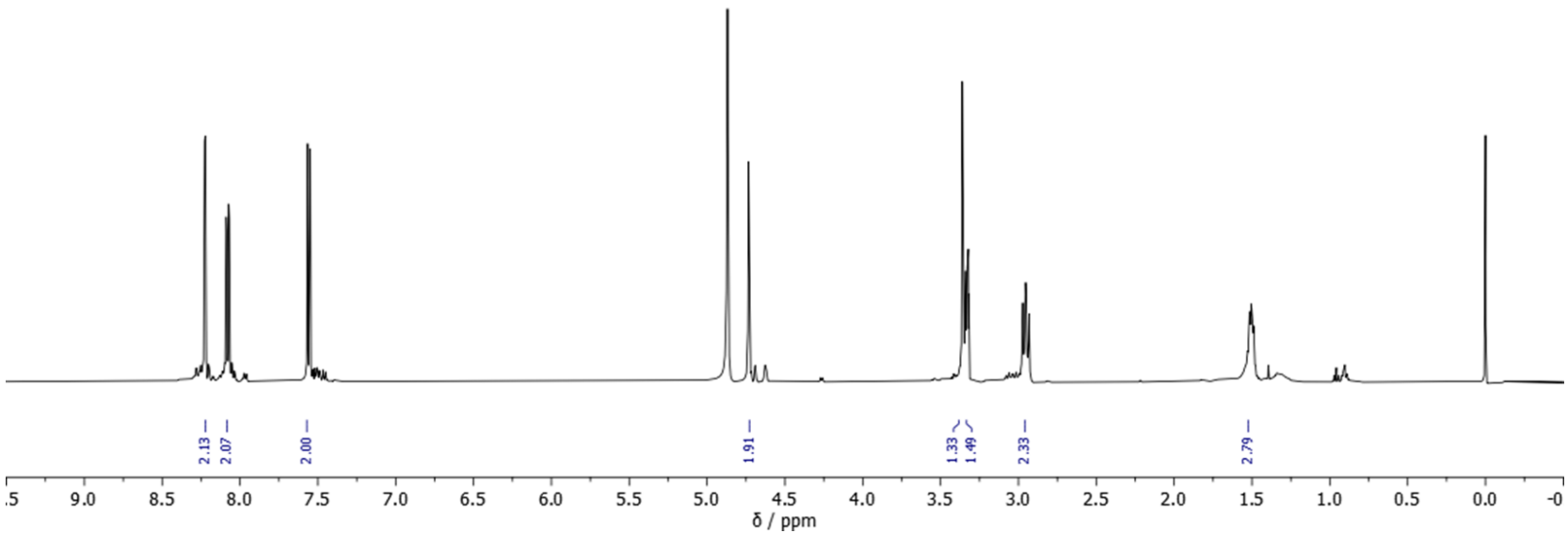

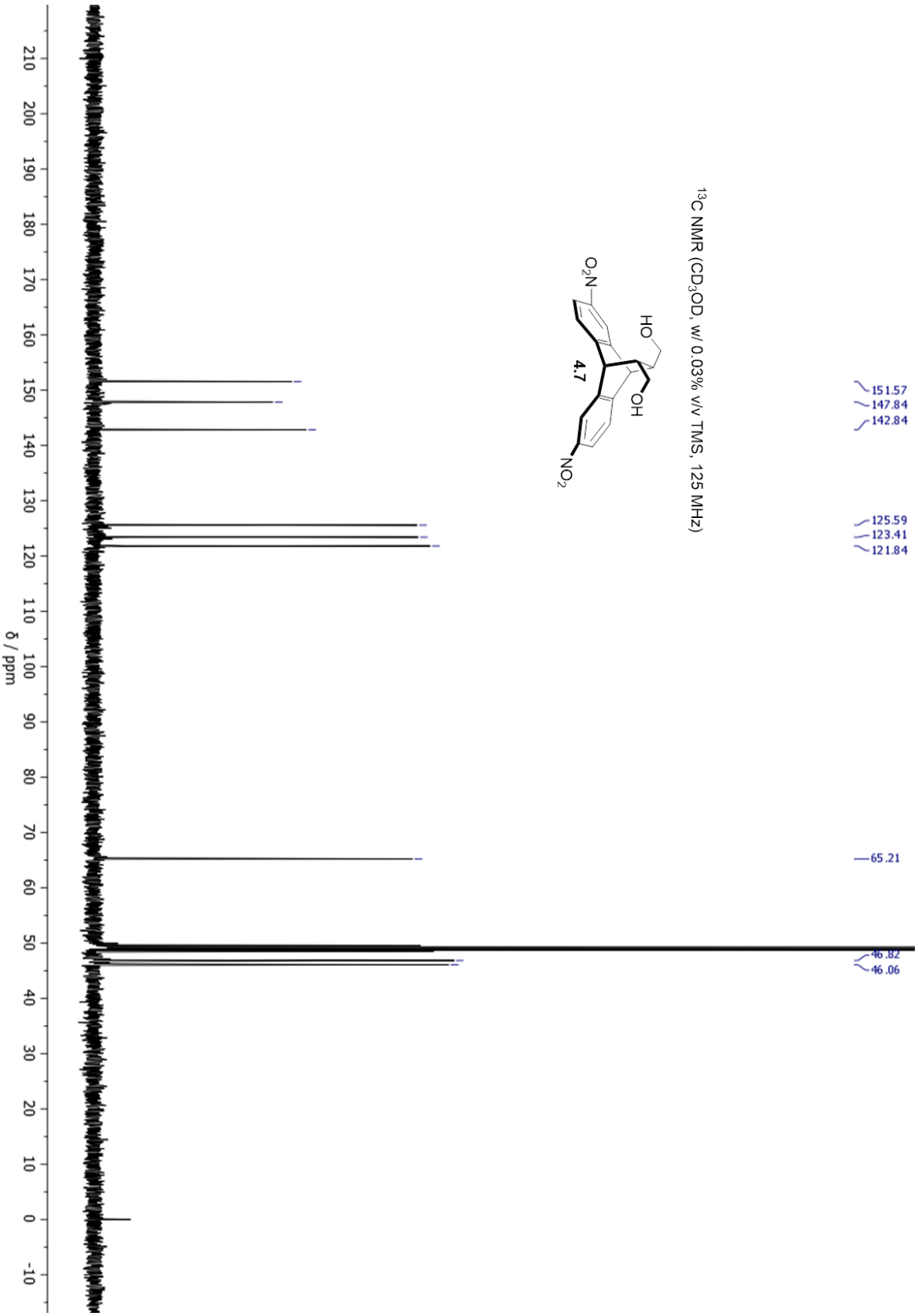
^{13}C NMR (CD_3OD, w/ 0.03% v/v TMS, 125 MHz)
4.7
O_2N
HO
OH
NO_2
151.57
147.84
142.84
125.59
123.41
121.84
65.21
46.82
46.06
δ / ppm

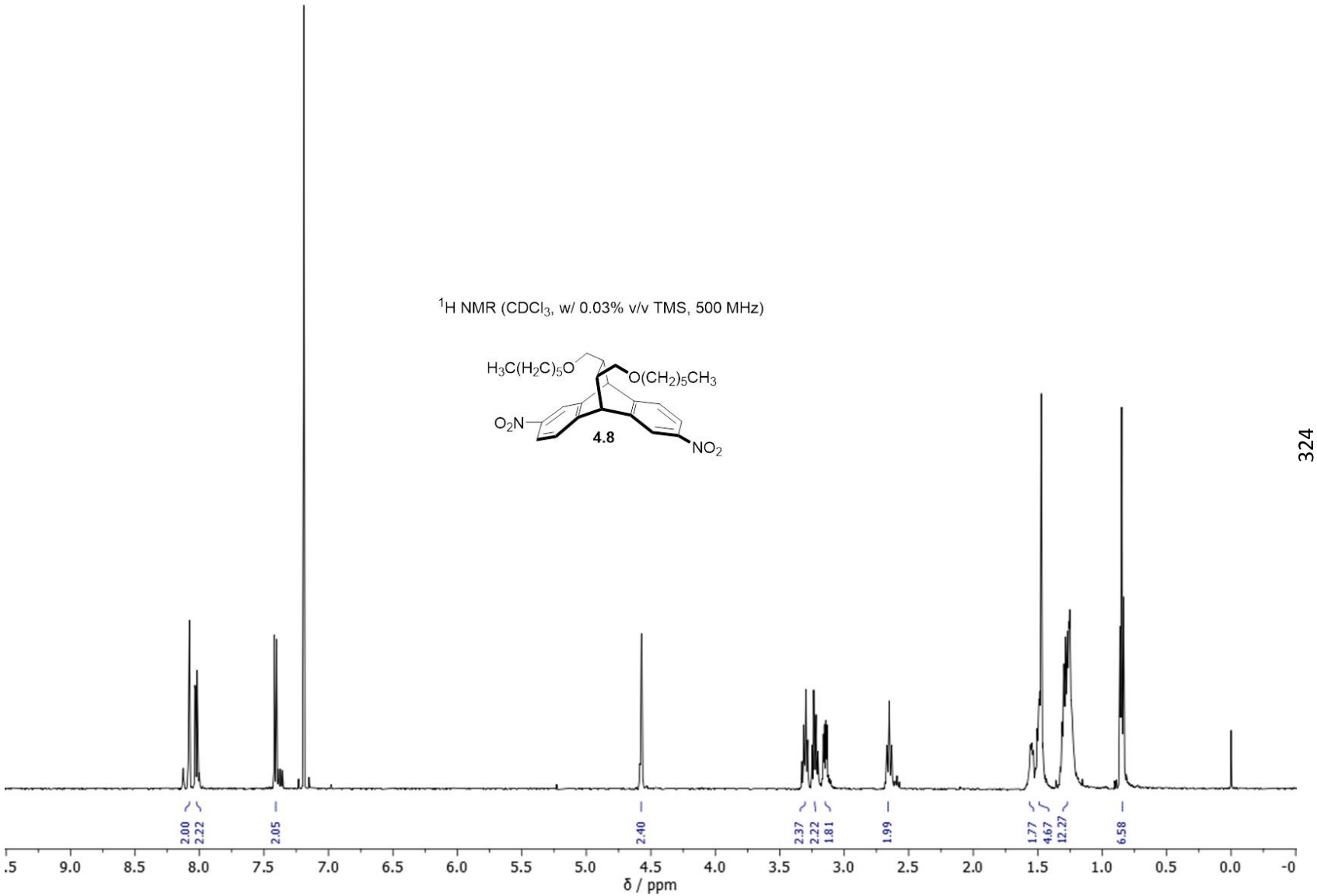
^{1}H NMR ($CDCl_3$, w/ 0.03% v/v TMS, 500 MHz)
$H_3C(H_2C)_5O$
$O(CH_2)_5CH_3$
O_2N
NO_2
4.8
2.00
2.22
2.05
2.40
2.37
2.22
1.81
1.99
1.77
4.67
12.27
6.58
δ / ppm

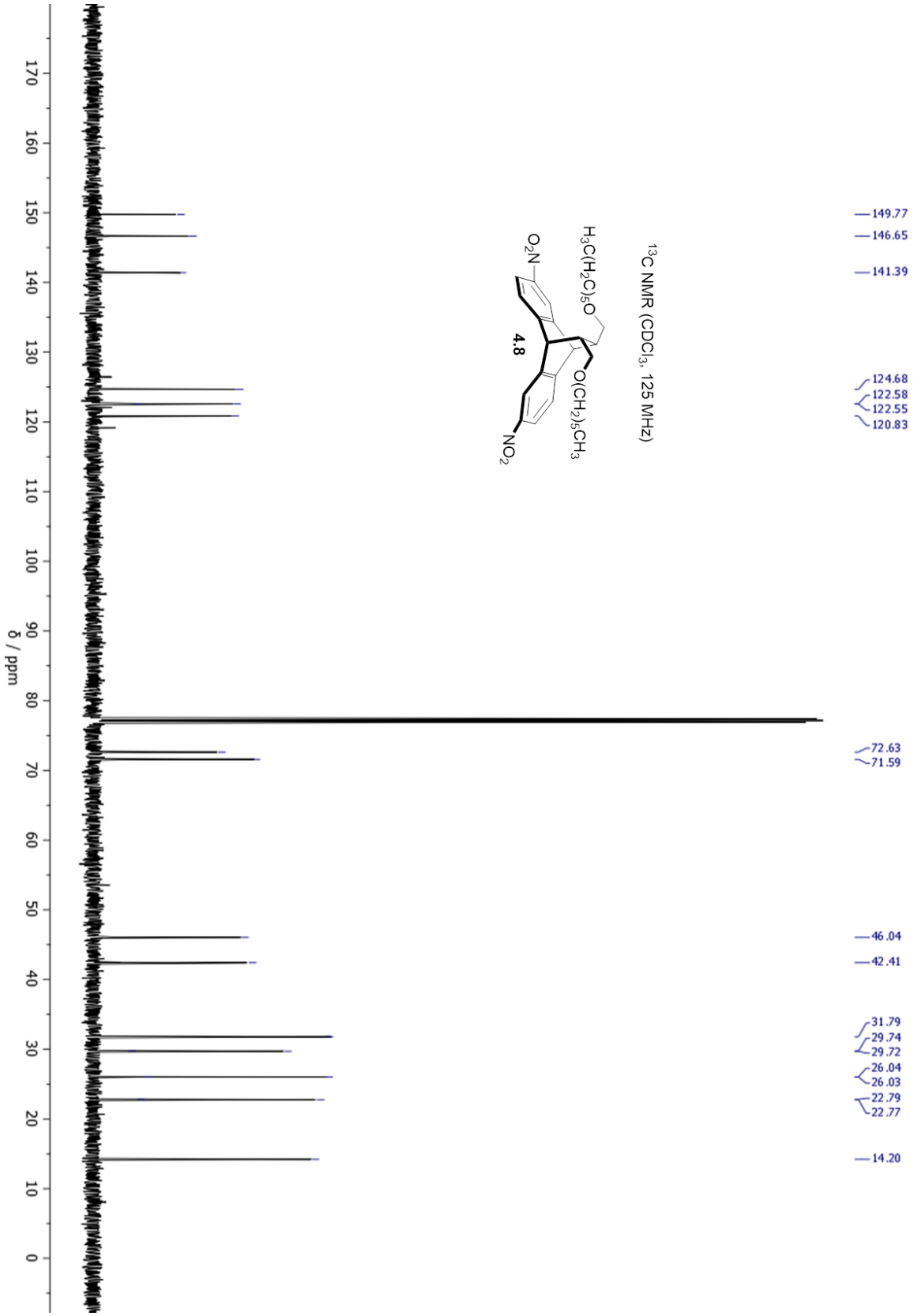
^{13}C NMR ($CDCl_3$, 125 MHz)
$H_3C(H_2C)_5O$
O_2N
4.8
$O(CH_2)_5CH_3$
NO_2
δ / ppm
149.77
146.65
141.39
124.68
122.58
122.55
120.83
72.63
71.59
46.04
42.41
31.79
29.74
29.72
26.04
26.03
22.79
22.77
14.20

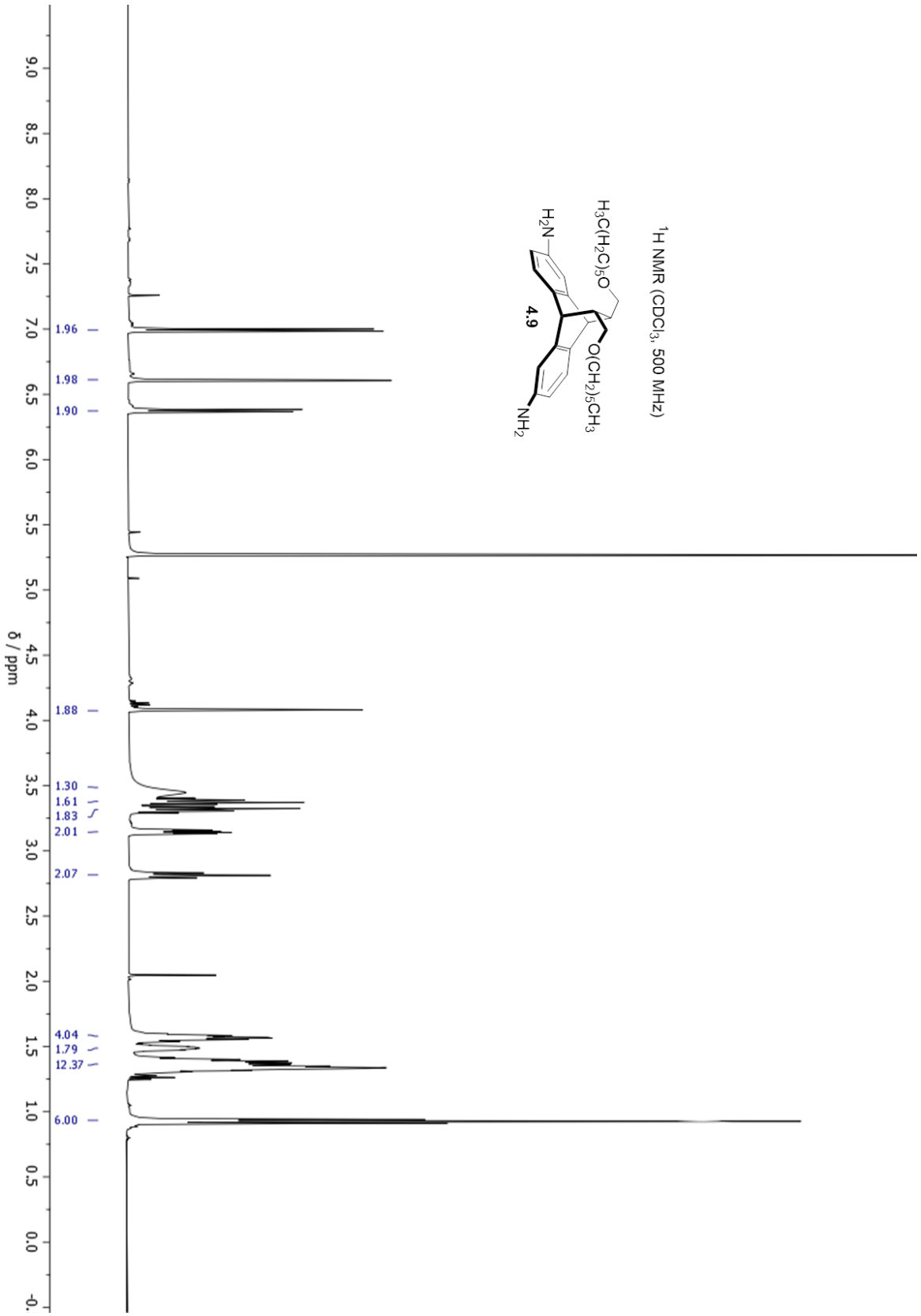
^{1}H NMR (CDCl$_3$, 500 MHz)
H$_2$N
H$_3$C(H$_2$C)$_5$O
O(CH$_2$)$_5$CH$_3$
NH$_2$
4.9
δ / ppm
9.0
8.5
8.0
7.5
7.0
6.5
6.0
5.5
5.0
4.5
4.0
3.5
3.0
2.5
2.0
1.5
1.0
0.5
0.0
-0.
1.96
1.98
1.90
1.88
1.30
1.61
1.83
2.01
2.07
4.04
1.79
12.37
6.00

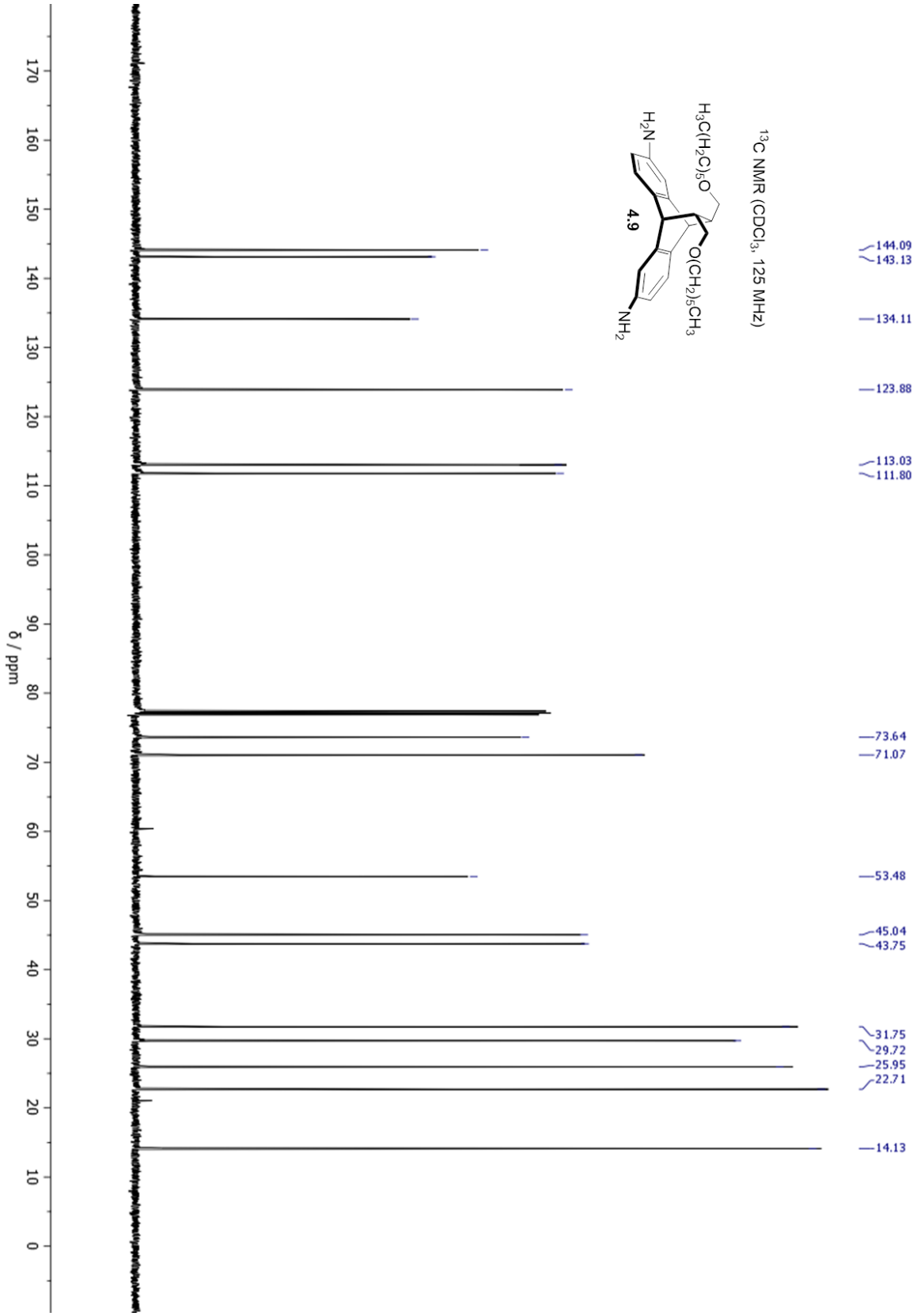
^{13}C NMR ($CDCl_3$, 125 MHz)
$H_3C(H_2C)_5O$
H_2N
4.9
$O(CH_2)_5CH_3$
NH_2
144.09
143.13
134.11
123.88
113.03
111.80
73.64
71.07
53.48
45.04
43.75
31.75
29.72
25.95
22.71
14.13
δ / ppm

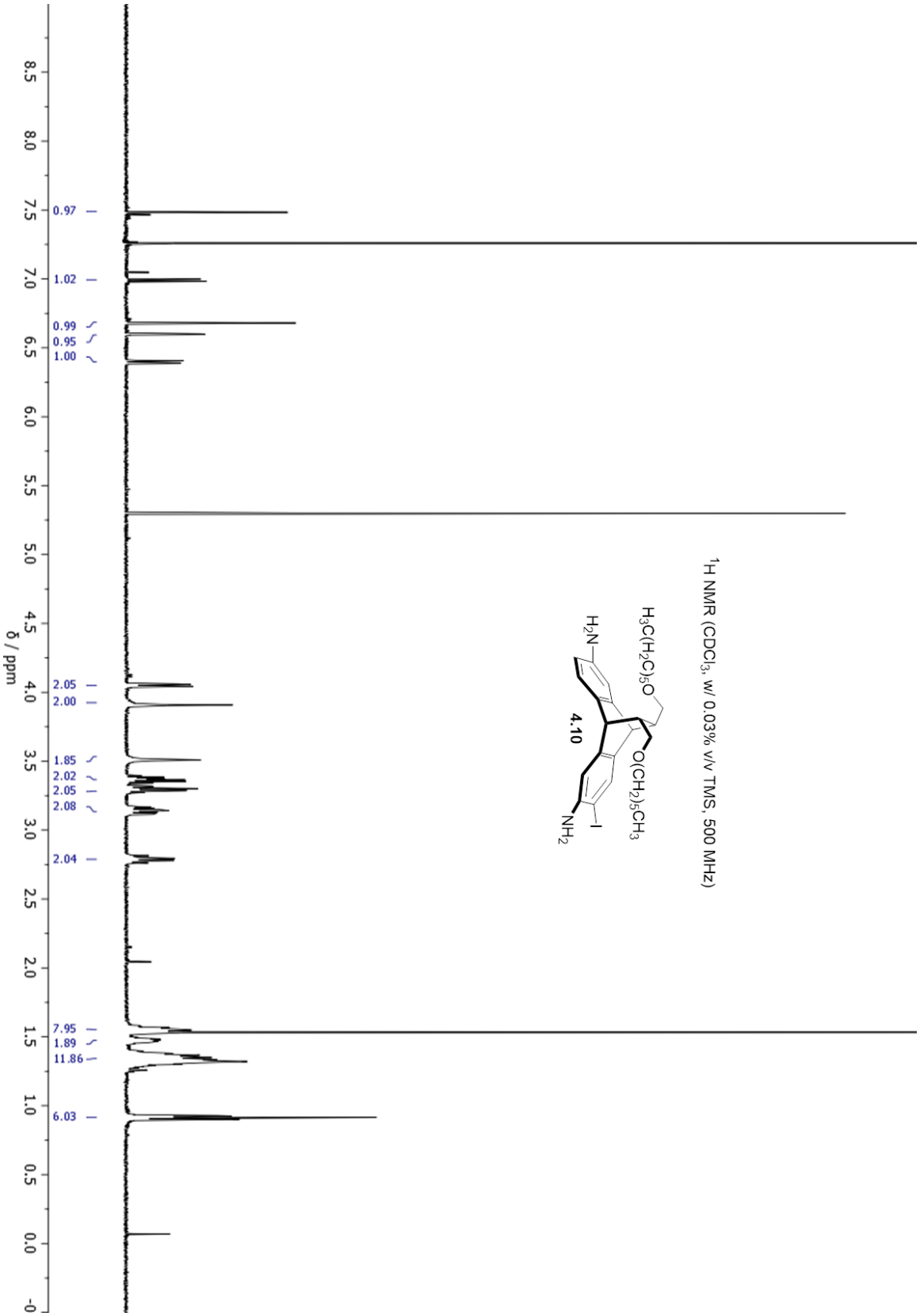
^{1}H NMR ($CDCl_3$, w/ 0.03% v/v TMS, 500 MHz)
$H_3C(H_2C)_5O$
$O(CH_2)_5CH_3$
H_2N
NH_2
I
4.10
δ / ppm
8.5
8.0
7.5
7.0
6.5
6.0
5.5
5.0
4.5
4.0
3.5
3.0
2.5
2.0
1.5
1.0
0.5
0.0
-0
0.97
1.02
0.99
0.95
1.00
2.05
2.00
1.85
2.02
2.05
2.08
2.04
7.95
1.89
11.86
6.03

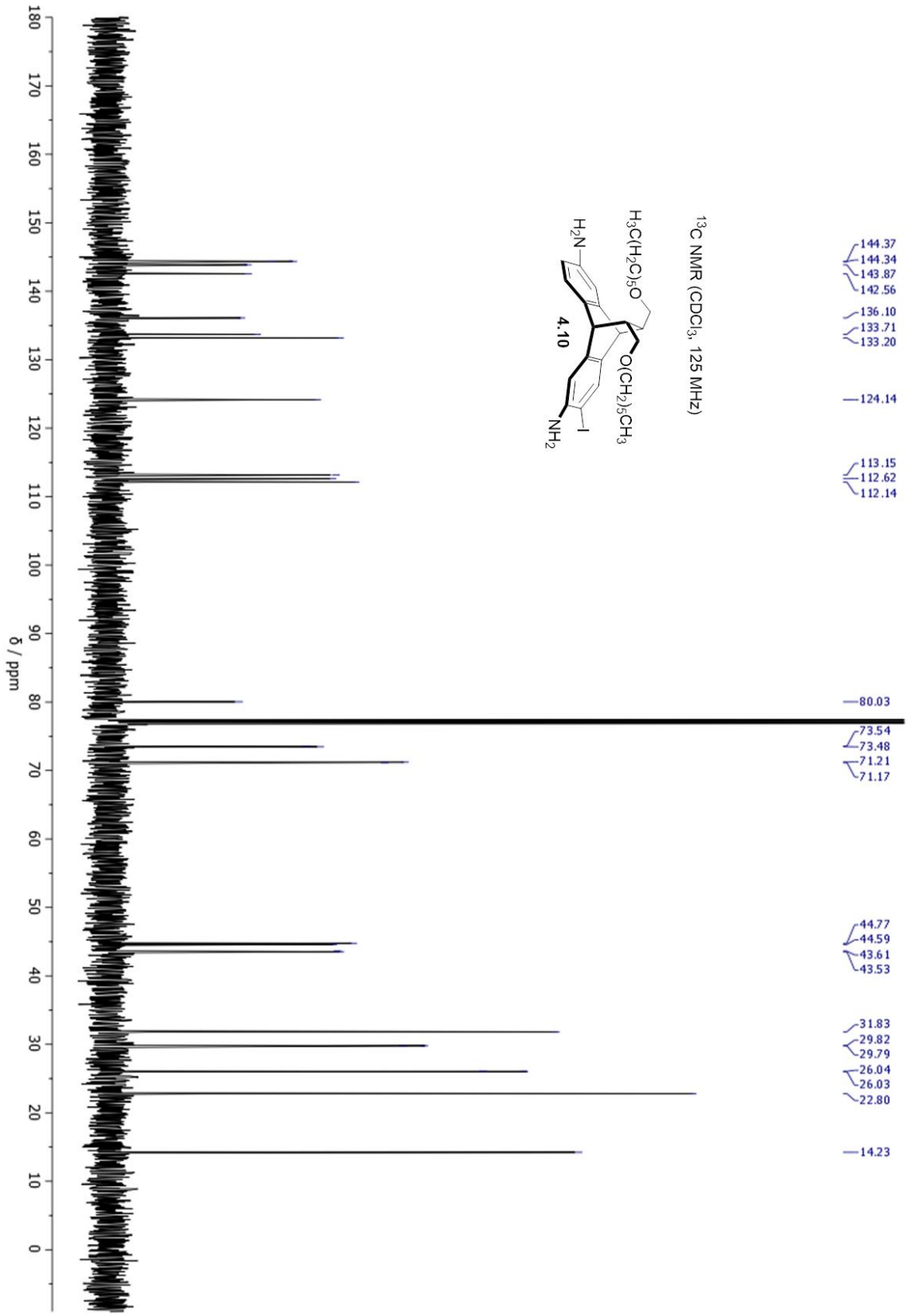
^{13}C NMR (CDCl$_3$, 125 MHz)
4.10
H$_2$N
H$_3$C(H$_2$C)$_5$O
O(CH$_2$)$_5$CH$_3$
I
NH$_2$
144.37
144.34
143.87
142.56
136.10
133.71
133.20
124.14
113.15
112.62
112.14
80.03
73.54
73.48
71.21
71.17
44.77
44.59
43.61
43.53
31.83
29.82
29.79
26.04
26.03
22.80
14.23
δ / ppm

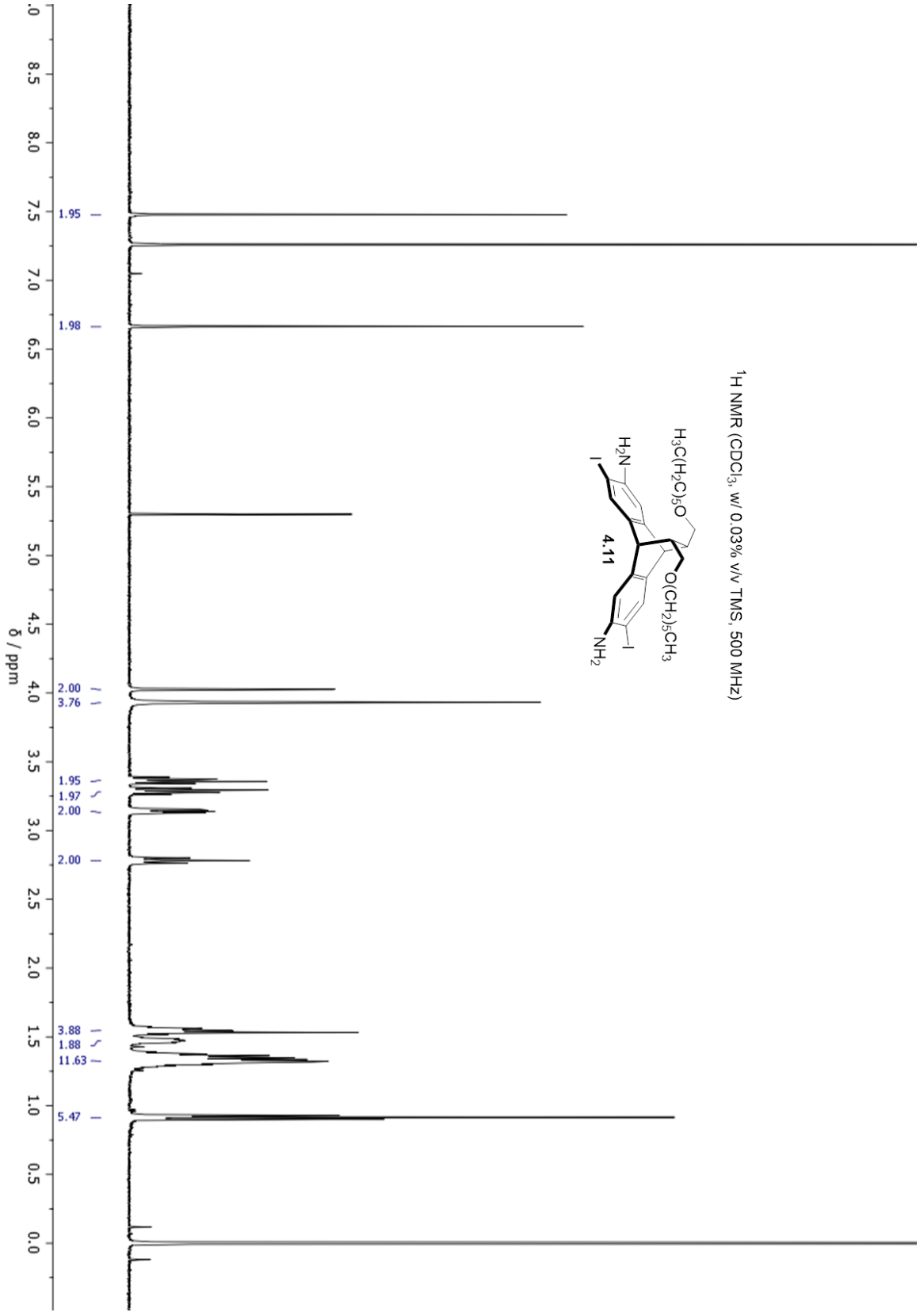
^{1}H NMR ($CDCl_3$, w/ 0.03% v/v TMS, 500 MHz)
$H_3C(H_2C)_5O$
H_2N
I
4.11
$O(CH_2)_5CH_3$
I
NH_2
δ / ppm
1.95
1.98
2.00
3.76
1.95
1.97
2.00
2.00
3.88
1.88
11.63
5.47

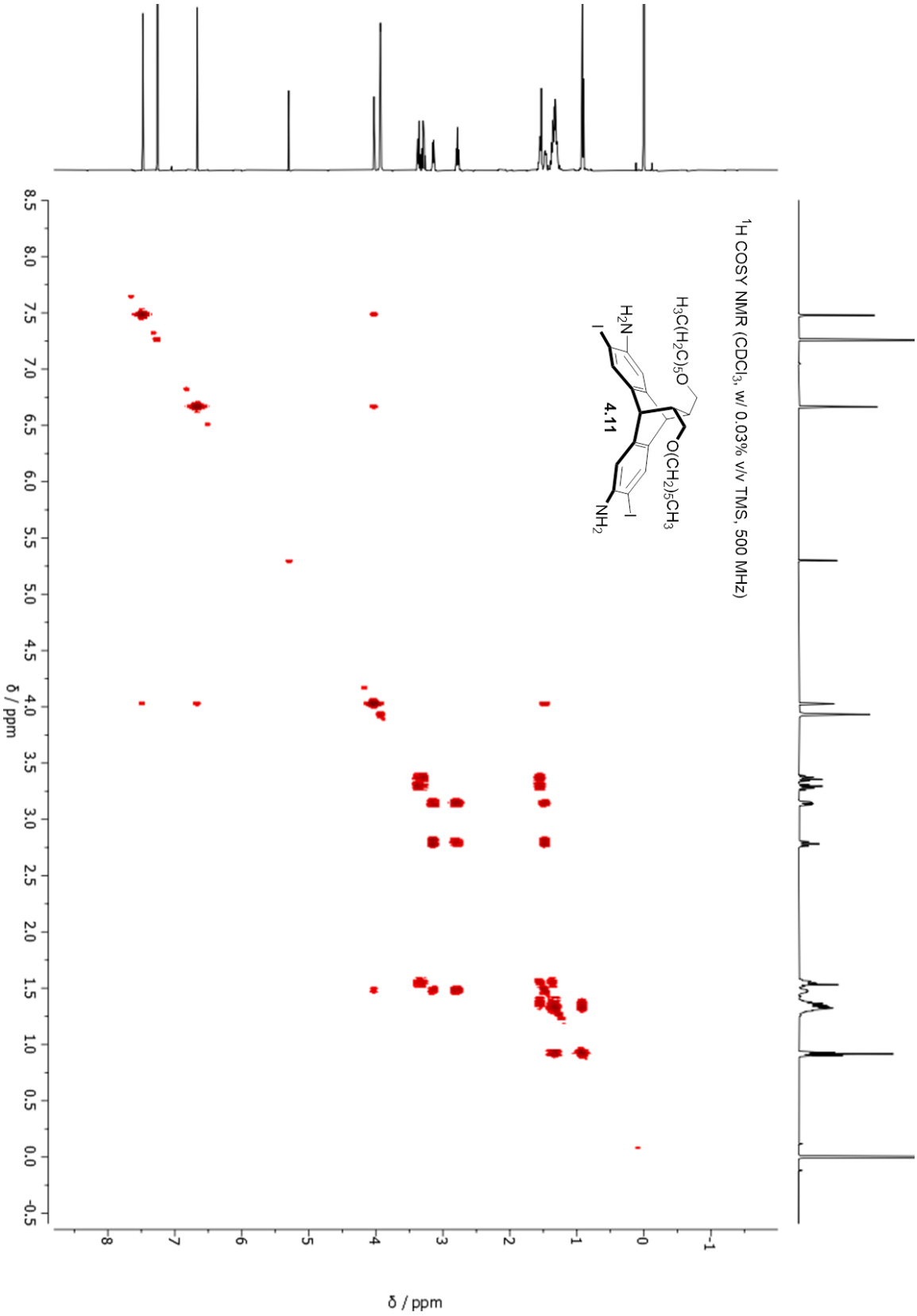
^{1}H COSY NMR (CDCl$_3$, w/ 0.03% v/v TMS, 500 MHz)
H$_3$C(H$_2$C)$_5$O
O(CH$_2$)$_5$CH$_3$
H$_2$N
NH$_2$
I
I
4.11
δ / ppm
δ / ppm

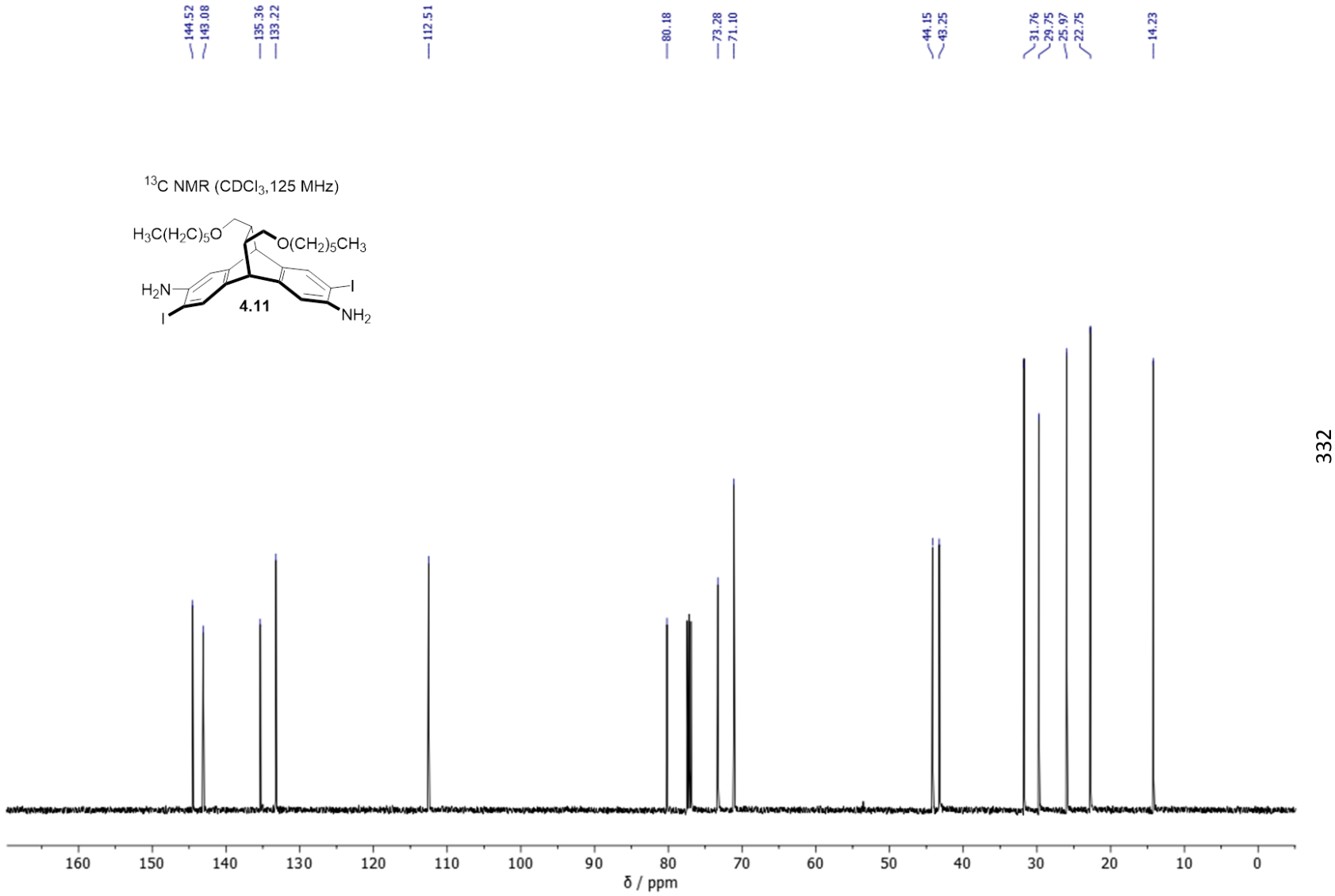
144.52
143.08
135.36
133.22
112.51
80.18
73.28
71.10
44.15
43.25
31.76
29.75
25.97
22.75
14.23
^{13}C NMR ($CDCl_3$,125 MHz)
$H_3C(H_2C)_5O$
$O(CH_2)_5CH_3$
H_2N
I
I
NH_2
4.11
160
150
140
130
120
110
100
90
80
70
60
50
40
30
20
10
0
δ / ppm

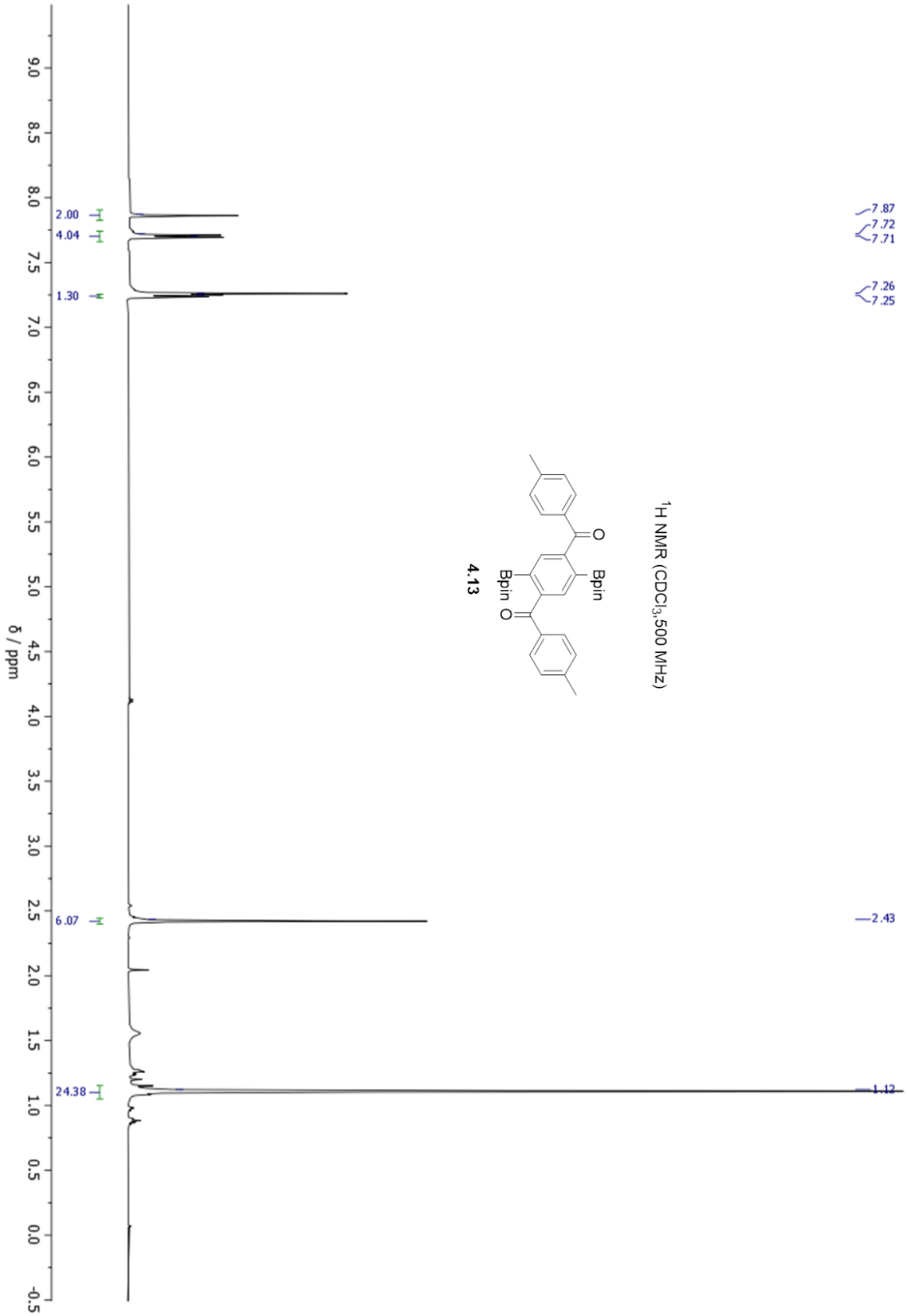

^{1}H NMR (CDCl$_3$,500 MHz)

4.13

^{13}C NMR ($CDCl_3$, 125 MHz)

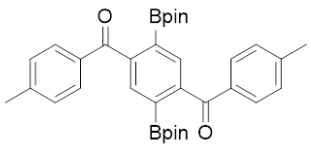

4.13

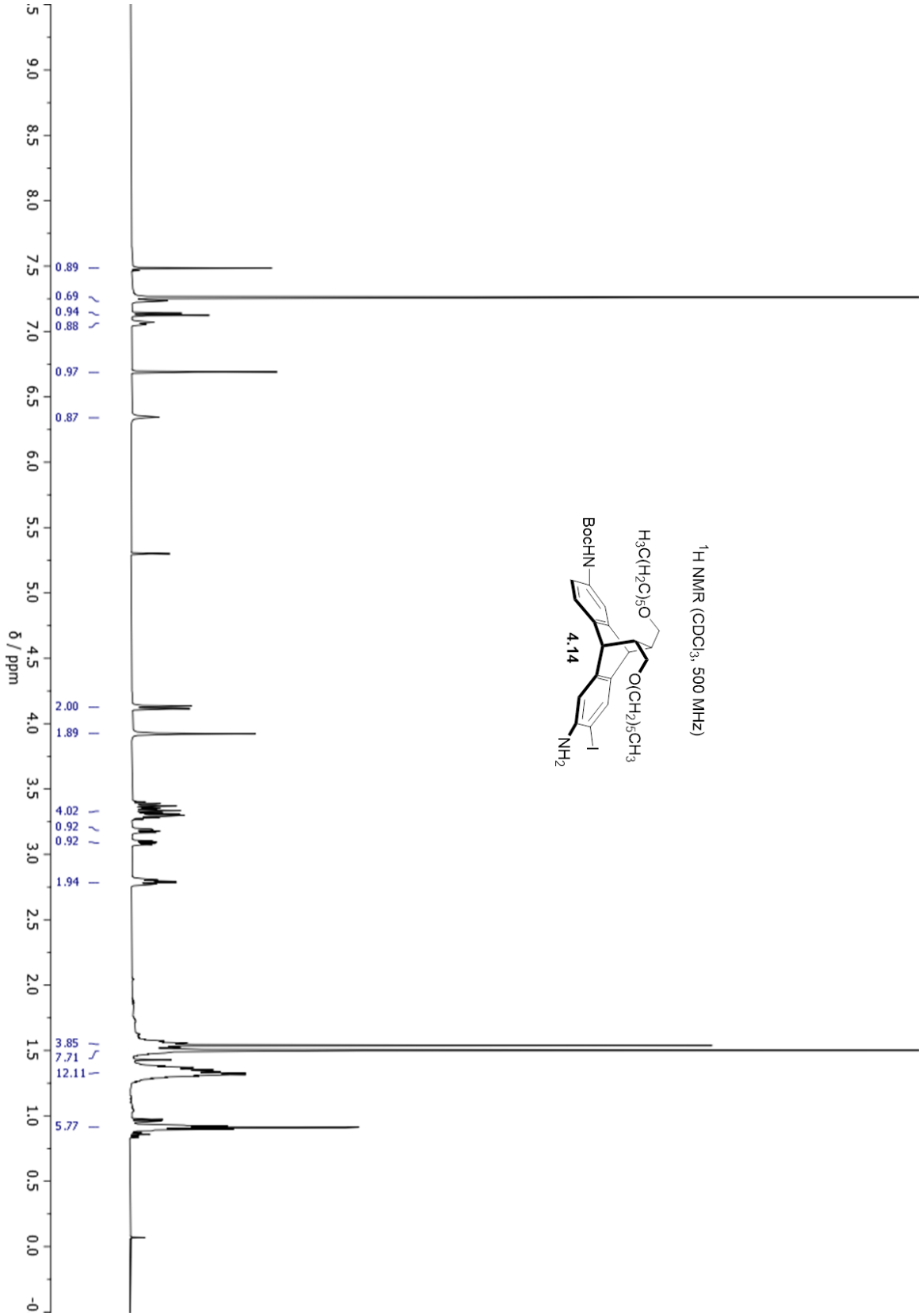
^{1}H NMR (CDCl$_3$, 500 MHz)
BocHN
H$_3$C(H$_2$C)$_5$O
O(CH$_2$)$_5$CH$_3$
I
NH$_2$
4.14
δ / ppm
0.89
0.69
0.94
0.88
0.97
0.87
2.00
1.89
4.02
0.92
0.92
1.94
3.85
7.71
12.11
5.77

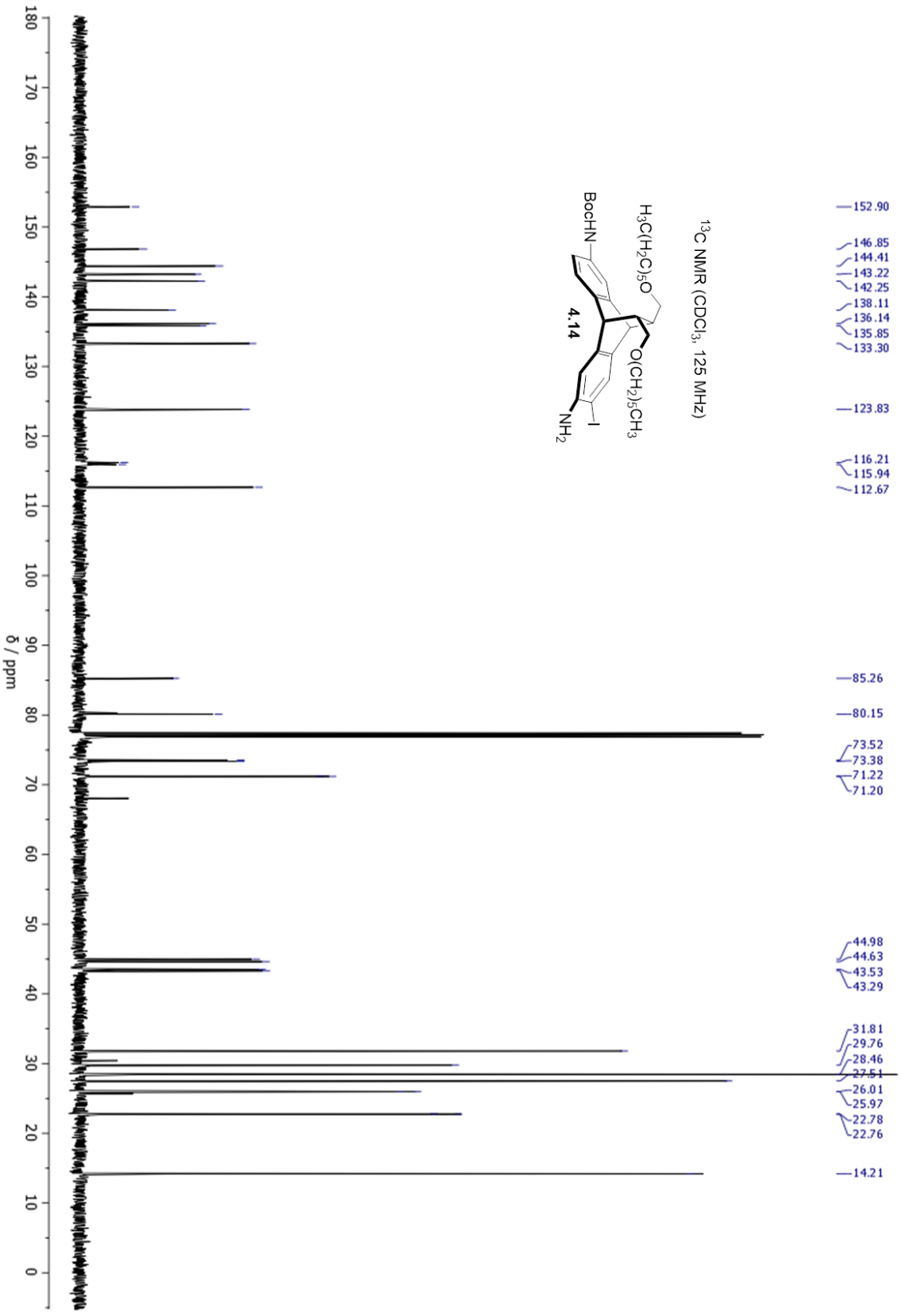
^{13}C NMR (CDCl$_3$, 125 MHz)
BocHN
H$_3$C(H$_2$C)$_5$O
O(CH$_2$)$_5$CH$_3$
NH$_2$
I
4.14
δ / ppm
152.90
146.85
144.41
143.22
142.25
138.11
136.14
135.85
133.30
123.83
116.21
115.94
112.67
85.26
80.15
73.52
73.38
71.22
71.20
44.98
44.63
43.53
43.29
31.81
29.76
28.46
27.51
26.01
25.97
22.78
22.76
14.21

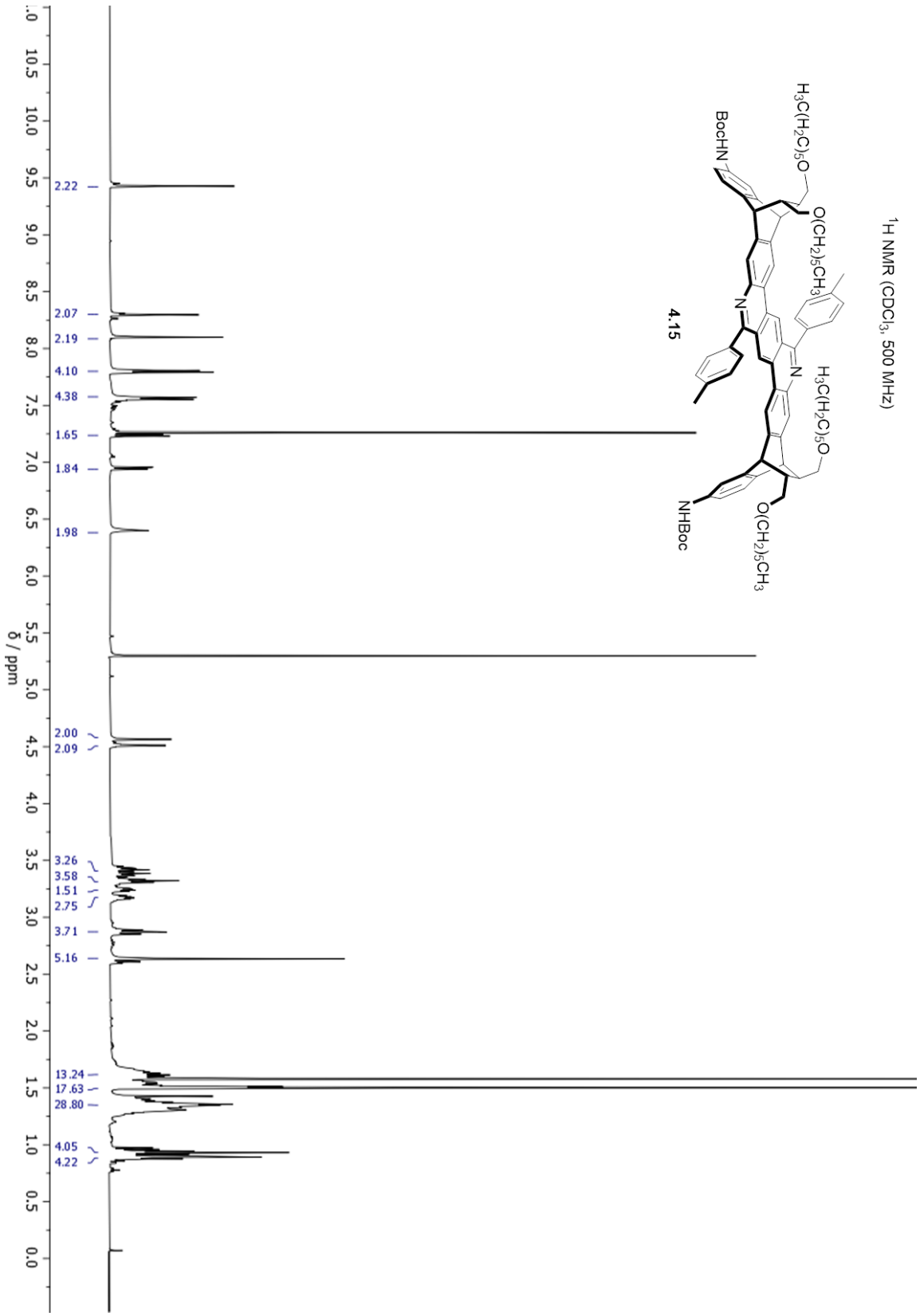
^{1}H NMR (CDCl$_3$, 500 MHz)
4.15
BocHN
NHBoc
H$_3$C(H$_2$C)$_5$O
O(CH$_2$)$_5$CH$_3$
δ / ppm
2.22
2.07
2.19
4.10
4.38
1.65
1.84
1.98
2.00
2.09
3.26
3.58
1.51
2.75
3.71
5.16
13.24
17.63
28.80
4.05
4.22

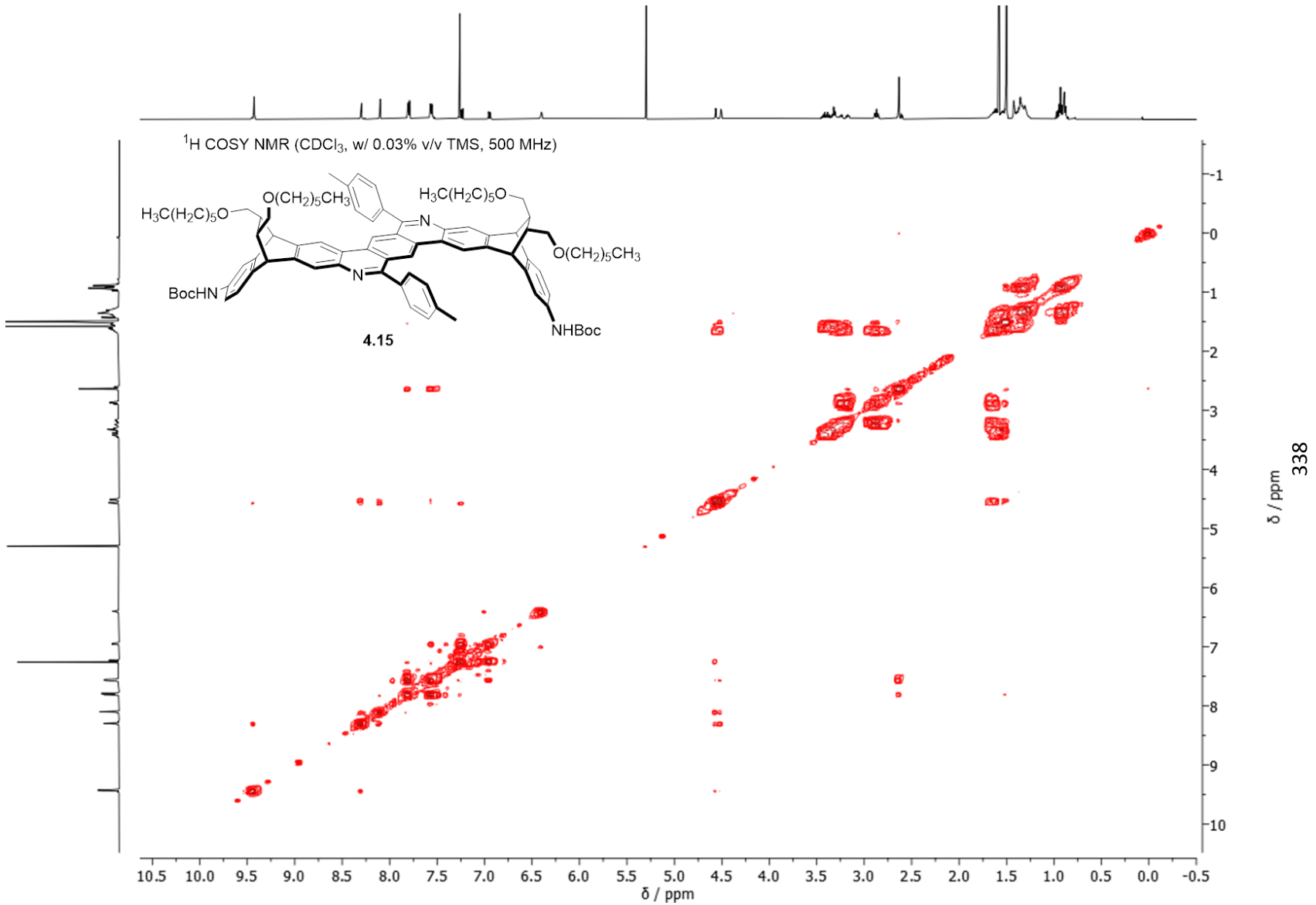
^{1}H COSY NMR ($CDCl_3$, w/ 0.03% v/v TMS, 500 MHz)
$H_3C(H_2C)_5O$
$O(CH_2)_5CH_3$
$H_3C(H_2C)_5O$
N
N
$O(CH_2)_5CH_3$
BocHN
NHBoc
4.15
δ / ppm
δ / ppm
338

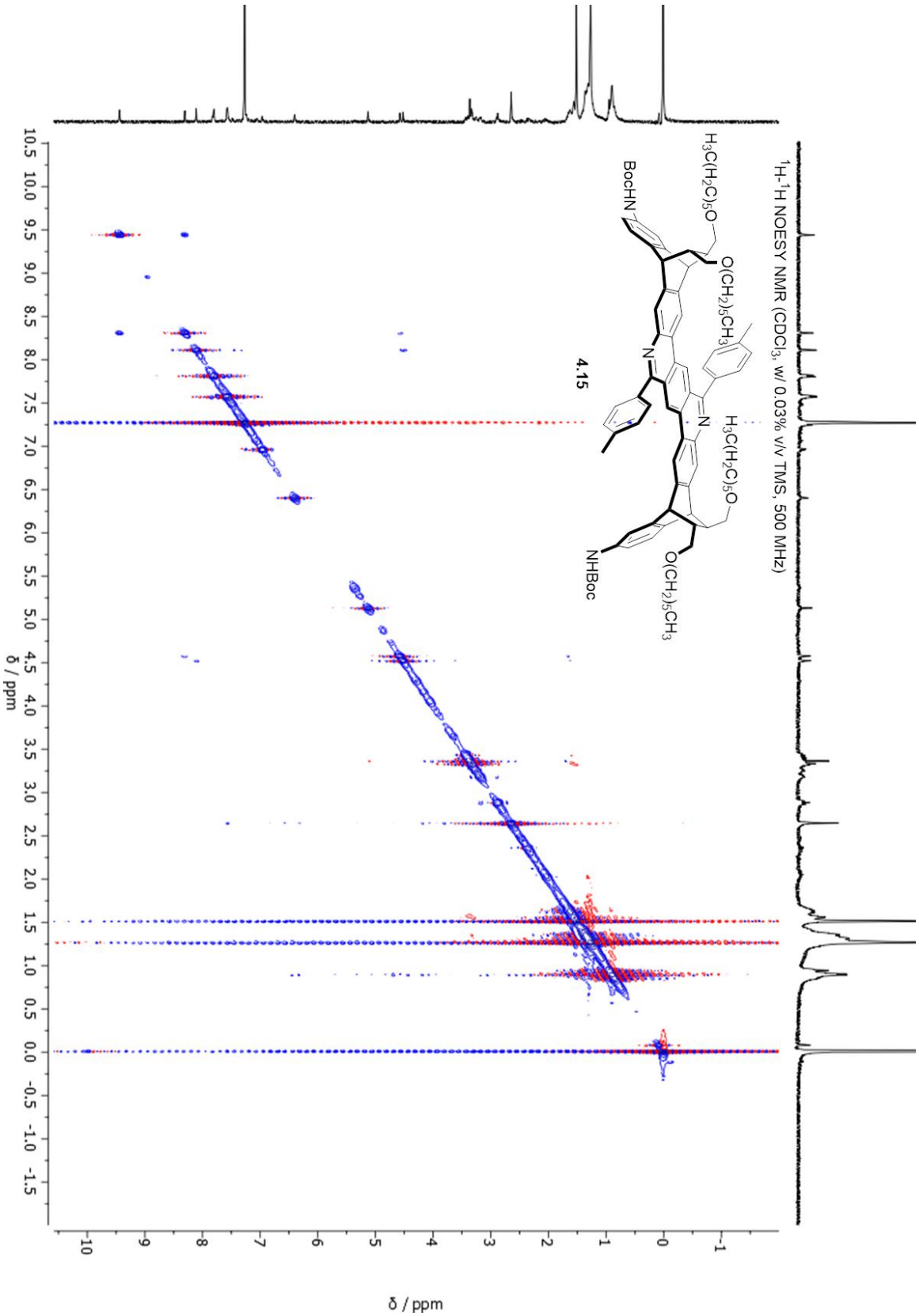
^{1}H-^{1}H NOESY NMR (CDCl$_3$, w/ 0.03% v/v TMS, 500 MHz)
4.15
BocHN
NHBoc
$H_3C(H_2C)_5O$
$O(CH_2)_5CH_3$
δ / ppm
δ / ppm

^{1}H NMR (1-to-4 $CDCl_3$-to-CD_3CN, 500 MHz)

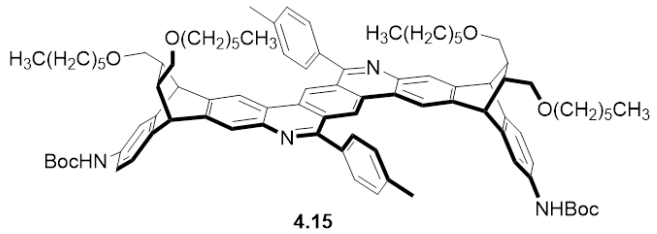

4.15

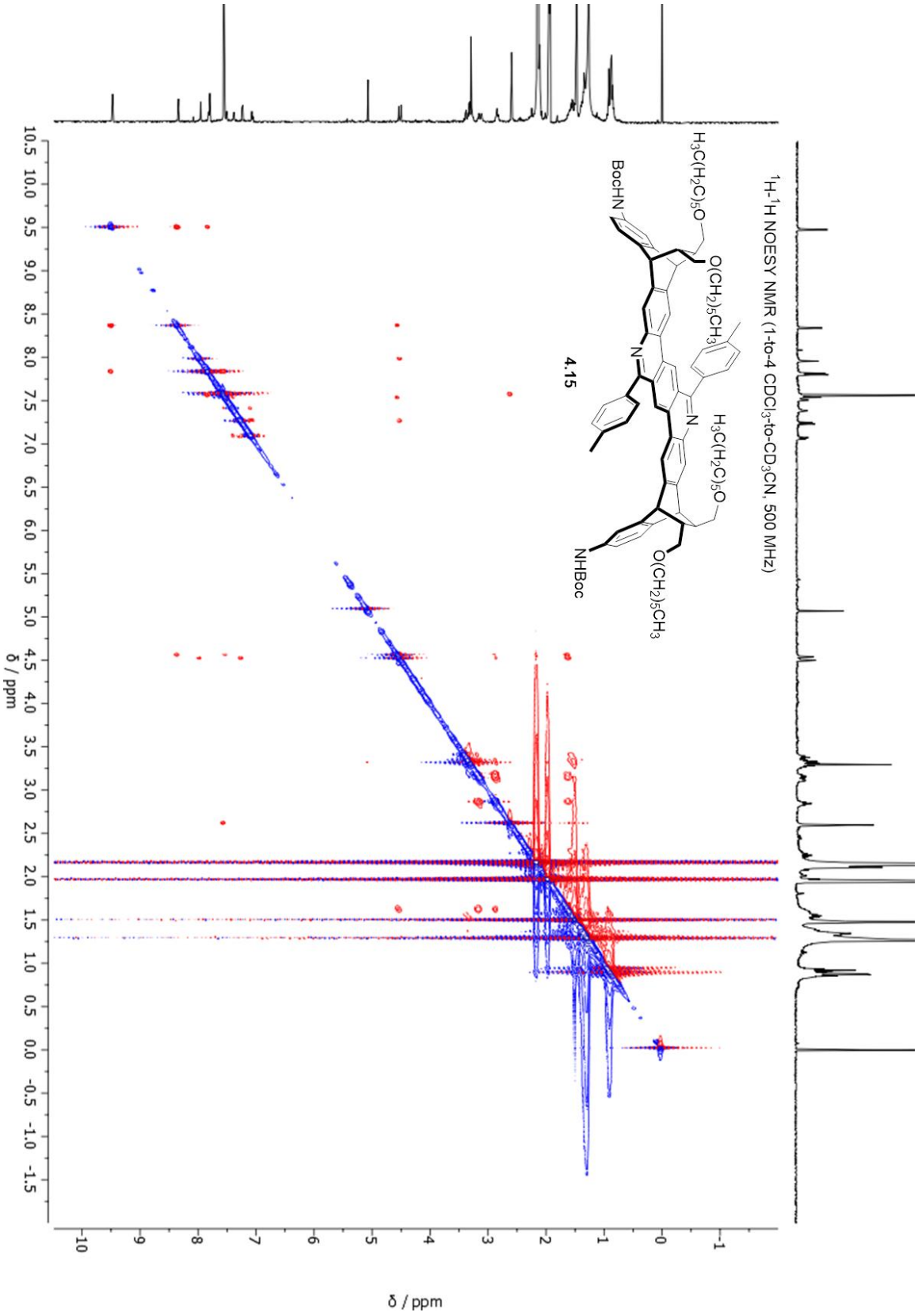
^{1}H-^{1}H NOESY NMR (1-to-4 $CDCl_3$-to-CD_3CN, 500 MHz)
$H_3C(H_2C)_5O$
$O(CH_2)_5CH_3$
BocHN
N
4.15
$H_3C(H_2C)_5O$
$O(CH_2)_5CH_3$
NHBoc
δ / ppm
δ / ppm

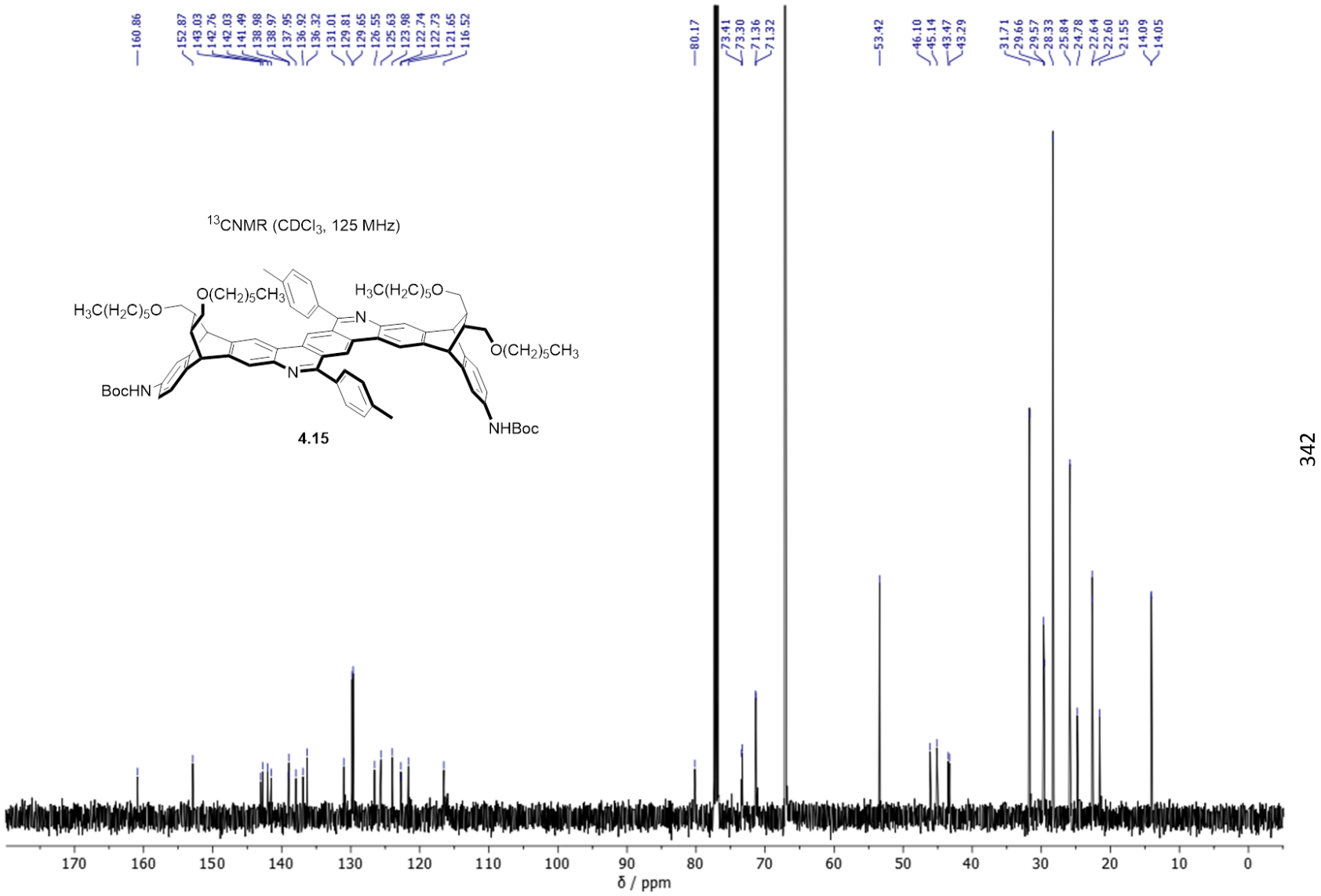
160.86
152.87
143.03
142.76
142.03
141.49
138.98
138.97
137.95
136.92
136.32
131.01
129.81
129.65
126.55
125.63
123.98
122.74
122.73
121.65
116.52
80.17
73.41
73.30
71.36
71.32
53.42
46.10
45.14
43.47
43.29
31.71
29.66
29.57
28.33
25.84
24.78
22.64
22.60
21.55
14.09
14.05
13CNMR (CDCl3, 125 MHz)
H3C(H2C)5O
O(CH2)5CH3
H3C(H2C)5O
N
N
O(CH2)5CH3
BocHN
NHBoc
4.15
170
160
150
140
130
120
110
100
90
80
70
60
50
40
30
20
10
0
δ / ppm

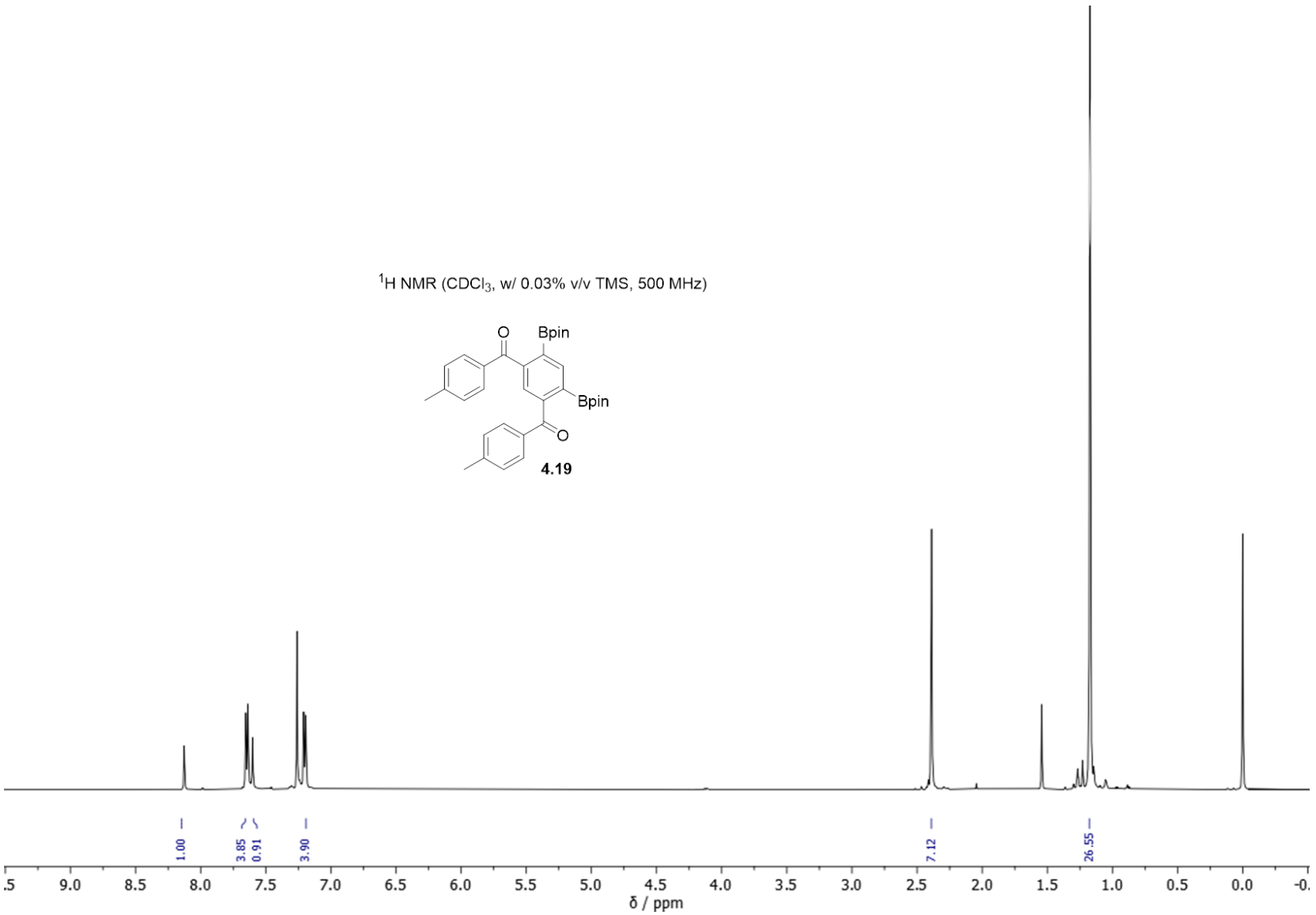
^{1}H NMR ($CDCl_3$, w/ 0.03% v/v TMS, 500 MHz)
O
Bpin
Bpin
O
4.19
1.00
3.85
0.91
3.90
7.12
26.55
δ / ppm

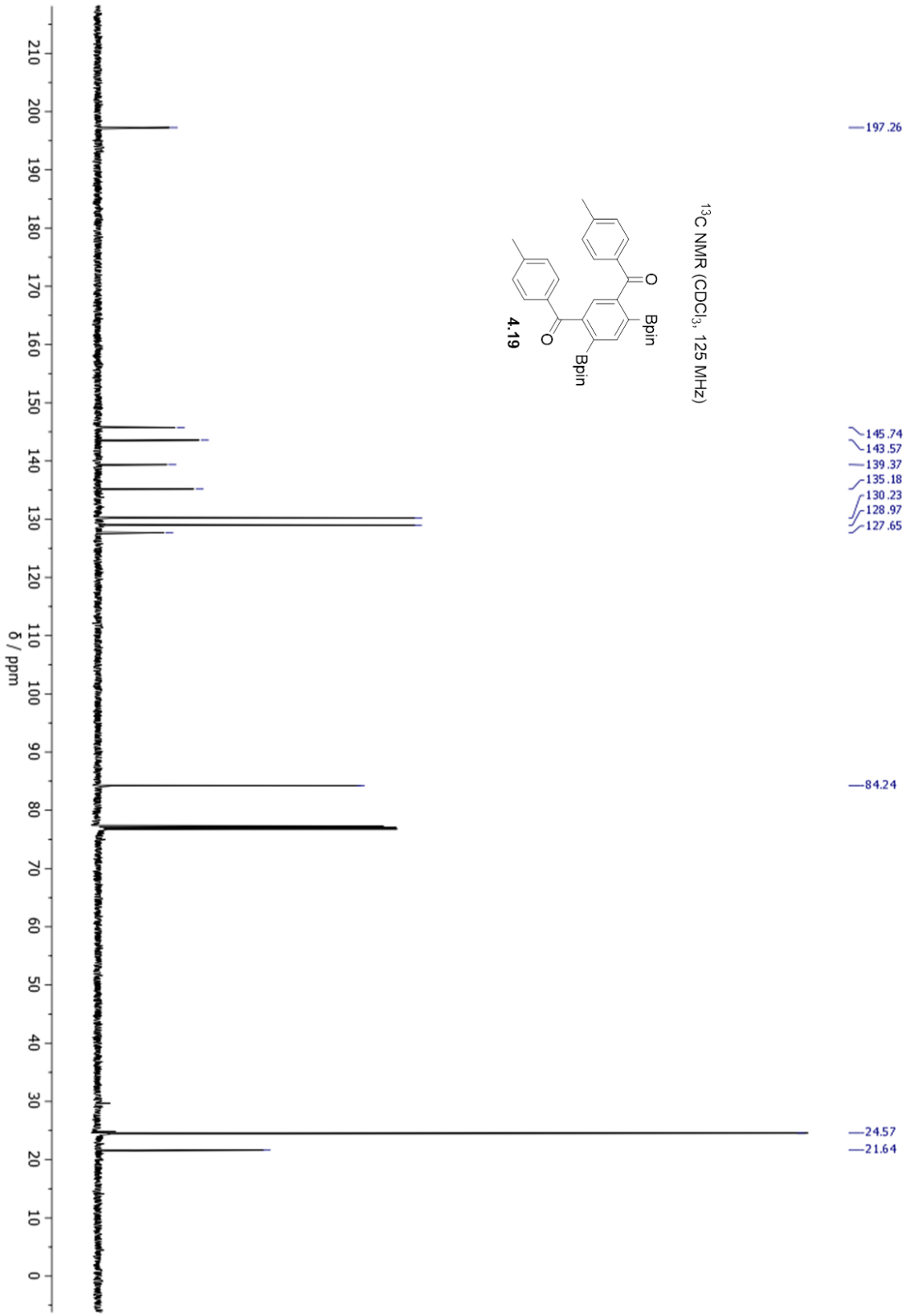
^{13}C NMR (CDCl$_3$, 125 MHz)
4.19
Bpin
Bpin
O
O
δ / ppm
197.26
145.74
143.57
139.37
135.18
130.23
128.97
127.65
84.24
24.57
21.64

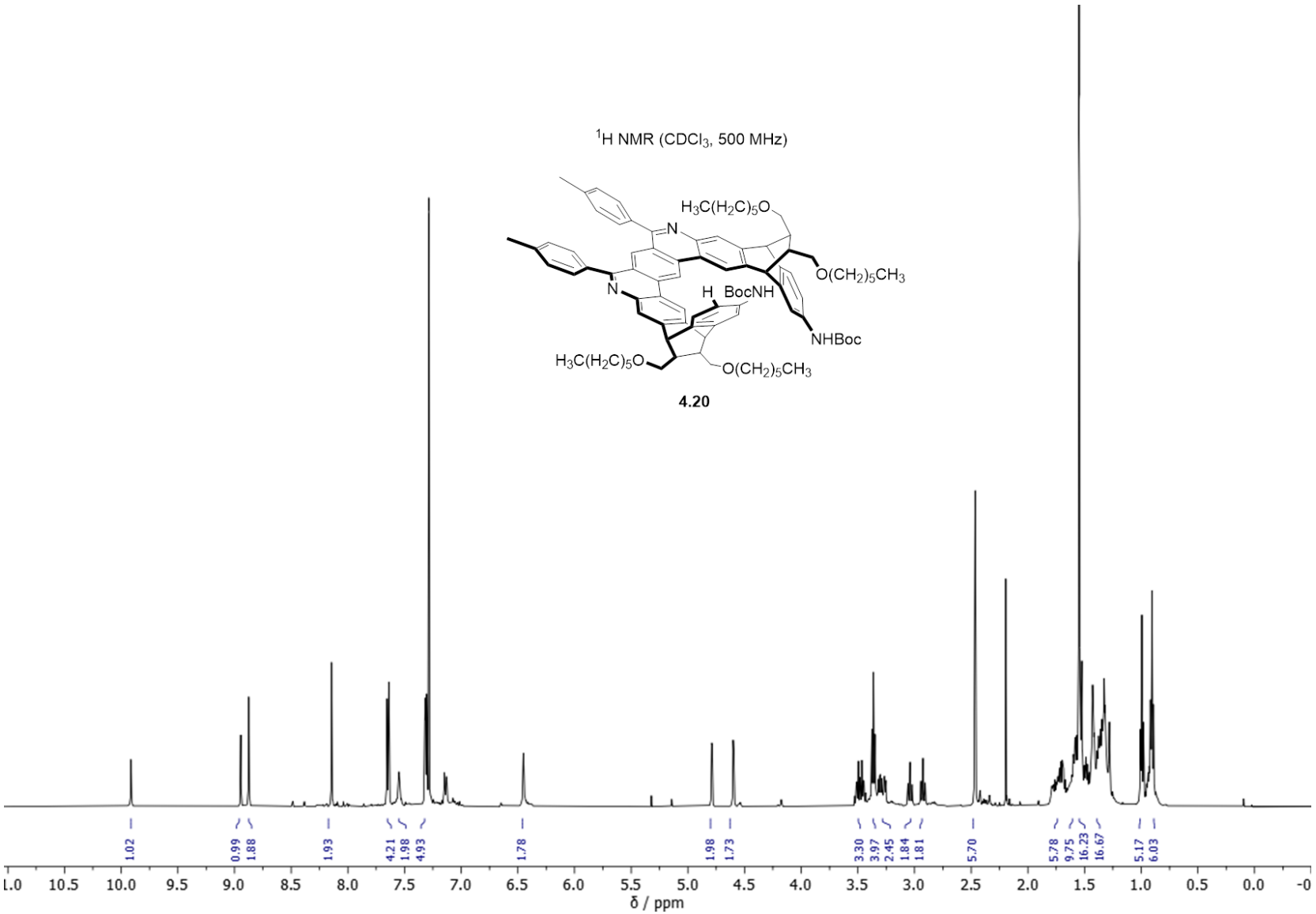
^{1}H NMR ($CDCl_3$, 500 MHz)
$H_3C(H_2C)_5O$
N
$O(CH_2)_5CH_3$
N
H BocNH
NHBoc
$H_3C(H_2C)_5O$
$O(CH_2)_5CH_3$
4.20
1.02
0.99
1.88
1.93
4.21
1.98
4.93
1.78
1.98
1.73
3.30
3.97
2.45
1.84
1.81
5.70
5.78
9.75
16.23
16.67
5.17
6.03
δ / ppm

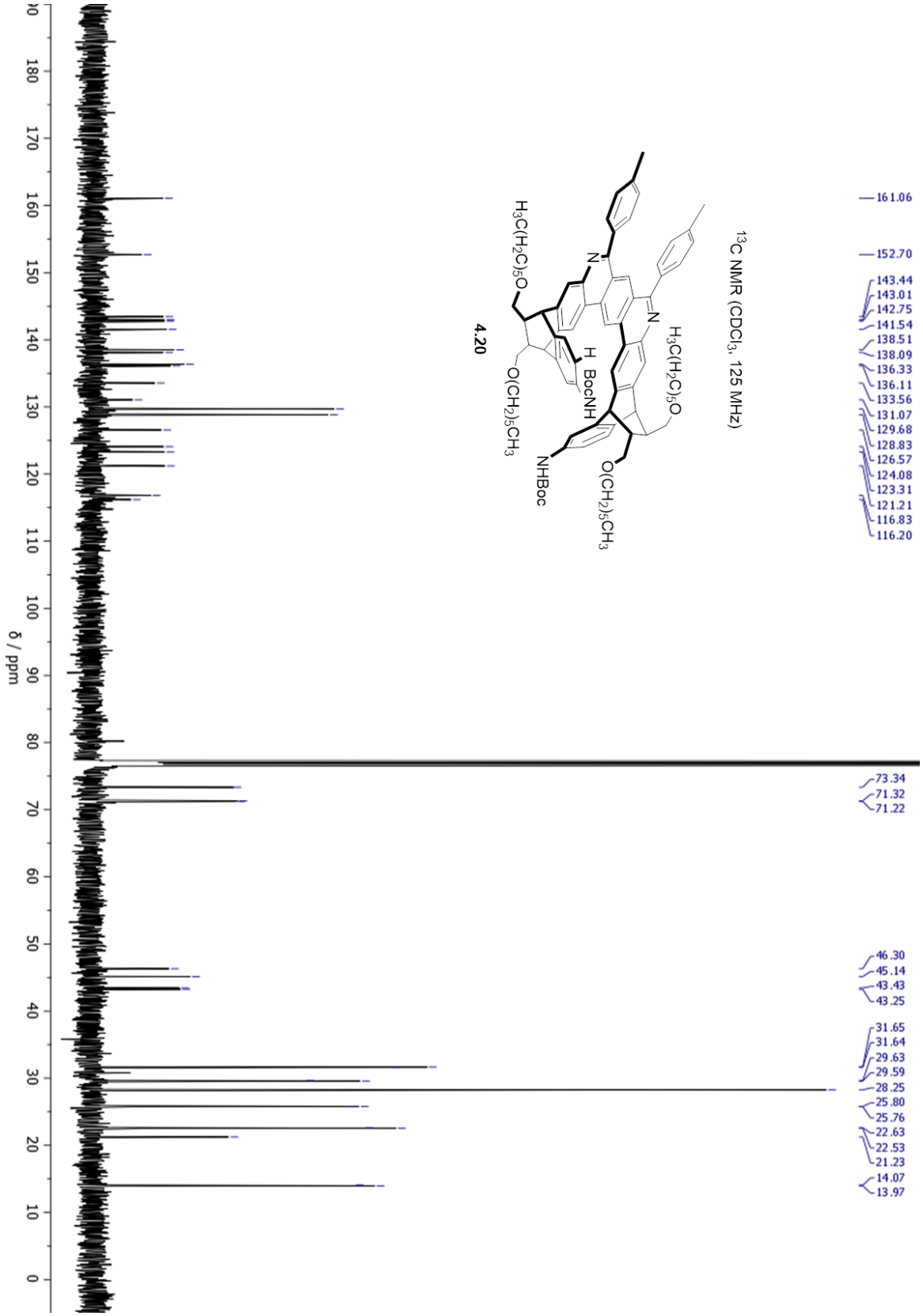
δ / ppm
0
10
20
30
40
50
60
70
80
90
100
110
120
130
140
150
160
170
180
190
4.20
^{13}C NMR ($CDCl_3$, 125 MHz)
161.06
152.70
143.44
143.01
142.75
141.54
138.51
138.09
136.33
136.11
133.56
131.07
129.68
128.83
126.57
124.08
123.31
121.21
116.83
116.20
73.34
71.32
71.22
46.30
45.14
43.43
43.25
31.65
31.64
29.63
29.59
28.25
25.80
25.76
22.63
22.53
21.23
14.07
13.97

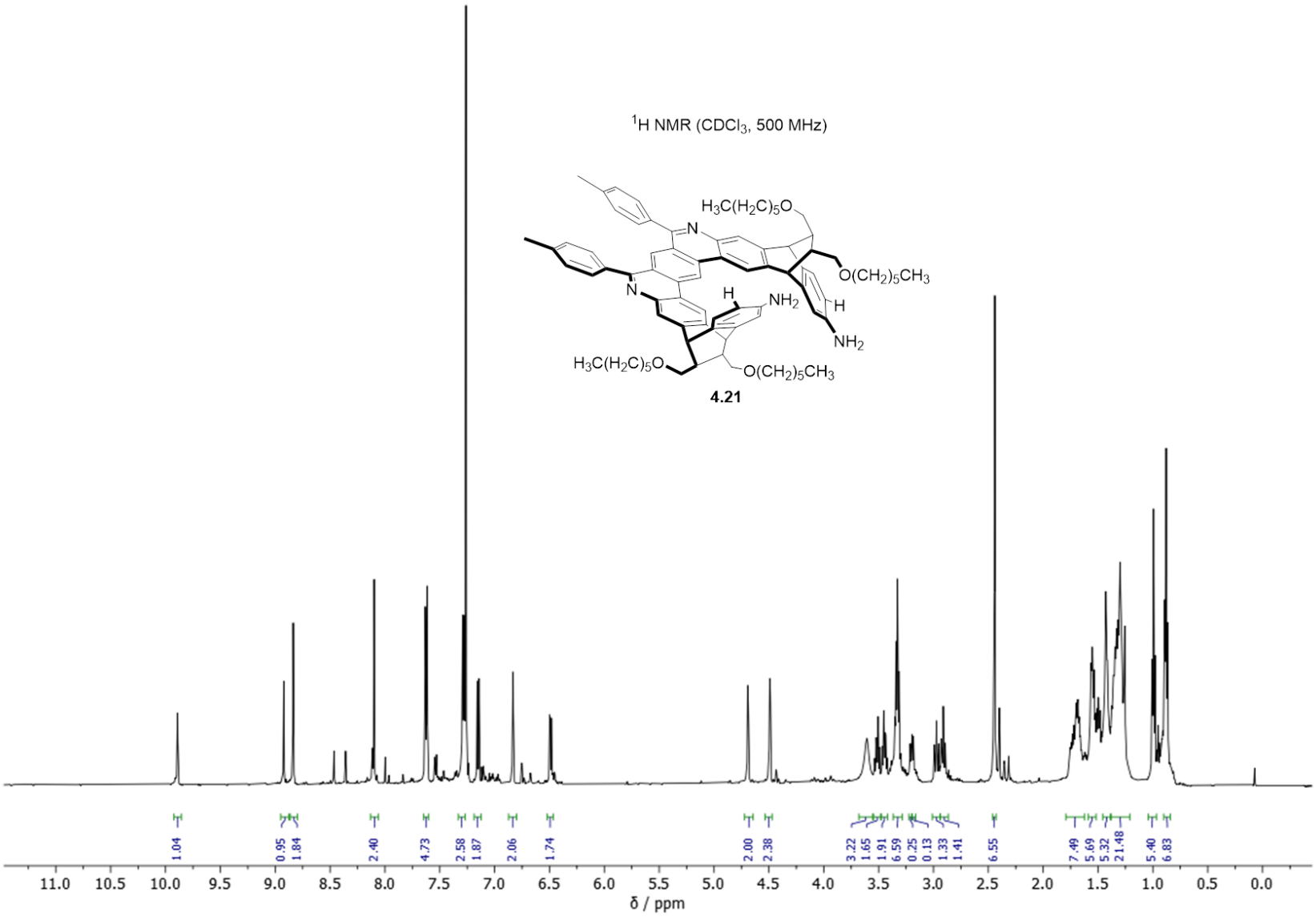
^{1}H NMR ($CDCl_3$, 500 MHz)
$H_3C(H_2C)_5O$
N
$O(CH_2)_5CH_3$
N
H
NH_2
H
NH_2
$H_3C(H_2C)_5O$
$O(CH_2)_5CH_3$
4.21
1.04
0.95
1.84
2.40
4.73
2.58
1.87
2.06
1.74
2.00
2.38
3.22
1.65
1.91
6.59
0.25
0.13
1.33
1.41
6.55
7.49
5.69
5.32
21.48
5.40
6.83
11.0
10.5
10.0
9.5
9.0
8.5
8.0
7.5
7.0
6.5
6.0
5.5
5.0
4.5
4.0
3.5
3.0
2.5
2.0
1.5
1.0
0.5
0.0
δ / ppm

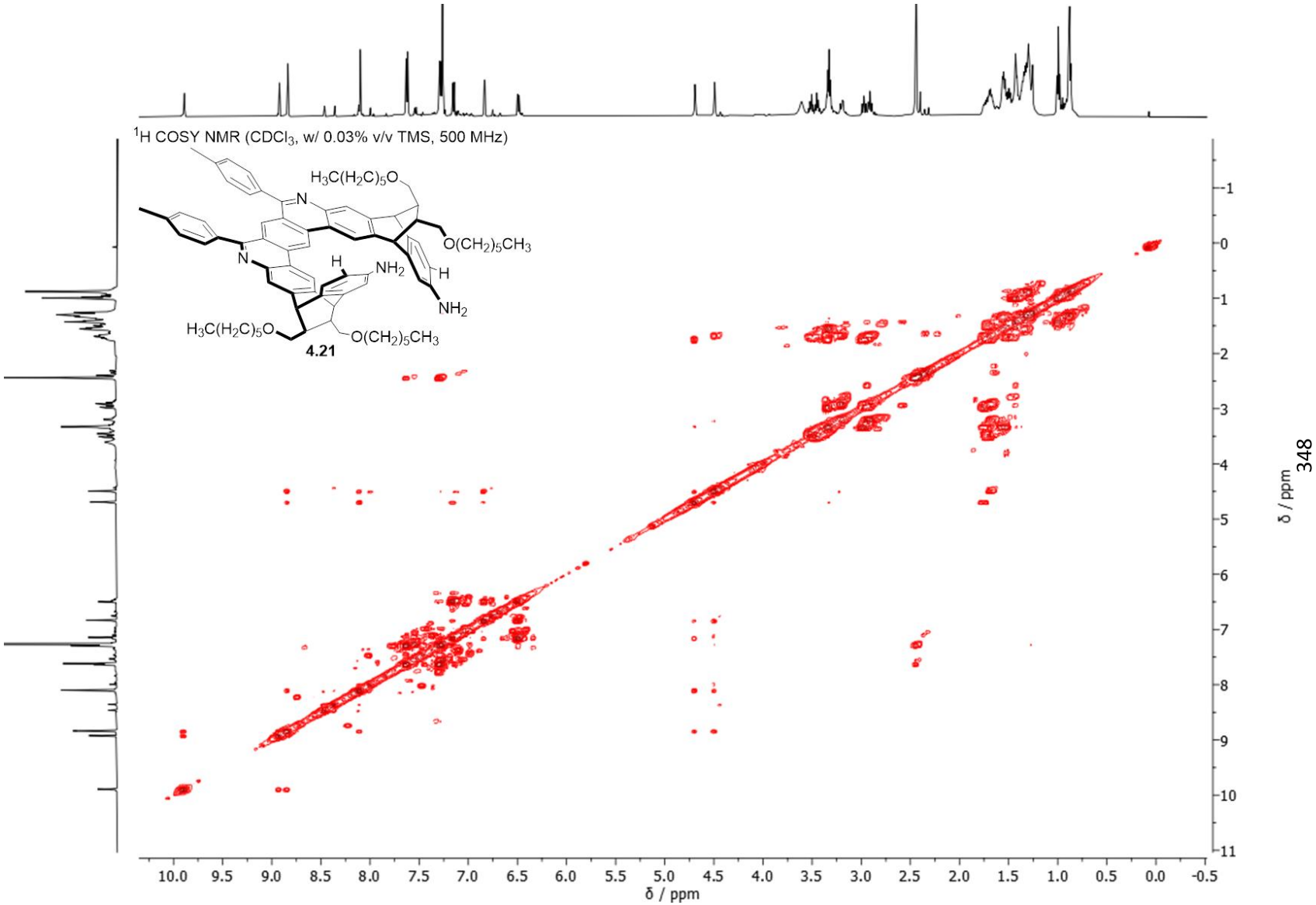
^{1}H COSY NMR ($CDCl_3$, w/ 0.03% v/v TMS, 500 MHz)
$H_3C(H_2C)_5O$
N
$O(CH_2)_5CH_3$
N
H
NH_2
H
NH_2
$H_3C(H_2C)_5O$
$O(CH_2)_5CH_3$
4.21
δ / ppm
δ / ppm

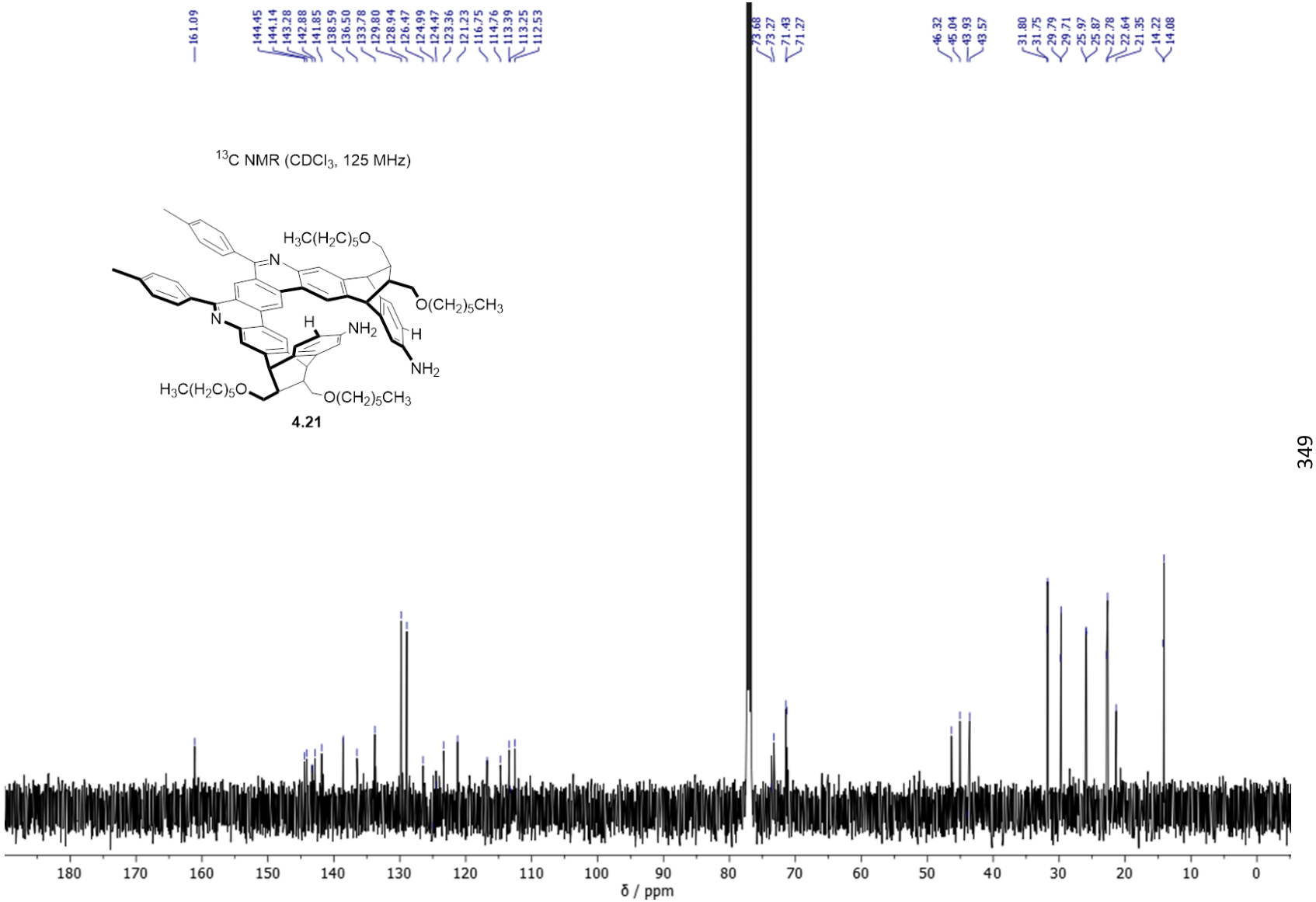

^{13}C NMR ($CDCl_3$, 125 MHz)

4.21

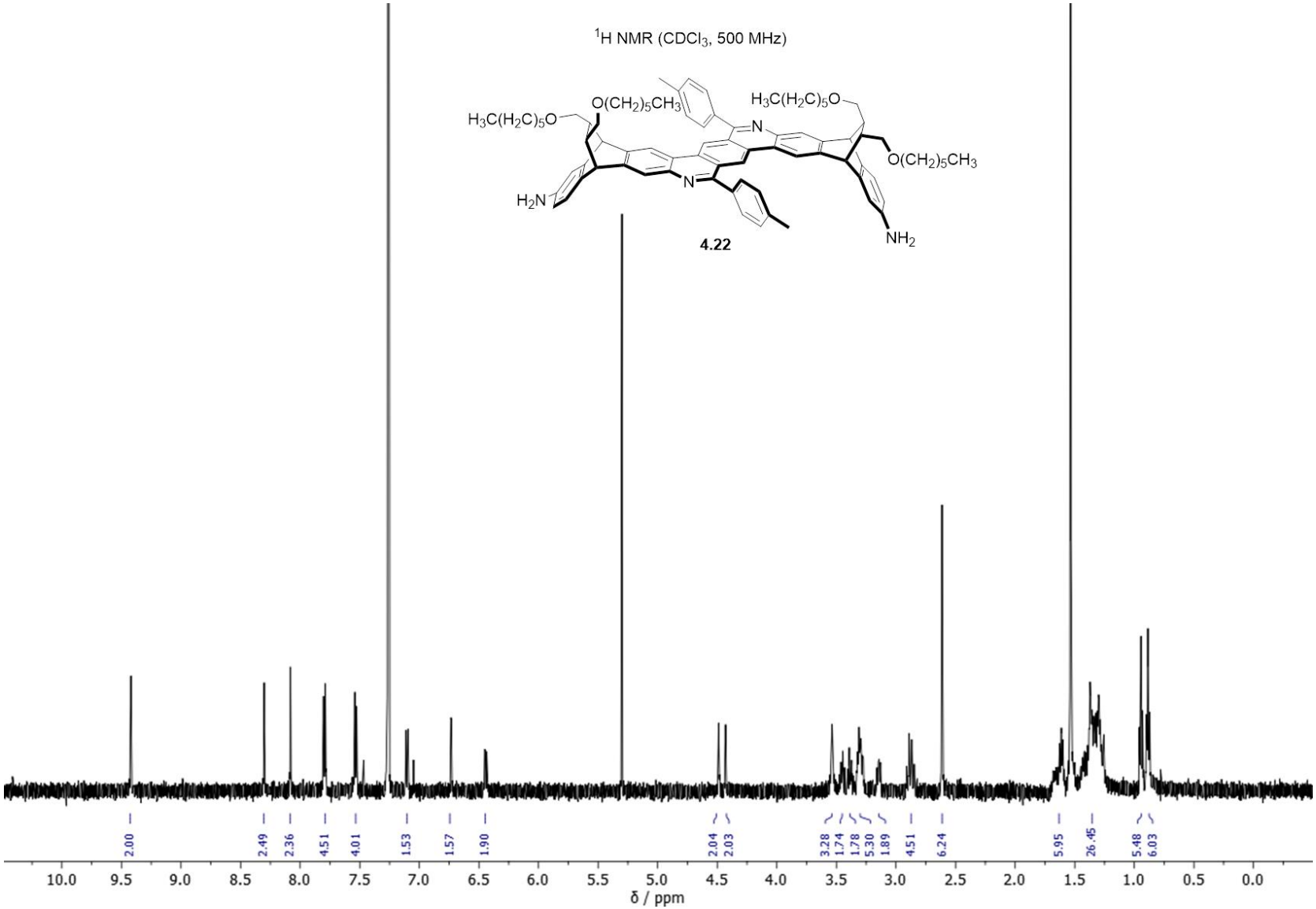
^{1}H NMR ($CDCl_3$, 500 MHz)
$H_3C(H_2C)_5O$
$O(CH_2)_5CH_3$
$H_3C(H_2C)_5O$
N
N
$O(CH_2)_5CH_3$
H_2N
NH_2
4.22
2.00
2.49
2.36
4.51
4.01
1.53
1.57
1.90
2.04
2.03
3.28
1.74
1.78
5.30
1.89
4.51
6.24
5.95
26.45
5.48
6.03
10.0
9.5
9.0
8.5
8.0
7.5
7.0
6.5
6.0
5.5
5.0
4.5
4.0
3.5
3.0
2.5
2.0
1.5
1.0
0.5
0.0
δ / ppm

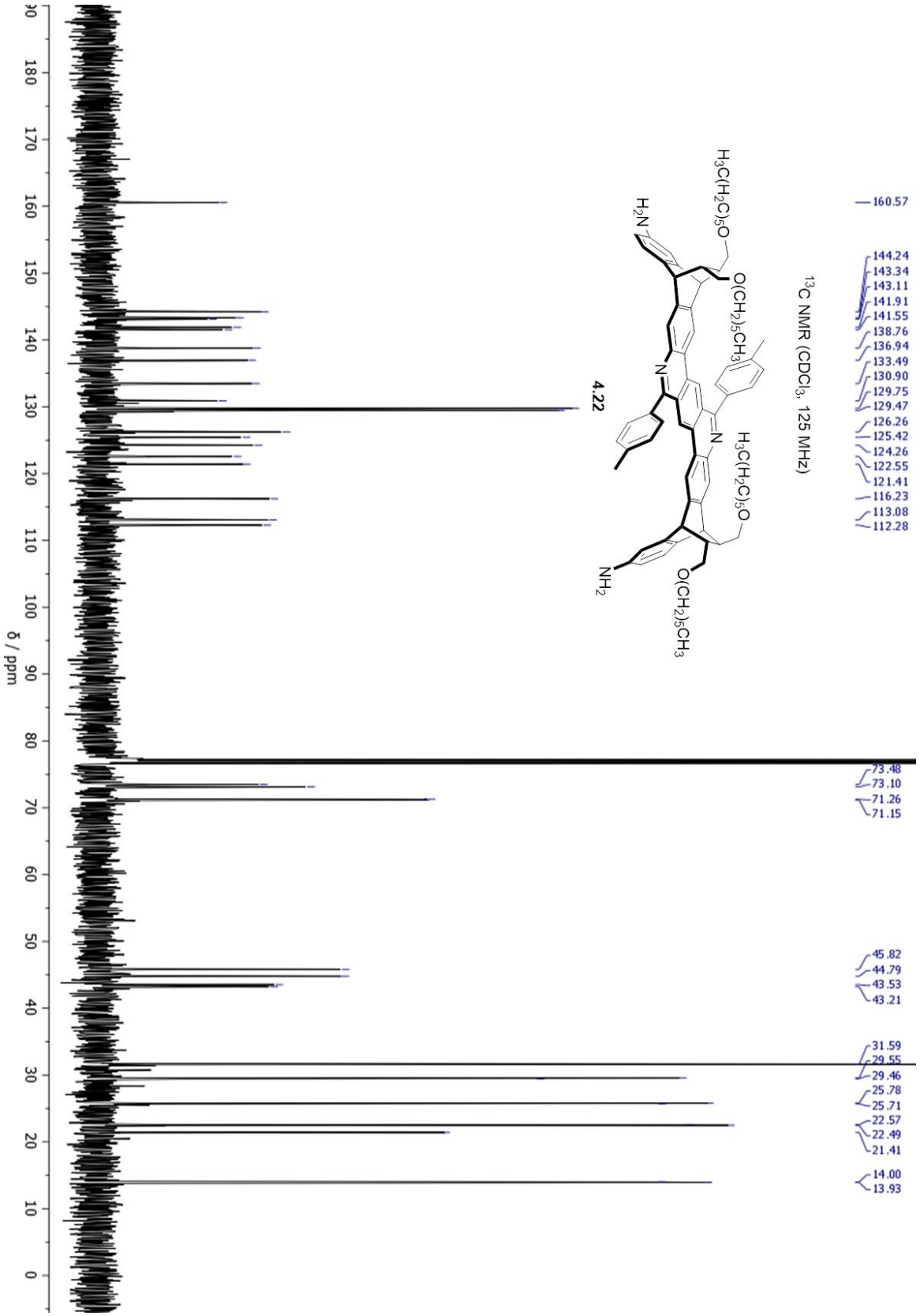
^{13}C NMR (CDCl$_3$, 125 MHz)
δ / ppm
4.22
H$_2$N
NH$_2$
H$_3$C(H$_2$C)$_5$O
O(CH$_2$)$_5$CH$_3$
160.57
144.24
143.34
143.11
141.91
141.55
138.76
136.94
133.49
130.90
129.75
129.47
126.26
125.42
124.26
122.55
121.41
116.23
113.08
112.28
73.48
73.10
71.26
71.15
45.82
44.79
43.53
43.21
31.59
29.55
29.46
25.78
25.71
22.57
22.49
21.41
14.00
13.93

^{1}H NMR ($CDCl_3$, w/ 0.03% v/v TMS, 500 MHz)

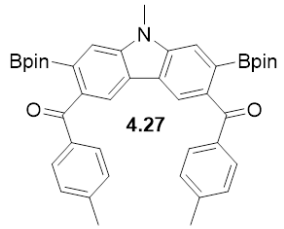

4.27

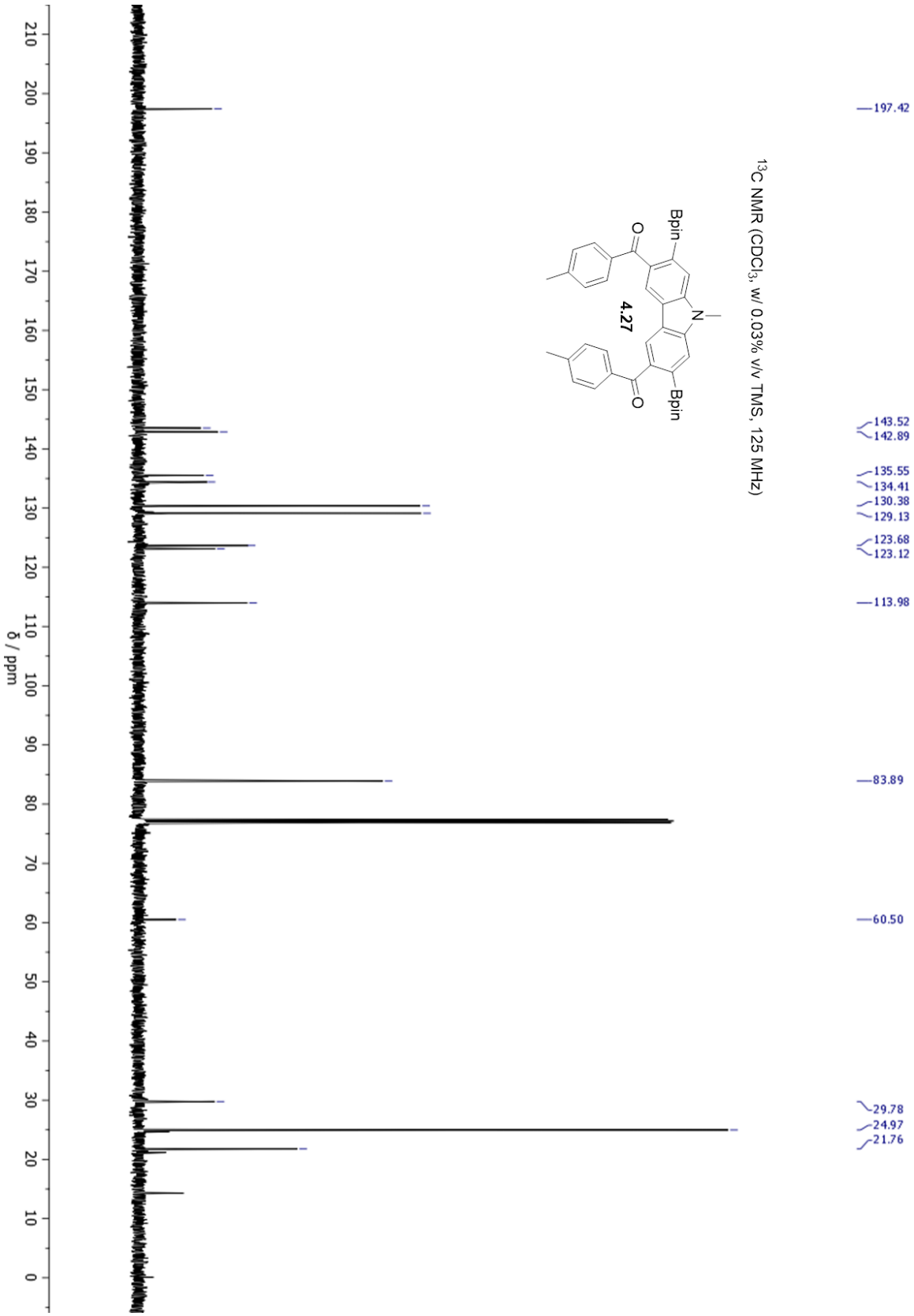
^{13}C NMR ($CDCl_3$, w/ 0.03% v/v TMS, 125 MHz)
4.27
Bpin
Bpin
O
O
N
δ / ppm
197.42
143.52
142.89
135.55
134.41
130.38
129.13
123.68
123.12
113.98
83.89
60.50
29.78
24.97
21.76

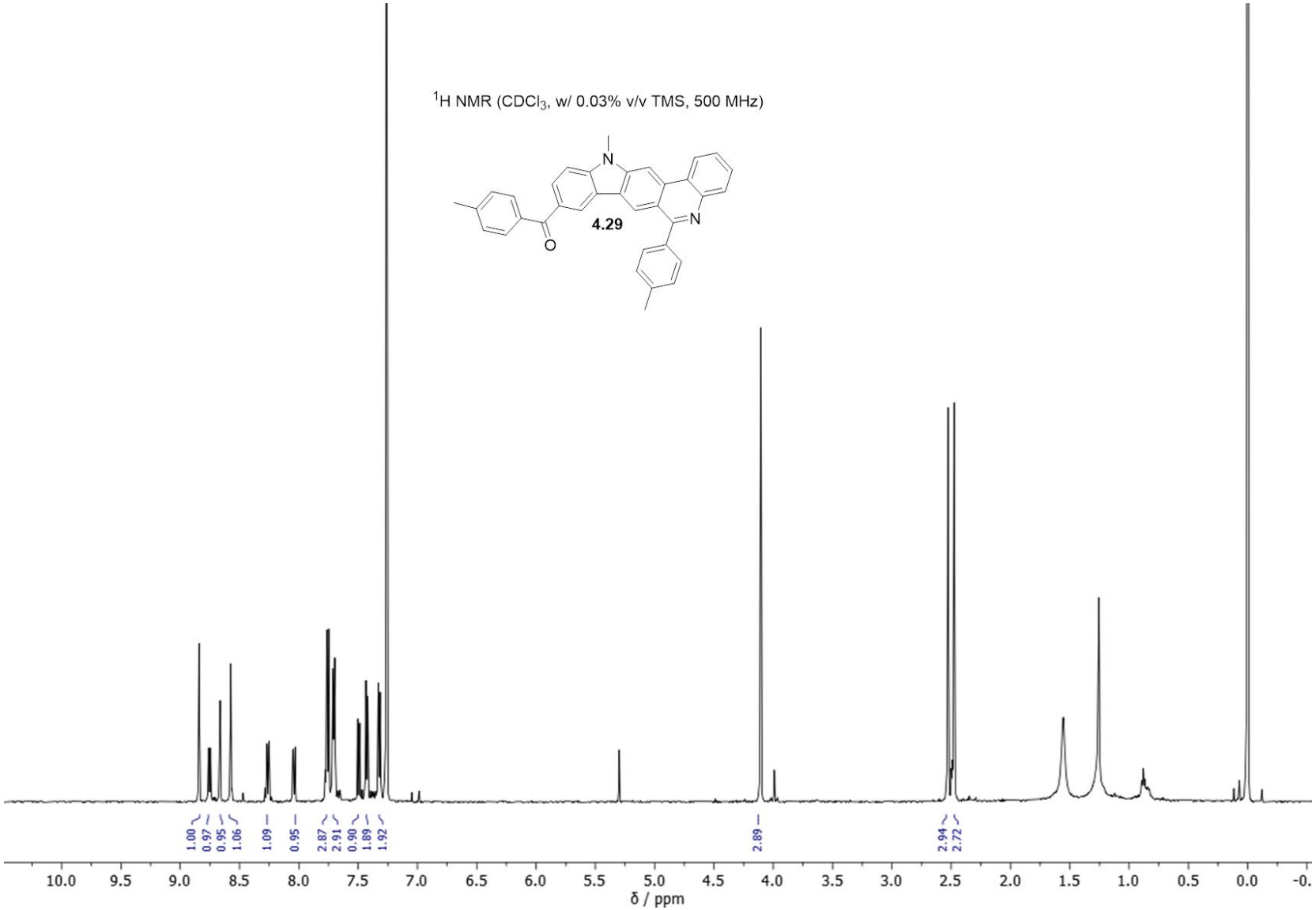
^{1}H NMR ($CDCl_3$, w/ 0.03% v/v TMS, 500 MHz)
4.29
1.00
0.97
0.95
1.06
1.09
0.95
2.87
2.91
0.90
1.89
1.92
2.89
2.94
2.72
δ / ppm

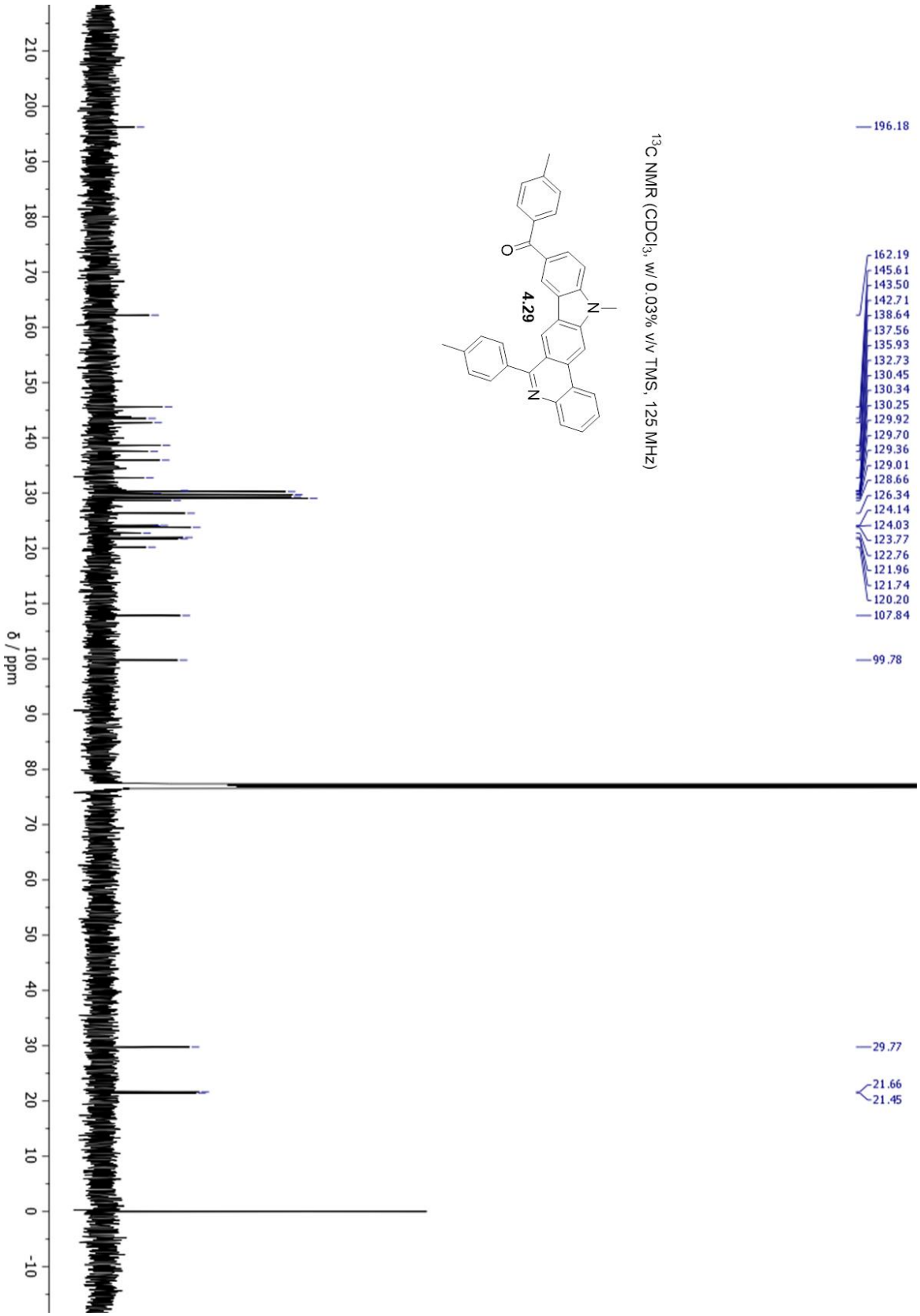
^{13}C NMR ($CDCl_3$, w/ 0.03% v/v TMS, 125 MHz)
4.29
δ / ppm
196.18
162.19
145.61
143.50
142.71
138.64
137.56
135.93
132.73
130.45
130.34
130.25
129.92
129.70
129.36
129.01
128.66
126.34
124.14
124.03
123.77
122.76
121.96
121.74
120.20
107.84
99.78
29.77
21.66
21.45

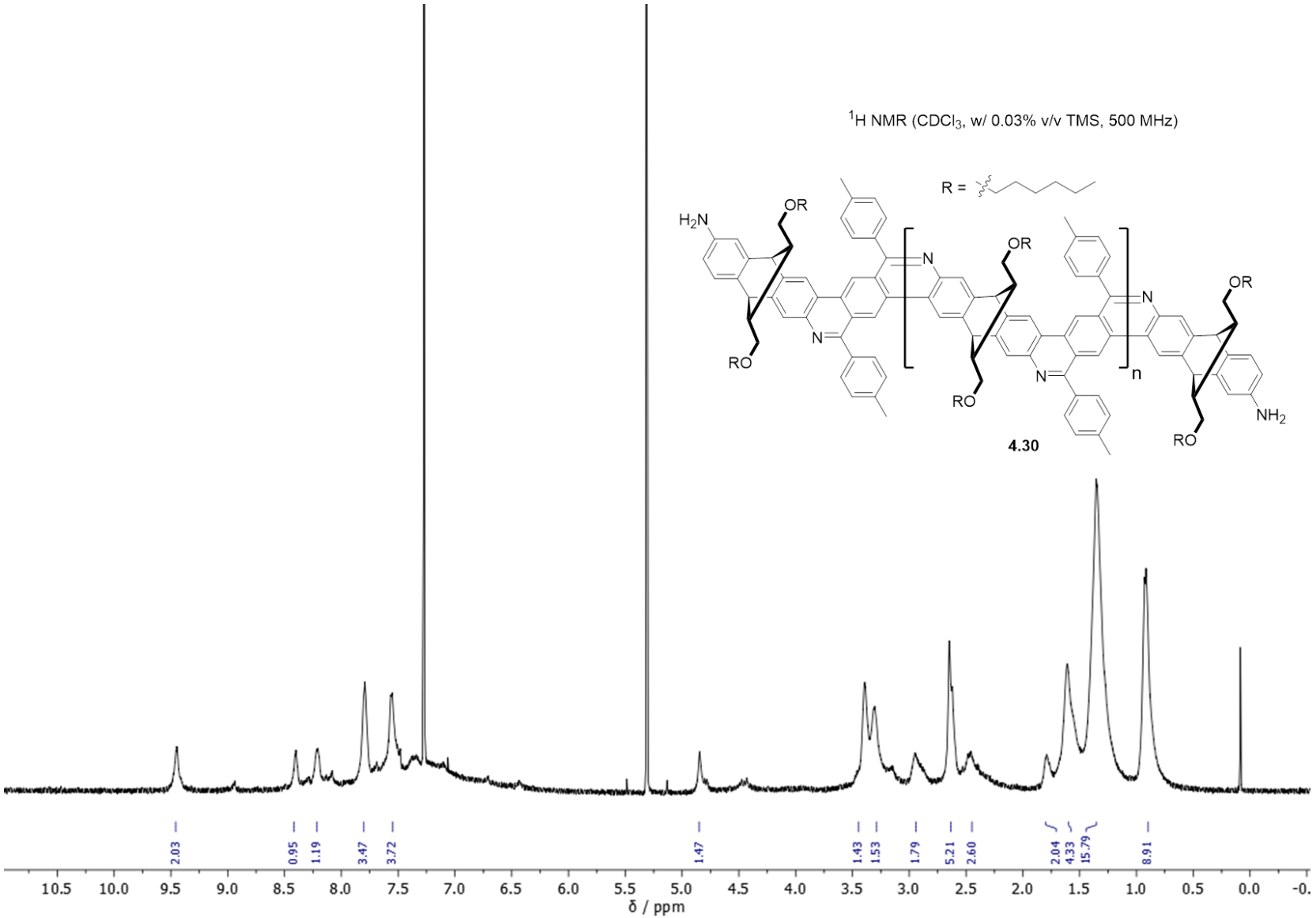
^{1}H NMR ($CDCl_3$, w/ 0.03% v/v TMS, 500 MHz)
R =
H_2N
OR
RO
N
n
NH_2
4.30
2.03
0.95
1.19
3.47
3.72
1.47
1.43
1.53
1.79
5.21
2.60
2.04
4.33
15.79
8.91
δ / ppm

^{1}H DOSY NMR ($CDCl_3$, w/ 0.03% v/v TMS, 500 MHz)

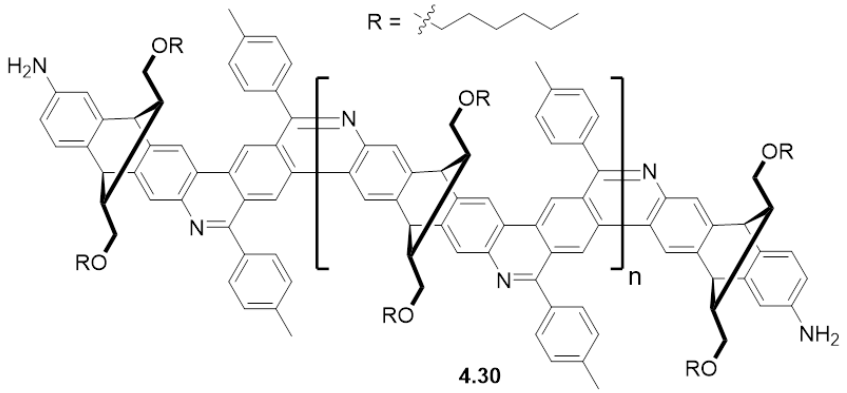

4.30

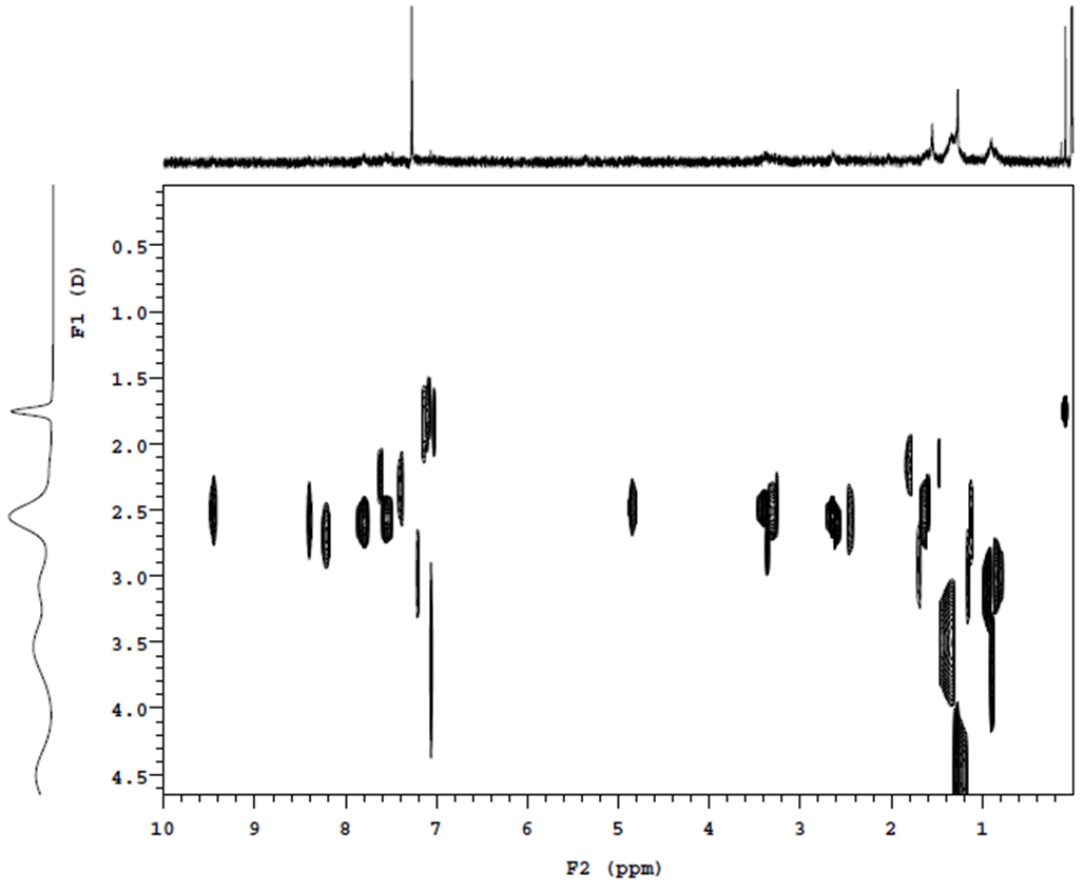

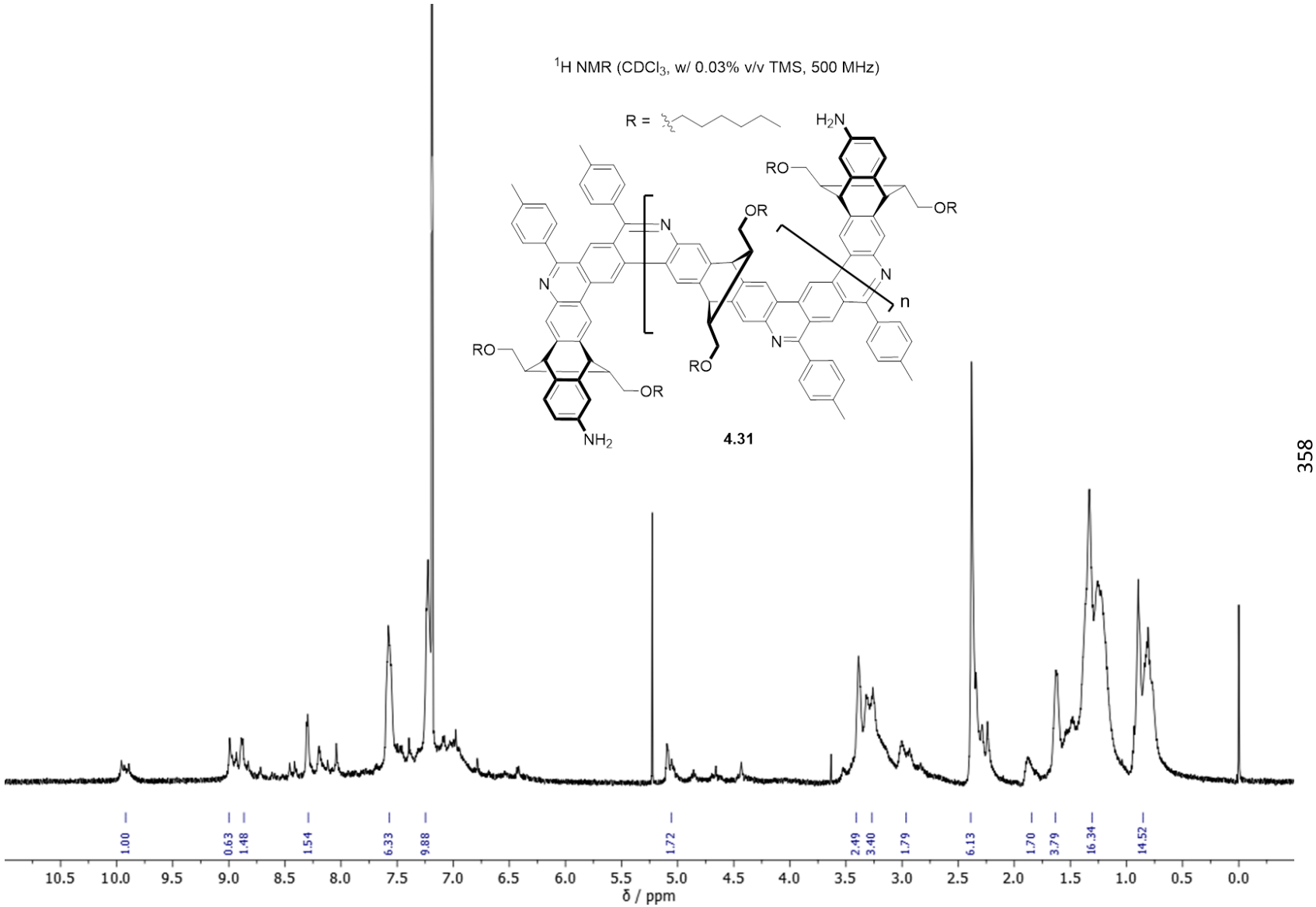
^{1}H NMR ($CDCl_3$, w/ 0.03% v/v TMS, 500 MHz)
R =
H_2N
RO
OR
N
n
NH_2
4.31
1.00
0.63
1.48
1.54
6.33
9.88
1.72
2.49
3.40
1.79
6.13
1.70
3.79
16.34
14.52
δ / ppm

^{1}H DOSY NMR ($CDCl_3$, w/ 0.03% v/v TMS, 500 MHz)

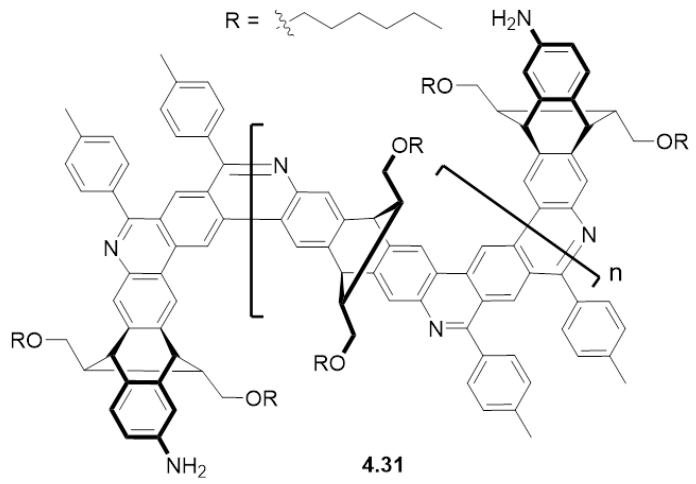

4.31

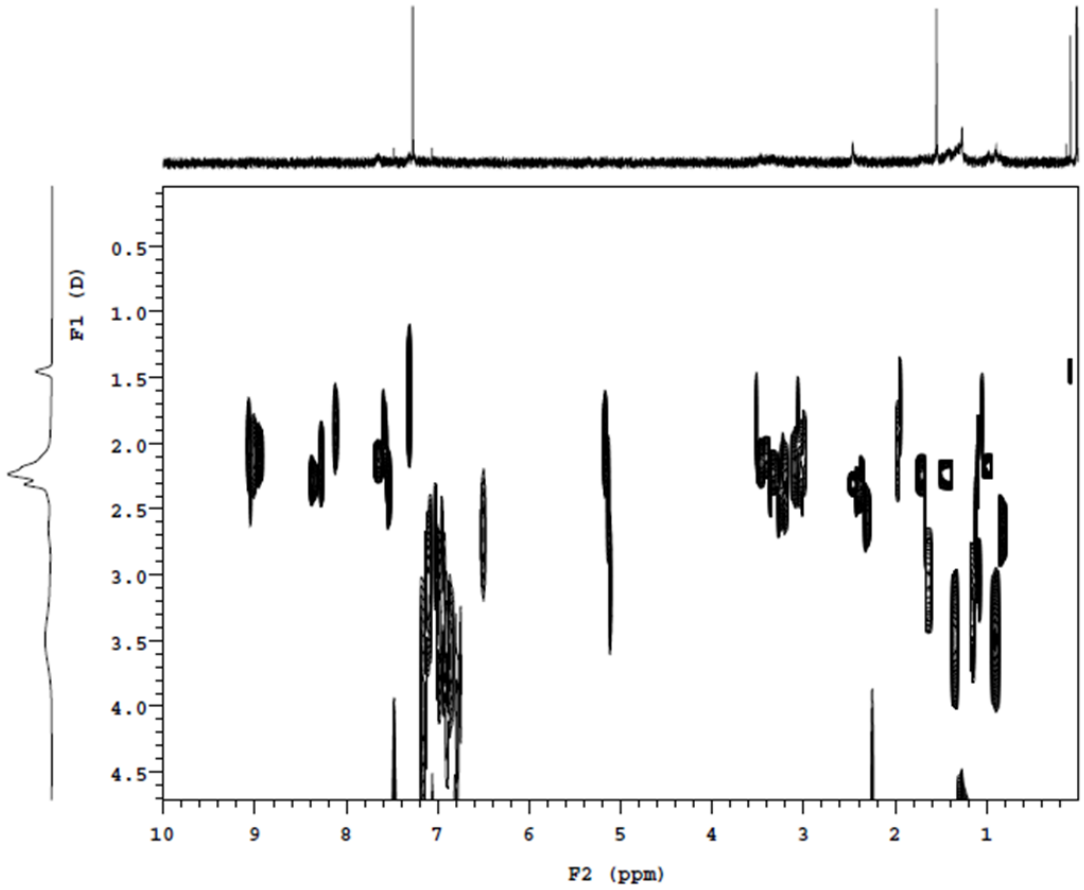

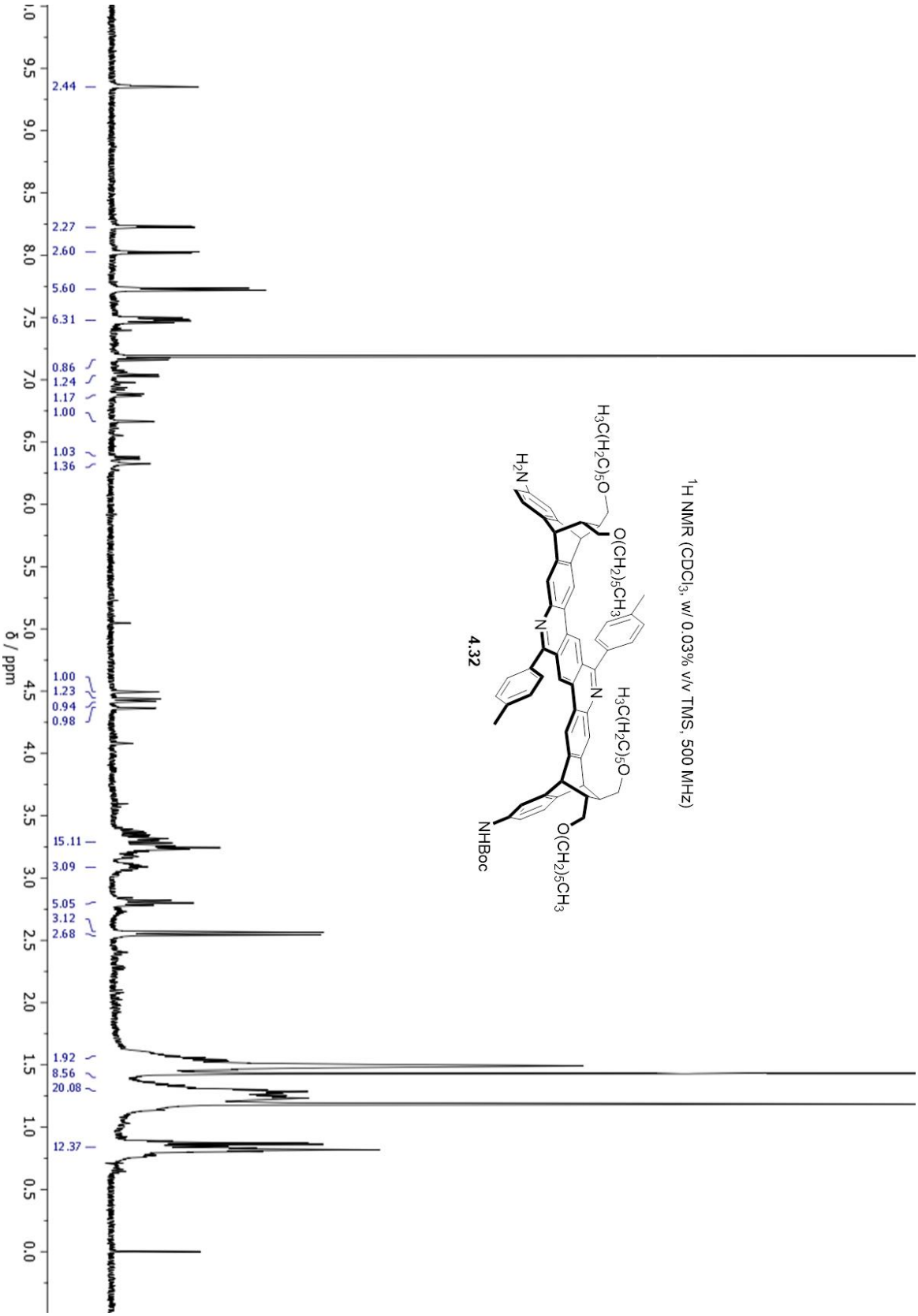
^{1}H NMR ($CDCl_3$, w/ 0.03% v/v TMS, 500 MHz)
4.32
H_2N
$H_3C(H_2C)_5O$
$O(CH_2)_5CH_3$
N
N
$H_3C(H_2C)_5O$
NHBoc
$O(CH_2)_5CH_3$
δ / ppm
2.44
2.27
2.60
5.60
6.31
0.86
1.24
1.17
1.00
1.03
1.36
1.00
1.23
0.94
0.98
15.11
3.09
5.05
3.12
2.68
1.92
8.56
20.08
12.37

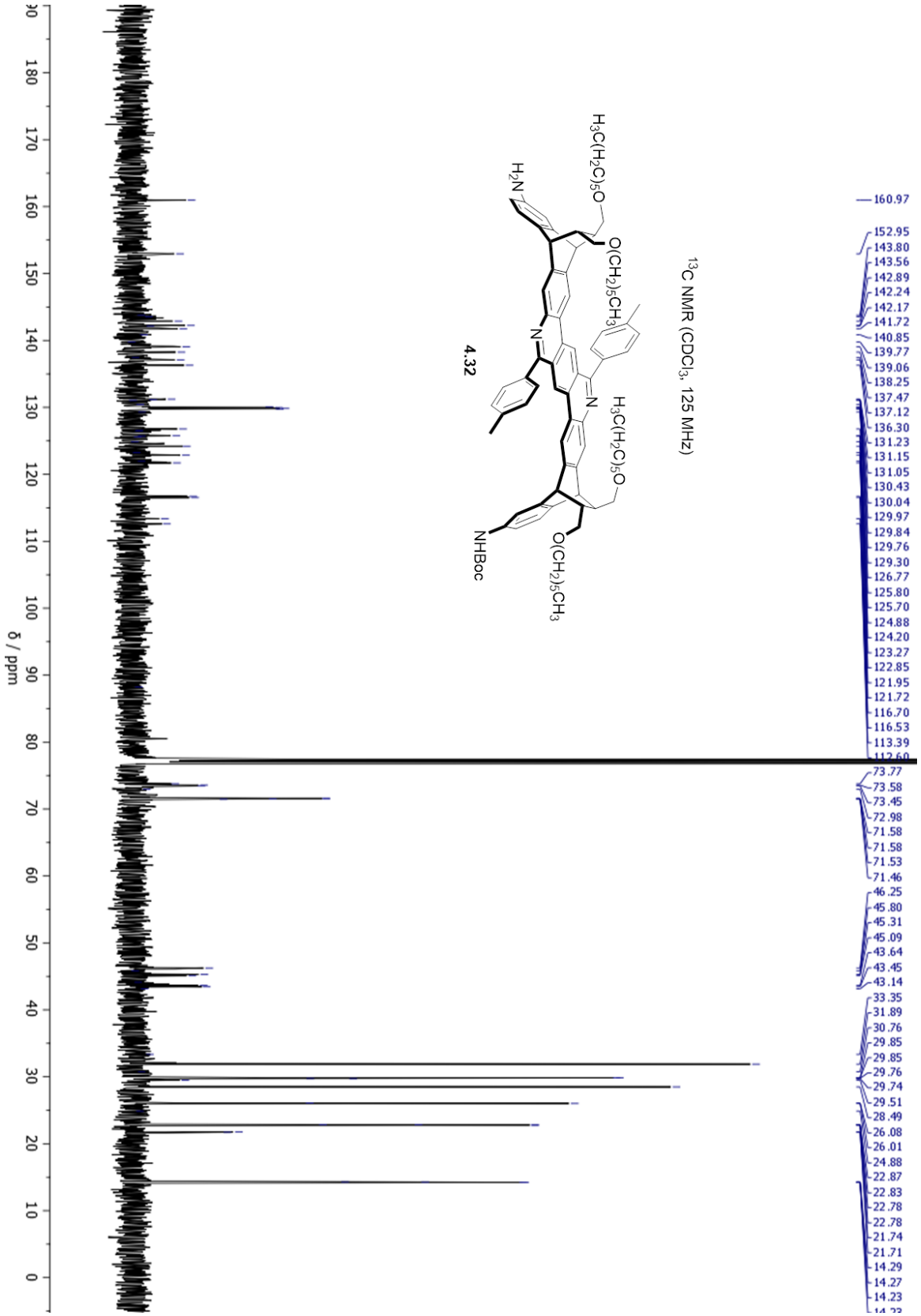
4.32
^{13}C NMR (CDCl$_3$, 125 MHz)
δ / ppm
160.97
152.95
143.80
143.56
142.89
142.24
142.17
141.72
140.85
139.77
139.06
138.25
137.47
137.12
136.30
131.23
131.15
131.05
130.43
130.04
129.97
129.84
129.76
129.30
126.77
125.80
125.70
124.88
124.20
123.27
122.85
121.95
121.72
116.70
116.53
113.39
73.77
73.58
73.45
72.98
71.58
71.58
71.53
71.46
46.25
45.80
45.31
45.09
43.64
43.45
43.14
33.35
31.89
30.76
29.85
29.85
29.76
29.74
29.51
28.49
26.08
26.01
24.88
22.87
22.83
22.78
22.78
21.74
21.71
14.29
14.27
14.23

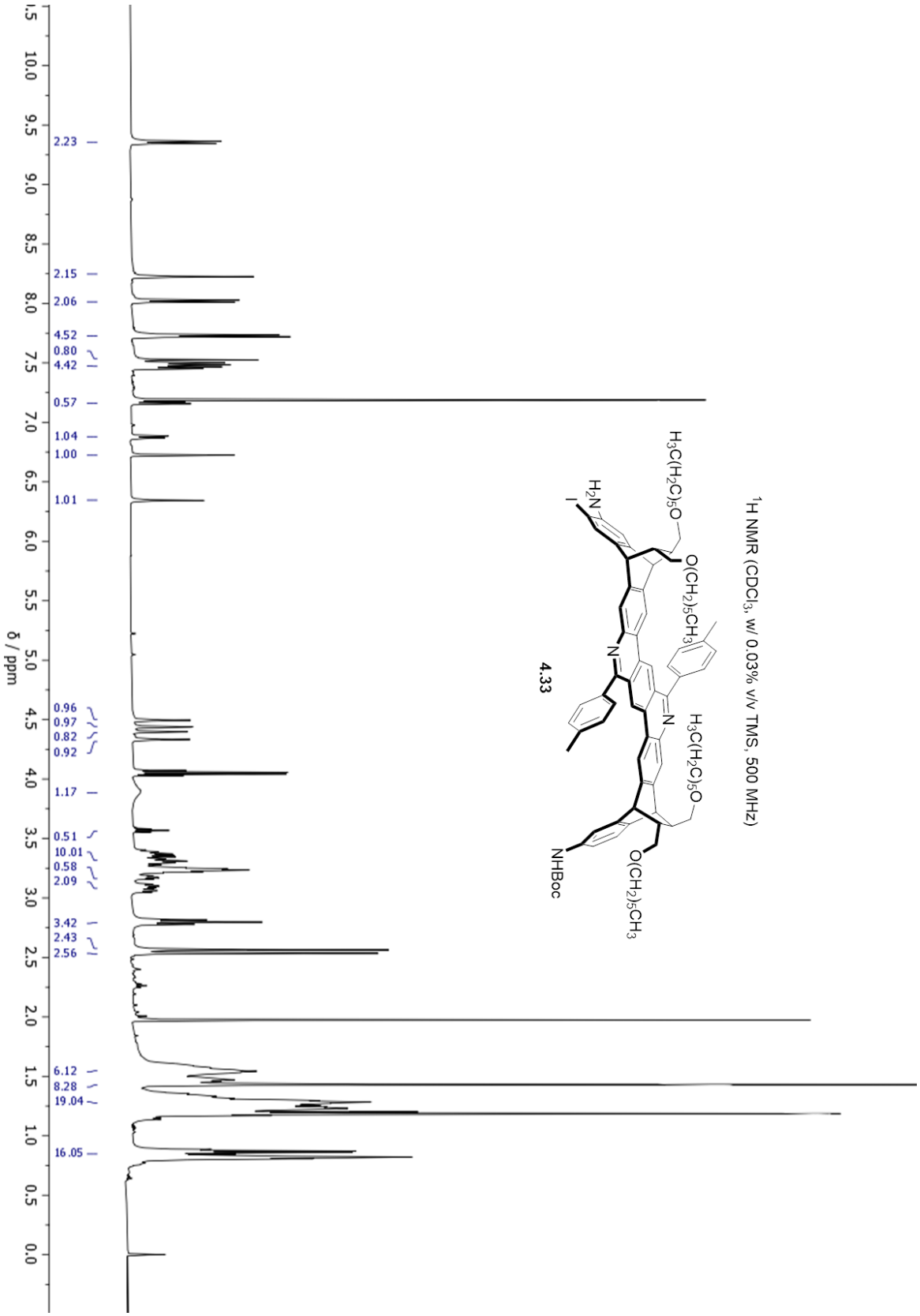
^{1}H NMR (CDCl$_3$, w/ 0.03% v/v TMS, 500 MHz)
4.33
δ / ppm
2.23
2.15
2.06
4.52
0.80
4.42
0.57
1.04
1.00
1.01
0.96
0.97
0.82
0.92
1.17
0.51
10.01
0.58
2.09
3.42
2.43
2.56
6.12
8.28
19.04
16.05

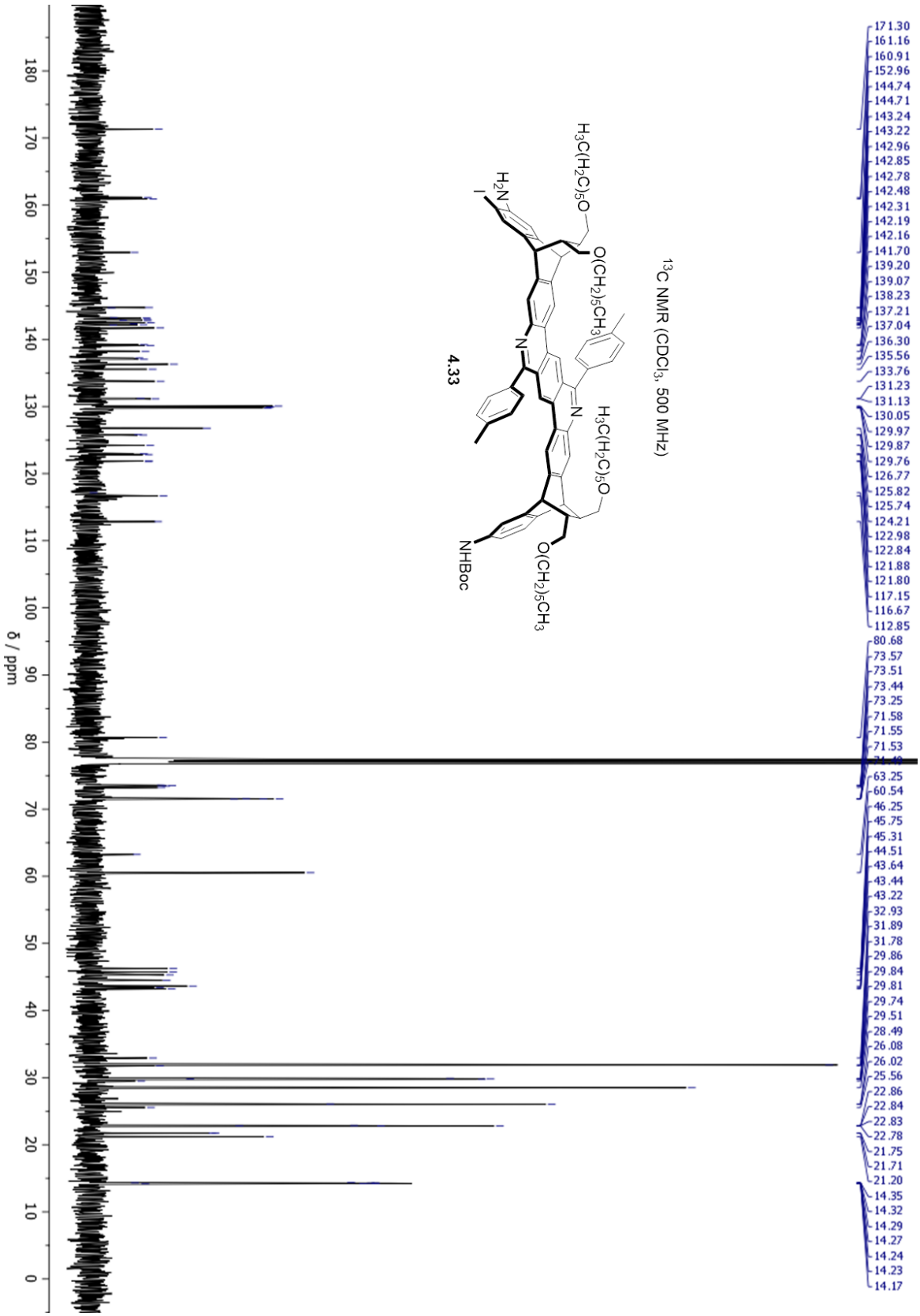
^{13}C NMR (CDCl$_3$, 500 MHz)
4.33
δ / ppm
171.30
161.16
160.91
152.96
144.74
144.71
143.24
143.22
142.96
142.85
142.78
142.48
142.31
142.19
142.16
141.70
139.20
139.07
138.23
137.21
137.04
136.30
135.56
133.76
131.23
131.13
130.05
129.97
129.87
129.76
126.77
125.82
125.74
124.21
122.98
122.84
121.88
121.80
117.15
116.67
112.85
80.68
73.57
73.51
73.44
73.25
71.58
71.55
71.53
63.25
60.54
46.25
45.75
45.31
44.51
43.64
43.44
43.22
32.93
31.89
31.78
29.86
29.84
29.81
29.74
29.51
28.49
26.08
26.02
25.56
22.86
22.84
22.83
22.78
21.75
21.71
21.20
14.35
14.32
14.29
14.27
14.24
14.23
14.17

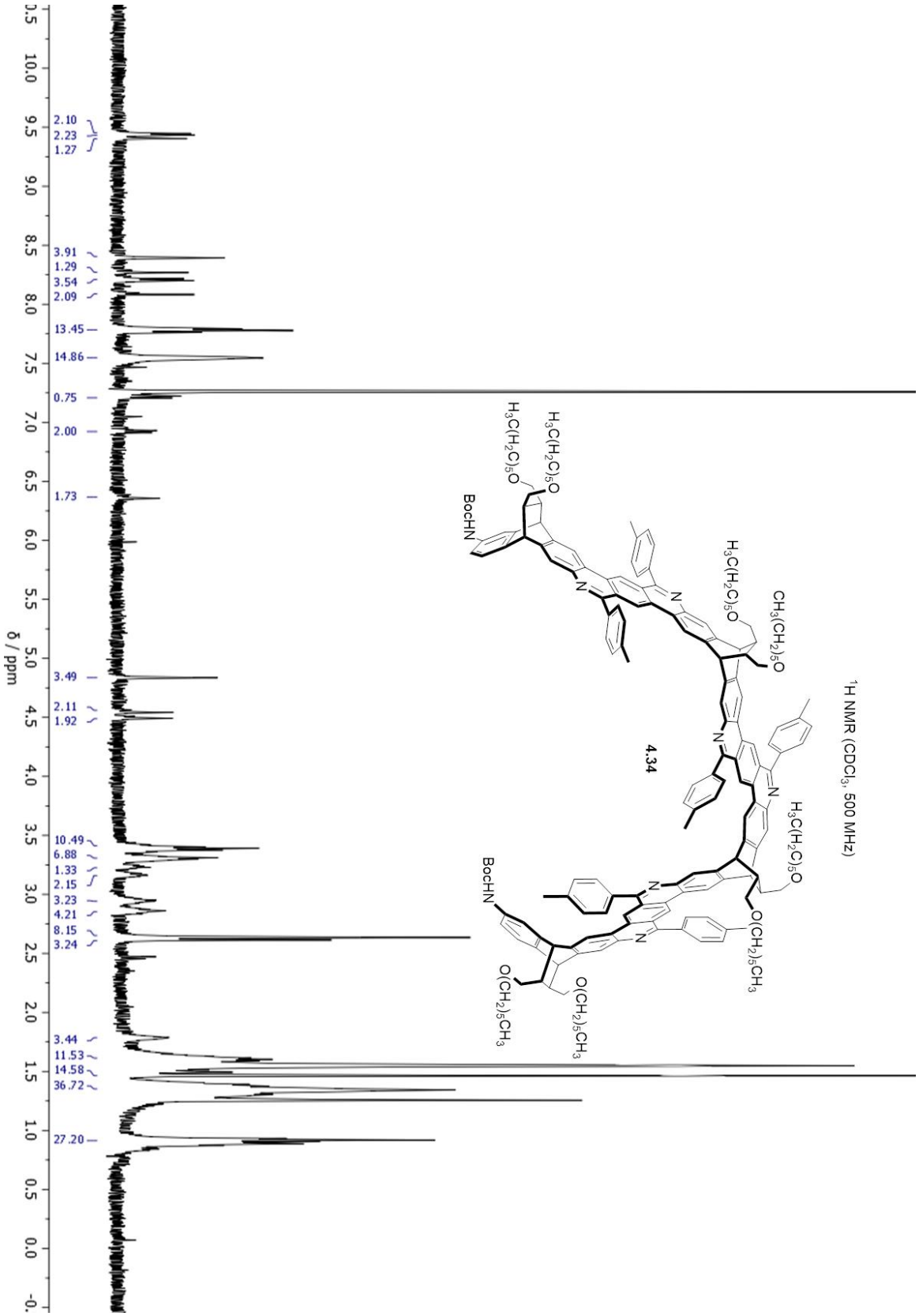
δ / ppm
10.5
10.0
9.5
9.0
8.5
8.0
7.5
7.0
6.5
6.0
5.5
5.0
4.5
4.0
3.5
3.0
2.5
2.0
1.5
1.0
0.5
0.0
-0.
2.10
2.23
1.27
3.91
1.29
3.54
2.09
13.45
14.86
0.75
2.00
1.73
3.49
2.11
1.92
10.49
6.88
1.33
2.15
3.23
4.21
8.15
3.24
3.44
11.53
14.58
36.72
27.20
4.34
BocHN
BocHN
$H_3C(H_2C)_5O$
$CH_3(CH_2)_5O$
$O(CH_2)_5CH_3$
N
^{1}H NMR ($CDCl_3$, 500 MHz)

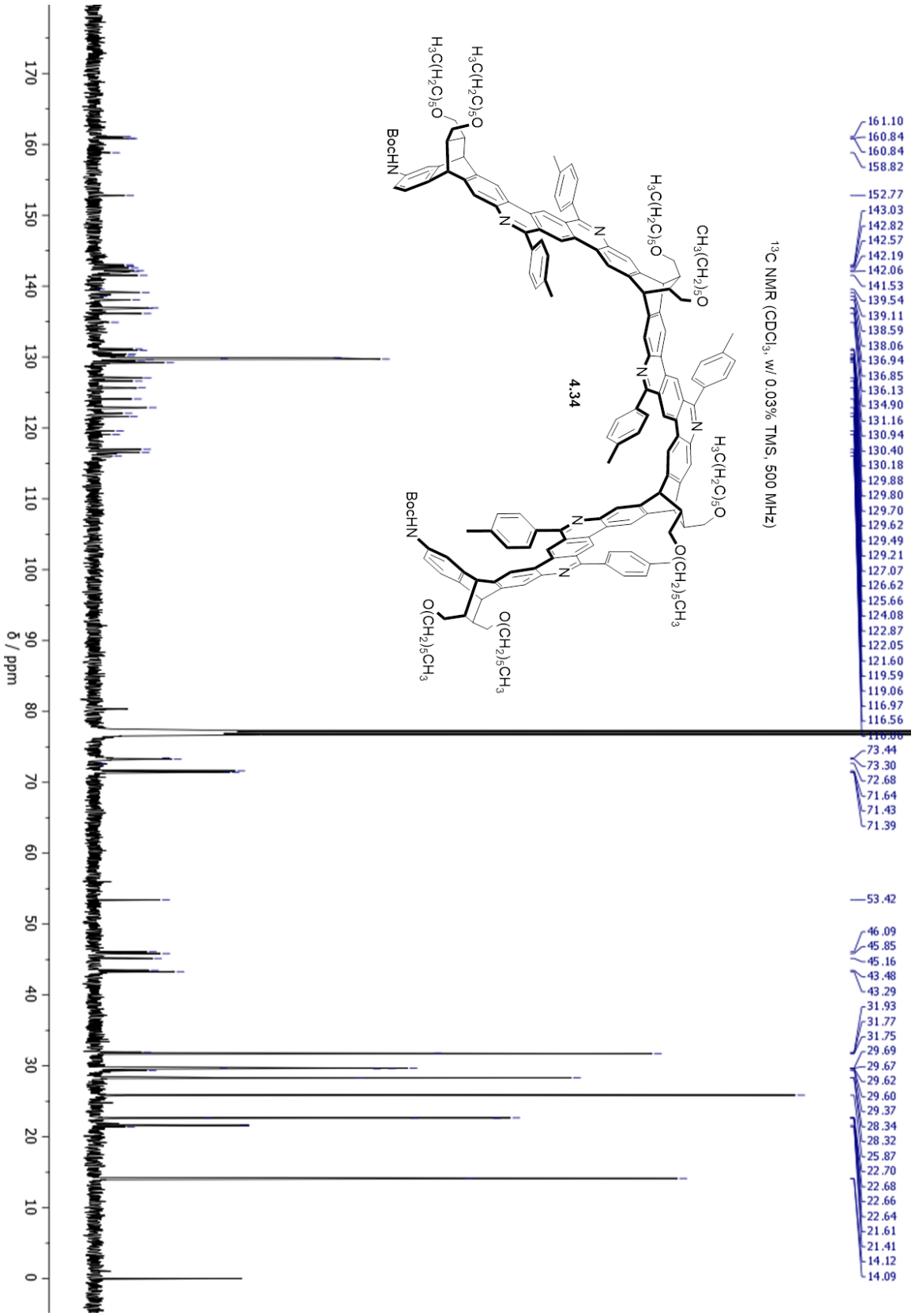
4.34
^{13}C NMR (CDCl$_3$, w/ 0.03% TMS, 500 MHz)
δ / ppm
161.10
160.84
160.84
158.82
152.77
143.03
142.82
142.57
142.19
142.06
141.53
139.54
139.11
138.59
138.06
136.94
136.85
136.13
134.90
131.16
130.94
130.40
130.18
129.88
129.80
129.70
129.62
129.49
129.21
127.07
126.62
125.66
124.08
122.87
122.05
121.60
119.59
119.06
116.97
116.56
73.44
73.30
72.68
71.64
71.43
71.39
53.42
46.09
45.85
45.16
43.48
43.29
31.93
31.77
31.75
29.69
29.67
29.62
29.60
29.37
28.34
28.32
25.87
22.70
22.68
22.66
22.64
21.61
21.41
14.12
14.09

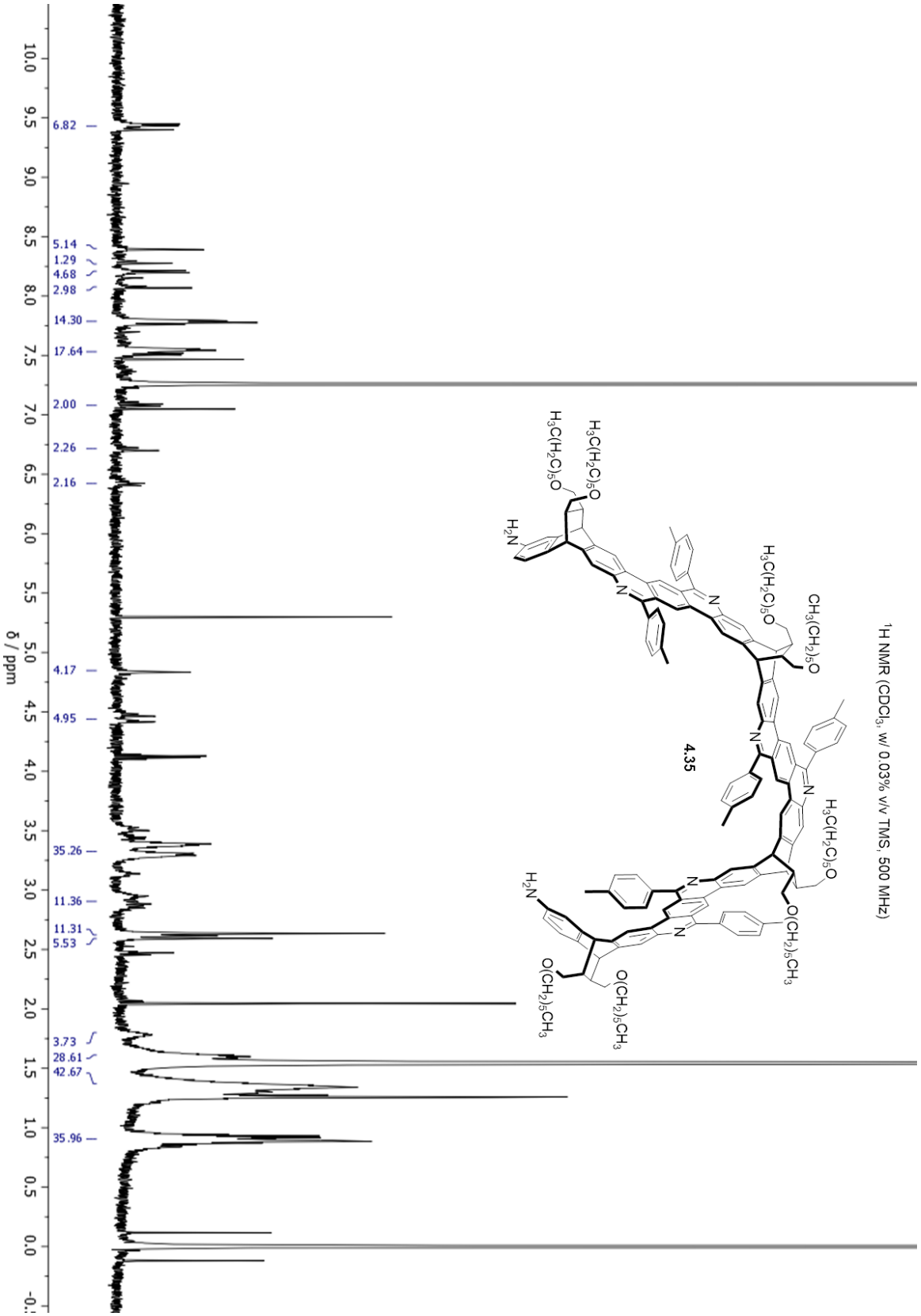
^{1}H NMR ($CDCl_3$, w/ 0.03% v/v TMS, 500 MHz)
4.35
δ / ppm
6.82
5.14
1.29
4.68
2.98
14.30
17.64
2.00
2.26
2.16
4.17
4.95
35.26
11.36
11.31
5.53
3.73
28.61
42.67
35.96

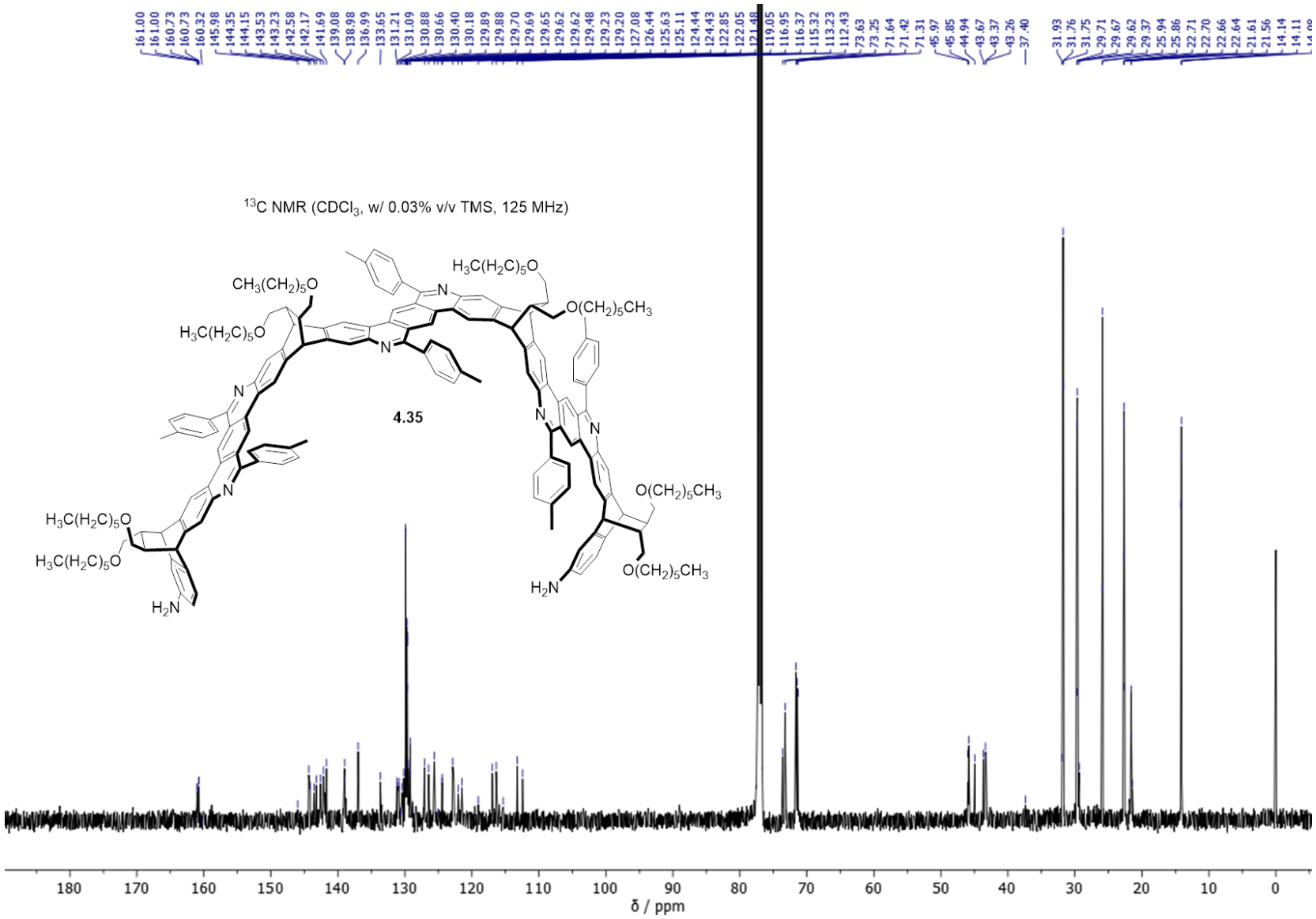
^{13}C NMR ($CDCl_3$, w/ 0.03% v/v TMS, 125 MHz)
4.35
δ / ppm

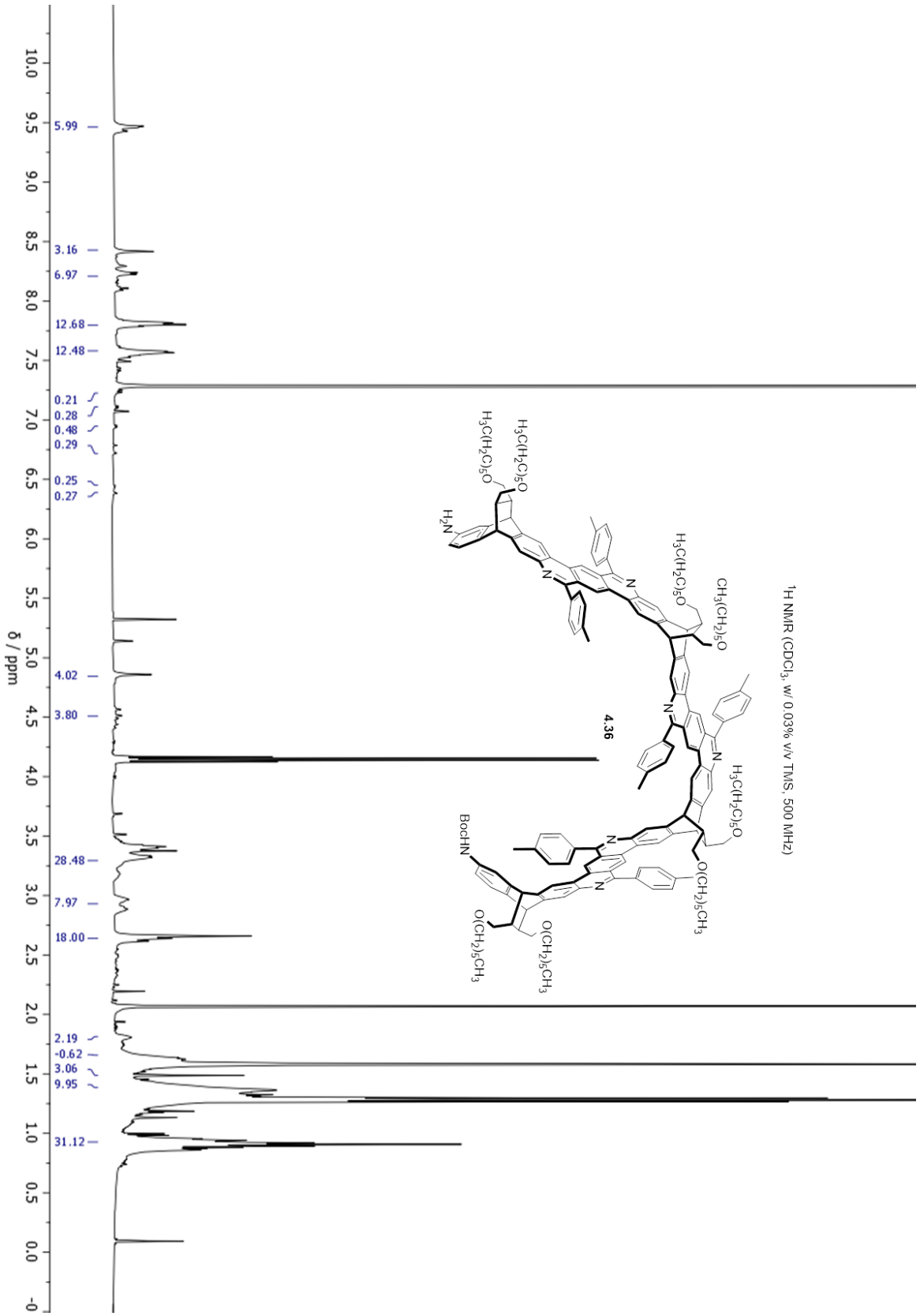
^{1}H NMR (CDCl$_3$, w/ 0.03% v/v TMS, 500 MHz)
δ / ppm
10.0
9.5
9.0
8.5
8.0
7.5
7.0
6.5
6.0
5.5
5.0
4.5
4.0
3.5
3.0
2.5
2.0
1.5
1.0
0.5
0.0
-0
5.99
3.16
6.97
12.68
12.48
0.21
0.28
0.48
0.29
0.25
0.27
4.02
3.80
28.48
7.97
18.00
2.19
-0.62
3.06
9.95
31.12
4.36
$H_3C(H_2C)_5O$
H_2N
$CH_3(CH_2)_5O$
BocHN
$O(CH_2)_5CH_3$
N

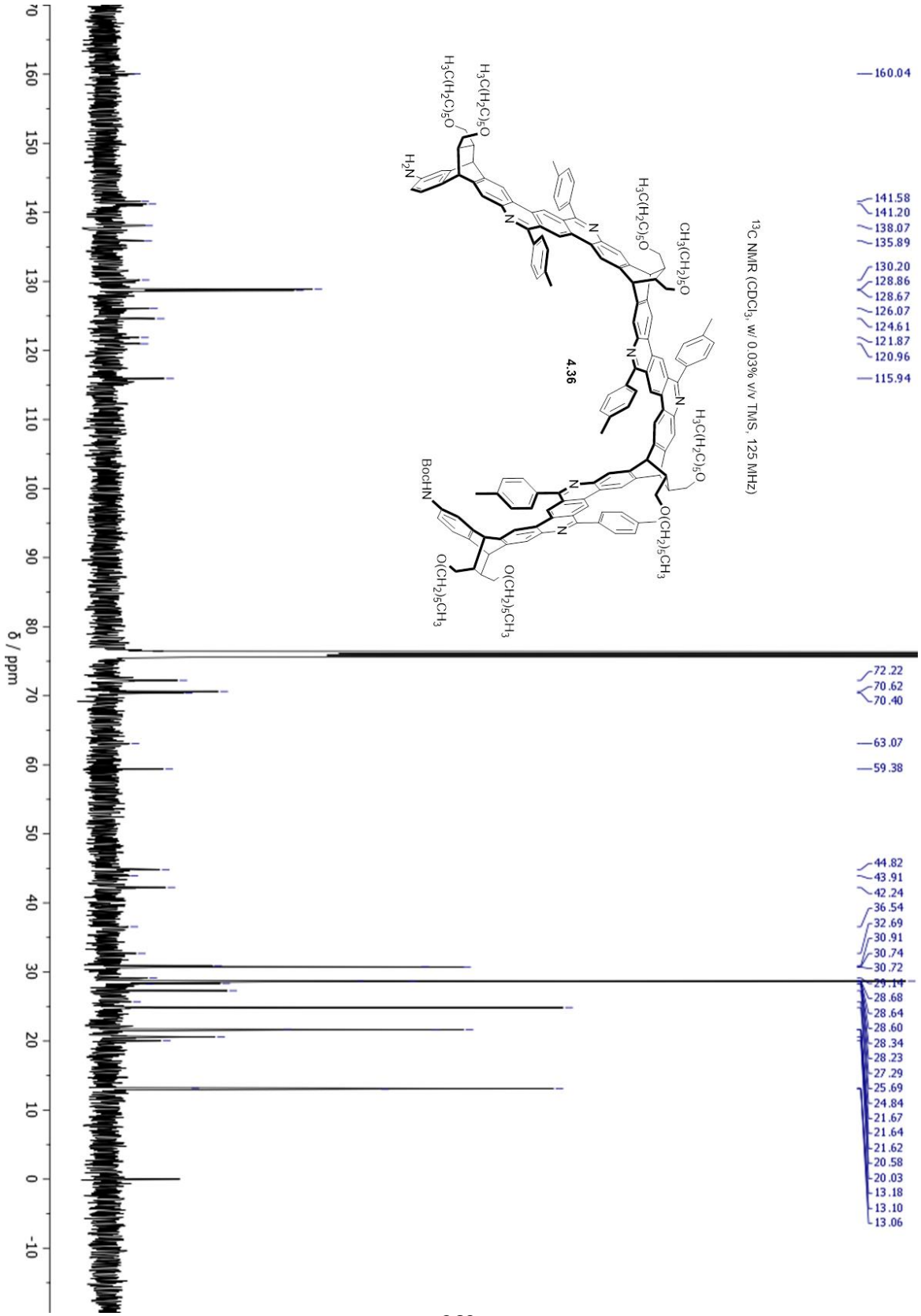
^{13}C NMR (CDCl$_3$, w/ 0.03% v/v TMS, 125 MHz)
4.36
δ / ppm
160.04
141.58
141.20
138.07
135.89
130.20
128.86
128.67
126.07
124.61
121.87
120.96
115.94
72.22
70.62
70.40
63.07
59.38
44.82
43.91
42.24
36.54
32.69
30.91
30.74
30.72
29.14
28.68
28.64
28.60
28.34
28.23
27.29
25.69
24.84
21.67
21.64
21.62
20.58
20.03
13.18
13.10
13.06

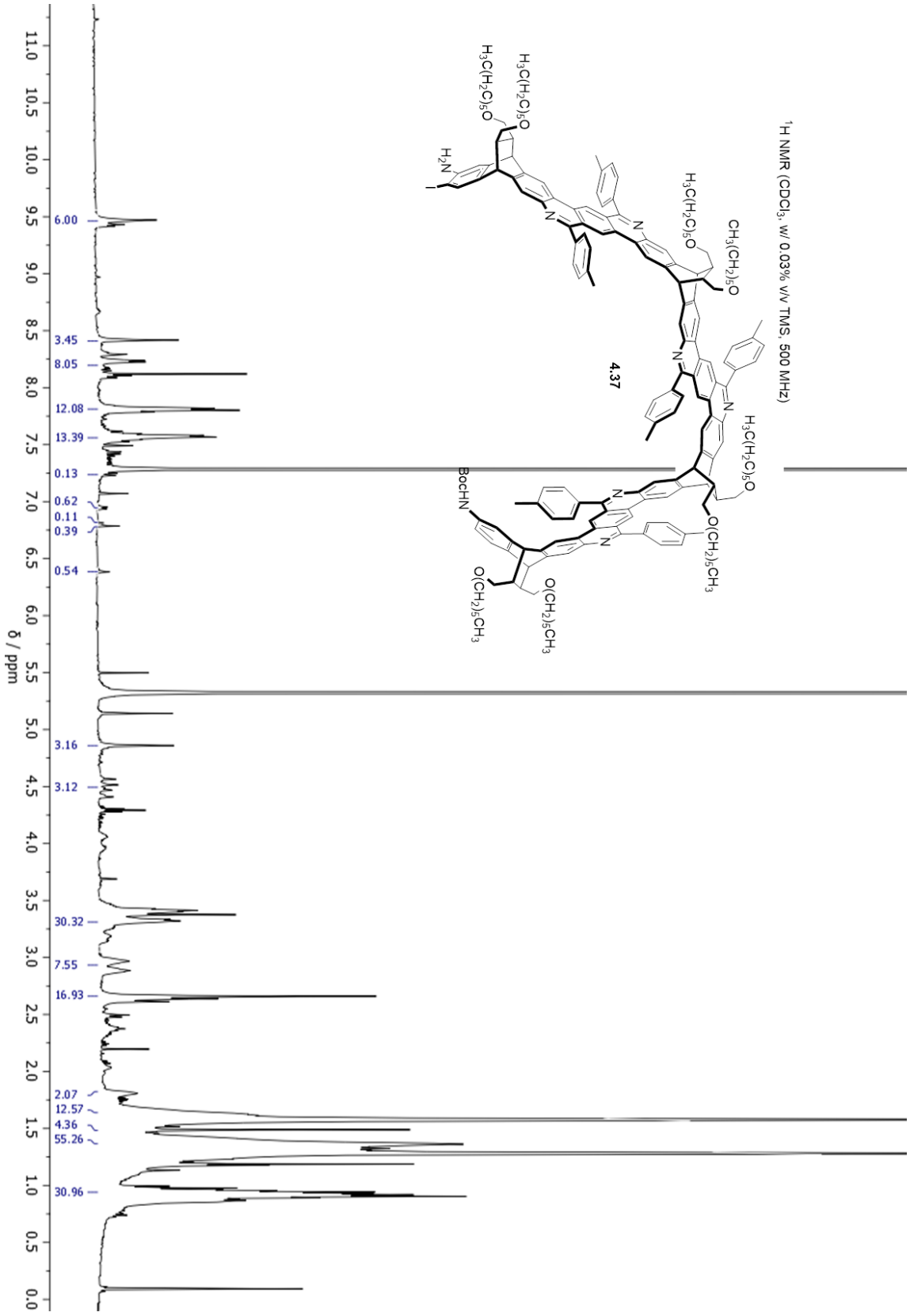
^{1}H NMR (CDCl$_3$, w/ 0.03% v/v TMS, 500 MHz)
4.37
δ / ppm
6.00
3.45
8.05
12.08
13.39
0.13
0.62
0.11
0.39
0.54
3.16
3.12
30.32
7.55
16.93
2.07
12.57
4.36
55.26
30.96

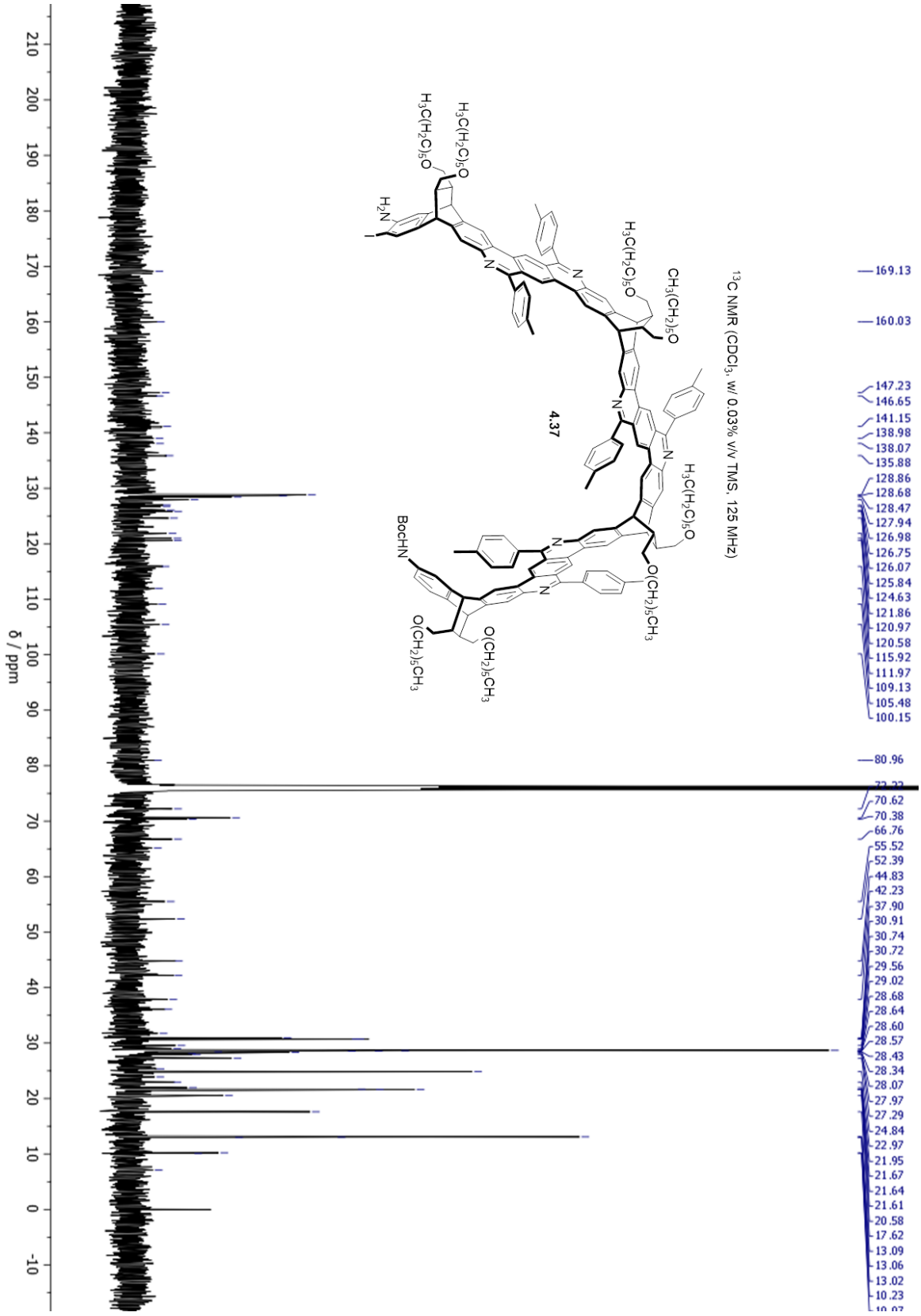
δ / ppm
210
200
190
180
170
160
150
140
130
120
110
100
90
80
70
60
50
40
30
20
10
0
-10
4.37
^{13}C NMR (CDCl$_3$, w/ 0.03% v/v TMS, 125 MHz)
169.13
160.03
147.23
146.65
141.15
138.98
138.07
135.88
128.86
128.68
128.47
127.94
126.98
126.75
126.07
125.84
124.63
121.86
120.97
120.58
115.92
111.97
109.13
105.48
100.15
80.96
70.62
70.38
66.76
55.52
52.39
44.83
42.23
37.90
30.91
30.74
30.72
29.56
29.02
28.68
28.64
28.60
28.57
28.43
28.34
28.07
27.97
27.29
24.84
22.97
21.95
21.67
21.64
21.61
20.58
17.62
13.09
13.06
13.02
10.23

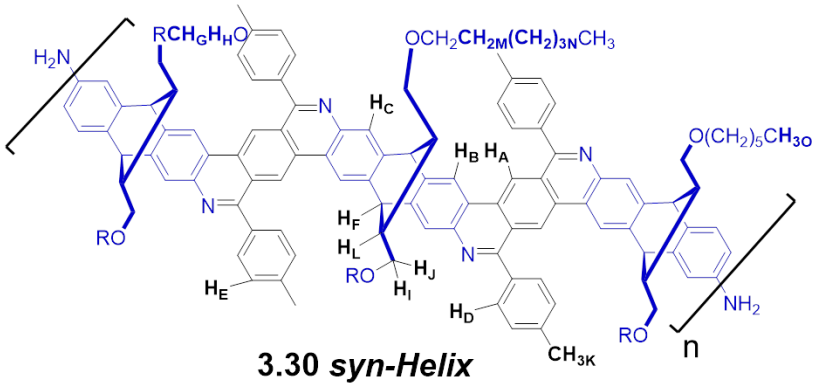

3.30 *syn-Helix*

***syn*-Helix T_1 Fit**

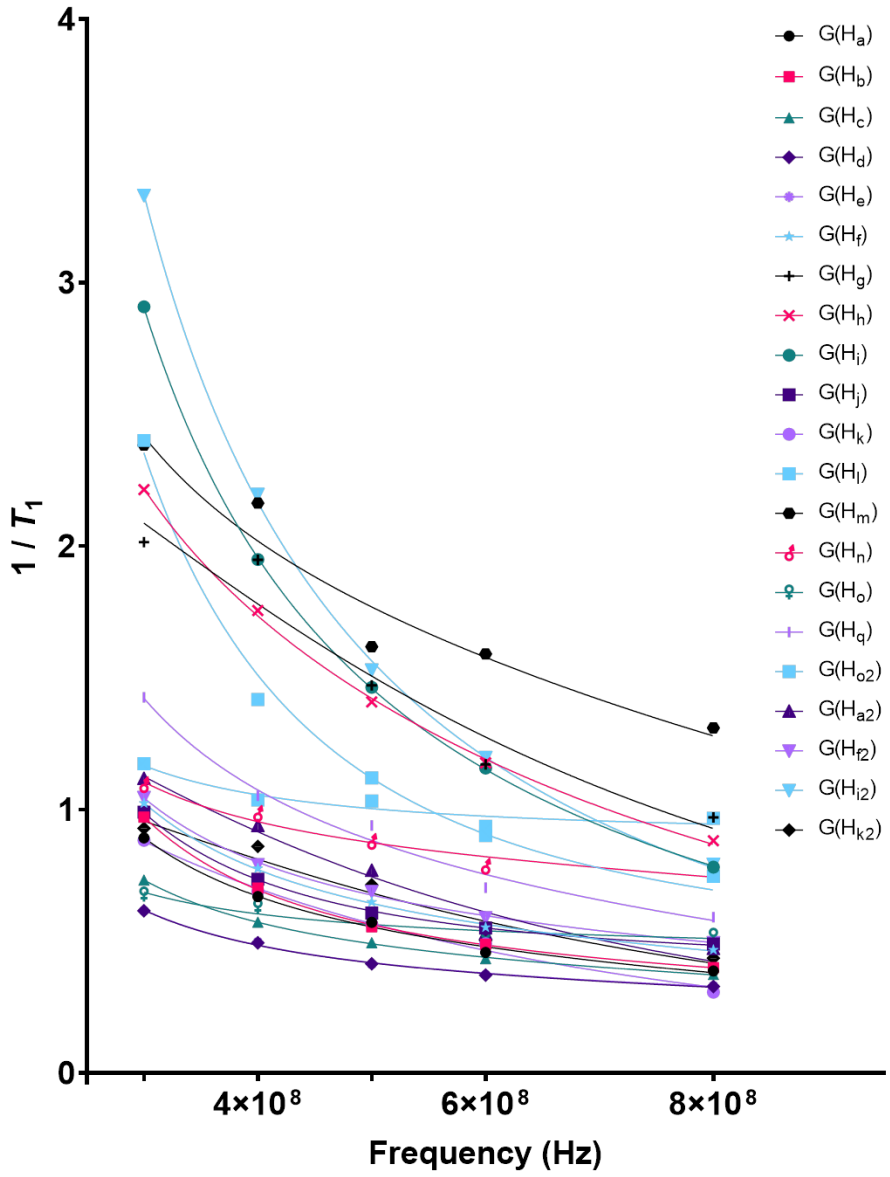

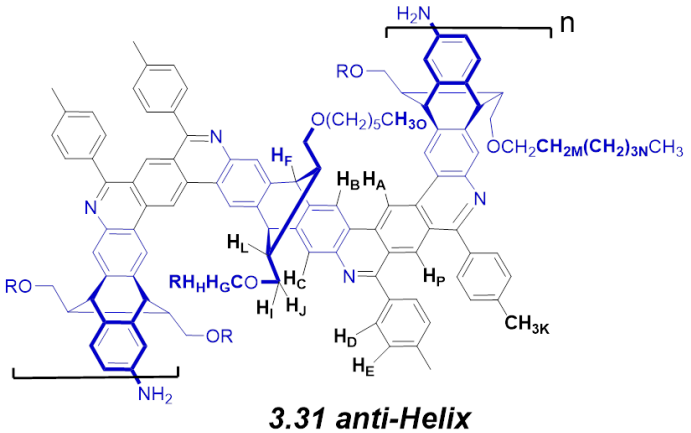

3.31 anti-Helix

anti-Helix T_1 Fit